Apolodor Aristotel Raduta

Nuclear Structure with Coherent States

Nuclear Structure with Coherent States

Apolodor Aristotel Raduta

Nuclear Structure with Coherent States

Apolodor Aristotel Raduta
Bucharest
Romania

Printed on acid-free paper

Preface

It is easy to understand that the structure as well as the value of a book depends essentially on the author's experience in the chosen field and on the readers for whom it is intended. After accumulating experience over many years of research and teaching, I felt the need to share my knowledge in theoretical nuclear physics with people whom I don't know.

Many of the procedures described in this book are different from the traditional ones, and also very powerful in describing the experimental data. In this context, I express my belief that real progress in our field may be achieved only by constantly trying something new. Although nowadays it is fashionable to concentrate on numerical analysis with complicated codes, this book is mostly based on analytical calculations which are to be used in numerical calculations. Over the years, I have had valuable collaborations with many outstanding physicists from all over the world. From each of them I have learned many new things. Now, it is a challenge for me to integrate their influences in a single style of presentation, so as to optimize the impact on readers. Let me mention the list of my collaborators from abroad to whom I will always be grateful for both illuminating discussions on the subject of this book and financial support: Profs. R.M. Dreizler, A. Faessler, N. Lo Iudice, E. Moya de Guerra, L. Zamick. Special thanks I owe to my friend Dr. A.C. Gheorghe for the wonderful and fruitful collaboration. Many of my Ph.D. students have chosen for their thesis subjects related to this work. To avoid forgetting to mention any one of them, I don't give the long list with their names but, instead, I thank them all at one go, but most heartily.

A special contribution was made by my wife Emilia who has always been near me, her affection helping me to have sufficient strength to accomplish this project and, at the same time, to continue with my normal activities. I thank her immensely for what she represents and does for me.

People who fail in explaining some of the existing data with the approaches they have at hand are advised to consult this work. I honestly hope that they will either find the solution here or be inspired to exploit the coherent state field to overcome the difficulties encountered. Of course readers will be the true judge of the validity and usefulness of my proposal. I certainly look forward to receive an echo from them.

<div style="text-align: right">Apolodor Aristotel Raduta</div>

Contents

Chapter 1
Introduction

It is customary to divide nuclear physics into two parts, one dealing with the nuclear structure and the other one with reaction mechanisms. The two domains interplay in treating common physics. In fact, the structural properties of nuclei are explored by various reactions and, in turn, the nuclear structure helps in interpreting reaction data. It is interesting to note that the range of subjects addressed by the nuclear structure field is closely related to the energy pumped to the projectiles which is further transferred to the target nucleus. Depending on the mass of the projectile ion, the populated levels are located at low or at large excitation energies. The intermediate compound nucleus loses neutrons or decays through α, proton or γ channels. To identify the final state of the residual nucleus, one has to interpret the data of γ-particle and γ-γ coincidence, angular distribution or the measurement through various methods of the lifetime of the metastable state. It is obvious that such achievements depend on the development of heavy ion accelerators as well as detection techniques. In this context we mention that nowadays many large heavy ion accelerators are in operation and sophisticated detectors (to give only few examples, we mention EUROGAM, GAMMASPHERE, EUROBALL, and JUROSPHERE) are functioning with a high efficiency. Both devices contribute to investigating a large number of nuclear states belonging to different bands and ranging from low up to a high and very high spins. The number of nuclei explored has been enlarged due to the experiments with radioactive beams, where the unstable nuclei used as projectile could be investigated.

Of course at the beginning of the 50's of the last century, the linear accelerators for protons and α particles could identify only few states. Therefore the theories were aimed mainly at explaining the observed properties related to these levels. In the meantime, as the experimental devices were improved, the volume of the data has continuously increased and, as expected, the existing theoretical approaches were not able to explain some of the newly accumulated information. Under these circumstances, it became necessary to improve the previous formalisms or to propose new approaches. In this way several models appeared over time, of which I shall refer only to the phenomenological ones. In chronological order the proposed formalisms were: (a) The liquid drop model proposed by Bohr and Mottelson; (b) The model of Wilets and Jean devoted to the γ unstable nuclei and possible phase transitions;

1

(c) The model of the triaxial rotor proposed by Davydov and Filippov; (d) The rotation–vibration model of Faessler and Greiner; (e) The model of Gneuss and Greiner which studies anharmonic Hamiltonians in the quadrupole shape coordinates; (f) The projection method proposed by Lipas; (g) The two-rotor model of Lo Iudice and Palumbo; (h) The interaction boson approximation which exploits the nuclear system symmetries, and (i) The coherent state model proposed by Raduta and his collaborators. Microscopic theories have also made notable progress but, due to the very large many body basis they require, it is not yet possible to approach the high spin states in heavy nuclei, although this target may not to be too far away.

Once many data as well as a wealth of theoretical results were accumulated, several books appeared with the ambitious goal of describing the current status of the field in an exhaustive manner. I think that all readers will have consulted at least one of the books authored by: Preston, Bohr and Mottelson, De Shalit and Talmi, De Shalit and Feshbach, Eisenberg and Greiner, Ring and Schuck, Williams, Suhonen, etc. The later the date on which the book appeared, the more complete is the description of the nuclear system.

As mentioned already, each model has specific merits and on the other hand many drawbacks. For this reason, the newly proposed approaches focus on the properties not explained by the preceding models. In this context one could assert that the coherent state model has the merit of covering the previous descriptions and of attacking new features.

The present book is structured as follows. We start by emphasizing the essential properties which recommend the use of the coherent states in describing nuclear systems. One knows that the coherent state has the defining property of minimizing the uncertainty equations associated with a pair of canonical conjugate coordinates. Also, the function does not obey some symmetries which must be fulfilled in the laboratory frame. The question we posed is whether these properties are preserved or violated, to a certain extent, when the broken symmetries are restored. Since in many circumstances one needs to factorize the coherent state involved in the specific treatment, a proof of the factorization theorem of Baker-Campbell-Haussdorf is given. All these issues are discussed in Chap. 2. In Chap. 3 we present the closed formula for the ground band energies proposed by Holmberg and Lipas (HL). Further another three compact formulas for these energies are proposed. All three describe the excitation energies in the ground band up to high and very high spin. They are distinct generalizations of the HL result.

Chapter 4 is devoted to a time-dependent variational principle (TDVP) description of a triaxial rotor. Several boson representations for the initial quantum mechanical object are described. A tilted rotor is semiclassically treated. Classical trajectories corresponding to various phases are analytically obtained and then quantized.

The use of a coherent state as a trial function for the TDVP equation associated with paired many body systems is presented in Chap. 5. Here it has been proved that the BCS, RPA (random phase approximation) and boson expansion approaches have a classical origin. With a coherent state as a variational state for a generalized BCS ground state one derives analytical expressions for the gauge and isospin projected states and corresponding energies. Comparing them with the exact results, for a single

j case one concludes that the projected states describe the irreducible representation of the O(5) group. Making use of a coherent state for the group SU(1,1), one obtains the full space of states describing a system of bosons correlated by pairing interaction.

Chapter 6 is devoted to the coherent state model for three interaction bands: ground, β and γ. Energies and transition rates are expressed in terms of a single overlap integral and its first derivative. These quantities are further analyzed in the extreme limits, vibrational and rotational. For these limits we provide compact analytical results which are easy to use in numerical applications. Also the model is presented in the intrinsic frame of reference. Numerical results for a large number of nuclei, possessing various symmetries, agree very well with the experimental data.

The CSM is extended to the pear-shaped nuclei in Chap. 7. To the three bands described by CSM one attaches three partner bands of negative parity. Besides that the dipole parity partner bands are considered. Thus, the mentioned extension describes simultaneously eight rotational bands, four of positive and four of negative parity. Signatures for the existence of a static octupole deformed shape are pointed out. Comparison with available experimental data reveals good agreement.

In Chap. 8, to a phenomenological CSM core we couple a set of interacting nucleons. Thus, we study the crossing of a collective and a two quasiparticle-core bands in even-even nuclei and of one quasiparticle and three quasiparticles bands in even-odd nuclei. These states are all of positive parity. Switching on the interaction with a system of octupole bosons, three pairs of parity partner bands in even-odd nuclei are presented.

Chapter 9 deals with a generalized coherent state model (GCSM) which distinguishes between the proton- and neutron-like bosons. The model describes simultaneously the ground, β and γ bands and an additional band built on the top of a magnetic state of scissors type. The model for the scissors-like state 1^+, contains the results of the two rotors (TRM) and two liquid drop models (TLDM) as limiting cases.

In Chap. 10, we study two applications of the GCSM: (a) Chiral symmetries in even-even nuclei and (b) Monopole charge properties of nuclei.

The results obtained by the author of this book and his collaboration concerning the quadrupole boson basis and its degeneracies are given in Chap. 11.

The overcomplete property of the coherent state allows it to be used as a generating function for a collective basis. Moreover, Chap. 12 gives a prescription for how to generate a projected spherical single particle basis, which may describe in an unified fashion the spherical and the deformed nuclei.

Chapter 13 describes semiclassically a fourth- and a solvable sixth-order boson Hamiltonian. For the first case one obtains a set of RPA like equations for small oscillations around a minimum value of the potential energy. Also, by a Fourier analysis of the classical action density, one obtains the quantal spectrum corresponding to a large amplitude motion of the system. In the second case analytical trajectories in a double well potential are provided. Also some signatures for the phase transition from one well to another are pointed out. A quantitative result for the tunneling process through the barrier separating the two wells is given. The trajectories in the two wells are quantized by a specific restriction on the classical action. Finally,

we consider another sixth-order boson Hamiltonian, which is diagonal in the SU(5) basis $|Nv\alpha JM\rangle$. Both the semiclassical and the quantal spectra are given by simple expressions in terms of the involved quantum numbers. These were successfully used to interpret some recent data concerning the monopole (0^+) and quadrupole (2^+) multiplets.

The 13 chapters have some common features: (a) Most results are presented in an analytical form; (b) In order not to alter the reading of the essential part of the concrete issue, the complicated formulas are collected in an Appendix, placed at the end of the book; (c) They are applied numerically for many nuclei and compared with the available experimental data as well as with those obtained through a different approach.

A detailed comparison of the CSM with five other phenomenological models is presented in Chap. 14, while Chap. 15 summarizes the main results of the present book. Back matter is a collection of appendices which either list the complex formulas referred to in the preceding chapters or are devoted to the mathematical tools needed in the book.

Chapter 2
Classical Versus Quantal Features in a Projected Coherent State

2.1 Definitions and Preliminaries

Most properties of the low lying spectra can be described in terms of few collective degrees of freedom. These can be given either phenomenologically [RBD95, RBF11] or in terms of single particle motion. Thus, projecting out the collective degrees of freedom from a many body system was always a central topic of nuclear structure theory [BaVe78, Vil77]. Accounting for collective motion and moreover for the coupling of the mentioned degrees of freedom with the non-collective coordinates is not an easy task. A significant simplification is achieved when one defines a semiclassical approach by means of a variational principle. Transferring the quantum mechanical many body problem to a semiclassical picture allows us to use the classical mechanical tools which are more developed and efficient. This operation is conventionally called dequantization procedure which is most reliable if the variational state is of the coherent type. The meaning of this statement is that the quantized classical trajectories lead to a spectrum, which is close to that corresponding to the initial many body Hamiltonian. Due to the overcomplete property of coherent states a full account of the dynamic in the whole Hilbert space is possible. Indeed, by expanding the coherent state in a Hilbert space basis, no expansion coefficient is vanishing. For example if we treat a boson Hamiltonian with coherent states the matrix elements include the contribution from all states of the boson space, which is not the case when a diagonalization method is adopted.

As a matter of fact this is the property which was exploited in many publications about the Coherent State Model (CSM) [RD76, RCGD82, HHL70]. This model uses an axially quadrupole deformed coherent state of Glauber type as an intrinsic ground state. Moreover, other two deformed states are defined by lowest order polynomial excitations of ground state, the excitations being defined so that some experimental data are satisfied. These states are modeling the intrinsic beta and gamma bands states, respectively. By angular momentum projection three sets of states are obtained which are to describe the main properties of the ground, beta and gamma bands. By construction the polynomial excitations are chosen such that the three intrinsic states

as well as the three sets of projected states are mutually orthogonal, respectively. Within the restricted boson space of projected states, obtained as described above, an effective Hamiltonian is defined such that the three bands are maximally decoupled. The CSM works especially well for high spin states. These states behave more or less semiclassically. This can be proved by the following simple reasoning. Suppose we have a spherical rigid rotor with the spectrum

$$E_J = \frac{J(J+1)\hbar^2}{2\mathcal{J}}. \tag{2.1.1}$$

Going with $\hbar$ to zero and with J to infinity like $k/\hbar$ with k constant one obtains that E_J is a constant with respect to J which in fact reclaims a classical behavior.

To prove the fact that a coherent state is suitable for accounting the classical properties we have to study the behavior of both unprojected and angular momentum projected state, from the point of view of the Heisenberg uncertainty relations.

Let us consider the coherent state defined with the z-component of the quadrupole boson operators $b_{2\mu}^\dagger$, $b_{2\mu}$ with $-2 \le \mu \le 2$:

$$|\Psi\rangle = e^{(db_{20}^\dagger - d^* b_{20})}|0\rangle, \tag{2.1.2}$$

where $|0\rangle$ stands for the boson vacuum state while d is a complex number. The coherent nature of this function is determined by:

$$b_{20}|\Psi\rangle = d|\Psi\rangle, \quad \langle\Psi|b_{20}^\dagger = d^*. \tag{2.1.3}$$

This equation can be proved by using the operator equation:

$$e^{\hat{A}} \hat{O} e^{-\hat{A}} = \sum_{n=0}^{\infty} \frac{1}{n!} [[A, \ldots [A, O]..]]. \tag{2.1.4}$$

Indeed, choosing $\hat{O} = b_{20}$ and $-\hat{A} = db_{20}^\dagger - d^* b_{20}$, one obtains:

$$b_{20}|\Psi\rangle = e^{-\hat{A}} e^{\hat{A}} b_{20} e^{-\hat{A}}|o\rangle = e^{-\hat{A}}(b_{20} + d)|0\rangle = d|\Psi\rangle \tag{2.1.5}$$

The second Eq. (2.1.3) is obtained from the first one by applying the Hermitian conjugation operation to it.

Using the Baker-Campbell-Hausdorff factorization:

$$e^{A+B} = e^A e^B e^{-\frac{1}{2}[A,B]}, \tag{2.1.6}$$

the coherent state is written in the form:

$$|\Psi\rangle = e^{-\frac{|d|^2}{2}} e^{db_{20}^\dagger}|0\rangle. \tag{2.1.7}$$

The average of the quadrupole operator:

$$Q_{20} = q_0 \left(b_{20}^{\dagger} + b_{20} \right), \tag{2.1.8}$$

with the coherent state has the expression:

$$\langle \Psi | Q_{20} | \Psi \rangle = 2q_0 Re\ d. \tag{2.1.9}$$

Thus the real part of d has the significance of the quadrupole deformation. Similarly, averaging the quadrupole momentum, conjugate of Q_{20}, with the coherent state one finds that the imaginary part of d is proportional with the classical quadrupole momentum. The function $|\Psi\rangle$ is a vacuum state for the shifted quadrupole boson operator:

$$(b_{20} - d) |\Psi\rangle = 0. \tag{2.1.10}$$

which is obvious from (2.1.5). The function $|\Psi\rangle$ has not a definite angular momentum, i.e. it is not eigenfunction of the angular momentum operator squared, $\hat{J}^2$. However it is eigenstate of $\hat{J}_z$. Due to this feature we say that $|\Psi\rangle$ is an axially deformed function. This statement can be easily proved by writing the r.h.s. of Eq. (2.1.7) as a boson power series:

$$|\Psi\rangle = e^{-\frac{|d|^2}{2}} \sum_{n=0} \frac{1}{n!} d^n \left(b_{20}^{\dagger} \right)^n |0\rangle. \tag{2.1.11}$$

The first term of the expansion is proportional to the vacuum state which is of zero angular momentum, the second term is a quadrupole state while the third one is proportional to

$$\sum_{J=0,2,4} C_{0\ 0\ 0}^{2\ 2\ J} \left(b_2^{\dagger} b_2^{\dagger} \right)_{J0} |0\rangle \equiv \sum_{J=0,2,4} \mathcal{A}_J |2, J, 0\rangle \tag{2.1.12}$$

where in the r.h.s. is a superposition of states of two bosons, angular momentum J (=0, 2, 4) and projection zero. Similarly, the three boson term is a superposition of states $|3, J, 0\rangle$ with $J = 0, 2, 3, 4, 6$. Therefore, the coherent state is a super-position of components with various angular momenta and vanishing projection. It is clear now that the state under consideration breaks two symmetries, namely the rotational and the gauge ones. The last symmetry breaking is evident since according to Eq. (2.1.11), $|\Psi\rangle$ is a sum of components with different number of bosons.

Since we want to discuss the classical features which might be described with the CSM we restrict our considerations to the case of real d. In terms of bosons, the quadrupole coordinate and its conjugate momentum can be defined as:

$$\alpha_{2\mu} = \frac{1}{k\sqrt{2}} \left(b_{2\mu}^{\dagger} + (-1)^{\mu} b_{2,-\mu} \right), \quad \pi_{2\mu} = \frac{ik}{\sqrt{2}} \left((-1)^{\mu} b_{2,-\mu}^{\dagger} - b_{2\mu} \right). \tag{2.1.13}$$

The above transformation is canonical irrespective of the value of the real constant k. The vacuum state $|0\rangle$ is a function of coordinate only. Indeed, the equation

$$b_{20}|0\rangle = 0, \qquad (2.1.14)$$

can be written as:

$$\frac{\partial}{\partial \alpha_{20}}|0\rangle = -k^2 \alpha_{20} \qquad (2.1.15)$$

This equation can be integrated with the result:

$$|0\rangle = C e^{-\frac{k^2 \alpha_{20}^2}{2}}. \qquad (2.1.16)$$

with C an integration constant. Therefore the vacuum state depends only on the quadrupole coordinate but not on the momenta. For the sake of simplicity let us denote by

$$F(\alpha_{2\mu}) = |0\rangle. \qquad (2.1.17)$$

The coherent state can be written as:

$$\Psi = e^{-i\frac{\sqrt{2}d}{k}\pi_{20}} F(\alpha_{2\mu}) = e^{-\frac{\sqrt{2}d}{k}\frac{\partial}{\partial \alpha_{20}}} F(\alpha_{2\mu})$$

$$= \sum_n \frac{(-\frac{\sqrt{2}d}{k})^n}{n!} \left(\frac{\partial}{\partial \alpha_{20}}\right)^n F(\alpha_{2\mu}) = F(\alpha_{2,-2}, \alpha_{2,-1}, \alpha_{20} - \frac{\sqrt{2}d}{k}, \alpha_{21}, \alpha_{22}).$$

$$(2.1.18)$$

This equation shows that the coherent state is just the vacuum state with the coordinate α_{20} shifted to $\alpha_{20} - \frac{d\sqrt{2}}{k}$. The shift operation is achieved by the displacement operator:

$$D(d) = e^{d(b_{20}^\dagger - b_{20})}. \qquad (2.1.19)$$

The mentioned operator breaks the rotational symmetry. Indeed, let us consider the simplest invariant, namely a harmonic Hamiltonian:

$$H = \omega \sum_\mu b_{2\mu}^\dagger b_{2\mu} \qquad (2.1.20)$$

Under the action of the operator D(d) one obtains a rotational non-invariant term:

$$D(d)HD(-d) = H - d\omega \left(b_{20}^\dagger + b_{20}\right) + \omega d^2. \qquad (2.1.21)$$

Note that the displacement operator transforms the scalar operator H into an operator which is not invariant to rotations. Let us consider now the Hermitian operator:

$$H^{'} = H + \lambda b_{20}^{\dagger} + \lambda^{*} b_{20} \tag{2.1.22}$$

Applying this equation on the coherent state Ψ, we obtain:

$$H^{'}\Psi = \left(\omega d b_{20}^{\dagger} + \lambda b_{20}^{\dagger} + \lambda^{*} d \right) \Psi \tag{2.1.23}$$

Choosing d such that $\omega d + \lambda = 0$, the above equation becomes:

$$H^{'}\Psi = -\frac{|\lambda|^2}{\omega} \Psi \tag{2.1.24}$$

From this equation it results that the deformed Hamiltonian $H^{'}$ admits the coherent state as eigenstate. Consider now that the coefficients λ and λ^{*} are functions of time in the Hamiltonian:

$$H(t) = \omega b_{20}^{\dagger} b_{20} + \lambda(t) b_{20}^{\dagger} + \lambda^{*}(t) b_{20} \equiv H_0 + H_{int} \tag{2.1.25}$$

The Hamiltonian H_0 has the eigenstates:

$$H_0|n\rangle = n\omega|n\rangle, \quad |n\rangle = \frac{1}{\sqrt{n!}} \left(b_{20}^{\dagger} \right)^n |0\rangle. \tag{2.1.26}$$

On the other hand the coherent state can be written as:

$$|\Psi\rangle \equiv |d\rangle = e^{-\frac{|d|^2}{2}} \sum_n \frac{1}{n!} \left(d b_{20}^{\dagger} \right)^n |0\rangle = e^{-\frac{|d|^2}{2}} \sum_n \frac{d^n}{\sqrt{n!}} |n\rangle \tag{2.1.27}$$

Within the interaction representation we define the time dependent state:

$$|d(t)\rangle = e^{-i H_0 t/\hbar} |d\rangle = e^{-\frac{|d|^2}{2}} \sum_n \frac{(de^{-i\omega t})^n}{\sqrt{n!}} |n\rangle = |de^{-i\omega t}\rangle \tag{2.1.28}$$

The time dependent Schrödinger equation associated to $H(t)$ reads:

$$i\frac{\partial}{\partial t}|\phi(t)\rangle = H(t)|\phi(t)\rangle = \left[\omega b_{20}^{\dagger} b_{20} + \lambda(t) b_{20}^{\dagger} + \lambda^{*}(t) b_{20} \right] |\phi(t)\rangle. \tag{2.1.29}$$

Supposing that at the initial moment of time the system stays in the vacuum state. Then the formal solution of the above equation is [ZH90]:

$$|\phi(t)\rangle = e^{-\frac{i}{\hbar}\int_0^t dt'\left(\hbar\omega b_{20}^\dagger b_{20}+\lambda(t')b_{20}^\dagger+\lambda^*(t')b_{20}\right)}|0\rangle$$
$$= \exp\left[d(t)b_{20}^\dagger - d^*(t)b_{20}\right]|0\rangle e^{i\eta(t)} = |d(t)\rangle e^{i\eta(t)}, \qquad (2.1.30)$$

where the following notations have been used:

$$d(t) = -ie^{-i\omega t}\int_0^t \lambda^*(\tau)e^{i\omega\tau}d\tau,$$

$$\eta(t) = -\frac{1}{2}\omega t - \int_0^t Re\left[\lambda(\tau)d(\tau)\right]d\tau \qquad (2.1.31)$$

This result says that the system remains always in a coherent state. Therefore, *if at the initial time the system is in a coherent state, including the extremal state, it will remain in a coherent state for ever.*

Now we shall present another definition of the coherent state based on the group theory. Let us note first that the set of operators $\{\hat{n} = b_{20}^\dagger b_{20}, b_{20}^\dagger, b_{20}, I\}$ where I stands for the unity operator, form a Lie algebra denoted by h_4. The corresponding group is conventionally called the Heisenberg-Weyl group and denoted by H_4. The Hilbert space of H_4 is spanned by the eigenstate of the number operator:

$$b_{20}^\dagger b_{20}|n\rangle = n|n\rangle. \qquad (2.1.32)$$

Using the notation $H_0 = b_{20}^\dagger b_{20}$, we have:

$$H_0|n\rangle = n|n\rangle \qquad (2.1.33)$$

It results that the vacuum state is the ground state of H_0. In that respect the vacuum state is an extremal state for H_0. We shall call stability subgroup that subgroup which leaves the extremal state invariant. For H_4 the stability subgroup is $U(1) \otimes U(1)$ with an algebra spanned by $\{\hat{n}, I\}$. The stability group consists of all operations of the form:

$$h = e^{i(\delta\hat{n}+\varphi I)}. \qquad (2.1.34)$$

Thus

$$h|0\rangle = |0\rangle e^{i\varphi}. \qquad (2.1.35)$$

The coset $H_4/U(1) \otimes U(1)$ is a set of elements Ω which provides for any element g from H_4 a unique decomposition:

$$g = Dh \tag{2.1.36}$$

A typical representative in the coset space $H_4/U(1) \otimes U(1)$ is:

$$D(d) = exp(db_{20}^\dagger - d^* b_{20}). \tag{2.1.37}$$

By definition a coherent state is the action of the coset elements on the extremal state.

$$\Psi = D(d)|0\rangle. \tag{2.1.38}$$

Remarkably, the coherent state of the Glauber type and the one defined on group theory grounds are identical. This is not generally true. This will be explicitly shown for the case of the $SU(2)$ group.

The properties mentioned above for the coherent states are the basic ones, which will be used in various contexts along this book. In this chapter we shall focus on the semiclassical features of the coherent states with symmetries restored.

2.2 Unprojected State

2.2.1 The Quadrupole Coordinate and Momentum

The conjugate coordinates:

$$\hat{\alpha}_{20} = \frac{1}{\sqrt{2}}\left(b_{20}^\dagger + b_{20}\right), \quad \hat{\pi}_{20} = \frac{i}{\sqrt{2}}\left(b_{20}^\dagger - b_{20}\right), \tag{2.2.1}$$

satisfy the equation:

$$[\hat{\alpha}_{20}, \hat{\pi}_{20}] = i, \tag{2.2.2}$$

where "i" denotes the imaginary unit. Conventionally, we use the units system where $\hbar = 1$.

The averages of $\hat{\alpha}$ and $\hat{\alpha}^2$ on $|\Psi\rangle$ are:

$$\langle\Psi|\hat{\alpha}_{20}|\Psi\rangle = \sqrt{2}d, \quad \langle\Psi|\hat{\alpha}_{20}^2|\Psi\rangle = 2d^2 + \frac{1}{2}. \tag{2.2.3}$$

The conjugate momentum and its square have the averages:

$$\langle\Psi|\hat{\pi}_{20}|\Psi\rangle = 0, \quad \langle\Psi|\hat{\pi}_{20}^2|\Psi\rangle = \frac{1}{2}. \tag{2.2.4}$$

Using these results, the uncertainty relation associated to the conjugate coordinates α and π has the form:

$$\Delta\hat{\alpha}_{20}\Delta\hat{\pi}_{20} = \frac{1}{2}, \tag{2.2.5}$$

where by Δx one denotes the dispersion of the coordinate x. Notice that the dispersion product reaches the minimum value of the set allowed by the Heisenberg uncertainty principle. Due to this feature one asserts that the coherent state $|\Psi\rangle$ is an optimal state to describe the properties which define the border of quantal and classical behavior.

2.2.2 The Boson Number and Its Conjugate Phase

In this subsection we consider again that d is a complex number. Let us denote by $\hat{N}_0$ the boson number operator:

$$\hat{N}_0 = b_{20}^\dagger b_{20}. \tag{2.2.6}$$

Writing the operator $\hat{N}_0^2$ in a normal order, the expectation values for $\hat{N}_0$ and $\hat{N}_0^2$ can be easily calculated:

$$\begin{aligned}\langle\Psi|\hat{N}_0|\Psi\rangle &= |d|^2 \equiv N_0, \\ \langle\Psi|\hat{N}_0^2|\Psi\rangle &= |d|^2 + |d|^4 = N_0 + N_0^2. \end{aligned} \tag{2.2.7}$$

Thus, the dispersion of the boson number operator can be easily calculated:

$$(\Delta\hat{N})^2 = |d|^2 \equiv N_0. \tag{2.2.8}$$

Writing the complex number d in the polar form

$$d = |d|e^{i\varphi} \tag{2.2.9}$$

and using Eq. (2.1.3) one obtains:

$$\begin{aligned}\langle\Psi|b_{20}|\Psi\rangle &= |d|e^{i\varphi} = N_0^{1/2}e^{i\varphi}, \\ e^{i\varphi} &= \langle\Psi|b_{20}|\Psi\rangle\left(\langle\Psi|\hat{N}_0|\Psi\rangle\right)^{-1/2}. \end{aligned} \tag{2.2.10}$$

The question which arises is whether such a factorization holds also for the operators whose averages are involved in the above equation. Before dealing with the quantum mechanical problem of the boson number and its conjugate phase we would like to present first the classical counterpart of this long standing problem.

Let H be a Hamiltonian defined in terms of the quadrupole boson operators $b_{2m}^{\dagger}, b_{2m}$ with $-2 \leq m \leq 2$ and consider the Time Dependent Variational Principle (*TDVP*) equation:

$$\delta \int_0^t \langle \Psi | H - i \frac{\partial}{\partial t'} | \Psi \rangle dt' = 0, \tag{2.2.11}$$

where the variational state is the coherent state $|\Psi\rangle$ (2.1.2), with d a complex number depending on time. Let us denote by

$$\mathcal{H} = \langle \Psi | H | \Psi \rangle. \tag{2.2.12}$$

The *TDVP* leads to the Hamilton equations of motion for the classical coordinates d and d^*.

$$\frac{\partial \mathcal{H}}{\partial d} = -i \, \overset{\bullet}{d}{}^*,$$
$$\frac{\partial \mathcal{H}}{\partial d^*} = i \, \overset{\bullet}{d}, \tag{2.2.13}$$

where "$\bullet$" indicates the time derivative. From these equations it results that d and d^* play the role of a classical coordinate and its conjugate momentum, respectively, while $\mathcal{H}$ is the classical energy function, or Hamilton function. Changing the classical coordinates d, d^* to the polar coordinates by the transformation

$$(d, d^*) \rightarrow (r, \varphi), \tag{2.2.14}$$

with $r = |d|^2$, the equations of motion become:

$$\frac{\partial \mathcal{H}}{\partial r} = - \overset{\bullet}{\varphi},$$
$$\frac{\partial \mathcal{H}}{\partial \varphi} = \overset{\bullet}{r} . \tag{2.2.15}$$

These equations suggest that the classical image (the average of $\hat{N}_0$ with Ψ) of the boson number operator, i.e. r, and the phase φ are, indeed, conjugate classical coordinates, namely r is a classical coordinate and φ its conjugate momentum. One can check that their Poisson bracket is equal to unity. Certainly, it would be desirable that a pair of Hermitian operators whose commutator is the imaginary unity exists

such that their averages with Ψ are just the canonical conjugate classical coordinates r and φ. In what follows we devote some space to the issue just formulated.

It is useful to introduce the off-diagonal operator

$$\hat{P}_0^\dagger = \hat{N}_0^{-1/2} b_{20}^\dagger \qquad (2.2.16)$$

which is the quantal counterpart of Eq. (2.2.10). The operator $\hat{N}_0^{-1/2}$ is defined by the following equation:

$$\hat{N}_0^{-1/2} = \frac{1}{\sqrt{\pi}} \int\limits_{-\infty}^{\infty} dx \exp\left(-x^2 \hat{N}_0\right). \qquad (2.2.17)$$

The Hermitian conjugate operator $\hat{P}_0$, satisfies the commutation relation:

$$\left[\hat{P}_0, \hat{N}_0\right] = \hat{P}_0. \qquad (2.2.18)$$

The conjugate coordinate corresponding to the boson number operator is:

$$\hat{\Phi}_0 = -i \ln \hat{P}_0. \qquad (2.2.19)$$

Indeed, considering the power expansion of the ln function in terms of $(\hat{P}_0 - 1)$, one checks that the operators $\hat{N}_0$ and $\hat{\Phi}_0$ satisfy the commutation relation:

$$\left[\hat{N}_0, \hat{\Phi}_0\right] = i. \qquad (2.2.20)$$

For monopole bosons, the conjugate coordinates of boson number and phase were described in details in Ref. [Hol80]. By contradistinction to the monopole case, here the rotation symmetry is broken. Indeed, while the boson number operator is a scalar, the phase operator $\hat{P}$ is a tensor of rank two and projection zero. It is an open question whether a construction of a scalar phase operator $\hat{P}$ is possible or not.

We note that our derivation of the phase operator is based on Eq. (2.2.18). Actually, this equation may be looked at as a defining equation for $\hat{P}_0$. Certainly the solution of this equation is not unique. For example, a possible solution is:

$$\hat{P}_0 = b_{20}. \qquad (2.2.21)$$

In this case we have:

$$\hat{\Phi}_0 = -i \ln b_{20}. \qquad (2.2.22)$$

One can check that the following equations for the expectation values hold:

$$\langle\Psi|\hat{\Phi}_0|\Psi\rangle = -i\ln d, \quad \langle\Psi|\hat{\Phi}_0^2|\Psi\rangle = -(\ln d)^2. \tag{2.2.23}$$

Consequently, the corresponding dispersion is vanishing:

$$\Delta\hat{\Phi}_0 = 0, \tag{2.2.24}$$

which reflects the fact that Ψ is an eigenfunction of $\hat{\Phi}_0$:

$$\hat{\Phi}_0|\Psi\rangle = -i(\ln d)|\Psi\rangle. \tag{2.2.25}$$

A direct use of Eq. (2.2.19) to calculate the uncertainty relation for the boson number and phase, is quite a cumbersome task especially due to the logarithm function. However, a considerable simplification is obtained by noticing that the deviation of $\hat{\Phi}_0$ from its expectation value can be expressed as:

$$\delta\hat{\Phi}_0 = -i\frac{\delta\hat{P}_0}{\hat{P}_0}. \tag{2.2.26}$$

We define a new dispersion of the phase operator by:

$$D\hat{\Phi}_0 = \frac{\Delta\hat{P}_0}{\langle\Psi|\hat{P}_0|\Psi\rangle}. \tag{2.2.27}$$

We shall prove [Hol80] that the newly defined quantity satisfies the Heisenberg uncertainty relation. Indeed, following the procedure of Ref. [CaNi68] one successively obtains:

$$\langle\Psi|\hat{P}_0|\Psi\rangle = de^{-|d|^2}\sum_{k=0}^{\infty}\frac{|d|^{2k}}{k!\sqrt{k+1}},$$

$$\langle\Psi|\hat{P}_0^2|\Psi\rangle = d^2e^{-|d|^2}\sum_{k=0}^{\infty}\frac{|d|^{2k}}{k!\sqrt{(k+1)(k+2)}}. \tag{2.2.28}$$

In the asymptotic region of $|d|$, compact forms for the sums involved in the above equation were obtained in Ref. [CaNi65], such that the final expressions for the considered expectation values are:

$$\langle\Psi|\hat{P}_0|\Psi\rangle = \frac{d}{|d|}\left[1 - \frac{1}{8|d|^2} + \cdots\right],$$

$$\langle\Psi|\hat{P}_0^2|\Psi\rangle = \frac{d^2}{|d|^2}\left[1 - \frac{1}{2|d|^2} - \frac{3}{8|d|^4} + \cdots\right]. \tag{2.2.29}$$

With these results one finds that for large values of $|d|$, the following uncertainty relation holds:

$$\Delta \hat{N}_0 D \hat{\Phi}_0 = \frac{1}{2}. \tag{2.2.30}$$

As we shall show in what follows, this equation is valid in the region of large number of bosons. Indeed, in the region of large $|d|$ the Ψ composing terms of maximal weights are those of large boson number.

  The uncertainty relation of the boson number operator and its conjugate phase has been first studied for photons by Dirac [Dir27] and for oscillator by Susskind and Glover [SuGl64]. The above equations have been obtained by representing the photon annihilation operator as a product of a unitary operator, written as $U = e^{i\phi}$, and a selfadjoint function of the boson number operator $f(\hat{N})$. The solution is $f = \hat{N}^{1/2}$ and is based on the assumption that ϕ is a self-adjoint operator. Later on it was proved that the conjugate phase variable is not well defined and therefore the corresponding uncertainty relation is doubtful. Indeed, one can check that the operator U is not unitary and, consequently, ϕ is not a self-adjoint operator and thereby cannot be assigned to a physical observable [CaNi65]. The reason for non-unitary is the presence of a vanishing boson number in the spectrum of $\hat{N}$. Even if we exclude this value, which prevents $\hat{N}$ to be invertible, the phase is not well defined for small values of N [Loui63]. Indeed, denoting by $|n_0\rangle$ the eigenstates of $\hat{N}_0$, the matrix elements of Eq. (2.2.20) lead to:

$$\langle n_0 | \hat{\Phi}_0 | m_0 \rangle = i \frac{\delta_{n_0, m_0}}{n_0 - m_0}, \tag{2.2.31}$$

which doesn't make sense for small values of the boson number. However, for large values of the boson number this can be assimilated with a continuous variable and the ratio from the right hand side of Eq. (2.2.31) is just the first derivative of the Dirac δ-function which is a well-defined entity.

  Positive attempts to define Hermitian operators depending on the phase, which together with the boson operator $\hat{N}_0$ satisfy the uncertainty relation, have been made by several authors [CaNi65, Loui63, CaNi68, Lev65]. Thus, the operators:

$$\hat{C}_0 = \frac{1}{2}(\hat{P}_0 + \hat{P}_0^\dagger),$$
$$\hat{S}_0 = \frac{1}{2i}(\hat{P}_0 - \hat{P}_0^\dagger) \tag{2.2.32}$$

are Hermitian and satisfy the uncertainty relations [CaNi68]:

$$\Delta \hat{N}_0 \Delta \hat{S}_0 \geq \frac{1}{2} \langle \hat{C}_0 \rangle,$$
$$\Delta \hat{N}_0 \Delta \hat{C}_0 \geq \frac{1}{2} \langle \hat{S}_0 \rangle, \tag{2.2.33}$$

where $\langle .. \rangle$ denotes the average of the operator involved, with the coherent state. The limitation on simultaneous measurement of observables S_0 and C_0 associated to the above mentioned Hermitian operators is expressed by the uncertainty product:

$$(\Delta \hat{S}_0)(\Delta \hat{C}_0) \geq \frac{1}{4} e^{-N_0}, \qquad (2.2.34)$$

with N_0 denoting the square of the dispersion $\Delta \hat{N}_0$. A more symmetric uncertainty relation in the regime of large $|d|$ is obtained by combining the already obtained results:

$$(\Delta \hat{N}_0)^2 \frac{(\Delta \hat{C}_0)^2 + (\Delta \hat{S}_0)^2}{(\langle \hat{C}_0 \rangle)^2 + (\langle \hat{S}_0 \rangle)^2} \geq \frac{1}{4}. \qquad (2.2.35)$$

Although here we deal with quadrupole bosons the proof of the uncertainty relations mentioned above goes identically with those given in Refs. [CaNi65, CaNi68].

2.3 Projected Spherical States

As already mentioned, the coherent state has neither a definite angular momentum nor a definite number of bosons. The question is whether the classical features, revealed by $|\Psi\rangle$ and reflected in the Heisenberg uncertainty equations of pairs of conjugate coordinates, are preserved when the rotational symmetry is restored, i.e. from the deformed state one projects out the components of a definite angular momentum. The same question is valid also for the gauge invariance restoration. A measure of the deviation from the classical behavior is again the departure of the dispersion product from the classical value. In what follows we attempt to answer these questions for the two pairs of conjugate coordinates considered above.

2.3.1 The Case of α, π Coordinates

As we proceeded above and, moreover, in order to keep close track to the CSM, which will be fully treated in one of the next chapters, for the case of (α, π) coordinates the parameter d is taken real.

Through angular momentum projection one generates a set of orthogonal states:

$$\phi_{JM}^{(g)} = N_J^{(g)} P_{M0}^J |\Psi\rangle, \qquad (2.3.1)$$

where P_{MK}^J denotes the angular momentum projection operator

$$P_{MK}^J = \frac{2J+1}{8\pi^2} \int D_{MK}^{J*}(\Omega) \hat{R}(\Omega) d\Omega, \qquad (2.3.2)$$

with D_{MK}^J standing for the Wigner function, or rotation matrix, $\hat{R}(\Omega)$ is the rotation defined by the Euler angles Ω, while $N_J^{(g)}$ is the normalization factor. The projected functions account for the main features of the rotational ground band [RCGD82]. For this reason the function is accompanied by the upper index "(g)". The norms have been analytically studied for any deformation and moreover very simple formulas for near vibrational and well deformed regimes have been obtained [RBF12]. For the sake of completeness we give the necessary expressions:

$$\left(N_J^{(g)}\right)^{-2} = (2J+1)I_J^{(0)}e^{-d^2}, \tag{2.3.3}$$

with

$$I_J^{(k)}(x) = \int_0^1 P_J(y)\,(P_2(y))^k\,e^{xP_2(y)}dy, \quad x = d^2, \tag{2.3.4}$$

where $P_k(x)$ is the Legendre polynomial of rank k. Expectation values of the conjugate coordinates and their squares have the expressions:

$$\langle\phi_{JM}^{(g)}|\hat{\alpha}|\phi_{JM}^{(g)}\rangle = \sqrt{2}d\,C_{M\,0\,M}^{J\,2\,J}C_{0\,0\,0}^{J\,2\,J},$$

$$\langle\phi_{JM}^{(g)}|\hat{\alpha}^2|\phi_{JM}^{(g)}\rangle = \frac{1}{2} + d^2\left[\sum_{J'=0,2,4} C_{M\,0\,M}^{J\,J'\,J}C_{0\,0\,0}^{J\,J'\,J}\left(C_{0\,0\,0}^{2\,2\,J'}\right)^2\right.$$

$$\left. + \sum_{J'=0,2,4}\left(C_{0\,0\,0}^{J'\,2\,J}\right)^2\left(C_{M\,0\,M}^{J'\,2\,J}\right)^2\left(\frac{N_J^{(g)}}{N_{J'}^{(g)}}\right)^2\right],$$

$$\langle\phi_{JM}^{(g)}|\hat{\pi}|\phi_{JM}^{(g)}\rangle = 0,$$

$$\langle\phi_{JM}^{(g)}|\hat{\pi}^2|\phi_{JM}^{(g)}\rangle = \frac{1}{2} + d^2\left[-\sum_{J'=0,2,4} C_{M\,0\,M}^{J\,J'\,J}C_{0\,0\,0}^{J\,J'\,J}\left(C_{0\,0\,0}^{2\,2\,J'}\right)^2\right.$$

$$\left. + \sum_{J'=0,2,4}\left(C_{0\,0\,0}^{J'\,2\,J}\right)^2\left(C_{M\,0\,M}^{J'\,2\,J}\right)^2\left(\frac{N_J^{(g)}}{N_{J'}^{(g)}}\right)^2\right]. \tag{2.3.5}$$

Standard notation, $C_{m_1\,m_2\,m}^{j_1\,j_2\,j}$, for the Clebsch-Gordan coefficient is used. From here the dispersions of $\hat{\alpha}$ and $\hat{\pi}$ are readily obtained and then the dispersion product is analytically expressed.

Now we simultaneously restore the rotation and gauge symmetries. The boson number projection operator is defined by:

$$\hat{P}_N = \frac{1}{2\pi} \int\limits_0^{2\pi} e^{i\phi(\hat{N}-N)} d\phi. \tag{2.3.6}$$

Applying successively the projection operators P^J_{MK} and $\hat{P}_N$ on the coherent state Ψ, one obtains a state of good angular momentum and boson number:

$$|NJM\rangle = \mathcal{N}_{NJ} \hat{P}_N P^J_{MK} |\Psi\rangle. \tag{2.3.7}$$

Here $\mathcal{N}_{JN}$ denotes the normalization factor and has the expression:

$$(\mathcal{N}_{NJ})^{-2} = e^{-d^2} \frac{d^{2N}}{N!} (2J+1) \mathcal{S}_{NJ}, \tag{2.3.8}$$

where the matrix $\mathcal{S}_{mJ}$ is defined by:

$$\mathcal{S}_{mJ} = \int\limits_0^1 (P_2(x))^m P_J(x) dx. \tag{2.3.9}$$

Following the path described in Ref. [RD76], one obtains:

$$\mathcal{S}_{lJ}(d) = \sum_{m=0}^l \frac{(-)^{l-m} 3^m (l)!(2m)!(m+\frac{1}{2}J)!}{2^{l-J} m!(l-m)!(m-\frac{1}{2}J)!(2m+J+1)!}. \tag{2.3.10}$$

The overlap matrix elements given above satisfy the restriction: they are nonvanishing only if $l \leq J/2$.

The explicit expression of the projected state is:

$$|NJM\rangle = \mathcal{N}_{NJ} e^{-d^2/2} \frac{d^N}{N!} \frac{2J+1}{8\pi^2} \int D^{J*}_{M0}(\Omega) \hat{R}(\Omega) \left(b^\dagger_{20}\right)^N d\Omega |0\rangle, \tag{2.3.11}$$

where $\hat{R}(\Omega)$ is the rotation defined by the set of Euler angles Ω.

The expectation values of the conjugate variables $\hat{\alpha}_{20}$ and $\hat{\pi}_{20}$ are equal to zero since each of the composing terms changes the boson number by one unit. Therefore, the corresponding dispersions squared are just the average values of their squares. By direct calculations one finds:

$$\Delta\hat{\alpha}_{20}\Delta\hat{\pi}_{20} = \frac{1}{2} + \sum_{J'=0,2,4} \left(C^{J'\,2\,J}_{M\,0\,M}\right)^2 \left(C^{J'\,2\,J}_{0\,0\,0}\right)^2 d^2 \left(\frac{\mathcal{N}_{NJ}}{\mathcal{N}_{(N-1)J'}}\right)^2. \tag{2.3.12}$$

2.3.2 Dispersions of $\hat{N}$ and $\hat{P}$ on Projected States

Note that while averaging the boson number operator with the coherent state $|\Psi\rangle$ only the component $b_{20}^{\dagger} b_{20}$ gives a non-vanishing contribution, when the average is performed with the angular momentum projected state all the terms involved in the expression of the boson number operator, contribute. Therefore in this case the boson number $\hat{N}_0$ is to be replaced with the boson total number operator:

$$\hat{N} = \sum_{-2 \leq m \leq 2} b_{2m}^{\dagger} b_{2m}. \tag{2.3.13}$$

The phase operator $\hat{P}$ satisfying the commutation relation

$$\left[\hat{P}, \hat{N}\right] = \hat{P}, \tag{2.3.14}$$

has the expression:

$$\hat{P} = \sum_{-2 \leq m \leq 2} b_{2m} \hat{N}^{-1/2}, \tag{2.3.15}$$

where the reciprocal square root operator is defined as in Eq. (2.2.17). Within the same spirit and with similar caution as before the conjugate phase operator is:

$$\hat{\Phi} = -i \ln \hat{P}. \tag{2.3.16}$$

The expectation values of the boson number operator $\hat{N}$ and its square $\hat{N}^2$ have been analytically obtained Ref. [RD76].

$$\langle \phi_{JM}^{(g)} | \hat{N} | \phi_{JM}^{(g)} \rangle = |d|^2 \frac{I_J^{(1)}}{I_J^{(0)}},$$

$$\langle \phi_{JM}^{(g)} | \hat{N}^2 | \phi_{JM}^{(g)} \rangle = |d|^2 \frac{I_J^{(1)}}{I_J^{(0)}} + |d|^4 \frac{I_J^{(2)}}{I_J^{(0)}}. \tag{2.3.17}$$

One can check that the overlap integral ratios involved in the above equations are related by the following equation [RCGD82, RBF12]:

$$x^2 \frac{I_J^{(2)}}{I_J^{(0)}} = \frac{1}{2} x(x-3) \frac{I_J^{(1)}}{I_J^{(0)}} + \frac{1}{4} \left(2x^2 + J(J+1)\right), \quad x = |d|^2. \tag{2.3.18}$$

From these equations one obtains the dispersion of $\hat{N}$:

$$
\left(\Delta \hat{N}\right)_J = -|d|^4 \left(\frac{I_J^{(1)}}{I_J^{(0)}}\right)^2 + \frac{1}{2}|d|^2(|d|^2 - 1)\frac{I_J^{(1)}}{I_J^{(0)}}
$$
$$
+ \frac{1}{4}\left(2|d|^4 + J(J+1)\right). \tag{2.3.19}
$$

The uncertainty relations will be calculated by choosing as conjugate operator the phase operator $\hat{P}$ divided by its average value [Hol80] and alternatively the Hermitian operators $\hat{C}$ and $\hat{S}$ defined as before [CaNi68]:

$$
\hat{C} = \frac{1}{2}\left(\hat{P} + \hat{P}^\dagger\right),
$$
$$
\hat{S} = \frac{1}{2i}\left(\hat{P} - \hat{P}^\dagger\right). \tag{2.3.20}
$$

In what follows we shall describe a method of calculating the dispersion of the associated phase operator $\hat{P}$. The average of $\hat{P}$ corresponding to the angular momentum projected state $|\phi_{JM}^{(g)}\rangle$ is:

$$
\langle \phi_{JM}^{(g)}|\hat{P}|\phi_{JM}^{(g)}\rangle = \left(N_J^{(g)}\right)^2 \langle\Psi|P_{M0}^{J\dagger}\sum_\mu b_{2\mu}P_{M0}^J \hat{N}^{-1/2}|\Psi\rangle
$$
$$
= e^{-\frac{|d|^2}{2}}\left(N_J^{(g)}\right)^2 \langle\Psi|P_{M0}^{J\dagger}\sum_\mu b_{2\mu}P_{M0}^J \frac{1}{\sqrt{\pi}}\int_{-\infty}^{+\infty}\frac{(-)^m x^{2m}}{m!}\hat{N}^m d^n \frac{b_{20}^{\dagger n}}{n!}dx|0\rangle
$$
$$
= e^{-\frac{|d|^2}{2}}\left(N_J^{(g)}\right)^2 \langle\Psi|P_{M0}^{J\dagger}\sum_\mu b_{2\mu}P_{M0}^J \frac{1}{\sqrt{n}}d^n \frac{b_{20}^{\dagger n}}{n!}|0\rangle
$$
$$
= e^{-\frac{d^2}{2}}C_{M\ 0\ M}^{J\ 2\ J}C_{0\ 0\ 0}^{J\ 2\ J}\left(N_J^{(g)}\right)^2 \langle\Psi|P_{00}^J\sum_{n=1}^{\infty}\frac{d^n}{\sqrt{n}}\frac{\left(b_{20}^\dagger\right)^{n-1}}{(n-1)!}|0\rangle
$$
$$
= de^{-|d|^2}C_{M\ 0\ M}^{J\ 2\ J}C_{0\ 0\ 0}^{J\ 2\ J}\left(N_J^{(g)}\right)^2 \frac{2J+1}{2}\int_{-1}^{+1}dx
$$
$$
\times \left[\sum_{m=0}^{\infty}\frac{1}{m!\sqrt{m+1}}\left(|d|^2 P_2(x)\right)^m P_J(x)\right]. \tag{2.3.21}
$$

The final result is:

$$
\langle \phi_{JM}^{(g)}|\hat{P}|\phi_{JM}^{(g)}\rangle = C_{M\ 0\ M}^{J\ 2\ J}C_{0\ 0\ 0}^{J\ 2\ J}d\frac{\mathcal{I}_J^{(0)}}{I_J^{(0)}}, \tag{2.3.22}
$$

where we denoted:

$$\mathcal{I}_J^{(0)} = \sum_{m=0}^{\infty} \frac{|d|^{2m}}{m!\sqrt{m+1}} \mathcal{S}_{mJ}. \tag{2.3.23}$$

Applying a similar procedure as before but for $\hat{P}^2$, one obtains the final result:

$$\langle \phi_{JM}^{(g)}|\hat{P}^2|\phi_{JM}^{(g)}\rangle = \mathcal{C}_M^J d^2 \frac{T_J^{(0)}}{I_J^{(0)}}, \tag{2.3.24}$$

with

$$\mathcal{C}_M^J = \sum_{J'=0,2,4} C_{0\,0\,0}^{2\,2\,J'} C_{0\,0\,0}^{J\,J'\,J} C_{M\,0\,M}^{J\,J'\,J} \sum_{\mu} C_{\mu\,-\mu\,0}^{2\,2\,J'},$$

$$T_J^0 = \sum_{m=0}^{\infty} \frac{|d|^{2m}}{m!\sqrt{(m+1)(m+2)}} \mathcal{S}_{mJ}. \tag{2.3.25}$$

Having the expressions of the expectation values of $\hat{P}$ and $\hat{P}^2$, the dispersion of P is readily obtained.

$$\left(\Delta\hat{P}\right)_{JM}^2 = \langle \phi_{JM}^{(g)}|\hat{P}^2|\phi_{JM}^{(g)}\rangle - \left(\langle \phi_{JM}^{(g)}|\hat{P}|\phi_{JM}^{(g)}\rangle\right)^2. \tag{2.3.26}$$

Although calculating the average of $\hat{\Phi}$ is quite a cumbersome task, that is possible. However according to Ref. [Hol80] the Heisenberg uncertainty inequality is satisfied by the dispersions of $\hat{N}$ and

$$(D\hat{P})_{JM} = \frac{(\Delta\hat{P})_{JM}}{|\langle \phi_{JM}^{(g)}|\hat{P}|\phi_{JM}^{(g)}\rangle|} \tag{2.3.27}$$

Therefore the departure from the classical limit is measured by $(\Delta\hat{N})_J(D\hat{P})_{JM}$.

The expectation values of the Hermitian operators $\hat{C}$ and $\hat{S}$, defined by

$$\hat{C} = \frac{1}{2}\left(\hat{P} + \hat{P}^\dagger\right),$$

$$\hat{S} = \frac{1}{2i}\left(\hat{P} - \hat{P}^\dagger\right) \tag{2.3.28}$$

are easily obtained from Eqs. (2.3.22) and (2.3.24).

$$\langle \phi_{J0}^{(g)}|\hat{C}|\phi_{J0}^{(g)}\rangle = \left(C_{0\,0\,0}^{J\,2\,J}\right)^2 (Re\ d) \frac{\mathcal{I}_J^{(0)}}{I_J^{(0)}},$$

$$\langle \phi_{J0}^{(g)} | \hat{S} | \phi_{J0}^{(g)} \rangle = \left(C_{0\,0\,0}^{J\,2\,J} \right)^2 (Im\, d) \frac{\mathcal{I}_J^{(0)}}{I_J^{(0)}}. \tag{2.3.29}$$

Following the procedure described above we obtain:

$$\langle \phi_{J0}^{(g)} | \hat{C}^2 + \hat{S}^2 | \phi_{J0}^{(g)} \rangle = |d|^2 \sum_{J'} \left(C_{0\,0\,0}^{J\,2\,J'} \right)^2 \frac{\mathcal{U}_{J'}^{(0)}}{I_J^{(0)}} + \frac{5}{2} \frac{\mathcal{U}_J^{(0)}}{I_J^{(0)}}, \tag{2.3.30}$$

with

$$\mathcal{U}_J^{(0)} = \sum_{k=0}^{\infty} \frac{|d|^{2k}}{(k+1)!} S_{kJ}. \tag{2.3.31}$$

The normalized sum of dispersions associated to the two observables $\hat{C}$ and $\hat{S}$ is:

$$\frac{(\Delta \hat{C})_{J0}^2 + (\Delta \hat{S})_{J0}^2}{\langle \hat{C} \rangle_{J0}^2 + \langle \hat{S} \rangle_{J0}^2} = \frac{1}{|d|^2 \left(C_{0\,0\,0}^{J\,2\,J} \right)^4}$$

$$\times \left[|d|^2 \sum_{J'} \left(C_{0\,0\,0}^{J\,2\,J'} \right)^2 \frac{\mathcal{U}_{J'}^{(0)} I_J^{(0)}}{(\mathcal{I}_J^{(0)})^2} + \frac{5}{2} \frac{\mathcal{U}_J^{(0)} I_J^{(0)}}{(\mathcal{I}_J^{(0)})^2} \right] - 1$$

$$\equiv (\Delta R)_J^2, \tag{2.3.32}$$

where the low index $J0$ suggests that the involved dispersions and average values correspond to the angular momentum projected state $\phi_{J0}^{(g)}$. Also, the notation $\langle \hat{O} \rangle_{J0}$ was used for the average value of $\hat{O}$ with the mentioned projected state.

The uncertainty relation associated to the two observables is obtained by equating

$$F_J = (\Delta \hat{N})_J \sqrt{\frac{(\Delta \hat{C})_{J0}^2 + (\Delta \hat{S})_{J0}^2}{\langle \hat{C} \rangle_{J0}^2 + \langle \hat{S} \rangle_{J0}^2}} \tag{2.3.33}$$

to the product of the right hand sides of Eq. (2.3.19) and $(\Delta R)_J$ given by (2.3.32). The departure of F from the value of $1/2$ constitutes a measure for the quantal nature of the system behavior.

Concerning the N, J projected states and the pair of coordinates $(\hat{N}, \hat{P})$ the results are as follows. The dispersion of $\hat{N}$ is vanishing since the projected state is eigenstate of $\hat{N}$. Also, the operators $\hat{P}$ and $\hat{P}^2$ violate the boson number conservation and therefore their corresponding averages are vanishing if the number of bosons N is nonvanishing. The mentioned averages are undetermined for the state with $N = 0$.

How the projection of symmetries affect the uncertainty inequalities and therefore how far from the classical limit one could go by these operations, will be quantitatively analyzed in several numerical applications.

2.4 Numerical Analysis

We start by giving the expansion weights of Ψ corresponding to various boson basis:

$$|\Psi\rangle = \sum_n C_n|n\rangle,$$

$$|\Psi\rangle = \sum_J C_{J0}|J0\rangle,$$

$$|\Psi\rangle = \sum_{NJ} C_{NJ0}|NJ0\rangle. \tag{2.4.1}$$

where $|n\rangle$ are eigenstates of the boson number operator $b_{20}^\dagger b_{20}$, $|J0\rangle$ denotes the eigenstates of angular momentum square, $\hat{J}^2$, and its projection on z-axis, J_0. The third basis $\{|NJ0\rangle\}$ is determined by the quantum numbers: the boson number N, the angular momentum J and z-projection of the angular momentum, 0. Actually, these expansions correspond just to the boson bases defined above by the studied symmetry projection.

Using the results described before, one finds out that the expansion weights have the following analytical expressions:

$$C_n = e^{-d^2/2}\frac{d^n}{\sqrt{n!}},$$

$$C_{J0} = \left(N_J^{(g)}\right)^{-1},$$

$$C_{NJ} = (\mathcal{N}_{NJ})^{-1}. \tag{2.4.2}$$

These weights have been plotted in Fig. 2.1a–c, as function of the deformation parameter d. The curves have maxima for some deformations which indicate that for such deformations the corresponding states, showing up in the expansion, are the dominant components.

The dispersions product of the conjugate coordinates $\hat{\alpha}_{20}$ and $\hat{\pi}_{20}$ calculated with the $J-$projected states is presented as function of d in Fig. 2.2c. It is well known that the classical limit of this quantity is 1/2 (units of $\hbar$). According to Fig. 2.2c the $J = 0$ projected state is the only projected state which behaves semiclassically in the region of small $d(\leq 1.5)$. The remaining states lay apart from the classical limit. The larger J, the larger the deviation from the classical limit. In the region of large $d(>3.)$ the deviation from the classical limit is an increasing function of d, irrespective the values

Fig. 2.1 Expansion
coefficients of the coherent
state $|\Psi\rangle$ in three distinct
basis, $|n\rangle$ (*panel* **a**), $|J0\rangle$
(*panel* **b**), and $|NJ0\rangle$ (*panel*
c), are plotted as function of
the deformation parameter d
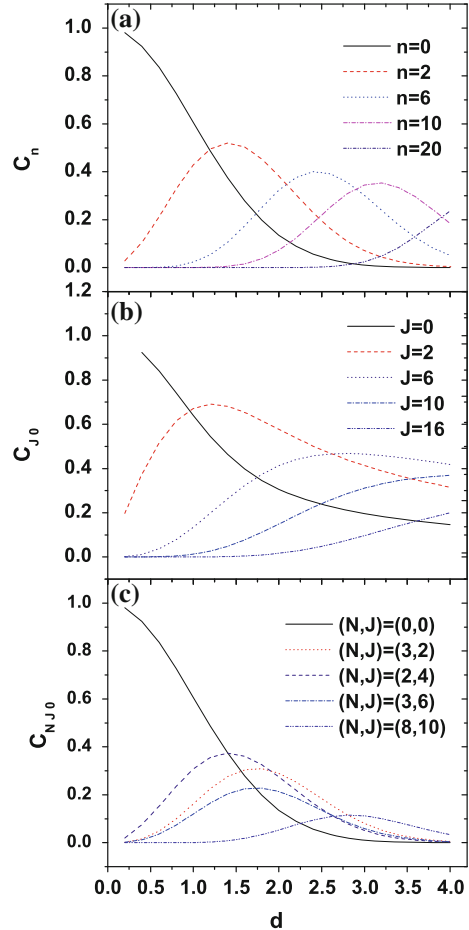
of J. This behavior trend is determined by the increasing nature of the dispersion of
$\hat{\alpha}_{20}$. Thus for both conjugate coordinates mentioned above, the nuclear deformation
favors the quantal behavior of the system.

In Fig. 2.3 we represented the product of $\hat{\alpha}_{20}$ and $\hat{\pi}_{20}$ dispersions as function of d,
using the states $|NJM\rangle$, which restore both symmetries mentioned above. As seen
in Fig. 2.3, the dispersion product has a strong J-dependence for small values of
d while for large valued of d, i.e. in the rotational limit, this tends to the classical
limit. In contrast to the case of the J-projected function here increasing d, favors the
classical behavior. This is reflected in the decreasing J-dependence of the dispersion
product as well as in approaching the classical value.

It is worth raising the question whether the features mentioned above depend on
the chosen pair of conjugate coordinates. We do not attempt to give a general answer
but analyze, for comparison, what happens when the pair of conjugate variables is

Fig. 2.2 Dispersions of the conjugate coordinates α_{20} and π_{20}, as well as their product are given as functions of d in *panels* **a**, **b** and **c** for angular momentum projected states
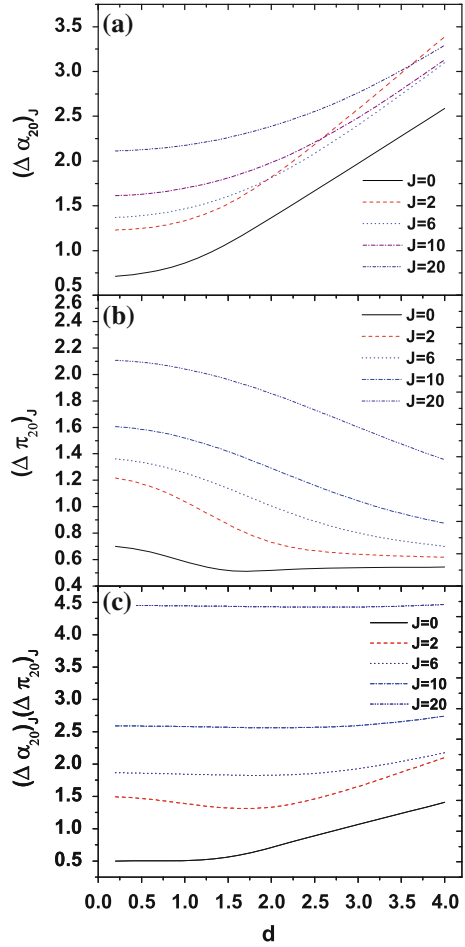
Fig. 2.3 Dispersion product for the conjugate coordinates $\hat{\alpha}_{20}$ and $\hat{\pi}_{20}$, corresponding to the NJ-projected states are plotted as function of the deformation parameter d
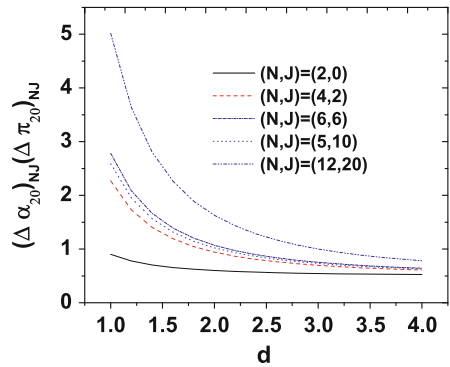
Fig. 2.4 Dispersions for the boson number operator (*panel* **a**) and the corresponding phase operator P (*panel* **b**) are plotted as function of d. Also, the dispersion product is given in *panel* **c**. Calculations are performed for angular momentum projected states
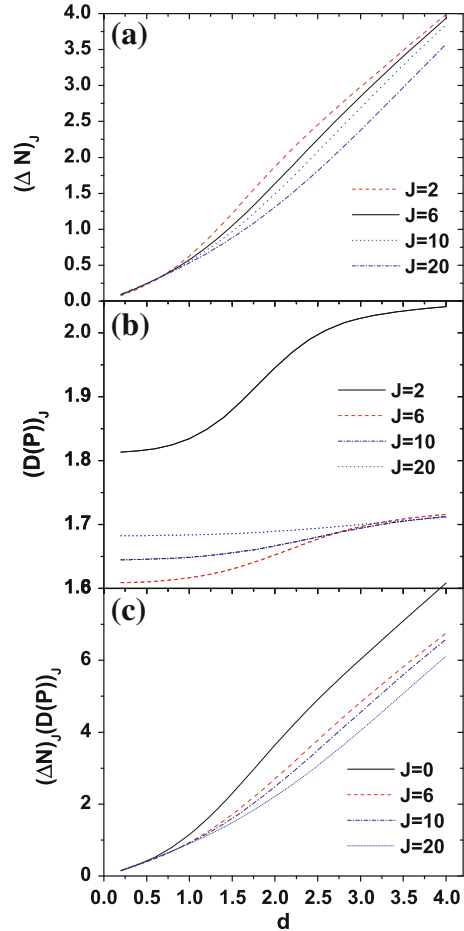
$(\hat{N}, \hat{P})$. The results are pictured in Fig. 2.4a–c. Dispersion of N increases with d and the split due to the J dependence increases slowly from zero within a narrow interval. Note that for d going to zero the projected function $\phi_{JM}^{(g)}$ goes to the state $|\frac{J}{2}, \frac{J}{2}, 0, J, M\rangle$ [RCGD82] with the standard notation $|N, v, \lambda, J, M\rangle$: N being the number of bosons, v the seniority, λ the missing quantum number, J the angular momentum and M the projection on the laboratory z-axis. Therefore, in the spherical limit N becomes a good quantum number and the dispersion is vanishing. By contrast, the normalized dispersion $D(P)$ has a large spread over J for small values of d but for large deformation the $J \neq 2$ dispersions attain a common value. Note that apart from the quantitative aspects, the dispersion product preserves the look of ΔN. The behavior of the pair of coordinates (N, R) is visualized in Fig. 2.5a–c. The split of R-dispersions due to their J-dependence is quite large for small deformation and is decreasing with d. The situation when dispersion of R_J with $J \neq 2$ get a

Fig. 2.5 Dispersions for the boson number operator (*panel* **a**) and for the observable $\hat{R}$ defined by (2.3.32) (*panel* **b**) as well as their product (**c**) are plotted as function of d for angular momentum projected states
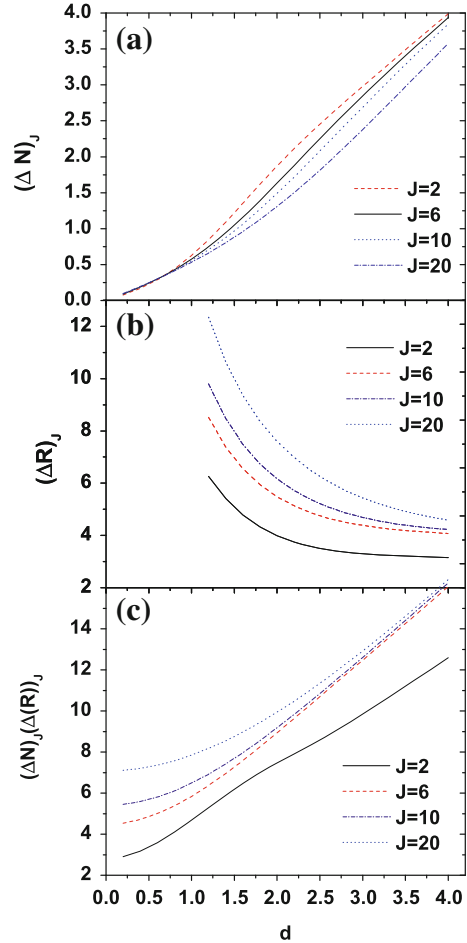
common value is reached for d larger than the maximum value shown in Fig. 2.4. The uncertainty relation for the pair (N, R) is shown in the plot of F_J (2.3.33) as a function of d. One notices that the departure from the classical limit is an increasing function of angular momentum. Also, this is increasing with the nuclear deformation. It is worth noticing that for large deformation, the $J \neq 2$ values become indistinguishable from each other.

The results obtained so far can be summarized as follows. The expansion weights of the coherent states in three distinct bases, exhibit a maximum when represented as function of the deformation parameter d. The larger are the selected quantum numbers the larger is the deformation for which the weight is maximum.

In the (α, π) representation only the $J = 0$ projected state behaves classically and that happens for small values of d. In the region of large d the departure from the classical picture is slightly increasing with the deformation.

The behavior of the (α, π) pair of conjugate coordinates in a NJ-projected state is different from that described above for a J-projected state. Indeed, from Fig. 2.3 we notice that the quantal features prevail for small deformation, while for the rotational limit of large d the associated Heisenberg relation approaches the classical limit. Also, in this limit the J-dependence of the uncertainty relations is very weak.

From Figs. 2.2c and 2.3 we conclude that in the (α, π) and J-projected states representation the system departs from the classical picture by increasing d while for the (N, J) projected states the larger the deformation the closer is the system to the classical behavior. In both cases the small deformation region is characterized by a quantal behavior reflected by the departure from the classical limits as well as by the split of the dispersion product due to the J-dependence. Comparing the figures referring to the uncertainty relations for the (α, π) in the J projected and NJ projected states respectively, one may conclude that the share of classical and quantal features depends on the symmetry of the wave function. In the specific situations the more symmetric is the system the closer is its behavior to the classical picture.

The delicate problem of boson number and the conjugate phase was treated by two alternative choices for the conjugate phase-like operator. In the first case the operator is $\hat{P}$ with a proper normalization. Although this is not a Hermitian operator the Heisenberg uncertainty relation holds for a large number of bosons. The dispersion product is quickly increasing with d starting with values close to zero (≈ 0.162). The behavior for small deformation is justified by the fact that the J-projected state becomes eigenstate of $\hat{N}$. For larger d the system behaves in a classical manner while for small deformation the quantal features prevail. The split of the dispersion product due to its J-dependence is not significant for $J \neq 2$. One may say that although the departure from the classical limit of the dispersion product is large the classical feature reclaiming a weak J-dependence, still persists. The dispersion product is increasing with d and is also J independent for large values of J.

For the second alternative situation the phase like operators $\hat{C}$ and $\hat{S}$ were used to define, for the sake of having a symmetrical form, the dispersion of the observable R. The dispersion product denoted by F_J is increasing with d. For small d the split over J is large while for large deformation the values of F_J for large J, are more or less the same. Here, as well as in the case of (α, π) coordinates, the coordinate dispersion is increasing with d, while the conjugate momentum dispersion is decreasing when d increases.

Comparing the results for (α, π) and (N, P) /or (N, R) coordinates we notice that the interplay of quantal and classical feature depends on the pair of conjugate coordinates under study.

Before the symmetries were restored the system behaves classically which is reflected by that the uncertainty relations achieve their minima, irrespective of the chosen pair of conjugate coordinate. Moreover, the expectation value for angular momentum square has a continuous value [RCGD82]:

$$\langle \Psi | \hat{J}^2 | \Psi \rangle = 6|d|^2. \tag{2.4.3}$$

Symmetry projection leads to a J (or NJ)-dependence for the uncertainty relations which is large for small deformation. Increasing $|d|$, the system tends to recover the classical behavior.

2.5 The Baker-Campbell-Hausdorff Formula for the SU(2) Algebra

Along this book we shall use, in several places, the coherent state for the SU(2) algebra. In order to handle it in a comfortable manner it is necessary to use a factorized form which will be derived in what follows. Therefore, here we try to factorize an operator of the form.

$$\hat{O} = e^{\hat{A}+\hat{B}}. \tag{2.5.1}$$

In some special cases such an operator can be written as a product of two exponential factors.

$$\hat{O} = e^{\hat{A}} e^{\hat{B}}. \tag{2.5.2}$$

For example this factorization holds if the operators A and B commute with each other. The factorization is still simple if the commutator of the two operators is a constant. In this case the following equation holds:

$$e^{\hat{A}+\hat{B}} = e^{\hat{A}} e^{\hat{B}} e^{-\frac{1}{2}\left[\hat{A},\hat{B}\right]}. \tag{2.5.3}$$

An example of an exponential operator which can be factorized in this manner is the Glauber function or equivalently *the coherent state for the Weyl group*:

$$|d\rangle = e^{db^{\dagger}-d^{*}b}|0\rangle, \tag{2.5.4}$$

where b and $b^{\dagger}$ are boson operators, while d a complex parameter and $|0\rangle$ is the vacuum state for the boson operator b. In this case one can verify that:

$$e^{db^{\dagger}-d^{*}b}|0\rangle = e^{db^{\dagger}} e^{-d^{*}b} e^{-\frac{|d|^{2}}{2}}|0\rangle. \tag{2.5.5}$$

This is a direct consequence of Eq. (2.5.3), but can be also obtained by direct calculation. Indeed, if the factorization mentioned is valid then the coherent state can be written in the form:

$$|d\rangle = C e^{db^{\dagger}}|0\rangle. \tag{2.5.6}$$

Remembering the fact that the coherent state is normalized to unity, we have:

$$\langle d|d \rangle = |C|^2 \langle 0|e^{d^*b}e^{db^\dagger}|0\rangle = |C|^2 e^{|d|^2} = 1. \tag{2.5.7}$$

It results that modulo a phase factor the coherent state can be written as:

$$|d\rangle = e^{-\frac{1}{2}|d|^2}e^{db^\dagger}|0\rangle. \tag{2.5.8}$$

Thus, up to a factor depending on the annihilation operator b, which acting on $|0\rangle$, it reproduces it, the exponential operator has the expression from Eq. (2.5.8).

Another case which will be considered here is that where the operators $\hat{A}$ and $\hat{B}$ are generators for the $SU(2)$ algebra. This case is often met in Nuclear Physics both in microscopic and phenomenological models. Indeed, we remember that the BCS function for the case where the space of correlated states is restricted to a single j state is written as an exponential of a sum of the quasispin generators S_+ and S_-. Working with this function is a difficult task since the associated power series must be rewritten in a normal order. Thereby it is much simpler to use from the beginning a factorized form, two of the factors being just the exponential operators of S_+ and S_-, respectively [KIR67].

Here we shall treat the case of a rotation around the axis OY, $e^{-i\theta_2 J_y}$, which will be expressed as product of three exponential operators corresponding to the rotation generators: J_+, J_- and J_z. Rotation around OY is a particular case, $s = 1$, of the more general rotation $e^{-is\theta_2 J_y}$. It is convenient to write this operator in the form:

$$e^{-i\theta_2 s J_y} = e^{F_1 J_-}e^{F_2 J_z}e^{F_3 J_+} \equiv B(s), \tag{2.5.9}$$

where F_1, F_2, F_3 are functions of s which are to be determined such that the following restrictions be satisfied:

$$F_1(0) = F_2(0) = F_3(0) = 0. \tag{2.5.10}$$

Notations for the raising and lowering operators are the standard ones:

$$J_+ = J_x + iJ_y, \quad J_- = J_x - iJ_y. \tag{2.5.11}$$

Their commutation relations are those characterizing the $SU(2)$ algebra:

$$[J_+, J_-] = 2J_z, \quad [J_\pm, J_z] = \mp J_\pm. \tag{2.5.12}$$

If we perform the first derivative of Eq. (12.1.34) with respect to s we obtain:

$$\dot{B} = \dot{F_1}\, J_- B + e^{F_1 J_-}\,\dot{F_2}\, J_z e^{F_2 J_z}e^{F_3 J_+} + e^{F_1 J_-}e^{F_2 J_z}\,\dot{F_3}\, J_+ e^{F_3 J_+}. \tag{2.5.13}$$

Now let us bring the non-exponential operators on the first position. To this aim one uses the identity

$$e^A B e^{-A} = B + \sum_{n=1} \frac{1}{n!} \underbrace{[A, [A, \ldots [A, B] \ldots]]}_{n \text{ times}}.$$ (2.5.14)

In the present case the mentioned identity becomes:

$$e^{F_1 J_-} J_z e^{-F_1 J_-} = J_z + F_1 [J_-, J_z] = J_z + F_1 J_-.$$ (2.5.15)

Hence:

$$e^{F_1 J_-} J_z = (J_z + F_1 J_-) e^{F_1 J_-}.$$ (2.5.16)

$$e^{F_2 J_z} J_+ e^{-F_2 J_z} = J_+ + F_2 [J_z, J_+] + \frac{1}{2!} F_2^2 [J_z, [J_z, J_+]] + \cdots$$

$$= J_+ + F_2 J_+ + \frac{1}{2!} F_2^2 J_+ + \cdots = J_+ e^{F_2}$$

$$e^{F_2 J_z} J_+ = J_+ e^{F_2} e^{F_2 J_z}$$

$$e^{F_1 J_-} J_+ e^{-F_1 J_-} = J_+ + F_1 [J_-, J_+] + \frac{1}{2!} F_1^2 [J_-, [J_-, J_+]] + \cdots$$

$$= J_+ - 2 F_1 J_z - F_1^2 J_-.$$ (2.5.17)

Therefore:

$$e^{F_1 J_-} e^{F_2 J_z} J_+ e^{F_3 J_+} = (J_+ - 2 F_1 J_z - F_1^2 J_-) e^{F_2} B.$$ (2.5.18)

Finally, the derivative of B becomes:

$$\dot{B} = \left[\dot{F_1} J_- + (J_z + F_1 J_-) \dot{F_2} + (J_+ - 2 F_1 J_z - F_1^2 J_-) e^{F_2} \dot{F_3} \right] B,$$

$$\frac{\theta_2}{2} (J_- - J_+) B = \left[(\dot{F_1} + F_1 \dot{F_2} - \dot{F_3} F_1^2 e^{F_2}) J_- + (\dot{F_2} - 2 F_1 e^{F_2} \dot{F_3}) J_z + J_+ e^{F_2} \dot{F_3} \right] B.$$ (2.5.19)

The generators J_+, J_- and J_z are linear independent operators, which result in having equal coefficients for the mentioned operators which show up in the l.h.s. and r.h.s. respectively.

$$\dot{F_1} + F_1 \dot{F_2} - F_1^2 \dot{F_3} e^{F_2} = \frac{\theta_2}{2} \Rightarrow \dot{F_1} = \frac{\theta_2}{2} (1 + F_1^2),$$

$$\dot{F_2} - 2 F_1 \dot{F_3} e^{F_2} = 0 \Rightarrow \dot{F_2} = -\theta_2 F_1,$$

$$\dot{F_3} e^{F_2} = -\frac{\theta_2}{2} \Rightarrow \dot{F_3} = -\frac{\theta_2}{2} e^{-F_2}.$$ (2.5.20)

The solutions of these equations, which obey the initial conditions, are:

$$F_1 = tg\frac{\theta_2}{2}s,$$

$$F_2 = 2\ln\cos\frac{\theta_2}{2}s,$$

$$F_3 = -F_1 = -tg\frac{\theta_2}{2}s. \tag{2.5.21}$$

For the rotation operator of interest the value $s = 1$ corresponds:

$$e^{-i\theta_2 J_y} = e^{(tg\frac{\theta_2}{2})J_-}e^{(2\ln\cos\frac{\theta_2}{2})J_z}e^{-(tg\frac{\theta_2}{2})J_+}. \tag{2.5.22}$$

Let us act with this equation on an eigenstate for J^2 and J_z of maximum projection and take into account the fact that $J_+|JJ\rangle = 0$. It results:

$$e^{-i\theta_2 J_y}|JJ\rangle = e^{(tg\frac{\theta_2}{2})J_-}\cos^{2J}\frac{\theta_2}{2}|JJ\rangle. \tag{2.5.23}$$

The same procedure could be applied to the operator

$$e^{zJ_- - z^*J_+}, \quad z = |z|e^{i\varphi}. \tag{2.5.24}$$

In this case the equations for the factor F_1, F_2, F_3 are:

$$\dot{F}_1 = F_1^2 z^* + z,$$

$$\dot{F}_2 = -2F_1 z^*,$$

$$\dot{F}_3 = -e^{-F_2}z^*. \tag{2.5.25}$$

Integrating these equations and then put $s = 1$, one obtains:

$$F_1 = e^{i\varphi}tg|z|,$$
$$F_2 = -ln(1 + tg^2|z|),$$
$$\dot{F}_3 = -e^{-i\varphi}tg|z|. \tag{2.5.26}$$

Using the notations

$$\zeta = e^{i\varphi}tg|z|, \quad \frac{\theta}{2} = |z|, \tag{2.5.27}$$

the following factorization is obtained:

$$e^{zJ_- - z^* J_+} = e^{\zeta J_-} e^{-ln(1+|\zeta|^2)J_z} e^{-\zeta^* J_+}. \tag{2.5.28}$$

If we want that the product to have as first factor the exponential operator corresponding to the raising operator J_+, one could repeat the previous procedure with the result:

$$e^{zJ_- - z^* J_+} = e^{-\zeta^* J_+} e^{-ln(1+|\zeta|^2)J_z} e^{\zeta J_-}. \tag{2.5.29}$$

Acting with the operators involved in Eq. (2.5.28) on the state of maximum weight $|JJ\rangle$ and taking into account that $J_+|JJ\rangle = 0$, $J_z|JJ\rangle = J|JJ\rangle$, one arrives at the following expression:

$$|J, z\rangle = e^{zJ_- - z^* J_+}|JJ\rangle = \frac{1}{(1+|\zeta|^2)^J} e^{\zeta J_-}|JJ\rangle. \tag{2.5.30}$$

This function is *the coherent state for the group SU*(2). Such property results from the following considerations:

(1) The function $|JJ\rangle$ is extremal for the set of eigenstates of J^2 and J_z. Indeed, all states of this set can be obtained by successively acting on the extremal state with the lowering operator:

$$|JM\rangle = \binom{2J}{J-M}^{-1/2} \frac{1}{(J-M)!} (J_-)^{J-M}|JJ\rangle. \tag{2.5.31}$$

(2) The stability subgroup G for this extremal is the group of rotations around the OZ axis.
(3) The exponential operator $e^{zJ_- - z^* J_+}$ is an element of the quotient group $SU(2)/G$.
(4) As shown before, the function $|J, z\rangle$ is obtained by acting with an element of the quotient group on the extremal state.

This function is often used in nuclear physics to study semiclassically the rotational degrees of freedom.

We notice that the stereographic projection of a sphere S^2 of a diameter equal to unity, $d = 1$, on a plane placed at the distance d from the sphere center, achieves an one to one correspondence of the sphere points of coordinates $(1/2, \theta/2, \varphi)$ and the points ζ of the complex plane. This correspondence is illustrated in Fig. 2.6. The mentioned sphere is known as the Bloch sphere. Adding to the complex plane the point from infinity, the complex plane can be compacted, according to the theorem of Alexandrov. In this manner the correspondence evidenced above becomes a homeomorphism of two compact manifold.

The coherent states corresponding to two different points z are not orthogonal except for those corresponding to the two sphere poles. Indeed, one can prove that

Fig. 2.6 The correspondence between the points of the sphere S^2 and those of the complex plane (ζ), achieved by the stereographic projection
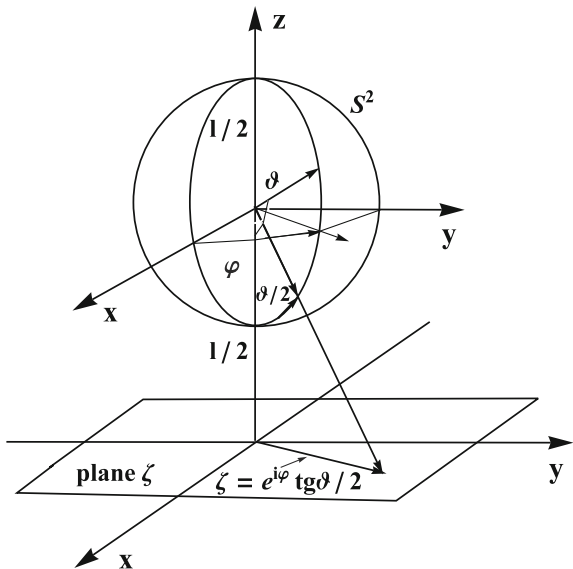
the scalar product of two coherent states corresponding to two different points of the complex plane is:

$$|\langle J, z'|J, z\rangle|^2 = \left[\frac{1 + \mathbf{n}(\Omega') \cdot \mathbf{n}(\Omega)}{2}\right]^{2J} = cos^{4J}\frac{\Theta}{2}, \qquad (2.5.32)$$

where $\mathbf{n}(\Omega)$ is the unity vector representing the point on the Bloch sphere of coordinate $(1/2, \theta/2, \varphi)$, while Θ is the angle of the two directions.

Resolution of unity for the spin coherent states is expressed by the relation:

$$\frac{2J + 1}{4\pi} \int d\Omega |J, z\rangle\langle J, z| = \sum_M |JM\rangle\langle JM| = 1. \qquad (2.5.33)$$

An extremely useful property of the coherent states is that the matrix element of any operator can be obtained by calculating the derivative of one of the generating function:

$$\langle J, z|e^{\alpha_+ J_+} e^{\alpha_0 J_0} e^{\alpha_- J_-}|J, z\rangle = \frac{1}{(1 + |\zeta|^2)^{2J}} \left[e^{\frac{\alpha_0}{2}} + (\alpha_- + \zeta)(\alpha_+ + \zeta^*)e^{-\frac{\alpha_0}{2}}\right]^{2J},$$

$$\langle J, z|e^{\alpha_- J_-} e^{\alpha_0 J_0} e^{\alpha_+ J_+}|J, z\rangle = \frac{1}{(1 + |\zeta|^2)^{2J}} \left[e^{\frac{\alpha_0}{2}}(1 + \alpha_+\zeta)(1 + \alpha_-\zeta^*) + |\zeta|^2 e^{-\frac{\alpha_0}{2}}\right]^{2J}.$$

$$ \qquad (2.5.34)$$

In order to derive these expressions some preliminaries are needed. Thus, the first relation can be obtained by a straightforward calculation and using the results:

$$e^{\alpha_- J_-}|J, z\rangle = \frac{1}{(1 + |\zeta|^2)^J} \left[|J, J\rangle + (\alpha_- + \zeta) \binom{2J}{1}^{1/2} |J, J - 1\rangle \right.$$

$$+ \cdots + (\alpha_- + \zeta)^k \binom{2J}{k}^{1/2} |J, J - k\rangle$$

$$\left. + (\alpha_- + \zeta)^{2J}|J, -J\rangle \right], \qquad (2.5.35)$$

$$e^{\alpha_0 J_0} e^{\alpha_- J_-}|J, z\rangle = \frac{1}{(1 + |\zeta|^2)^J} \left[e^{\alpha_0 J}|J, J\rangle + (\alpha_- + \zeta) \binom{2J}{1}^{1/2} \right.$$

$$\times e^{\alpha_0 (J-1)}|J, J - 1\rangle$$

$$\left. + \cdots + (\alpha_- + \zeta)^{2J} e^{-\alpha_0 J}|J, -J\rangle \right], \qquad (2.5.36)$$

$$\langle J, z|e^{\alpha_+ J_+} = \frac{1}{(1 + |\zeta|^2)^J} \left[\langle J, J| + (\alpha_+ + \zeta^*) \binom{2J}{1}^{1/2} \right.$$

$$\times \langle J, J - 1|$$

$$\left. + \cdots + (\alpha_+ + \zeta^*)^{2J} \binom{2J}{2J}^{1/2} \langle J, -J| \right]. \qquad (2.5.37)$$

Concerning the second generating function, the intermediary steps lead to the result:

$$|J, z\rangle = \frac{1}{(1 + |\zeta|^2)^J}$$

$$\times \left[|J, J\rangle + z \binom{2J}{1}^{1/2} |J, J - 1\rangle + \cdots + z^k \binom{2J}{k}^{1/2} |J.J - k\rangle \right.$$

$$\left. + \cdots + z^{2J}|J, -J\rangle \right], \qquad (2.5.38)$$

$$e^{\alpha_+ J_+}|J, z\rangle = \frac{1}{(1 + |\zeta|^2)^J}$$

$$\times \left[|J, J\rangle(1 + \alpha_+\zeta)^{2J} + |J, J - 1\rangle(1 + \alpha_+\zeta)^{2J-1}\zeta \begin{pmatrix} 2J \\ 1 \end{pmatrix}^{1/2} \right.$$

$$\left. + |J, J - 2\rangle(1 + \alpha_+\zeta)^{2J-2}\zeta^2 \begin{pmatrix} 2J \\ 2 \end{pmatrix}^{1/2} + \cdots + |J, -J\rangle\zeta^{2J} \right],$$

$$(2.5.39)$$

$$e^{\alpha_0 J_0} e^{\alpha_+ J_+}|J, z\rangle = \frac{1}{(1 + |\zeta|^2)^J}$$

$$\times \left[|J, J\rangle e^{\alpha_0 J}(1 + \alpha_+\zeta)^{2J} + |J, J - 1\rangle(1 + \alpha_+\zeta)^{2J-1}\zeta \begin{pmatrix} 2J \\ 1 \end{pmatrix}^{1/2} e^{\alpha_0(J-1)} \right.$$

$$+ |J, J - 2\rangle(1 + \alpha_+\zeta)^{2J-2}\zeta^2 \begin{pmatrix} 2J \\ 2 \end{pmatrix}^{1/2} e^{\alpha_0(J-2)}$$

$$\left. + \cdots + |J, -J\rangle\zeta^{2J} e^{-\alpha_0 J} \right], \qquad (2.5.40)$$

$$\langle J, z|e^{\alpha_- J_-} = \frac{1}{(1 + |\zeta|^2)^J}$$

$$\times \left[\langle J, J|(1 + \alpha_-\zeta^*)^{2J} + \langle J, J - 1|(1 + \alpha_-\zeta^*)^{2J-1}\zeta^* \begin{pmatrix} 2J \\ 1 \end{pmatrix}^{1/2} \right.$$

$$\left. + \langle J, J - 2|(1 + \alpha_-\zeta^*)^{2J-2}(\zeta^*)^2 \begin{pmatrix} 2J \\ 2 \end{pmatrix}^{1/2} + \cdots + \langle J, -J|(\zeta^*)^{2J} \right].$$

$$(2.5.41)$$

Chapter 3
Compact Formulas for Ground Band Energies

3.1 Introduction

One of the big merits of the liquid drop model is that it defines in a consistent way the rotational bands. Many theoretical efforts have been made to describe excitation energies and electromagnetic transitions probabilities. One of the early claims, was to obtain a closed formula for the ground band energies which explains the deviations from the $J(J + 1)$ pattern. Various methods have been proposed which were mainly based on the principle of variable moment of inertia [MSB69, Harr65, DDK70]. These approaches proposed for ground band energies a series expansion in terms of $J(J + 1)$ term. The weak point of these expansions is that they do not converge for high angular momenta. The first attempt to avoid this difficulty was due to Holmberg and Lipas [HoLi68] who proposed a square root of a linear expression of $J(J + 1)$. This expression proves to work better than a quadratic expression in $J(J + 1)$.

Here we raise the question whether this formula can be improved so that it can be extended to the region of states with high angular momenta. In what follows we describe four solutions for this problem, each of them being obtained in a distinct manner. One solution is based on a semiclassical treatment of a second order quadrupole boson Hamiltonian. Two different expressions for the ground band energies are given by asymptotic and near vibrational expansions respectively, of an angular momentum projection formula. Finally, a compact formula is possible within a cranking approach. The four expressions obtained for energies are used for a large number of nuclei.

To conclude, in this chapter we derive analytical formulas for the rotational ground band energies, which are suitable for a realistic description of a large class of nuclei.

3.2 Holmberg-Lipas Formula for the Ground Band Energies

A systematic analysis of the spectra in nuclei from the regions $150 < A < 190$ and $A > 220$ confirmed, in the beginning of 60s of the last century, the description proposed by Bohr and Mottelson for the low lying states from the ground band of deformed nuclei:

$$E = \frac{\hbar^2}{2\mathcal{I}} J(J+1) \equiv A J(J+1). \tag{3.2.1}$$

Later on, the experimental technique development allowed to populate states of higher angular momenta for which the above simple formula does not work any longer. It was thus necessary to correct this simple formula by terms of higher power in $J(J+1)$. A more realistic expression could be:

$$E = A J(J+1) + B J^2 (J+1)^2. \tag{3.2.2}$$

For states of high and very high spin even this new equation does not suffice for a realistic description. Attempts to extend the Eq. (3.2.2) have been made from both the microscopic side, by a cranking formalism, and the phenomenological framework generalizing the above equation to the series:

$$E = A J(J+1) + B J^2 (J+1)^2 + C J^3 (J+1)^3 + \cdots, \tag{3.2.3}$$

Unfortunately, this expansion is not useful since for high angular momentum is divergent. An alternative solution has been proposed by Holmberg and Lipas (HL) in Ref. [HoLi68], which will be described below. The authors noticed that the moment of inertia is not a constant with respect to the angular momentum. If the l.h.s of Eq. (3.2.1) one considers the experimental energies corresponding to the angular momentum J, one could extract then the moment of inertia. Plotting further the moment of inertia vs energy one obtains a linear dependence excepting the first excited energy levels:

$$\mathcal{I} = c_1 + c_2 E. \tag{3.2.4}$$

This linear dependence is shown in Fig. 3.1. Inserting the moment of inertia as given in Eq. (3.2.4) in (3.2.1) we obtain a second rank equation for energy.

$$2 c_2 E^2 + 2 c_1 E - J(J+1) = 0. \tag{3.2.5}$$

The solution of this equation is:

$$E = a \left[\sqrt{1 + b J(J+1)} - 1 \right], \tag{3.2.6}$$

Fig. 3.1 The moment of inertia is represented as function of energy for several nuclei
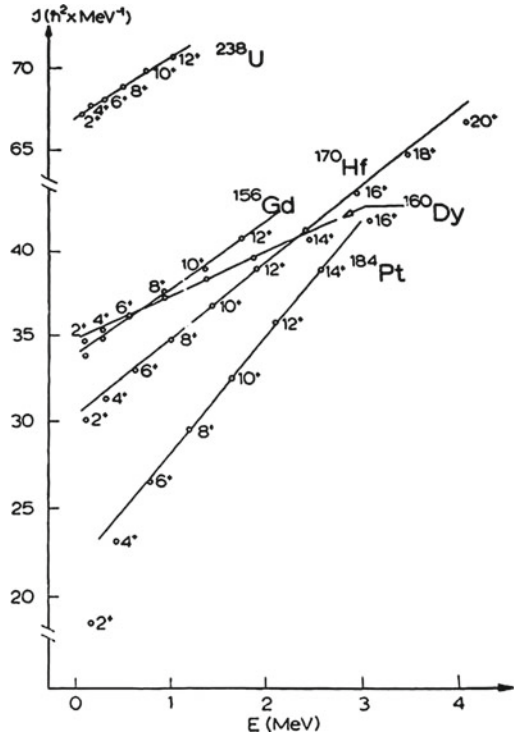
where the new constants a and b are given by:

$$a = \frac{c_1}{2c_2}, \quad b = \frac{2c_2}{c_1^2}. \tag{3.2.7}$$

HL formula (3.2.6) can be also obtained on the ground of hydrodynamic model. Indeed, the energy of a deformed nucleus may be written as:

$$E(\beta) = \frac{\hbar^2}{2\mathcal{I}(\beta)} J(J+1) + \frac{1}{2}(\beta - \beta_0)^2, \tag{3.2.8}$$

where β_0 is the nuclear static deformation, while β is the dynamic deformation. Within the hydrodynamic model the moment of inertia is proportional to the square of the nuclear deformation:

$$\mathcal{I} = 3\mathcal{B}\beta^2. \tag{3.2.9}$$

The deformation which assures the system equilibrium is obtained from the condition

$$\frac{\partial E(\beta)}{\partial \beta} = 0. \tag{3.2.10}$$

The result is:

$$\beta - \beta_0 \equiv \Delta\beta = \frac{2E}{C\beta_0} + \mathcal{O}(\Delta\beta^2). \tag{3.2.11}$$

Using now this result in connection with (3.2.9), we obtain:

$$\mathcal{I} = 3\mathcal{B}\left[\beta_0^2 + \frac{4E}{C} + \mathcal{O}(\Delta\beta^2)\right]. \tag{3.2.12}$$

This equation confirms the linear dependence on energy of the moment of inertia. Replacing the moment of inertia from Eq. (3.2.8) with the expression (3.2.12) and neglecting the terms $\mathcal{O}(\Delta\beta^2)$, one obtains a second degree equation for the energy E:

$$24\frac{\mathcal{B}}{C}E^2 + 6\mathcal{B}\beta_0^2 E - \hbar^2 J(J+1) = 0. \tag{3.2.13}$$

The solution for this equation is of the form (3.2.6) with the parameters a and b given by:

$$a = \frac{1}{8}C\beta_0^2, \quad b = \frac{8}{3}\frac{\hbar^2}{\mathcal{B}C\beta_0^4}. \tag{3.2.14}$$

For illustration, in Fig. 3.2 one presents the results for the ground band energies obtained with formulas (3.2.2) and (3.2.6) [HoLi68]. Comparing the theoretical results, (3.2.2) and (3.2.6), with the corresponding experimental data one notices that the HL formula provides a better agreement.
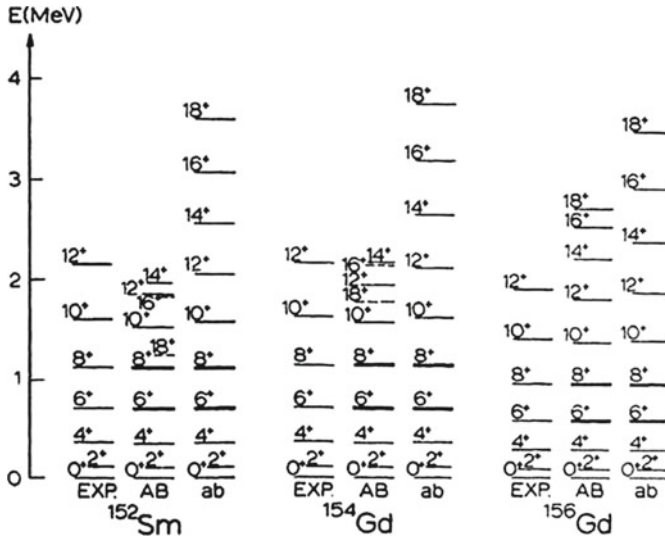
Fig. 3.2 Ground band energies calculated with Eq. (3.2.2) (AB) as well as with the Holmberg-Lipas formula (3.2.6)

3.3 Angular Momentum Projected State

As variational state we choose the axial symmetric coherent function

$$|\Psi_g\rangle = e^{d(b_{20}^\dagger - b_{20})}|0\rangle, \tag{3.3.1}$$

This function will be used in connection with the boson Hamiltonian:

$$H = A_1 \sum_\mu b_{2\mu}^\dagger b_{2\mu} + A_2 \hat{J}^2. \tag{3.3.2}$$

The vacuum state for the quadrupole boson operators, $b_{2\mu}^\dagger$, $b_{2\mu}$, is denoted by $|0\rangle$, while d is a real quantity which plays the role of the deformation parameter. As explained already in the previous chapter, the reason is the fact that the average value of the quadrupole moment written in the lowest order in terms of quadrupole boson operator, with the function $|\Psi_g\rangle$ is proportional to d. The component of a given angular momentum is obtained by a projection procedure:

$$\varphi_{JM}^{(g)} = N_J^{(g)} P_{M0}^J \Psi_g, \tag{3.3.3}$$

where P_{MK}^J is the angular momentum projection operator:

$$P_{MK}^J = \frac{2J+1}{8\pi^2} \int D_{MK}^{J*}(\Omega) \hat{R}(\Omega) d\Omega, \tag{3.3.4}$$

and D_{MK}^J the Wigner function, while $\hat{R}(\Omega)$ is a rotation operator defined by the Euler angles Ω. The system energy is defined as the average value of H with the projected state:

$$E_J^{(g)} \equiv \langle \varphi_{JM}^{(g)}|H|\varphi_{JM}^{(g)}\rangle = A_1 d^2 \frac{I_J^{(1)}(d^2)}{I_J^{(0)}(d^2)} + A_2 J(J+1), \tag{3.3.5}$$

where we denoted by $I_J^{(0)}$ the overlap integral:

$$I_J^{(0)}(x) = \int_0^1 P_J(y) e^{x P_2(y)} dy, \quad x = d^2. \tag{3.3.6}$$

with P_J standing for the Legendre polynomial of rank J. The kth derivative of this integral is denoted by:

$$I_J^{(k)}(x) = \frac{d^k I_J^{(0)}}{dx^k}. \tag{3.3.7}$$

The normalization factor for the projected state has the expression:

$$\left(N_J^{(g)}\right)^{-2} = (2J + 1)I_J^{(0)}e^{-d^2}. \tag{3.3.8}$$

These integrals have been analytically calculated in Ref. [RCGD82]. Actually, the energies presented here refer to the ground band described by the coherent state model (CSM) which considers simultaneously three interacting bands, ground, beta and gamma. In the asymptotic limit of the deformation parameter d, the ground band energies have the expression [RS83]

$$E_J^{(g,asym)} = \frac{A_1}{2}\left[\frac{x-1}{2} + G_J^{1/2}\right] + A_2 J(J + 1), \tag{3.3.9}$$

with

$$G_J = \frac{9}{4}x(x-2) + \left(J + \frac{1}{2}\right)^2 - \frac{4}{9x}\left(3 + \frac{10}{x} + \frac{37}{x^2}\right)$$
$$+ \frac{2}{3x}\left(1 + \frac{10}{3x} + \frac{13}{x^2}\right)J(J+1) - \frac{2}{9x^3}J^2(J+1)^2, \quad x = d^2. \tag{3.3.10}$$

The parameter $x = d^2$ describes the deformation and is involved in the ansatz for the variational state (3.3.1). It is worth mentioning that Eq. (3.3.9) generalizes the Holmberg-Lipas (HL) formula, the $J(J + 1)$ dependence being more complex. The expression (3.3.9) is obtained by replacing the series expansion in $1/x$, associated to the ratio $x\frac{I_J^{(1)}}{I_J^{(0)}}$,

$$x\frac{I_J^{(1)}}{I_J^{(0)}} = x - 1 - \frac{1}{3x} - \frac{5}{9x^2} - \frac{37}{27x^3} + \left(\frac{1}{6x} + \frac{5}{18x^2} + \frac{13}{18x^3}\right)J(J+1)$$
$$- \frac{1}{54x^3}J^2(J+1)^2 + \mathcal{O}(x^{-4}), \tag{3.3.11}$$

by a faster convergent one.

According to Ref. [RCGP84], for the near vibrational regime (d–close to zero) the ground state band energies have the expressions:

$$E_J^{g,vib} = A_1\left[\frac{J}{2} + \frac{J}{2(2J+3)}x + \frac{9}{2}\frac{(J+1)(J+2)}{(2J+3)^2(2J+5)}x^2\right.$$
$$\left. + \frac{27}{2}\frac{(J+1)(J+2)}{(2J+3)^3(2J+5)(2J+7)}x^3\right] + A_2 J(J+1). \tag{3.3.12}$$

For the sake of completeness we present the derivation of the two expressions for the ground band energies, in the rotational and near vibrational limits.

3.3.1 Vibrational and Large Deformation Regime

By direct calculations we can check that the overlap integral $I_J^{(0)}$ and its first and second derivatives satisfy the following differential equation:

$$\frac{d^2 I_J^{(0)}}{dx^2} - \frac{x-3}{2x}\frac{dI_J^{(0)}}{dx} - \frac{2x^2 + J(J+1)}{4x^2}I_J^{(0)} = 0, \quad (x = d^2). \tag{3.3.13}$$

By a suitable change of function this equation can be brought to the differential equation characterizing the hypergeometric function of the first rank. Thus, the final result for $I_J^{(0)}$ is:

$$I_J^{(0)} = \frac{(J!)^2}{(\frac{J}{2})!(2J+1)!}(6d^2)^{\frac{J}{2}}e^{-\frac{d^2}{2}}{}_1F_1\left(\frac{1}{2}(J+1), J+\frac{3}{2}; \frac{3}{2}d^2\right). \tag{3.3.14}$$

This expression is further used for describing both the asymptotic and vibrational behavior for the excitation energies in the ground band. Indeed, in the asymptotic region of d, the hypergeometric function behaves like:

$$_1F_1(a, c; z) = \frac{\Gamma(c)}{\Gamma(a)}e^z z^{a-c}[1 + \mathcal{O}(|z|^{-1})]. \tag{3.3.15}$$

Due to this expression, the dominant term of $I_J^{(0)}$ is:

$$I_J^{(0)} \sim \frac{e^x}{3x}. \tag{3.3.16}$$

This expression suggests an alternative expression for $I_J^{(0)}$, valid in the asymptotic region, of the following form:

$$I_J^{(0)} = e^x \sum_{n=1} A_n x^{-n}. \tag{3.3.17}$$

Inserting this expression into the above differential equation, one obtains the recursion relation for the expansion coefficients A_k:

$$A_{n+1} = \frac{A_n}{6n}(2n+J)(2n-J-1). \tag{3.3.18}$$

The leading term (3.3.16) gives $A_1 = \frac{1}{3}$ and then (3.3.18) determines the whole set of the expansion coefficients. This way we obtain for the ratio $d^2 I_J^{(1)}/I_J^{(0)}$ the expression:

$$x \frac{I_J^{(1)}}{I_J^{(0)}} = x - 1 - \frac{1}{3x} - \frac{5}{9x^2} - \frac{37}{27x^3} + \left(\frac{1}{6x} + \frac{5}{18x^2} + \frac{13}{18x^3} \right) J(J+1)$$

$$- \frac{1}{54x^3} J^2(J+1)^2 + \mathcal{O}(x^{-4}). \tag{3.3.19}$$

The convergence in terms of $1/x$ for the excitation energy may be improved in two steps. First we write the differential equation for $I_J^{(0)}$ in a different form:

$$x \left(x \frac{I_J^{(1)}}{I_J^{(0)}} \right)' + \left(x \frac{I_J^{(1)}}{I_J^{(0)}} \right)^2 - \frac{x-1}{2} \left(x \frac{I_J^{(1)}}{I_J^{(0)}} \right) - \frac{2x^2 + J(J+1)}{4} = 0. \tag{3.3.20}$$

The derivative $\left(x \frac{I_J^{(1)}}{I_J^{(0)}} \right)'$ is further calculated by using (3.3.19) and thus the above equation becomes a second degree algebraic equation for $x \frac{I_J^{(1)}}{I_J^{(0)}}$. Solving this equation one obtains:

$$x \frac{I_J^{(1)}}{I_J^{(0)}} = \frac{1}{2} \left[\frac{x-2}{2} + \sqrt{G_J} \right], \tag{3.3.21}$$

where G_J is defined by Eq. (3.3.10).

Concerning the near vibrational regime the final expression for energies is obtained in two steps. First, one derives the vibrational limit of the kth derivative:

$$\lim_{d \to 0} \left(d^2 \frac{I_J^{(1)}}{I_J^{(0)}} \right)^{(k)} = \frac{1}{(2J+3)^k} \left[\frac{J}{2} (\delta_{k,0} + \delta_{k,1}) + 9 \frac{(J+1)(J+2)}{2J+5} \right.$$

$$\left. \times \left((\delta_{k,2} + 9 \frac{\delta_{k,3}}{2J+7}) \right) \right], \quad k = 0, 1, 2, 3. \tag{3.3.22}$$

Then, truncating the Taylor expansion of $x \frac{I_J^{(1)}}{I_J^{(0)}}$, around the point $x = 0$, at the third order, one obtains:

$$x \frac{I_J^{(1)}}{I_J^{(0)}} = \frac{J}{2} + \frac{J}{2(2J+3)} x + \frac{9}{2} \frac{(J+1)(J+2)}{(2J+3)^2(2J+5)} x^2$$

$$+ \frac{27}{2} \frac{(J+1)(J+2)}{(2J+3)^3(2J+5)(2J+7)} x^3 + \mathcal{O}(x^4). \tag{3.3.23}$$

Therefore (3.3.9) and (3.3.12) describe the energies in the ground band in the asymptotic and vibrational regions of d, respectively.

3.4 Semiclassical Treatment of a Second Order Quadrupole Boson Hamiltonian

For a moment we consider the simplest quadrupole boson $(b_{2,\mu}^\dagger, -2 \leq \mu \leq 2)$ Hamiltonian:

$$H = A_1 \sum_\mu b_\mu^\dagger b_\mu + A_2 \sum_\mu (b_\mu^\dagger b_{-\mu}^\dagger + b_\mu b_{-\mu})(-)^\mu. \qquad (3.4.1)$$

Here we are interested to study the classical equations provided by the time dependent variational principle associated to H:

$$\delta \int_0^t \langle \Psi | H - i\hbar \frac{\partial}{\partial t'} | \Psi \rangle dt' = 0, \qquad (3.4.2)$$

If the variational states span the whole Hilbert space of the boson states, then solving the variational equations is equivalent to solving the time dependent Schrödinger equation which is, in general, a difficult task. Therefore, we restrict the trial function to a coherent state which, we hope, is suitable for describing the semiclassical feature of the chosen system:

$$|\Psi\rangle = \exp\left[z_0 b_0^\dagger - z_0^* b_0 + z_2(b_2^\dagger + b_{-2}^\dagger) - z_2^*(b_2 + b_{-2})\right]|0\rangle. \qquad (3.4.3)$$

Indeed, the coherence property results from the obvious equation:

$$b_\mu |\Psi\rangle = (\delta_{\mu 0} z_0 + (\delta_{\mu 2} + \delta_{\mu -2}) z_2)|\Psi\rangle. \qquad (3.4.4)$$

In order to write explicitly the equations emerging from (3.4.2) we have to calculate first the averages of H

$$\mathcal{H} = \langle \Psi | H | \Psi \rangle, \qquad (3.4.5)$$

as well as of the action operator $-i\hbar\frac{\partial}{\partial t}$. The variational equation (3.4.2) yields the following classical equations for the complex coordinates z_k and z_k^*:

$$\begin{aligned}
\frac{\partial \mathcal{H}}{\partial z_0} &= -i\hbar \, \dot{z}_0^*, \quad \frac{\partial \mathcal{H}}{\partial z_0^*} = i\hbar \, \dot{z}_0, \\
\frac{\partial \mathcal{H}}{\partial z_2} &= -2i\hbar \, \dot{z}_2^*, \quad \frac{\partial \mathcal{H}}{\partial z_2^*} = 2i\hbar \, \dot{z}_2.
\end{aligned} \qquad (3.4.6)$$

Note that the coordinates z_k and z_k^* define a classical phase space, while $\mathcal{H}$ plays the role of a classical Hamilton function. For what follows it is useful to bring these equations to a canonical form. This is achieved by the transformation:

$$q_i = 2^{(k+2)/4} \mathrm{Re}(z_k), \quad p_i = \hbar 2^{(k+2)/4} \mathrm{Im}(z_k), \quad k = 0, 2, \quad i = \frac{k+2}{2}. \quad (3.4.7)$$

Indeed, in the new coordinates the classical equations of motion become:

$$\frac{\partial \mathcal{H}}{\partial q_k} = -\dot{p}_k, \quad \frac{\partial \mathcal{H}}{\partial p_k} = \dot{q}_k. \quad (3.4.8)$$

In terms of the new coordinates, the Hamilton function is written as:

$$\mathcal{H} = \frac{A_1 + 2A_2}{2}(q_1^2 + q_2^2) + \frac{A_1 - 2A_2}{2\hbar^2}(p_1^2 + p_2^2)$$
$$= \frac{A}{2}(q_1^2 + q_2^2) + \frac{A'}{2\hbar^2}(p_1^2 + p_2^2), \quad (3.4.9)$$

where we denoted by $A = A_1 + 2A_2$ and $A' = A_1 - 2A_2$. Equation (3.4.8) provides the connection between the generalized momenta and the coordinates time derivatives:

$$p_1 = \frac{\hbar^2 \dot{q}_1}{A'}, \quad p_2 = \frac{\hbar^2 \dot{q}_2}{A'}. \quad (3.4.10)$$

Taking into account these relations, the classical energy function becomes:

$$\mathcal{H} = \frac{\hbar^2}{2A'}(\dot{q}_1^2 + \dot{q}_2^2) + \frac{A}{2}(q_1^2 + q_2^2). \quad (3.4.11)$$

For what follows it is useful to use the polar coordinates:

$$q_1 = r \cos\theta, \quad q_2 = r \sin\theta, \quad (3.4.12)$$

for the Hamilton function:

$$\mathcal{H} = \frac{\hbar^2}{2A'}(\dot{r}^2 + r^2 \dot{\theta}^2) + \frac{A}{2}r^2. \quad (3.4.13)$$

For what follows it is useful to introduce the quantities:

$$\mathcal{L}_1 = \frac{\hbar}{4}((q_1^2 + p_1^2 - q_2^2 - p_2^2),$$
$$\mathcal{L}_2 = \frac{\hbar}{2}(q_1 q_2 + p_1 p_2),$$
$$\mathcal{L}_3 = \frac{\hbar}{2}(q_1 p_2 - q_2 p_1) = \frac{\hbar^2}{A'}r^2\dot{\theta} \quad (3.4.14)$$

One can check that

$$\{\mathcal{L}_i, \mathcal{L}_k\} = \hbar \epsilon_{ikj} \mathcal{L}_l, \quad (3.4.15)$$

where $\{,\}$ denotes the Poisson bracket while ϵ_{ikj} the antisymmetric unit tensor. In virtue of Eq. (3.4.15) the set of functions $\mathcal{L}_k$ with the Poisson brackets as multiplication operation, form a classical $SU_c(2)$ algebra. Moreover, they could be obtained by averaging with $\mid \Psi\rangle$, the generators $\hat{L}_k$

$$\mathcal{L}_k = \langle \Psi \mid \hat{L}_k \mid \Psi\rangle; \ k = 1, 2, 3, \tag{3.4.16}$$

of a boson $SU_b(2)$ algebra defined with the operators $b_0^\dagger, b_{\pm 2}^\dagger$, as:

$$\hat{L}_1 = \frac{\hbar}{4}\left[2b_0^\dagger b_0 - (b_2^\dagger + b_{-2}^\dagger)(b_2 + b_{-2})\right],$$

$$\hat{L}_2 = \frac{\hbar}{2\sqrt{2}}\left[b_0^\dagger(b_2 + b_{-2}) + (b_2^\dagger + b_{-2}^\dagger)b_0\right],$$

$$\hat{L}_3 = \frac{\hbar}{2\sqrt{2}i}\left[b_0^\dagger(b_2 + b_{-2}) - (b_2^\dagger + b_{-2}^\dagger)b_0\right]. \tag{3.4.17}$$

The equation

$$\hat{L}_k \to \hat{\mathcal{L}}_k, \ k = 1, 2, 3, \tag{3.4.18}$$

and the correspondence between commutators and Poisson brackets

$$[,] \to \frac{1}{i}\{,\}, \tag{3.4.19}$$

define a homeomorphism of the boson and classical algebras generated by $\{\hat{L}_k\}_{k=1,2,3}$ and $\{\mathcal{L}_k\}_{k=1,2,3}$ respectively. Note that the boson $SU_b(2)$ algebra does not describe the rotations in the real configuration space but in a fictitious space. Due to this fact we shall refer to $\hat{L}_k$ as to the components of a pseudo-angular momentum. Using the equations of motion for the conjugate variables, one can prove that

$$\dot{\mathcal{L}}_3 = 0 \ , \quad \dot{\mathcal{H}} = 0, \tag{3.4.20}$$

The first conservation law expressed by (3.4.20) is determined by the invariance against rotation around the 3rd axis in the fictitious space mentioned above: $[H, \hat{L}_3] = 0$. The second equation asserts that the energy is conserved and that is a consequence of the variational principle. Since the classical system is characterized by two degrees of freedom and, on the other hand, there are two constants of motion

$$\mathcal{H} = E \ , \quad \mathcal{L}_3 = L, \tag{3.4.21}$$

the equations of motion are exactly solvable.

The constant value of $\mathcal{L}_3$ is conventionally taken to be:

$$\frac{\hbar^2}{2A'}r^2\,\dot{\theta} = L\hbar, \tag{3.4.22}$$

which allows us to express the angular variable derivative in terms of the radial one:

$$\dot{\theta} = \frac{2A'L}{\hbar r^2}. \tag{3.4.23}$$

Thus, the energy function written in the reduced space, becomes:

$$\mathcal{H} = \frac{\hbar^2}{2A'} \dot{r}^2 + \frac{2A'L^2}{r^2} + \frac{A}{2}r^2 \equiv \frac{\hbar^2}{2A'} \dot{r}^2 + V_{\text{eff}}(r). \tag{3.4.24}$$

We recognize in the effective potential energy:

$$V_{\text{eff}}(r) = \frac{2A'L^2}{r^2} + \frac{A}{2}r^2, \tag{3.4.25}$$

just the Davidson potential [Dav32].

Instead of finding the classical trajectories and then quantizing them, here we first quantize the energy by replacing

$$\frac{\hbar^2 \dot{r}}{A'} \rightarrow -i\hbar \frac{\partial}{\partial r}. \tag{3.4.26}$$

Thus, one arrives at the Schrödinger equation:

$$\left[-\frac{A'}{2} \frac{\partial^2}{\partial r^2} + \frac{2A'L^2}{r^2} + \frac{A}{2}r^2 \right] u(r) = \epsilon u(r). \tag{3.4.27}$$

Making use of the change of variable and function:

$$x = \sqrt{\frac{A}{A'}} r^2, \quad u(r) = e^{-\frac{x}{2}} x^s f(x), \tag{3.4.28}$$

one obtains the following differential equation:

$$\left[x \frac{\partial^2}{\partial x^2} + \left(2s + \frac{1}{2} - x \right) \frac{\partial}{\partial x} + \left(\frac{2s^2 - s - 2L^2}{2x} + \frac{\epsilon}{2\sqrt{AA'}} - \frac{1}{4} - s \right) \right] f(x) = 0. \tag{3.4.29}$$

This should be compared with the differential equation for the Laguerre polynomials:

$$\left[x \frac{\partial^2}{\partial x^2} + (m + 1 - x) \frac{\partial}{\partial x} + n \right] L_n^m(x) = 0. \tag{3.4.30}$$

Indeed, the two equations are identical provided the following equations hold:

$$1 + m = 2s + \frac{1}{2}, \quad n = \frac{\epsilon}{2\sqrt{AA'}} - \frac{1}{4} - s, \quad 2s^2 - s - 2L^2 = 0. \tag{3.4.31}$$

From the last equation we derive the expression of s as a function of L. The positive solution is:

$$s = \frac{1}{4}(1 + \sqrt{1 + 16L^2}).$$ (3.4.32)

The second equation (3.4.31) yields for the energy ϵ the following expression:

$$\epsilon_{nL} = 2\sqrt{(A_1^2 - 4A_2^2)}\left(n + \frac{1}{2} + \frac{1}{4}\sqrt{1 + 16L^2}\right), \quad n = 0, 1, 2, \ldots \ L = 0, 1, 2, \ldots$$ (3.4.33)

An approximate expression may be obtained by expanding first the Davidson potential V_{eff} around its minimum r_0 given by the equation:

$$r_0^2 = 2L\sqrt{\frac{A'}{A}},$$ (3.4.34)

and truncating the expansion at the quadratic term. The result for the energy function is:

$$\mathcal{H} = \frac{\hbar^2}{2A'}\dot{r}^2 + 2A(r - r_0)^2 + 2L\sqrt{AA'}.$$ (3.4.35)

Quantizing this Hamilton function we obtain an eigenvalue equation for a harmonic oscillator whose energy is:

$$E_{nL} = 2\sqrt{AA'}\left(n + \frac{1}{2}\right) + 2L\sqrt{AA'}$$

$$= 2\sqrt{(A_1^2 - 4A_2^2)}\left(n + \frac{1}{2} + L\right), \quad n = 0, 1, 2, \ldots$$ (3.4.36)

We remark the fact that the two spectra, exact and semiclassical coincide when L is large:

$$E_{nL} \approx \epsilon_{n,L}, \text{ for } L = \text{large}.$$ (3.4.37)

Note that the initial boson Hamiltonian could be easily diagonalized by a suitable chosen canonical transformation:

$$\tilde{b}_\mu^\dagger = Ub_\mu^\dagger - V(-)^\mu b_{-\mu},$$
$$\tilde{b}_\mu = Ub_\mu - V(-)^\mu b_{-\mu}^\dagger.$$ (3.4.38)

Indeed, the coefficients U and V may be chosen such that:

$$\left[\tilde{b}_\mu, \tilde{b}_{\mu'}^\dagger\right] = \delta_{\mu\mu'}, \left[H, \tilde{b}_\mu^\dagger\right] = E\tilde{b}_\mu^\dagger.$$ (3.4.39)

The second equation provides a homogeneous system of equations for the transformation coefficients

$$\begin{pmatrix} A_1 & 2A_2 \\ -2A_2 & -A_1 \end{pmatrix} \begin{pmatrix} U \\ V \end{pmatrix} = E \begin{pmatrix} U \\ V \end{pmatrix},$$
                                          (3.4.40)

This determines U and V up to a multiplicative constant to be fixed by the first equation which gives:

$$U^2 - V^2 = 1.$$ (3.4.41)

The compatibility condition for Eq. (3.4.40) gives $E = \sqrt{A_1^2 - 4A_2^2}$, and therefore the eigenvalues of H are:

$$E_n = \sqrt{A_1^2 - 4A_2^2} \left(n + \frac{5}{2} \right).$$ (3.4.42)

The frequency obtained is half the one obtained through the semiclassical approach. The reason is that here the frequency is associated to each of the 5 degrees of freedom while semiclassically the frequency is characterizing a plane oscillator. Note that the pseudo-angular momentum L is different from the angular momentum in the laboratory frame describing rotations in the quadrupole boson space:

$$\hat{J}_\mu = \sqrt{10} \left(b_2^\dagger b_2 \right)_{1\mu}.$$ (3.4.43)

The expected value of the angular momentum square is:

$$\langle \Psi | \hat{J}^2 | \Psi \rangle = 3 \left[q_1^2 + q_2^2 + \frac{1}{\hbar^2} \left(p_1^2 + p_2^2 \right) \right].$$ (3.4.44)

Since the variational function $|\Psi\rangle$ is not eigenstate of $\hat{J}^2$, the above mentioned average value is not a constant of motion. Indeed, it is easy to check that:

$$\frac{\partial \langle \Psi | \hat{J}^2 | \Psi \rangle}{\partial t} = \frac{6}{\hbar^2} \left(A' - A \right) (q_1 p_1 + q_2 p_2) \neq 0.$$ (3.4.45)

It is instructive to see whether we could crank the system so that the magnitude of angular momentum is preserved, i.e.

$$\langle \Psi | \hat{J}^2 | \Psi \rangle = \hbar^2 J (J + 1).$$ (3.4.46)

Using the polar coordinates the above equation becomes:

$$\frac{3\hbar^2}{A'^2} \dot{r}^2 + \frac{12L^2}{r^2} + 3r^2 = J(J + 1).$$ (3.4.47)

This equation is treated similarly with the energy equation. Thus by the quantization:

$$\frac{A'^2}{\hbar^2}\dot{r} \rightarrow -i\hbar\frac{\partial}{\partial r},\tag{3.4.48}$$

Equation (3.4.47) becomes a differential equation for the wave function describing the angular momentum:

$$-\frac{\partial^2\Phi}{\partial r^2} + \left(\frac{4L^2}{A'^2 r^2} + \frac{r^2}{A'^2}\right)\Phi = \frac{J(J+1)}{3A'^2}\Phi.\tag{3.4.49}$$

Making the change of variable and function:

$$x = \frac{r^2}{A'}, \quad \Phi = e^{-\frac{x}{2}}x^s\Psi,\tag{3.4.50}$$

we obtain the following equation for Ψ:

$$x\frac{\partial^2\Psi}{\partial x^2} + \left(2s - x + \frac{1}{2}\right)\frac{\partial\Psi}{\partial x} + \left(\frac{2s^2 - s - \frac{2L^2}{A'^2}}{2x} + \frac{J(J+1)}{12A'} - s - \frac{1}{2}\right)\Psi = 0.\tag{3.4.51}$$

This equation admits the Laguerre polynomials $L_{n'}^{m'}(x)$ with the quantum numbers determined as follows:

$$m' = 2s - \frac{1}{2}, \quad s = \frac{1}{4} + \frac{1}{4}\sqrt{1 + \frac{16L^2}{A'^2}}, \quad \frac{J(J+1)}{12A'} = n' + \frac{1}{2} + \frac{1}{4}\sqrt{1 + \frac{16L^2}{A'^2}}.\tag{3.4.52}$$

The last relation (3.4.52) can be viewed as an equation determining L:

$$L = \left[\left(\frac{J(J+1)}{12} - A'(n' + \frac{1}{2})\right)^2 - \left(\frac{A'}{4}\right)^2\right]^{1/2}.\tag{3.4.53}$$

On the other hand taking the harmonic approximation for the potential term in Eq. (3.4.47) one obtains the classical equation for a harmonic oscillator from which we get:

$$J(J+1) = 12A'\left(n' + \frac{1}{2}\right) + 12L.\tag{3.4.54}$$

Reversing this equation one can express the pseudo-angular momentum L in terms of the angular momentum J:

$$L = \frac{J(J+1)}{12} - A'\left(n' + \frac{1}{2}\right).\tag{3.4.55}$$

Replacing, successively, the expressions for L, (3.4.53 and 3.4.55), into energy Eqs. (3.4.33 and 3.4.36), we obtain four distinct expressions for the energies characterizing the starting Hamiltonian H.

$$
E^{(1)}_{nn'J} = \sqrt{AA'}\left[2n + 1 + \frac{J(J+1)}{6} - A'\left(2n' + 1\right)\right],
$$

$$
E^{(2)}_{nn'J} = \sqrt{AA'}\left[2n + 1 + 2\sqrt{\left[\frac{J(J+1)}{12} - A'\left(n' + \frac{1}{2}\right)\right]^2 - \left(\frac{A'}{4}\right)^2}\right],
$$

$$
E^{(3)}_{nn'J} = \sqrt{AA'}\left[2n + 1 + \frac{1}{2}\sqrt{1 + 4\left[\frac{J(J+1)}{6} - A'\left(2n' + 1\right)\right]^2}\right],
$$

$$
E^{(4)}_{nn'J} = \sqrt{AA'}\left[2n + 1 + \frac{1}{2}\sqrt{1 + 4\left[\frac{J(J+1)}{6} - A'\left(2n' + 1\right)\right]^2 - (A')^2}\right].
$$

$$(3.4.56)$$

Notice the fact that for a fixed pair of (n, n') each of the above equations define a rotational band: The lowest band corresponds to $(n, n') = (0, 0)$ and defines the ground band. Except for the band energies $E^{(1)}_{00J}$ which exhibits a $J(J+1)$ pattern the other three bands have the same generic expressions. Thus, the excitation energies have the form:

$$
E_J = a\left[\sqrt{1 + bJ(J+1) + cJ^2(J+1)^2} - 1\right]. \qquad (3.4.57)
$$

which is a generalization of the Holmberg-Lipas formula [HoLi68]. The parameters a, b and c are to be fixed by fitting three particular experimental energies.

We recall that we required that the average value of $\hat{J}^2$ equals $\hbar^2 J(J+1)$. Subsequently we eliminated the energy dependence on the pseudo-angular momentum L. This way we projected approximately the angular momentum from the variational state.

3.5 Numerical Results

Since the expressions (3.3.9), (3.3.11) and (3.3.12) are based on series expansion in $1/x$ and x, respectively, it is worth showing how far the truncated expansions are from the exact energies. Aiming at this goal in Figs. 3.3 and 3.4 we plotted the ratio $d^2 \frac{I_J^{(1)}}{I_J^{(0)}}$ and the associated truncated series for large and small values of d, respectively, as functions of d for two angular momenta: $J = 12$ and $J = 16$. In the case of asymptotic regime we considered also the square root expression (3.3.21). In this case one defines an existence interval of d for which $G_J \geq 0$. The lower bounds
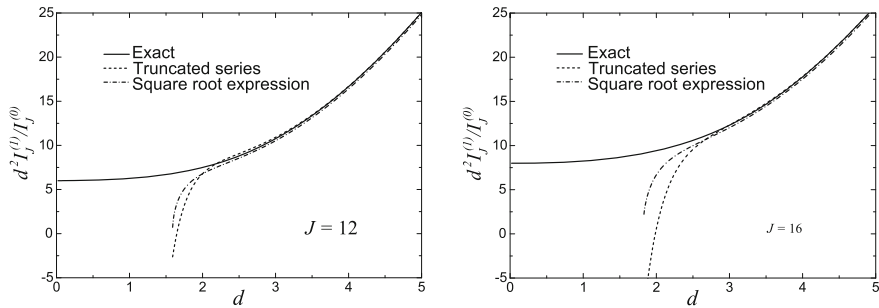
Fig. 3.3 $d^2 I_J^{(1)}/I_J^{(0)}$ is plotted as a function of d for J $= 12$ *left* and J $= 16$ *right*. Two approximations of this function are also presented. One is a truncated expansion in $1/x$ (Eq. 3.3.23), while the other one is given by a square root expression (Eq. 3.3.21) which is slightly faster convergent than the previously mentioned expansion
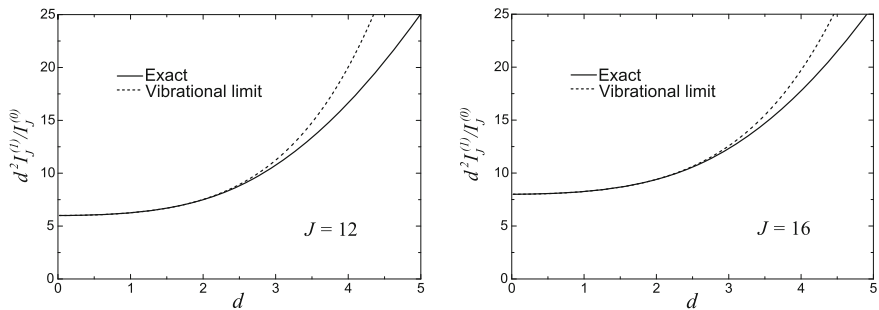
Fig. 3.4 $d^2 I_J^{(1)}/I_J^{(0)}$ is plotted as a function of d for J $= 12$ *left* and J $= 16$ *right*. This is compared with the function given by the near vibrational approximation used in Eq. (3.3.12) (see the factor multiplied with A_1)

of these intervals for J running from 0 to 30 are listed in Table 3.1. From Fig. 3.3 we see that for $d \geq 3$ the used expressions for energies achieve the convergence even for high angular momenta. Concerning the energies for the near vibrational regime one notes that we use a power series of x and therefore one may think that such an expansion is valid only for $x \leq 1$. However, we notice that the coefficients of this expansion are depending on J and moreover are less than unity. The larger J the smaller are these coefficients. This fact infers that the convergence radius is larger than unity and is an increasing function of the angular momentum. As a matter of fact this is confirmed in the plot shown in Fig. 3.4. Comparing the curves from Figs. 3.3 and 3.4 one may say that there is a small interval of d were the asymptotic and small x expansions are matched. This allows us to assert that the reunion of the two formulas, (3.3.9) and (3.3.12), assures an overall description of nuclei ranging from small to large deformation.

In Fig. 3.5 we plotted the term G_J involved in the energy expression (3.3.9) as a function of the deformation parameter d. Except for $J = 0$ and $J = 2$ all the other functions vanish for a specific value of d which are, in fact, the lower

Table 3.1 The smallest value of d, for which G_J is positive

J	0	2	4	6	8	10	12	14	16	18	20	22	24	26	28	30
d_{min}	1.55	0	0	0.65	1.21	1.43	1.59	1.71	1.82	1.91	1.99	2.07	2.14	2.21	2.27	2.33

Fig. 3.5 G_J is plotted as function of d for some angular momenta. Note that excepting the cases of $J = 2, 4$ all other functions G_J get negative for d smaller than a critical value. These limiting values are listed in Table 3.1
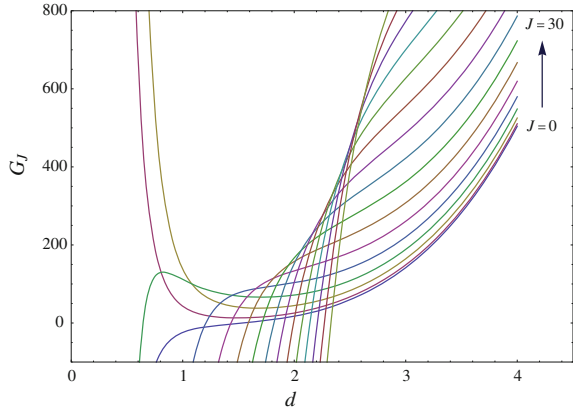
bounds of the existence interval. The basic expressions for energies (3.4.57), (3.3.9) and (3.3.12) have been used for a large number of nuclei grouped according to the nuclear phase to which they belong. Thus, for well deformed nuclei behaving like axially deformed rotor the ratio E_{4+}/E_{2+} should be close to the value of 3.3, while for the near vibrational region one expects a ratio close to the value 2. Between these two extreme values are placed gamma unstable nuclei where the ratio may run in the interval of 2.5–3.0. The deviation from axial symmetry can affect the ratio mentioned above. Thus ^{228}Th exhibits some specific feature of a triaxial nucleus with an equilibrium value $\gamma^0 = 30^0$. The corresponding ratio E_{4+}/E_{2+} is equal to 3.24. According to the IBA (Interacting Boson Approximation) model [AI76, IAAR87] the nuclei belonging to the three groups mentioned above are described by the irreducible representations of some dynamic groups as $SU(3)$, $SU(5)$ and $O(6)$. Since the nuclei described by a certain symmetry group exhibit some specific properties one says that these form a certain nuclear phase. According to Casten [CAIA81] all nuclei of the periodic table may be placed on the sides of a triangle having in vertexes the three symmetries mentioned above. On each side which links two adjacent symmetries one expects a critical transition point. Few years ago, Iachello [Iac00, IA01] advanced the idea that each of the critical nuclei laying on the three triangle sides correspond to specific symmetries. Thus, the transition $O(6) \rightarrow SU(5)$ is characterized by a critical symmetry which is $E(5)$. Representatives for the $E(5)$ symmetry are ^{104}Ru and ^{102}Pd characterized by specific ratios $E_{4+}/E_{2+} = 2.48, 2.29$, respectively. In the transition $SU(5) \rightarrow SU(3)$, the critical point is close to 3. Such nuclei are ^{150}Nd, ^{152}Sm, ^{154}Gd and ^{156}Dy. Indeed, they prove to be critical points for the mentioned phase transition when the entire isotopic chains are considered. Recently, it was shown that some nuclei lay inside the Casten's triangle.

The question to answer is whether the compact energy formulas obtained are able to describe the ground band energies for all nuclei mentioned above. The theoretical values for energies labeled by Th(1) are obtained with Eq. (3.3.9) if d is large or with Eq. (3.3.12) when d is smaller than 2. The calculated energies labeled by Th(2) are obtained with Eq. (3.4.57). The parameters A_1, A_2, d were obtained by a least mean square fitting procedure while a, b, c by fixing the energies of three particular levels. The fitted energies were chosen so as to obtain an overall good agreement with experimental data. The best set of a, b, c would be obtained by minimizing the r.m.s. value of deviations which, for this case, is a more tedious procedure.

The agreement of calculated and experimental excitation energies is judged by the r.m.s (root mean square) values of the deviation, denoted by

$$\chi = \sqrt{\sum_i^N \frac{(E_i^{Th} - E_i^{Exp})^2}{N}}. \tag{3.5.1}$$

The fitting procedure yields for the coefficients b and c double precision numbers, which are presented, in tables, in a truncated form. Since the square root formula provides energies which are quite sensitive to small variations for the parameters b and c, we give their values with a suitable large number of digits. Indeed, with the listed parameters we get the energies corresponding to the exact parameters yielded by the fitting procedure. Comparing the values of c for different nuclei, one notices that the parameter acquires larger values for smaller deformation parameter.

Table 3.2 shows the results for some isotopes of Th and U. Except for ^{228}Th, these isotopes are characterized by large values for the deformation parameter d. As we already mentioned, ^{228}Th has features which are specific to the triaxial nuclei. We notice the small values for the r.m.s. obtained in these cases.

The nuclei presented in Table 3.3, are characterized by small d and moreover they satisfy the $O(6)$ symmetry. For these nuclei, the defining Eq. (3.3.12) was used. One notices that this formula for the near vibrational picture describes the excitation energies better than the generalized HL formula. This is reflected by the relative r.m.s. values.

In Table 3.4 one finds the results for some isotopes of Nd, Sm and Dy obtained with the formula characterizing the near vibrational regime. These nuclei may be viewed as critical points for the phase transition $SU(5) \rightarrow SU(3)$ [RF05, RGF05, RGBF09]. However, one expects that for nuclei close to the critical point the other formula using an asymptotic expansion in terms of $1/x$ works as well.

Finally, Table 3.5 presents two nuclei which satisfy the $E(5)$ symmetry. These are described with the closed formulas (3.3.12) and (3.4.57). We remark that also in this case the r.m.s. values are small. The experimental data for these nuclei were considered up to the angular momentum were the first backbending shows up.

Before closing this section we summarize our results presented in Tables 3.2, 3.3, 3.4 and 3.5. For nuclei characterized by ratios $E_g^{4^\dagger}/E_g^{2^\dagger}$ larger than 2.93 we used the asymptotic expansion for energies (Eq. (3.3.9)) while for values of this ratio smaller than 3.02 the expansion for small d, i.e. that given by Eq. (3.3.12), was used. Within the overlapping interval of d, both formulas are valid.

Table 3.2 Experimental (Exp.) and theoretical (Th(1) and Th(2)) excitation energies, for several nuclei, ^{228}Th [Art97], ^{232}Th [Schm91], ^{232}U [Schm91], ^{234}U [Akov02], ^{236}U [Sch91], ^{238}U [ChSi04], are given in units of keV

J^π	^{228}Th			^{232}Th			^{234}U			^{236}U			^{238}U		
	Exp.	Th(1)	Th(2)	Exp.	Th(1)	Th(2)	Exp.	Th(1)	Th(2)	Exp.	Th(1)	Th(2)	Exp.	Th(1)	Th(2)
2^+	57.76	57.61	57.485	49.37	49.66	49.31	43.50	43.72	43.49	45.24	45.516	45.22	44.92	44.73	44.88
4^+	186.82	186.90	186.82	162.12	162.966	162.12	143.35	143.93	143.35	149.48	150.33	149.48	148.38	147.93	148.38
6^+	378.18	378.51	378.78	333.2	334.64	333.63	296.07	296.84	296.07	309.78	311.34	309.97	307.18	306.90	307.71
8^+	622.50	622.73	623.29	556.90	558.25	557.65	497.04	497.63	497.02	522.24	524.29	522.724	518.10	517.8	518.96
10^+	911.80	911.49	911.80	827.0	827.44	827.69	741.2	741.3	741.15	782.3	784.32	783.07	775.9	776.26	777.492
12^+	1239.4	1238.58	1237.99	1137.1	1136.62	1137.77	1023.8	1023.38	1023.69	1085.3	1086.49	1086.07	1076.7	1077.35	1078.41
14^+	1599.5	1599.27	1597.63	1482.8	1481.12	1482.77	1340.8	1339.79	1340.41	1426.3	1426.07	1426.86	1415.5	1416.33	1416.88
16^+	1988.1	1989.81	1988.1	1858.6	1857.14	1858.6	1687.8	1687.24	1687.8	1800.9	1798.79	1800.9	1788.4	1788.68	1788.4
18^+	2407.9	2407.05	2407.9	2262.9	2261.56	2262.1	2063.0	2062.99	2063.08	2203.9	2200.85	2204.11	2191.1	2190.24	2188.89
20^+		2848.18	2856.32	2691.5	2691.82	2690.9	2464.2	2464.74	2464.12	2631.7	2628.97	2632.91	2619.1	2617.29	2614.76
22^+		3310.53	3333.13	3144.2	3145.71	3143.29	2889.7	2890.57	2889.32	3081.2	3080.31	3084.22	3068.1	3066.53	3062.93
24^+		3791.4	3838.43	3619.6	3621.32	3618.06	3339	3338.8	3337.54	(3550)	3552.43	3555.4	3535.3	3535.05	3530.78
26^+		4287.89	4372.51	4116.2	4116.88	4114.4	3808	3807.96	3808.0	(4039)	4043.2	4044.28	4018.1	4020.31	4016.08
28^+		4796.81	4935.76	(4631.8)	4630.77	4631.8	(4297)	4296.74	4300.17	(4549)	4550.77	4549.0	4517	4520.08	4517.0
30^+		5314.41	5528.64	(5162)	5161.41	5169.96		4803.88	4813.74	(5077)	5073.52	5068.04	5035	5032.4	5031.98
$\frac{E_g^{4+}}{E_g^{2+}}$	3.23			3.28			3.30			3.30			3.30		
χ		0.56	0.66		1.13	2.2		0.53	0.95		2.21	3.16		1.40	2.48

(continued)

Table 3.2 (continued)

J^π		228Th Exp.	Th(1)	Th(2)	232Th Exp.	Th(1)	Th(2)	234U Exp.	Th(1)	Th(2)	236U Exp.	Th(1)	Th(2)	238U Exp.	Th(1)	Th(2)
A_1	a	182.8720	1909.4426		233.4401	3339.3037		221.7839	3443.7877		386.4548	5932.3853		502.4456	5945.5847	
A_2	b	4.0861	0.0101534		3.2430	0.00495222		2.9879	0.00423038		1.9129	0.00254985		1.0667	0.00252536	
d	c	2.7062	5.4707523×10^{-6}		3.0822	1.026518×10^{-6}		3.2192	9.425528×10^{-7}		3.6189	7.754542×10^{-8}		3.8524	6.979548×10^{-8}	

The predictions labeled by Th(1) are obtained with the square root formula given by the asymptotic expansion of the CSM-ground band energies (Eq. (3.3.9)), while Th(2) are obtained by the generalized HL expression (Eq. (3.4.57)). The parameters for Th(1) calculations, i.e. A_1, A_2, d, were obtained by a least mean square procedure while those of the set Th(2), a, b, c, by fixing three particular energy levels, which are underlined. The parameters obtained are also listed. To have a hint about the agreement between the theoretical and experimental excitation energies, for each case the r.m.s value of discrepancies, denoted by χ, is also given. The values of A_1, A_2, a, χ are given in keV while, d, b, c are dimensionless. Having in view a possible classification of the considered nuclei, the ratio E_g^{4+}/E_g^{2+} is also given

Table 3.3 The same as in Table 3.2 but for a different set of nuclei: ^{170}W [Ba02], ^{174}Os [BrJu99], ^{178}Os [BrJu98], ^{176}Pt [BrJu99], ^{178}Os [Br94], ^{176}Pt [BrJu98], ^{178}Pt [Br94], ^{180}Pt [WuNi03]

J^π	^{174}Os			^{178}Os			^{176}Pt			^{178}Pt			^{180}Pt		
	Exp.	Th(1)	Th(2)	Exp.	Th(1)	Th(2)	Exp.	Th(1)	Th(2)	Exp.	Th(1)	Th(2)	Exp.	Th(1)	Th(2)
2^+	158.60	152.02	149.25	131.6	119.27	129.07	264.0	233.81	220.91	(170.1)	149.29	149.75	153.21	143.63	138.40
4^+	435.00	432.32	435.0	397.7	404.65	397.7	564.1	549.32	564.1	(427.1)	426.55	427.1	410.74	414.33	410.74
6^+	778.99	796.32	761.00	769.78	762.39	905.6	918.39	952.62	(764.6)	779.04	778.67	757.07	765.22	768.11	
8^+	1171.93	1177.95	1206.54	1193.8	1196.31	1194.95	1305.7	1332.77	1372.98	(1177.6)	1194.67	1189.99	1181.50	1185.52	1190.82
10^+	1617.5	1624.47	1656.71	1681.6	1678.19	1681.6	1764.8	1789.52	1824.74	(1660.4)	1669.39	1660.4	1674.28	1671.64	1674.28
12^+	2113.8	2116.53	2144.95	2219.4	2212.86	2216.81	2277.0	2287.36	2310.5	(2207.6)	2201.46	2192.86	2229.2	2222.0	2219.37
14^+	2656.3	2653.1	2672.04	2804.3	2799.02	2799.12	2833.5	2825.61	2833.5	(2811.9)	2789.99	2790.85	2841.5	2835.83	2828.63
16^+	3239.8	3233.59	3239.8	(3429)	3435.95	3429.0	3423.8	3403.88	3396.93	(3457.5)	3434.47	3457.5	3504.8	3512.67	3504.8
18^+	3861.8	3857.66	3850.29		4123.2	4107.78	4041.80	4021.95	4003.64	(4107.9)	4134.61	4195.33	4252.8	4252.27	4250.34
20^+	4524.9	4525.07	4505.56		4860.49	4837.1	4690.40	4679.66	4656.13		4890.21	5006.32		5054.43	5067.32
22^+	5233.0	5235.69	5207.47		5647.65	5618.61	5377.0	5376.91	5356.52		5701.14	5892.01		5919.06	5957.41
24^+	5987.10	5989.4	5957.69		6484.53	6453.89	6106.60	6113.64	6106.6		6567.32	6853.56		6846.07	6921.93
26^+	6786.1	6786.12	6757.65		7371.04	7344.39	6878.6	6889.78	6907.87		7488.66	7891.85		7835.39	7961.93
28^+	7628.4	7625.81	7608.61												
30^+	8511.6	8508.41	8511.60												
32^+	9429.7	9433.9	9467.53												
$\dfrac{E_g^{4+}}{E_g^{2+}}$	2.74			3.02			2.14			2.51			2.68		
χ		4.01	23.78		7.20	2.33		17.29	37.15		17.56	31.75		6.15	8.80
A_1, a		253.6741	801.1928		1297.25			277.2380	407.296		222.5347	551.9787		198.9086	761.038
A_2, b		5.3413	0.0673811		0.0346			4.9031	0.2278488		6.8660	0.10072468		7.7625	0.0650988
c		1.5935	8.260490×10^{-5}		3.88×10^{-5}			1.4494	3.279647×10^{-4}		1.5878	3.293427×10^{-4}		1.5869	1.71825×10^{-4}
d		1.6566						1.4494			1.5878			1.5869	

Also the predictions Th(1) are obtained with the expression (3.3.12) corresponding to the expansion characterized by d-small

Table 3.4 The same as in Table 3.2 but for a different set of nuclei: ^{150}Nd [MATU95], ^{152}Sm [Art96], ^{156}Dy [Rei03]

J^π		^{150}Nd			^{152}Sm			^{156}Dy		
		Exp.	Th(1)	Th(2)	Exp.	Th(1)	Th(2)	Exp.	Th(1)	Th(2)
2^+		130.21	122.59	126.16	121.78	107.02	118.00	137.77	83.82	128.88
4^+		381.45	386.14	381.45	366.48	372.03	366.48	404.19	398.35	404.19
6^+		720.4	726.86	722.89	706.88	719.04	709.74	770.44	797.667	786.22
8^+		1129.7	1130.85	1129.70	1125.35	1131.97	1125.35	1215.61	1252.12	1242.82
10^+		1599.00	1593.52	1595.26	1609.23	1605.59	1603.21	1725.02	1752.12	1753.75
12^+		(2119.00)	2112.90	2119.0	2148.51	2137.63	2140.1	2285.88	2293.59	2307.61
14^+		(2682.50)	2687.99	2702.57	(2736.01)	2726.97	2736.01	2887.82	2874.50	2898.42
16^+			3318.23	3348.22	(3362.0)	3372.98	3392.27	3523.3	3493.72	3523.30
18^+			4003.30	4058.16		4075.29	4110.63	4178.10	4150.56	4181.18
20^+			4742.97	4834.33		4833.64	4892.87	4859.00	4844.58	4871.98
22^+			5537.10	5678.39		5647.87	5740.62	5573.00	5575.48	5596.23
24^+			6385.58	6591.67		6517.87	6655.29	6328.70	6343.07	6354.73
26^+			7288.35	7575.26		7443.56	7638.09	7130.30	7147.20	7148.47
28^+			8245.35	8630.02		8424.87	8690.01	7978.50	7987.76	7978.50
30^+			9256.53	9756.66		9461.76	9811.89	8875.90	8864.66	8845.86
$\frac{E_g^{4+}}{E_g^{2+}}$		2.93			3.01			2.93		
χ			5.61	7.92		9.84	11.43		23.86	18.45
A_1	a		215.8125	2867.41		221.5088	1187.15		348.6711	1913.4867
A_2	b		6.7513	0.0513		6.9223	0.0344		4.4983	0.0231439
d	c		1.6321	1.17×10^{-4}		1.6640	6.11×10^{-5}		1.7089	1.051357×10^{-5}

Table 3.5 The same as in Table 3.2 but for a different set of nuclei: ^{104}Ru [Bl91], ^{102}Pd [FJ98]. These nuclei obey the E(5) symmetry

J^π		^{104}Ru			^{102}Pd		
		Exp.	Th(1)	Th(2)	Exp.	Th(1)	Th(2)
2^+		358.03	348.13	358.03	556.43	563.02	520.03
4^+		888.49	901.59	910.87	1275.87	1280.12	1275.87
6^+		1556.30	1561.29	1556.30	2111.35	2100.12	2114.71
8^+		2320.30	2303.22	2287.30	3013.06	3006.50	3019.06
10^+		3111.80	3119.23	3111.80	3992.71	3993.31	3992.71
12^+			4005.75	4039.35	5055.10	5057.87	5043.55
14^+			4960.97	5078.09	6179.80	6198.80	6179.80
16^+			5983.88	6234.53	7428.80	7415.32	7408.97
18^+			7073.86	7513.64		8706.93	8737.58
20^+			8230.5	8919.18		10073.30	10171.10
$\frac{E_g^{4^+}}{E_g^{2^+}}$		2.48			2.29		
χ			11.33	17.84		9.88	15.41
A_1	a	522.4864	562.6938		649.8648	710.6779	
A_2	b	8.1960	0.2738559		9.2391	0.329923	
d	c	1.5466	9.51995×10^{-4}		1.4174	5.317905×10^{-4}	

3.6 Another Compact Formula for the Ground Band Energies

The work with coherent states is particularly simple especially when we want to calculate matrix elements. This beauty is somehow altered when we pass to the angular momentum projected states, although even there the matrix element are analytically estimated. Here we address the question whether for a given angular momentum there exists a deformation parameter such that the matrix elements with the projected states are equal to those corresponding to unprojected states. To answer this question we consider the most general four order quadrupole boson Hamiltonian:

$$
\begin{aligned}
H = & \left\{ \frac{1}{2} D_{11}(b_2^\dagger b_2)_0 + D_{20}(b_2^\dagger b_2^\dagger)_0 + D_{30}(b_2^\dagger b_2^\dagger b^\dagger)_0 \right. \\
& + D_{21}(b_2^\dagger b_2^\dagger b_2)_0 + \frac{1}{2} \sum_J D_{22}^{(J)} \left[(b_2^\dagger b_2^\dagger)_J (b_2 b_2)_J \right]_0 \\
& \left. + D_{40}(b_2^\dagger b_2^\dagger)_0 (b_2^\dagger b_2^\dagger)_0 + D_{31}(b_2^\dagger b_2^\dagger)_0 (b_2^\dagger b_2^\dagger)_0 \right\} + h.c. \quad (3.6.1)
\end{aligned}
$$

Within the coherent state model the lowest eigenvalues of H are approximated by its average values with the angular momentum projected states:

$$E_J^{(g)}(d) = \langle \varphi_J^{(g)} | H | \varphi_J^{(g)} \rangle,$$

$$\varphi_{JM}^{(g)} = N_J^{(g)} P_{M0}^J \psi^{(g)}(d), \quad \psi^{(g)}(d) = e^{d(b_{20}^\dagger - b_{20})} |0\rangle, \tag{3.6.2}$$

where $N_J^{(g)}$ denotes the normalization constant expressed in terms of the overlap integral $I_J^{(0)}$, defined before, by

$$(N_J^{(g)})^{-2} = (2J + 1)e^{-d^2} I_J^{(0)}, \tag{3.6.3}$$

while $|0\rangle$ stands for the vacuum state of the quadrupole boson operators. Now, we shall crank the coherent state function such that the angular momentum squared

$$\hat{J}^2 = \sum_{\mu=\pm 1,0} (-)^\mu J_\mu J_{-\mu}, \quad J_\mu = \sqrt{10}(b_2^\dagger b_2)_{1\mu}. \tag{3.6.4}$$

is preserved in the average, i.e.,

$$\langle \hat{J}^2 \rangle = J(J + 1). \tag{3.6.5}$$

This restriction provides an equation determining the deformation parameter d:

$$d^2 = \frac{1}{6} J(J + 1) \equiv d_J^2. \tag{3.6.6}$$

Note that this restriction transforms a continuous variable into a discrete one. The same happens with the energy $E(d)$, the average of H with Ψ, if the deformation parameter d is replaced by d_J:

$$E(d_J) = A_1 J(J + 1) + A_2 J^2 (J + 1)^2 + A_3 [J(J + 1)]^{3/2} \equiv E_J, \tag{3.6.7}$$

where the following notation was used:

$$A_1 = \frac{1}{6\sqrt{5}}, \tag{3.6.8}$$

$$A_2 = \frac{7}{45} \left[7D_{22}^{(0)} + 6D_{22}^{(4)} + 2\sqrt{5}D_{22}^{(2)} + 14(D_{40} + D_{31}) \right],$$

$$A_3 = \frac{-1}{3\sqrt{105}} (D_{30} + D_{21}). \tag{3.6.9}$$

Equation (3.6.7) represents a compact three parameters formula for the ground band excitation energies. The parameters involved are to be determined by a least square

procedure. The results for several nuclei are given in Tables 3.6 and 3.7. As seen in these tables, the agreement between calculated and experimental excitation energies is quite good. From Eq. (3.6.7) one can check that the energy spacing $E_J - E_{J-2}$ is a multivalued function of J. Due to this feature one expects that such a simple formula is able to describe the energy levels in the backbending region. As a matter of fact among the nuclei treated here the following backbenders are included: ^{166}Yb, ^{184}Os, ^{166}Hf, ^{168}Hf, ^{172}Hf, ^{174}Hf, ^{158}Er.

In what follows we shall analyze more closely the relationship between the wave functions $\psi_J = \psi(d_J)$ and $\varphi_{JM}^{(g)}$ as well as between E_J as given by (3.6.7) and $\langle \varphi_{JM}^{(g)} | H | \varphi_{JM}^{(g)} \rangle$.

To this aim we mention first a few properties for ψ_J. The set $\{\psi_J\}$ is not orthogonal. Indeed:

$$\langle \psi_J | \psi_{J'} \rangle = \exp\left[-\frac{1}{2}(d_J - d_{J'})^2 \right]. \tag{3.6.10}$$

Expanding ψ in terms of $\varphi_{J0}^{(g)}$, one obtains:

$$\psi(d) = \sum_{J'} C_{J'}(d) \varphi_{J'0}^{(g)}(d). \tag{3.6.11}$$

Denoting $C_{JJ'} = C_{J'}(d_J)$, we notice that the average of the angular momentum operator squared with the above function yields:

$$\sum_{J'} C_{JJ'} J'(J' + 1) = J(J + 1). \tag{3.6.12}$$

Replacing d with d_J in Eq. (3.6.11) and then taking the scalar product of the resulting equation with $\varphi_{J'0}^{(g)}$ it results:

$$C_{JJ'} = [N_{J'}(d_J)]^{-1}. \tag{3.6.13}$$

Moreover, the norm of ψ has the expression:

$$1 = \sum_{J'} (C_{J'}(d))^2 \tag{3.6.14}$$

which for $d = d_J$ yields

$$\sum_{J'} \left(N_{J'}^{(g)}(d_J) \right)^{-2} = 1. \tag{3.6.15}$$

Table 3.6 Excitation energies in ground band given in keV, calculated with the compact formula (3.6.7) are compared with the corresponding experimental data

	^{154}Gd		^{156}Dy		^{158}Er		^{166}Yb		^{166}Hf		^{168}Hf		^{170}Hf	
2^+	123	122	138	127	192	176	102	107	159	171	124	129	100	103
4^+	371	376	404	392	527	525	330	342	471	508	385	398	321	324
6^+	717	729	770	765	970	983	668	685	898	953	756	774	641	642
8^+	1,144	1,158	1,215	1,218	1,493	1,502	1,098	1,115	1,407	1,454	1,212	1,226	1,041	1,039
10^+	1,637	1,645	1,725	1,732	2,072	2,046	1,606	1,613	1,971	1,975	1,734	1,729	1,503	1,501
12^+	2,184	2,180	2,286	2,290	2,680	2,594	2,175	2,156	2,565	2,492	2,304	2,264	2,013	2,017
14^+	2,777	2,759	2,888	2,885	3,190	3,139	2,779	2,723	3,178	2,990	2,910	2,814	2,564	2,577
16^+	3,404	3,387	3,523	3,512	3,663	3,688	3,273	3,292		3,470		3,367	3,147	3,177
18^+	4,016	4,074	4,179	4,171	4,229	4,260	3,782	3,840		3,941		3,918		3,814
20^+		4,837	4,860	4,871		4,891	4,371	4,343		4,427		4,464		4,490
A_1		22.49		23.17		33.64		18.87		32.44		23.61		18.47
A_2		0.018		0.014		0.036		-0.001		0.031		0.012		0.008
A_3		-0.911		-0.859		-1.81		-0.386		-1.71		-0.876		-0.5437

The results for the coefficients A_i with $i = 1, 2, 3$ obtained with a least square procedure are also listed

Table 3.7 The same as in Table 3.6 for another set of nuclei

	172Hf		174Hf		182Os		184Os		182Pt		184Pt		186Pt		238U	
2+	95	96	91	92	127	145	120	142	154	136	162	139	191	168	45	45
4+	308	308	298	299	400	437	384	439	416	411	435	419	490	493	148	149
6+	627	626	609	613	794	832	774	852	771	783	797	795	877	911	307	307
8+	1,036	1,034	1,010	1,020	1,278	1,293	1,275	1,345	1,202	1,219	1,229	1,235	1,341	1,375	518	516
10+	1,519	1,518	1,502	1,507	1,813	1,790	1,871	1,886	1,695	1,694	1,705	1,712	1,856	1,852	776	773
12+	2,063	2,062		2,056	2,347	2,306	2,546	2,446	2,238	2,196	2,201	2,212	2,407	2,327	1,076	1,074
14+	2,651	2,648	2,650	2,841	2,828	3,259		2,998		2,717		2,730		2,802	1,415	1,413
16+	3,273	3,259		3,265	3,321	3,354		3,519		3,262		3,271		3,292	1,788	1,787
18+		3,876		3,880	3,858	3,890		3,989		3,843		3,848		3,833	2,191	2,190
20+		4,478		4,468	4,481	4,453		4,391		4,483		4,487		4,474	2,618	2,618
A_1		16.51		15.65		27.06		25.90		25.50		26.12		32.43		7.72
A_2		−0.003		−0.0059		0.0225		0.0081		0.0239		0.0253		0.0424		−0.0007
A_3		−0.230		−0.124		−1.265		−0.919		−1.213		−1.273		−1.931		−0.0058

Now, we want to see whether the expansion coefficients (3.6.11) exhibit an extremal as function of J', and how does this depend on d. Recall that the norm of the projected state has an analytical expression:

$$(C_J(d))^2 = e^{-d^2}(2J+1)I_J^{(0)}(d) \equiv M_J(d). \qquad (3.6.16)$$

Taking into account the analytical expression of the overlap integral $I_J^{(0)}$ one can prove that the first derivative of $M(d)$ with respect to d^2 has only one zero. Moreover, $\frac{\partial M}{\partial(d^2)}$ is positive for $d \to 0$ and negative for $d \to \infty$ Therefore, the function $M(d)$ has a sole extremal and this is a maxim. Now, we search for the value of d which maximizes $M_J(d)$ by using the asymptotic behavior of the Legendre polynomial P_J involved in the expression of the mentioned overlap integral. To this end it is useful to expand $P_J(x)$ as:

$$P_J(\sqrt{1-t}) = \sum_{p=0}^{J/2} f_p t^p, \quad J - even. \qquad (3.6.17)$$

where the coefficients f_p are determined from the identity:

$$P_J(\sqrt{1-t}) =_1 F_1\left(\frac{J+1}{2}, -\frac{J}{2}, 1, t\right), \qquad (3.6.18)$$

with $_1F_1$ denoting the hypergeometric function. This relation can be proved by showing that the two functions, P_J and F, satisfy the same differential equation with similar boundary conditions. The above expansion allows us to write the function $M_J(d)$ in a more suitable form:

$$M_J(d) = \frac{2J+1}{2} \sum_{p=0}^{J/2} \lambda_p \mathcal{R}_p,$$

$$\mathcal{R}_p = \int_0^1 t^p (1-t)^{-\frac{1}{2}} e^{-\frac{3}{2}d^2 t} dt. \qquad (3.6.19)$$

The asymptotic behavior of $\mathcal{R}_p(d)$ is given in Ref. [BE53]:

$$\mathcal{R}_p = p!\left(\frac{2}{3d^2}\right)^{p+1}\left[1 + \frac{p+1}{3d^2} + \mathcal{O}\left(\frac{1}{d^4}\right)\right]. \qquad (3.6.20)$$

Consequently, $M_J(d)$ becomes:

$$M_J(d) = \frac{2J+1}{2d^2} e^{-y}\left[1 + \frac{1}{18d^2}(4y^2 - 15y + 6) + \mathcal{O}\left(\frac{1}{d^2}\right)\right], \qquad (3.6.21)$$

where

$$y = \frac{J(J+1)}{6d^2}. \tag{3.6.22}$$

Now, the solution of the equation:

$$\frac{\partial(M_J(d))}{\partial(d^2)} = 0, \tag{3.6.23}$$

is found to be:

$$d_0^2 = \frac{J(J+1)}{6} - \frac{2}{3} + \mathcal{O}\left(\frac{1}{d_0^2}\right). \tag{3.6.24}$$

Thus for large J we have:

$$d_0 \approx d_J. \tag{3.6.25}$$

In what follows we shall compare the m.e. of $\hat{N}$, $\hat{N}^2$. To begin with we start with $\hat{N}$:

$$\langle\psi(d)|\hat{N}|\psi(d)\rangle = d^2,$$
$$\langle\varphi_{J0}^{(g)}(d)|\hat{N}|\varphi_{J0}^{(g)}(d)\rangle = d^2\frac{I_J^{(1)}(d)}{I_J^{(0)}(d)}. \tag{3.6.26}$$

The right hand side can be written in a different form:

$$d^2\frac{I_J^{(1)}(d)}{I_J^{(0)}(d)} = d^2 + \frac{e^{d^2}}{(2J+1)I_J^{(0)}}\frac{\partial[M_J(d)]}{\partial(d^2)}. \tag{3.6.27}$$

Since d_0 is solution for Eq. (3.6.23) one obtains:

$$\langle\varphi_{J0}^{(g)}(d_0)|\hat{N}|\varphi_{J0}^{(g)}(d_0)\rangle = \langle\psi(d_0)|\hat{N}|\psi(d_0)\rangle. \tag{3.6.28}$$

When J is large the above equation becomes:

$$\langle\varphi_{J0}^{(g)}(d_J)|\hat{N}|\varphi_{J0}^{(g)}(d_J)\rangle = \langle\psi(d_J)|\hat{N}|\psi(d_J)\rangle. \tag{3.6.29}$$

Similarly, the following result for the average of $\hat{N}^2$ is obtained

$$\langle\varphi_{J0}^{(g)}(d_0)|\hat{N}^2|\varphi_{J0}^{(g)}(d_0)\rangle = \langle\varphi_{J0}^{(g)}(d_0)|\hat{N}|\varphi_{J0}^{(g)}(d_0)\rangle + d_0^4\frac{I_J^{(2)}(d_0)}{I_J^{(0)}(d_0)}. \tag{3.6.30}$$

From the expression of M_J one gets:

$$d_0^4 \frac{I_J^{(2)}(d_0)}{I_J^{(0)}(d_0)} = d_0^4 + \frac{d_0^4}{M_J(d_0)} \frac{\partial^2 M_J(d)}{\partial (d^2)^2}|_{d_0},$$

$$\frac{d_0^4}{M_J(d_0)} \frac{\partial^2 M_J}{\partial (d^2)^2}|_{d_0} = -1 + \mathcal{O}\left(\frac{1}{d_0^2}\right). \tag{3.6.31}$$

From the above relations one concludes:

$$\langle \varphi_{J0}^{(g)}(d_J)|\hat{N}^2|\varphi_{J0}^{(g)}(d_J)\rangle = \langle \psi(d_J)|\hat{N}^2|\psi(d_J)\rangle, \quad J - \text{large}. \tag{3.6.32}$$

The matrix elements of the terms involved in H corresponding to the projected state $\varphi_{J0}^{(g)}$ are either a monomial of d or proportional to the matrix element of $\hat{N}$ and $\hat{N}^2$. In virtue of the results presented above we have:

$$\langle \psi_J|H|\psi_J\rangle \approx \langle \varphi_{J0}^{(g)}(d_J)|H|\varphi_{J0}^{(g)}(d_J)\rangle. \tag{3.6.33}$$

This proves in fact that spectra of H corresponding to the cranking procedure and the basis of angular momentum projected states respectively, are about the same in the regime of J large. Also, the deformation parameter fixed by the cranking restriction maximizes the overlap of unprojected and projected states.

3.7 Conclusions

The results of this chapter can be summarized as follows. By a dequantization procedure we associated to a quantum mechanical Hamiltonian, quadratic in the quadrupole bosons, a time dependent classical equation. The classical Hamiltonian has a separated form, i.e. is a sum of a kinetic and a potential energy terms. The latter one does not depend on momenta and is of the Davidson type. This actually says nothing but the fact that the Davidson potential has a classical origin. The centrifugal term is determined by a pseudo-angular momentum associated to the intrinsic coordinates. It is worth mentioning that the constraint for the angular momentum in the laboratory frame yields a differential equation which is connected to that one corresponding to the energy conservation, which results in obtaining a specific angular momentum dependence for the quantal energy. Actually, the expression obtained generalizes the Holmberg-Lipas formula, involving under the square root symbol a $J^2(J+1)^2$ term as well. A similar expression is also obtainable within the coherent state model (CSM) for a large deformation regime. Another compact expression was proposed by CSM for the near vibrational regime, i.e. small nuclear deformation. Numerical applications prove that the two compact expressions provided by CSM are able to describe the ground state energies for deformed, near vibrational and transitional

nuclei. By matching the two expressions, one obtains a unitary description for nuclei satisfying different symmetries or, with other words, belonging to various nuclear phases. Also a crancking formula is obtained with a quartic Hamiltonian. Although results were obtained for a large number of nuclei (44), here however only few examples are presented. The agreement between results and experimental excitation energies is quite impressive.

The chosen nuclei range from near vibrational to well deformed nuclei and belong to various symmetries. Thus, the nuclei from Table 3.2 are axially symmetric deformed nuclei except for ^{228}Th which exhibits the features of a triaxial nucleus. Nuclei characterized by relatively small values of d are considered in Tables 3.3 and 3.4. They satisfy $O(6)$ Table 3.3 and $X(5)$ Table 3.4 symmetries. Two nuclei satisfying the symmetry $E(5)$ are presented in Table 3.5.

Chapter 4
Description of the Triaxial Rotor

4.1 The Triaxial Rotor. Diagonalization

The angular momentum components, given in units of $\hbar$, will be denoted by $\hat{L}_x, \hat{L}_y, \hat{L}_z$ in the laboratory frame (L) and by $\hat{L}_1, \hat{L}_2, \hat{L}_3$ in the body fixed reference frame (B). In the two frames the commutation relations are different:

$$\left[\hat{L}_x, \hat{L}_y\right] = i\hat{L}_z; \quad \left[\hat{L}_y, \hat{L}_z\right] = i\hat{L}_x; \quad \left[\hat{L}_z, \hat{L}_x\right] = i\hat{L}_y;$$
$$\left[\hat{L}_1, \hat{L}_2\right] = -i\hat{L}_3; \quad \left[\hat{L}_2, \hat{L}_3\right] = -i\hat{L}_1; \quad \left[\hat{L}_3, \hat{L}_1\right] = -i\hat{L}_2. \quad (4.1.1)$$

Let $\Omega = (\theta_1, \theta_2, \theta_3)$ be the Euler angles defining the rotation which transforms (L) in (B):

$$(L) \overset{\hat{R}(\Omega)}{\rightarrow} (B).$$

Since rotation does not change the vector length it results:

$$\hat{L}_x^2 + \hat{L}_y^2 + \hat{L}_z^2 = \hat{L}_1^2 + \hat{L}_2^2 + \hat{L}_3^2.$$

Denoting by $|LMK\rangle$ the common eigenfunctions of $\hat{L}^2, \hat{L}_z, \hat{L}_3$, we have:

$$\hat{L}^2|LMK\rangle = L(L+1)|LMK\rangle,$$
$$\hat{L}_z|LMK\rangle = M|LMK\rangle,$$
$$\hat{L}_3|LMK\rangle = K|LMK\rangle. \quad (4.1.2)$$

Consider now a rigid body having the moments of inertia with respect to axes 1, 2, 3 equal to $\mathcal{I}_1, \mathcal{I}_2, \mathcal{I}_3$, respectively. The body can perform rotations around the axes 1, 2, 3. Usually, one calls a triaxial rigid body an object described by the Hamiltonian:

$$H_R = \frac{\hbar^2}{2} \left[\frac{\hat{L}_1^2}{\mathcal{I}_1} + \frac{\hat{L}_2^2}{\mathcal{I}_2} + \frac{\hat{L}_3^2}{\mathcal{I}_3} \right]. \tag{4.1.3}$$

To describe the motion of the considered rigid body means to solve the eigenvalue problem associated to H_R. It is instructive to study separately the particular situations:

(1) The isotropic rotor: $\mathcal{I}_1 = \mathcal{I}_2 = \mathcal{I}_3 \equiv \mathcal{I}_0$. In this case we have:

$$\hat{H} = \frac{\hbar^2 \mathbf{L}^2}{2\mathcal{I}_0},$$

$$\hat{H}|LMK\rangle = \frac{\hbar^2 L(L+1)}{2\mathcal{I}_0}|LMK\rangle \equiv E_{sym}|LMK\rangle.$$

Hence

$$E_{sym} = \frac{\hbar^2}{2\mathcal{I}_0} L(L+1). \tag{4.1.4}$$

H_R is rotationally invariant i.e. commutes with the R_3 generators L_x, L_y and L_z. Due to this property the isotropic rotor is called the *symmetric rotor*. The state $|LMK\rangle$ is degenerate over both M and K. What are the possible values of K? Note that classically, the rotor can rotate around any axis. From the quantum mechanical point of view the situation is different. Indeed, under a given rotation a point on a sphere goes to another point of the sphere. In principle the final state cannot be distinguished from the initial one since they correspond to the same energy. Since a transformation is sizable only if something is changed, one says that such rotations are not possible. Within the frame B, the axes are usually chosen to coincide with the principal axes of the inertial ellipsoid. Let 3 be the symmetry axis. In the case of symmetric rotor any axis can be chosen as symmetry axis. The system is also invariant against rotations around the axis 3. Therefore this is also a not allowed rotation axis. If the system rotates with the angle φ around axis 3, the wave function transforms as follows:

$$|LMK\rangle \equiv \Phi(\theta_1, \theta_2, \theta_3) \rightarrow \Phi(\theta_1, \theta_2, \theta_3 + \varphi) = e^{-iK\varphi}\Phi(\theta_1, \theta_2, \theta_3). \tag{4.1.5}$$

In order that the wave function be invariant to rotations around the axis 3 it is necessary that $K = 0$. This selection for K is equivalent to forbidding the rotations around the axis 3. Indeed, in this case the angular momentum is perpendicular to the axis 3. Another symmetry to be satisfied by the wave function is that determined by the change of z' in $-z'$, which is equivalent to the transformations of the Euler angles: $(\theta_1, \theta_2, \theta_3) \rightarrow (\theta_1, \pi - \theta_2, \pi - \theta_3)$. When such transformation is performed the wave functions modify as:

$$\Phi(\theta_1, \pi - \theta_2, \pi - \theta_3) = (-1)^{L-K}\Phi(\theta_1, \theta_2, \theta_3). \tag{4.1.6}$$

Fig. 4.1 A rotational band
where the excitation energies
are proportional to $L(L + 1)$,
with L even
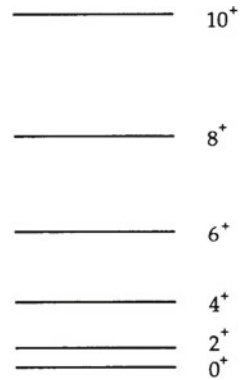
Since $K = 0$, it results that L must be even. Concluding, for the isotropic rotor, the spectrum is given by Eq. (4.1.4), with L-even. The wave function corresponding to a given L is $|LM0\rangle$. In Fig. 4.1 the spectrum of a symmetric rotor is represented.

(2) Rotor with axial symmetry:

$$\mathcal{I}_1 = \mathcal{I}_2 \equiv \mathcal{I}_0 \neq \mathcal{I}_3. \tag{4.1.7}$$

H_R is invariant to rotations around axis z but not around the other axes.

$$H_R|LMK\rangle = E_{asym}|LMK\rangle, \text{(asym} = \text{axial symmetric)},$$

$$E_{asym} = \frac{\hbar^2}{2}\left[\frac{L(L+1)}{\mathcal{I}_0} + (\frac{1}{\mathcal{I}_3} - \frac{1}{\mathcal{I}_0})K^2\right]. \tag{4.1.8}$$

From the above equation one sees that the eigenstates are degenerate over the quantum number M but not with respect to K. Taking into account the explicit expression of the angular momentum in the frame (L) and (B), one could prove that a possible realization of the eigenfunctions $|LMK\rangle$ is:

$$|LMK\rangle = D_{MK}^{L*}, \tag{4.1.9}$$

where D_{MK}^L denotes the rotation matrix:

$$D_{MK}^L(\Omega) = \langle LM|e^{-i\theta_1 L_z}e^{-i\theta_2 L_y}e^{-i\theta_3 L_z}|LK\rangle. \tag{4.1.10}$$

(3) The general case: $\mathcal{I}_1 \neq \mathcal{I}_2 \neq \mathcal{I}_3$. In Fig. 4.2 one can see the energy levels for a triaxial rotor whose moments of inertia are those of a liquid drop. These are represented as function of the deformation γ. We notice that the ground band energies have a degenerate minimum for $\gamma = 0°$ and $\gamma = 60°$. The energies of the gamma band states, $2_2^+, 3_1^+, 5_1^+$, have a minimum in $\gamma = 30°$. Energies for the states $4_2^+, 6_2^+, 8_2^+, \ldots$, from the γ band have a minimum for γ close to $40°$. One remarks

Fig. 4.2 The energies of the triaxial rotor with hydrodynamic moments of inertia, as function of the γ deformation. $\mathcal{J}_0$ stands for the moment of inertia corresponding to $\gamma = 0$
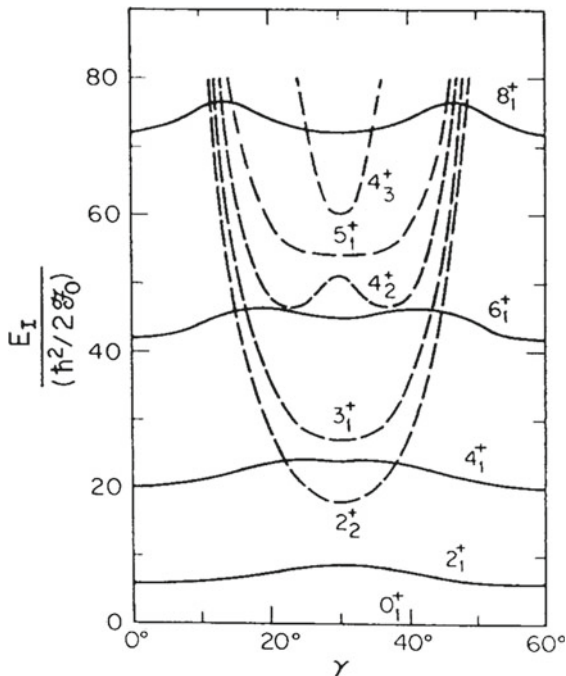
that the rotor has only one state 0^+. Indeed, for a given I there are $2I + 1$ eigenstates
for the rotor Hamiltonian. It is worth mentioning that the energy levels of the ground
band described by a rotor with hydrodynamic moments of inertia look like being γ
unstable states while the states from the γ band are very well localized. Also, we
notice that the curves corresponding to the γ band states $J \neq 2$ are localized inside
the curve of 2_2^+. Therefore, the stability of the gamma states is an increasing function
of the angular momentum.

Consequently, within the rigid rotor formalism the β band does not exist, this
being of non-collective nature.

Since the system exhibits no symmetry axis, the eigenstate $|LM\rangle$ has the form:

$$|LM\rangle = \sum_{K=-L}^{L} A_K |LMK\rangle. \tag{4.1.11}$$

To obtain the expansion coefficients A_K, the associated matrix of H_R is to be
diagonalized in the basis $|LMK\rangle$. Aiming at this goal we need to know the matrix
elements of L_μ, the spherical components of angular momentum:

$$\langle LMK'|L_\mu|LMK\rangle = \sqrt{L(L+1)}C_{K-\mu K'}^{L1L}(-1)^\mu, \mu = 0, \pm 1. \tag{4.1.12}$$

Obviously for H_R (4.1.3), the non-vanishing matrix elements are characterized by $\Delta K = 0, \pm 2$. Thus we distinguish two classes of states for the rigid rotor: one with states which are linear combinations of $|LMK\rangle$ with K-even and one of states having only odd K components.

To obtain Eq. (4.1.12) we used the fact that in the body fixed frame the operator

$$\hat{L}_+ = \hat{L}_1 + i\hat{L}_2, \tag{4.1.13}$$

plays the role of K-lowering operator while

$$\hat{L}_- = L_1 - i\hat{L}_2, \tag{4.1.14}$$

that of raising operator. Indeed, acting on the function $|LMK\rangle$ first with L_+ and then with L_3 we obtain:

$$\hat{L}_3\hat{L}_+|LMK\rangle = \left(\left[\hat{L}_3, \hat{L}_+\right] + \hat{L}_+\hat{L}_3\right)|LMK\rangle$$
$$= (K - 1)\hat{L}_+|LMK\rangle. \tag{4.1.15}$$

It is instructive to calculate the matrix elements of operators $\hat{L}_\pm$:

$$\langle LMK \mp 1|\hat{L}_\pm|LMK\rangle = \sqrt{(L \pm K)(L \mp K + 1)}. \tag{4.1.16}$$

From this equation by a direct calculation one obtains the matrix elements for the Cartesian components of the angular momentum.

$$\langle L, MK'|L_1|LMK\rangle = \frac{1}{2}\left[\sqrt{(L - K)(L + K + 1)}\delta_{K',K+1}\right.$$
$$\left. + \sqrt{(L + K)(L - K + 1)}\delta_{K',K-1}\right],$$
$$\langle L, MK'|L_2|LMK\rangle = -\frac{i}{2}\left[-\sqrt{(L - K)(L + K + 1)}\delta_{K',K+1}\right.$$
$$\left. + \sqrt{(L + K)(L - K + 1)}\delta_{K',K-1}\right],$$
$$\langle L, MK'|L_3|LMK\rangle = M\delta_{K',K}. \tag{4.1.17}$$

Thus $\hat{L}_1$ has, formally, the same m.e. as the operator L_x, in the frame (L) while m.e. of $\hat{L}_2$ differ from the m.e. of $\hat{L}_y$ by a global sign.

As we have seen, the structure of $\hat{H}_R$ is such that the components with even K are not mixed with those of odd K. Therefore, the diagonalization of $\hat{H}_R$ for each of the cases, K-even and K-odd, is performed in a space of lower dimension. Further, in order to reduce even more the number of independent expansion coefficients A_K (4.1.11) we want to exploit the D_2 symmetry.

Notice that the labels 1, 2, 3 are arbitrarily chosen. On other hand the observables should not depend on the way we numerate the axes. It is easy to show that there are 24 distinct ways to form a right thriedral and also 24 choices for a skew thriedral. Among each class we can transform one system to another without changing the system physics. To obtain the transformations relating two frames of the same kind (right or skew) we need the operators:

$$\text{(a) } T_1 : 1 \leftrightarrow -1; \ 3 \leftrightarrow -3,$$
$$T_1^2 = 1; \ T_1 = R_\pi^2.$$

T_1 is a rotation around the axis 2 with π.

$$\text{(b) } T_2 : 1 \leftrightarrow 2; \ 2 \leftrightarrow -1,$$
$$T_2 \equiv R_3(\frac{\pi}{2}); T_2^4 = 1; T_2^2 = R_\pi^3.$$

Thus, T_2 describes a rotation of angle $\frac{\pi}{2}$ around the axis 3.

$$\text{(c) } T_3 : 1 \rightarrow 2 \rightarrow 3 \rightarrow 1,$$
$$T_3^3 = 1.$$

Obviously, any transformation of right thriedral to another right thriedral can be written in the form:

$$T = T_1^i T_2^j T_3^k; i = 1, 2; j = 1, 2, 3, 4; k = 1, 2, 3 \ (24 \text{ distinct transformations}).$$

It is instructive to show how do the transformations T_k, with k $= 1$,2, 3 act on the carthesian coordinates from (B), (x, y, z), on the Euler angles $(\theta_1, \theta_2, \theta_3)$, as well as on the deformations β, γ. It is easy to check that:

$$T_1(x, y, z) = (x, -y, -z), \quad T_1(\theta_1, \theta_2, \theta_3) = (\theta_1 + \pi, \pi - \theta_2, -\theta_3), \quad T_1(\beta, \gamma) = (\beta, \gamma)$$
$$T_2(x, y, z) = (y, -x, z), \quad T_2(\theta_1, \theta_2, \theta_3) = (\theta_1, \theta_2, \theta_3 + \frac{\pi}{2}), \quad T_2(\beta, \gamma) = (\beta, -\gamma)$$
$$T_3(x, y, z) = (y, z, x), \quad T_3(\theta_1, \theta_2, \theta_3) = (\theta_1, \theta_2 + \frac{\pi}{2}, \theta_3 + \frac{\pi}{2}), \quad T_1(\beta, \gamma) = (\beta, \gamma + \frac{2\pi}{3}).$$
$$(4.1.18)$$

Concerning the Hamiltonian eigenfunction, it should be the same in all the 24 points related by the 24 choices of the coordinate system:

$$(T_1) : \psi(\beta, \gamma, \theta_1, \theta_2, \theta_3) = \psi(\beta, \gamma, \theta_1 + \pi, \pi - \theta_2, -\theta_3),$$
$$(T_2) : \psi(\beta, \gamma, \theta_1, \theta_2, \theta_3) = \psi(\beta, -\gamma, \theta_1, \theta_2, \theta_3 + \frac{\pi}{2}),$$
$$(T_3) : \psi(\beta, \gamma, \theta_1, \theta_2, \theta_3) = \psi(\beta, \gamma + \frac{2\pi}{3}, \theta_1, \theta_2 + \frac{\pi}{2}, \theta_3 + \frac{\pi}{2}). \quad (4.1.19)$$

A subgroup of the octahedral group is that of D_2, whose irreducible representations are discussed in Appendix A. This group is defined as a set of rotations of angle equal to π around the axes 1, 2, 3, respectively.

In particular, the rotation of angle π around the axis 2, that is R_π^2, is just T_1 while the rotation with angle π around the axis 3 is $(T_2)^2$. Since, the elements of D_2 commute with $\hat{H}_R$, there exists a set of common eigenfunctions. Therefore, we are interested in those linear combinations (4.1.11) for which the following conditions are fulfilled:

$$
\begin{aligned}
T_1|LM\rangle = \pm|LM\rangle &= R_\pi^2|LM\rangle = D_{00}^L|LM\rangle \\
&= P_L(\cos\pi)|LM\rangle = \pm|LM\rangle, \\
T_2^2|LM\rangle = \pm|LM\rangle &= R_\pi^3|LM\rangle = \sum A_k R_\pi^3|LMK\rangle \\
&= \sum A_k(-)^K|LMK\rangle = \pm|LM\rangle.
\end{aligned}
\tag{4.1.20}
$$

There are 4 sets of states for the rigid rotor which correspond to the four sign choices in (4.1.20), respectively. Actually, these are the four irreducible representations of the group D_2. Since H_R (Eq. 4.1.3) commutes with the elements of D_2, it is natural to classify the eigenstates of H_R by the irreducible representations of D_2. The restriction (4.1.20) for the trial function (4.1.11) implies certain constraints for the expansion coefficients and therefore a reduction of the dimension for the diagonalization space. To obtain these constraints, we need some properties of the Wigner functions D_{MK}^L.

Let us denote by $|LK\rangle^{(B)}$ the eigenfunctions of $\hat{L}^2$, L_3 in the frame (B), while in the frame (L) the eigenfunctions of $\hat{L}^2$, L_z are $|LM\rangle^{(L)}$. The connection between the two functions is:

(i) $\quad |L, K\rangle^{(B)} = \sum_M D_{MK}^L |LM\rangle^L,$

(ii) $\quad D_{MK}^L(-\theta_3, -\theta_2, -\theta_1) = D_{KM}^{L*}(\theta_1, \theta_2, \theta_3) = (-)^{M-K} D_{-K,-M}^L(\theta_1, \theta_2, \theta_3),$

(iii) $\quad T_1 = R_2(0, \pi, 0).$ (4.1.21)

$$
\begin{aligned}
T_1(\varphi_1, \varphi_2, \varphi_3) D_{MK}^L &= \sum_{K'} D_{MK'}^L(\varphi_1, \varphi_2, \varphi_3) D_{K'K}^L(\theta_1, \theta_2, \theta_3) \\
&= \sum_{K'} D_{MK'}^L(0, \pi, 0) D_{K'K}^L(\theta_1, \theta_2, \theta_3) \\
&= \sum_{K'} (-)^{L+K'} \delta_{M,-K'} D_{K'K}^L(\theta_1, \theta_2, \theta_3) \\
&= (-)^{L-M} D_{-M,K}^L(\theta_1, \theta_2, \theta_3).
\end{aligned}
\tag{4.1.22}
$$

Considering the Euler angles $\Omega = (-\theta_3, -\theta_2, -\theta_1)$ and the relation of the Wigner functions with this argument and $\theta_1, \theta_2, \theta_3$, respectively, one obtains:

$$T_1 D_{MK}^{L*} = (-)^{L-K} D_{M,-K}^{L*}.$$ (4.1.23)

(iv) Similarly, one estimates the action of $T_2^2 = R_\pi^3$ on the Wigner function D_{MK}^I:

$$T_2^2 D_{MK}^I = \sum_{K'} D_{MK'}^I(\varphi_1, \varphi_2, \varphi_3) D_{K'K}^I(\theta_1, \theta_2, \theta_3)$$

$$= \sum D_{MK'}^I(0, 0, \pi) D_{K',K}^I(\theta_1, \theta_2, \theta_3)$$

$$= \sum_{K'} e^{-iK'\pi} \delta_{K'M} D_{K'K}^I(\theta_1, \theta_2, \theta_3)$$

$$= e^{-iM\pi} D_{MK}^I(\theta_1, \theta_2, \theta_3).$$ (4.1.24)

To change D_{MK}^I in D_{MK}^{I*}, one proceeds as before and obtains:

$$T_2^2 D_{MK}^{I*}(\Omega) = (-)^{-iK\pi} D_{MK}^{I*}(\Omega).$$ (4.1.25)

Finally, the results are:

$$T_1 |LMK\rangle = (-)^{L-K} |LM - K\rangle,$$
$$T_2^2 |LMK\rangle = (-)^K |LMK\rangle.$$ (4.1.26)

In what follows, we show that the coefficients A_k from the expansion (4.1.11) are not all independent if $|LM\rangle$ are irreducible representations of D_2. Indeed, suppose that the trial function (4.1.11) is a representation of type A for D_2. We distinguish several situations:
Case K-even and the irreducible representation of type A. According to the character Table from Appendix A, the coefficients A must satisfy:

$$T_1 |LM\rangle = |LM\rangle, (\chi(R_\pi^2) = 1),$$
$$T_2^2 |LM\rangle = |LM\rangle, (\chi(R_\pi^3) = 1).$$ (4.1.27)

One sees that in order for the second equation to be fulfilled it is necessary that K be even. Under the given circumstances the second equation is automatically satisfied. Using this result in connection with the first equation (4.1.27) we obtain:

$$T_1 |LM\rangle = \sum_K A_K (-)^{L-K} |LM - K\rangle$$

$$= \sum_K A_{-K} (-)^L |LMK\rangle = \sum_K A_K |LMK\rangle \Rightarrow$$

$$A_K = (-)^L A_{-K}.$$ (4.1.28)

As for the second equation, this is naturally obeyed. Indeed:

$$T_2^2|LM\rangle = \sum_{K-par} A_K(-)^K|LMK\rangle = \sum_{K-par} A_K|LMK\rangle = |LM\rangle.$$

Let K be even and $|LM\rangle$ a irreducible representation of type B_1.

$$T_1|LM\rangle = -|LM\rangle, \quad \chi(R_\pi^2) = -1,$$
$$T_2^2|LM\rangle = |LM\rangle, \quad \chi(R_\pi^3) = +1,$$
$$\Rightarrow \quad A_{-K} = (-)^{L+1}A_K. \tag{4.1.29}$$

Case K-odd and $|LM\rangle$ a representation of type B_2:

$$T_1|LM\rangle = |LM\rangle, \chi(R_\pi^2) = +1,$$
$$T_2^2|LM\rangle = -|LM\rangle, \chi(R_\pi^3) = -1,$$
$$\Rightarrow A_{-K} = -(-)^L A_K. \tag{4.1.30}$$

Case K-odd and a representation of type B_3:

$$T_1|LM\rangle = -|LM\rangle, \chi(R_\pi^2) = -1,$$
$$T_2^2|LM\rangle = -|LM\rangle, \chi(R_\pi^3) = -1,$$
$$\Rightarrow A_{-K} = (-)^L A_K. \tag{4.1.31}$$

The results above are collected in Table 4.1. Note that the number of A_K in (4.1.11) gives the number of linear independent functions provided by the diagonalization procedure. Thus, among the states of type A we have one state with $L = 0$, none with $L = 1$, two states of $L = 2$, one state with $L = 3$, three states $L = 4$ and two states with $L = 5$. In Table 4.1 we give the number of states of a given angular momentum which show up in a certain irreducible representation of the group D_2.

Table 4.1 Symmetries for A_K in case the wave function (4.1.11) is a irreducible representation of D_2

	K	A_K/A_{-K}	$T_1\|LM\rangle$ $= s\|LM\rangle$ $s = \pm$	$T_2^2\|LM\rangle$ $= s'\|LM\rangle$ $s' = \pm$	Nr. of allowed values for $\|K\|$ L = even	in Eq. (4.1.11) L = odd
A	Even	$(-)^L$	$+$	$+$	$\frac{L+2}{2}$	$\frac{L-1}{2}$
B_1	Even	$-(-)^L$	$-$	$+$	$\frac{L}{2}$	$\frac{L+1}{2}$
B_2	Odd	$-(-)^L$	$+$	$-$	$\frac{L}{2}$	$\frac{L+1}{2}$
B_3	Odd	$(-)^L$	$-$	$-$	$\frac{L}{2}$	$\frac{L+1}{2}$

Table 4.2 The number of
states of a given angular
momentum, appearing in
each irreducible
representation of D_2

L	0	1	2	3	4	5
A	1	0	2	1	3	2
B_1	0	1	1	2	2	3
B_2	0	1	1	2	2	3
B_3	0	1	1	2	2	3

In what follows we consider separately the representations of type A and B and
list the corresponding wave function and eigenvalues. To begin with we start with
the representation A (Table 4.2).
There is one state with $L = 0$:

$$|0, 0\rangle = |0, 0, 0\rangle. \tag{4.1.32}$$

The corresponding eigenvalue is 0.
For $L = 2$, there are two states (because there are two nonvanishing independent
coefficients A_K):

$$|2M\rangle_{(N)} = A_0^{(N)}|2M0\rangle + \frac{A_2^{(N)}}{\sqrt{2}}(|2M2\rangle + |2M, -2\rangle), \tag{4.1.33}$$

where N specifies the ordering number of the two solutions. The corresponding
energies are:

$$E(2N, A) = \hbar^2 \left(\frac{1}{\mathcal{I}_1} + \frac{1}{\mathcal{I}_2} + \frac{1}{\mathcal{I}_2} \right) + (-)^N \hbar^2 \left[\left(\frac{1}{\mathcal{I}_1\mathcal{I}_2\mathcal{I}_3} \right)^2 \right.$$
$$\left. -3 \left(\frac{1}{\mathcal{I}_1\mathcal{I}_2} + \frac{1}{\mathcal{I}_1\mathcal{I}_3} + \frac{1}{\mathcal{I}_2\mathcal{I}_3} \right) \right]^{1/2}. \tag{4.1.34}$$

For $L = 3$, there is only one state:

$$|3M\rangle = \frac{1}{\sqrt{2}}(|3M2\rangle - |3M, -2\rangle), \tag{4.1.35}$$

with energy:

$$E(3, A) = 2\hbar^2 \left(\frac{1}{\mathcal{I}_1} + \frac{1}{\mathcal{I}_2} + \frac{1}{\mathcal{I}_3} \right). \tag{4.1.36}$$

It is worth noting that these energies are invariant to the way one labels the axes 1,
2, 3. One checks that the following identity holds:

$$E(21, A) + E(22, A) = E(3, A). \tag{4.1.37}$$

The model of rigid rotor was introduced, in 1958, by Davydov and Filippov to explain the collective properties of some particular nuclei. The authors noticed that there are nuclei where the sum of energies for the first two states of angular momentum 2 is equal or close to the energy of the first 3^+, i.e. Eq. (4.1.37) is obeyed. Also, some properties of the neighboring nuclei are essentially influenced by the fact that Eq. (4.1.37) is satisfied [Dav32].

Despite the fact that for higher values of L analytical expressions for energies are no longer possible, one obtains, however, recurrence relations for the excitation energies which are similar to Eq. (4.1.37).

Indeed, in order to calculate the trace of $\hat{H}_R$ we need the diagonal m.e. of L_k^2.

$$\langle LMK|L_{1,2}^2|LMK\rangle = \frac{1}{2}\left[L(L+1) - K^2\right],$$

$$\langle LMK|L_3^2|LMK\rangle = K^2 \Rightarrow \tag{4.1.38}$$

$$Tr H_R = \sum_N E(L, N) = \sum_K \langle LMK|H_R|LMK\rangle \tag{4.1.39}$$

$$= \frac{\hbar^2}{4}\left[\left(\frac{1}{\mathcal{I}_1} + \frac{1}{\mathcal{I}_2}\right)L(L+1)\sum_{K=0}^{L}1 + \left(\frac{2}{\mathcal{I}_3} - \frac{1}{\mathcal{I}_1} - \frac{1}{\mathcal{I}_2}\right)\underbrace{\sum_{K=0}^{L}K^2}_{\frac{L(L+1)(L+2)}{6}}\right].$$

Thus we obtain:

$$\sum_N E(L, N) = \frac{\hbar^2}{12}L(L+1)(L+2)\left(\frac{1}{\mathcal{I}_1} + \frac{1}{\mathcal{I}_2} + \frac{1}{\mathcal{I}_3}\right), L = \text{par},$$

$$\sum_N E(L, N) = \frac{\hbar^2}{12}(L-1)L(L+1)\left(\frac{1}{\mathcal{I}_1} + \frac{1}{\mathcal{I}_2} + \frac{1}{\mathcal{I}_3}\right), L = \text{odd},$$

$$\Rightarrow \sum_N E(L, N) = \sum_{N'} E(L+1, N'), L = \text{par}. \tag{4.1.40}$$

which is a generalization of Eq. (4.1.37).

Let us turn now our attention to the states of type B. We consider first the states with L = 1:

$$|1M\rangle = |1M0\rangle, \quad \text{representation of type } B_1,$$

$$|1M\rangle = \frac{1}{\sqrt{2}}(|1M1\rangle + |1M-1\rangle), \quad \text{representation of type } B_2,$$

$$|1M\rangle = \frac{1}{\sqrt{2}}(|1M1\rangle - |1M-1\rangle), \quad \text{representation of type } B_3.$$

Their energies are:

$$E(1, B_1) = \frac{\hbar^2}{2}\left(\frac{1}{\mathcal{I}_1} + \frac{1}{\mathcal{I}_2}\right),$$

$$E(1, B_2) = \frac{\hbar^2}{2}\left(\frac{1}{\mathcal{I}_1} + \frac{1}{\mathcal{I}_3}\right),$$

$$E(1, B_3) = \frac{\hbar^2}{2}\left(\frac{1}{\mathcal{I}_2} + \frac{1}{\mathcal{I}_3}\right). \qquad (4.1.41)$$

For L = 2, there are three states. There is only one state B_1 with $|K| = 2$:

$$|2M\rangle = \frac{1}{\sqrt{2}}(|2M2\rangle - |2M - 2\rangle),$$

$$E(2, B_1) = \frac{\hbar^2}{2}\left(\frac{4}{\mathcal{I}_3} + \frac{1}{\mathcal{I}_1} + \frac{1}{\mathcal{I}_2}\right).$$

The other two states are of the type B_2 and B_3, respectively. They have $|K| = 1$ and energies which are obtainable from one another by permuting the axes 1, 2, 3.

Now we raise the question *what is the parity of the states described above?* The parity of a state is taken relatively to the parity of the ground state which is conventionally taken to be "+". As the spin of the ground state is zero it results that such state is of type A. In general, one may connect the parity of a state with the representation of the group D_2 to which the state belongs. Let C be the operator of complex conjugation. In the framework of angular momentum formalism, C could be viewed as a reflexion transformation with respect to the plane $y = 0$. Indeed:

$$CL_\pm = C(L_x \pm iL_y) = L_x \mp iL_y = L_\mp,$$

which is equivalent to the reflection $y \to -y$.

The parity transformation can be defined either as a reflection with respect to the origin ($x \to -x, y \to -y, z \to -z$), or as a product of a reflection with respect to a plane, for example the plane $y = 0$, and a rotation of angle π around the axis perpendicular on the reflection axis.

$$P = R_\pi^y C = e^{-i\pi L_y}C,$$

$$PD_{MK}^{L*} = R_\pi^y C D_{MK}^{L*} = R_\pi^y D_{MK}^L = (-)^{L+M} D_{-M,K}^L = (-)^{L-K} D_{M,-K}^{L*}.$$

Using the transformation rules $A_K \to A_{-K}$ for different representations one obtains:

$$P|LM\rangle = +|LM\rangle, \quad \text{for A and } B_2,$$

$$P|LM\rangle = -|LM\rangle, \quad \text{for } B_1 \text{ and } B_3.$$

The first equation is consistent with the fact that the ground state is of parity +. The second equation takes place for both even and odd K.

4.2 Semiclassical Description and Quantization

4.2.1 Introduction

Many collective properties of the low lying states are related to the quadrupole collective coordinates. The simplest phenomenological scheme of describing them is the liquid drop model (LD) proposed by Bohr and Mottelson [BM53]. In the intrinsic frame of reference the Schrödinger equation for the five coordinates, β, γ, Ω can be separated and an uncoupled equation for the variable β is obtained [GRC78, RCG78]. However, the rotational degrees of freedom, the Euler angles describing the position of the intrinsic frame with respect to the laboratory frame and the variable γ, the deviation from the axial symmetry, are coupled together. Under certain approximations [CA04] the equation describing the dynamic deformation γ is separated from the ones associated to the rotational degrees of freedom. Recently, many papers were devoted to the study of the resulting equation for the gamma variable [IA01, BONA04, BLMPY05, BLMPY07, GRF07].

Here we focus on the rotational degrees of freedom by considering a triaxial rotor with rigid moments of inertia. The coupling to other degrees of freedom, collective or individual, will not be treated in this chapter. We attempt to describe, by a semiclassical procedure, the wobbling motion corresponding to various ordering relations for the moments of inertia. We present four pairs of canonical conjugate variables to which four distinct boson representations for the angular momentum correspond, respectively. These could be alternatively used for a boson description of the wobbling motion. We stress on the fact that the semiclassical description provides a better estimate of the zero point energy. Another advantage of the method presented here over the boson descriptions consists in separating the potential and kinetic energies.

4.2.2 Semiclassical Description of a Triaxial Rotor

We consider a triaxial rigid rotor with the moments of inertia $\mathcal{I}_k$, k = 1, 2, 3, corresponding to the axes of the laboratory frame, described by the Hamiltonian:

$$\hat{H}_R = \frac{\hat{I}_1^2}{2\mathcal{I}_1} + \frac{\hat{I}_2^2}{2\mathcal{I}_2} + \frac{\hat{I}_3^2}{2\mathcal{I}_3}. \tag{4.2.1}$$

The angular momentum components are denoted by $\hat{I}_k$. They satisfy the following commutation relations:

$$\left[\hat{I}_1, \hat{I}_2\right] = i\hat{I}_3; \left[\hat{I}_2, \hat{I}_3\right] = i\hat{I}_1; \left[\hat{I}_3, \hat{I}_1\right] = i\hat{I}_2. \tag{4.2.2}$$

The raising and lowering angular momentum operators are defined in the standard way, i.e. $\hat{I}_\pm = \hat{I}_1 \pm i\hat{I}_2$. They satisfy the mutual commutation relations:

$$[\hat{I}_+, \hat{I}_-] = 2\hat{I}_3; \ [\hat{I}_+, \hat{I}_3] = -\hat{I}_+; \ [\hat{I}_-, \hat{I}_3] = \hat{I}_-. \qquad (4.2.3)$$

The case of rigid rotor in the intrinsic frame with the axes taken as principal axes of the inertia ellipsoid is formally obtained by changing the sign of one component, $\hat{I}_2 \rightarrow -\hat{I}_2$, and replacing the moments of inertia with respect to axes 1, 2, 3 with those corresponding to the principal axes of the inertia ellipsoid. Thus if I_k, with $k = 1, 2, 3$ were the angular momentum components in the intrinsic frame the r.h.s. of Eq. (4.2.2) would have the sign minus. The difference in sign with respect to the case of the laboratory frame comes from the fact that in the product, for example $I_1 I_2$, the second rotation is performed around the axis "1" which in the case of the body fixed frame was already affected by the first rotation, i.e. the one around the axis "2".

This quantum mechanical object has been extensively studied in various contexts [CAS31], including that of nuclear physics. Indeed, in Ref. [DF58], the authors noticed that there are some nuclei whose low lying excitations might be described by the eigenvalues of a rotor Hamiltonian with a suitable choice for the moments of inertia. Since then, many extensions of the rotor picture have been considered. We just mention a few: particle-rotor model [MSD74, BM81], two rotors model [LOPA78] used for describing the scissors mode, the cranked triaxial rotor [GRC78, IY83]. The extensions provide a simple description of the data but also lead to new findings like scissors mode [LOPA78], finite magnetic bands, chiral symmetry [FRA01].

In principle it is easy to find the eigenvalues of H_R by using a diagonalization procedure within a basis exhibiting the D_2 symmetry. However, when we restrict the considerations to the yrast band it is by far more convenient to use a closed expression for the excitation energies.

An intuitive picture is obtained when two moments of inertia, say those corresponding to axes 1 and 2, are close to each other, in magnitude, and much smaller than the moment of inertia of the third axis. The system will rotate around an axis which lies close to the third axis. Since the third axis is almost a symmetry axis, this is conventionally called the quantization axis. Indeed, a basis having one of the quantum numbers the angular momentum projection on this axis is suitable for describing excitation energies and transition probabilities. Small deviations of angular momentum from the symmetry axis can be quantized, which results in having a boson description of the wobbling motion. This quantization can be performed in several distinct ways. The most popular one consists in choosing the Holstein-Primakoff (HP) boson representation [HolPr40] for the angular momentum components and truncating the resulting boson Hamiltonian at the second order. However, the second order expansion for the rotor Hamiltonian is not sufficient in order to realistically describe the system rotating around an axis which makes a large angle with the quantization axis. Actually, there is a critical angle where the results obtained by diagonalizing the expanded boson Hamiltonian is not converging. On the other hand, one knows from

the liquid drop model that a prolate system in its ground state rotates around an axis which is perpendicular to the symmetry axis. Clearly, such a picture corresponds to an angle between the symmetry and rotation axes, equal to $\pi/2$ which is larger than the critical angle mentioned above. Therefore, this situation cannot be described with a boson representation of the HP type. In order to treat the system exhibiting such behavior one has two options: (a) to change the quantization axis by a rotation of an angle equal to $\pi/2$ and to proceed as before in the rotated frame; (b) to keep the quantization axis but change the HP representation with the Dyson (D) boson expansion.

Note that if we deal with the yrast states, the zero point oscillation energy corresponding to the wobbling frequency contributes to the state energies. There are experimental data which cannot be described unless some anharmonic terms of H_R are taken into account. It should be mentioned that anharmonicities may renormalize both the ground state energy and the wobbling frequency.

In what follows we describe a simple semiclassical procedure where these two effects are obtained in a compact form.

We suppose that a certain class of properties of the Hamiltonian H_R can be obtained by solving the time dependent equations provided by the variational principle:

$$\delta \int_0^t \langle \psi(z)|H_R - i\frac{\partial}{\partial t'}|\psi(z)\rangle dt' = 0. \tag{4.2.4}$$

If the trial function $|\psi(z)\rangle$ spans the whole Hilbert space of the wave functions describing the system, solving the equations provided by the variational principle is equivalent to solving the time dependent Schrödinger equation associated to H_R. Here we restrict the Hilbert space to the subspace spanned by the variational state:

$$|\psi(z)\rangle = \mathcal{N}e^{z\hat{I}_-}|II\rangle, \tag{4.2.5}$$

where z is a complex number depending on time and $|IM\rangle$ denotes the eigenstates of the angular momentum operators $\hat{I}^2$ and $\hat{I}_3$. $\mathcal{N}$ is a factor which assures that the function $|\psi\rangle$ is normalized to unity.

$$\mathcal{N} = (1+|z|^2)^{-I}. \tag{4.2.6}$$

The function (4.2.5) is a coherent state for the group $SU(2)$ [KS80], generated by the angular momentum components and, therefore, is suitable for the description of the classical features of the rotational degrees of freedom.

In order to make explicit the variational equations, we have to calculate the average values of H_R and the time derivative operator, with the trial function $\psi(z)$. For the sake of saving the space these will be denoted by $\langle .. \rangle$. The average values of the involved operators can be obtained by the derivatives of the norm function:

$$\langle \hat{I}_- \rangle = \mathcal{N}^2 \frac{\partial}{\partial z}(\mathcal{N}^{-2}) = \frac{2Iz^*}{1 + zz^*},$$

$$\langle \hat{I}_+ \rangle = \mathcal{N}^2 \frac{\partial}{\partial z^*}(\mathcal{N}^{-2}) = \frac{2Iz}{1 + zz^*},$$

$$\langle \hat{I}_+ \hat{I}_- \rangle = \mathcal{N}^2 \frac{\partial^2}{\partial z \partial z^*}(\mathcal{N}^{-2}) = \frac{2I}{1 + zz^*} + \frac{2I(2I - 1)zz^*}{(1 + zz^*)^2},$$

$$\langle \hat{I}_+^2 \rangle = \mathcal{N}^2 \frac{\partial^2}{\partial z^{*2}}(\mathcal{N}^{-2}) = \frac{2I(2I - 1)z^2}{(1 + zz^*)^2},$$

$$\langle \hat{I}_-^2 \rangle = \mathcal{N}^2 \frac{\partial^2}{\partial z^2}(\mathcal{N}^{-2}) = \frac{2I(2I - 1)z^{*2}}{(1 + zz^*)^2}. \tag{4.2.7}$$

In what follows we shall make use of the equation

$$e^{\hat{S}} \hat{A} e^{-\hat{S}} = \hat{A} + \frac{1}{1!}[\hat{S}, \hat{A}] + \frac{1}{2!}[\hat{S}, [\hat{S}, \hat{A}]] + \cdots, \tag{4.2.8}$$

which holds for any operators $\hat{S}$ and $\hat{A}$, to obtain the averages of I_3

$$\langle \hat{I}_3 \rangle = I - z\langle \hat{I}_- \rangle = I - \frac{2Izz^*}{1 + zz^*}, \tag{4.2.9}$$

as well as of the angular momentum squared:

$$\langle \hat{I}_3^2 \rangle = \langle (\hat{I}_3 - z\hat{I}_-)(I - z\hat{I}_-) \rangle = I^2 - \frac{2I(2I - 1)zz^*}{(1 + zz^*)^2}$$

$$\langle \hat{I}_1^2 \rangle = \frac{1}{4}\left[2I + \frac{2I(2I - 1)}{(1 + zz^*)^2}(z + z^*)^2 \right],$$

$$\langle \hat{I}_2^2 \rangle = -\frac{1}{4}\left[-2I + \frac{2I(2I - 1)}{(1 + zz^*)^2}(z - z^*)^2 \right]. \tag{4.2.10}$$

From here it results immediately that the average of $\sum_k \hat{I}_k^2$ is $I(I + 1)$

$$\langle \hat{I}_1^2 \rangle + \langle \hat{I}_2^2 \rangle + \langle \hat{I}_3^2 \rangle = I(I + 1). \tag{4.2.11}$$

This, actually, reflects the fact that $\psi(z)$ is an eigenfunction of $\hat{I}^2$.

The averages of H_R and the time derivative operator have the expressions:

$$\langle \hat{H} \rangle = \frac{I}{4}\left(\frac{1}{\mathcal{I}_1} + \frac{1}{\mathcal{I}_2} \right) + \frac{I^2}{2\mathcal{I}_3} + \frac{I(2I - 1)}{2(1 + zz^*)^2}\left[\frac{(z + z^*)^2}{2\mathcal{I}_1} - \frac{(z - z^*)^2}{2\mathcal{I}_2} - \frac{2zz^*}{\mathcal{I}_3} \right],$$

$$\langle \frac{\partial}{\partial t} \rangle = \frac{I(\dot{z}z^* - z\dot{z}^*)}{1 + zz^*}. \tag{4.2.12}$$

Denoting the average of H_R by $\mathcal{H}$, the time dependent variational equation yields:

$$\frac{\partial \mathcal{H}}{\partial z} = -\frac{2i I \dot{z}^*}{(1+zz^*)^2},$$

$$\frac{\partial \mathcal{H}}{\partial z^*} = \frac{2i I \dot{z}}{(1+zz^*)^2}. \tag{4.2.13}$$

Using the polar coordinate representation of the complex variables $z = \rho e^{i\varphi}$, the equations of motion for the new variables are:

$$\frac{\partial \mathcal{H}}{\partial \rho} = -\frac{4\rho I \dot{\varphi}}{(1+\rho^2)^2},$$

$$\frac{\partial \mathcal{H}}{\partial \varphi} = \frac{4I\rho \dot{\rho}}{(1+\rho^2)^2}. \tag{4.2.14}$$

It is convenient to choose that pair of conjugate variables which brings the classical equations of motion in the canonical Hamilton form. This goal is touched by changing ρ to

$$r = \frac{2I}{1+\rho^2}, \quad 0 \le r \le 2I. \tag{4.2.15}$$

Indeed, in the new variables the equations of motion are:

$$\frac{\partial \mathcal{H}}{\partial r} = \dot{\varphi},$$

$$\frac{\partial \mathcal{H}}{\partial \varphi} = -\dot{r}. \tag{4.2.16}$$

The sign "$-$" from the second line of the above equations suggests that φ and r play the role of generalized coordinate and momentum respectively. In terms of the new variables, the classical energy function acquires the expression:

$$\mathcal{H}(r,\varphi) = \frac{I}{4}\left(\frac{1}{\mathcal{I}_1} + \frac{1}{\mathcal{I}_2}\right) + \frac{I^2}{2\mathcal{I}_3} + \frac{(2I-1)r(2I-r)}{4I}\left[\frac{\cos^2 \varphi}{\mathcal{I}_1} + \frac{\sin^2 \varphi}{\mathcal{I}_2} - \frac{1}{\mathcal{I}_3}\right]. \tag{4.2.17}$$

The angular momentum components can be written in an alternative form:

$$\langle I_1 \rangle = \frac{2I\rho}{1+\rho^2}\cos\varphi, \quad \langle I_2 \rangle = \frac{2I\rho}{1+\rho^2}\sin\varphi, \quad \langle I_3 \rangle = I\frac{1-\rho^2}{1+\rho^2}. \tag{4.2.18}$$

We notice that the pair of coordinates:

$$\xi = I\frac{1 - \rho^2}{1 + \rho^2} = \langle I_3 \rangle, \text{ and } \phi = -\varphi, \tag{4.2.19}$$

are canonically conjugate variables and

$$\frac{\partial \mathcal{H}}{\partial \xi} = -\overset{\bullet}{\phi}, \quad \frac{\partial \mathcal{H}}{\partial \phi} = \overset{\bullet}{\xi}. \tag{4.2.20}$$

Taking the Poisson bracket defined in terms of the new conjugate coordinates one finds:

$$\{\langle I_1 \rangle, \langle I_2 \rangle\} = \langle I_3 \rangle, \quad \{\langle I_2 \rangle, \langle I_3 \rangle\} = \langle I_1 \rangle, \quad \{\langle I_3 \rangle, \langle I_1 \rangle\} = \langle I_2 \rangle \tag{4.2.21}$$

These equations assert that the averages for the angular momentum components form a classical algebra with the inner product $\{, \}$. The correspondence

$$\{\langle I_k \rangle, \{, \}i\} \longrightarrow \{I_k, [,]\}, \tag{4.2.22}$$

is an isomorphism of $SU(2)$ algebras. Due to the constraint (4.2.11) among the three averages of angular momentum components only two are independent. Sometimes it is convenient to work with two real coordinates, say $\langle I_1 \rangle$ and $\langle I_2 \rangle$, instead of the pair (ξ, ϕ).

4.2.3 Boson Representation for Angular Momentum

In general, treating the classical equations is an easier task than solving the time dependent Schrödinger equation. For some particular cases analytical solutions are possible to be found. Moreover, good approximation for solutions in a certain region of the coordinate space can be achieved. The usefulness of this procedure is seen when from the classical picture we could come back to the initial quantum mechanical problem. This desire is accomplished by transcribing the above equations in the complex variables and then quantizing the conjugate complex coordinate. A recipe to find a pair of canonical complex variable is provided by Cartan's theorem [CAR22]. For the case to be treated here, we suggest four pairs of canonical complex coordinates.

To begin with, let us consider the average of the angular momentum components, expressed in terms of the (φ, r):

$$
\begin{aligned}
J_+^{cl} &\equiv \langle \hat{I}_+ \rangle = \sqrt{r(2I - r)} \cdot e^{i\varphi}, \\
J_-^{cl} &\equiv \langle \hat{I}_- \rangle = \sqrt{r(2I - r)} \cdot e^{-i\varphi}, \\
J_3^{cl} &\equiv \langle \hat{I}_3 \rangle = I - (2I - r) = r - I.
\end{aligned} \tag{4.2.23}
$$

The method of associating to a model Hamiltonian, a system of classical equations by means of a time dependent variational principle is usually called *dequantization procedure*. Accordingly, the average of H_R is the classical energy function, while $\langle \hat{I}_k \rangle$ the kth component of the classical angular momentum.

Let f and g be two complex functions defined on the phase space spanned by the canonical conjugate variables (φ, r). The Poisson bracket associated to these functions is defined by:

$$\{f, g\} = \frac{\partial f}{\partial \varphi} \frac{\partial g}{\partial r} - \frac{\partial f}{\partial r} \frac{\partial g}{\partial \varphi}. \tag{4.2.24}$$

With this definition Eq. (4.2.16) can be written as:

$$\{r, \mathcal{H}\} = \dot{r}, \quad \{\varphi, \mathcal{H}\} = \dot{\varphi}, \quad \{\varphi, r\} = 1. \tag{4.2.25}$$

The classical angular momentum components satisfy the equations:

$$\{J_+^{cl}, J_-^{cl}\} = -2i\, J_3^{cl}, \quad \{J^{cl}{}_\pm, J_3^{cl}\} = \pm i\, J^{cl}{}_\pm. \tag{4.2.26}$$

The functions $J_\pm^{cl}$, J_3^{cl} with the inner product defined by the Poisson brackets generate a classical algebra which will be denoted by $SU_{cl}(2)$.

4.2.4 Holstein-Primakoff Boson Expansion

Let us consider the complex coordinate

$$\mathcal{C} = \sqrt{2I - r} \cdot e^{i\varphi}, \tag{4.2.27}$$

and denote by $\mathcal{C}^*$ the corresponding complex conjugate variable. They obey the equations:

$$\{\mathcal{C}^*, \mathcal{C}\} = i, \quad \{\mathcal{C}, \mathcal{H}\} = \dot{\mathcal{C}}, \quad \{\mathcal{C}^*, \mathcal{H}\} = \dot{\mathcal{C}}^*. \tag{4.2.28}$$

These equations suggest that the complex coordinates are of canonical type. To quantize the classical phase space means to achieve a homeomorphism between the algebra of the $\mathcal{C}, \mathcal{C}^*$ with the multiplication operation $\{,\}$ and the algebra of the operators $a, a^\dagger$ with the commutator as inner multiplier:

$$\left(\mathcal{C}, \mathcal{C}^*, \{,\}\right) \longrightarrow \left(a, a^\dagger, -i[,]\right). \tag{4.2.29}$$

A consequence of this homeomorphism is the boson character of the operators $a, a^\dagger$, expressed through the relation:

$$[a, a^\dagger] = 1. \tag{4.2.30}$$

The quantization of an arbitrary function $f(\mathcal{C}, \mathcal{C}^*)$ is performed by replacing $\mathcal{C}$ and $\mathcal{C}^*$ by the operators a and $a^\dagger$, respectively. Concerning the terms containing mixed product of $\mathcal{C}$ and $\mathcal{C}^*$, the product must be symmetrized first and then the complex coordinates be replaced by the boson operators. The simplest example is the angular momentum components which after quantization become the operators:

$$\hat{J}_+ = \sqrt{2I} \left(1 - \frac{a^\dagger a}{2I}\right)^{\frac{1}{2}} a,$$

$$\hat{J}_- = \sqrt{2I}\, a^\dagger \left(1 - \frac{a^\dagger a}{2I}\right)^{\frac{1}{2}},$$

$$\hat{J}_3 = I - a^\dagger a. \tag{4.2.31}$$

One can check that these boson operators obey the commutation relations (4.2.3) and, consequently, generate an $SU(2)$ algebra which hereafter will be denoted by $SU_b(2)$. The product of the two successive homeomorphisms:

$$SU(2) \to SU_{cl}(2) \to SU_b(2) \tag{4.2.32}$$

is the homeomorphism $SU(2) \to SU_b(2)$ which is in fact the boson representation of the angular momentum algebra. Equation (4.2.31) are known under the name of *boson expansion* of the angular momentum components. They were found out, long time ago, by Holstein and Primakoff [HolPr40] by a different method. We shall refer to it as to the HP boson expansion. The interpretation of I results from the following equation:

$$\sum_{k=1}^{3} \hat{I}_k^2 = I(I+1).$$

Thus, I acquires the significance of the angular momentum magnitude. Replacing the angular momentum components by their boson representations, the rotor Hamiltonian H_R receives a boson realization.

$$H^{HP} = \mathcal{B} + \mathcal{C}\left[2I\left(\hat{n} + \frac{1}{2}\right) - \hat{n}^2\right]$$

$$+ 2I\mathcal{A}\left[a^+ a^+ \left(1 - \frac{\hat{n}+1}{2I}\right)^{1/2}\left(1 - \frac{\hat{n}}{2I}\right)^{1/2} + \text{h.c.}\right], \tag{4.2.33}$$

where

$$\mathcal{B} = \frac{I(I+1)}{2\mathcal{I}_3}; \quad \mathcal{C} = \frac{1}{4}(\frac{1}{\mathcal{I}_1} + \frac{1}{\mathcal{I}_2} - \frac{2}{\mathcal{I}_3}); \quad \mathcal{A} = \frac{1}{8}(\frac{1}{\mathcal{I}_1} - \frac{1}{\mathcal{I}_2}),$$

while "h.c." denotes the Hermitian conjugate of the preceding expression. The boson Hamiltonian (4.2.33) can be diagonalized in the basis:

$$|m\rangle = \frac{1}{\sqrt{m!}}(a^+)^m|0\rangle. \qquad (4.2.34)$$

The matrix elements of H^R are :

$$H_{n,n}^{HP} = \mathcal{B} + \mathcal{C}\left[I(2n+1) - n^2\right],$$

$$H_{n,n-2}^{HP} = \mathcal{A}\left[n(n-1)(2I-n+1)(2I-n+2)\right]^{1/2},$$

$$H_{n,n+2}^{HP} = \mathcal{A}\left[(n+1)(n+2)(2I-n)(2I-n-1)\right]^{1/2},$$

$$I_0|m\rangle = \underbrace{(I-m)}_{K}|m\rangle; \; -I \leq K \leq I \Rightarrow m \leq 2I.$$

The states $|m\rangle$ defined by Eq. (4.2.34) are eigenstates for $\hat{I}_3$.

$$\hat{I}_3|m\rangle = (I-m)|m\rangle. \qquad (4.2.35)$$

From this equation it clearly results the connection between the number of bosons m and the quantum number K:

$$K = I - m. \qquad (4.2.36)$$

Taking into account that $-I \leq K \leq I$, it results that the number of bosons of the basis states is subject to the restriction $0 \leq m \leq 2I$. We distinguish, in the boson Hamiltonian, three terms: (a) a constant, which describes a spherical rotor with the moment of inertia $\mathcal{I}_3$; (b) a term with the coefficient $\mathcal{C}$ which describes the deviation from spherical symmetry; (c) an off-diagonal term having $\mathcal{A}$ as factor, which describes the deviation from the axial symmetry.

Let us analyze the contribution coming from each of the three terms. Remember an important result concerning the semiclassical behavior of the rigid rotor. If this is axially symmetric or close to that form it prefers to rotate around the axis of maximal moment of inertia. On the other hand a high spin state implies a semiclassical behavior. This feature determines a certain selection of the quantum number K in a state of high spin. If $\mathcal{I}_3$ is maximum, the shape of the system is *oblate* and according to Eq. (4.2.36), only the state with a small number of bosons contributes. If by contrary $\mathcal{I}_3$ is minimum the shape is prolate and the states with large number of bosons contribute to the state of high spin. Due to the above mentioned arguments it is obvious that the above defined basis is suitable for the description of the situation when $\mathcal{I}_3$ is maximum. In this case the square root operator can be expanded in power series of $\frac{\hat{n}}{2I}$ and the resulting series can be truncated by keeping only few terms. This approximation is good for I large. In this case one could use the zeroth order

expansion where besides the diagonal term the cross term $a^+a^+ + aa$ shows up. This term can be brought to a diagonal form by the Bogoliubov transformation:

$$a^+ = U\alpha^+ - V\alpha,$$

determined such that the new operators be of boson type and moreover in the transformed Hamiltonian the term $\alpha^+\alpha^+ + \alpha\alpha$ has a vanishing coefficient. The final form for H^{HP} is:

$$H^{HP} = \frac{I(I+1)}{2\mathcal{I}_3} + I\left[\left(\frac{1}{\mathcal{I}_1} - \frac{1}{\mathcal{I}_3}\right)\left(\frac{1}{\mathcal{I}_2} - \frac{1}{\mathcal{I}_3}\right)\right]^{1/2}\left(\alpha^+\alpha + \frac{1}{2}\right).$$

The first term describes a precession motion, while the second one a *wobbling* motion. This expression has been obtained by Bohr and Mottelson [BM74]. A possible improvement of the wobbling frequency was introduced by Tanabe [TT73] by adding some anharmonic corrections to the boson Hamiltonian which describes the wobbling motion. We note that when the quantization axis is intermediary, i.e. the corresponding moment of inertia is neither maximum nor minimum, the wobbling frequency obtained by Bohr and Mottelson, hereafter denoted by ω_{BM}, becomes imaginary which reflects, in fact, that the old vacuum state is favored with respect to the vacuum state of the new boson operators. Also if $\mathcal{I}_3$ is minimum and $\mathcal{I}_1 > \mathcal{I}_2$, the energy provided by H^{HP} exceeds $\frac{I(I+1)}{2\mathcal{I}_3}$, which actually is the upper limit for the eigenvalues of the initial Hamiltonian.

Certainly both cases, when $\mathcal{I}_3$ is intermediary or minimum, could be treated by relabeling the axes such that the final situation corresponds to the picture with OZ of maximum moment of inertia. However, keeping the axis OZ as quantization axis even in one of the cases with non-maximum $\mathcal{I}_3$ has a major importance since such situation is common to different fields. For example for the random phase approximation (RPA) applied to the many body motion of *large amplitude*, for a critical value of the attractive two body interaction strength the ground state becomes unstable. Like in that case where the RPA vacuum state can be stabilized by some renormalization effects, here we ask the question whether the ground state can be recovered if renormalization effects due to the correlations with the multi-boson states are properly accounted for.

Concretely, H^{HP} will not be truncated and then subject to the Bogoliubov transformation; by contrary the canonical transformation will be first performed and subsequently the resulting terms will be put in a normal order. This way all terms of the power series will contribute to the ground state, due to the normal ordering. Transformation coefficients are determined by minimizing the correlated ground state energy.

According to this scheme, after performing the canonical transformation and then the normal ordering of boson monomials, the final Hamiltonian is:

$$H^{HP} = H_{00} + \omega_I\alpha^\dagger\alpha + \cdots \tag{4.2.37}$$

In what follows we attempt to obtain analytical expressions for H_{00} and ω_I. To this aim we define first the vacuum state and excited states corresponding to the new bosons.

$$\alpha|\tilde{0}\rangle = 0, \quad |\tilde{m}\rangle = \frac{\alpha^{\dagger m}}{\sqrt{m!}}|\tilde{0}\rangle. \tag{4.2.38}$$

These states are linear combinations of the states constructed by means of bosons $a, a^{\dagger}$:

$$|\tilde{m}\rangle = \sum_n A_{mn}|n\rangle. \tag{4.2.39}$$

The expansion coefficients were analytically calculated in Ref. [RBB77].

$$A_{mn} = \sqrt{m!n!}\, U^{-\frac{m+n+1}{2}} \sum_q \frac{(-1)^{q-m} 2^{\frac{m+n}{2}-q} \left(\frac{V}{2}\right)^{\frac{m+n}{2}-q}}{q!\left(\frac{n-q}{2}\right)!\left(\frac{m-q}{2}\right)!},$$
$$n - q = even, \ m - q = even, \ q \le min(m,n). \tag{4.2.40}$$

Using the expansion (4.2.39) we obtain:

$$H_{00} = \langle\tilde{0}|H^{HP}|\tilde{0}\rangle = \sum_m (A_{0m})^2 H_{mm}^{HP} + 2\sum_m A_{0m} A_{0,m+2} H_{m,m+2},$$
$$H_{00} + \omega_I = \langle\tilde{1}|H^{HP}|\tilde{1}\rangle = \sum_m (A_{1m})^2 H_{mm}^{HP} + 2\sum_m A_{1m} A_{1,m+2} H_{m,m+2}.$$
$$\tag{4.2.41}$$

Inserting A_{0m} and A_{1m} in these equations and then using the identities:

$$\sum_{k=0}^{\infty} \frac{(2k)!}{(k!)^2}\left(\frac{V}{2U}\right)^{2k} = U,$$
$$\sum_{k=0}^{\infty} \frac{(2k)!2k}{(k!)^2}\left(\frac{V}{2U}\right)^{2k} = UV^2, \tag{4.2.42}$$

it results:

$$H_{00} = \mathcal{B} + \mathcal{C}\left[2I\left(V^2 + \frac{1}{2}\right) - (2U^2V^2 + V^4)\right] - 2\mathcal{A}UVS_0(U,V),$$
$$H_{00} + \omega_I = \mathcal{B} + \mathcal{C}\left[2I\left(U^2 + V^2 + \frac{1}{2}\right) - (U^4 + 3V^4 + 8U^2V^2)\right]$$
$$- 2\mathcal{A}UVS_1(U,V). \tag{4.2.43}$$

Here the following notations were used:

$$S_0(U, V) = \sum_{k=0}^{\infty} \frac{(2k+1)!}{(k!)^2} \left(\frac{V}{2U}\right)^{2k} \frac{1}{U^3} \left[(2I - 2k - 1)(2I - 2k)\right]^{1/2},$$

$$S_1(U, V) = \sum_{k=0}^{\infty} \frac{(2k+3)!}{(k!)(k+1)!} \left(\frac{V}{2U}\right)^{2k} \frac{1}{2U^5} \left[(2I - 2k - 2)(2I - 2k - 1)\right]^{1/2}.$$

$$(4.2.44)$$

These sums satisfy the inequalities:

$$0 < S_0 < 2I + 1 + 3V^2,$$
$$0 < S_1 < 4I + 5 + 12V^2, \qquad (4.2.45)$$

which assures that the series S_0 and S_1 are convergent.

This formalism has been used for all three situations distinguished by the relative values of $\mathcal{I}_3$, with the results: (a) When $\mathcal{I}_3$ is maximum the yrast state energies obtained with H_{00} are almost identical with those obtained by diagonalization.

(b) When $\mathcal{I}_3$ is minimum, H_{00} exhibits a local minimum staying far from the ground state.

(c) When $\mathcal{I}_3$ has an intermediary value, H_{00} has no minimum as a function of V.

To conclude, the canonical transformation formalism seems to be an efficient tool to describe the yrast energies for the case when $\mathcal{I}_3$ is maximum.

4.2.5 The Dyson Boson Expansion

One canonical pair is:

$$\mathcal{C}_1 = \frac{1}{\sqrt{2I}} \sqrt{r(2I - r)} e^{i\varphi},$$

$$\mathcal{B}_1^* = \sqrt{2I} \sqrt{\frac{2I - r}{r}} e^{-i\varphi}. \qquad (4.2.46)$$

Indeed, calculating their Poisson bracket, one obtains:

$$\{\mathcal{B}_1^*, \mathcal{C}_1\} = i. \qquad (4.2.47)$$

Through the quantization

$$\left(\mathcal{C}_1, \mathcal{B}_1^*, \{,\}\right) \longrightarrow \left(b, b^\dagger, -i[,]\right), \qquad (4.2.48)$$

one obtains the Dyson's boson representation (D) of angular momentum [DYS56]:

$$\hat{J}_+^D = \sqrt{2I}b$$
$$\hat{J}_-^D = \sqrt{2I}\left(b^\dagger - \frac{(b^\dagger)^2 b}{2I}\right),$$
$$\hat{J}_3^D = I - b^\dagger b. \tag{4.2.49}$$

Note that while the HP expansion preserves the hermiticity property, the D expansion does not have such a virtue. Indeed, the Hermitian conjugate of J_+^D is not equal to J_-^D, although the classical component J_-^{cl} is the complex conjugate of J_+^{cl}. Also, the Hermitian conjugate of the boson operator b is $b^\dagger$, despite the fact that their classical counterparts are not related by a complex conjugation operation.

Consider one of the orderings for the moments of inertia:

$$\mathcal{I}_2 < \mathcal{I}_3 < \mathcal{I}_1, \ \frac{1}{\mathcal{I}_3} > \frac{1}{2}\left(\frac{1}{\mathcal{I}_1} + \frac{1}{\mathcal{I}_2}\right).$$

The D-boson expansion associated to H_R is:

$$H^D = \frac{I(I+1)}{2\mathcal{I}_3} + \frac{I}{4}\left(\frac{1}{\mathcal{I}_1} + \frac{1}{\mathcal{I}_2} - \frac{2}{\mathcal{I}_3}\right) - \mathcal{C}H', \text{ where,}$$
$$H' = -(2I-1)b^+b + b^{+2}b^2$$
$$- k\left[Ib^{+2} + \left(I - \frac{1}{2}\right)b^2 + \left(\frac{1}{2I} - 1\right)b^+b^3 + \frac{1}{4I}b^{+2}b^4\right],$$
$$k = \frac{\frac{1}{\mathcal{I}_2} - \frac{1}{\mathcal{I}_1}}{\frac{2}{\mathcal{I}_3} - \frac{1}{\mathcal{I}_1} - \frac{1}{\mathcal{I}_2}}.$$

In one of the following subsection we will show that H^D can be written as a sum of one kinetic and one potential energy terms.

Expanding the potential around one minimum and neglecting the powers larger than 2, one obtains an oscillator equation which gives the H^D spectrum the following form:

$$E_n = \frac{I(I+1)}{2\mathcal{I}_1} + \left[\left(\frac{1}{\mathcal{I}_2} - \frac{1}{\mathcal{I}_1}\right)\left(\frac{1}{\mathcal{I}_3} - \frac{1}{\mathcal{I}_1}\right)I(I+1)\right]^{1/2}\left(n + \frac{1}{2}\right).$$

The first term describes a precession around the axis OX while the second one a wobbling for angular momentum. Notice that for both expansions, HP and D, for high spins the system prefers to rotate around the maximal moment of inertia. Indeed, the dominant term for the HP expansion is $\frac{I(I+1)}{2\mathcal{I}_3}$ while for the D representation the term $\frac{I(I+1)}{2\mathcal{I}_1}$ prevails.

Now we want to relate the HP and D boson representation defined with the help of the bosons a and b, respectively. To this aim, let us consider the transformation:

$$Ta^+T^{-1} = A^+ = b^+ \left(1 - \frac{b^+b}{2I}\right)^{-1/2},$$

$$TaT^{-1} = a' = \left(1 - \frac{b^+b}{2I}\right)^{1/2} b \qquad (4.2.50)$$

One can easily prove the properties:
   (a) T is not unitary since $\left(A^+\right)^+ \neq a'$,
   (b) $T[a, a^\dagger]T^{-1} = 1 = [a', A^+] = [b, b^+]$,
   (c) $Ta^+aT^{-1} = A^+a' = b^+b$.
Using these relations it results:
   (d) $T \hat{I}_k^{HP} T^{-1} = \hat{I}_k^D, \quad k = \pm, 3$,
   (e) $T \hat{H}^{HP} T^{-1} = \hat{H}^D$.
Let T' the transformation which diagonalizes $\hat{H}^{HP}$

$$(T')^{-1} \hat{H}^{HP} T' = \hat{H}^{HP}_{diag}, \qquad (4.2.51)$$

Then

$$(TT')^{-1} \hat{H}^D (TT') = \hat{H}^{HP}_{diag}. \qquad (4.2.52)$$

This equation shows that, although $\hat{H}^D$ is not Hermitian, it has real eigenvalues. Let us denote by $|m\rangle_D$ the states built with the bosons b involved in the D representation:

$$|m\rangle_D = \frac{(b^+)^m}{\sqrt{m!}} |0\rangle_D. \qquad (4.2.53)$$

What is the relation between the two sets of states $|m\rangle_{HP}$ and $|m\rangle_D$? The m.e. of the D Hamiltonian in the above defined basis are:

$$H^D_{n,n} = \mathcal{B} + \mathcal{C}(2In - n^2),$$
$$H^D_{n,n-2} = 2\mathcal{A}I\sqrt{n(n-1)},$$
$$H^D_{n,n+2} = \frac{\mathcal{A}}{2I}(2I - n)(2I - n - 1)\left[(n+1)(n+2)\right]^{1/2}. \qquad (4.2.54)$$

The connection with the m.e. of the HP Hamiltonian is:

$$H^D_{n,n+k} = L_{n,n+k} H^{HP}_{n,n+k}, k = 0, \pm 2, \qquad (4.2.55)$$
$$L_{n,n+k} = (2I)^{-k/2} \left[(2I - n)!/(2I - n - k)!\right]^{1/2}, \text{ if } n, n + k \leq 2I,$$
$$L_{n,n+k} = (2I)^{-k/2} \left[(-2I + n + k - 1)!/(-2I + n - 1)!\right]^{1/2}, \text{ if } n, n + k \geq 2I + 1,$$
$$\qquad (4.2.56)$$

With the transformation T the above relation becomes:

$$_D\langle n|T\hat{H}^{HP}T^{-1}|n+k\rangle_D = L_{n,n+k\,HP}\langle n|\hat{H}^{HP}|n+k\rangle_{HP}. \qquad (4.2.57)$$

From here we get a possible solution for T:

$$T|m\rangle = (2I)^{\frac{m}{2}} \begin{cases} ((2I-m)!)^{1/2}|m\rangle_D, & \text{if } m \le 2I, \\ ((m-2I-1)!)^{-1/2}|m\rangle_D, & \text{if } m \ge 2I+1. \end{cases} \qquad (4.2.58)$$

$$_{HP}\langle m|T^{-1} = (2I)^{-\frac{m}{2}} \begin{cases} ((2I-m)!)^{-1/2}\,_D\langle m|, & \text{if } m \le 2I, \\ ((m-2I-1)!)^{1/2}\,_D\langle m|, & \text{if } m \ge 2I+1 \end{cases}. \qquad (4.2.59)$$

Using the equality:

$$(A^+)^m = (b^+)^m \left[\left(1 - \frac{b^+b+m-1}{2I}\right)\left(1 - \frac{b^+b+m-2}{2I}\right)\cdots \right.$$
$$\left. \left(1 - \frac{b^+b+1}{2I}\right)\right]^{-1/2}. \qquad (4.2.60)$$

one finds that the expression of T is consistent with Eq. (4.2.50).

4.2.6 An Exponential Boson Expansion

Consider now the complex coordinates:

$$\mathcal{C}_2 = \frac{1}{\sqrt{2}}(r - i\varphi), \quad \mathcal{C}_2^* = \frac{1}{\sqrt{2}}(r + i\varphi). \qquad (4.2.61)$$

These coordinates are also canonically conjugate since $\{\mathcal{C}_2^*, \mathcal{C}_2\} = i$. The isomorphism

$$\left(\mathcal{C}_2, \mathcal{C}_2^*, \{,\}\right) \longrightarrow \left(a, a^\dagger, -i[,]\right) \qquad (4.2.62)$$

yields a third boson representation of angular momentum:

$$\hat{J}_+^R = \sqrt{\frac{1}{\sqrt{2}}(a^\dagger + a)}\, e^{\frac{1}{\sqrt{2}}(a^\dagger - a)} \sqrt{2I - \frac{1}{\sqrt{2}}(a^\dagger + a)},$$

$$\hat{J}_-^R = \sqrt{2I - \frac{1}{\sqrt{2}}(a^\dagger + a)}\, e^{-\frac{1}{\sqrt{2}}(a^\dagger - a)} \sqrt{\frac{1}{\sqrt{2}}(a^\dagger + a)},$$

$$\hat{I}_3^R = \frac{1}{\sqrt{2}}(a^\dagger + a) - I. \qquad (4.2.63)$$

This boson expansion has been derived in Ref. [RCGP84] for the generators of the quasispin algebra. Obviously, this expansion preserves the hermiticity.

4.2.7 A New Boson Expansion

The pair of coordinates:

$$\mathcal{C}_3 = \frac{r}{\sqrt{2I}}, \ \mathcal{D}_3^* = i\sqrt{2I}\varphi. \tag{4.2.64}$$

satisfy the equation

$$\{\mathcal{D}_3^*, \mathcal{C}_3\} = i. \tag{4.2.65}$$

The quantization

$$\left(\mathcal{C}_3, \mathcal{D}_3^*, \{,\}\right) \longrightarrow \left(b, b^\dagger, -i[,]\right), \tag{4.2.66}$$

provides a new boson representation for the angular momentum:

$$
\begin{aligned}
J_+ &= 2I\sqrt{\frac{b}{\sqrt{2I}}}e^{\frac{b^\dagger}{\sqrt{2I}}}\sqrt{1 - \frac{b}{\sqrt{2I}}}, \\
J_- &= 2I\sqrt{1 - \frac{b}{\sqrt{2I}}}e^{-\frac{b^\dagger}{\sqrt{2I}}}\sqrt{\frac{b}{\sqrt{2I}}}, \\
J_3 &= \sqrt{2I}b - I.
\end{aligned}
\tag{4.2.67}
$$

These boson expressions satisfy the commutation relations (4.2.3) and, therefore, represents a new boson expansion for the angular momentum components operators. This expansion does not preserve the hermiticity.

Each of these four boson expansions can be used to study the wobbling motion associated to the Hamiltonian H_R.

The achievements in the field of boson expansion for both phenomenological and microscopic operators were reviewed in Ref. [KLMA91].

4.3 A Harmonic Approximation for Energy

Solving the classical equations of motion (4.2.16) one finds the classical trajectories given by $\varphi = \varphi(t), \ r = r(t)$. Due to Eq. (4.2.16), one finds that the time derivative of $\mathcal{H}$ is vanishing. That means that the system energy is a constant of motion and, therefore, the trajectory lies on the surface $\mathcal{H} = const$. Another restriction for

trajectory consists in the fact that the classical angular momentum square is equal to $I(I+1)$. The intersection of the two surfaces, defined by the two constants of motion, determines the manifold on which the trajectory characterizing the system is placed. According to Eq. (4.2.16), the stationary points, where the time derivatives are vanishing, can be found just by solving the equations:

$$\frac{\partial \mathcal{H}}{\partial \varphi} = 0, \quad \frac{\partial \mathcal{H}}{\partial r} = 0. \tag{4.3.1}$$

These equations are satisfied by two points of the phase space: $(\varphi, r) = (0, I)$, $(\frac{\pi}{2}, I)$. Each of these stationary points might be minimum for the constant energy surface provided that the moments of inertia are ordered in a suitable way.

Studying the sign of the Hessian associated to $\mathcal{H}$, one obtains:

(a) If $\mathcal{I}_1 > \mathcal{I}_2 > \mathcal{I}_3$, then $(0, I)$ is a minimum point for energy, while $(\frac{\pi}{2}, I)$ a maximum.

This situation is illustrated in Fig. 4.3. Expanding the energy function around minimum and truncating the resulting series at second order, one obtains:

$$\mathcal{H} = \frac{I}{4}\left(\frac{1}{\mathcal{I}_2} + \frac{1}{\mathcal{I}_3}\right) + \frac{I^2}{2\mathcal{I}_1} - \frac{2I-1}{4I}\left(\frac{1}{\mathcal{I}_1} - \frac{1}{\mathcal{I}_3}\right)r'^2 + \frac{I(2I-1)}{4}\left(\frac{1}{\mathcal{I}_2} - \frac{1}{\mathcal{I}_1}\right)\varphi^2, \tag{4.3.2}$$

where $r' = r - I$. This energy function describes a classical oscillator characterized by the frequency:

$$\omega = \left(I - \frac{1}{2}\right)\sqrt{\left(\frac{1}{\mathcal{I}_3} - \frac{1}{\mathcal{I}_1}\right)\left(\frac{1}{\mathcal{I}_2} - \frac{1}{\mathcal{I}_1}\right)}. \tag{4.3.3}$$
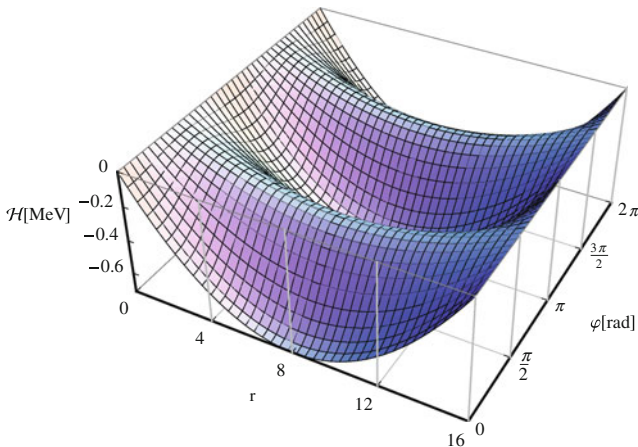
Fig. 4.3 The classical energy, given in MeV, is represented as function of the phase space coordinates r (dimensionless) and $\varphi[rad]$. The rotor is characterized by the following moments of inertia: $\mathcal{I}_1 = 125\hbar^2$ MeV^{-1}, $\mathcal{I}_2 = 42\hbar^2$ MeV^{-1}, $\mathcal{I}_3 = 31.4\hbar^2$ MeV^{-1} (color figure online)
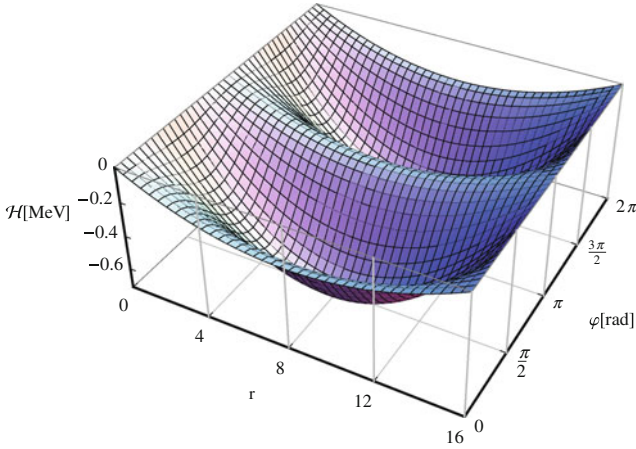
Fig. 4.4 The classical energy, given in MeV, versus the phase space coordinates r (dimensionless) and $\varphi[rad]$. The energy corresponds to the following moments of inertia: $\mathcal{I}_1 = 42\hbar^2 \, \text{MeV}^{-1}$, $\mathcal{I}_2 = 125\hbar^2 \, \text{MeV}^{-1}$, $\mathcal{I}_3 = 31.4\hbar^2 \, \text{MeV}^{-1}$ (color figure online)

(b) If $\mathcal{I}_2 > \mathcal{I}_1 > \mathcal{I}_3$, then $(0, I)$ is a maximum point for energy while in $(\frac{\pi}{2}, I)$ the energy is minimum. Under these conditions the energy function looks as shown in Fig. 4.4. Considering the second order expansion for the energy function around the minimum point one obtains:

$$\mathcal{H} = \frac{I}{4}\left(\frac{1}{\mathcal{I}_1} + \frac{1}{\mathcal{I}_3}\right) + \frac{I^2}{2\mathcal{I}_2} - \frac{2I-1}{4I}\left(\frac{1}{\mathcal{I}_2} - \frac{1}{\mathcal{I}_3}\right)r'^2 + \frac{I(2I-1)}{4}\left(\frac{1}{\mathcal{I}_1} - \frac{1}{\mathcal{I}_2}\right)\varphi'^2,$$
(4.3.4)

where $r' = r - I$, $\varphi' = \varphi - \frac{\pi}{2}$. Again, we got a Hamilton function for a classical oscillator with the frequency:

$$\omega = \left(I - \frac{1}{2}\right)\sqrt{\left(\frac{1}{\mathcal{I}_3} - \frac{1}{\mathcal{I}_2}\right)\left(\frac{1}{\mathcal{I}_1} - \frac{1}{\mathcal{I}_2}\right)}.$$
(4.3.5)

(c) In order to treat the situation when $\mathcal{I}_3$ is the maximal moment of inertia we change the trial function to:

$$|\Psi(z)\rangle = \mathcal{N}_1 e^{z\hat{I}_-}|I, I\rangle,$$
(4.3.6)

where $|I, I\rangle$ is eigenstate of $\hat{I}^2$ and $\hat{I}_1$. It is obtained by applying to $\psi(z)$ a rotation of angle $\pi/2$ around the axis OY.

$$|I, I\rangle = e^{-i\frac{\pi}{2}}|I, I\rangle.$$
(4.3.7)

The new lowering operator corresponds to the new quantization axis:

$$\hat{\tilde{I}}_\pm = \hat{I}_2 \pm i\hat{I}_3. \tag{4.3.8}$$

Following the same path as for the old trial function, one obtains the equations of motion for the new classical variables. In polar coordinates the energy function is:

$$\tilde{\mathcal{H}}(r, \varphi) = \frac{I}{4}\left(\frac{1}{\mathcal{I}_2} + \frac{1}{\mathcal{I}_3}\right) + \frac{I^2}{2\mathcal{I}_1} + \frac{(2I-1)r(2I-r)}{4I}\left[\frac{\cos^2\varphi}{\mathcal{I}_2} + \frac{\sin^2\varphi}{\mathcal{I}_3} - \frac{1}{\mathcal{I}_1}\right]. \tag{4.3.9}$$

When $\mathcal{I}_3 > \mathcal{I}_2 > \mathcal{I}_1$ the system has a minimal energy in $(\varphi, r) = (\frac{\pi}{2}, I)$. For a set of moments of inertia satisfying the restrictions mentioned before, $\tilde{\mathcal{H}}$ is represented in Fig. 4.5 as function of (r, φ).

The second order expansion for $\tilde{\mathcal{H}}(r, \varphi)$ yields:

$$\tilde{\mathcal{H}}(r, \varphi) = \frac{I}{4}\left(\frac{1}{\mathcal{I}_1} + \frac{1}{\mathcal{I}_2}\right) + \frac{I^2}{2\mathcal{I}_3} + \frac{2I-1}{4I}\left(\frac{1}{\mathcal{I}_1} - \frac{1}{\mathcal{I}_3}\right)r'^2$$
$$+ \frac{(2I-1)2I}{4}\left(\frac{1}{\mathcal{I}_2} - \frac{1}{\mathcal{I}_3}\right)\varphi'^2. \tag{4.3.10}$$

The oscillator frequency is:

$$\omega = \left(I - \frac{1}{2}\right)\sqrt{\left(\frac{1}{\mathcal{I}_1} - \frac{1}{\mathcal{I}_3}\right)\left(\frac{1}{\mathcal{I}_2} - \frac{1}{\mathcal{I}_3}\right)}. \tag{4.3.11}$$
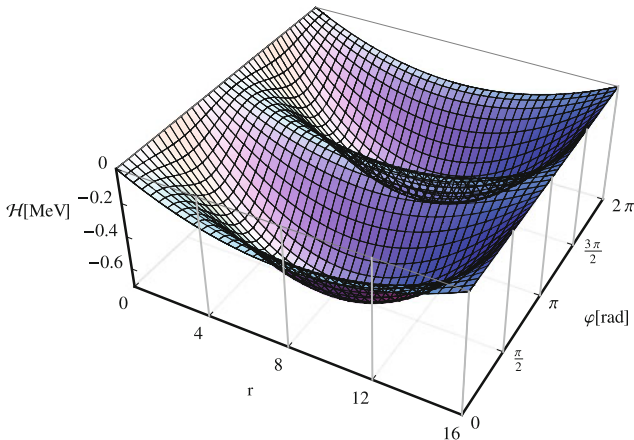
Fig. 4.5 The classical energy versus the phase space coordinates r (dimensionless) and $\varphi[rad]$. Energy is determined by the following moments of inertia: $\mathcal{I}_1 = 42\hbar^2\,\text{MeV}^{-1}$, $\mathcal{I}_2 = 31.4\hbar^2\,\text{MeV}^{-1}$, $\mathcal{I}_3 = 125\hbar^2\,\text{MeV}^{-1}$. The represented energy is given in units of MeV (color figure online)

4.3.1 The Potential Energy

In a previous section we described four distinct boson expansions for the angular momentum. Inserting a chosen boson representation of the angular momentum into the starting Hamiltonian, we are faced with finding the eigenvalues of the resulting boson operator. Alternatively, we could express first the classical Hamilton function in terms of the canonical complex coordinates and then, in virtue of the quantization rules, the complex coordinates are replaced with the corresponding bosons. The two procedures yield boson Hamiltonians which differ by terms multiplied with coefficients like $\frac{1}{2I}$. This suggests that the two procedures coincide in the limit of large angular momentum.

The classical energy function comprises mixed terms of coordinate and conjugate momentum. Therefore, it is desirable to prescribe a procedure to separate the potential and kinetic energies. As a matter of fact this is the goal of this sub-section. We consider the pair of complex coordinates $(\mathcal{C}_1, \mathcal{B}_1^*)$. In terms of these coordinates the classical energy function looks like:

$$
\mathcal{H} = \frac{I}{4} \left(\frac{1}{\mathcal{I}_1} + \frac{1}{\mathcal{I}_2} \right) + \frac{I^2}{2\mathcal{I}_3}
$$
$$
+ \frac{2I-1}{8I} \left(\frac{1}{\mathcal{I}_1} + \frac{1}{\mathcal{I}_2} - \frac{2}{\mathcal{I}_3} \right) \left[r(2I-r) + \frac{k}{4I} \left(r^2 \mathcal{B}_1^{*2} + 4I^2 \mathcal{C}_1^2 \right) \right].
$$

$$(4.3.12)$$

where:

$$
r = 2I - \mathcal{B}_1^* \mathcal{C}_1, \quad 2I - r = \mathcal{B}_1^* \mathcal{C}_1,
$$
$$
k = \frac{\frac{1}{\mathcal{I}_1} - \frac{1}{\mathcal{I}_2}}{\frac{1}{\mathcal{I}_1} + \frac{1}{\mathcal{I}_2} - \frac{2}{\mathcal{I}_3}}.
$$

$$(4.3.13)$$

The components of classical angular momentum have the expressions:

$$
\langle \hat{I}_+ \rangle = \sqrt{2I} \left(\mathcal{B}_1^* - \frac{\mathcal{B}_1^{*2} \mathcal{C}_1}{2I} \right),
$$
$$
\langle \hat{I}_- \rangle = \sqrt{2I} \mathcal{C}_1,
$$
$$
\langle \hat{I}_3 \rangle = I - \mathcal{B}_1^* \mathcal{C}_1.
$$

$$(4.3.14)$$

Here we consider the classical rotor Hamilton function as being obtained by replacing the operators $\hat{I}_k$ by the classical components expressed in terms of the complex coordinates $\mathcal{B}_1^*$ and $\mathcal{C}_1$.

$$
\mathcal{H} = \frac{I}{4} \left(\frac{1}{\mathcal{I}_1} + \frac{1}{\mathcal{I}_2} \right) + \frac{I^2}{2\mathcal{I}_3} - \frac{1}{4} \left(\frac{1}{\mathcal{I}_1} + \frac{1}{\mathcal{I}_2} - \frac{2}{\mathcal{I}_3} \right) \tilde{\mathcal{H}}(\mathcal{B}_1^*, \mathcal{C}_1). \qquad (4.3.15)
$$

Here $\tilde{\mathcal{H}}$ denotes the term depending on the complex coordinates. Its quantization is performed by the following correspondence:

$$\mathcal{B}_1^* \to x, \quad \mathcal{C}_1 \to \frac{d}{dx}. \tag{4.3.16}$$

By this association, a second order differential operator corresponds to $\tilde{\mathcal{H}}$, whose eigenvalues are obtained by solving the equation:

$$\left[\left(-\frac{k}{4I}x^4 + x^2 - kI \right) \frac{d^2}{dx^2} + (2I - 1)\left(\frac{k}{2I}x^3 - x \right)\frac{d}{dx} - k\left(I - \frac{1}{2} \right)x^2 \right] G = E'G. \tag{4.3.17}$$

Performing now the change of function and variable:

$$G = \left(\frac{k}{4I}x^4 - x^2 + kI \right)^{I/2} F,$$

$$t = \int_{\sqrt{2I}}^{x} \frac{dy}{\sqrt{\frac{k}{4I}y^4 - y^2 + kI}}, \tag{4.3.18}$$

Equation (4.3.17) is transformed into a second order differential Schrödinger equation:

$$-\frac{d^2 F}{dt^2} + V(t)F = E'F, \tag{4.3.19}$$

with

$$V(t) = \frac{I(I+1)}{4} \frac{\left(\frac{k}{I}x^3 - 2x \right)^2}{\frac{k}{4I}x^4 - x^2 + kI} - k(I+1)x^2 + I. \tag{4.3.20}$$

We consider for the moments of inertia an ordering such that $k > 1$. Under this circumstance the potential $V(t)$ has two minima for $x = \pm\sqrt{2I}$, and a maximum for $x = 0$. For a set of moments of inertia which satisfies the restriction mentioned above, the potential is illustrated in Fig. 4.6 for few angular momenta. A similar potential obtained by a different method was given in Ref. [KLLI81].

The minimum value for the potential energy is:

$$V_{min} = -kI(I+1) - I^2. \tag{4.3.21}$$

Note that the potential is symmetric in the variable x. Due to this feature the potential behavior around the two minima are identical. To illustrate the potential behavior around its minima we make the option for the minimum $x = \sqrt{2I}$. To this value of
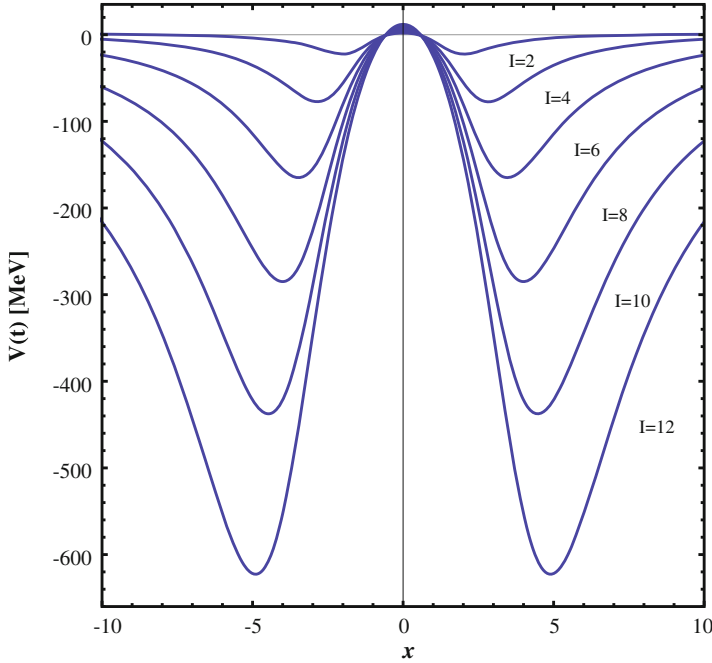
Fig. 4.6 The potential energy involved in Eq. (4.5.1), associated to the Hamiltonian H_R and determined by the moments of inertia $\mathcal{I}_1 = 125\hbar^2 \, \text{MeV}^{-1}$, $\mathcal{I}_2 = 42\hbar^2 \, \text{MeV}^{-1}$, $\mathcal{I}_3 = 31.4\hbar^2 \, \text{MeV}^{-1}$, is plotted as function of the dimensionless variable x, defined in the text. The defining equation (4.3.20) was used (color figure online)

x it corresponds $t = 0$. Expanding $V(t)$ around $t = 0$ and truncating the expansion at second order we obtain:

$$V(t) = -kI(I+1) - I^2 + 2k(k+1)I(I+1)t^2. \qquad (4.3.22)$$

Inserting this expansion in Eq. (4.3.19), one arrives at a Schrödinger equation for a harmonic oscillator. The eigenvalues are

$$E'_n = -kI(I+1) - I^2 + [2k(k+1)I(I+1)]^{1/2}(2n+1). \qquad (4.3.23)$$

The quantized Hamiltonian associated to $\mathcal{H}$ has an eigenvalue which is obtained from the above expression. The final result is:

$$E_n = \frac{I(I+1)}{2\mathcal{I}_1} + \left[\left(\frac{1}{\mathcal{I}_2} - \frac{1}{\mathcal{I}_1}\right)\left(\frac{1}{\mathcal{I}_3} - \frac{1}{\mathcal{I}_1}\right)I(I+1)\right]^{1/2}\left(n + \frac{1}{2}\right). \qquad (4.3.24)$$

4.3.2 Numerical Application

In the previous sections we provided several expressions for the wobbling frequency corresponding to different ordering relations for the moments of inertia. Here we attempt to prove that these results are useful for describing realistically the yrast energies. The application refers to ^{158}Er, where data up to very high angular momentum are available [Hel04]. We consider the case where the maximum moment of inertia corresponds to the axis OX. In our description the yrast state energies are, therefore, given by

$$E_I = \frac{I}{4}\left(\frac{1}{\mathcal{I}_2} + \frac{1}{\mathcal{I}_3}\right) + \frac{I^2}{2\mathcal{I}_1} + \frac{\omega_I}{2}. \tag{4.3.25}$$

The last term in the above expression is caused by the zero point energy of the wobbling oscillation. The wobbling frequency has been derived before, with the result:

$$\omega_I = \left(I - \frac{1}{2}\right)\sqrt{\left(\frac{1}{\mathcal{I}_3} - \frac{1}{\mathcal{I}_1}\right)\left(\frac{1}{\mathcal{I}_2} - \frac{1}{\mathcal{I}_1}\right)}. \tag{4.3.26}$$

We applied a least square procedure to fix the moments of inertia. Since the derivatives of the χ^2 function with respect to $\frac{1}{\mathcal{I}_2}$ and $\frac{1}{\mathcal{I}_3}$ respectively, are identical, the applied procedure provides only two variables $\frac{1}{\mathcal{I}_1}$ and

$$\kappa = \frac{1}{2}\left(\frac{1}{\mathcal{I}_2} + \frac{1}{\mathcal{I}_2}\right) + \sqrt{\left(\frac{1}{\mathcal{I}_3} - \frac{1}{\mathcal{I}_1}\right)\left(\frac{1}{\mathcal{I}_2} - \frac{1}{\mathcal{I}_1}\right)}. \tag{4.3.27}$$

The mentioned variables are the coefficients of $I^2/2$ and $I/2$ in the expression of the yrast energies normalized to the state of vanishing angular momentum.

The results of calculations are shown in Fig. 4.7 where, for comparison, the experimental data and the results obtained in Ref. [TT73] by a different method, are also plotted. As shown in Fig. 4.7, the agreement between the calculated and the experimental energies is very good. Also, the figure suggests that the description presented above of the yrast states in the considered nucleus is better than that reported in Ref. [TATA06].
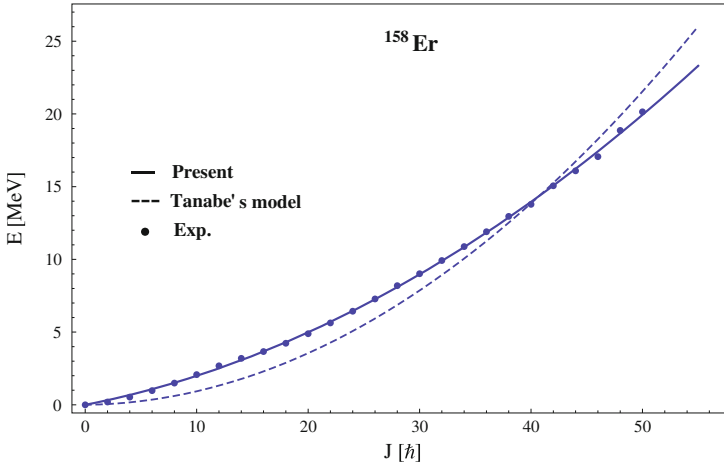
Fig. 4.7 The excitation energies of yrast states, calculated with Eq. (4.3.25), are compared with the results obtained in Ref. [TT73] by a different method as well as with the experimental data from Ref. [Hel04]. The moments of inertia were fixed by a least *square* procedure with the results: $\mathcal{I}_1 = 100.168\hbar^2\,\text{MeV}^{-1}$. Inserting the value of κ provided by the fitting procedure one obtains the following equation relating the moments of inertia $\mathcal{I}_2$ and $\mathcal{I}_3$: $\frac{1}{\mathcal{I}_2} = 0.576837 + \frac{1}{\mathcal{I}_3} \pm 1.519\sqrt{\frac{1}{\mathcal{I}_3} - 0.00998318}$ (color figure online)

4.4 The Tilted Rotor, Symmetries and Nuclear Phases

Let us consider a Hamiltonian which is a polynomial of second order in the angular momentum components:

$$H = A_1 J_1^2 + A_2 J_2^2 + A_3 J_3^2 + B_1 J_1 + B_2 J_2 + B_3 J_3 \tag{4.4.1}$$

Since this commutes with the total angular momentum squared, we have:

$$J_1^2 + J_2^2 + J_3^2 = j(j+1)I. \tag{4.4.2}$$

where I denotes the unity operator. The operator H acts in the Hilbert space V. It is clear that the symmetry group for H is

$$G = SU(2). \tag{4.4.3}$$

Let R be an unitary representation of $SU(2)$ in V. For what follows it is worth mentioning which are the invariance groups

$$G_0 = \{R(g) \mid g \in G, R(g)H = HR(g)\} \tag{4.4.4}$$

for a given set of parameters $\{A_i, B_k\}$ with $1 \le i, k \le 3$.

It can be easily checked that the Hamiltonians, characterized by distinct invariance groups, are obtained by the following constraints on the coefficients A and B.
(a) $A_1 = A_2 = A_3 \equiv A$, $B_1 = B_2 = 0$, $B_3 \equiv B$
For this case H and G_0 take the form

$$H = BJ_3 + AJ^2,$$
$$G_0 = \begin{cases} R(SU(2)) & if \ B = 0 \\ \{\exp(i\varphi J_3) \mid 0 \le \varphi < 2\pi\} \ if \ B \neq 0 \end{cases} \tag{4.4.5}$$

(b) $\mid A_1 - A_3 \mid \ge \mid A_1 - A_2 \mid$, $A_1 \neq A_3$, $B_1 = B_2 = 0$, $B_3 = B$, $B(A_1 - A_2) \ge 0$.
This implies

$$H = (A_1 - A_2)(J_1^2 + uJ_2^2 + 2v_0 J_3) + A_3 \mathbf{J}^2,$$
$$u = \frac{A_2 - A_3}{A_1 - A_3}, \quad v_0 = \frac{B}{2(A_1 - A_3)}, \quad -1 \le u \le 1, \ v_0 \ge 0. \tag{4.4.6}$$

Under these circumstances, one distinguishes several situations:
(b1) $v_0 > 0$, $u < 1$. *In this case the symmetry group is*

$$G_0 = \begin{cases} \{I, R_3, R_0 R_3, R_0\} \sim Z_4, \ if \ 2j = odd, \\ \{I, R_3\} \qquad \sim Z_2, \ if \ 2j = even, \end{cases} \tag{4.4.7}$$

where

$$R_0 = R(-i\sigma_0), \ R_k = R(i\sigma_k), \ k = 1, 2, 3 \tag{4.4.8}$$

and the sign $\sim$ stands for the isomorphism relationship. $\sigma_i (0 \le i \le 3)$ are the Pauli matrices.

When $u = -1$ one obtains for H an *expression identical to that proposed bu Glik-Lipkin-Meshkov, modulo a contraction and an additional diagonal term. For $v_0 \neq 0$ and $u = 0$ the model of Bohr and Mottelson, describing the particle-core interaction, is obtained.*
(b2) If $v_0 = 0$ and $u \neq 0, 1$, then

$$G_0 = \begin{cases} \{I, R_1, R_2, R_3\} \sim D_2, & if \ 2j = even, \\ \{I, R_0, R_k, R_0 R_k \mid k = 1, 2, 3\} \sim Q, & if \ 2j = odd \end{cases}. \tag{4.4.9}$$

where D_2 and Q denote the dihedral and quaternion groups, respectively. This situation corresponds to a triaxial rotor.
(b3) The case of a symmetrical prolate rotor is described by $u = v_0 = 0$ which corresponds to:

$$G_0 = \{\exp(i\varphi J_1), \ R_2 \exp(i\varphi J_1) \mid 0 \le \varphi < 2\pi\}. \tag{4.4.10}$$

(b4) *The axially symmetrical rotor with an oblate deformation correspond to $u = 1$, $v_0 = 0$ and has the invariance group*

$$G_0 = \{\exp(i\varphi J_3),\, R_2 \exp(i\varphi J_3) \mid 0 \leq \varphi < 2\pi\} \tag{4.4.11}$$

(b5) *The system with axial symmetry* is described by $u = 1$, $v_0 > 0$ and

$$G_0 = \{\exp(i\varphi J_3) \mid 0 \leq \varphi < 2\pi\} \tag{4.4.12}$$

Any other Hamiltonian of the family (4.4.1) *can be obtained from one of those specified by the restrictions* (a) *and* (b) *through a rotation transformation.*

As for the Hamiltonians of class (b) these are fully described once we know to characterize the Hamiltonian:

$$h = J_1^2 + u J_2^2 + 2v_0 J_3. \tag{4.4.13}$$

Normalizing the coordinates $x_i = \langle J_i \rangle$ with the radius of the sphere determined by the angular momentum constraint we are faced with the problem of finding the motion of a point (x_1, x_2, x_3) on a sphere of a radius equal to unity:

$$x_1^2 + x_2^2 + x_3^2 = 1 \tag{4.4.14}$$

determined by the classical Hamiltonian:

$$h = x_1^2 + u x_2^2 + 2v x_3, |u| \leq 1, \quad v \geq 0. \tag{4.4.15}$$

The two parameters u and v are functions of the weight of the $SU(2)$ representation (j). The explicit dependence on j is determined by the specific way the dequantization was performed. Through the dequantization procedure the commutation relations for the components of angular momentum become

$$\{x_i, x_k\} = \epsilon_{ikl} x_l \tag{4.4.16}$$

where $\{,\}$ denotes the inner product for the classical $SU(2)$-Lie algebra. The equations of motion for classical variables (see Eq. 4.2.16) are:

$$\overset{\bullet}{x_k} = \{x_k, h\}, \ k = 1, 2, 3. \tag{4.4.17}$$

Taking into account the expression of h and the constraint (4.4.14), one obtains the equations governing the motion of x_k.

$$
\begin{aligned}
\overset{\bullet}{x}_1 &= 2x_2(u x_3 - v), \\
\overset{\bullet}{x}_2 &= 2x_1(x_3 - v), \\
\overset{\bullet}{x}_3 &= 2(1 - u)x_1 x_2.
\end{aligned}
\tag{4.4.18}
$$

From (4.4.15) and (4.4.18) it results

$$\overset{\bullet}{h} = 0 \tag{4.4.19}$$

Therefore h is a constant of motion which will be hereafter denoted by E. The classical trajectory will be a curve determined by intersecting the sphere (4.4.14) with the surface

$$x_1^2 + u x_2^2 + 2v x_3 = E. \tag{4.4.20}$$

It is well known that a good signature for the time evolution of the point (x_1, x_2, x_3) is the set of critical points of this curve. These are determined by equations:

$$\frac{\partial h}{\partial x_k} = 0, \ k = 1, 2, 3. \tag{4.4.21}$$

Some of the critical points are also satisfying the equation

$$\det \left(\frac{\partial^2 h}{\partial x_i \partial x_k} \right)_{1 \le i,k \le 3} = 0 \tag{4.4.22}$$

if the parameters u and v take some particular values. In this case the critical points are degenerate, otherwise they are called non-degenerate. The set of (u, v) to which degenerate critical points correspond is given by the equation:

$$f(u, v) \equiv (1 - u)(1 - v)(u^2 - v^2) = 0 \tag{4.4.23}$$

The product set

$$\mathcal{B} = \{(x_1, x_2, x_3, u, v) \mid \frac{\partial h}{\partial x_k} = 0, \ k = 1, 2, 3; \ f(u, v) = 0\} \tag{4.4.24}$$

will be conventionally called bifurcation set.

The critical points are listed in Table 4.3. There, the corresponding energy (E) values are also given. From Table 4.3 one sees that E takes 4 critical values which are denoted by E_1, E_2, E_+ and E_-, respectively. The solutions (u, v) of the Eq. (4.4.23) are plotted in Fig. 4.8. Here we have also plotted the curve $v^2 = u$ where the critical energies E_1 and E_2 are equal. The curves given in Fig. 4.8 are conventionally called separatrices. The dependence of critical energies on the parameters u and v is visualized in Fig. 4.9.

There are several sets (u, v, E) for which the solutions of equations of motion can be expressed in terms of elementary functions. If the system energy takes one of critical values, the equations of motion can be easily integrated. Below, we shall give the list for final solutions, $P(t) = (x_1(t), x_2(t), x_3(t))$:

$1°$ $E = -2v$, $P(t) = (0, 0, -1)$.

$2°$ $E = 2v$. For this case one distinguishes several situations:

Table 4.3 Critical energies characterizing various sets of the (u,v) parameters are presented

Energy	Restrictions for (u, v)	Critical points	Type
$E_1 = 1 + v^2$	$u < 1, \ v < 1$	$((1 - v^2)^{\frac{1}{1}}, 0, v)$	M
		$(-(1 - v^2)^{\frac{1}{1}}, 0, v)$	M
	$u = 1, \ v < 1$	$((1 - v^2)^{\frac{1}{2}} \cos\varphi, (1 - v^2)^{\frac{1}{2}} \sin\varphi, v)$	M
		$\varphi \in (-\frac{\pi}{2}, \frac{\pi}{2}) \cup (\frac{\pi}{2}, \frac{3\pi}{2})$	
$E_2 = \frac{v^2}{u} + u$	$0 < u < 1, \ v <\mid u \mid$	$(0, (1 - \frac{v^2}{u^2})^{\frac{1}{2}}, \frac{v}{u})$	s
		$-(0, (1 - \frac{v^2}{u^2})^{\frac{1}{2}}, \frac{v}{u})$	s
	$u < 0, \ v <\mid u \mid$	$(0, (1 - \frac{v^2}{u^2})^{\frac{1}{2}}, \frac{v}{u})$	m
		$-(0, (1 - \frac{v^2}{u^2})^{\frac{1}{2}}, \frac{v}{u})$	m
	$u = 1, \ v < 1$	$((1 - v^2)^{\frac{1}{2}} \cos\varphi, (1 - v^2)^{\frac{1}{2}} \sin\varphi, v)$	M
		$\varphi \in (0, \pi) \cup (\pi, 2\pi)$	
$E_+ = 2v$	$v < u$	$(0, 0, 1)$	m
	$v = u = 0$	$(0, 0, 1)$	m
	$0 < v = u < 1$	$(0, 0, 1)$	s
	$u < v < 1$	$(0, 0, 1)$	s
	$u \leq 1$	$(0, 0, 1)$	M
	$v > 1$	$(0, 0, 1)$	M
$E_- = -2v$	$u + v > 0$	$(0, 0, -1)$	m
	$u + v = 0$	$(0, 0, -1)$	m
	$u + v < 0$	$(0, 0, -1)$	s

These are the values of the energy function corresponding to critical points (x_1, x_2, x_3). Notations M, m, s stand for maxima, minima and saddle points, respectively

Fig. 4.8 The separatrix described by solutions of Eq. (4.4.23)
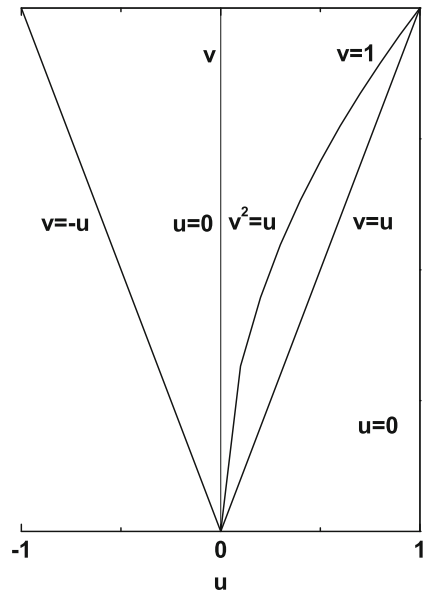
Fig. 4.9 For a given value of u the critical energies are given as function of v
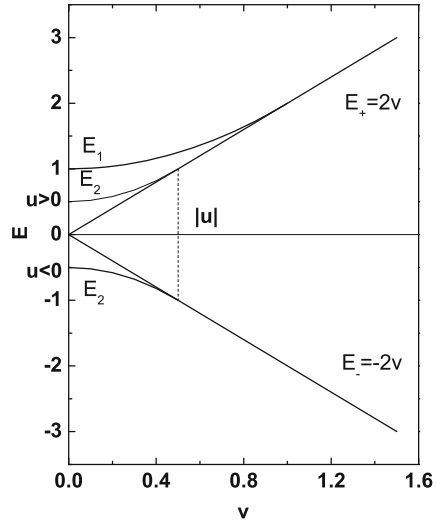
(a) $v < u < 1$, with the solution:

$$x_k(t) = [A_1\delta_{k,1}\sin\frac{2\pi t}{T_1} + A_2\delta_{k,2}\cos\frac{2\pi t}{T_1} + \delta_{k,3}(A'_3 + A_3\cos\frac{4\pi t}{T_1})][B + C\cos\frac{4\pi t}{T_1}]^{-1}.$$

(4.4.25)

The following notations were used:

$$T_1 = \pi[(1-v)(u-v)]^{-\frac{1}{2}},$$
$$A_1 = 4(u-v)[v(1-v)]^{\frac{1}{2}}, \quad A_2 = 4(1-v)[v(u-v)]^{\frac{1}{2}},$$
$$A_3 = v(1-u), \quad A'_3 = 3uv + 3v - 2u - 4v^2,$$
$$B = 2u - uv - v, \quad C = v(1-u).$$

(4.4.26)

From (4.4.25), one easily obtains:

$$\lim_{t\to 0} P(t) = (0, \frac{2}{u}[v(u-v)]^{\frac{1}{2}}, \frac{2v}{u} - 1)$$
$$\lim_{v\to u} P(t) = (0, 0, 1).$$

(4.4.27)

(b) If the parameters u and v satisfy one of the ordering relations $0 < u < v < 1$, $0 < v < -u$, $0 < -u < v$, the solutions $x_k(t)$ are :

$$x_k(t) = [\delta_{k,1}A_1\cosh\frac{2\pi t}{T_1} - iA_2\delta_{k,2}\sinh\frac{2\pi t}{T_1} + \delta_{k,3}(-A'_3 + A_3\cosh\frac{4\pi t}{T_1})]$$
$$\times [-B + C\cosh\frac{4\pi t}{T_1}]^{-1}.$$

(4.4.28)

These orbits have the properties:

$$\lim_{t\to 0} P(t) = (2[v(1-v)]^{\frac{1}{2}}, 0, 2v - 1),$$

$$\lim_{t\to\infty} P(t) = (0, 0, 1),$$

$$\lim_{v\to u} P(t) = (2[v(1-v)]^{\frac{1}{2}}, 0, 2v - 1), \quad \text{for } 0 < u < v < 1. \quad (4.4.29)$$

(c) $u < 1 < v$, $P(t) = (0, 0, 1)$.

3° $E = v^2 + 1$, $v \le 1$, $P(t) = (\pm\sqrt{1 - v^2}, 0, v)$.

4° $E = \frac{v^2}{u} + u$. Again, the solution depends on the relative magnitudes of the parameters u and v.

(a) *If $u < v, 1$, then*

$$x_k(t) = [D_1\delta_{k,1} + D_2\delta_{k,2} \sinh \frac{2\pi t}{T_2} + (D_3' + D_3 \cosh \frac{2\pi t}{T_2})][F_1 + F_2 \cosh \frac{2\pi t}{T_2}]^{-1}.$$
$$(4.4.30)$$

where the following notations were used:

$$T_2 = \pi u^{\frac{1}{2}}[(1-u)(v^2 - u^2)]^{-\frac{1}{2}},$$
$$D_1 = (u^2 - v^2)(1-u)^{\frac{1}{2}}u^{-\frac{1}{2}},$$
$$D_2 = [u^{-1}(1-u)(u-v^2)(u^2 - v^2)]^{\frac{1}{2}},$$
$$D_3' = -u(1-u), \; D_3 = v(\alpha_2 - v),$$
$$F_1 = -v(1-u), \; F_2 = u(\alpha_2 - v). \quad (4.4.31)$$

In the limits $t \to 0$ and $t \to \infty$ one obtains:

$$\lim_{t\to 0} P(t) = (\frac{v - \alpha_1 u}{\sqrt{u(1-u)}}, 0, \alpha_1),$$

$$\lim_{t\to\infty} P(t) = (0, \frac{\sqrt{u^2 - v^2}}{u}, \frac{v}{u}). \quad (4.4.32)$$

(b) For $v < u < 1$ the solutions are:

$$x_k(t) = [D_1\delta_{k,1} + D_2\delta_{k,2} \sinh \frac{2\pi t}{T_2} + (-D_3' + D_3 \cosh \frac{2\pi t}{T_2})][-F_1 + F_2 \cosh \frac{2\pi t}{T_2}]^{-1}.$$
$$(4.4.33)$$

The limits for initial and infinity times respectively, are:

$$\lim_{t\to 0} P(t) = (\frac{u^{-\frac{1}{2}}(1-u)^{\frac{1}{2}}(u^2 - v^2)}{v - \alpha_1 u}, 0, \alpha_2),$$

$$\lim_{t\to\infty} P(t) = (0, u^{-1}(u^2 - v^2)^{\frac{1}{2}}, u^{-1}v) \quad (4.4.34)$$

(c) In the interval of $1 > \sqrt{u} > v > u$, the solution reads:

$$x_k(t) = [\pm D_1 \delta_{k,1} \mp i D_2 \delta_{k,2} \sin \frac{2\pi t}{T_2} + (D'_3 + D_3 \cos \frac{2\pi t}{T_2})][F_1 + F_2 \cos \frac{2\pi t}{T_2}]^{-1}.$$

$$\lim_{t \to 0} P(t) = (\frac{u^{-\frac{1}{2}}(1-u)^{\frac{1}{2}}(v^2-u^2)}{v - \alpha_2 u}, 0, \alpha_1). \tag{4.4.35}$$

Notice that among the solutions corresponding to the critical points, two are periodic functions of time.

It is also interesting to see the expressions of the solutions corresponding to some particular values for the parameters u and v as well as for the constant of motion E. Here is the list of them:

(A) For $u = 1$ the solutions are:

$$x_3(t) = const.,$$

$$x_1(t) = \sqrt{1 - x_3^2} \cos 2(x_3 - v)t,$$

$$x_2(t) = -\sqrt{1 - x_3^2} \sin 2(x_3 - v)t, \tag{4.4.36}$$

with initial conditions:

$$P(t) |_{t=0} \equiv (x_1(t), x_2(t), x_3(t)) |_{t=0} = (\sqrt{1 - x_3^2}, 0, x_3) \tag{4.4.37}$$

(B) If $u = v = 0, 0 < E < 1$, then

$$x_1(t) = \pm\sqrt{E},$$
$$x_2(t) = \pm\sqrt{1 - E} \sin 2\sqrt{E}t,$$
$$x_3(t) = -\sqrt{1 - E} \cos 2\sqrt{E}t.$$
$$P(0) = (\pm\sqrt{E}, 0, -\sqrt{1 - E}). \tag{4.4.38}$$

(C) $v = 0, \ u = -1, E = 0$. In this case the solutions are:

$$x_1(t) = \pm\sqrt{\frac{1 - p^2}{2}} e^{-\frac{t}{2}},$$

$$x_2(t) = x_1(t),$$

$$x_3(t) = [1 - (1 - p^2)e^{-t}]^{\frac{1}{2}}, \ 1 > p > 0$$

$$P(0) = \left(\pm\sqrt{\frac{1 - p^2}{2}}, \pm\sqrt{\frac{1 - p^2}{2}}, p\right), \tag{4.4.39}$$

Note that for t going to infinity the curve reaches the north pole:

$$\lim_{t \to \infty} P(t) = (0, 0, 1). \tag{4.4.40}$$

(D) $v = u < 1, \ E = 2v$. **For this case the solutions are**:

$$x_1(t) = \pm \frac{2\sqrt{v(1-v)}}{1 + 4v(1-v)t^2},$$

$$x_2(t) = \pm \frac{4(1-v)t}{1 + 4v(1-v^2)t^2} \sqrt{\frac{v(1-v)}{1-u}},$$

$$x_3(t) = \frac{2v - 1 + 4v(1-v)t^2}{1 + 4v(1-v)t^2},$$

$$\lim_{t \to 0} P(t) = (\pm \sqrt{4v(1-v)}, 0, 2v - 1),$$

$$\lim_{t \to \infty} P(t) = (0, 0, 1). \tag{4.4.41}$$

Analyzing the trajectories from various phases one may conclude:

(a) For certain ranges of the (u, v) parameters, critical points are surrounded by periodic trajectories. The periods exhibit discontinuities when separatrices are approached.

(b) There are specific intervals for (u, v), where some critical points are saddle points. Around such critical points the classical Hamiltonian is unstable against the variation of one coordinate but stable with respect to another one. For such a situation the linearization procedure is not a confident way of approximating the real situations. This assertion will become more clear at the end of this section.

(c) It is to be noticed that the periods of the exact trajectories obtained for the energy critical values $E_+ = 2v$ with $v < u < 1$ and $E_2 = \frac{v^2}{u} + u$ with $u < v, \sqrt{u} < 1$ are exactly the same as the periods of trajectories given by the linearized equations of motion (see Eqs.(4.4.25), (4.4.35) and Table 4.5).

Now let us turn our attention to the exact solutions of Eqs. (4.4.18) with constraints (4.4.14) and (4.4.20). Due to the constraint relations there is only one independent variable. For the sake of convenience, let us take x_3 as independent coordinate. The equation of motion for x_3 can be formally integrated:

$$t - t_0 = \int_{x_{30}}^{x_3} \frac{dx}{2\sqrt{|u|}[(x - \alpha_1)(x - \alpha_2)(x - \alpha_3)(x - \alpha_4)]^{\frac{1}{2}}}, \tag{4.4.42}$$

where we denoted:

$$\alpha_1 = v - \sqrt{E_1 - E},$$

$$\alpha_2 = v + \sqrt{E_1 - E},$$

$$\alpha_3 = \frac{1}{u}[v - \sqrt{u(E_2 - E)}],$$

$$\alpha_4 = \frac{1}{u}[v + \sqrt{u(E_2 - E)}], \tag{4.4.43}$$

The limits for the integral (4.4.42) are chosen so that the integrand is a real number for any $x \in (x_{30}, x_3)$. Obviously, the integral (4.4.42) depends on the relative positions of the poles $\alpha_i\,(i = 1, 2, 3, 4)$. By means of (4.4.42) the time dependence of x_3 is expressed in terms of the elliptic function of first kind [ERD55].

$$t - t_0 = \frac{1}{\sqrt{C}} F(\varphi, k). \tag{4.4.44}$$

where

$$\varphi = \begin{cases} \arcsin k_1 & \text{if all } \alpha_i \text{ are real} \\ \arctan k_1 & \text{if two } \alpha_i \text{ are C-numbers} \end{cases} \tag{4.4.45}$$

The explicit expressions for C, k_1^2, k^2 are collected in Table 4.4. Therein, k^2 is given in terms of

Table 4.4 The arguments k_1 and k of the elliptic function F defining the solution of equations of motion (4.4.44) and (4.4.45)

E and (u, v)	C	k_1^2	k
$u = 0,\ v < 1$			
$-2v < E < 2v$	$2v(\alpha_2 - \alpha_1)$	$\frac{2v(x_3-\alpha_1)}{E-2v\alpha_1}$	$\sqrt{\frac{1-\rho}{2}}$
$u = 0,\ v < 1$			
$2v < E < v^2 + 1$	$E - 2v\alpha_1$	$\frac{x_3-\alpha_1}{\alpha_2-\alpha_1}$	$\sqrt{\frac{2}{1-\rho}}$
$0 < v < \sqrt{u} < 1$			
$E_2 < E < E_1$	$4(1-u)\sqrt{(1-\alpha_1^2)(1-\alpha_2^2)}$	$\frac{(1-\alpha_1^2)(\alpha_2-\alpha_1-x_3)}{(1-\alpha_2^2)x_3}$	$\frac{1}{2}(1 + \frac{\rho}{\sqrt{\rho^2-1}})$
$u > 0$			
$-2v < E < 2v$	$u(\alpha_4 - \alpha_3)(\alpha_2 - \alpha_1)$	$\frac{(\alpha_4-\alpha_3)(x_3-\alpha_1)}{(\alpha_3-\alpha_1)(\alpha_4-x_3)}$	$\sqrt{\frac{1-\rho}{2}}$
$u < 0$			
$-2v < E < 2v$	$u(\alpha_4 - \alpha_3)(\alpha_2 - \alpha_1)$	$\frac{(\alpha_1-\alpha_2)(x_3-\alpha_3)}{(\alpha_1-\alpha_3)(x_3-\alpha_2)}$	$\sqrt{\frac{1-\rho}{2}}$
$u = -1,\ 0 \le v < 1$			
$-(v^2 + 1) < E < -2v$	$u(\alpha_3 - \alpha_1)(\alpha_4 - \alpha_2)$	$\frac{(\alpha_4-\alpha_2)(x_3-\alpha_3)}{(\alpha_4-\alpha_3)(x_3-\alpha_2)}$	$\sqrt{\frac{2}{1-\rho}}$
$1 > \sqrt{u} > v > u > 0$			
$2v < E < E_2$	$u(\alpha_4 - \alpha_2)(\alpha_3 - \alpha_1)$	$\frac{(\alpha_2-\alpha_3)(x_3-\alpha_1)}{(\alpha_3-\alpha_1)(\alpha_2-x_3)}$	$\sqrt{\frac{\rho-1}{\rho+1}}$
$1 > v > \sqrt{u},\ u > 0$			
$2v < E < v^2 + 1$	$u(\alpha_4 - \alpha_2)(\alpha_3 - \alpha_1)$	$\frac{(\alpha_4-\alpha_1)(x_3-\alpha_2)}{(\alpha_2-\alpha_4)(\alpha_1-x_3)}$	$\sqrt{\frac{\rho-1}{\rho+1}}$
$v < u < 1$			
$2v < E < E_2$	$u(\alpha_2 - \alpha_3)(\alpha_4 - \alpha_1)$	$\frac{(\alpha_4-\alpha_2)(x_3-\alpha_1)}{(\alpha_2-\alpha_1)(\alpha_4-x_3)}$	$\sqrt{\frac{2}{1-\rho}}$
$u < 0$			
$2v < E < E_1$	$-u(\alpha_4 - \alpha_2)(\alpha_1 - \alpha_3)$	$\frac{(\alpha_1-\alpha_3)(x_3-\alpha_2)}{(\alpha_1-\alpha_2)(x_3-\alpha_3)}$	$\sqrt{\frac{2}{1-\rho}}$

Also the normalization constant C is given. The first order periods T are listed

$$\rho = \frac{2v^2 - E}{v(\alpha_2 - \alpha_1)} \tag{4.4.46}$$

Taking into account the properties for the elliptic functions, the solution $x_3(t)$ described by (4.4.42) is a periodic function of time with the period:

$$T = \frac{\pi}{\sqrt{C}} {}_2F_1(\frac{1}{2}, \frac{1}{2}, 1; k^2) \tag{4.4.47}$$

where ${}_2F_1$ is the hypergeometric function. In Table 4.5 we also give expressions of T corresponding to an energy E lying close to a critical energy. For the sake of saving space we did not list in Table 4.4 situations where at least two poles α_i are equal and their common values belong to the interval $[-1, 1]$. In such cases trajectories, satisfying the equations of motion (4.4.18) might be:

(I) a steady point if

   (a) $\alpha_{i_1} = \alpha_{i_2} \in [-1, 1], \alpha_{i_3}, \alpha_{i_4} \notin [-1, 1]$ with $i_k \in 1, 2, 3, 4$ and $i_k \neq i_{k'}$, for $k \neq k'$

   (b) $\alpha_{i_1} = \alpha_{i_2} \in [-1, 1]$ and $\alpha_{i_3}, \alpha_{i_4}$ are complex numbers.

   (c) $\alpha_{i_1} = \alpha_{i_2} = \alpha_{i_3} = \alpha_{i_4} \in [-1, 1]$

(II) two steady points if $\alpha_{i_1} = \alpha_{i_2} \in [-1, 1], \alpha_{i_3} = \alpha_{i_4} \neq \alpha_{i_1}$ and $\alpha_{i_3} \in [-1, 1]$

(III) one steady point and one circle if $\alpha_{i_k} \in [-1, 1]$ for any k and $\alpha_{i_1} = \alpha_{i_2}, \alpha_{i_3} = \alpha_{i_4}, \alpha_{i_1}, \alpha_{i_2} \notin [\alpha_{i_3}, \alpha_{i_4}]$ In Table 4.4, two kinds of orbits are analyzed.

(IV) One circle when $\alpha_{i_1} = \alpha_{i_2} \in [-1, 1], \alpha_{i_1} \neq \alpha_{i_2}$ and $\alpha_{i_3}, \alpha_{i_4}$ are either lying outside the interval [-1,1] or are complex numbers.

(V) Two circles when the poles are all different and their modulus are smaller than 1. It is well understood that whenever there are two possible orbits they correspond to the same energy. The system chooses one of the two possibilities according to its initial position. One should notice that the periods we have obtained by linearizing the equations of motion correspond to the zero order expansion of the period for the exact solution. By contrary, the expansion of T around a saddle point of energy function exhibits a logarithmic singularity. Now it is clear why the linearization procedure is not applicable around a saddle point. Such singularities reflect the fact that a system lying in a saddle point is unstable against perturbation. From Fig. 4.8 one sees that the manifold $\{(u, v)||u| \leq 1, v \geq 0\}$ is divided in several regions by separatrices. On other hand from Table 4.5 it results that the period of any classical trajectory has singularities for (u, v) belonging to one separatrix. In other words, a given trajectory cannot be continuously deformed by varying (u, v) so that a separatrix is crossed over. In this sense one could say that separatrix are borders for a domain of (u, v) characterized by a specific behavior of the system under consideration. Conventionally, we shall call these domains as *phases of the classical motion*. It can be shown that two different phases correspond to two different symmetries for the elementary classical system. Also, it is obvious

Table 4.5 The arguments k_1 and k of the elliptic function F defining the solution of equations of motion (4.4.44) and (4.4.45)

E and (u,v)	First orders expansion for T
$-2v < E < 2v$ $u=0,\ v<1$	$\dfrac{\pi}{2\sqrt{v(v+1)}}\left(1 + \dfrac{\epsilon}{4v(v+1)}\right);\quad E=-2v+\epsilon$ $\dfrac{\pi}{\sqrt{v(1-v)}}\left(1 - \dfrac{(2v+1)\epsilon}{8v(1-v)^2}\right);\ E=2v-\epsilon$
$2v < E < v^2+1$ $u=0,\ v<1$	$\dfrac{\pi}{\sqrt{v(1-v)}}\left(1 - \dfrac{\epsilon}{4v(1-v)}\right);\quad E=2v+\epsilon$ $\dfrac{\pi}{\sqrt{1-v^2}}\left(1 + \dfrac{6v\epsilon+\epsilon^2}{2(1-v^2)}\right);\ E=v^2+1-\epsilon^2$
$E_2 < E < E_1$	$\pi\sqrt{\dfrac{u}{(1-u)(u^2-v^2)}}\left(1 - \epsilon\dfrac{u[(1-u)(u^2+v^2)+u(u-v^2)]}{2(u^2-v^2)^2(1-u)}\right);\quad E=E_2+\epsilon;\ v<u$
$0 < v < \sqrt{u} < 1$	$\dfrac{\pi}{2}\sqrt{\dfrac{u}{(1-u)(v^2-u^2)}}\left(1 - \dfrac{u(u+1)\epsilon}{2(1-u)(v^2-u^2)}\right);\ E=E_2+\epsilon;\ v>u$ $\dfrac{\pi}{2\sqrt{(1-u)(1-v^2)}}\left(1 + \dfrac{(1+u)\epsilon}{2(1-u)(1-v^2)}\right);\ E=E_1-\epsilon$
$-2v < E < 2v$	$\dfrac{\pi}{2\sqrt{(1+v)(u+v)}}\left(1 + \dfrac{(u-v)(1+u)(1-v)+8uv}{4(u+v)^2(1+v)^2}\epsilon\right);\ E=-2v+\epsilon$
$u > 0$	$\dfrac{\pi}{2\sqrt{(1-v)(u-v)}}\left(1 - \dfrac{(1+u)\epsilon}{4(1-v)(u-v)}\right);\ E=2v-\epsilon,\ u>v$ $\dfrac{\pi}{2\sqrt{(1-v)(v-u)}}\left(1 + \dfrac{v(1-u)^2-4u(1+v)^2-4(u-v)^2}{4(v-u)^2(1-v)^2}\epsilon\right);\ E=2v-\epsilon,\ v>u$
$-2v < E < 2v$	$\dfrac{\pi}{2\sqrt{(1+v)(v+u)}}\left(1 + \dfrac{-v(1-u)^2+u(1+v)^2+(u+v)^2}{4(v+u)^2(1+v)^2}\epsilon\right);\ E=-2v+\epsilon,\ u+v>0$
$u < 0$	$\dfrac{\pi}{\sqrt{-(1+v)(v+u)}}\left(1 - \dfrac{v(1-u)(2v+u+1)}{4(v+u)^2(1+v)^2}\epsilon\right);\ E=-2v+\epsilon,\ u+v<0$ $\dfrac{\pi}{\sqrt{(1-v)(v-u)}}\left(1 + \dfrac{(v+uv-2v)(2v-u-1)}{8(v-u)^2(1-v)^2}\epsilon\right);\ E=2v-\epsilon$
$-(v^2+1) < E < -2v$	$\dfrac{\pi}{\sqrt{2(1-v^2)}}\left[1 + \dfrac{9}{4}\sqrt{\dfrac{2(1+v^2)}{1-v^2}}\,\epsilon - \dfrac{\epsilon^2}{1-v^2}\left[\dfrac{1}{8}+\dfrac{9}{2}\dfrac{1+v^2}{1-v^2}\right]\right];\ E=-(v^2+1)+\epsilon^2$
$u=-1,\ 0\le v<1$	$\pi\sqrt{\dfrac{2}{1-v^2}}\left(1 - \dfrac{3}{4}\dfrac{\epsilon v}{(1-v^2)^2}\right);\ E=-2v-\epsilon$
$2v < E < E_2$	$\dfrac{\pi}{\sqrt{(1-v)(v-u)}}\left(1 - \epsilon\dfrac{v(1-u)(1-2v+u)+4u(1-v)^2+4(v-u)^2}{16(1-v)^2(v-u)^2}\right);\ E=2v+\epsilon;\ \text{if}\ E=E_2-\epsilon^2$

(continued)

Table 4.5 (continued)

E and (u,v)	First orders expansion for T
$1 > \sqrt{u} > v > u > 0$	$\pi\sqrt{\dfrac{u}{(1-u)(v^2-u^2)}}\left[1 + \dfrac{9}{2}\dfrac{u}{v^2-u^2}\sqrt{\dfrac{u-v^2}{1-u}}\,\epsilon - \epsilon^2\left[\dfrac{1}{4}\dfrac{u(1+u)}{(1-v)(v^2-u^2)} + 9\dfrac{u^2(u-v^2)}{(1-u)(v^2-u^2)^2}\right]\right];$
$2v < E < v^2 + 1$	$\dfrac{\pi}{\sqrt{(1-u)(1-v^2)}}\left[1 + \dfrac{7}{2}\dfrac{1}{1-v^2}\sqrt{\dfrac{v^2-u}{1-u}}\,\epsilon + \dfrac{\epsilon^2}{1-v^2}\left(\dfrac{1}{4} + 3\dfrac{v^2-u}{(1-u)(1-v^2)}\right)\right];$
$1 > v > \sqrt{u},\ u > 0$	$E = v^2 + 1 - \epsilon^2$
$2v < E < E_2$	$\dfrac{\pi}{2\sqrt{(1-v)(u-v)}}\left[1 + \dfrac{\epsilon u[-(1+u-2v)(2u-v-uv)+4(1-u)^2 v]}{16(1-v)^2(u-v)^2}\right];\quad E = 2v + \epsilon$
$v < u < 1$	$2\pi\sqrt{\dfrac{u}{(1-u)(u^2-v^2)}}\left[1 - \dfrac{3}{2}\epsilon\dfrac{u}{u^2-v^2}\sqrt{\dfrac{u-v^2}{1-u}} + \dfrac{1}{4}\dfrac{u(1+u)}{(1-u)(u^2-v^2)}\epsilon^2\right];\quad E = E_2 - \epsilon^2$
$2v < E < E_1$	$\dfrac{\pi}{\sqrt{(v-u)(1-v)}}\left(1 - \epsilon\dfrac{(1+u-2v)(v-2u+uv)+4u(1-v)^2+4(v-u)^2}{16(v-u)^2(1-v)^2}\right);\quad E = 2v + \epsilon$
$u < 0$	$\dfrac{\pi}{\sqrt{(1-u)(1-v^2)}}\left[1 + \dfrac{9}{2}\dfrac{1}{1-v^2}\sqrt{\dfrac{v^2-u}{1-u}}\,\epsilon - \dfrac{\epsilon^2}{1-v^2}\left(\dfrac{1}{4}\dfrac{1+u}{1-u} + 9\dfrac{v^2-u}{(1-u)(1-v^2)}\right)\right];\quad E = E_1 - \epsilon^2$

Also the normalization constant C is given. The first order periods T are listed

that by perturbing a trajectory of a given phase, one obtains a trajectory of the same phase. A more rigorous definition for the classical phases pointing to their relation to the underlying group symmetry as well as to their stability properties against perturbations exceeds the goal of this book.

4.4.1 Quantization of Periodic Orbits

Now, once we have a full classical description of the classical system, we want to investigate whether starting from there it is possible to get some information about the quantal system. This can be achieved by quantizing the classical trajectories, i.e. by enforcing the classical action to be an integer multiple of 2π. This provides an equation for the quantized energy which is supposed to be an approximation for the eigenvalues of the quantum mechanical Hamiltonian. The restriction for the classical action is similar to the well-known quantization rule of Bohr and Sommerfeld. The resulting energies define the so called semiclassical spectrum of H. How good this approximation is, can be judged only by comparing the semiclassical spectrum with the exact one. This comparison will be made in the next section.

Let us now write down explicitly the quantization condition. To this purpose we shall define first the classical action. For the time being we suppose that (u, v) is fixed and moreover does not belong to a separatrix. Further we consider an extremal point P on the sphere S_1^2 to which the energy E_0 corresponds. There is a continuous family (with respect to the energy E) of trajectories surrounding P. For an arbitrary value of E we shall define the action as the magnitude of the area of the calhote containing P and having the trajectory of energy E as border.

$$\mathcal{L}(E) = \int d\Omega = \int_{E_0}^{E} \int_{0}^{T} dE' \, dt' = \int_{E_0}^{E} T(E') \, dE', \qquad (4.4.48)$$

where $T(E')$ denotes the period of the orbit of energy E' and is given analytically in Table 4.5. Then the quantization rules reads:

$$\mathcal{L}(E) = 2\pi n. \qquad (4.4.49)$$

Since $\mathcal{L}(E)$ is an increasing function of E, the Eq. (4.4.49) can be reversed:

$$E_n = f(u, v, n) \qquad (4.4.50)$$

By a formal derivation of $\mathcal{L}(E)$ one easily obtains:

$$\frac{\partial \mathcal{L}(E)}{\partial E} = T(E) = \frac{\partial \mathcal{L}(E)}{\partial n} \frac{\partial n}{\partial E},$$
$$\frac{\partial E}{\partial n} = \frac{2\pi}{T(E)}. \qquad (4.4.51)$$

From here it is manifest that a linear dependence of E on n is obtained when $T(E)$ is approximated by its zero order expansion around E_0. In Table 4.5 results for cases when such expansions are not singular with respect to the deviation $\epsilon = E - E_{cr}$ are given. Note that this happens in our case since E_0 is an extremal value for the energy function. Energies obtained in this way are identical with those obtained by quantizing the trajectory provided by the linearized equations of motion. It is worth mentioning that for the latter case the quantization condition is just that of Bohr and Sommerfeld. Thus, it becomes clear that solving Eq. (4.4.49) one goes beyond the standard result obtainable through the Bohr-Sommerfeld rule. The quantization method presented here has several limitations, induced by the fact that $T(E)$ has singularities when (u, v) belongs to a separatrix as well as when the trajectory on S_1^2 lies close to a saddle point. Therefore $\mathcal{L}(E)$ defined by (4.4.48) is only locally a continuous function of E and (u, v). It is an open question how to extend the quantization condition (4.4.49) to a region which intersects two different phases.

4.5 The Quantum Hamiltonian

Here we shall study the Schrödinger equation:

$$H\Psi = E\Psi, \quad \text{with}$$
$$H = J_1^2 + uJ_2^2 + 2v_0J_3 \tag{4.5.1}$$

For what follows it is useful to write H in terms of the lowering ($J_- = J_1 - iJ_2$) and raising angular momentum operators ($J_+ = J_1 + iJ_2$).

$$H = \frac{1-u}{4}(J_+^2 + J_-^2) + \frac{1+u}{4}(J_+J_- + J_-J_+) + 2v_0J_0 \tag{4.5.2}$$

Here J_0 denotes the third component of angular momentum operator. It is convenient to write the Schrödinger Eq. (4.5.1) in such a form that the potential energy is demixed from the kinetic energy. To this aim we shall write the operators $J_\pm$, J_0 as differential operators with respect to a real variable q, chosen so that the commutation relations

$$[J_+, J_-] = 2J_0, \ [J_\pm, J_0] = \mp J_\pm, \tag{4.5.3}$$

are preserved. A possible representation for the operators $J_k (k = 0, \pm)$, satisfying this condition and $J_1^2 + J_2^2 + J_3^2 = j(j+1)$, is:

$$J_\pm = i\frac{c \pm d}{k's}(j \mp J_0),$$
$$J_0 = jcd - s\frac{d}{dq} \tag{4.5.4}$$

where c,s,d denote the elliptic functions [ERD55]:

$$s = sn(q, k), c = cn(q, k), d = dn(q, k) \text{ with}$$

$$k = \sqrt{u}, \ u > 0, \ q = \int_0^{\varphi} (1 - k^2 \sin t^2)^{-\frac{1}{2}} dt \equiv F(\varphi, k),$$

$$k' = \sqrt{1 - k^2} \tag{4.5.5}$$

The functions s, c, d are related with the usual trigonometric functions by:

$$s = \sin \varphi, \ c = \cos \varphi, \ d = \sqrt{1 - k^2 \sin \varphi^2}, \tag{4.5.6}$$

and have the periods $4K, \ 4K, \ 2K$, respectively, with

$$K = F(\frac{\pi}{2}, k) = \frac{\pi}{2} {}_2F_1(\frac{1}{2}, \frac{1}{2}, 1; k^2) \tag{4.5.7}$$

To check the commutation relations (4.5.3) for the boson representation (4.5.4) one needs the derivatives of the involved elliptic functions:

$$\frac{d}{dq} sn(q) = cn(q) dn(q),$$

$$\frac{d}{dq} cn(q) = -sn(q) dn(q),$$

$$\frac{d}{dq} dn(q) = -k^2 sn(q) cn(q). \tag{4.5.8}$$

In the new representation the Hamiltonian H (14.1.1) has the form:

$$H = -\frac{d^2}{dq^2} - 2v_0 s \frac{d}{dq} + j(j+1)s^2 k^2 + 2v_0 cdj \tag{4.5.9}$$

Now changing the function Ψ to the function Φ by

$$\Psi = (d - kc)^{-\frac{v}{k}} \Phi \tag{4.5.10}$$

the Schrödinger Eq. (4.5.1) becomes:

$$[-\frac{d^2}{dq^2} + V(q)]\Phi = E\Phi \tag{4.5.11}$$

where

$$V(q) = (j(j+1)k^2 + v_0^2)s^2 + (2j+1)v_0 cd \tag{4.5.12}$$

Let us consider first the particular case $v_0 = 0$. In this special case $V(q)$ has two minima for

$$\varphi_m = 0, \pi \tag{4.5.13}$$

The minimum values of $V(q)$ are equal and the common value is

$$V_m = 0. \tag{4.5.14}$$

The second order expansion of $V(q)$ around one chosen minimum point, $q_m = q(\varphi_m)$ is:

$$\tilde{V}(q) = j(j+1)k^2 q^2 \tag{4.5.15}$$

Approximating $V(q)$ by $\tilde{V}(q)$, the Eq. (4.5.11) describes the harmonic oscillation of q around q_m. Therefore the eigenvalues are given by

$$E_n = \sqrt{j(j+1)u}(2n+1) \tag{4.5.16}$$

This situation corresponds to the triaxial rotor. Indeed, writing H (14.1.1) in a different form:

$$H = -j(j+1) + H' \tag{4.5.17}$$

the new Hamiltonian has the form

$$H' = 2J_1^2 + (u+1)J_2^2 + J_3^2 \tag{4.5.18}$$

describes a triaxial rotor characterized by the moments of inertia $\mathcal{I}_i (i = 1, 2, 3)$ given by:

$$2 = \frac{1}{2\mathcal{I}_1}, \quad u+1 = \frac{1}{2\mathcal{I}_2}, \quad 1 = \frac{1}{2\mathcal{I}_3}. \tag{4.5.19}$$

Certainly, they satisfy the ordering relation:

$$\mathcal{I}_3 > \mathcal{I}_2 > \mathcal{I}_1 \tag{4.5.20}$$

From the Schrödinger Eq. (4.5.11) corresponding to H' can be derived the equation obtained in Ref. [BR79] for arbitrary inertial momenta satisfying the ordering relations (4.5.20) if the restrictions (4.5.19) are adopted. By the same transformation the spectrum obtained in Ref. [BR79]

$$E_n' = \frac{j(j+1)}{2\mathcal{I}_3} + [(\frac{1}{\mathcal{I}_1} - \frac{1}{\mathcal{I}_3})(\frac{1}{\mathcal{I}_2} - \frac{1}{\mathcal{I}_3})]^{\frac{1}{2}}\sqrt{j(j+1)}(n+\frac{1}{2}), \tag{4.5.21}$$

goes to the spectrum of H'.

Coming back to the general case, that of $v_0 \neq 0$, the absolute minimum of $V(q)$ is reached for $\varphi_m = \pi$:

$$V_m \equiv V(q_m) = -(2j + 1)v_0,$$
$$q_m \equiv q(\varphi_m) = 2k. \tag{4.5.22}$$

The second derivative of $V(q)$ in the minimum point is

$$V''(\varphi_m) = 2[j(j+1)k^2 + v_0^2] + (2j+1)v_0(1 + k^2) \tag{4.5.23}$$

The Schrödinger equation corresponding to the harmonic approximation for $V(q)$ is:

$$\{-\frac{d^2}{dq^2} - (2j+1)v_0 + \frac{1}{4}[(2j+1+2v_0)(k^2(2j+1)+2v_0) - k^2]\}\Phi = E\Phi \tag{4.5.24}$$

Therefore the eigenvalues are:

$$E_n = -(2j+1)v_0 + \sqrt{(2j+1+2v_0)(u(2j+1)+2v_0)} - u(n + \frac{1}{2}) \tag{4.5.25}$$

Taking now $v = \frac{v_0}{j}$, which corresponds to a specific dequantization procedure [GRC98], and neglecting the $\frac{1}{j}$-order terms, one obtains:

$$E_n = j[-2vj + \sqrt{(u+v)(1+v)}(n + \frac{1}{2})] \tag{4.5.26}$$

This result coincides, up to a contraction factor, with that obtained through the semi-classical procedure for the case $u > 0$, $-2v < E < 2v$ mentioned in Table 4.4. It is worth noting that replacing the conjugate variables q and $-i\frac{d}{dq}$ by the corresponding expressions in terms of the boson operators a and $a^\dagger$:

$$q = \frac{1}{\sqrt{2}}(a + a^\dagger),$$
$$-i\frac{d}{dq} = \frac{i}{\sqrt{2}}(a^\dagger - a), \tag{4.5.27}$$

the equation (4.5.4) provides a new boson representation for the $SU(2)$ algebra generators. For practical purposes it is more convenient to use the bosons:

$$q = B^\dagger, \quad \frac{d}{dq} = B. \tag{4.5.28}$$

A similar result for the quantal spectrum can be obtained by using the Holstein Primakoff representation [HolPr40] for the angular momentum operator

$$J_+ = \sqrt{2j}a^\dagger(1 - \frac{a^\dagger a}{2j})^{\frac{1}{2}}, \ J_- = \sqrt{2j}a(1 - \frac{a^\dagger a}{2j})^{\frac{1}{2}}, \ J_0 = -j + a^\dagger a, \quad (4.5.29)$$

where a, a^+ are boson operators

$$[a, a^\dagger] = 1. \tag{4.5.30}$$

By this boson representation the commutation relations (4.5.3) are exactly satisfied. Inserting the expressions (4.5.29) for the angular momentum operators in the equation (4.5.2) one obtains a boson representation for the cranked Hamiltonian. Expanding the square-root operators and ignoring the corrective terms of the order $\frac{1}{j}$, one obtains a quadratic expressions in boson operators:

$$H = [j(u+1) + 2v_0]a^\dagger a + \frac{1-u}{2}j(a^{\dagger 2} + a^2) + \frac{j(1+u)}{2} - 2v_0 j. \quad (4.5.31)$$

Further, H is diagonalized by the canonical transformation

$$a^\dagger = Ub^\dagger + Vb, \ a = Ub + Vb^\dagger \tag{4.5.32}$$

with

$$V = \frac{1}{2}[(\frac{v_0 + ju}{v_0 + j})^{\frac{1}{4}} - (\frac{v_0 + j}{v_0 + ju})^{\frac{1}{4}}],$$
$$U^2 = 1 - V^2, \ [b, b^\dagger] = 1. \tag{4.5.33}$$

The new boson representation of H is

$$H = -v_0(2j+1) + \sqrt{(v_0 + j)(v_0 + ju)}(b^\dagger b + \frac{1}{2}). \tag{4.5.34}$$

The excitation energies are:

$$E_n = -v_0(2j+1) + \sqrt{(v_0 + j)(v_0 + ju)}(n + \frac{1}{2}). \tag{4.5.35}$$

It is worth noting that the two procedures provide the same zero point energy. Moreover, up to some corrective terms of the order $\frac{1}{2}$, the excitation energies coincide.

Concluding this chapter we may say that the triaxial as well as the tilted rotors were treated semiclassically and several boson representations were derived. The most geeral tilted rotor was considered in various phases of the parameters space, separated by separatrices. Analytical trajectories were obtained for each phase and in particular for the critical energies. The periods for the latter cases coincide with those obtained by linearizing the equations of motion around a minimum point. The periodic orbits are quantized through a restriction which generalizes the Bohr-Sommerfeld quantization rule. The method can be applied also for large amplitude

motion. For the Dyson boson expansion, the kinetic and potential energies of the
rotor Hamiltonian are fully separated. Further the harmonic approximation around
the minimum point of the potential yields the wobbling frequency. The symmetries
of the rotor Hamiltonian were discussed. Thus, the eigenstates are interpreted in
terms of the irreducible representation of the group D_2. The corresponding energies
are also analytically given for the low spin states.

Chapter 5
Semiclassical Description of Many Body Systems

5.1 The Coupling of Individual and Collective Degrees of Freedom

The competition of collective and individual degrees of freedom plays an important role in the study of nuclear systems. Chiefly, one attempts to reduce the number of degrees of freedom to a small number of relevant ones and to understand the nuclear spectra in terms of the competition between them. The projection of the optimal collective coordinates is done either by a time dependent formalism using a constrained variational principle for the classical action [Vil77, MOY77, BaVe78, RB76, Ma77, RG78, MP82], or through a variational principle for the Schrödinger equation [MSMUH82, KMU82]. The first case has the advantage of keeping close contact with the classical features but brings in difficulties in re-quantizing the classical trajectories [RE80, LNP80, KGLD79, SU83]. The second method provides a full quantum mechanical solution for projecting the maximally decoupled collective space out of the many fermionic states but in spite of its beauty seems to be still far from quantitative applications.

Alternatively, the semi-phenomenological models assume one phenomenological Hamiltonian describing the motion of a collective core and another one coupling a set of interacting particles to the core [BMR73, FA76, MV75, KS73, TF75, NVR75, TNVF77, BHM78, HA76, GSF79, ISO73, IKMO79, IO83, I81, RCD76, RLF83, Ma78, BM81, HMO83]. On this line, effects like alignment of the angular momentum of the single particle motion either to the symmetry axis or to the rotation axis of the core, and the transition from the superconducting phase to the normal one were intensively studied.

In what follows we shall use a model Hamiltonians such that the collective part is described by a phenomenological quadrupole boson and the rest of nucleons interact through a pairing force. The coupling of the particle and core simulates a specific dependence of the gap parameters on the angular momentum of a rotational non-invariant core, described in terms of quadrupole bosons (b_μ, $-2 \leq \mu \leq 2$).

$$H = \Omega \hat{N}_b + \sum_{k=1}^{n_s} (\epsilon_k - \lambda) \hat{N}_k - \frac{1}{4} G \sum_{k,k'=1}^{n_s} P_k^+ P_{k'} + H_{coup} + H_c, \qquad (5.1.1)$$

where the following notations were used:

$$\hat{N}_b = \sum_{\mu=-2}^{2} b_\mu^+ b_\mu, \quad \hat{N}_k = \sum_{m=-j_k}^{j_k} c_{km}^+ c_{km},$$

$$P_k^+ = \hat{j}_k (c_k^+ c_k^+)_0, \quad \hat{j}_k = (2j_k + 1)^{1/2},$$

$$H_{coup} = \eta \sum_{k=1}^{n_s} \left[b_0^+ P_k + b_0 P_k^+ \right],$$

$$H_c = -\lambda_1 \hat{J}^2. \qquad (5.1.2)$$

Here $c_{km}^+ (c_{km})$ denotes the creation (annihilation) operator of one particle in the spherical shell model state $|km\rangle = |nljm\rangle$. The lower label k is the ordering index for single particle energies: $\epsilon_1 < \epsilon_2 < \epsilon_3 < \cdots < \epsilon_{n_s}$. $\hat{J}$ stands for the core angular momentum and has the expression:

$$\hat{J}^2 = 2\hat{N}_b(2\hat{N}_b + 1) - 10(b^+ b^+)_0(bb)_0 - 7\sqrt{5} \left[(b^+ b^+)_2 (bb)_2 \right]_0. \qquad (5.1.3)$$

Also, $\hat{N}_p$ denotes the total number of particles operator, i.e., $\hat{N}_p = \sum_{k=1}^{n_s} \hat{N}_k$, while n_s represents the number of states under consideration.

Instead of solving the stationary eigenvalue problem associated to the Hamiltonian H, we seek the time dependent solution $|\psi_{p,b}^{(k)}(t)\rangle$ of the variational principle equation:

$$\delta \int_{t_0}^{t} \langle \psi_{p,b}(t') | i \frac{\partial}{\partial t'} - H | \psi_{p,b}(t') \rangle dt' = 0. \qquad (5.1.4)$$

Obviously in the above equation the unit system where $\hbar = 1$ was used. One can prove that if the trial function spans the whole Hilbert space of the particle-core Hilbert space then solving the variational principle equation is equivalent to solving the time dependent Schrödinger equation. We shall restrict the particle-core space to the set of states:

$$|\psi_{p,b}(t)\rangle = e^{T_b(t)} e^{T_p(t)} |0\rangle_p |0\rangle_b,$$

$$T_b(t) = z_0(t) b_0^+ - z_0^*(t) b_0, \quad T_p(t) = \sum_{k=1}^{n_s} \left(z_k(t) P_k^+ - z_k^*(t) P_k \right), \qquad (5.1.5)$$

where $|0\rangle_b$, $|0\rangle_p$ are vacuum states for boson and particle annihilation operators respectively, while $z_k(t)$ are smooth complex functions of time and $z_k^*(t)$ their complex conjugates.

The set $M(t) = (z_0, z_1, \ldots, z_{n_s}, z_0^*, z_1^*, \ldots, z_{n_s}^*)$ is interpreted as a point in the classical phase-space coordinates associated with the $n_s + 1$ degrees of freedom. Solving the variational principle equations, one determines the time dependence of the functions $M(t)$ when the initial conditions, $M(t_0) = M_0$, are specified. The set of points $M(t)$ obeying the initial condition mentioned above, defines the classical trajectory in the classical phase space.

Let us denote by $\mathcal{M}$ the submanifold of the particle-core space, $S_p \otimes S_c$, spanned by $|\psi_{p,b}(t)\rangle$ for $(z_0, z_1, \ldots, z_{n_s}) \in C^{n_s+1}$. Once the classical equations of motion for the coordinates z_k are solved, the function $|\psi_{p,b}(t)\rangle$ is determined and finally the system time evolution becomes:

$$|\psi_{p,b}^C(t)\rangle = |\psi_{p,b}(t_0)\rangle \exp\{i \int_{t_0}^{t} \langle \psi_{p,b}(t')|i\frac{\partial}{\partial t'} - H|\psi_{p,b}(t')\rangle dt'\} \qquad (5.1.6)$$

Indeed, one can show that the above function obeys the variational principle on the manifold $C \otimes \mathcal{M}$ [KGLD79]. The factor multiplying $\psi_{p,b}$ in (5.1.6) results from a "parallel" variation of $\psi_{p,b}^C$, i.e., on C. This way the time evolution of the "space" independent phase is uniquely determined. Note that the structure of $\psi_{p,b}^C$ is similar to that of a stationary state of the Schrödinger equation. This result actually ensures the independence of the results of a measurement on the time observation. This property is also valid for $\psi_{p,b}^C$ requiring that the gauge invariant factor

$$|\Psi_{p,b}^G\rangle = |\psi_{p,b}\rangle \exp\{i \int_{t_0}^{t} \langle \psi_{p,b}(t')|i\frac{\partial}{\partial t'}|\psi_{p,b}\rangle dt'\} \qquad (5.1.7)$$

be periodic

$$|\psi_{pb}^G(t+T)\rangle = |\psi_{pb}^G(t)\rangle \qquad (5.1.8)$$

and by redefining, as a result of a measurement, the time average of the operator associated to the physical observable in an interval much longer than T. The above restriction is conventionally called the gauge invariant periodic (GIP) condition [KGLD79] which implies that $|\psi_{p,b}\rangle$ is a periodic function and

$$\int_{0}^{T} \langle \psi_{p,b}|i\frac{\partial}{\partial t'}|\psi_{p,b}\rangle dt' = 2m\pi, \quad m = 0, 1, 2, \ldots \qquad (5.1.9)$$

This relation is similar to the Bohr-Sommerfeld quantization rule [T81, FG80]. This condition fixes the integration constants of the classical equations of motion and

consequently, the classical energy $\langle \psi_{p,b}|H|\psi_{p,b}\rangle$, which is a constant of motion, becomes a discrete spectrum [P73].

Therefore, the path to be followed in studying the particle-core Hamiltonians is: *(i) dequantization of the quantal systems described by the model Hamiltonian H; (ii) solving the classical equations of motion and depicting the periodic orbits; (iii) quantization of the classical periodic trajectories.*

It is worth noting that the variational state is a product of $n_s + 1$ coherent states, one of Weyl type, describing the collective core, whereas the remaining n_s are coherent states for $SU(2)$ algebras associated to the single j shells, respectively. Thus, here we give an example about how the coherent states might be used for treating a many body system.

5.1.1 The Classical Description of H

We shall suppose that the core is in a state of angular momentum J which is achieved by the restriction:

$$\langle \psi_{p,b}|\hat{J}^2|\psi_{p,b}\rangle = J(J+1). \tag{5.1.10}$$

It is convenient to write the classical coordinates in a polar form:

$$z_k = \rho_k e^{i\varphi}, \quad 0 \leq k \leq n_s, \ 0 \leq \varphi_k < 2\pi, \ \rho_0 > 0, \ 0 < \rho_k < \pi/4, \ k > 1 \tag{5.1.11}$$

To make explicit the classical equations of motion we need the transformation relations:

$$e^{T_b}b_m e^{-T_b} = b_m - z_0 \delta_{m,0},$$
$$e^{T_p}c^+_{km} e^{-T_p} = U_k c^+_{km} - s_{km}V_k c_{k,-m} \equiv a^+_{km},$$
$$U_k = \cos 2\rho, \quad V_k = \sin 2\rho e^{-i\varphi_k}, \ s_{km} = (-1)^{j_k - m}, \quad 1 \leq k \leq n_s. \tag{5.1.12}$$

The exponential excitation of the vacuum state is vacuum for the transformed operators.

$$a_{km}e^{T_p}|0\rangle_p = 0, \quad (b_m - z_0\delta_{m,0})e^{T_b}|0\rangle_b = 0. \tag{5.1.13}$$

The classical energy function has the expression:

$$\mathcal{H} = \langle \psi_{p,b}|H|\psi_{p,b}\rangle = (\Omega - 6\lambda_1)\rho_0^2 + \sum_{k=1}^{n_s} 2(\epsilon_k - \lambda)\Omega_k |V_k|^2$$

$$- \frac{|\Delta|^2}{G} + \frac{\eta}{G}\rho_0(\Delta e^{i\varphi_0} + \Delta^* e^{-i\varphi_0}),$$

$$\Delta = \frac{1}{2}G\sum_{k=1}^{n_s}\Omega_k \sin 4\rho_k e^{-i\varphi}, \ \Omega_k = j_k + \frac{1}{2}. \tag{5.1.14}$$

The constraint can be explicitly calculated:

$$6\rho_0^2 = J(J+1). \tag{5.1.15}$$

In order to calculate the average of the operator $i\frac{\partial}{\partial t}$ it is useful to write the vacuum states in a factorized form by using the Baker-Campbell-Hausdorff transformation:

$$e^{T_b}|0\rangle_b = e^{-\rho_0^2/2} e^{z_0 b_0^+}|0\rangle_b,$$

$$e_p^T|0\rangle_p = \left[\prod_{k=1}^{n_s} U_k^{\Omega_k}\right]\left[\exp\left(\sum_{k=1}^{n_s}\sum_{m>0}\frac{V_k^*}{U_k}c_{km}^+ c_{k,-m}^+ s_{km}\right)\right]|0\rangle_p. \tag{5.1.16}$$

By a straightforward calculation one finds:

$$\langle\psi_{p,b}|i\frac{\partial}{\partial t}|\psi_{p,b}\rangle = -\left(\rho_0^2\dot{\varphi}_0 + \sum_{k=1}^{n_s}\Omega_k \sin^2 2\rho_k\dot{\varphi}_k\right), \tag{5.1.17}$$

where the "$\bullet$" specifies the time derivative.

The variational principle yields the equations:

$$-2\rho_0\dot{\varphi}_0 = \frac{\partial\mathcal{H}}{\partial\rho_0}, \quad -2\Omega_k\dot{\varphi}_k\sin(4\rho_k) = \frac{\partial\mathcal{H}}{\partial\rho_k},$$

$$2\rho_0\dot{\rho}_0 = \frac{\partial\mathcal{H}}{\partial\varphi_0}, \quad 2\Omega_k\dot{\rho}_k\sin(4\rho_k) = \frac{\partial\mathcal{H}}{\partial\varphi_k}. \tag{5.1.18}$$

Changing the variables ρ_k, $k = 0, 1, \ldots, n_s$ by

$$r_0 = \rho_0^2, \quad r_k = \Omega_k \sin^2 2\rho_k, \quad k = 1, 2, \ldots, n_s, \tag{5.1.19}$$

otherwise keeping the same angles as before, the classical equations of motion acquire the canonical Hamilton form:

$$-\dot{\varphi}_k = \frac{\partial\mathcal{H}}{\partial r_k}, \quad \dot{r}_k = \frac{\partial\mathcal{H}}{\partial\varphi_k}, \quad k = 0, 1, \ldots, n_s. \tag{5.1.20}$$

Due to these equations the variables r_k, φ_k are called canonically conjugate variables, namely r_k are coordinates and φ_k the corresponding conjugate momenta. For any pair of complex functions f_1, f_2 of $(r_0, r_1, \ldots, r_{n_s}, \varphi_0, \varphi_1, \ldots, \varphi_{n_s})$, the associated Poisson bracket is defined as:

$$\{f_1, f_2\} = \sum_{i=0}^{n_s}\left(\frac{\partial f_1}{\partial r_i}\frac{\partial f_2}{\partial\varphi_i} - \frac{\partial f_1}{\partial\varphi_i}\frac{\partial f_2}{\partial r_i}\right). \tag{5.1.21}$$

In particular we have:

$$\{r_i, \varphi_i\} = 1, \quad i = 0, 1, \ldots, n_s. \tag{5.1.22}$$

Inserting the expressions of the partial derivatives in Eq. (5.1.20) one obtains:

$$
\begin{aligned}
-\dot{\varphi} &= 2\left(\epsilon_k - \lambda - G|V_k|^2\right) \\
&\quad - \frac{U_k^2 - |V_k|^2}{2U_k|V_k|}\left[\Delta e^{i\varphi_k} + \Delta^* e^{-i\varphi_k} - 2\eta\rho_0\cos(\varphi_0 - \varphi_k)\right], \\
\dot{r}_k &= -i\Omega_k U_k|V_k|\left[\Delta e^{i\varphi_k} - \Delta^* e^{-i\varphi_k} + i\eta\rho_0\sin(\varphi_0 - \varphi_k)\right], \quad k = 1, 2, \ldots, n_s, \\
-\dot{\varphi}_0 &= \Omega - 6\lambda_1 + \frac{\eta}{2\rho_0 G}\left(\Delta e^{i\varphi_0} + \Delta^* e^{-i\varphi_0}\right), \\
\dot{r}_0 &= i\frac{\eta}{G}\rho_0\left(\Delta e^{i\varphi_0} - \Delta^* e^{-i\varphi_0}\right).
\end{aligned}
\tag{5.1.23}
$$

There exist two constants of motion:

$$
\mathcal{R}_0 = \sum_{i=0}^{n_s} r_i, \quad E = \mathcal{H}(r_0, \ldots, r_{n_s}; \varphi_0, \ldots, \varphi_{n_s}). \tag{5.1.24}
$$

with $r_0, \ldots, r_{n_s}$ and $\varphi_0, \ldots, \varphi_{n_s}$ satisfying the equations of motion (5.1.23). The first constant of motion reflects the fact that the operator $\hat{N}_b + \frac{1}{2}\hat{N}_p$ commutes with H while the second one is a common feature of any time dependent treatment resulting from a variational principle. The defining relations for the two constants of motion represent two surfaces in the phase space, whose intersection provides the support for the classical trajectory describing the system time evolution. The constant energy function exhibits several stationary points obtained from (5.1.23) by canceling the time derivatives of coordinates and momenta. From the stationary points we are interested in those which make the classical energy minimum. Moreover, we keep only minima satisfying the constraint (5.1.15). For this analysis we consider $\eta < 0$. Thus, we find a degenerate minimum with

$$
r_0 = \frac{1}{6}J(J+1), \quad \varphi_0 = \varphi_1 = \cdots = \varphi_{n_s}, \quad 6\lambda_1 = \Omega + \frac{\eta}{G}|\Delta|\left(\frac{6}{J(J+1)}\right)^{1/2}, \tag{5.1.25}
$$

and r_k obeying the equations:

$$
2\left[(\epsilon_k - \lambda) - G|V_k|^2\right]U_k|V_k| - (U_k^2 - |V_k|^2)(|\Delta| - \eta r_0) = 0, \quad k = 1, \ldots, n_s. \tag{5.1.26}
$$

Note that the classical equations determining the energy minima satisfying the constraint (5.1.15) represent the BCS equations to determine the occupation probabilities U_k and $|V_k|$.

For the sake of simplicity we choose vanishing angles

$$
\varphi_k = 0, \quad k = 0, \ldots, n_s. \tag{5.1.27}
$$

which results in obtaining real value for the energy gap $\Delta^* = \Delta$ this, actually, characterizing the uncoupled system of $\eta = 0$. In order to make an easier comparison with the case of standard BCS formalism we ignore the single particle energy renormalization term due to the pairing correlations, i.e. $G|V_k|^2$. Also the coordinates of the minimum point will be accompanied by an superscript "°". Since the gap parameter (5.1.14) depends on J it results that its value in the minimum point will also depend on J and denoted by $\overset{\circ}{\Delta}_J$. Also, the following notation will be used:

$$\overset{\circ}{\Delta}_0 = \overset{\circ}{\Delta}_J - \eta \left(\frac{1}{6}J(J+1)\right)^{1/2}. \tag{5.1.28}$$

One can be proved that the classical energy exhibits a unique minimum. The solutions of constrained BCS equations are:

$$|\overset{\circ}{V}_k|^2 = \frac{1}{2}\left[1 - \frac{\epsilon_k - \lambda}{E_k}\right], \quad \overset{\circ}{U}_k^2 = \frac{1}{2}\left[1 + \frac{\epsilon_k - \lambda}{E_k}\right] \tag{5.1.29}$$

with $E_k = [(\epsilon_k - \lambda)^2 + (\overset{\circ}{\Delta}_0)]^{1/2}$ while the gap and the Fermi sea level satisfy the equations:

$$\frac{1}{2}G\sum_{k=1}^{n_s} \frac{\Omega_k}{E_k} = 1 + \frac{\eta}{\overset{\circ}{\Delta}_0}\left(\frac{1}{6}J(J+1)\right)^{1/2},$$

$$\mathcal{R}_0 = \frac{1}{6}J(J+1) + \sum_{k=1}^{n_s} \Omega_k|V_k|^2. \tag{5.1.30}$$

The minimum value of $\mathcal{H}$ is:

$$E_J^{(0)} = \sum_{k+1}^{n_s} 2(\epsilon_k - \lambda)\Omega_k|\overset{\circ}{V}_k|^2 - \frac{\overset{\circ}{\Delta}_J \overset{\circ}{\Delta}_0}{G} \tag{5.1.31}$$

Of course, for the particular case of $\eta = 0$, the results of BCS formalism are fully recovered. For nonvanishing η the BCS equations depend on the state angular momentum of the core due to the coupling and the cranking terms.

We conclude by saying that based on a semiclassical approach the results of the many body formalism called BCS (Bardeen-Cooper-Schrieffer) are recovered. Obviously, this proves that the BCS formalism has a classical origin.

In what follows we shall study the small oscillations around the minimum point. We shall prove that the oscillation amplitudes are described by a system of homogeneous linear equations of random phase approximation (RPA) type. The condition to be fulfilled in order that the system of algebraic equations be compatible, provides a dispersion equation for oscillation energies.

Aiming at this goal we shall perform a Taylor expansion of the r.h.s. of (5.1.23) around the minimum point described above and keep only the linear terms. Writing the resulting equations in terms of the deviations:

$$q_k = r_k - \overset{\circ}{r}_k, \quad p_k = \varphi_k - \overset{\circ}{\varphi}_k, \tag{5.1.32}$$

one obtains:

$$-\dot{p}_k = A_k q_k - \frac{1}{2} G F_k \sum_{k=0}^{n_s} F_i q_i,$$

$$\dot{q}_k = 2D_k \left(\overset{\circ}{\Delta}_0 p_k - G \sum_{i=0}^{n_s} D_i p_i \right), \quad k = 0, 1, \ldots, n_s. \tag{5.1.33}$$

with the notations:

$$A_k = -\frac{\overset{\circ}{\Delta}_0 \eta}{2G(\overset{\circ}{r}_0)^{3/2}} \delta_{k,0} + \frac{\overset{\circ}{\Delta}_0}{2\Omega_k (\overset{\circ}{U}_k \overset{\circ}{V}_k)^3} (1 - \delta_{k,0}),$$

$$F_k = -\frac{\eta}{G \overset{\circ}{r}_0^{1/2}} \delta_{k,0} + \frac{\overset{\circ}{U}_k^2 - \overset{\circ}{V}_k^2}{\overset{\circ}{U}_k \overset{\circ}{V}_k} (1 - \delta_{k,0}),$$

$$D_k = -\frac{\eta}{G} \overset{\circ}{r}_0^{1/2} \delta_{k,0} + \Omega_k \overset{\circ}{U}_k \overset{\circ}{V}_k (1 - \delta_{k,0}), \quad k = 0, 1, \ldots, n_s. \tag{5.1.34}$$

It is worth noting that the linearization process does not alter the conservation law for the quantity $\mathcal{R}_0$. Indeed, one can check that the quantity

$$Q_0 = \sum_{i=0}^{n_s} q_i, \tag{5.1.35}$$

is a constant of motion and on other hand Q_0 and $\mathcal{R}_0$ are, up to a constant in time, identical. In terms of the new coordinates and momenta the second order expansion of energy is:

$$\mathcal{H} = E_J^{(0)} + \sum_{i,k=0}^{n_s} (\gamma_{ik} q_i q_k + \mu_{ik} p_i p_k), \tag{5.1.36}$$

where

$$\gamma_{ik} = \frac{1}{4} (2A_k \delta_{ik} - G F_i F_k), \quad \mu_{ik} = \overset{\circ}{\Delta}_0 D_k \delta_{ik} - G D_i D_k. \tag{5.1.37}$$

Now we shall integrate the linear system of equations (5.1.33). To this end we shall determine the transformation:

$$\begin{pmatrix} P \\ Q \end{pmatrix} = \begin{pmatrix} \mathcal{G} & \mathcal{F} \\ \mathcal{U} & \mathcal{V} \end{pmatrix} \begin{pmatrix} p \\ q \end{pmatrix},$$

(5.1.38)

where $\mathcal{G}, \mathcal{F}, \mathcal{U}, \mathcal{V}$ are row vectors with $n_s + 1$ components, so that:

$$\dot{P} = -\omega Q, \quad \dot{Q} = \omega P, \quad \{Q, P\} = 1.$$

(5.1.39)

From Eq. (5.1.39) one finds a particular solution for $\mathcal{U}$ and $\mathcal{V}$:

$$\mathcal{U} = -\mathcal{G}, \quad \mathcal{V} = \mathcal{F}.$$

(5.1.40)

We can make the option for this solution without any loss of generality. Indeed, if there is a solution (P, Q, ω) of Eq. (5.1.39) then ω is unique, while P, Q are determined up to a canonical transformation which leaves the Poisson bracket invariant. Eq. (5.1.39) provides a set of equations for $\mathcal{G}_k, \mathcal{F}_k$

$$\omega \mathcal{G}_k = 2\overset{\circ}{\Delta}_0 D_k \mathcal{F}_k - 2G D_k X,$$

$$-\omega \mathcal{F}_k = -A_k \mathcal{G}_k + \frac{1}{2} G F_k \Lambda.$$

(5.1.41)

Here we used the notations:

$$X = \sum_{k=0}^{n_s} \mathcal{F}_k D_k, \quad \Lambda = \sum_{k=0}^{n_s} \mathcal{G}_k F_k.$$

(5.1.42)

Further, the solution of Eq. (5.1.41) is found following the algorithm: (i) $\mathcal{G}_k$ and $\mathcal{F}_k$ are expressed in terms of X and Λ; (ii) Inserting the results in (5.1.42) one obtains a linear and homogeneous system of equations for X and Λ; The compatibility condition provides the equation for the frequency ω:

$$\omega^2 \tilde{a} \left(\omega^2 \tilde{a} + 4\overset{\circ}{\Delta}_0^2 a \right) = \omega^2 \tilde{b},$$

(5.1.43)

where

$$\tilde{a} = \frac{\eta \overset{\circ}{r}_0^{1/2}}{\overset{\circ}{\Delta}_0 (\tilde{\eta}^2 - \omega^2)} - a, \quad \tilde{b} = b + \frac{\eta^2}{G(\tilde{\eta}^2 - \omega^2)}, \quad \tilde{\eta} = \frac{\eta \overset{\circ}{\Delta}_0}{G \overset{\circ}{r}_0^{1/2}}$$

$$a = G \sum_{k=1}^{n_s} \frac{2j_k + 1}{4E_k(4E_k^2 - \omega^2)}, \quad b = G \sum_{k=1}^{n_s} \frac{(2j_k + 1)(\epsilon_k - \lambda)}{2E_k(4E_k^2 - \omega^2)}$$

(5.1.44)

We notice that $\omega = 0$ is a solution for Eq. (5.1.43). This solution deserves a special attention and therefore will be separately treated. For $\omega \neq 0$ the dispersion equation can be written in a more suitable form:

$$\frac{\mathcal{A}_0^J}{\tilde{\eta}^2 - \omega^2} + G \sum_{k=1}^{n_s} \frac{(2j_k + 1)\mathcal{A}_k^J}{4E_k(4E_k^2 - \omega^2)} = 0, \tag{5.1.45}$$

with the notation:

$$\mathcal{A}_0^J = -\frac{\overset{\circ}{\Delta}_J - \overset{\circ}{\Delta}_0}{\overset{\circ}{\Delta}_0}\left(2\tilde{\eta}b(\tilde{\eta}) + 2(\tilde{\eta}^2 - 2\overset{\circ}{\Delta}_0^2)a(\tilde{\eta}) + \frac{\overset{\circ}{\Delta}_J - \overset{\circ}{\Delta}_0}{\overset{\circ}{\Delta}_0}\right),$$

$$\mathcal{A}_j^J = 4\frac{\overset{\circ}{\Delta}_J - \overset{\circ}{\Delta}_0}{\overset{\circ}{\Delta}_0}\frac{1}{4E_j^2 - \tilde{\eta}^2}\left[2E_j^2 - \overset{\circ}{\Delta}_0^2 + \tilde{\eta}(\epsilon_j - \lambda)\right]$$

$$-\frac{1}{2}G\sum_{k=1}^{n_s}\frac{(2j_k + 1)(\epsilon_j - \lambda)}{E_k(\epsilon_j + \epsilon_k - 2\lambda)}. \tag{5.1.46}$$

Equation (5.1.45) admits n_s solutions:

$$0 < \omega_1 < \omega_2 < \cdots < \omega_{n_s}. \tag{5.1.47}$$

For each frequency the homogeneous system of equations for X and Λ is solved up to a multiplicative constant which is later determined from Eq. $\{Q, P\} = 1$. The amplitudes $\mathcal{G}$ and $\mathcal{F}$ are determined from (5.1.41) (for details see Ref. [RCGP84]). In order to save space here we don't give their analytical expressions. One can be proved that the matrices just determined satisfy the relations:

$$\sum_{k=0}^{n_s}\mathcal{G}_{ik} = 0, \; 1 \leq i \leq n_s, \;\; \mathcal{F}\mathcal{G}^T = \mathcal{G}\mathcal{F}^T, \;\; 2\mathcal{F}\mathcal{G}^T = I, \tag{5.1.48}$$

with $I_{i,k} = \delta_{ik}, 1 \leq i \leq n_s, \; 0 \leq k \leq n_s$. In virtue of these relations the following equations hold:

$$\{Q_i, Q_k\} = \{P_i, P_k\} = 0, \;\; \{Q_i, P_k\} = \delta_{ik}, \;\;\; 1 \leq i, k \leq n_s. \tag{5.1.49}$$

The above equations assert that Q_i, P_i are canonically conjugate variables and moreover, they are mutually independent.

Now let us turn our attention to the solution $\omega = 0$. Note that there are $n_s + 1$ degrees of freedom but due to Eq. (5.1.35) only n_s are independent. As we have seen there are n_s nonvanishing frequencies characterizing n_s independent modes,

respectively. It results that $\omega = 0$ is a spurious solution. From (5.1.41), for $\omega = 0$, one obtains:

$$\mathcal{F}_k = \frac{G}{\overset{\circ}{\Delta}_0} X, \quad \mathcal{G}_k = 0, \quad 0 \leq k \leq n_s. \tag{5.1.50}$$

Inserting these in (5.1.38), one readily obtains:

$$P = Q = \frac{GX}{\overset{\circ}{\Delta}_0} Q_0, \tag{5.1.51}$$

where Q_0 is the constant of motion defined by (5.1.35). These coordinates have the Poisson bracket equal to zero and not unity as it must be according to the constraint in (5.1.39). It can be shown that Q_0 is an independent variable with respect to the conjugate coordinates Q_i, P_i with $i = 1, 2, \ldots, n_s$ since the following equations hold:

$$\{Q_0, Q_i\} = \{Q_0, P_i\} = 0, \quad 1 \leq i \leq n_s. \tag{5.1.52}$$

Moreover, since Q_0 is a constant of motion it results:

$$\{Q_0, \mathcal{H}\} = 0. \tag{5.1.53}$$

However it is possible to define a new momentum

$$P_0 = \sum_{i=0}^{n_s} f_i p_i, \tag{5.1.54}$$

so that the following relations are fulfilled:

$$\{Q_0, P_0\} = 1, \quad \{P_0, \mathcal{H}\} = -\omega_0 Q_0. \tag{5.1.55}$$

The solutions for ω_0 and f_i are:

$$\omega_0 = 2a_0 G \left(\tilde{b}_0^2 + 4a_0 \tilde{a}_0 \overset{\circ}{\Delta}_0^{\,2} \right)^{-1},$$

$$f_k = \omega_0 \left\{ \left[\frac{\Omega_k (\epsilon_k - \lambda)}{8a_0 \tilde{\eta} E_k^3} \left(b_0 \tilde{\eta} + \frac{\overset{\circ}{\Delta}_J - \overset{\circ}{\Delta}_0}{\overset{\circ}{\Delta}_0} \right) + \frac{\Omega_k \overset{\circ}{\Delta}_0^{\,2}}{4 E_k^3} \right] (1 - \delta_{k0}) \right.$$

$$\left. + \left[\frac{b_0 \tilde{\eta} + (\overset{\circ}{\Delta}_J - \overset{\circ}{\Delta}_0)/\overset{\circ}{\Delta}_0}{2a_0 \tilde{\eta}^2 G} \frac{\overset{\circ}{\Delta}_J - \overset{\circ}{\Delta}_0}{\overset{\circ}{\Delta}_0} - \frac{2G}{\overset{\circ}{\Delta}_0 \eta} r_0^{\circ 3/2} \right] \delta_{k0} \right\}. \tag{5.1.56}$$

where $a_0, b_0, \tilde{a}_0, \tilde{b}_0$ correspond to the functions $a, b, \tilde{a}, \tilde{b}$ values for $\omega = 0$. By brute calculations one finds:

$$\sum_{k=0}^{n_s} \mathcal{F}_{ik} f_k = 0, \quad 1 \leq i \leq n_s. \tag{5.1.57}$$

From here the Poisson brackets of P_0 with Q_i and P_i are obtained:

$$\{P_0, Q_i\} = \{P_0, P_i\} = 0, \quad 1 \leq i \leq n_s \tag{5.1.58}$$

Then Eq. (5.1.55) yields:

$$\overset{\bullet}{P}_0 = -\omega_0 Q_0. \tag{5.1.59}$$

The transformation (5.1.38) can be reversed for $\omega = \omega_i$ with $i = 1, 2, \ldots, n_s$:

$$q_i = \sum_{k=1}^{n_s} (P_k + Q_k) \mathcal{G}_{ki} + f_i Q_0, \quad 0 \leq i \leq n_s,$$

$$p_i = = \sum_{k=1}^{n_s} (P_k - Q_k) \mathcal{F}_{ki} + P_0, \quad 0 \leq i \leq n_s. \tag{5.1.60}$$

The time evolution of the coordinates Q_i and P_i can be obtained by integrating Eqs. (5.1.39) and (5.1.59). The result is:

$$Q_k = A_k \sin(\omega_k t + \delta_k), \quad P_k = A_k \cos(\omega_k + \delta_k), \quad 1 \leq k \leq n_s,$$
$$Q_0 = const., \quad P_0 = -\omega_0 Q_0 t + \delta_0. \tag{5.1.61}$$

The initial conditions determine the integration constants $Q_0, \delta_0, A_i, \delta_i (1 \leq i \leq n_s)$. Writing the energy function in terms of the new coordinates Q, P, the equations of motion become:

$$\frac{\partial \mathcal{H}}{\partial Pi} = \omega_i P_i (1 - \delta_{i0}), \quad \frac{\partial \mathcal{H}}{\partial Qi} = \omega_i Q_i, \quad 0 \leq i \leq n_s. \tag{5.1.62}$$

These equations can be integrated. Taking into account the relation for the minimum energy one obtains:

$$\mathcal{H} = E_J^{(0)} + \frac{1}{2} \omega_0 Q_0^2 + \sum_{i=1}^{n_s} \frac{1}{2} \omega_i (Q_i^2 + P_i^2). \tag{5.1.63}$$

Note that the energy function depends on the integration constants Q_0 and A_i. These will be determined by the quantization condition and by this the classical smooth function becomes a discrete energy. To this end we express first the action:

$$\langle \psi_{p,b} | i \frac{\partial}{\partial t} | \psi_{p,b} \rangle = \sum_{k=1}^{n_s} \frac{1}{2} \omega_k (Q_k + P_k)^2 + \omega_0 Q_0^2. \tag{5.1.64}$$

Since in the new representation the modes are decoupled from each other then to fulfill the quantization condition is sufficient that this restriction is separately obeyed by each mode:

$$\int_0^{T_k} \frac{1}{2}\omega_k(Q_k + P_k)^2 dt = 2n_k\pi, \quad 1 \le k \le n_s, \quad n_k = 0, 1, 2, \ldots,$$

$$\int_0^{T_0} \omega_0 Q_0^2 dt = 2n_0\pi, \quad n_0 = 0, 1, 2, \ldots, \tag{5.1.65}$$

where
$$T_k = 2\pi/\omega_k, \quad T_0 = 2\pi/\omega_0 Q_0. \tag{5.1.66}$$

The quantization conditions yield:

$$Q_0 = n_0, \quad \frac{1}{2}A_k^2 = n_k, \quad 1 \le k \le n_s. \tag{5.1.67}$$

Thus, one obtains the quantized form for the system energy:

$$E_{1,J} = E_{1,J}^0 + \frac{1}{2}\omega_0^{(J)} n_0^2 + \sum_{k=1}^{n_s} n_k \omega_k^{(J)}. \tag{5.1.68}$$

The additional index "(J)" suggests that ω_0 and ω_k with $k = 1, 2, \ldots, n_s$ depend on the core's angular momentum.

Concerning the second relation from (5.1.65), some additional comments are necessary. We have seen that P_0 is a linear function on time. Then p_i is a superposition of periodic functions of time plus a linear function of time. The latter term implies also a periodic time dependence for the coordinates z_i since p_i is nothing but the coordinate phase. This allows us to define a pair of conjugate periodic functions:

$$\tilde{Q}_0 = \sqrt{2Q_0} \sin P_0, \quad \tilde{P}_0 = -\sqrt{2Q_0} \cos P_0. \tag{5.1.69}$$

For the new coordinates Eq. (5.1.65) becomes just the Bohr-Sommerfeld quantization rule for the periodic orbit of $\tilde{Q}_0, \tilde{P}_0$. Energies given by (5.1.68) represent the semiclassical spectrum and are an approximation for the spectrum of the quantal system described by H. The time evolution of the quantal system is given by $\psi_{p,b}$ with z, z^* dependence on time as described before. We note that the collective and individual degrees of freedom are coupled with each other in both in the stationary solution and the state describing the system's fluctuations around the equilibrium state. Now it is instructive to consider two particular situations.

(a) If the strength interactions η and G are so that the sums in (5.1.33) can be ignored, the collective and individual degrees of freedom are decoupled and through a direct integration one obtains the frequencies:

$$\omega_{coll} = |\tilde{\eta}|, \quad \omega_i = 2E_i, \quad i1, 2, \ldots, n_s. \tag{5.1.70}$$

Moreover, there is no spurious solution since the Eq. (5.1.35) is no longer valid. Actually, this is the quasiparticle approximation. The factor 2 involved in the expression of ω_i reflects the fact that we deal with an even system.

(b) The subsystem of shell model nucleons interacting through pairing is obtained as a particular case by considering $\Omega = \lambda_1 = \eta = 0$. In this case the constant of motion is:

$$Q_0' = \sum_{i=1}^{n_s} q_i. \tag{5.1.71}$$

Thus, the number of particles is conserved at the classical level. Consequently, there is no need for the particle-number equation to determine the stationary solutions. The dispersion equation for this case becomes:

$$\omega^2(\omega^2 - 4\overset{\circ}{\Delta}_0)a^2 = \omega^2 b^2. \tag{5.1.72}$$

For $\omega \neq 0$ the above equation splits into two distinct equations:

$$\sum_{k=1}^{n_s} \frac{2j_k + 1}{4E_k(2(\epsilon_k - \lambda) \pm y_k)} = 0, \quad y_k = (\omega_k^2 - 4\overset{\circ}{\Delta}_0{}^2)^{1/2}. \tag{5.1.73}$$

An alternative form for the dispersion equation giving the nonvanishing frequencies is obtained from (5.1.45):

$$\sum_{k=1}^{n_s} \frac{(2j_k + 1)\mathcal{A}_k^0}{4E_k(4E_k^2 - \omega^2)} = 0, \tag{5.1.74}$$

$$\mathcal{A}_k^0 = \sum_{k'=1}^{n_s} \frac{(2j_{k'} + 1)(\epsilon_k - \lambda)}{E_{k'}(\epsilon_k + \epsilon_{k'} - 2\lambda)} \tag{5.1.75}$$

The frequency ω_0 characterizing the spurious mode (Q_0', P_0') is:

$$\omega_0 = \frac{2a_0 G}{b_0^2 - 4a_0^2 \overset{\circ}{\Delta}_0{}^2}, \tag{5.1.76}$$

while the amplitudes f_k defining the momentum P_0' are:

$$f_k = \frac{\omega_0 \Omega_k}{8a_0 E_k^3}((\epsilon_k - \lambda)b_0 + a_0 \overset{\circ}{\Delta}_0{}^2). \tag{5.1.77}$$

To conclude, so far we have presented a time dependent formalism to treat a set of pairing correlated particles interacting with a phenomenological core. The variational state is a product of coherent states for the Weyl and SU(2) groups, respectively. The

equations for the stationary points are identical with those provided by the standard many body approach specific to the BCS formalism. The linearized equations of motion describe the system fluctuations around the minimum point of the energy function. A canonical transformation for the coordinate deviations from the equilibrium values and their conjugate momenta can be determined such that a normal mode is defined. The compatibility condition for the matrix transformation to exist yields a dispersion relation for the normal modes. The spurious solution is commented separately. The equations for mode frequencies coincide with the standard random phase approximation (RPA) equations. This way we proved that the many body approaches like BCS and RPA have a classical origin.

Of course we have to ask ourselves whether the higher RPA formalisms can be recovered through a semiclassical treatment. This feature will be treated in the following subsection.

5.1.2 On the Classical Origin of Boson Expansions

The method of boson mapping came about in the solid-state physics and has been applied to interacting electrons by Holstein and Primakoff (HP) [HolPr40] and Dyson [DYS56]. It consists in replacing the algebra of density and pair-of-particles operators by an equivalent algebra of bosons, hopefully leading to a simplification of the many fermion problem. Indeed, the problem is simpler provided the number of bosons describing the collective features of the many fermion system is small and, moreover, their interaction with other types of bosons is negligible.

Boson mapping has been consistently employed for nuclear systems from the early sixties of the last century. Several collateral subjects were opened in the field of boson mappings such those of projecting out the physical states, which satisfy the Pauli Principle, and the expansion convergence [MYT64, MYTT64, JDFJ71, BZ62, S67, P68, PW70, KT71, M7174, RS77, Ho68, DO81, RCSS73, YK81, KY81]. Various view points were presented in connection with the boson mapping. We mention only two of them namely (a) that of Yamamura and Kuriama, and Marumori which achieve the HP mapping for the particle-hole operators through the classical phase space [YK81, KY81] associated to the quantal system and (b) that of Dobaczewski who mapped a fermion sub-algebra onto the classical holomorphic functions [DO81].

The procedure described below is somewhat related to that of Yamamura and Kuriama. Indeed, we quantize first the canonical complex coordinates and consequently the classical images of the algebra elements become generators for a boson realization of the considered algebra.

In this context we consider here the quasispin operators:

$$S_0^k = \frac{1}{2}(\hat{N}_k - \Omega_k),$$

$$S_+^k = \frac{1}{2}\sum_{m=-j_k}^{j_k} s_{k,m} c_{k,m}^+ c_{k,-m}^+,$$

$$S_-^k = \frac{1}{2} \sum_{m=-j_k}^{j_k} s_{k,m} c_{k,-m} c_{km}, \quad s_{k,m} = (-)^{j_k-m}. \tag{5.1.78}$$

associated to a single shell j_k. These operators satisfy the commutation relations:

$$[S_0^k, S_\pm^k] = \pm S_\pm^k, \quad [S_+^k, S_-^k] = 2S_0^k. \tag{5.1.79}$$

which are specific to the fermionic $SU_f(2)$ algebra. Let us introduce now the complex coordinates C_k, C_k^*, related with the canonical conjugate variables r_k and φ_k defined before, by:

$$C_k = \sqrt{\frac{1}{2}}(r_k + i\varphi_k), \quad C_k^* = \sqrt{\frac{1}{2}}(r_k - i\varphi_k), \quad k = 0, 1, \dots, n_s. \tag{5.1.80}$$

The equations of motion for the complex variables C_k, C_k^* are:

$$\{C_k, \mathcal{H}\} = \dot{C}_k, \quad \{C_k^*, \mathcal{H}\} = \dot{C}_k^*. \tag{5.1.81}$$

The Poisson bracket of the two complex coordinates is:

$$\{C_k^*, C_{k'}\} = i\delta_{k,k'}. \tag{5.1.82}$$

The average values of the algebra elements with the trial function $\psi_{p,b}$ are:

$$\begin{aligned}
\mathcal{S}_0^k &\equiv \langle \psi_{p,b} | S_0^k | \psi_{p,b} \rangle = \Omega_k (V_k V_k^* - \frac{1}{2}) = \sqrt{\frac{1}{2}}(C_k + C_k^*) - \frac{1}{2}\Omega_k, \\
\mathcal{S}_+^k &\equiv \langle \psi_{p,b} | S_+^k | \psi_{p,b} \rangle = \Omega_k U_k V_k = \Omega_k \\
&\quad \times e^{(C_k - C_k^*)/2\sqrt{2}} \left[\left(1 - \frac{C_k + C_k^*}{\sqrt{2}\Omega_k}\right)\left(\frac{C_k + C_k^*}{\sqrt{2}\Omega_k}\right)\right]^{1/2} e^{(C_k - C_k^*)/2\sqrt{2}}, \\
\mathcal{S}_-^k &\equiv \langle \psi_{p,b} | S_-^k | \psi_{p,b} \rangle = \Omega_k U_k V_k^* = \Omega_k \\
&\quad \times e^{-(C_k - C_k^*)/2\sqrt{2}} \left[\frac{C_k + C_k^*}{\sqrt{2}\Omega_k} \left(1 - \frac{C_k + C_k^*}{\sqrt{2}\Omega_k}\right)\right]^{1/2} e^{-(C_k - C_k^*)/2\sqrt{2}}.
\end{aligned}$$
$$\tag{5.1.83}$$

The classical functions defined above satisfy the relations:

$$\{\mathcal{S}_0^k, \mathcal{S}_\pm^k\} = \pm i\mathcal{S}_\pm^k, \quad \{\mathcal{S}_+^k, \mathcal{S}_-^k\} = -2i\mathcal{S}_0^k. \tag{5.1.84}$$

In virtue of these relations, the complex functions $\mathcal{S}_0^k$, $\mathcal{S}_+^k$, $\mathcal{S}_-^k$ are the generators of a classical $SU_c(2)$ algebra having the multiplication operation defined through the Poisson bracket.

To the pair of conjugate coordinates we shall associate the operators B_k and B_k^+

$$C_k \to B_k, \quad C_k^* \to B_k^+, \tag{5.1.85}$$

obeying the commutation relations:

$$[B_k, B_{k'}^+] = \delta_{kk'}, \quad [B_k, B_{k'}] = [B_k^+, B_{k'}^+] = 0. \tag{5.1.86}$$

The images of $\mathcal{S}_i^k$ ($i = 0, \pm$) through the above transformations are:

$$S_{0,B}^k = \sqrt{\frac{1}{2}} \left(B_k^+ + B_k \right) - \frac{1}{2}\Omega_k,$$

$$S_{+,B}^k = \Omega_k e^{(B_k^+ - B_k)/2\sqrt{2}} \left[\left(1 - \frac{B_k^+ + B_k}{\sqrt{2}\Omega_k} \right) \frac{B_k^+ + B_k}{\sqrt{2}\Omega_k} \right]^{1/2} e^{(B_k^+ - B_k)/2\sqrt{2}},$$

$$S_{-,B}^k = \Omega_k e^{-(B_k^+ - B_k)/2\sqrt{2}} \left[\frac{B_k^+ + B_k}{\sqrt{2}\Omega_k} \left(1 - \frac{B_k^+ + B_k}{\sqrt{2}\Omega_k} \right) \right]^{1/2} e^{-(B_k^+ - B_k)/2\sqrt{2}}.$$

$$\tag{5.1.87}$$

Using now the commutation relation:

$$[B_k^+ + B_k, e^{\pm(B_k^+ - B_k)/2\sqrt{2}}] = \pm\sqrt{\frac{1}{2}} e^{\pm(B_k^+ - B_k)/2\sqrt{2}}, \tag{5.1.88}$$

it can be proved that the operators $S_{i,B}^k, i = 0, \pm$ obey the same commutation relations as the initial quasi-spin components operators. Therefore, they are generators of the boson representation of the $SU_b(2)$ algebra. The homeomorphism of the two representations of the SU(2) algebra is conventionally called the boson expansion or representation of the fermionic SU(2) algebra. Concluding, the boson mapping of the fermionic SU(2) algebra is achieved according to the following diagram:

$$\begin{array}{ccc} \mathcal{S}_i^k, \; [\mathcal{S}_i^k, \mathcal{S}_j^k] & & \\ \downarrow & \searrow & \\ \mathcal{S}_i^k, \; i\{\mathcal{S}_i^k, \mathcal{S}_j^k\} \longrightarrow & S_{i,B}^k, \; [S_{i,B}^k, S_{j,B}^k] \end{array} \tag{5.1.89}$$

The above diagram shows that the mapping of the fermionic algebra onto the boson algebra is a product of two mappings, one which links the fermionic algebra to the classical one and another from the classical $SU_c(2)$ algebra to the boson type one. Such property makes the diagram commutative. Note that the construction described above depends essentially on the complex coordinates defined with the canonical

ones, r_k and φ_k. Are these coordinates unique? The answer is "no". There are also other coordinates determined, according to the Frobenius Darboux theorem [CAR22] by the equation:

$$\sum_{k=1}^{ns}\left[\langle\psi_{p,b}|\frac{\partial}{\partial C_k}|\psi_{p,b}\rangle dC_k + \langle\psi_{p,b}|\frac{\partial}{\partial C_k^*}|\psi_{p,b}\rangle dC_k^*\right] = \sum_{k=1}^{n_s}[C_k^* dC_k - C_k dC_k^*].$$

(5.1.90)

A solution of this equation is:

$$C_k^* = \sqrt{\Omega_k}V_k, \quad C_k = \sqrt{\Omega_k}V_k^*.$$

(5.1.91)

It is worthwhile noting that these coordinates satisfy the Eqs. (5.1.81) and (5.1.82). The averages of the fermionic algebra $S_i^k, i = 0, \pm$ with the function $\psi_{p,b}$ can be expressed in terms of the newly introduced coordinates:

$$\mathcal{S}_0^k = C_k^* C_k - \frac{1}{2}\Omega_k,$$

$$\mathcal{S}_+^k = \sqrt{\Omega_k}C_k^*(1 - C_k^* C_k/\Omega_k)^{1/2},$$

$$\mathcal{S}_-^k = \sqrt{\Omega_k}(1 - C_k^* C_k/\Omega_k)^{1/2}C_k.$$

(5.1.92)

The complex functions $\mathcal{S}_i^k, \ i = 0, \pm$ obey the commutation relations for the classical $SU_c(2)$ algebra having the Poisson bracket as multiplication operation. Further, this algebra is mapped onto the boson algebra by:

$$C_k \rightarrow B_k, C_k^* \rightarrow B_k^+.$$

(5.1.93)

This way one obtains the HF boson mapping of the quasispin algebra:

$$S_{0,HP}^k = B_k^+ B_k - \frac{1}{2}\Omega_k,$$

$$S_{+,HP}^k = \sqrt{\Omega_k}B_k^+(1 - B_k^+ B_k/\Omega_k)^{1/2},$$

$$S_{-,HP}^k = \sqrt{\Omega_k}(1 - B_k^+ B_k/\Omega_k)^{1/2}B_k.$$

(5.1.94)

Concerning the D boson mapping of the quasispin algebra this is generated by the complex coordinates:

$$C_k^* = \sqrt{\Omega_k}U_k V_k, \quad C_{1,k} = \sqrt{\Omega_k}\frac{V_k^*}{U_k}.$$

(5.1.95)

Expressing the averages $\langle\psi_{p,b}|S_i^k|\psi_{p,b}\rangle$ with $i = 0, \pm$, in terms of the complex coordinates $C_k^*, C_{1,k}$ and then quantizing the classical complex coordinates by

$$C_k^* \rightarrow b_k^+, \quad C_1, k \rightarrow b_k,$$

(5.1.96)

one obtains the D boson mapping:

$$S_{0,D}^{k} = b_{k}^{+} b_{k} - \frac{1}{2}\Omega_{k},$$

$$S_{+,D}^{k} = \sqrt{\Omega_{k}} b_{k}^{+},$$

$$S_{-,D}^{k} = \sqrt{\Omega_{k}}(1 - b_{k}^{+} b_{k}/\Omega_{k}) b_{k}. \tag{5.1.97}$$

The three boson representation described above exhibit two common features: (i) all three satisfy the Eqs. (5.1.81), (5.1.82) and (5.1.84); (ii) the diagram (5.1.89) is commutative. In contrast to the others, the D-representation is a "finite" expansion, which does not preserve the hermiticity. Indeed, one could check that $S_{+,D}^{k} \neq (S_{-,D}^{k})^{+}$. In the classical representation it is easy to relate the coordinates generating the three boson expansions, respectively. Further, after quantization, one obtains the relation between the three kinds of bosons. In general, any transformation preserving their Poisson bracket yields a new boson expansion for the quasispin operators. This property proves the fact that the boson expansions can be determined up to a canonical transformation.

Note that each choice of the coordinates in the phase space implies a boson mapping of the initial many body Hamiltonian H which, of course, deviates from the harmonic picture. Certainly, the most suitable boson expansion for a given Hamiltonian H is that for which H_B is closest to its harmonic approximation. To be more specific let us consider the bosons $\mathcal{B}_i$, $\mathcal{B}_i^{+}$ and $\tilde{\mathcal{B}}_0$, $\tilde{\mathcal{B}}_0^{+}$ corresponding to the coordinate Q_i, P_i and $\tilde{Q}_0, \tilde{P}_0$ according to the procedure described above.

$$(H)_B = E_J^{(0)} + \frac{1}{2}\omega_0^{(J)}(\tilde{\mathcal{B}}_0^{+}\tilde{\mathcal{B}}_0)^2 + \sum_{i=1}^{n_s} \omega_i^{(J)}(\mathcal{B}_i^{+}\mathcal{B}_i + \frac{1}{2}). \tag{5.1.98}$$

Denoting by $\mathcal{C}_i$, $\mathcal{C}_i^{+}$ the boson operators corresponding to the q and p coordinates (5.1.32), and using the canonical transformation which defines Q_i, P_i on obtains the relations of these bosons with $\mathcal{B}_i, \mathcal{B}_i^{+}$.

$$\mathcal{B}_j^{+} = \frac{1}{2}(1-i)\sum_{k=0}^{n_s}\left[(\mathcal{F}_{jk}+\mathcal{G}_{jk})\mathcal{C}_k^{+} + (\mathcal{F}_{jk}-\mathcal{G}_{jk})\mathcal{C}_k\right],$$

$$\mathcal{B}_0^{+} = \frac{1}{2}\sum_{k=0}^{n_s}\left[(1+f_k)\mathcal{C}_k^{+} + (1-f_k)\mathcal{C}_k\right],$$

$$\tilde{\mathcal{B}}_0^{+} = \left(\sqrt{\frac{1}{2}}(\mathcal{B}_0^{+}+\mathcal{B}_0)\right)^{1/2} \exp(\mathcal{B}_0^{+}-\mathcal{B}_0)/\sqrt{2}. \tag{5.1.99}$$

This way $\mathcal{B}_j^{+}$ are expressed as linear combination of $\mathcal{C}_k^{+}$ and $\mathcal{C}_k$ which are the images of the classical coordinates r_k and φ_k through the boson-mapping transformation. We may conclude that the described procedure is equivalent to a local quasi-boson

approximation for $\hat{N}_k$ and its canonical conjugate ϕ_k. Alternatively, one can use the boson mapping of H by using the transformations (5.1.80) and (5.1.85):

$$H \rightarrow \mathcal{H}(r, \varphi) \rightarrow \mathcal{H}(C, C^*) \rightarrow H_B(B, B^+). \tag{5.1.100}$$

It is obvious that H_B contains complicated anharmonicities. How suitable is the above mentioned mapping to describe the eigenvalues of H is decided by the magnitude of $|\mathcal{H}(r, \varphi) - \mathcal{H}(q, p)|$. Actually, the boson expansion convergence is determined by the convergence of the Taylor expansion $\mathcal{H}(q, p)$ around the minimum point $(\overset{\circ}{r}_k, \overset{\circ}{\varphi}_k)$.

Concluding, some results concerning a powerful higher RPA procedure, namely boson expansion, are derived via classical phase space coordinates. Specific features like expansion convergence are defined by the associated Taylor expansions of the corresponding classical functions. Finally, one could say that boson expansion is based on classical arguments.

5.1.3 Short Numerical Application

In order to see how the classical treatment of the BCS and RPA approaches works, we consider the case of the lowest three bands in ^{188}Pt [FI72]. The space of the single particle states is restricted to the major neutron shell:

$2f_{7/2}, 2h_{9/2}, 1i_{13/2}, 3p_{3/2}, 2f_{5/2}, 3p_{1/2}$. The corresponding energies ϵ_k, are determined by the spherical shell model with the strength parameters for the $\mathbf{l} \cdot \mathbf{s}$ and $\mathbf{l}^2 - \langle \mathbf{l}^2 \rangle$ taken as:

$$\hbar\omega_0 = 41A^{-1/3} \text{ (MeV)}, \quad C = -0.1274 \text{ (MeV)}, \quad D = -0.0268 \text{ (MeV)}, \tag{5.1.101}$$

where A stands for the atomic mass. To the gap equation we added the condition for the particle number conservation. The paring equations have been solved taking for the pairing strength $G = 23/A$ while for the particle-core interaction strength, the values $\eta = -0.1G$. Once $\overset{\circ}{\Delta}_0$ and λ are determined one finds the quasiparticle energies as given in Table 5.1.

Table 5.1 Quasiparticle energies given in units of MeV for different values of the core-s angular momentum

	E_j				
j	J = 0	2	4	6	8
$\frac{13}{2}$	0.973	0.995	1.012	1.029	1.046
$\frac{3}{2}$	1.197	1.215	1.229	1.243	1.256
$\frac{5}{2}$	1.486	1.501	1.512	1.524	1.535
$\frac{9}{2}$	1.508	1.522	1.533	1.544	1.555
$\frac{7}{2}$	2.090	2.101	2.109	2.117	2.125
$\frac{1}{2}$	2.389	2.398	2.405	2.412	2.419

Table 5.2 The solutions $\omega_i^{(J)}$ of the dispersion equation for $0 \leq J \leq 8$

i	$\omega_i^{(J)}$				
	J = 0	2	4	6	8
1		0.272	0.361	0.437	0.503
2	1.991	2.042	2.082	2.121	2.158
3	2.634	2.666	2.691	2.717	2.742
4	2.730	2.762	2.788	2.814	2.839
5	3.923	3.945	3.962	3.979	3.996
6	4.673	4.691	4.706	4.721	4.736

Having the quasiparticle energies determined, the dispersion equation yields the system frequencies. The results are collected in Table 5.2. In the case of $J = 0$ the modes $\omega_i^{(0)}$ with $2 \leq i \leq 6$ characterize exclusively the neutron system. When $J \neq 0$ an additional mode shows up, whose energy is smaller than the lowest two-quasiparticle state, i.e. $(\nu i_{13/2})^2$. This mode is the most collective one and is located close to ω_{coll} in the quasiparticle approximation. All modes $\omega_i^{(J)}$ depend on both the collective and individual degrees of freedom. Denoting the l.h.s. of Eqs. (5.1.45) and (5.1.73) by $f_J(\omega)$ and $f_0(\omega)$ respectively, and plotting these as functions of ω and $(\omega^2 - 4\Delta^2)$ respectively, we get a picture of the mode energy distribution (Figs. 5.1 and 5.2).

These calculations involve only one free parameter, that is Ω, involved in the expression $E_J^{(0)}$ defining the ground band energies. This was slightly varied to yield for $E_2^{(0)} - E_0^{(0)}$ a value lying close to the experimental energy. Tentatively, we associate the energies

$$\bar{E}_J^{(g)} = E_J^{(0)} - E_0^{(0)}, \quad \bar{E}_J^{(1)} = \bar{E}_J^{(g)} + \omega_1^{(J)}, \quad \bar{E}_J^{(3)} = \bar{E}_J^{(g)} + 3\omega_1^{(J)}, \qquad (5.1.102)$$
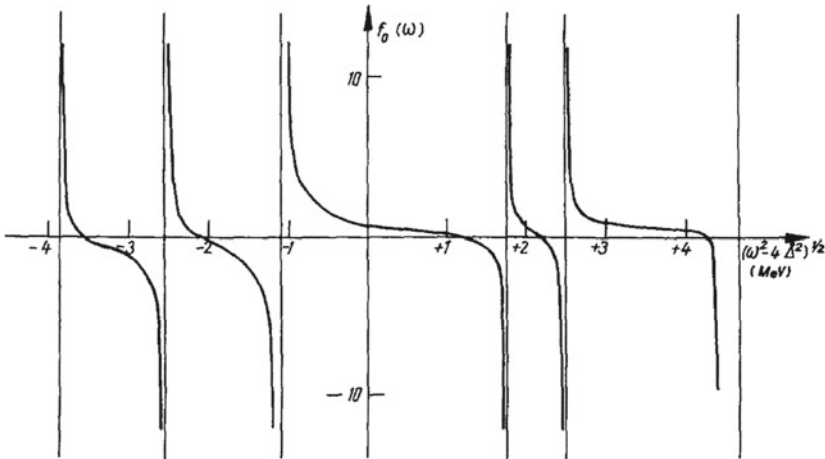
Fig. 5.1 f_0, denoting the l.h.s. of Eq. (5.1.73) is plotted as function of $(\omega^2 - 4\overset{\circ}{\Delta}{}^2)^{1/2}$
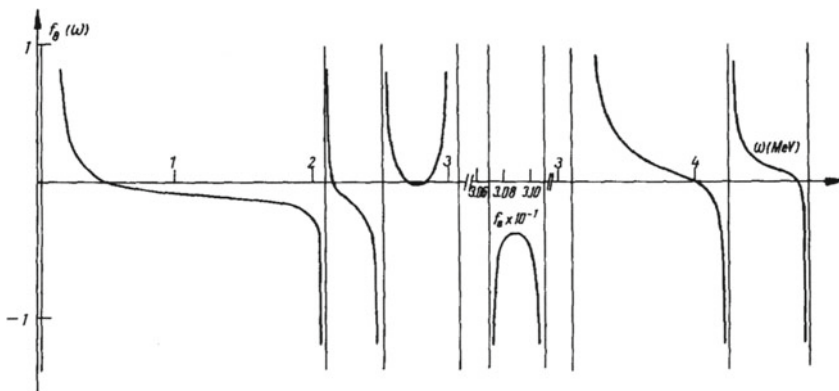
Fig. 5.2 f_8, denoting the l.h.s. of Eq. (5.1.45) for $J = 8$ is plotted as a function of ω

to the ground, gamma and beta bands states. Thus, a state of even angular momentum J from the gamma band is interpreted as one phonon state built on the top of the stationary state J_g^+ belonging to the ground band. Similarly, the state J_β^+ appears to be a three phonon state relative to the ground band state J_g^+. Note that in this picture the head state of the beta band cannot be described since there is no non-spurious mode with vanishing angular momentum. We note the good quality of the agreement of the predicted and experimental excitation energies. Discrepancies are increasing functions with the core-s angular momentum. However, for high angular momentum the anharmonicities, which are ignored here, play an important role. Also, the experimental difference $E_{2_\beta^+} - E_{2_g^+}$ is quite well described by $3\omega_1^{(2)}$ which is consistent with the viewpoint about the beta band in the Pt region, as a three phonon excitation of the ground band.

This concept is different from the traditional one where the bands are constructed in a "vertical" fashion starting with the vacuum state and the first modes of the β and γ deformation for the ground, β and γ bands, respectively (Figs. 5.3 and 5.4).

Fig. 5.3 The theoretical (Th) excitation energies $\bar{E}_J^{(g)}, \bar{E}_J^{(1)}, \bar{E}_J^{(3)}$ given in units of MeV are compared with the corresponding experimental data
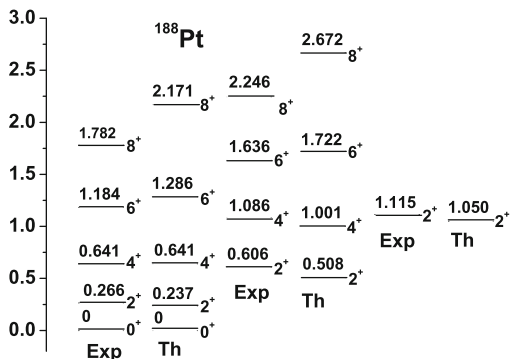
Fig. 5.4 Excitation energies in the horizontal bands $\omega_1^{(J)}$ and $3\omega_1^{(2)}$, given in units of MeV, are compared with the corresponding experimental data for ^{188}Pt [FI72], i.e. $E_{J_\gamma^+} - E_{J_\gamma^+}$ and $E_{2_\beta^+} - E_{2_g^+}$, respectively
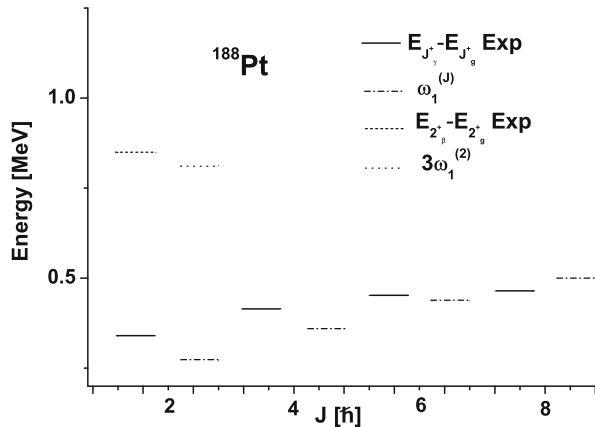
To conclude, the time dependent variational principle in a space spanned by the product of two coherent states, formulated for a particle-core Hamiltonian, yields the classical equations of motion for both the collective and individual degrees of freedom. The stationary points equations are identical to those given by the BCS formalism. Equations for classical small oscillations around the energy minimum are specific to RPA. Even the higher order RPA many-body approaches can be recovered at the classical level. This was shown for the boson representation of the quasispin algebra. A short numerical application for ^{188}Pt is presented for the formalism described in detail in this section. The RPA equations were solved for a restricted single particle space. The yrast states are given by energies in the minimum point for various core angular momenta. Adding for each J the multiphonon excitations one develops "horizontal bands" with states of equal angular momenta. Technical details necessary for deriving some of the equations in this section may be found in Ref. [RCGP84].

5.2 Generalized Nucleon-Nucleon Pairing with Isospin and Particle Number Projection

The pairing correlations of nucleons of the same charge have been extensively studied in the last five decades [BEL59, BAY60, CHA63, KISO60, RISH64, FOM70]. Some properties like the gap parameter, moments of inertia, spectroscopic factors, pairing versus nuclear deformation and angular momentum have been nicely described by many groups of theoreticians. Though not so extensively the Cooper pairs of one proton and one neutron have been also investigated [GOS64, CCJ66, JM69, WFS70, TAK71, GOO79, GOO98]. The results reported there demonstrate that the generalized Bogoliubov-Valatin transformation including *pp*, *nn* and *pn* pairing is appropriate for treating the pairing correlations in a self-consistent way, in spite of some earlier pessimistic views on this issue [LA64, FLVU63]. It turns out the proton-neutron

pairing interaction is an appealing subject not only because it is by itself an interesting issue but also because by taking it into consideration various phenomena like stability of the ground state against the particle-particle proton-neutron interaction, the structure of nuclei lying close to the proton drip-line, the structure of the $N = Z$ nuclei, the structure of super-dense nuclear matter, might be realistically approached.

In finite nuclei the standard way to account for pairing interaction is the BCS approach, where several symmetries are broken. Indeed, there are many properties which are not affected by considering the quantum numbers as average values. However, there are many features which depend strongly on the fluctuations in the ground state and therefore the broken symmetries should be rigorously restored. In particular, in a BCS treatment of a heterogeneous system of nucleons the total number of particles, the isospin (T) and the third isospin component (T_3) are not conserved. For homogeneous system the particle number is projected out by using, for example the method proposed by Fomenko in Ref. [FOM70]. If the proton and neutron systems are simultaneously considered but only alike nucleons are paired, the product of particle number projected states is a linear superposition of states $|TT_3\rangle$, with T ranging from $\frac{N-Z}{2}$ to $\frac{N+Z}{2}$. For such situations techniques to project out components of good isospin are available.

Here we treat the particle number and isospin projection under the general circumstance when one deals not only with proton-proton (pp) and neutron-neutron (nn) Cooper pairs but also with proton-neutron (pn) Cooper pairs. For realistic calculations the pairing Hamiltonian alone may not yield a good result and the quadrupole-quadrupole interaction has to be included too [KISO63]. We consider only $T = 1$ (pn) pairs since adding the $T = 0$ pairs does not change the isospin of the total wave function. Since the isospin projection operator commutes with the $T = 0$ pairs, the method discussed here is also valid when $T = 0$ pairing is included.

5.2.1 Tensorial Properties

Since the isospin projection of the BCS ground state involves rotations in the space of isospin, we shall define first the conventions about the tensorial properties of single particle creation ($c^\dagger_{\tau jm}$) and annihilation operators ($c_{\tau jm}$) for a particle in the shell model state $|\tau jm\rangle \equiv |\tau; nljm\rangle$ with τ taking the value p for protons and n for neutrons. In the space of isospin, the rotation transformations are generated by the operators:

$$\tau_{+1} = -\frac{1}{\sqrt{2}} \sum_{jm} c^\dagger_{pjm} c_{njm},$$

$$\tau_{-1} = \frac{1}{\sqrt{2}} \sum_{jm} c^\dagger_{njm} c_{pjm},$$

$$\tau_0 = \frac{1}{2}(\hat{N}_p - \hat{N}_n). \tag{5.2.1}$$

An operator T_K^I is conventionally called a tensor of rank I and projection K, with respect to the rotations in the space of isospin, if the following commutation relations are fulfilled:

$$[\tau_{\pm 1}, T_K^I] = \mp [\frac{1}{2}(I \mp K)(I \pm K + 1)]^{\frac{1}{2}} T_{K\pm 1}^I, \quad [\tau_0, T_K^I] = K T_K^I. \qquad (5.2.2)$$

It is easy to check the following commutation relations for the particle creation operators:

$$[\tau_{+1}, c_{pjm}^\dagger] = 0, \quad [\tau_{-1}, c_{pjm}^\dagger] = \frac{1}{2} c_{njm}^\dagger, \quad [\tau_0, c_{pjm}^\dagger] = \frac{1}{2} c_{pjm}^\dagger, \qquad (5.2.3)$$

$$[\tau_{+1}, c_{njm}^\dagger] = -\frac{1}{2} c_{pjm}^\dagger, \quad [\tau_{-1}, c_{njm}^\dagger] = 0, \quad [\tau_0, c_{njm}^\dagger] = -\frac{1}{2} c_{njm}^\dagger. \qquad (5.2.4)$$

Consequently, the operators $c_{pjm}^\dagger$, $c_{njm}^\dagger$ are tensors of rank $\frac{1}{2}$ and projections $\frac{1}{2}$ and $-\frac{1}{2}$, respectively. Writing the Hermitian conjugate operation for the Eqs. (5.2.3 and 5.2.4), one obtains the commutation relations of the proton and neutron annihilation operators. Thus, one obtains that c_{pjm} and $-c_{njm}$ are tensors of ranks $\frac{1}{2}$ and projections $-\frac{1}{2}$ and $\frac{1}{2}$ respectively. Analogously, one proves that the operators $\sum_m c_{pjm}^\dagger c_{\widetilde{pjm}}^\dagger$, $\sum_m c_{njm}^\dagger c_{\widetilde{njm}}^\dagger$, $\sqrt{2} \sum_m c_{pjm}^\dagger c_{\widetilde{njm}}^\dagger$ are the components $+1, -1, 0$, respectively, of a tensor of rank one.

5.2.2 pp, nn and pn Pairing

Let us consider, to begin with, a many-body Hamiltonian describing the spherical shell model single particle motion of a system of protons and neutrons interacting among themselves through proton-neutron pairing interaction

$$H_1 = \sum_{\tau=p,n;jm} (\epsilon_{\tau j} - \lambda_\tau) c_{\tau jm}^\dagger c_{\tau jm} - \frac{G_{pn}}{4} \sum_{jm;j'm'} c_{pjm}^\dagger c_{\widetilde{njm}}^\dagger c_{\widetilde{nj'm'}} c_{pj'm'}. \qquad (5.2.5)$$

This Hamiltonian can be quasi-diagonalized by a suitable Bogoliubov-Valatin (BV) transformation:

$$e^T c_{\tau jm}^\dagger e^{-T} = U_j c_{\tau jm}^\dagger - V_j c_{\widetilde{\tau' jm}} \equiv a_{\tau jm}^\dagger,$$

$$e^T c_{\tau jm} e^{-T} = U_j c_{\tau jm} - V_j^* c_{\widetilde{\tau' jm}}^\dagger \equiv a_{\tau jm},$$

$$\tau = p, n; \quad \tau' \neq \tau, \qquad (5.2.6)$$

Here $c_{\tau jm}^\dagger (c_{\tau jm})$ denotes the creation (annihilation) operator for a τ-particle in the spherical shell model state $|\tau; nljm\rangle \equiv |\tau jm\rangle$. The time reversed state corresponding

to $|\tau jm\rangle$ is $\widetilde{|\tau jm\rangle} = (-)^{j-m}|\tau j-m\rangle$. The operator $\mathcal{T}$ defining the BV transformation is:

$$\mathcal{T} = \sum_{jm}[z_{pn,j}c_{pjm}^{\dagger}c_{\widetilde{njm}}^{\dagger} - z_{pn,j}^{*}c_{\widetilde{njm}}c_{pjm}]. \tag{5.2.7}$$

The coefficients U_j, V_j are related with the amplitudes $z_{pn,j}z_{pn,j}^{*}$ by the equations:

$$z_{pn,j} = \rho_{pn}e^{i\phi_{pn}}, \quad U_j = \cos(\rho_{pn}), \quad V_j = e^{-i\phi_{pn}}\sin(\rho_{pn}). \tag{5.2.8}$$

The new operators $a_{\tau jm}^{\dagger}$, $a_{\tau jm}$ are fermionic operators. Since the *third component of the isospin is not changed by the BV transformation*, in Eq. (5.2.6), the new operators carry the same label τ as the corresponding particle operators. The vacuum state of the quasiparticle operator $a_{\tau}^{\dagger}$ is:

$$|BCS\rangle_{pn} = e^{\mathcal{T}}|0\rangle \equiv \prod_{jm}(U_j + V_j^{*}c_{pjm}^{\dagger}c_{\widetilde{njm}}^{\dagger})|0\rangle. \tag{5.2.9}$$

where $|0\rangle$ denotes the particle vacuum state. Factorizing the BV transformation, one obtains an equivalent form for the BCS wave function:

$$|BCS\rangle_{pn} = N_{pn}exp[\sum_{jm}\frac{V_j^{*}}{U_j}c_{pjm}^{\dagger}c_{\widetilde{njm}}^{\dagger}]|0\rangle,$$

$$N_{pn} = \prod_{j}U^{2\Omega_j}. \tag{5.2.10}$$

where Ω_j denotes the semi-degeneracy of the state $|\tau jm\rangle$. Since each pair has $t_3 = 0$ and $t = 1$, the $|BCS\rangle_{pn}$ function is formed by $T_3 = 0$, $0 \le T \le \sum_{j}2\Omega_j$ components. Let us now consider a more complex Hamiltonian which involves not only the p-n pairing interaction but also the proton-proton and neutron-neutron pairing interaction:

$$H = H_1 - \sum_{\tau=p,n}\frac{G_{\tau}}{4}\sum_{jm,j'm'}c_{\tau jm}^{\dagger}c_{\widetilde{\tau jm}}^{\dagger}c_{\widetilde{\tau j'm'}}c_{\tau j'm'}. \tag{5.2.11}$$

In this case the BV transformation defined above is not sufficient to include the pairing two body interaction in the mean field of the single particle motion. Therefore we have to generalize it to:

$$\alpha_{1jm}^{\dagger} = U_{ppj}c_{pjm}^{\dagger} + U_{pnj}c_{njm}^{\dagger} - V_{ppj}c_{\widetilde{pjm}} - V_{pnj}c_{\widetilde{njm}},$$

$$\alpha_{2jm}^{\dagger} = U_{npj}c_{pjm}^{\dagger} + U_{nnj}c_{njm}^{\dagger} - V_{npj}c_{\widetilde{pjm}} - V_{nnj}c_{\widetilde{njm}},$$

$$\alpha_{\widetilde{1jm}} = V_{ppj}^{*}c_{pjm}^{\dagger} + V_{pnj}^{*}c_{njm}^{\dagger} + U_{ppj}^{*}c_{\widetilde{pjm}} + U_{pnj}^{*}c_{\widetilde{njm}},$$

$$\alpha_{\widetilde{2jm}} = V_{npj}^{*}c_{pjm}^{\dagger} + V_{nnj}^{*}c_{njm}^{\dagger} + U_{npj}^{*}c_{\widetilde{pjm}} + U_{nnj}^{*}c_{\widetilde{njm}}, \tag{5.2.12}$$

The condition that the α operators describe independent fermions yield the following equations for the coefficients defining the generalized BV transformation:

$$|U_{ppj}|^2 + |U_{pnj}|^2 + |V_{ppj}|^2 + |V_{pnj}|^2 = 1,$$

$$|U_{npj}|^2 + |U_{nnj}|^2 + |V_{npj}|^2 + |V_{nnj}|^2 = 1,$$

$$U_{ppj}U_{npj}^* + U_{pnj}U_{nnj}^* + V_{ppj}V_{npj}^* + V_{pnj}V_{nnj}^* = 0,$$

$$U_{ppj}V_{npj} + U_{pnj}V_{nnj} - V_{ppj}U_{npj} - V_{pnj}U_{nnj} = 0. \tag{5.2.13}$$

To keep close to the case of a Hartree-Fock transformation in the isospin space we consider the situation where the matrix elements $U_{\tau\tau'j}$ with $\tau, \tau' = p, n$ satisfy the constraints:

$$U_{ppj} = U_{nnj} = real, \quad U_{pnj} = -U_{npj}^* \tag{5.2.14}$$

For a given isospin, the transformation satisfying these conditions and the Eq. (5.2.12) depend on 5 independent real parameters.

According to the Bloch-Messiah theorem [BLME62], the most general BV transformation can be written as a product of two Hartree-Fock transformations in the isospin variables and a simple BV transformation. In the particular case specified above, the transformation can be written as a product of one BV transformation and a rotation in the space of the isospin. Indeed, let us consider a rotation defined by a given set of Euler angles $\Omega_0^{(j)}$ and denote by α's the images of the a operators (see Eq. (5.2.6)) through this rotation:

$$\begin{pmatrix} \alpha_{1jm}^\dagger \\ \alpha_{2jm}^\dagger \end{pmatrix} = \hat{R}(\Omega_0^{(j)}) \begin{pmatrix} a_{pjm}^\dagger \\ a_{njm}^\dagger \end{pmatrix} \hat{R}(\Omega_0^{(j)})^\dagger. \tag{5.2.15}$$

Here and in what follows the superscript (j) on the Euler angles Ω_0 is used to indicate that the rotation acts only on the j-shell and that the Euler angles may depend on j. Rotating first the operators $a^\dagger$ and then expressing the result in terms of particle creation operators one obtains:

$$\alpha_{1jm}^\dagger = D_{\frac{1}{2}\frac{1}{2}}^{\frac{1}{2}} U_j c_{pjm}^\dagger + D_{-\frac{1}{2}\frac{1}{2}}^{\frac{1}{2}} U_j c_{njm}^\dagger + D_{\frac{1}{2}\frac{1}{2}}^{\frac{1}{2}} V_j c_{\widetilde{pjm}} - D_{\frac{1}{2}\frac{1}{2}}^{\frac{1}{2}} V_j c_{\widetilde{njm}},$$

$$\alpha_{2jm}^\dagger = D_{\frac{1}{2}-\frac{1}{2}}^{\frac{1}{2}} U_j c_{pjm}^\dagger + D_{-\frac{1}{2}-\frac{1}{2}}^{\frac{1}{2}} U_j c_{njm}^\dagger - D_{\frac{1}{2}-\frac{1}{2}}^{\frac{1}{2}} V_j c_{\widetilde{pjm}} + D_{-\frac{1}{2}-\frac{1}{2}}^{\frac{1}{2}} V_j c_{\widetilde{njm}},$$

$$\alpha_{\widetilde{1jm}} = -D_{-\frac{1}{2}\frac{1}{2}}^{\frac{1}{2}*} V_j^* c_{pjm}^\dagger + D_{\frac{1}{2}\frac{1}{2}}^{\frac{1}{2}*} V_j^* c_{njm}^\dagger + D_{\frac{1}{2}\frac{1}{2}}^{\frac{1}{2}*} U_j c_{\widetilde{pjm}} + D_{-\frac{1}{2}\frac{1}{2}}^{\frac{1}{2}*} U_j c_{\widetilde{njm}},$$

$$\alpha_{\widetilde{2jm}} = D_{-\frac{1}{2}-\frac{1}{2}}^{\frac{1}{2}*} V_j^* c_{pjm}^\dagger - D_{\frac{1}{2}-\frac{1}{2}}^{\frac{1}{2}*} V_j^* c_{njm}^\dagger + D_{\frac{1}{2}-\frac{1}{2}}^{\frac{1}{2}*} U_j c_{\widetilde{pjm}} + D_{-\frac{1}{2}-\frac{1}{2}}^{\frac{1}{2}*} U_j c_{\widetilde{njm}}. \tag{5.2.16}$$

where D_{MK}^J denotes the Wigner function describing the matrix element of the rotation transformation defined by the Euler angles $\Omega_0^{(j)}$. Thus, the transformation matrix

from the operators c to the operators α depend on three Euler angles $\Omega_0^{(j)}$ and two independent variables specified by U_j and $|V_j|$ coefficients. Due to this fact one could establish a one to one correspondence between the matrices involved in Eq. (5.2.12) satisfying the conditions (5.2.13) and (5.2.14) and the matrices of the coefficients of the linear equations (5.2.16).

Here we restrict our consideration to this class of matrices. A particular situation is obtained when the rotation is performed around an axes in the (X, Y) plane of the isospin space:

$$
\begin{aligned}
e^{\mathcal{T}_1} c_{pjm}^\dagger e^{-\mathcal{T}_1} &= U_j^1 c_{pjm}^\dagger - V_j^1 c_{njm}^\dagger, \\
e^{\mathcal{T}_1} c_{njm}^\dagger e^{-\mathcal{T}_1} &= U_j^1 c_{njm}^\dagger + V_j^{1*} c_{pjm}^\dagger.
\end{aligned}
\tag{5.2.17}
$$

with the Hartree Fock transformation in isospin space:

$$
\mathcal{T}_1 = \sum_{jm} [z c_{pjm}^\dagger c_{njm} - z^* c_{njm}^\dagger c_{pjm}], \quad z = \rho e^{i\phi},
$$

$$
U_j^1 = \cos(\rho), \quad V_{jm}^1 = e^{-i\phi} \sin(\rho).
\tag{5.2.18}
$$

The product of the transformations given by the Eqs. (5.2.17) and (5.2.6) yield:

$$
\begin{pmatrix}
\alpha_{1jm}^\dagger \\
\alpha_{2jm}^\dagger \\
\alpha_{\widetilde{1jm}} \\
\alpha_{\widetilde{2jm}}
\end{pmatrix}
\equiv e^{\mathcal{T}_1} e^{\mathcal{T}}
\begin{pmatrix}
c_{pjm}^\dagger \\
c_{njm}^\dagger \\
c_{\widetilde{pjm}} \\
c_{\widetilde{njm}}
\end{pmatrix}
e^{-\mathcal{T}} e^{-\mathcal{T}_1}
$$

$$
=
\begin{pmatrix}
U_j U_j^1 & -U_j V_j^1 & -V_j V_j^1 & -V_j U_j^1 \\
U_j V_j^{1*} & U_j U_j^1 & -V_j U_j^1 & V_j V_j^1 \\
V_j^* V_j^{1*} & V_j^* U_j^1 & U_j U_j^1 & -U_j V_j^{1*} \\
V_j^* U_j^1 & -V_j^* V_j^1 & U_j V_j^1 & U_j U_j^1
\end{pmatrix}
\begin{pmatrix}
c_{pjm}^\dagger \\
c_{njm}^\dagger \\
c_{\widetilde{pjm}} \\
c_{\widetilde{njm}}
\end{pmatrix}.
\tag{5.2.19}
$$

Supplementing this transformation with a rotation in the isospin space around the z axis one obtains again a five parameters transformation.

The vacuum state for the operators $\alpha_{1jm}^\dagger$, $\alpha_{2jm}^\dagger$, defined by the Eq. (5.2.19), is:

$$
|BCS\rangle \equiv \prod_{jm} \hat{R}(\Omega_0^{(j)})(U_j + V_j^* c_{pjm}^\dagger c_{\widetilde{njm}}^\dagger)|0\rangle = N_{pn}
$$

$$
\times \exp \sum_{jm} \left[\frac{V_j^*}{U_j} (c_{pjm}^\dagger c_{\widetilde{njm}}^\dagger D_{00}^1(\Omega_0^{(j)}) + \frac{1}{\sqrt{2}} c_{pjm}^\dagger c_{\widetilde{pjm}}^\dagger D_{10}^1(\Omega_0^{(j)}) \right.
$$

$$
\left. + \frac{1}{\sqrt{2}} c_{njm}^\dagger c_{\widetilde{njm}}^\dagger D_{-10}^1(\Omega_0^{(j)}))] |0\rangle
\tag{5.2.20}
$$

Clearly, the $|BCS\rangle$ state (5.2.20) obtained by the transformation (5.2.19) is as general as that corresponding to the transformation (5.2.12) and has the important advantages of providing a simpler framework for projection of particle and isospin quantum numbers. Since this function is proportional to the exponential of a sum of tensor components of isospin one, it has not definite values for T and T_3. Moreover, the total number of particles is also not preserved. The upper index (j) accompanying the Euler angles Ω_0 indicates that the rotation is to be considered on the operators associated to the orbit j. This allows that the two distinct factors entering the wave function (5.2.20) are parametrized by independent sets of parameters for each j. Note that the role of $\hat{R}(\Omega_0^{(j)})$ is to add pp and nn pairs to the system, which will eventually change the K value. If the Euler angles $\Omega_0^{(j)}$ do not depend on angular momentum then the rotation $\hat{R}(\Omega_0^{(j)})$ has the meaning of a collective rotation which fixes the orientation of the intrinsic-like frame in the space of isospin. In what follows we refer to the $|BCS\rangle$ state in Eq. (5.2.20) as the intrinsic state and to the $|BCS\rangle_{pn}$ state in Eq. (5.2.10) as the auxiliary intrinsic state.

In the next sections we derive analytical expressions for the states which are simultaneously eigenstates of the particle total number($\hat{N}$), isospin squared $\hat{T}^2$, and isospin third component ($\hat{T}_3$) operators. Such a state is projected out from the state $|BCS\rangle$ defined by the Eq. (5.2.20).

5.2.3 The Projection of the Particle Number

Here we shall project [VIL66] out the total number of particles from the generalized BCS function. Although the method adopted here is well known we are giving few details in order to make the reading easier. Suppose that one deals with a many body state $|\Phi\rangle$ which can be written as a linear combination of eigenstates of the total number of particles

$$|\Phi\rangle = \sum_m X_m |m\rangle, \qquad (5.2.21)$$

with

$$\hat{N}|m\rangle = m|m\rangle,$$
$$\hat{N} = \hat{N}_p + \hat{N}_n,$$
$$\hat{N}_\tau = \sum_{jm} c^\dagger_{\tau jm} c_{\tau jm}, \quad \tau = p, n, \qquad (5.2.22)$$

The operator

$$P_N = \frac{1}{2\pi} \int_0^{2\pi} e^{i(\hat{N}-N)\phi} d\phi \qquad (5.2.23)$$

is a projection operator for the particle number components:

$$P_N|\Phi\rangle = X_N|N\rangle \tag{5.2.24}$$

and therefore can be written in the alternative form:

$$P_N = |N\rangle\langle N| \tag{5.2.25}$$

To project out the components of a definite number of particles from the function $|BCS\rangle$ we note first that the following equations hold:

$$e^{i\hat{N}\phi}|BCS\rangle_{pn} = N_{pn}\exp[e^{i2\phi}\sum_{jm}\frac{V_j^*}{U_j}c_{pjm}^\dagger c_{\widetilde{njm}}^\dagger]|0\rangle,$$

$$\left[\hat{N}, \tau_k\right] = 0, k = \pm 1, 0 \tag{5.2.26}$$

where $\hat{\tau}_k$ are the generator operators for rotations in the space of isospin. With these preliminaries given it is easy to project the components of good particle number:

$$|N; BCS\rangle \equiv \mathcal{N}_N P_N|BCS\rangle$$

$$= \mathcal{N}_N N_{pn}\sum_{k_{j_1}+\cdots+k_{jmax}=\frac{N}{2}}\left[\prod_i\frac{1}{(k_{j_i})!}(V_{j_i}^*)^{k_{j_i}}U_{j_i}^{2\Omega_{j_i}-k_{j_i}}\hat{R}(\Omega_0^{(j_i)})\right.$$

$$\left.\times (\sum_m c_{pj_im}^\dagger c_{\widetilde{nj_im}}^\dagger)^{k_{j_i}}\right]|0\rangle \tag{5.2.27}$$

The normalization factor is denoted by $\mathcal{N}_N$ and has the expression

$$\mathcal{N}_N^{-2} = \sum_{k_{j_1}+\cdots+k_{jmax}=\frac{N}{2}}\prod_i\binom{2\Omega_{j_i}}{k_{j_i}}V_{j_i}^{2k_{j_i}}U_{j_i}^{4\Omega_{j_i}-2k_{j_i}}. \tag{5.2.28}$$

In practice, it is useful to relate the matrix elements between projected states to the matrix elements between unprojected states. To this aim it is worth expressing the projected state as being obtained by acting with an operator on the state $|BCS\rangle_{pn}$.

$$|N; BCS\rangle = \frac{\mathcal{N}_N}{2\pi}\int_0^{2\pi}e^{-iN\phi}\exp[(e^{i2\phi}-1)\sum_j\frac{V_j^*}{U_j}\hat{R}(\Omega_0^{(j)})\sum_m c_{pjm}^\dagger c_{\widetilde{njm}}^\dagger]|BCS\rangle_{pn},$$

$$\tag{5.2.29}$$

Further, the particle creation operators are expressed in terms of the quasiparticle operators which admit $|BCS\rangle_{pn}$ as a vacuum state. To have a compact form for the final result the following notation is used:

$$\widetilde{V}_j = \frac{V_j^*}{U_j}(e^{2i\phi} - 1), \ A_j^\dagger = \frac{1}{\sqrt{2\Omega_j}} \sum_m a_{pjm}^\dagger a_{\widetilde{njm}}^\dagger, \ A = (A^\dagger)^\dagger. \tag{5.2.30}$$

The exponential can be written in a more convenient form:

$$\exp[\sum_{jm} \widetilde{V}_j c_{pjm}^\dagger c_{\widetilde{njm}}^\dagger]|BCS\rangle_{pn} = \prod_j \exp[\widetilde{V}_j U_j^2 \sqrt{2\Omega_j}A_j^\dagger - \widetilde{V}_j V_j^2 \sqrt{2\Omega_j}A_j$$

$$+\widetilde{V}_j V_j U_j 2\Omega_j (1 - \frac{\hat{N}_{qp}^{(j)} + \hat{N}_{qn}^{(j)}}{2\Omega_j})]$$

$$|BCS\rangle_{pn}, \tag{5.2.31}$$

where $\hat{N}_{q\tau}^{(j)}$ denotes the τ-quasiparticle number operator for the orbit j. Since the operators involved in the r.h.s. of the Eq. (5.2.31) form a closed algebra, the exponential operator can be written as a product of three exponentials as shown and Refs. [KIR67, RG00]. Furthermore, an equivalent and simpler form is obtained for the above equation:

$$\exp[\sum_{jm} \widetilde{V}_j c_{pjm}^\dagger c_{\widetilde{njm}}^\dagger]|BCS\rangle_{pn} = \prod_j e^{\alpha_j(1)a_j A_j^\dagger} e^{\gamma_j(1)c_j}|BCS\rangle_{pn}, \tag{5.2.32}$$

where the following notations were used:

$$a_j = \widetilde{V}_j U_j^2 \sqrt{2\Omega_j}, \quad c_j = \widetilde{V}_j U_j V_j 2\Omega_j,$$

$$\alpha_j(1) = \frac{1}{1 + \frac{c_j}{\Omega_j}}, \quad \gamma_j(1) = \frac{1}{2} + \frac{1}{2}\frac{\Omega_j}{c_j} \ln\left(1 + \frac{c_j}{\Omega_j}\right). \tag{5.2.33}$$

The functions α and γ are analytically given in Ref. [RG00]. The final form for the projected state is:

$$|N; BCS\rangle = \mathcal{N}_N \sum_{k_{j_1}+\cdots+k_{jmax}=\frac{N}{2}} T_{k_{j_1}k_{j_2}\dots k_{jmax}} \prod_{i=1}^{max} \hat{R}(\Omega_0^{(j_i)})(A_{j_i}^\dagger)^{k_{j_i}}|BCS\rangle_{pn}. \tag{5.2.34}$$

The coefficients T have the expressions:

$$T_{k_{j_1}k_{j_2}\dots k_{jmax}} = \frac{1}{2\pi} \int_0^{2\pi} e^{-iN\phi} \prod_{i=1}^{max} \frac{1}{k_i!}(\alpha_{j_i}(1)a_{j_i})^{k_{j_i}} e^{\gamma_{j_i}(1)c_{j_i}} d\phi. \tag{5.2.35}$$

Analytical expressions for these coefficients are given in Ref. [RG00]. For the case of a system of nucleons of the same charge, a similar expansion was derived by Fomenko [FOM70], with the important difference that the author of Ref. [FOM70] considered the deformed single particle basis where the pairs are non-degenerate while in the case considered here pairs have the degeneracy $(2\Omega_j)$. This gives a different result for the $A^\dagger$ coefficients. For illustration let us consider the linear term in $A_j^\dagger$. In the Fomenko case the coefficient for this operator is determined exclusively by the linear term in the operator $\widetilde{V}_j c_{pjm}^\dagger c_{\widetilde{njm}}^\dagger$ while in the present paper all terms of the exponential series contribute to the final expression of the above mentioned coefficient.

5.2.4 The Projection of the Isospin

The unprojected state $|BCS\rangle$ can be written in an equivalent form:

$$|BCS\rangle = \prod_{jm}(U_j + V_j^*(D_{00}^1(\Omega_0^{(j)})c_{pjm}^\dagger c_{\widetilde{njm}}^\dagger + \frac{1}{\sqrt{2}}D_{10}^1(\Omega_0^{(j)})c_{pjm}^\dagger c_{\widetilde{pjm}}^\dagger$$

$$+ \frac{1}{\sqrt{2}}D_{-10}^1(\Omega_0^{(j)})c_{njm}^\dagger c_{\widetilde{njm}}^\dagger))|0\rangle. \tag{5.2.36}$$

From this equation it is obvious that the state $|BCS\rangle$ has not good isospin and isospin third component. Given T and T_3 values can be projected out with the operator [MOY86, VIL66, RCGD82]:

$$P_{MK}^T = \frac{2T+1}{8\pi^2}\int D_{MK}^T{}^*(\Omega)\hat{R}(\Omega)d\Omega. \tag{5.2.37}$$

Indeed, acting with this operator on a "deformed" function, considered in the intrinsic frame:

$$|\Phi\rangle = \sum_{TK}C_{TK}|TK\rangle, \tag{5.2.38}$$

where $|TK\rangle$ are eigenstates for the $\hat{T}^2$ and $\hat{T}_3$ operators, one obtains:

$$P_{MK}^T|\Phi\rangle = C_{TK}|TM\rangle. \tag{5.2.39}$$

For the sake of simplicity let us consider first the situation when the Euler angles $\Omega_0^{(j)}$ are independent of the j-value:

$$\Omega_0^{(j)} = \Omega_0. \tag{5.2.40}$$

The state of good isospin projected out of the state $|BCS\rangle$ is:

$$\phi_{TMK} = \mathcal{N}_T \frac{2T+1}{8\pi^2} \int D_{MK}^{T}{}^{*}(\Omega)\hat{R}(\Omega)\hat{R}(\Omega_0)|BCS\rangle_{pn}d\Omega. \qquad (5.2.41)$$

If Ω_0 is such that $\hat{R}(\Omega_0)$ corresponds to the unity transformation, the above equation defines the normalized state projected from $|BCS\rangle_{pn}$. Denoting by Ω' the Euler angles for the rotation $\hat{R}(\Omega)\hat{R}(\Omega_0)$, i.e.,

$$\hat{R}(\Omega') = \hat{R}(\Omega)\hat{R}(\Omega_0) \equiv \hat{R}(\Omega\Omega_0) \qquad (5.2.42)$$

the projected state can be written as follows:

$$\phi_{TMK} = \mathcal{N}_T \frac{2T+1}{8\pi^2} \sum_{K'} D_{KK'}^{T}(\Omega_0) \int D_{MK'}^{T}{}^{*}(\Omega')\hat{R}(\Omega')|BCS\rangle_{pn}d\Omega'. \qquad (5.2.43)$$

Since the state $|BCS\rangle_{pn}$ has only $K = 0$ components, in the sum involved in the above expression, only the term $K' = 0$ survives. Therefore, the final expression for the projected state is:

$$\phi_{TMK} = \mathcal{N}_T \frac{2T+1}{8\pi^2} D_{K0}^{T}(\Omega_0) \int D_{M0}^{T}{}^{*}(\Omega)\hat{R}(\Omega)|BCS\rangle_{pn}d\Omega \qquad (5.2.44)$$

From the above equation one derives the analytical expression for the normalization factor:

$$\mathcal{N}_T^{-2} = |D_{K0}^{T}(\Omega_0)|^2 {}_{pn}\langle BCS|P_{00}^{T}|BCS\rangle_{pn}. \qquad (5.2.45)$$

The matrix elements of the projector P_{00}^{T} is given analytically in Ref. [RG00]. Note that the K quantum number is associated to the projection of the isospin on the third axis of the intrinsic frame and corresponds to the $\frac{N_p - N_n}{2}$ value of the nuclear system. The reference frame where the wave function contains only $K = 0$ pairs is conventionally called auxiliary intrinsic frame. By rotating this auxiliary system with the angle Ω_0, one obtains the actual intrinsic system. According to the calculations shown in the present section, working in the subsidiary intermediate intrinsic frame brings substantial technical simplifications.

One can easily prove that the general case, where $\Omega_0^{(j)}$ may be different for each j can be obtained from (5.2.20) by the replacement:

$$\Omega_0 = \bigotimes_j \Omega_0^{(j)}. \qquad (5.2.46)$$

where the notation $\bigotimes$ stands for a shell dependent rotation of the product wave function.

Indeed, according to (5.2.20) the following relations hold:

$$\hat{R}(\Omega)|BCS\rangle = \hat{R}(\Omega) \prod_{jm} \hat{R}(\Omega_0^{(j)})(U_j + V_j^* c_{pjm}^\dagger c_{\widetilde{njm}}^\dagger)|0\rangle = \hat{R}(\Omega \bigotimes_j \Omega_0^{(j)})|BCS\rangle_{pn}.$$

(5.2.47)

Changing the integration variable from Ω to $\Omega \bigotimes_j \Omega_0^{(j)}$ and then using the addition theorem for the functions D one arrives at an expression analogous to (5.2.43). Some additional comments about how to calculate the D-function for the argument $\bigotimes_j \Omega_0^{(j)}$ are necessary. The path described before can be followed successively for each value of j. For example for the first value of the angular momentum j_1 one obtains:

$$\hat{R}(\Omega)\hat{R}(\bigotimes_j \Omega_0^{(j)}) = \hat{R}(\Omega\Omega_0^{(j_1)})\hat{R}(\bigotimes_{j\neq j_1} \Omega_0^{(j)}).$$

(5.2.48)

Changing the integration variable to

$$\Omega' = \Omega\Omega_0^{(j_1)},$$

(5.2.49)

and using

$$D_{MK}^{T}{}^*(\Omega'\Omega_0^{(j_1)^{-1}}) = \sum_{K'} D_{KK'}^{T}(\Omega_0^{(j_1)})D_{MK'}^{T}{}^*(\Omega'),$$

(5.2.50)

one separates the $\Omega^{(j_1)}$ dependence of the projected wave function. The procedure should be repeated for $j_2, j_3, \ldots, j_{max}$. The final result is:

$$\phi_{TMK} = \frac{2T+1}{8\pi^2}\mathcal{N}_T D_{K0}^{T}(\bigotimes_j \Omega_0^{(j)}) \int D_{M0}^{T}{}^*(\Omega)\hat{R}(\Omega)|BCS\rangle_{pn} d\Omega,$$

(5.2.51)

where

$$D_{K0}^{T}(\bigotimes_j \Omega_0^{(j)}) = \sum_{K_1,K_2,\ldots,K_{max-1}} D_{KK_1}^{T}(\Omega_0^{(j_1)})D_{K_1K_2}^{T}(\Omega_0^{(j_2)})\ldots D_{K_{max-1}0}^{T}(\Omega_0^{(j_{max})}),$$

$$\mathcal{N}_T^{-2} = |D_{K0}^{T}{}^*(\bigotimes_j \Omega_0^{(j)})|^2 {}_{pn}\langle BCS|P_{00}^T|BCS\rangle_{pn}.$$

(5.2.52)

5.3 Projection of Particle Number and Isospin

Combining the two projection procedures described in the previous subsections one constructs the projected state having, at a time, good particle number and good isospin and isospin third component:

$$|NTMK\rangle = \frac{2T+1}{16\pi^3}\mathcal{N}_{NT} \int D_{MK}^{T}{}^* e^{i(\hat{N}-N)\phi}\hat{R}(\Omega)\hat{R}(\Omega_0)|BCS\rangle_{pn} d\Omega d\phi,$$

(5.3.1)

where $\mathcal{N}_{NT}$ denotes the normalization factor. Since the total particle number operator $\hat{N}$ commutes with the rotation operator it is convenient to act first with the number operator on the state $|BCS\rangle_{pn}$.

$$|NTMK\rangle = \frac{2T+1}{16\pi^3}\mathcal{N}_{NT}N_{pn}\int\limits_0^{2\pi}d\phi e^{-iN\phi}$$

$$\times \int D_{MK}^{T}{}^*(\Omega)\hat{R}(\Omega\Omega_0)e^{\sum_{jm}[\frac{V_j^*}{U_j}e^{2i\phi}c_{pjm}^\dagger c_{\widetilde{njm}}^\dagger]}|0\rangle d\Omega. \tag{5.3.2}$$

Now we change the Haar measure for rotations from Ω to $\Omega' = \Omega\Omega_0$ and the argument Ω_0 is taken out of the integral by using the composition rule of the rotation matrices as described before. Thus, one obtains:

$$|NTMK\rangle = \frac{2T+1}{16\pi^3}\mathcal{N}_{NT}N_{pn}D_{K0}^T(\Omega_0)\int\limits_0^{2\pi}d\phi e^{-iN\phi}$$

$$\times \int D_{MK}^{T}{}^*(\Omega')\hat{R}(\Omega')e^{\sum_{jm}[\frac{V_j^*}{U_j}e^{2i\phi}c_{pjm}^\dagger c_{\widetilde{njm}}^\dagger]}|0\rangle d\Omega'. \tag{5.3.3}$$

The norm of the state can be calculated in a way similar to that adopted in the previous subsection where only the isospin was projected out. The result is:

$$\mathcal{N}_{NT}^{-2} = \frac{1}{2\pi}|D_{K0}^T(\Omega_0)|^2\int\limits_0^{2\pi}e^{-iN\psi}{}_{pn}\langle BCS|P_{00}^T e^{i\hat{N}\psi}|BCS\rangle_{pn}d\psi \tag{5.3.4}$$

The matrix element involved in the above equation was calculated in Ref. [RG00]. Again, we remark that the general case is obtained by considering Ω_0 given by (5.2.46).

If one wants to calculate the matrix elements for operators given in the quasiparticle representation, the projected state should be written as a many-body quasiparticle state. To this aim the isospin projection operator is to be applied to the particle number projected state given by the Eq. (5.2.34):

$$|NTKM\rangle = \frac{2T+1}{8\pi^2}\mathcal{N}_{NT}D_{K0}^T(\bigotimes_{j_i}\Omega_0^{(j_i)})\sum_{k_{j_1}+\cdots+k_{j_{max}}=\frac{N}{2}}T_{k_{j_1}k_{j_2}\ldots k_{j_{max}}}$$

$$\times \int D_{M0}^{T*}(\Omega')\hat{R}(\Omega')\prod_{i=1}^{max}(A_{j_i}^\dagger)^{k_{j_i}}|BCS\rangle_{pn}d\Omega'. \tag{5.3.5}$$

The norm is given by:

$$\mathcal{N}_{NT}^{-2} = |D_{K0}^{T}(\bigotimes_{j_i} \Omega_0^{(j_i)})|^2 \sum_{k'_{j_1},\ldots,k'_{jmax}} \sum_{k_{j_1}+\cdots+k_{jmax}=\frac{N}{2}} T^*_{k'_{j_1}k'_{j_2}\ldots k'_{jmax}} T_{k_{j_1}k_{j_2}\ldots k_{jmax}}$$

$$\times {}_{pn}\langle BCS|\left(\prod_{l=1}^{max}(A_{j_l})^{k'_{j_l}}\right)P_{00}^T\left(\prod_{i=1}^{max}(A_{j_i}^{\dagger})^{k_{j_i}}\right)|BCS\rangle_{pn}. \qquad (5.3.6)$$

The matrix element of the projector operator P_{00}^T is given explicitly in Ref. [RG00].

5.4 Numerical Application for a Single J Shell

In order to compare the results of the present approach with the exact result we consider the case of a single j for which the iso-scalar Hamiltonian considered in the previous section is exactly solvable [TAK71, FLO52]. In this case we could also derive analytical results for the unprojected BCS formalism as well as for the situations where only a partial projection, i.e. either the particle number or the isospin, is achieved. These cases are separately treated in what follows.

5.4.1 Unprojected BCS

In order to calculate the average of the model Hamiltonian on the unprojected BCS state , we use the inverse of the B-V transformation (5.2.16):

$$\begin{pmatrix} c_{pjm}^{\dagger} \\ c_{njm}^{\dagger} \\ c_{\widetilde{pjm}} \\ c_{\widetilde{njm}} \end{pmatrix} = \begin{pmatrix} sU_j\cos\frac{\beta}{2} & -\delta U_j\sin\frac{\beta}{2} & -\delta V_j\sin\frac{\beta}{2} & sV_j\cos\frac{\beta}{2} \\ \delta^*U_j\sin\frac{\beta}{2} & s^*U_j\cos\frac{\beta}{2} & s^*V_j\cos\frac{\beta}{2} & \delta^*V_j\sin\frac{\beta}{2} \\ \delta^*V_j^*\sin\frac{\beta}{2} & -s^*V_j^*\cos\frac{\beta}{2} & s^*U_j\cos\frac{\beta}{2} & -\delta^*U_j\sin\frac{\beta}{2} \\ -sV_j^*\cos\frac{\beta}{2} & -\delta V_j^*\sin\frac{\beta}{2} & \delta U_j\sin\frac{\beta}{2} & sU_j\cos\frac{\beta}{2} \end{pmatrix} \begin{pmatrix} \alpha_{1jm}^{\dagger} \\ \alpha_{2jm}^{\dagger} \\ \alpha_{\widetilde{1jm}} \\ \alpha_{\widetilde{2jm}} \end{pmatrix}.$$

$$(5.4.1)$$

where s and δ stand for the phase factors:

$$s = e^{\frac{i}{2}(\alpha+\gamma)}, \quad \delta = e^{\frac{i}{2}(\alpha-\gamma)}. \qquad (5.4.2)$$

Using the inverse transformation we calculate the gap parameters:

$$\Delta_p \equiv \langle BCS|\frac{G}{2}\sum_m c_{pjm}^{\dagger}c_{\widetilde{pjm}}^{\dagger}|BCS\rangle = G\Omega_j U_j V_j e^{i\alpha}\sin\beta,$$

$$\Delta_n \equiv \langle BCS| \frac{G}{2} \sum_m c^\dagger_{njm} c^\dagger_{\widetilde{njm}} |BCS\rangle = G\Omega_j U_j V_j e^{-i\alpha} \sin\beta,$$

$$\Delta_{pn} \equiv \langle BCS| \frac{G}{2} \sum_m c^\dagger_{pjm} c^\dagger_{\widetilde{njm}} |BCS\rangle = G\Omega_j U_j V_j \cos\beta. \qquad (5.4.3)$$

An effective gap parameter may be defined by:

$$\Delta = G\Omega_j U_j V_j. \qquad (5.4.4)$$

This gap parameter does not depend on the Euler angles (α, β, γ) and is related to the gaps defined in (5.4.3) by:

$$2|\Delta|^2 = |\Delta_p|^2 + |\Delta_n|^2 + 2|\Delta_{pn}|^2. \qquad (5.4.5)$$

The constraint for the total number of particles

$$\langle BCS|\hat{N}_p + \hat{N}_n|BCS\rangle = N, \qquad (5.4.6)$$

determines the modulus of the V parameter:

$$|V_j|^2 = \frac{N}{4\Omega_j}. \qquad (5.4.7)$$

The average of the model Hamiltonian on the BCS state is:

$$E_1 = 2\Omega_j(2\epsilon|V_j|^2 - G\Omega U_j^2|V_j|^2 - 6G|V_j|^4). \qquad (5.4.8)$$

As a function of V, the energy has a minimum and, moreover, the constraint (5.4.6) is obeyed provided the parameters ϵ and G, defining the model Hamiltonian, are related by:

$$|V_j|^2 = \frac{1}{2}(1 - \frac{\epsilon}{G\frac{\Omega_j}{2}}). \qquad (5.4.9)$$

From the above equation one extracts the expression for the quasiparticle energy

$$E_q = \frac{G\Omega_j}{2}, \qquad (5.4.10)$$

which is related to the effective gap by:

$$E_q = \sqrt{\epsilon^2 + \Delta^2}. \qquad (5.4.11)$$

The ground state energy can be expressed in terms of the total number of particles:

$$E_1 = \epsilon N - G\frac{N}{4}\left(\frac{4\Omega_j - N}{2} + \frac{3N}{4\Omega_j}\right). \qquad (5.4.12)$$

5.4.2 N-Projected BCS

In the case of a single j, the normalized N-projected BCS state has a simple form:

$$|N; BCS\rangle = \left(\frac{(2\Omega_j - \frac{N}{2})!}{(\frac{N}{2})!(2\Omega_j)!} \right)^{\frac{1}{2}} \left(\sum_m c_{pjm}^{\dagger} c_{n\overline{jm}}^{\dagger} \right)^{\frac{N}{2}} |0\rangle. \qquad (5.4.13)$$

By a direct calculation one finds the following expression for the expectation value of the model Hamiltonian in the N-projected state:

$$E_2 \equiv \langle N; BCS|H|N; BCS\rangle$$
$$= \epsilon N - G \frac{N}{4} \left[(\frac{N}{2} - 1) \frac{2}{2\Omega_j - 1} + \frac{1}{2}(4\Omega_j - N + 2) \right]. \qquad (5.4.14)$$

5.4.3 Isospin Projected BCS State

In this case the projected state $|TMK; BCS\rangle$ is given by Eq. (5.2.51). Since the model Hamiltonian is invariant to any rotation in the isospin space it commutes with the projection operator. Therefore, when its matrix element between projected states is evaluated, H can be brought aside the state $|BCS\rangle_{pn}$. Having H in this position we write it in terms of quasiparticles accepting the above mentioned state as a vacuum. The final expression for the desired average is:

$$E_3 \equiv \langle TMK; BCS|H|TMK; BCS\rangle = \epsilon N - G \frac{N}{4} \left(\frac{4\Omega_j - N}{2} + \frac{3N}{4\Omega_j} \right). \qquad (5.4.15)$$

Note that E_3 is identical to E_1. This happens because the model Hamiltonian is an isoscalar operator and there is no projection on the number of particles. For simultaneous number and isospin projection the analytical expression is more involved.

5.4.4 The Exact Eigenvalues of H

The isoscalar pairing interaction involved in our model Hamiltonian, $\hat{T}_{pair}$, can be expressed in terms of the quadratic Casimir operator of the group O(5) generated by the proton-proton, neutron-neutron and proton-neutron quasispin operators [TAK71]. Therefore, its eigenvalues have simple expressions in terms of the highest weight of the irreducible representations of the $O(5)$ group. These weights are determined by the reduced isospin t [FLO52] and seniority quantum numbers v:

$$T_{pair} = -\frac{G}{2} \left(\frac{1}{4}(N - v)(4\Omega_j - N - v + 6) + t(t + 1) - T(T + 1) \right). \qquad (5.4.16)$$

Since in our calculations both the BCS and the projected states have vanishing seniority and reduced isospin (the isospin carried by the unpaired particles) we compare our results with those of Eq. (5.4.16) for $v = t = 0$:

$$E_4 = \epsilon N - \frac{G}{2} \left(\frac{N}{4}(4\Omega_j - N + 6) - T(T+1) \right). \tag{5.4.17}$$

5.4.5 Particle Number and Isospin Projection

In numerical calculation we consider a system with four protons and eight neutrons. The states occupied by protons and neutron have equal angular momenta, $j = \frac{23}{2}$. We consider the projected states with $K = -2$ which corresponds to the T_3 value for the given system. The structure of the BCS state depends on the Euler angle Ω_0 $(=(\alpha, \beta, \gamma))$. In our application we take $\beta = \frac{\pi}{3}, \alpha = \gamma = 0$. The matrix elements of H between projected states can be derived by direct calculation. In order to get them in a compact form the following relations are very useful.

$$P_p(P_p^\dagger)^l(P_n^\dagger)^s(P_{pn}^\dagger)^m|0\rangle = 4l(\Omega_j - l - m + 1)(P_p^\dagger)^{l-1}(P_n^\dagger)^s(P_{pn}^\dagger)^m|0\rangle$$

$$- m(m-1)(P_p^\dagger)^l(P_n^\dagger)^{s+1}(P_{pn}^\dagger)^{m-2}|0\rangle,$$

$$\langle 0|(P_n)^s(P_{pn})^m(P_{pn}^\dagger)^m(P_n^\dagger)^s|0\rangle = \frac{m!(2\Omega_j - 2s)!}{(2\Omega_j - 2s - m)!} \frac{4^s s! \Omega_j!}{(\Omega_j - s)!}. \tag{5.4.18}$$

where the operators $P^\dagger$, P are particle pair operators (To simplify, we omit here the j-argument). The final result for energies is:

$$E_{NT} \equiv \langle NTMK|H|NTMK\rangle = \epsilon N - G\frac{N}{4}(2\Omega_j - \frac{N}{2} + 1)$$

$$- \frac{G}{2}\mathcal{N}_{NT}^2(N_{pn})^2|D_{K0}^T(\Omega_0)|^2 \sum_p S_p Z(\frac{N}{2}; p), \tag{5.4.19}$$

where

$$S_p = \left[4p(\Omega_j - \frac{N}{2} + p + 1)(-2)^p \binom{\Omega_j}{p} \binom{2\Omega_j - 2p}{\frac{N}{2} - 2p} \right. \tag{5.4.20}$$

$$\left. + 4(-2)^p(p+1)^2 \binom{\Omega_j}{p+1} \binom{2\Omega_j - 2(p+1)}{\frac{N}{2} - 2(p+1)} \right] (\frac{V_j}{U_j})^N.$$

The function $Z(\frac{N}{2}, p)$ involved in (5.4.19) has the expression:

$$Z(\frac{N}{2}, p) = \frac{2T+1}{2} \int_0^\pi d_{00}^T(\beta)(d_{00}^1(\beta))^{\frac{N}{2}-2p}(d_{10}^1(\beta)d_{-10}^1(\beta))^p \sin(\beta)d\beta, .$$

$$= \sum_{k,m,n}(-)^{p+k+n}\frac{(2T+1)2^{-T-p}}{m+n+\frac{N}{2}-2p+1}\binom{T}{k}^2\binom{T+p-k}{m}\binom{k+p}{n}$$

(5.4.21)

The second term in (5.4.19) is determined by the *pn* pairing while the third one is due to the *pp* and *nn* pairings which have equal contributions.

The numerical results obtained for all the cases described are represented in Fig. 5.5 for $\epsilon = 0$ and $G = 0.125$ MeV. From there one notices several features which are worth mentioning. The number projection alone has a small influence on the ground state energy. Indeed, it lowers the BCS energy by an amount of about 257 KeV. According to Ref. [FDO98] this feature depends on the number of particles considered. The isospin projection alone does not affect at all the BCS energy. This is caused by the isoscalar character of the chosen model Hamiltonian. In both cases, of N and T projection, the projected states are degenerate. If the model Hamiltonian was not isospin invariant the effect coming from the T-projection alone would lift up the corresponding degeneracy.
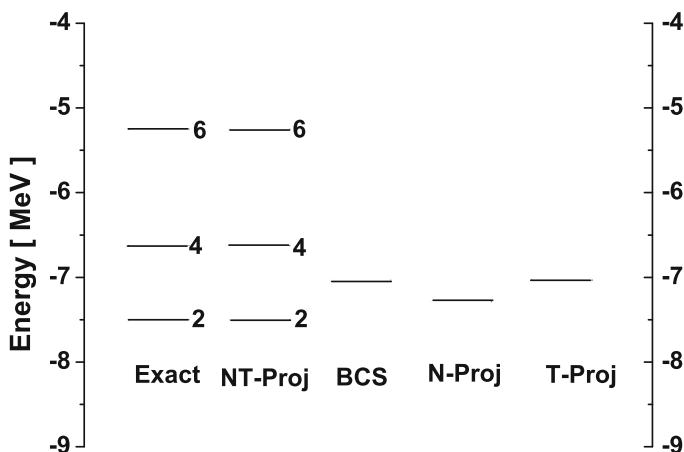
Fig. 5.5 Energies of a system of eight neutrons and four protons distributed in a shell with $j = \frac{23}{2}$ and interacting through pairing forces of a strength $G = 0.125$ MeV, obtained by different approaches—the present formalism (*second column*), BCS (*third column*), N-projected BCS (*fourth column*) and T-projected BCS (*last column*)—are compared with the exact energies given on the first column. Results are given in units of MeV. States from the first two columns are labeled by their isospin quantum number

Considering the two projections at a time, a big effect appears on the ground state energy and moreover the degeneracy is lifted up. The values of the projected isospin, for the case under study i.e., eight neutrons and four protons in the shell $j = 23/2$, are 2, 4 and 6. The selection is given by the function Z which is vanishing for odd isospin. *Remarkable the fact that the energies obtained within the present projection approach are identical with the exact ones. This proves that the NT projected states are exact eigenfunctions of H and, moreover, irreducible representation for the $O(5)$ group.*

5.4.6 Transition Probabilities

Since the $N + T$ projection has an important effect on energies and moreover modifies essentially the structure of the unprojected state we may expect an important correction to the transition probabilities. In order to get a flavor of how large such corrections could be, we study here the β^- and β^+ Fermi transitions. The corresponding transition operators are the raising (T_+) and lowering (T_-) isospin operators

$$T_+ = \sum_m c^\dagger_{pjm} c_{njm}, \quad T_- = \sum_m c^\dagger_{njm} c_{pjm}. \tag{5.4.22}$$

For the unprojected BCS state such a transition may take place from the ground state of the (N, Z) system ($N = 8, Z = 4$ in our case), described by $|BCS\rangle$, to one of the three quasiparticle states:

$$|11\rangle = \frac{1}{2\sqrt{\Omega_j}} \sum_{m>0} \alpha^\dagger_{1jm} \alpha^\dagger_{\widetilde{1jm}} |BCS\rangle,$$

$$|22\rangle = \frac{1}{2\sqrt{\Omega_j}} \sum_{m>0} \alpha^\dagger_{2jm} \alpha^\dagger_{\widetilde{2jm}} |BCS\rangle,$$

$$|12\rangle = \frac{1}{\sqrt{2\Omega_j}} \sum_m \alpha^\dagger_{1jm} \alpha^\dagger_{\widetilde{2jm}} |BCS\rangle. \tag{5.4.23}$$

Keeping in mind the structure of the quasiparticle operators and the fact that the major component of the state $|BCS\rangle$ is associated to the nucleus (N, Z) one realizes that the two quasiparticle states have components describing the neighboring nuclei $(N, Z+2), (N-1, Z-1), (N-1, Z+1), (N+1, Z-1), (N+1, Z+1), (N, Z-2), (N+2, Z), (N-2, Z)$. The third and fourth components mentioned above are the daughter nuclei of the β^- and β^+ decay processes. Writing the transition operators in terms of the quasiparticle operators one obtains the following expressions for the transition amplitudes:

$$\langle BCS|T_-|11\rangle = \sqrt{4\Omega_j} s^{*2} U_j V_j \cos^2 \frac{\beta}{2},$$

$$\langle BCS|T_-|22\rangle = -\sqrt{4\Omega_j} \delta^{*2} U_j V_j \sin^2 \frac{\beta}{2},$$

$$\langle BCS|T_-|12\rangle = 0,$$

$$\langle BCS|T_+|11\rangle = -\sqrt{4\Omega_j}\delta^2 U_j V_j \sin^2\frac{\beta}{2},$$

$$\langle BCS|T_+|22\rangle = \sqrt{4\Omega_j}s^2 U_j V_j \cos^2\frac{\beta}{2},$$

$$\langle BCS|T_+|12\rangle = 0. \tag{5.4.24}$$

Squaring these amplitudes and considering the data mentioned above for a single j case we obtain the following probabilities for the β^- transitions:

$$|\langle BCS|T_-|11\rangle|^2 = 5.06,$$
$$|\langle BCS|T_-|22\rangle|^2 = 0.56,$$
$$|\langle BCS|T_-|12\rangle|^2 = 0. \tag{5.4.25}$$

In a similar way one calculates the probabilities for the β^+ decay.

$$\langle BCS|T_+|11\rangle|^2 = 0.56,$$
$$\langle BCS|T_+|22\rangle|^2 = 5.06,$$
$$\langle BCS|T_+|12\rangle|^2 = 0. \tag{5.4.26}$$

The total strengths for beta minus and beta plus transitions are equal to each other:

$$\beta^{(-)} = \beta^{(+)} = 5.62 \tag{5.4.27}$$

In virtue of the above equation the $N - Z$ sum rule is drastically violated, unless we consider the $N = Z$ case. Indeed, in the unprojected BCS case the sum rule is vanishing while the $N - Z$ value is equal to 4.

Now let us focus our attention on the T and N projected states. Due to the structure of the unprojected BCS state one could project out the isospin and the total number of particles simultaneously for even-even and the neighboring odd-odd nuclei. The projected states for the mother and daughter nuclei are characterized by the same isospin and total number of particles. The K quantum number differ by one unit, i.e. $\Delta K = \pm 1$. Since the transition operator acts on the many body state, as defined before, the transition amplitudes for the β^- and β^+ are readily obtained:

$$\langle NTMK|T_-|NTMK+1\rangle = \sqrt{(T-K)(T+K+1)},$$
$$\langle NTMK|T_+|NTMK-1\rangle = \sqrt{(T+K)(T-K+1)}. \tag{5.4.28}$$

In contrast to the unprojected state, here the mother nucleus may be in any of the three projected states with isospin 2, 4 and 6. For each of these situations the mother nucleus decays to only one state by a β^- transition and to another single state by a β^+ transition. Therefore the strengths for the three beta minus transitions are equal to 4, 18 and 40 respectively. The strengths for the β^+ transition from the projected states with T equal to 2, 4 and 6 are equal to 0, 14 and 36, respectively. Taking the

square of the above equations and subtracting the result for the second from the result for the first equation one obtains the sum rule:

$$\beta^{(-)} - \beta^{(+)} = -2K = N - Z. \qquad (5.4.29)$$

To conclude, the sum rule is obeyed by any of the three $(T = 2, 4, 6)$ projected states. Comparing the magnitudes of the probabilities for the three transitions we remark on a strong dependence on the T quantum number. Comparing the results for the ground state $(T = 2)$ decay probabilities with the corresponding probabilities of the unprojected BCS state the following conclusions may be drawn. For $|BCS\rangle$ the β^- strength is 5.62 and this is comparable to the corresponding data for the $T = 2$ state, which is 4. By contrary, concerning the β^+ strength the discrepancy is large. For unprojected case the strength is 5.62 while for the projected $T = 2$ state the β^+ transition is forbidden.

Let us summarize the main results described in this section. We addressed the problem of isospin and particle number projection from the quasiparticle ground state of a system with isovector proton-neutron pairing, in addition to proton-proton and neutron-neutron pairing. In this case, the resulting BCS state also breaks, in general, the charge symmetry and does not have good T_3 value. For this general case we presented a formalism to restore gauge and isospin symmetries that is based on a specific form of the corresponding Bogoliubov-Valatin (BV) transformation.

We show that within a given j-shell the general 5 parameter BV transformation can be expressed as a rotation in the space of isospin performed on a simpler two-parameter dependent BV transformation that involves only one kind of pairs in the isovector pair multiplet. We can therefore express the vacuum of the corresponding 5-parameter dependent quasiparticles as a product of such transformations applied on the particle vacuum. This quasiparticle BCS vacuum has neither a definite particle number nor a good isospin. For clarity, we restored the symmetries in several steps. First we projected out the total number of particles and then from the same "deformed" state we projected out the components of good isospin. Finally both symmetries are restored at a time. The projected states are written alternatively in the particle and quasiparticle representations. Therefore the results can be used for treating operators written both in the particle and the quasiparticle representation.

The fact that the BCS state can be expressed in terms of isospin rotations of an auxiliary BCS state, made only of proton-neutron pairs, allows to perform analytically the integration over the gauge variable and Euler angles involved in the particle number and isospin projection respectively. This fact is fully exploited to provide analytical expressions for the norms of the projected states as well as their energy expectation values and transition matrix elements of one body operators.

The effect of projection on energies and transition probabilities was quantitatively studied for a single j case where the model Hamiltonian is solvable. The conclusion is that the projection is very important for both energies and transition probabilities. *Concerning energies, the results for the projected states are identical with the exact ones. This proves that the NT-projected state is in fact an irreducible representation of the group $O(5)$. In fact this is a nice example of generating a basis from a coherent state.*

5.5 Bogoliubov Transformation for Bosons

We consider separately the case of bosons with vanishing momentum and that of bosons carrying nonvanishing momentum.

5.5.1 Bosons with Zero Momentum

Let $a^\dagger$ and a be the creation and annihilation operators for a particle of boson type:

$$\left[a, a^\dagger\right] = 1. \tag{5.5.1}$$

This boson has no angular momentum and no linear momentum. The Fock space, $\mathcal{F}_a$, generated by this boson is spanned by the multi-boson states::

$$|m\rangle = \left(1/\sqrt{m!}\right)\left(a^\dagger\right)^m |0\rangle, \tag{5.5.2}$$

where $|0\rangle$ is the vacuum state defined as:

$$a|0\rangle = 0. \tag{5.5.3}$$

The Bogoliubov (B) transformation for bosons is defined by the operator:

$$T = e^S, \quad S = -\frac{1}{2}y\left(a^{\dagger 2} - a^2\right), \quad y = \text{real}. \tag{5.5.4}$$

This operator transforms linearly the boson operators $a^\dagger$ and a:

$$Ta^\dagger T^\dagger = Ua^\dagger + Va \equiv b^\dagger,$$
$$TaT^\dagger = Ua + Va^\dagger \equiv b, \tag{5.5.5}$$

where the following notations have been used:

$$U = \cosh y, \quad V = \sinh y. \tag{5.5.6}$$

Te new operators obey boson type commutation relations

$$\left[b, b^\dagger\right] = 1. \tag{5.5.7}$$

In virtue of this relation the B transformation is called *canonical transformation*.
    The Fock space corresponding to the new bosons, $\mathcal{F}_b$, is spanned by the states:

$$|\tilde{m}\rangle = T|m\rangle = \left(1/\sqrt{m!}\right)\left(b^\dagger\right)^m |\tilde{0}\rangle, \quad b|\tilde{0}\rangle = 0. \tag{5.5.8}$$

In many circumstances one needs to know the *overlap matrix* of states from the two Fock spaces [RBB77]:

$$G_{n,m}(y) = \langle n | \tilde{m} \rangle. \tag{5.5.9}$$

Aiming to this goal we define the oscillator Hamiltonian:

$$H = \frac{p^2}{2M} + Kx^2 \tag{5.5.10}$$

associated to the conjugate coordinates defined with the boson operators a si $a^\dagger$:

$$x = \alpha(a^\dagger + a), \quad p = \frac{i}{2\alpha}(a^\dagger - a) \tag{5.5.11}$$

where $\alpha = (8KM)^{-1/4}$. In terms of bosons H can be written as:

$$H = \omega(a^\dagger a + \frac{1}{2}), \quad \omega = \left(\frac{2K}{M}\right)^{\frac{1}{2}}. \tag{5.5.12}$$

Obviously, the states $|n\rangle$ of the space $\mathcal{F}_a$ are eigenfunctions of H corresponding to the eigenvalues $\omega(n + 1/2)$. In the configuration space these states have the expression:

$$|n\rangle = N_n(\alpha) \exp\left(-x^2/4\alpha^2\right) H_n\left(x/\sqrt{2}\alpha\right),$$

$$N_n(\alpha) = \left(2^n n! \alpha \sqrt{2\pi}\right)^{-1/2}, \tag{5.5.13}$$

with H_n Hermite polynomial of rank n. The image of H through B is:

$$H' \equiv THT^+ = \omega\left[\left(U^2 + V^2\right)a^\dagger a + UV\left(a^{\dagger 2} + a^2\right) + \left(V^2 + \frac{1}{2}\right)\right]. \tag{5.5.14}$$

Alternatively, H can be written in terms of the new bosons:

$$H' = \omega\left(b^\dagger b + \frac{1}{2}\right). \tag{5.5.15}$$

On other hand the Hamiltonian H' can be also written in terms of the variables (x, p) defined above:

$$H' = \omega\alpha^2(U - V)^2 p^2 + \left[\omega(U + V)^2/4\alpha^2\right]x^2. \tag{5.5.16}$$

We recognize the oscillator Hamiltonian characterized by:

$$M_1 = \left[2\omega\alpha^2(U - V)^2\right]^{-1}, \quad K_1 = \omega(U + V)^2/4\alpha^2,$$

$$\alpha_1 = e^{-y}\alpha, \quad \omega_1 = \omega. \tag{5.5.17}$$

From Eq. (5.5.15) it results that the state $|\tilde{m}\rangle$ is eigenfunction of H' corresponding to the eigenvalue $\omega(m + \frac{1}{2})$ and therefore have the expressions:

$$|\tilde{m}\rangle = N_m(\alpha_1) \exp(-x^2/4\alpha_1^2) H_m(x/\sqrt{(2\alpha_1)}). \qquad (5.5.18)$$

Thus, *the overlap matrix* becomes:

$$G_{n,m}(x) = N_n(\alpha)N_m(\alpha_1)\alpha\sqrt{2}I_{nm}, \qquad (5.5.19)$$

with the notation:

$$I_{nm} = \int\limits_{-\infty}^{\infty} \exp\left[-z^2(\beta^2 + 1)/2\right] H_n(z)H_m(\beta z)dz, \quad \beta = e^y. \qquad (5.5.20)$$

This way, to calculate the overlap matrix we have to perform the integrals I_{nm}. To this end we use the generator function method which defines the Hermite polynomial as coefficients of a power series expansion:

$$\exp\left(-t^2 + 2tz\right) = \sum_{n=0}^{\infty} \frac{t^n}{n!} H_n(z),$$

$$\exp\left(-s^2 + 2s\beta z\right) = \sum_{m=0}^{\infty} \frac{s^m}{m!} H_m(\beta z). \qquad (5.5.21)$$

Multiplying the Eq. (5.5.21), side by side, and integrating the result with the weighting function $\exp\left[-z^2(\beta^2 + 1)/2\right]$, one obtains:

$$(\pi/\beta U)^{1/2} \exp\left(-\frac{V}{U}t^2 - \frac{V}{U}s^2 + \frac{2}{U}ts\right) = \sum \frac{t^n s^m}{n!m!} I_{nm}. \qquad (5.5.22)$$

Expanding the l.h.s. of this relation in power series of t and s and then identifying the coefficients of the series from the two sides we obtain I_{nm} and then:

$$G_{n,m}(y) = \sqrt{n!m!}\,(\cosh)^{-(m+n+1)/2}$$

$$\times \sum_q \frac{(-1)^{(n-q)/2}}{q!\left[(n-q)/2\right]!\left[(m-q)/2\right]!} \left(\frac{1}{2}\sinh\right)^{(m+n)/2-q}. \qquad (5.5.23)$$

Summation in Eq. (5.5.23) must obey the constraints:

$$n - q = \text{even}, \quad m - q = \text{even}, \quad q \leq \min(m, n). \qquad (5.5.24)$$

Having $G_{n,m}$ determined we can express the states from $\mathcal{F}_b$ in terms of those from $\mathcal{F}_a$:

$$|\tilde{m}\rangle = \sum_n G_{nm}(y)|n\rangle. \qquad (5.5.25)$$

Note that the transformation T is actually a coherent state for the group $SU(1, 1)$, generated by:

$$K_+ = \frac{1}{2}(a^\dagger)^2, \quad K_- = \frac{1}{2}a^2, \quad K_0 = \frac{1}{2}\left(a^\dagger a + \frac{1}{2}\right). \tag{5.5.26}$$

5.5.2 Boson with Linear Momentum

Here we consider a set of boson operators $\{a_\beta^\dagger\}_{\beta=\pm k}$ which create a particle in a state of momentum $\beta \neq 0$. They satisfy the commutation relations:

$$[a_\beta, a_{\beta'}^\dagger] = \delta_{\beta,\beta'}, \quad [a_\beta, a_{\beta'}] = [a_\beta^\dagger, a_{\beta'}^\dagger] = 0, \quad \beta, \beta' = \pm k \neq 0. \tag{5.5.27}$$

The Fock space is spanned by:

$$|m, n\rangle = \left[(a_k^\dagger)^m (a_{-k}^\dagger)^n / \sqrt{m!n!}\right] |0, 0\rangle,$$
$$a_\beta|0, 0\rangle = 0, \quad \beta = \pm k. \tag{5.5.28}$$

The conjugate states are defined in a standard way:

$$\langle m, n| = (|n, m\rangle)^\dagger. \tag{5.5.29}$$

The B transformation is generalized to:

$$T = e^S, \quad S = -y(a_k^\dagger a_{-k}^\dagger - a_{-k}a_k), \quad k \neq 0. \tag{5.5.30}$$

The images of boson operators through the B transformation are:

$$Ta_\beta^\dagger T^+ = Ua_\beta^\dagger + Va_{-\beta} \equiv b_\beta^\dagger,$$
$$Ta_\beta T^+ = Ua_\beta + Va_{-\beta}^\dagger \equiv b_\beta, \tag{5.5.31}$$

where $U = \cosh y$, $V = \sinh y$. Also the Fock states defined above are brought to a new Fock space:

$$\widetilde{|m, n\rangle} = T|m, n\rangle = \left[(b_k^\dagger)^m (b_{-k}^\dagger)^n / \sqrt{m!n!}\right] \widetilde{|0, 0\rangle},$$
$$b_\beta\widetilde{|0, 0\rangle} = 0, \quad \beta = \pm k. \tag{5.5.32}$$

In what follows we are interested in the overlap matrix:

$$G_{pl,mn} = \langle p, l|\widetilde{m, n\rangle}. \tag{5.5.33}$$

To this goal we introduce the Hamiltonian:

$$\mathcal{H} = \frac{1}{2M} \left(p_k^2 + p_{-k}^2 \right) + \eta(x_k^2 + x_k^2), \qquad (5.5.34)$$

where x and p are conjugate variables defined with the boson operators:

$$x_\beta = \alpha \left(a_\beta^\dagger + a_\beta \right), \quad p_\beta = \frac{i}{2\alpha} \left(a_\beta^\dagger - a_\beta \right),$$

$$\beta = \pm k, \quad \alpha = (8M\eta)^{-1/4}. \qquad (5.5.35)$$

The Hamiltonian (5.5.34) can be expressed in terms of boson operators:

$$\mathcal{H} = \omega \left(a_k^\dagger a_k + a_{-k}^\dagger a_{-k} + 1 \right), \quad \omega = (2\eta/M)^{1/2}. \qquad (5.5.36)$$

Using the two forms of the Hamiltonian $\mathcal{H}$ one obtains the eigenvalues and eigenfunctions:

$$\mathcal{H}|l, p\rangle = \omega(p + l + 1)|l, p\rangle,$$

$$|l, p\rangle = N_l(\alpha)N_p(\alpha) \exp\left[-\frac{1}{4\alpha^2} \left(x_k^2 + x_{-k}^2 \right) \right] H_l \left(\frac{x_k}{\sqrt{2}\alpha} \right) H_p \left(\frac{x_{-k}}{\sqrt{2}\alpha} \right). \qquad (5.5.37)$$

Here H_l and H_p are Hermite polynomials and N_l, N_p normalization constants. Through the B transformation the Hamiltonian $\mathcal{H}$ becomes:

$$\mathcal{H}' \equiv T\mathcal{H}T^\dagger = \omega \left(U^2 + V^2 \right) \left(a_k^\dagger a_k + a_{-k}^\dagger a_{-k} \right) + 2\omega UV \left(a_k^\dagger a_{-k}^\dagger + a_{-k} a_k \right)$$

$$+ \omega \left(2V^2 + 1 \right), \qquad (5.5.38)$$

or, alternatively:

$$\mathcal{H}' = \omega \left(b_k^\dagger b_k + b_{-k}^\dagger b_{-k} + 1 \right). \qquad (5.5.39)$$

For what follows it is useful to introduce the operators:

$$X_\beta = Ux_\beta + Vx_{-\beta}, \quad P_\beta = Up_\beta - Vp_{-\beta}, \quad \beta = \pm k. \qquad (5.5.40)$$

These variables are conjugate to each other.

$$\left[X_\beta, P_{\beta'} \right] = i\delta_{\beta,\beta'}. \qquad (5.5.41)$$

In the new variables the Hamiltonian $\mathcal{H}'$, looks as:

$$\mathcal{H}' = \omega\alpha^2 \left(P_k^2 + P_{-k}^2 \right) + \frac{\omega}{4\alpha^2} \left(X_k^2 + X_{-k}^2 \right) - 3\omega(U^2 + V^2). \qquad (5.5.42)$$

Obviously, the eigenfunctions of H are:

$$\mathcal{H}'\widetilde{|m,n\rangle} = \omega(m+n+1)\widetilde{|m,n\rangle},$$

$$\widetilde{|m,n\rangle} = N_m(\alpha)N_n(\alpha)\exp\left[-\frac{1}{4\alpha^2}\left(X_k^2 + X_{-k}^2\right)\right]H_m(\frac{X_k}{\sqrt{2}\alpha})H_n(\frac{X_{-k}}{\sqrt{2}\alpha}).$$

$$(5.5.43)$$

Thus the overlap matrix to be found is a weighted integral of four Hermite polynomials:

$$G_{pl,mn} = N_p(\alpha)N_l(\alpha)N_m(\alpha)N_n(\alpha)2\alpha^2 I_{pl,mn},$$

$$I_{pl,mn} = \int_{-\infty}^{\infty}\int_{-\infty}^{\infty}\exp\left[-\left(U^2y^2 + U^2z^2 + 2UVz\right)\right]$$

$$\times\ H_p(z)H_l(y)H_m(Uy+Vz)H_n(Uz+Vy)dy\ dz.\qquad (5.5.44)$$

The integration is performed in the manner described above for the simple case of bosons without momentum. The final result is:

$$\frac{\pi}{U}\exp\left[\frac{2}{U}(\lambda h - V\lambda t + tw + Vwh)\right] = \sum\frac{\lambda^p t^l w^m h^n}{p!l!m!n!}I_{pl,mn}.\qquad (5.5.45)$$

Expanding the l.h.s. in power series of the variables λ, t, w, h and then identifying the coefficients of the two sides the overlap matrix is readily obtained:

$$G_{pl,mn} = \sqrt{p!l!m!n!}(\cosh y)^{-(l+n+1)}\sum_q\frac{(-1)^{l-m+q}(\sinh y)^{l-m+2q}}{q!(n-q)!(m-q)!(l-m+q)!}.$$

$$(5.5.46)$$

Summation is to be performed according to the restrictions:

$$q \leq \min(m,n),\quad q \geq m-1.\qquad (5.5.47)$$

The compatibility conditions for the quantum numbers is:

$$m - l = n - p.\qquad (5.5.48)$$

In Ref. [RBB76] the overlap matrix was obtained by a different method which makes use of the identities:

$$\left(Ua^\dagger + Va\right)^n = \sum_{i,m}\frac{n!}{2^i i!m!(n-2i-m)!}U^{n-i-m}V^{i+m}\left(a^\dagger\right)^{n-2i-m}a^m,$$

$$\left[a^l_\beta,(a^\dagger_\beta)^n\right] = \sum_{s=1}\frac{l!n!}{s!(n-s)!(l-s)!}(a^\dagger_\beta)^{n-s}a^{l-s}_\beta.\qquad (5.5.49)$$

In conclusion, here we used the SU(1, 1) coherent states in order to describe the space of correlated bosons.

Chapter 6
The Coherent State Model

6.1 The Coherent State Model

CSM defines [RCGD82] first a restricted collective space whose vectors are modeling the states of ground, β and γ bands. In choosing these states we were guided by some experimental information as well as by some previous theoretical investigations.

The original classification of collective states in terms of bands relies on the weak coupling limit, in which the angular momentum projection on the intrinsic symmetry axis (K) is a good quantum number. Departing from this extreme, as it happens in realistic cases, the band mixing description is necessary.

On the basis of energy values three typical experimental situations can be distinguished: (a) The lowest member of the γ band lies above the lowest member of the β band: $E_{2^+_\gamma} > E_{0^+_\beta}$. This is the case for the Sm region [EIGR70]. (b) States of the β and γ bands with the same angular momentum are almost degenerate. A good example is the nucleus ^{232}Th [Sa76]. (c) The 2^+ state of the γ-band lies below the 0^+ state of β band. Such situation is met in the Pt region [FUN75]. Group theoretical interpretation of these features are based on SU(5), SU(3) and O(6) symmetries [AI76], respectively.

Since the situation for Pt isotopes guides us in choosing the model states, two more information are to be added, (i)The E2 transitions between members of ground and β bands are relatively weak and the ratio $B(E2; 0^+_\beta \rightarrow 2^+_\gamma)/B(E2; 0^+_\beta \rightarrow 2^+_g)$ is much larger than unity; (ii) States of γ band has a doublet structure as for example $E_{4^+_\gamma} - E_{3^+_\gamma} < E_{3^+_\gamma} - E_{2^+_\gamma}$.

The boson structure of the low spin states in the Pt isotopes was studied by diagonalizing a fourth order boson Hamiltonian. One found that 2^+_γ has a structure similar to that predicted by the empirical rule of Sheline and Sakai (SS) [Sa76, Sh60], i.e. the dominant component is a two boson state, while 0^+_β is dominantly a three boson state [JAJO76, ROUL78]. This modified SS scheme is in accord with the experimental feature (i) and seems to be a common result for all models using a γ soft potential energy surface. Extensive studies of ground state band performed by Lipas and collaborators [LHH76] show that an axially symmetric coherent state is a good

basis for the description of small oscillations around a deformed equilibrium shape.
States of excited bands could be constructed either by using independent coherent
states or by exciting the ground band states with low rank polynomials in quadrupole
bosons $b_m^\dagger$ ($-2 \leq m \leq 2$).

In view of the statements (i) and (ii) as well as the modified SS scheme we chose
the deformed basis to satisfy the following conditions:

(a) In the limit of small deformation the projected states yield the highest seniority
states of the N-phonon multiplet while in the large deformation regime a rotational
behavior should be reproduced.

(b) The projected states describing the members of ground and beta bands are
only weakly coupled by the E2 transition operator.

(c) The states should be orthogonal before and after the angular momentum pro-
jection was performed.

All these conditions are fulfilled by the following set of three deformed states:

$$\psi_g = e^{[d(b_0^\dagger - b_0)]}|0\rangle \equiv T|0\rangle, \ \ \psi_\gamma = \Omega_{\gamma,2}^\dagger \psi_g, \ \ \psi_\beta = \Omega_\beta^\dagger \psi_g. \tag{6.1.1}$$

where the excitation operators for γ and β bands are defined by:

$$\Omega_{\gamma 2}^\dagger = (b^\dagger b^\dagger)_{2,2} + d\sqrt{\frac{2}{7}} b_2^\dagger, \ \ \Omega_\beta = (b^\dagger b^\dagger b^\dagger)_0 + \frac{3d}{\sqrt{14}}(b^\dagger b^\dagger)_0 - \frac{d^3}{\sqrt{70}}. \tag{6.1.2}$$

For practical aims it is useful to list few properties of the deformed states ψ_i with
i = g, β, γ:

$$\langle \psi_k | \psi_{k'} \rangle = \delta_{k,k'}, \ \ \Omega_\beta \psi_g = \Omega_{\gamma 2} \psi_g = \Omega_\beta \psi_\gamma = 0,$$

$$b_{-2} \psi_\beta = \frac{3}{\sqrt{5}} \psi_\gamma, \ \ b_{-1} b_{-2} \psi_i = (b_{-2})^2 \psi_i = 0, \ \ i = g, \beta, \gamma,$$

$$H_{def} \psi_i = \epsilon_i \psi_i, \ \ T \left[(b^\dagger b^\dagger)_4 (bb)_4 \right]_0 T^\dagger \psi_i = 0, \ \ i = g, \beta, \gamma. \tag{6.1.3}$$

The deformed Hamiltonian which admits ψ_i as eigenstates, is defined in terms of the
boson number operator $(\hat{N})$, angular momentum squared $(\hat{J}^2)$ and the z-component
of the angular momentum operator, $(\hat{J}_z)$. The eigenvalues are simple expressions of
the strengths of the terms involved in H_{def}:

$$H_{def} \psi_i = T \left[3A\hat{N}(\hat{N} - 3) + 3B(b^+ b^+)_0(bb)_0 + (B - A)(b^+ b^+ b^+)_0(bbb)_0 \right.$$

$$\left. + B\hat{J}^2 + C\hat{J}_z \right] T^\dagger, \ \epsilon_g = 0, \ \epsilon_\beta = 6(B - A), \ \epsilon_\gamma = 6(B - A) + 2C. \tag{6.1.4}$$

Denoting by Q_i^h (i = g, β, γ) the expectation value of the harmonic quadrupole
operator

$$Q_{2\mu} = q_0(b_\mu^\dagger + (-)^\mu b_{-\mu}), \tag{6.1.5}$$

on the state ψ_i, one obtains the following ordering equation:

$$Q_g^h < Q_\gamma^h < Q_\beta^h. \tag{6.1.6}$$

Since Q_g^h is proportional to d, this parameter will be hereafter called the deformation parameter. From the three deformed and orthogonal functions one generates through projection, three sets of mutually orthogonal states

$$\phi_{JM}^i = N_J^i P_{M0}^J \psi_i, \, i = g, \beta, \gamma, \tag{6.1.7}$$

where P_{MK}^J denotes the projection operator defined as:

$$P_{MK}^J = \frac{2J+1}{8\pi^2} \int D_{MK}^{J*} \hat{R}(\Omega) d\Omega, \tag{6.1.8}$$

and N_J^i the normalization factors. Deformed and projected states satisfy the required conditions mentioned before and therefore contain the salient features of the major collective bands. Since we attempt to set up a very simple model we relay on the experimental feature saying that the β band is largely decoupled from the ground as well as from the γ bands and choose a model Hamiltonian whose matrix elements between beta states and states belonging either to the ground or to the gamma band are all equal to zero. The simplest Hamiltonian obeying this restriction is

$$\tilde{H} = A_1(22\hat{N} + 5\Omega_{\beta'}^\dagger \Omega_{\beta'}) + A_2\hat{J}^2 + A_3\Omega_\beta^\dagger \Omega_\beta, \text{ with}$$
$$\Omega_{\beta'}^\dagger = (b^\dagger b^\dagger)_0 - \frac{1}{\sqrt{5}} d^2. \tag{6.1.9}$$

Since the following relations

$$\Omega_\beta \phi_{JM}^i = \Omega_{\beta'}^2 \phi_{JM}^i = 0, \, i = g, \gamma, \tag{6.1.10}$$

hold, new terms can be added to the Hamiltonian $\tilde{H}$ without altering the decoupling condition for the β band. This way, one arrived at the following model Hamiltonian:

$$H = A_1[22\hat{N} + 5\Omega_{\beta'}^\dagger \Omega_{\beta'}] + A_2\hat{J}^2 + A_3\Omega_\beta^\dagger \Omega_\beta + A_4(\Omega_\beta^\dagger \Omega_{\beta'}^2 + h.c.) + A_5\Omega_{\beta'}^{\dagger 2} \Omega_{\beta'}^2. \tag{6.1.11}$$

Note that the three sets of projected states corresponding to ψ_β and

$$\psi_{\beta'} = \Omega_{\beta'}^\dagger \psi_g, \, \psi_{\beta''} = (\Omega_{\beta'}^\dagger)^2 \psi_g, \tag{6.1.12}$$

respectively, are linearly independent and possible candidates for the description of the β band. Since in the vibrational limit $(d \to 0)$, $\phi_{JM}^{\beta'}$ satisfy the standard SS

scheme we used these functions to describe the beta bands of nuclei from the Sm region [RASA86]. The resulting formalism, called CSM2, is an alternative version of CSM for Sm region. However, most of the specific features for this region could be obtained in a description with ϕ^{β}_{JM} given by Eq. (6.1.7) as model states for the beta band, by choosing a suitable set of structure coefficients in the model Hamiltonian.

It is worth noting that the procedure adopted to construct the restricted collective basis and the effective Hamiltonian is to some extent similar to the Lanczos method of generating a suitable basis for treating a given interaction [LANC90].

As a further test for the model set up in this fashion, we consider the E2 transition rates. We take for the quadrupole operator the following structure

$$Q_{2\mu} = q_0(b^{\dagger}_{\mu} + (-)^{\mu}b_{-\mu}) + q_1(b^{\mu}b)_{\mu} + q_2((b^{\dagger}b^{\dagger})_{2\mu} + (bb)_{2\mu}). \qquad (6.1.13)$$

In the limit of small d, the mixing of ground and gamma band states is negligible. The states from the ground and beta bands may be connected only through the q_2 term of the quadrupole operator. Indeed, it can be proved that:

$$\langle \phi^{\beta}_{JM}|b^{\dagger}_{\mu} + (-)^{\mu}b_{-\mu}|\phi^{g}_{J'M'}\rangle = 0, \quad \langle \phi^{\beta}_{JM}|(b^{\dagger}b)_{2\mu}|\phi^{g}_{J'M'}\rangle = 0. \qquad (6.1.14)$$

Due to this feature, in the Pt region, which is close to the vibrational limit, we can use a two parameter version of the quadrupole operator, with $q_1 = 0$.

The matrix elements of any boson operator between two projected states can be easily expressed in terms of the following overlap integrals:

$$I^{(k)}_J(d^2) = \int_0^1 P_J(x)\,[P_2(x)]^k\,exp\left[d^2 P_2(x)\right]dx,$$

$$\mathcal{I}^{(k)}_J(d^2) = \int_0^{\pi} d^J_{22}(\theta)d^k_{22}(\theta)exp\left[d^2 P_2(\cos\theta)\right]\sin\theta d\theta, \ \ k = 2, 3, 4,$$

$$I^{J2}_{02}(d^2) = \int_0^{\pi} d^J_{02}(\theta)d^2_{20}(\theta)exp\left[d^2 P_2(\cos\theta)\right]\sin\theta d\theta. \qquad (6.1.15)$$

For example the projected states norms are:

$$(N^g_J)^{-2} = (2J+1)I^{(0)}_J(d)e^{-d^2},$$

$$(N^{\beta}_J)^{-2} = (2J+1)(6+\frac{9}{7}d^2)I^{(0)}_J + \frac{18}{5}I^{(1)}_J]e^{-d^2},$$

$$(N^{\gamma}_J)^{-2} = \frac{1}{49}(2J+1)[(49+29d^2)\mathcal{I}^{(2)}_J + 28d^2\mathcal{I}^{(3)}_J + 6d^2\mathcal{I}^{(4)}_J]e^{-d^2}. \quad (6.1.16)$$

In Appendix B, the last two integrals of Eq. (6.1.15) are expressed in terms of $I_J^{(0)}$, which can be calculated by a direct integration:

$$I_J^{(0)}(d^2) = e^{-\frac{1}{2}d^2} \sum_{k=0}^{\infty} \frac{3^k (2k)!(k + \frac{1}{2}J)!}{2^{k-J} k!(k - \frac{1}{2}J)!(2k + J + 1)!} d^{2k}. \tag{6.1.17}$$

The summation involved can be analytically performed with the result:

$$I_J^{(0)}(d^2) = \frac{(J!)^2}{(\frac{1}{2}J)!(2J + 1)!}(6d^2)^{J/2} e^{-d^2/2}\,_1F_1(\frac{1}{2}(J + 1), J + \frac{3}{2}; \frac{3}{2}d^2), \tag{6.1.18}$$

where $_1F_1$ denotes the confluent hypergeometric function. Considering the expression of the angular momentum spherical component in term of the quadrupole bosons:

$$J_\mu = \sqrt{10}(b^\dagger b)_{1\mu}, \quad \mu = \pm 1, 0, \tag{6.1.19}$$

one obtains for the angular momentum squared, the following expression:

$$\hat{J}^2 = 2\hat{N}_b(2\hat{N}_b + 1) - 10(b^+ b^+)_0(bb)_0 - 7\sqrt{5}\left[(b^+ b^+)_2(bb)_2\right]_0. \tag{6.1.20}$$

Averaging this equation with the projected ground band state one obtains that the overlap integral $I_J^{(0)}$ satisfies the differential equation:

$$\frac{d^2 I_J^{(0)}}{dx^2} - \frac{x - 3}{2x}\frac{d I_J^{(0)}}{dx} - \frac{2x^2 + J(J + 1)}{4x^2} I_J^{(0)} = 0. \tag{6.1.21}$$

With a suitable change of function this equation is brought to the form of the equation satisfied by a hypergeometric function and finally the form (6.1.18) is, again, obtained.

To conclude, the CSM formalism consists in: (a) defining, through a projection technique, three sets of mutually orthogonal states whose properties recommend them as model states for the ground, beta and gamma bands, respectively; (b) in the restricted space of projected states one finds an effective Hamiltonian having vanishing matrix elements between beta band states and states from either ground or gamma band; (c) the E2 transitions between states of the restricted space are described by the transition operator $Q_{2\mu}$ given by Eq. (6.1.13).

Note that the model states are generated through projection from a coherent state and two excitations of that through simple polynomial boson operators. Since the coherent state achieves the minimum value for the uncertainty relations for the quadrupole collective coordinate and its conjugate momentum, it is expected that this is an ideal state to account for the semiclassical behavior of the nuclear system staying in a state of high spin.

Moreover, the states are infinite series of bosons and thus highly deformed states can be described.

The model Hamiltonian is not commuting with the boson number operator and because of this property a basis generated from a coherent state is expected to be most suitable.

In the reduced model space of the angular momentum projected states the eigenvalues of the model Hamiltonian (either $\tilde{H}$ of H) are obtained as follows: Those corresponding to the β band states and to states of odd angular momentum from the γ band, are determined by averaging the model Hamiltonian with the respective model states. Energies from ground band and gamma band states with even angular momenta are obtained by diagonalizing a 2×2 matrix. Thus, energies of the three bands, ground, β and γ, have analytical expressions in terms of the overlap integral $I_J^{(0)}$ and its low order derivatives.

Before presenting several notable applications of CSM, we shall describe in more details the vibrational and rotational limits of the CSM. Also, the description of the wave function in the intrinsic system of reference will point out new useful features of the model. As a result, energies are described by compact formulas depending on $J(J+1)$. Also, the reduced transition probabilities acquire simple expressions.

6.2 The Vibrational and Near Vibrational Regimes

6.2.1 Energies

As already mentioned, in Refs. [RGB77, RAD83, RSS84], it was proved that the projected states go to the first three highest seniority states respectively, when the parameter d goes to zero. For a easier writing, let us denote:

$$
\begin{aligned}
\varphi_{JM}^{i,v} &= \lim_{d \to 0} \varphi_{JM}^{i}(d), \\
H^v &= \lim_{d \to 0} H.
\end{aligned}
\tag{6.2.1}
$$

According to Refs. [RGB77, RAD83, RSS84], the vibrational limits for the projected states are:

$$
\begin{aligned}
\varphi_{JM}^{g,v} &= |\frac{J}{2}, \frac{J}{2}, 0, J, M\rangle, \\
\varphi_{JM}^{\gamma,v} &= |\left[\frac{J+3}{2}\right], \left[\frac{J+3}{2}\right], 0, J, M\rangle, \quad [\ldots] - \text{integer part}, \\
\varphi_{JM}^{\beta,v} &= \left[1 - \frac{6}{7} \frac{J(2J+3)}{(J+7)(3J+10)}\right]^{\frac{1}{2}} |\frac{J}{2}+3, \frac{J}{2}+3, 1, J, M\rangle
\end{aligned}
$$

$$+\left[\frac{6}{7}\frac{J(2J+3)}{(J+7)(3J+10)}\right]^{\frac{1}{2}}|\frac{J}{2}+3, \frac{J}{2}+1, 0, J, M\rangle$$

$$\equiv \varphi_{JM}^{\beta v,1} + \varphi_{JM}^{\beta v,2}. \tag{6.2.2}$$

where, the standard notations for the states $|N, v, \alpha, J, M\rangle$, labeled by the number of bosons (N), seniority (v), missing quantum number (α), angular momentum (J) and its projection on z axis (M), are used. These quantum numbers, except α, are given by the Casimir operators eigenvalues of the groups in the chain $SU(5) \supset R(5) \supset R(3) \supset R(2)$. A complete description of these states may be found in Refs. [GRC78, RCG78]. The vibrational limits are related by the following equations:

$$\varphi_{JM}^{\beta v,1} = \left[\frac{3}{5}(3J+10)\right]^{-\frac{1}{2}}(b^\dagger b^\dagger b^\dagger)_0 \varphi_{JM}^{g,v},$$

$$\varphi_{JM}^{\beta v,2} = \left[\frac{15}{7}\frac{J(2J+3)}{(J+7)^2(3J+10)}\right]^{\frac{1}{2}}(b^\dagger b^\dagger)_0 \varphi_{JM}^{\gamma,v}. \tag{6.2.3}$$

Note that due to Eq. (6.2.3), the vibrational limit of the head state of β band is a pure three boson state. The vibrational limit for the band energies are:

$$E_J^{g,v} = 11A_1 J + A_2 J(J+1),$$

$$E^{\gamma,v} = 22A_1\left[\frac{J+3}{2}\right] + A_2 J(J+1),$$

$$E_J^{\beta,v} = A_1\left(11(J+6) + \frac{12}{7}\frac{J(2J+3)}{3J+10}\right)$$

$$+ A_2 J(J+1) + \frac{3}{5}(3J+10)A_3. \tag{6.2.4}$$

where $[..]$ denotes the integer part. Since the matrix elements of the model Hamiltonian between states of ground and gamma bands are vanishing in the vibrational limit, it results that the vibrational states are eigenstates of H in the restricted collective space. Moreover, one can prove that this is true in the whole boson space for ground and gamma band states of any angular momentum. Concerning the beta band states, this property holds only for the $J = 0$ state. However, if one ignores the component $\varphi_{JM}^{\beta v,2}$ of the vibrational beta states, the remaining component, i.e. $\varphi_{JM}^{\beta v,1}$, is an eigenstate of the vibrational Hamiltonian:

$$H^v \varphi_{JM}^{\beta v,1} = \left[11A_1(J+6) + A_2 J(J+1)\right.$$

$$\left. + \frac{3}{5}(3J+10)A_3\right]\varphi_{JM}^{\beta v,1}. \tag{6.2.5}$$

For small values of the deformation parameter, the exact energies can be expressed as a power series in d. As a result the excitation energies of the three bands are written as compact formulas depending on powers of $J(J+1)$ which are easy to be handled in numerical calculations. As we have already mentioned the matrix elements of the model Hamiltonian between the angular momentum projected states can be written as function of the overlap integral $I_J^{(0)}$ and its kth derivatives, $I_J^{(k)}$. Taking into account the composition rule as well as the recurrence relations for the Legendre polynomial one can prove that the basic integrals satisfy the differential equation:

$$\frac{d^2 I_J^{(0)}}{dx^2} - \frac{x-3}{2x}\frac{dI_J^{(0)}}{dx} - \frac{2x^2 + J(J+1)}{4x^2}I_J^{(0)} = 0, \quad (x = d^2). \tag{6.2.6}$$

The solution for this equation is:

$$I_J^{(0)}(d^2) = \frac{(J!)^2}{(\frac{J}{2})!(2J+1)!}(6d^2)^{\frac{J}{2}}e^{-\frac{d^2}{2}}{}_1F_1\left(\frac{1}{2}(J+1), J+\frac{3}{2}; \frac{3}{2}d^2\right), \tag{6.2.7}$$

where ${}_1F_1(a, b, z)$ is the hypergeometric function of the first kind. The excitation energies of the ground, beta and gamma bands are functions of the ratio $d^2\frac{I_J^{(1)}}{I_J^{(0)}}$ and its first three derivatives with respect to d^2. These quantities have the following vibrational limits:

$$\lim_{d\to 0}\left(d^2\frac{I_J^{(1)}}{I_J^{(0)}}\right)^{(k)} = \frac{1}{(2J+3)^k}\left[\frac{J}{2}(\delta_{k,0} + \delta_{k,1}) + 9\frac{(J+1)(J+2)}{2J+5}\right.$$
$$\left.\times\left(\delta_{k,2} + 9\frac{\delta_{k,3}}{2J+7}\right)\right], k = 0, 1, 2, 3. \tag{6.2.8}$$

These relations allow us to write down the Taylor expansion of $xI_J^{(1)}/I_J^{(0)}$ up to the third order in $x\ (= d^2)$:

$$x\frac{I_J^{(1)}}{I_J^{(0)}} = \frac{J}{2} + \frac{J}{2(2J+3)}x + \frac{9}{2}\frac{(J+1)(J+2)}{(2J+3)^2(2J+5)}x^2$$
$$+ \frac{27}{2}\frac{(J+1)(J+2)}{(2J+3)^3(2J+5)(2J+7)}x^3. \tag{6.2.9}$$

Inserting the truncated power series of the $xI_J^{(1)}/I_J^{(0)}$, into the excitation energy expressions one obtains [RS83]:

$$E_J^g = 22A_1\sum_{k=0}^{3}A_{J,k}^{(g)}x^k + A_2 J(J+1) - \Delta E_J, \tag{6.2.10}$$

$$E_J^\gamma = 44A_1 + \frac{A_1}{\sum_{k=0}^{3} Q_{J,k}^{(\gamma,0)} x^k} \left[\sum_{k=0}^{3} \left(22R_{J,k}^{(\gamma,0)} + 5U_{J,k}^{(\gamma,0)} \right) x^k \right]$$

$$+ A_2 J(J+1) + \Delta E_J, \quad J = even, \tag{6.2.11}$$

$$E_J^\gamma = 44A_1 + \frac{A_1}{\sum_{k=0}^{3} Q_{J,k}^{(\gamma,1)} x^k} \left[\sum_{k=0}^{3} \left(22R_{J,k}^{(\gamma,1)} + 5U_{J,k}^{(\gamma,1)} \right) x^k \right]$$

$$+ A_2 J(J+1), \quad J = odd, \tag{6.2.12}$$

$$E_J^\beta = \frac{1}{\sum_{k=0}^{3} Q_{J,k}^{(\beta)} x^k} \left\{ A_1 \sum_{k=0}^{3} \left(22R_{J,k}^{(\beta)} + 5U_{J,k}^{(\beta)} \right) x^k \right.$$

$$\left. + \sum_{k=0}^{3} \left(A_3 V_{J,k}^{(\beta)} + A_4 d Z_{J,k}^{(\beta)} + A_5 B_{J,k}^{(\beta)} \right) x^k \right\}$$

$$+ A_2 J(J+1). \tag{6.2.13}$$

The expansion coefficients A, Q, R, U, V, Z, B and the quantity ΔE are given in Appendix C.

6.2.1.1 The Vibrational Structure of the β Band States

Here we shall prove the relation (6.2.2) which expresses the states of β band in the spherical limit.

By means of Eqs. (6.1.17) and (6.2.9) and the expansion

$$\left(\frac{N_J^\beta}{N_J^g} \right)^{-2} = \frac{3}{5}(3J+10) + \frac{9}{35}\frac{17J+15}{2J+3}x$$

$$+ \frac{81}{5}\frac{(J+1)(J+2)}{(2J+3)^2(2J+5)}x^2$$

$$+ \frac{243}{5}\frac{(J+1)(J+2)}{(2J+3)^2(2J+5)(2J+7)}x^3 + \mathcal{O}(x^4). \tag{6.2.14}$$

one obtains:

$$\lim_{d \to 0} \varphi_{JM}^{(\beta)} = \mathcal{A}(b^+ b^+ b^+)_0 | \frac{J}{2}, \frac{J}{2}, 0, J, M \rangle, \quad \mathcal{A} = \left[\frac{3}{5}(3J+10) \right]^{-1/2}. \tag{6.2.15}$$

According to Ref. [RCG78] the r.h.s. of Eq. (6.2.15) can be written as:

$$\mathcal{A}(b^+ b^+ b^+)_0 | \frac{J}{2}, \frac{J}{2}, 0, J, M \rangle = \eta | \frac{J}{2}+3, \frac{J}{2}+3, 1, J, M \rangle$$

$$+ \epsilon | \frac{J}{2}+3, \frac{J}{2}+1, 0, J, M \rangle \tag{6.2.16}$$

Indeed, the inequality satisfied by the completeness quantum number α

$$v - J \leq 3\alpha \leq v - \frac{J}{2}, \, \alpha - \text{integer} \tag{6.2.17}$$

has solutions only for two values of the seniority quantum number v: $\frac{J}{2} + 3$ and $\frac{J}{2} + 1$. For $v = \frac{J}{2} + 3$ the solutions for α are:

$$\alpha = \begin{cases} 1 & \text{for } J < 6 \\ 0, 1 & \text{for } J \geq 6 \end{cases} \tag{6.2.18}$$

As shown in Ref. [RCG78] the state $|\frac{J}{2} + 3, \frac{J}{2} + 3, 0, J, M\rangle$ does not appear in the expansion:

$$(b^+ b^+ b^+)_0 |\frac{J}{2}, \frac{J}{2}, 0, J, M\rangle = \sum_{\alpha, v \leq \frac{J}{2} + 3} C_{v,\alpha} |\frac{J}{2} + 3, v, \alpha, J, M\rangle. \tag{6.2.19}$$

Now, we proceed with calculating the amplitudes η, ϵ. To this end we calculate the function:

$$F(J) = \lim_{d \to 0} \langle \varphi^{\beta}_{JM} | 5\Omega^+_{\beta'} \Omega_{\beta'} | \varphi^{\beta}_{JM} \rangle. \tag{6.2.20}$$

By direct calculations one obtains:

$$F(J) = \frac{12}{7} \frac{J(2J + 3)}{3J + 10}. \tag{6.2.21}$$

On the other hand

$$F(J) = \epsilon^2 \langle \frac{J}{2} + 3, \frac{J}{2} + 1, 0, JM | \hat{\Lambda}^2 - \hat{N}(\hat{N} + 3) | \frac{J}{2} + 3, \frac{J}{2} + 1, 0, JM \rangle, \tag{6.2.22}$$

where $\hat{\Lambda}^2$ is the Casimir operator of the group R5 while $\hat{N}$ stands for the boson number operator.

$$\hat{\Lambda}^2 | N, v, \alpha, JM \rangle = v(v + 3) | N, v, \alpha, JM \rangle,$$
$$\hat{N} | N, v, \alpha, JM \rangle = N | N, v, \alpha, JM \rangle. \tag{6.2.23}$$

Finally one obtains:
$$F(J) = 2\epsilon^2 (J + 7). \tag{6.2.24}$$

Comparing the two results for the function $F(J)$ one obtains:

$$\epsilon = \left(\frac{6}{7} \frac{J(2J + 3)}{(J + 7)(3J + 10)} \right)^{\frac{1}{2}}. \tag{6.2.25}$$

Since $\lim_{d\to 0} \varphi_J^{(\beta)}$ is normalized to unity, the amplitude η is:

$$\eta = \left(1 - \frac{6}{7} \frac{J(2J+3)}{(J+7)(3J+10)}\right)^{\frac{1}{2}}. \tag{6.2.26}$$

6.2.2 Reduced Probability for E2 Transitions

As already mentioned, the CSM uses for the quadrupole transition operator the following expression:

$$Q_{2\mu} = q_h(b_\mu^\dagger + (-)^\mu b_{-\mu}) + q_{anh}((b^\dagger b^\dagger)_{2\mu} + (bb)_{2\mu})$$
$$\equiv Q_{2\mu}^h + Q_{2\mu}^{anh}. \tag{6.2.27}$$

The anharmonic term is the lowest order term in bosons which brings a non-vanishing contribution to the E2 transition between a state from the beta band and a state from the ground band.

Analytical expressions for transition probabilities are also possible. First we list the results for the limit $d \to 0$ of the non-vanishing matrix elements of the terms involved in the transition operator. The final results are [RAD83, RSS84]:

$$\lim_{d\to 0} \langle \varphi_J^g || Q_2^h || \varphi_{J'}^g \rangle = (1 - \delta_{J,J'}) \left[\frac{2}{3} \frac{(J+J'+3)(J+J'+1)}{J+J'}\right]^{1/2} C_{0\,0\,0}^{J\,2\,J'} q_h,$$

$$\lim_{d\to 0} \langle \varphi_J^\beta || Q_2^h || \varphi_{J'}^\beta \rangle = (1 - \delta_{J,J'}) \left[\frac{2}{3} \frac{(J+J'+1)(J+J'+3)(3(J+J')+26)}{(J+J')(3(J+J')+14)}\right]^{1/2}$$
$$\times C_{0\,0\,0}^{J\,2\,J'} q_h,$$

$$\lim_{d\to 0} \langle \varphi_J^\gamma || Q_2^h || \varphi_J^g \rangle = 2 \left[\frac{(J+1)(2J+3)}{3(J-1)(J+2)}\right]^{1/2} C_{2\,-2\,0}^{J\,2\,J} q_h, \quad J = \text{even},$$

$$\lim_{d\to 0} \langle \varphi_J^\gamma || Q_2^h || \varphi_{J+1}^g \rangle = -\left[\frac{6(J+1)(J+2)^2(2J+3)}{J(2J+1)(2J^2+5J+11)}\right]^{1/2} C_{2\,-2\,0}^{J\,2\,J+1} q_h, \quad J = \text{odd},$$

$$\lim_{d\to 0} \langle \varphi_J^\beta || Q_2^h || \varphi_{J+2}^\gamma \rangle = 2 \left[\frac{6(2J+3)(2J+5)(2J+7)}{7(J+3)(J+4)(3J+10)}\right]^{1/2} C_{0\,2\,2}^{J\,2\,J+2} q_h,$$

$$\lim_{d\to 0} \langle \varphi_J^\beta || Q_2^h || \varphi_{J+1}^\gamma \rangle = -\left[\frac{108(J+2)(J+3)^2}{7(3J+10)(2J^2+9J+18)}\right]^{1/2} C_{0\,2\,2}^{J\,2\,J+1} q_h,$$

$$\lim_{d\to 0} \langle \varphi_J^\gamma || Q_2^h || \varphi_{J+2}^\gamma \rangle = \left[\frac{(J+1)(J+2)(2J+5)(2J+7)}{3(J-1)(J+3)(J+4)}\right]^{1/2} C_{2\,0\,2}^{J\,2\,J+2} q_h, \quad J = \text{even},$$

$$\lim_{d\to 0} \langle \varphi_J^\gamma || Q_2^h || \varphi_{J+2}^\gamma \rangle = \left[\frac{(J+3)(2J+3)(4J^3+18J^2+45J+23)^2}{3J(2J+1)(J+1)(2J^2+13J+29)(2J^2+5J+11)}\right]^{1/2}$$
$$\times C_{2\,0\,2}^{J\,2\,J+2} q_h, \quad J = \text{odd},$$

$$\lim_{d\to 0}\langle \varphi_J^\gamma||Q_2^h||\varphi_{J+1}^\gamma\rangle = -\left[\frac{3(J+1)(J+2)^2(J+3)^2}{2(J-1)(2J+3)(2J^2+9J+18)}\right]^{1/2}$$
$$\times\, C_{2\ 0\ 2}^{J\ 2\ J+1}q_h,\ J = even,$$

$$\lim_{d\to 0}\langle \varphi_J^g||Q_2^{anh}||\varphi_{J-2}^\beta\rangle = \left[\frac{4(J-1)J^2}{(2J-1)(2J+1)(3J+4)}\right]^{1/2}\, C_{0\ 0\ 0}^{J\ 2\ J-2}q_h. \qquad (6.2.28)$$

Note that in the limit of large J, the Alaga's rule [AL57] is valid even for the vibrational regime.

It is well known that the $B(E2)$ values are very sensitive to the small variation in both the wave functions and transition operator. Therefore we include in the expression of the matrix elements of the transition operator the first order Taylor expansion in terms of the deformation parameter d. Then the $B(E2)$ value characterizing a certain transition is obtained, in the Rose convention [ROSE57], by squaring the corresponding reduced matrix element. Intraband transition matrix elements are:

$$\langle\phi_J^g||Q_2||\phi_{J-2}^g\rangle = \sqrt{\frac{J}{2}}\,(q_h - q_{anh}d)\,,$$

$$\langle\phi_J^\beta||Q_2||\phi_{J-2}^\beta\rangle = \sqrt{\frac{J(3J+10)}{2(3J+4)}}\left[q_h - \frac{q_{anh}d(3J+4)}{3J+10}\right],$$

$$\langle\phi_{J+2}^\gamma||Q_2||\phi_J^\gamma\rangle = \sqrt{\frac{J(2J+7)}{2(2J+3)}}\left[q_h - \frac{q_{anh}d(2J-13)}{2J+7}\sqrt{\frac{2}{7}}\right],\quad J = even,$$

$$\langle\phi_J^\gamma||Q_2||\phi_{J-1}^\gamma\rangle = q_h d\sqrt{\frac{2(J-2)}{J(J-1)(2J+3)}}\left[8 - \frac{J-8}{2J-1}\right.$$
$$\left. + \frac{(J+2)(2J+3)}{(J+1)(2J+1)} + \frac{2(J-5)(J-1)(4J+3)}{(J+1)(2J-1)(2J+1)}\right],\quad J = even,$$

$$\langle\phi_{J+1}^\gamma||Q_2||\phi_J^\gamma\rangle = \sqrt{\frac{6(J+3)}{J(2J+3)}}\left[q_h - \frac{5q_{anh}d}{J+3}\sqrt{\frac{2}{7}}\right],\quad J = even,$$

$$\langle\phi_{J+2}^\gamma||Q_2||\phi_J^\gamma\rangle = \sqrt{\frac{(J-1)(J+3)(J+4)}{2(J+1)(J+2)}}\left[q_h - q_{anh}d\frac{J+6}{J+4}\sqrt{\frac{2}{7}}\right],\quad J = odd.$$
$$(6.2.29)$$

The interband transition matrix elements are:

$$\langle\phi_J^g||Q_2||\phi_{J-2}^\beta\rangle = q_{anh}\sqrt{\frac{6J}{(3J+4)}}\left[1 - \frac{3(34J^2+34J-29)}{14(2J-1)(2J+3)(3J+4)}d^2\right],$$

$$\langle\phi_J^g||Q_2||\phi_J^\beta\rangle = -2q_{anh}d\sqrt{\frac{3J(J+1)}{(2J-1)(2J+3)(3J+10)}},$$

$$\langle\phi_{J-2}^g||Q_2||\phi_J^\beta\rangle = q_{anh}d^2\frac{3(J-1)}{2J-1}\sqrt{\frac{6J}{(2J-3)(2J+1)(3J+10)}}, \qquad (6.2.30)$$

$$\langle \phi_J^\gamma || Q_2 || \phi_J^g \rangle = \sqrt{\frac{2(J+1)}{2J-1}}$$
$$\times \left[q_h + \frac{2q_{anh}d(44J^4 - 210J^3 - 533J^2 - 15J + 378)}{7(J-1)(J+1)(2J+3)^2} \sqrt{\frac{2}{7}} \right],$$

$$(6.2.31)$$

$$\langle \phi_J^\gamma || Q_2 || \phi_{J-2}^g \rangle = \sqrt{(2J+3)} \left[q_{anh}\sqrt{\frac{2}{7}} + \frac{3q_h d}{(2J+3)(2J-1)} \right],$$

$$\langle \phi_J^\gamma || Q_2 || \phi_{J+2}^g \rangle = \frac{6q_h d(J-1)}{(J+1)(2J+3)} \sqrt{\frac{J(J+2)(2J+5)}{(2J+1)(2J+3)}},$$

$$\langle \phi_{J-1}^\gamma || Q_2 || \phi_J^g \rangle = -\sqrt{\frac{(J-2)(2J+1)}{(J-1)(2J-1)}} \left[q_h + q_{anh}d\frac{(J+3)(J+4)}{(2J+1)(J+1)}\sqrt{\frac{2}{7}} \right],$$

$$\langle \phi_{J+1}^\gamma || Q_2 || \phi_J^g \rangle = -\sqrt{3(J+3)} \left[q_{anh}\sqrt{\frac{2}{7}} + \frac{q_h d}{(2J+3)} \right], \qquad (6.2.32)$$

$$\langle \phi_J^\beta || Q_2 || \phi_{J+2}^\gamma \rangle = \sqrt{\frac{6(2J+5)(2J+7)}{7(2J+1)(3J+10)}} \left[q_h + q_{anh}d\frac{8J^2 + 42J + 21}{(2J+3)(2J+7)}\sqrt{\frac{2}{7}} \right],$$

$$\langle \phi_J^\beta || Q_2 || \phi_J^\gamma \rangle = 4(J+5)\sqrt{\frac{3(J+1)}{7(2J-1)(3J+10)}}$$
$$\times \left[q_{anh}\sqrt{\frac{2}{7}} + q_h d\frac{10J^2 + 13J - 33}{2(J+1)(J+5)} \right],$$

$$\langle \phi_{J+2}^\beta || Q_2 || \phi_J^\gamma \rangle = q_{anh}d\sqrt{\frac{3J(J+2)}{(2J+3)(3J+16)}}\frac{8(5J^2 + 17J - 27)}{7(J+1)(2J+3)}. \qquad (6.2.33)$$

In the limit $d \to 0$ these expressions reproduce the m.e. corresponding to vibrational case (6.2.28), where some transitions are forbidden [RASA86, RAD83]. Taking the next leading order of the transition m.e., the mentioned selection rules are washed out.

6.3 Large Deformation Regime

One salient feature of CSM is the behavior of the projected states as function of the deformation parameter especially for the extreme limits of $d \to 0$ and large d. While in the vibrational limit these are just multiphonon states in the rotational

regime, i.e. for asymptotic values for deformation parameter d, the wave functions of the ground, beta and gamma band states predicted by the liquid drop model [BM53] in the large deformation regime are nicely simulated. Indeed, as proved in Ref. [RCGD82], writing the projected states in the intrinsic reference frame and then considering a large deformation d, one obtains:

$$
\begin{aligned}
\varphi^i_{JM} = C_J \beta^{-1} e^{-(d - \frac{k\beta}{\sqrt{2}})^2} \Big[& \delta_{i,g} D^{J*}_{M0}(\Omega_0) + \delta_{i,\beta} \frac{4d^2}{9\sqrt{114}} D^{J*}_{M0}(\Omega_0) \\
& + \delta_{i,\gamma} \beta f_J k\gamma (D^{J*}_{M2}(\Omega_0) + (-)^J D^{J*}_{M,-2},(\Omega_0)) \Big],
\end{aligned}
$$

$$(6.3.1)$$

where k is a constant defining the canonical transformation relating the quadrupole bosons and the quadrupole collective conjugate coordinates:

$$
\alpha_\mu = \frac{1}{k\sqrt{2}} (b^\dagger_\mu + (-)^\mu b_{-\mu}), \quad \pi_\mu = \frac{ik}{\sqrt{2}} ((-)^\mu b^\dagger_{-\mu} - b_\mu), \qquad (6.3.2)
$$

while the constants C_J and f_J are

$$
C_J = \frac{2}{3} \pi^{-\frac{1}{4}} k^{2/3} (2J + 1)^{1/2}, \quad f_J = -\sqrt{2}(8 + (-)^{J+1})^{-1/2}. \qquad (6.3.3)
$$

It is worth noticing that the model Hamiltonian yields for the ground band similar excitation energies as the effective Hamiltonian

$$
H_{eff} = 22A_1 \hat{N} + A_2 \hat{J}^2. \qquad (6.3.4)
$$

Averaging this Hamiltonian on a vibrational ground band state one obtains a quadratic expression in N, the number of bosons in the considered state:

$$
\langle H_{eff} \rangle = 2N(11A_1 + A_2 + 2A_2N). \qquad (6.3.5)
$$

In the asymptotic region for d the average matrix element of H_{eff} is [RGB77] proportional to $J(J + 1)$:

$$
\langle H_{eff} \rangle = J(J + 1) \left(\frac{11A_1}{3d^2} + A_2 \right). \qquad (6.3.6)
$$

For the intermediate values of the deformation parameter d, we may use for energies either rational functions of d with the coefficients being functions of the angular momentum as given in the previous section, or asymptotic expansion for the matrix elements in power of $1/x$. The latter version was described in Ref. [RS83]. Here we sketch the ideas and give the final results.

6.3.1 Energies

The asymptotic expressions for the matrix elements are obtained by considering the behavior of the overlap integral $I_J^{(0)}$ for large d. This is obtained by using the asymptotic expression for the hypergeometric function:

$$_1F_1(a, c; z) = \frac{\Gamma(c)}{\Gamma(a)} e^z z^{a-c} [1 + \mathcal{O}(|z|^{-1})], \tag{6.3.7}$$

One finds that the dominant term of the asymptotic form of $I_J^{(0)}$ is:

$$I_J^{(0)} \sim \frac{e^x}{3x}. \tag{6.3.8}$$

This suggests as trial function for the equantity $I_J^{(0)}$ satisfying the differential equation (6.2.6), the following series:

$$I_J^{(0)} = e^x \sum_{n=1} A_n x^{-n}. \tag{6.3.9}$$

This series expansion together with the differential equation, offer a recurrence relation for the coefficients A_n:

$$A_{n+1} = \frac{A_n}{6n} (2n + J)(2n - J - 1). \tag{6.3.10}$$

Using the asymptotic form (6.3.8) as the limit condition, which infers $A_1 = \frac{1}{3}$, the solution (6.3.9) is completely determined.

For large values of the deformation parameter, the series can be approximated by a truncation, such that one arrives at the following expression

$$x \frac{I_J^{(1)}}{I_J^{(0)}} = x - 1 - \frac{1}{3x} - \frac{5}{9x^2} - \frac{37}{27x^3} + \left(\frac{1}{6x} + \frac{5}{18x^2} + \frac{13}{18x^3} \right) J(J+1)$$

$$- \frac{1}{54x^3} J^2(J+1)^2 + \mathcal{O}(x^{-4}). \tag{6.3.11}$$

This approximation can be substantially improved. Indeed, let us write the differential equation (6.2.6) in the form

$$x \left(x \frac{I_J^{(1)}}{I_J^{(0)}} \right)' + \left(x \frac{I_J^{(1)}}{I_J^{(0)}} \right)^2 - \frac{x-1}{2} \left(x \frac{I_J^{(1)}}{I_J^{(0)}} \right) - \frac{2x^2 + J(J+1)}{4} = 0 \tag{6.3.12}$$

and replace the first term by the derivative of the expression (6.3.11). Obviously, one obtains a quadratic equation for the quantity $x I_J^{(1)}/I_J^{(0)}$ whose positive solution is:

$$x \frac{I_J^{(1)}}{I_J^{(0)}} = \frac{1}{2}\left[\frac{x-2}{2} + \sqrt{G_J}\right], \tag{6.3.13}$$

where

$$G_J = \frac{9}{4}x(x-2) + \left(J + \frac{1}{2}\right)^2 - \frac{4}{9x}\left(3 + \frac{10}{x} + \frac{37}{x^2}\right)$$
$$+ \frac{2}{3x}\left(1 + \frac{10}{3x} + \frac{13}{x^2}\right)J(J+1) - \frac{2J^2}{9x^3}(J+1)^2. \tag{6.3.14}$$

Note that the m.e. between ground and γ states are negligible within the approximation of large deformation.

Using the approximation (6.3.11), the energies of the β and γ bands can be written as follows:

$$E_J^\beta = \frac{1}{P_J^\beta}\left[A_1 S_J^\beta + A_3 F_J^\beta\right] + A_2 J(J+1), \tag{6.3.15}$$

$$E_J^\gamma = A_1 \frac{S_J^\gamma}{P_J^\gamma} + A_2 J(J+1), \tag{6.3.16}$$

The polynomials P, S, F, in $J(J+1)$, are given in Appendix D. To these equations we add the equations determining the excitation energies in the ground band:

$$E_J^g = 11A_1\left[\frac{x-2}{2} + \sqrt{G}\right] + A_2 J(J+1). \tag{6.3.17}$$

In order to obtain a good agreement for β-band energies, for some cases, the use of an additional term accompanied by the A_4 or A_5 parameter is necessary. For these additional terms the following asymptotic relations are used:

$$\langle\phi_{JM}^\beta|\Omega_\beta^\dagger\Omega_{\beta'}^2 + h.c.|\phi_{JM}^\beta\rangle = \frac{96d}{5\sqrt{70}}\left(\frac{x}{2} - \frac{T_J^{4,\beta}}{P_J^\beta}\right),$$

$$\langle\phi_{JM}^\beta|\Omega_\beta^{\dagger 2}\Omega_{\beta'}^2|\phi_{JM}^\beta\rangle = \frac{32}{875}\frac{T^{5,\beta}}{P_J^\beta}, \tag{6.3.18}$$

with the factors $T_J^{n,\beta}$, with n = 4, 5, and P_J^β defined in Appendix D.

6.3.2 Reduced Probabilities for the E2 Transitions

Taking the asymptotic limit of the exact m.e. of the quadrupole operator, one obtains very simple formulas for transition m.e. in the large deformation case. The asymptotic expressions for the reduced m.e. of the harmonic quadrupole transition operator are [RS83]:

$$\langle \phi_J^i || Q_2^h || \phi_{J'}^i \rangle = 2dq_h C_{K_i 0 K_i}^{J\,2\,J'}, \quad i = g, \beta, \gamma, \quad K_i = -2\delta_{i\gamma}, \quad (6.3.19)$$

$$\langle \phi_J^\gamma || Q_2^h || \phi_{J'}^g \rangle = \sqrt{2} q_h C_{-2\,2\,0}^{J\,2\,J'}, \quad (6.3.20)$$

$$\langle \phi_J^\beta || Q_2^h || \phi_{J'}^\gamma \rangle = \frac{2}{3\sqrt{19}} q_h C_{0\,-2\,-2}^{J\,2\,J'}, \quad (6.3.21)$$

while the β and ground band states are connected by anharmonic part of $Q_{2\mu}$:

$$\langle \phi_J^\beta || Q_2^{anh} || \phi_{J'}^g \rangle = 2\sqrt{\frac{7}{19}} q_{anh} C_{0\,0\,0}^{J\,2\,J'}. \quad (6.3.22)$$

Note that in the asymptotic limit of the deformation parameter d, the projected functions are similar to that of the liquid drop model in the strong coupling regime. The Clebsch-Gordan factorization of the transition probabilities is known in literature as Alaga's rule [AL57]. Thus, we may say that our description of the deformed nuclei is consistent with the Alaga's rule.

As already mentioned before, the connection between the vibrational and rotational spectra, within the CSM, is achieved according to the Sheline-Sakai scheme [Sa76, Sh60]. This property is illustrated in Fig. 6.1 where the spectrum of $\hat{N}$, the boson number operator, is represented as function of the deformation parameter d. Note that in the vibrational limit the energy levels are equidistant, being multi-boson
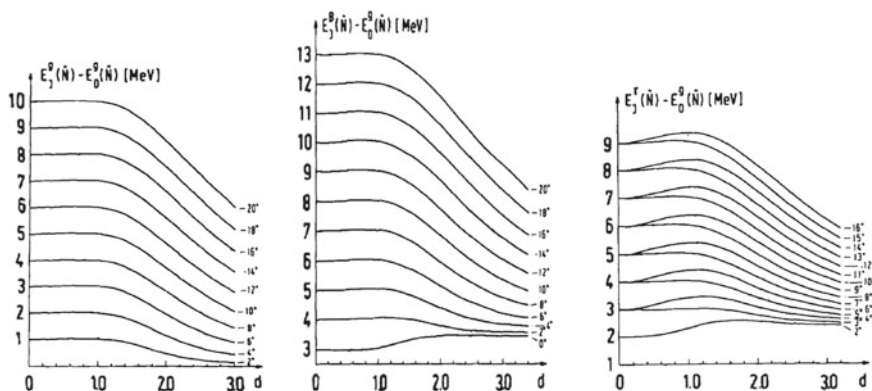
Fig. 6.1 Excitation energies of ground, beta and gamma bands states are represented as function of d, for the boson number operator $\hat{N}$

states, while in the rotational limit they have a $J(J+1)$ like pattern. A special atten-
tion deserves the case of γ band. The degeneracies (3,4), (5,6), (7,8),…, etc. seen
in the limit of $d \to 0$ transforms into a doublet structure once the deformation is
going apart from zero. This staggering order is changed into another one (2,3), (4,5),
(6,7),…, etc., in the regime of large deformation. The transition between the two
extreme nuclear phases, spherical and well deformed, crosses, unavoidably, a criti-
cal point. The specific features of this phase transition are suggested in Fig. 6.2 where
the deformation dependence of the intraband E2 transition probability is shown. It is
to be noticed that the intraband probability for the transition $J \to (J-2)$ follows
more or less similar pattern, as a function of d, with the excitation energy functions.
The situation for the gamma band transitions $(J+1) \to J$ is, however, different.
Indeed, the transitions between states which are degenerate in the vibrational limit
are vanishing in the beginning of interval then they split and increase with different
slopes, reach maximum values and then decrease continuously. On the ascendant
part the transitions to odd spins increase faster and therefore intersect the curves cor-
responding to the transitions to the next even spin levels. The curves crossings take
place for d about 1.5. Close to this deformation, all transitions undertake a maximal
value. The corresponding deformation may be interpreted as a critical value for the
phase transition from spherical to rotational regime. To conclude, the behavior of
the $(J+1) \to J$ transitions in the γ band, can be considered as a signature of the
critical point characterizing the spherical-rotational phase transition.

Fig. 6.2 The normalized B(E2) values characterizing the intraband transitions $J \to (J-2)$ for ground (**a**), β (**b**) and γ (**d**) bands. For γ band the transitions $(J+1) \to J$ are also considered (**c**)
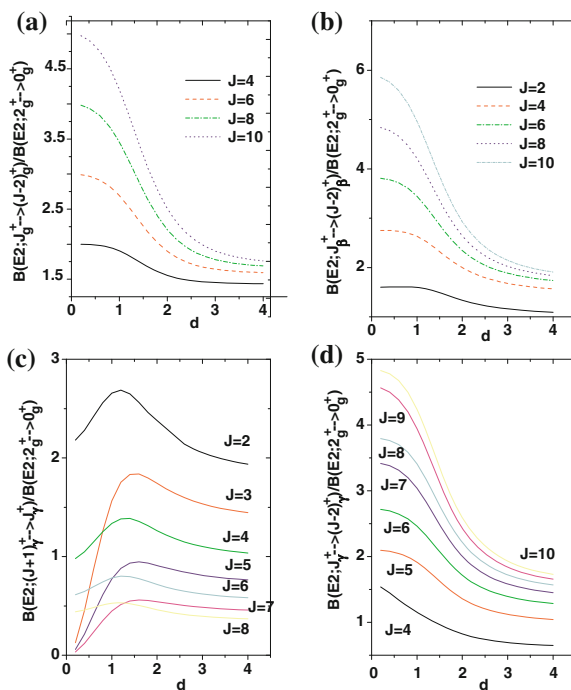
6.4 The Intrinsic Frame of Reference

Some virtues of the projected states, to describe certain specific properties of nuclear systems, can be revealed by going to the intrinsic reference frame, obtained by a rotation of Eulerian angle Ω_0 from the laboratory frame. The intrinsic coordinates are defined by rotating with the angle Ω_0 the collective coordinates α_μ, related to the boson operators by Eq. (6.3.2):

$$a_\mu = R(\Omega_0)\alpha_\mu R(\Omega_0^{-1}) = \beta\left[\delta_{\mu,0}\cos\gamma + \frac{\sin\gamma}{\sqrt{2}}(\delta_{\mu,2} + \delta_{\mu,-2})\right],$$

$$R(\Omega)a_m R(\Omega^{-1}) = \sum_{m_1} D^2_{m_1 m}(\Omega_0^{-1}\Omega\Omega_0)a_{m_1}. \tag{6.4.1}$$

As suggests the second equation of (6.4.1), the intrinsic coordinates are not components of a tensor with a definite rank. Written in quadrupole coordinates, the equation for the boson vacuum can be integrated with the result:

$$|0\rangle = 2\left(\frac{2k^5}{3\pi^{1/2}}\right)^{1/2} e^{-\frac{k^2\beta^2}{2}}. \tag{6.4.2}$$

After elementary algebraic manipulations, the projected states (6.1.7) can be written in terms of Ω_0, and the dynamic quadrupole deformations β and γ:

$$\phi^i_{JM} = \mathcal{N}^i_J \sum_K D^{J*}_{MK}(\Omega_0)\Gamma^i_{JK}(d,\beta,\gamma)e^{-\frac{k^2\beta^2}{2}}, \quad i = g,\beta,\gamma. \tag{6.4.3}$$

The normalization factors are given by:

$$\mathcal{N}^i_J = K_J N^i_J(d), \quad K_J = (24)^{-\frac{1}{2}}\pi^{-\frac{9}{4}}k^{\frac{5}{2}}(2J+1)e^{-d^2}, \tag{6.4.4}$$

while the coefficients Γ have the expressions:

$$\Gamma^g_{JK}(d,\beta,\gamma) = \int D^{J*}_{K0}(\Omega)F(\Omega,d,a)d\Omega,$$

$$\Gamma^\beta_{JK}(d,\beta,\gamma) = \int D^{J*}_{K0}(\Omega)\left[T^\beta_{00}(\alpha) + \sum_m D^2_{m0}(\Omega)T^\beta_{2,m}(\alpha)\right]F(\Omega,d,a)d\Omega,$$

$$\Gamma^\gamma_{JK}(d,\beta,\gamma) = \sum_m \int D^{J*}_{K2}(\Omega)D^2_{m2}(\Omega)T^\gamma_{2,m}(\alpha)F(\Omega,d,a)d\Omega,$$

$$F(\Omega,d,a) = \exp\left[\sqrt{2}kd\sum_m D^2_{m'0}(\Omega)a_{m'}\right]. \tag{6.4.5}$$

The notations $T_{0,0}^{\beta}$ and $T_{2,0}^{\beta}$ stand for the scalar and second order tensor parts of the operator $\Omega_{\beta}^{\dagger}$ and depend only on the coordinates α. Similarly, a tensor term T^{γ}, for the γ band, is defined:

$$\Omega_{\beta}^{\dagger}\psi_g = \left[T_{0,0}^{\beta}(\alpha) + T_{2,0}^{\beta}(\alpha)\right]exp(-d^2 + \sqrt{2}kd\alpha_0)|0\rangle,$$
$$\Omega_{\gamma}^{\dagger}\psi_g = T_{2,2}^{\gamma}(\alpha)exp(-d^2 + \sqrt{2}kd\alpha_0)|0\rangle. \tag{6.4.6}$$

The three Eulerian angles and the two deformation coordinates β and γ span the manifold

$$S_5 = [0, 2\pi] \times [0, \pi] \times [0, 2\pi] \times [0, \infty] \times [0, 2\pi] \tag{6.4.7}$$

The scalar product of two functions ϕ_{JM}^{i} and $\phi_{J'M'}^{i'}$ defined on S_5 is:

$$(\phi_{JM}^{i}, \phi_{J'M'}^{i'}) = \frac{1}{24} \int_{S_5} \phi_{JM}^{i*}\phi_{J'M'}^{i'}d^5\tau,$$

$$\text{with } d^5\tau = \frac{3}{4\pi^2}|\sin 3\gamma|\beta^4 d\beta d\gamma. \tag{6.4.8}$$

In the regime of large d, the leading terms of ϕ_{JM}^{i} are those given in Eq. (6.3.1). The ground state amplitude $\Gamma_{JK}^{g}(d, \beta, \gamma)$ can be analytically evaluated:

$$\Gamma_{JK}^{g}(d, \beta, \gamma) = \frac{4\pi^3}{[\Gamma\left(\frac{1}{2}\right)]^2} \frac{[(J-K)!(J+K)!]^{1/2}}{(\frac{J-K}{2})!\,(\frac{J+K}{2})!}(-)^{\frac{J+K}{2}} \sum_{m,n,s}(-)^s 2^{\frac{m+n}{2}+s+1}3^{\frac{m}{2}+s}(dk\beta)^{m+n}$$

$$\times \frac{(m+s+\frac{K}{2})!\,(m+s-\frac{K}{2})!\,(m+s+\frac{J}{2})!(\cos\gamma)^n(\sin\gamma)^m}{s!(n-s)!\,(\frac{2m+K}{4})!\,(\frac{2m-K}{4})!\,(m+s-\frac{J}{2})!(2m+2s+J+1)!}$$

$$\equiv \sum_{m,n}X_{m,n}^{J,K}(dk\beta)^{m+n}(\cos\gamma)^m(\sin\gamma)^n, \text{ if K = even and 0 otherwise.} \tag{6.4.9}$$

Alternatively, this amplitude can be written as a series of d with the coefficients depending on β and γ:

$$\Gamma_{JK}^{g}(d, \beta, \gamma)e^{-\frac{k^2\beta^2}{2}} = \sum_{J\le J', J'=even} C_{J'K}^{J}(-)^{\frac{J'-J}{2}}(6d^2)^{J'/4}e^{\sqrt{2}dk\beta\cos\gamma}f_{J'K}(\beta, \gamma), \tag{6.4.10}$$

where

$$C_{J'K}^{J} = \left(\frac{24\pi^{9/2}}{k^5}\right)^{1/2} \frac{F(J+K)F(J-K)}{F(J'+K)F(J'-K)} \frac{\left(\frac{J+J'}{2}\right)!}{(J+J'+1)!}\left[\frac{(2J')!}{(J'/2)!}\right]^{1/2},$$

$$F(m) = \frac{(m!)^{1/2}}{(m/2)!}, \quad m = even,$$

$$f_{JK}(\beta, \gamma) = \pi^{-1/4} k^{5/2} 2^{\frac{J+3}{2}} 3^{\frac{J-2}{4}} \left[\frac{(J-K)!(J+K)! \left(\frac{J}{2}\right)!}{(2J)!} \right]^{1/2} e^{-\frac{k^2 \beta^2}{2}}$$

$$\times (k\beta)^{J/2} \sum_v \frac{(\cos \gamma)^{\frac{J-K}{2} - 2v} \left(\frac{1}{2\sqrt{3}} \sin \gamma\right)^{\frac{K}{2} + 2v}}{v! \left(v + \frac{K}{2}\right)! \left(\frac{J-K}{2} - 2v\right)!}. \qquad (6.4.11)$$

As shown in Appendix F, the functions Γ^{β}_{JK} and Γ^{γ}_{JK} can be expressed as linear combination of Γ^{g}_{JK}.

From Eqs. (6.4.3) and (6.4.10) one immediately finds:

$$\lim_{d \to 0} \phi^g_{JM} = |\frac{J}{2}, \frac{J}{2}, 0, J, M\rangle = \sum_K f_{JK}(\beta, \gamma) D^{J*}_{MK}. \qquad (6.4.12)$$

Thus, for the highest seniority states one has been found a very compact formula, in terms of intrinsic variables. As a matter of fact, this is a nice example showing how to generate a basis sub-set from a coherent state. A full $\{|N v \alpha J M\rangle\}$ basis was projected in Ref. [GRC78], by using a coherent state with respect to b_0 and $b_2 + b_{-2}$ boson operators as generating function. In the quoted paper the corresponding coherence parameters c_0 and c_2, multiplying the bosons $b_0^{\dagger}$ and $b_2^{\dagger} + b_{-2}^{\dagger}$ respectively, are c-numbers. In fact this feature of coherent states, to comprise any vector state of a complete basis, is caused by their over-completeness property.

Using the analytical expression (6.4.9), one can easily prove the following symmetry relations for the ground band states amplitudes:

$$\Gamma^g_{JK}(d, \beta, \gamma) = \Gamma^g_{J-K}(d, \beta, \gamma),$$
$$\Gamma^g_{JK}(d, \beta, -\gamma) = (-)^{K/2} \Gamma^g_{JK}(d, \beta, \gamma),$$
$$\Gamma^g_{JK}(-d, -\beta, \gamma) = \Gamma^g_{JK}(d, \beta, \gamma). \qquad (6.4.13)$$

From the results of Appendix F, one finds that Γ^{β}_{JK} satisfies the same symmetry relations as Γ^g_{JK}. As for Γ^{γ}_{JK}, the only modified equation is:

$$\Gamma^{\gamma}_{JK} = (-)^J \Gamma^{\gamma}_{J-K}. \qquad (6.4.14)$$

Making use of these symmetries, the projected states can be written in the form:

$$\varphi^i_{JM} = \mathcal{N}^i_J e^{-\frac{k^2 \beta^2}{2}} \sum_{K \geq 0} \frac{\Gamma^i_{JK}}{(1 + \delta_{K0})} (D^{J*}_{MK} + (-)^J D^{J*}_{J-K}), \quad i = g, \beta, \gamma. \quad (6.4.15)$$

The wave functions in the intrinsic frame satisfy the following ortho-normalization equation:

$$\frac{(\mathcal{N}_J^i)^2}{4(2J+1)} \sum_K \int \left(\Gamma_{JK}^i\right)^2 \beta^4 e^{-k^2\beta^2} |\sin 3\gamma| d\beta d\gamma = 1,$$

$$\sum_K \int \Gamma_{JK}^i \Gamma_{JK}^{i'} \beta^4 e^{-k^2\beta^2} |\sin 3\gamma| d\beta d\gamma = 0, \text{ if } i \neq i'. \quad (6.4.16)$$

In order to use the projected states for a practical scope, one needs to know the matrix elements of an arbitrary function of β and γ variable:

$$I_{JK,J',K'}^{i,i'}(a,b,c) = k^5 \int e^{-k^2\beta^2} \Gamma_{JK}^i \Gamma_{J'K'}^{i'}(k\beta)^a \cos^b \gamma \sin^c \gamma |\sin 3\gamma| \beta^4 d\beta d\gamma, \ i, i'$$

$$= g, \beta, \gamma. \quad (6.4.17)$$

The analytical expression for this integral is given in Appendix F.

6.4.1 Useful Information Coming from the Intrinsic Frame

Here we present a comparison of the CSM predictions and the fully microscopic model of Koppel et al. [KOP81]. In Ref. [KOP81], Koppel studied the Bohr-Mottelson Hamiltonian with the potential energy and inertial parameters microscopically calculated. First, one defines the single particle states by using, as a mean field, the Woods Saxon potential with the Coulomb interaction included for protons. Then, the potential energy is calculated by including the Strutinski corrections [STR68] due to the single particle motion. The parameters for the liquid drop model are taken from the mass formula of Meyers-Swiatecki [MS67] amended by the corrections introduced by Pauli and Ledergerber [PL71]. The gap parameter is taken equal to $12A^{-1/2}$. The moments of inertia and the three mass parameters are determined by means of a cranking formalism which includes the pairing interaction. The Schrodinger equation for the collective motion is solved by the procedure developed by Kumar and Baranger [KB68]. This way one finds the energies and corresponding eigenstates:

$$\Psi_{\alpha JM}(\beta, \gamma, \Omega) = \sum_{K \geq 0, even} A_{\alpha JK}(\beta, \gamma) \Phi_{MK}^J(\Omega), \alpha = g, \beta, \gamma$$

$$\Phi_{MK}^J = \left[\frac{2J+1}{16\pi^2(1+\delta_{K,0})}\right]^{1/2} \{D_{MK}^{J*}(\Omega) + (-)^J D_{M-K}^{J*}(\Omega)\}.$$

$$(6.4.18)$$

The probability for the component K to be realized is:

$$N_K = \int |A_{\alpha JK}|^2 dV_{\beta,\gamma} \tag{6.4.19}$$

In Ref. [RKF83] one may find the amplitudes $A_{\alpha IK}$ for the states 0_g^+, 2_γ^+, 0_β^+, 10_g^+, 10_γ^+, 10_β^+ plotted as function of the β and γ variables, respectively. For ^{190}Pt, the results corresponding to the first three mentioned states are given in Fig. 6.3, while those of the last three, in Fig. 6.4. From the panel a) of Fig. 6.3, one sees that the ground state γ probability has a flat maximum, for a non-vanishing value of β, which practically does not depend on γ. The amplitude $A_{\beta 00}$ characterizing the state 0_β^+, exhibits two maxima, one for prolate and one for oblate deformation. The same structure has $A_{\gamma 20}$, while $A_{\gamma 22}$ has only one maximum at $\gamma = 60°$. It is nice to remark that this result is consistent with the CSM prediction for Pt region, saying that the quadrupole moments for the states 2_g^+ and 2_γ^+ have opposite signs. The $K = 2$ component for the state 2_γ^+ prevails, its probability being $N_2 = 0.652$, which is to be compared with $N_0 = 0.348$ corresponding to the $K = 0$ amplitude. In the high spin states (see Fig. 6.4), several K components are contributing with
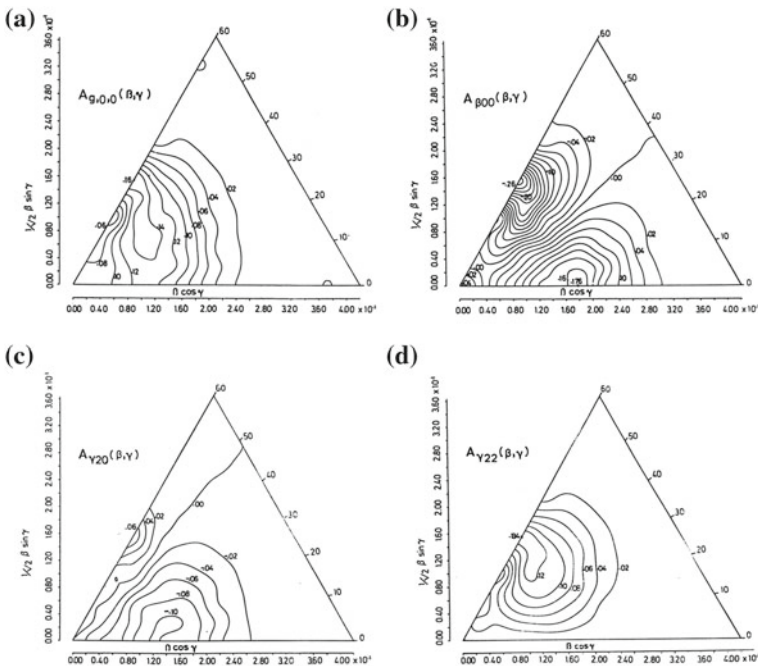
Fig. 6.3 The K amplitudes, defined by Eq. (6.4.18) are plotted as function of the dynamic β and γ variables for the states $0_g^\dagger$ (**a**), $0_\beta^\dagger$ (**b**) and $2_\gamma^\dagger$ (**c**) and (**d**)
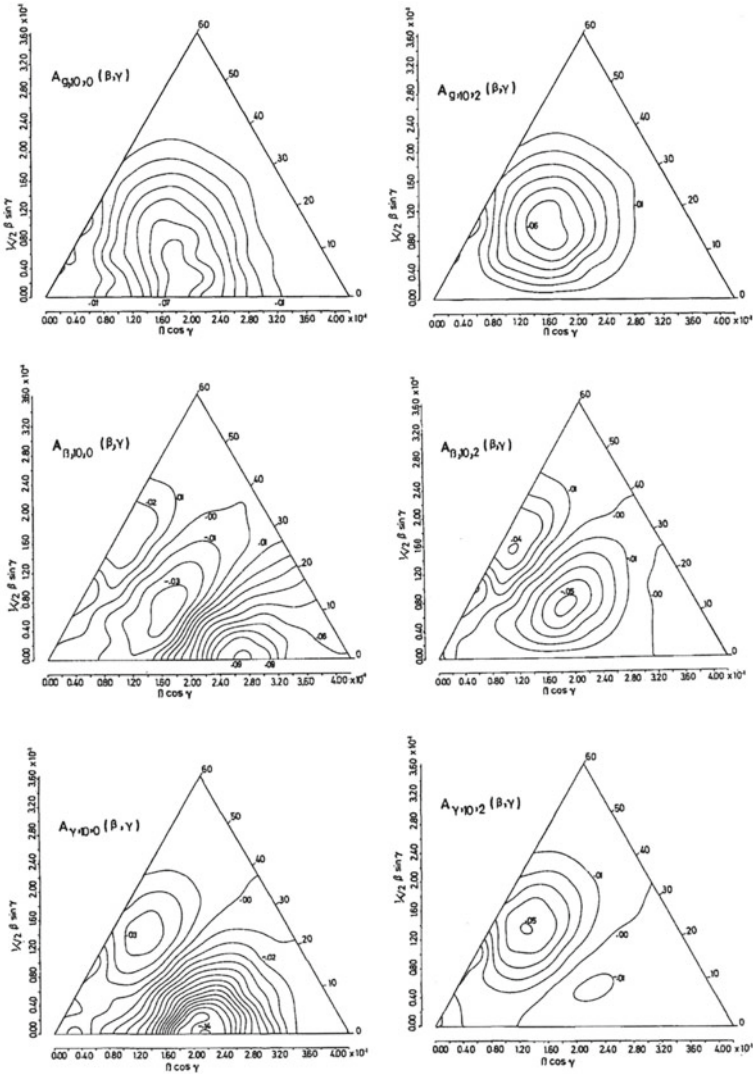
Fig. 6.4 The K amplitudes, defined by Eq. (6.4.19) are plotted as function of the dynamic γ variables for the states $10_g^\dagger$, $K = 0$ (*upper left*), $10_g^\dagger$, $K = 2$ (*upper right*) $10_\beta^\dagger$, $K = 0$ (*middle left*) and $K = 2$ (*middle right*), $10_\gamma^\dagger$, $K = 0$ (*bottom left*) and $K = 2$ (*bottom right*)

comparable weights. For example the state 10_g^+ consists mainly of three components with $K = 0$ ($N_0 = 0.4847$), $K = 2$ ($N_2 = 0.3714$) and $K = 4$ ($N_4 = 0.104$) exhibiting maxima at γ equal to $0°$, $30°$ and $40°$. The state 10_β^+ has a dominant $K = 0$ component ($N_0 = 0.4818$) and two small components with $K = 2$ ($N_2 = 0.1781$) and $K = 4$ ($N_4 = 0.0514$). The dominant component has three maxima, one for

$\gamma = 0°$, which prevails over the other ones, one at $35°$ and the third one at $55°$. The state 10_γ^+ has also three K-components with the weights $N_0 = 0.6284$, $N_2 = 0.1178$, and $N_4 = 0.1279$. The dominant component has two maxima at γ equal to $0°$ and $60°$. The K $= 2$ component has also two maxima at γ equal $15°$ and $45°$, while the third component only one maximum at $\gamma = 45°$.

Within the CSM, one defines the probability distributions for γ and β deformations by the following equations:

$$f_J^{(i)}(d, \gamma) = \int |\phi_{JM}^i|^2 \beta^4 d\beta d\Omega, \, i = g, \gamma, \beta,$$

$$g_J^{(i)}(k\beta) = \frac{1}{32\pi^2 k^5} \int |\phi_{JM}^i|^2 d\Omega |\sin 3\gamma| d\gamma. \tag{6.4.20}$$

These functions are plotted in Fig. 6.5. In the case of $g_J^i(k\beta)$, for a better presentation, a scaling factor k_i is used. In panel e) the function

$$F_J^i(k\beta) = (k\beta)^4 g_J^i(k\beta), \tag{6.4.21}$$

is plotted versus $k\beta$. If one denotes by

$$\beta_0^2 = \langle \psi_g | \beta^2 | \psi_g \rangle, \tag{6.4.22}$$

and then one evaluates the expectation value involved in the defining equation, one arrives at:

$$(k\beta_0)^2 = \frac{1}{2}(4d^2 + \frac{5}{2}). \tag{6.4.23}$$

According to Ref. [RCGD82], for ^{190}Pt d $= 0.62$ and consequently $k\beta_0 = 1.5$ which is, as shown in Fig. 6.5, just the value where the function $F_J^g(k\beta)$ reaches its maximum. This feature allows us to interpret the value of beta where the functions F_J^i achieve their maxima as the static deformation of the given nucleus, in the state ϕ_J^i. In this respect, one may say that the deformation in ground state is smaller than that in the state 2_γ^+ which at its turn, is smaller than that of 0_β^+. Corroborating this result with that earlier mentioned concerning the ordering relations of the quadrupole moments in the unprojected states, one may say that, at least for these states, the projection does not alter the ordering of quadrupole moments. The plot in panel a) of Fig. 6.5 shows an unstable structure for the ground state and a flat maximum at around $45°$ due to the admixture of the K $\neq 0$ components for the state 10_g^+. The state 0_β^+ exhibits two equal maxima for $\gamma = 0°$ and $60°$ respectively, which fully agrees with what the generalized Bohr Mottelson model predicts. The plot for 10_β^+ shows two lower maxima at $\gamma = 15°$ and $50°$. This picture is similar to that for the K $= 2$ component of the state 10_β^+. One notices that 2_γ^+ has a broad but not high maximum, centered at about $30°$. This structure is specific to a triaxial rotor state. The bright of the γ distribution function may reclaim the importance of the kinetic energy in the γ
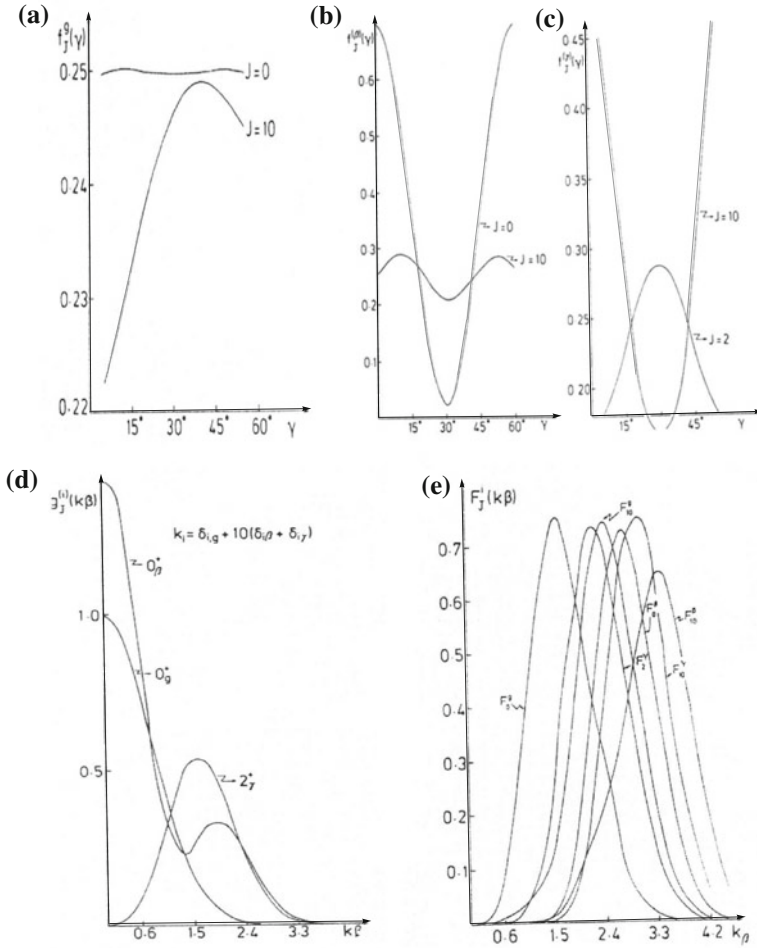
Fig. 6.5 The γ probability is plotted for low and high angular momenta in ground (**a**), β (**b**) and γ (**c**) bands. The probability distribution for the β variable is presented in the panels (**e**). The same function as in (**e**) multiplied with the factor β^4 which enter the definition of the measure in the β space, is plotted in panel (**d**)

vibrational state. Such a soft maximum appears also in the $K = 0$ amplitude of the microscopic formalism described before, which keeps the picture close to the gamma unstable situation. Indeed, for γ unstable model the $K = 0$ component is just $\cos 2\gamma$ which produces a prolate maximum while the $K = 2$ component is proportional to $\sin 2\gamma$ which has a maximum at $45°$. Within the CSM, the γ distribution function associated to the state 10_γ^+ has two equal maxima, one for γ close to $0°$ and one close to $60°$. This behavior is identical with that shown by the plot of $A_{\gamma,10,0}$ in Ref. [RKF83] (Fig. 6.6).

Fig. 6.6 The ground *left*, gamma *right* and beta *middle* band energies predicted by CSM in ^{232}Th are compared with experimental data. The structure coefficients and the deformation parameters, fitted as explained in the text, are given in the figure legend
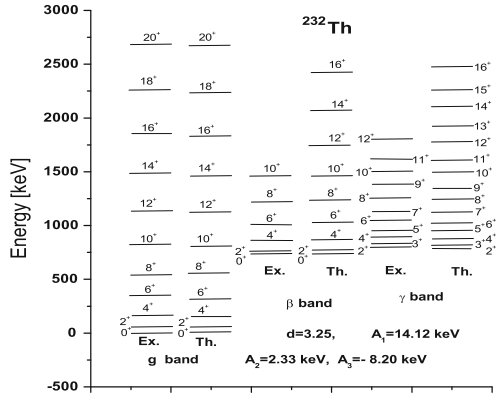
In conclusion, for low spin the model states for gamma band used by CSM have a γ asymmetric structure. Moreover, due to the fact that the energies in the ground and gamma bands are obtained by diagonalizing a 2/2 matrix, it is expected that such a γ asymmetric structure is met for both eigenstates of the model Hamiltonian. This explains why the CSM formalism is able to describe the data for the triaxial like nuclei. According to the comparison performed before, the CSM predictions for ^{190}Pt are in full agreement with those obtained microscopically in Ref. [KOP81]. This confirms once more that the choice for the three vector states, modeling the ground beta and gamma bands, is the appropriate one (Figs. 6.7 and 6.8).

6.5 Some Numerical Applications

6.5.1 Energies

The CSM formalism was applied, in Refs. [RPB03, RASA86, RS83, RSS84, MRF98], to several even-even nuclei: $^{188-194}$Pt, $^{188-192}$Os, ^{194,196}Hg, ^{156,162}Dy, $^{150-160}$Gd, ^{228,232}Th, ^{126}Xe and ^{130}Ba. Among these, one finds nuclei satisfying one of the three symmetries mentioned above, i.e., O(6), SU(5) and SU(3). From each of these sets, we chose a representative which is shown graphically. Thus, in Figs. 6.6, 6.7, 6.8 and 6.9 we compare the calculated and experimental energies for ground, beta and gamma bands for ^{232}Th(SU(3)), ^{156}Dy(SU(5)), ^{162}Dy(O(6)), ^{192}Pt(O(6)). We also present the situation of the O(6) nuclei ^{126}Xe and ^{130}Ba (Figs. 6.10 and 6.11), which seem to exhibit the characteristics of a triaxial rotor. Another triaxial rotor considered [MRF98] is ^{228}Th (Figs. 6.12 and 6.13). The arguments supporting this label consist in the following: The static values for the γ deformation estimated within the triaxial rotation-vibration model (TRVM) are about 25° for ^{126}Xe and ^{130}Ba and 13° for ^{228}Th [MRF98]. It is well known that the triaxial rotor predicts that the sum of the energies for the first two states 2^+ is equal to the energy of the
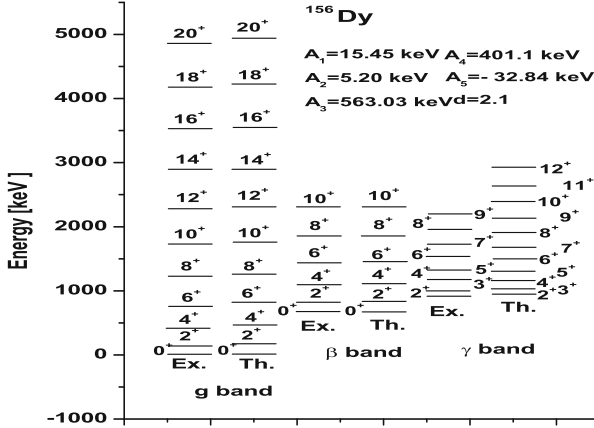
Fig. 6.7 The same as in Fig. 6.6 but for ^{156}Dy
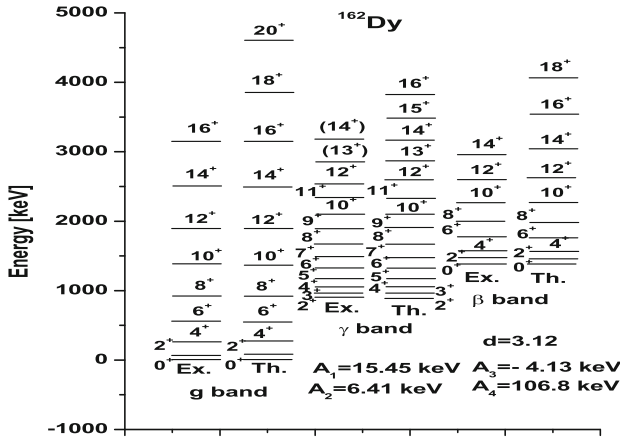
Fig. 6.8 The same as in Fig. 6.6 but for ^{162}Dy

first 3^+ state. The differences for the two quantities, which should be equal to each other in the rotor picture, are 2, 47 and 95 keV for ^{228}Th, ^{126}Xe and ^{130}Ba, respectively. The deviation from the rotor picture for the Xe and Ba isotopes, reflects an additional interaction of ground and gamma bands. Note that in the quoted figures for the triaxial nuclei the β states energies are not given. The reason is that only very few beta state energies are available, one or two. Moreover the coefficient A_3 was fixed such that the calculated energy of the heading state and the corresponding experimental value are equal.

The energies for the beta band and those for the odd-J states of gamma band are obtained as expectation values of the model Hamiltonian on the corresponding model states. The energies of the ground band states as well as of gamma band

Fig. 6.9 The ground *left*, gamma *middle* and beta *right* band energies predicted by CSM in ^{192}Pt, are compared with experimental data. The structure coefficients and the deformation parameters, fitted as explained in the text, are given in the figure legend
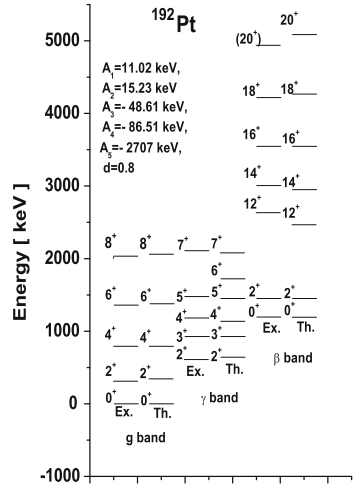
Fig. 6.10 The experimental (exp.) and the CSM predicted excitation energies for ^{126}Xe are represented in units of keV for g.s. and γ bands
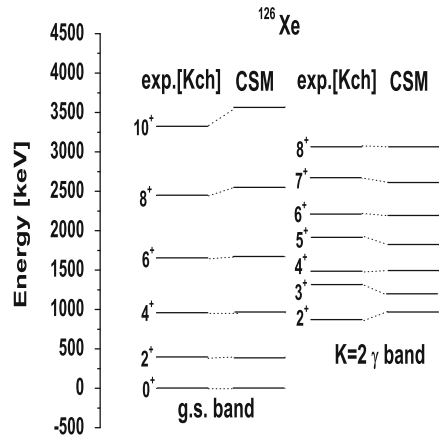
states with even angular momentum, were obtained by diagonalizing, for each J, a 2×2 matrix. The results depend on the structure coefficients A_i (i = 1, 2, ..., 5), and the deformation parameter d. For most nuclei, especially for the well deformed ones, only three structure coefficients (A_1, A_2 and A_3) are needed to obtain a good description of the data. These parameters were fixed in the following manner. For a given d the parameters A_i are fixed by fitting the energies of the lowest states in ground, beta and gamma bands. The parameter d is fixed so that an overall agreement in the three bands is obtained. Since the parameters A_3, A_4, A_5 affect only the beta band energies, they were fixed by fitting some energy levels from the beta bands. As a matter of fact, this confers the model certain flexibility in describing the detailed features of the beta band. Due to this aspect, in Ref. [RPB03] it was attempted to attribute the non-yrast states J^+, with $J \geq 12$ and even, to the beta band. As we

Fig. 6.11 The same as in
Fig. 6.10 but for ^{130}Ba
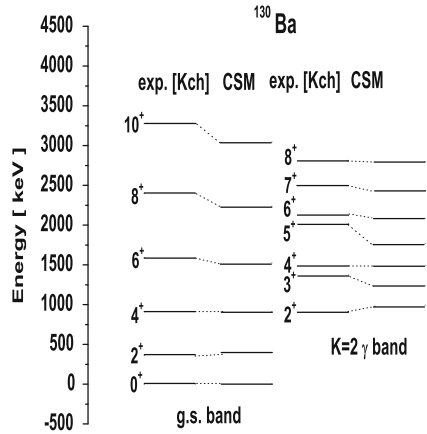
Fig. 6.12 The experimental
(exp.), the triaxial rotation
vibration model (TRVM) and
the CSM predicted energies
for ^{228}Th, are represented in
keV for the ground band
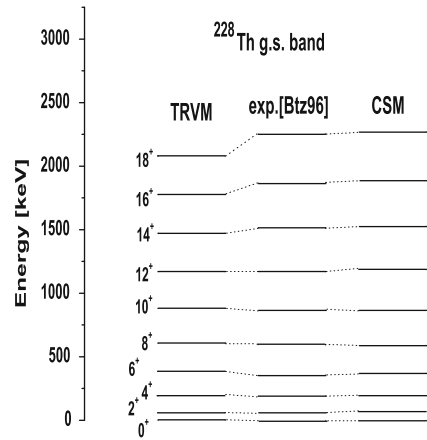
shall see in the next section a better description for these states is obtained when
the coupling to the quasiparticle degrees of freedom is taken into account. In Ref.
[RS83], one reported on the case of ^{232}Th where a least square procedure was used to
get the best fit of the available data. In the ground band, states with very high angular
momentum, up to 30^+, were included and the agreement with the experimental data
was within a deviation of 20 keV in gamma band and 8 keV in ground and beta
bands.

A common feature for spherical-deformed transitional nuclei is the staggering of
some levels of gamma band: $(3^+, 4^+)$, $(5^+, 6^+)$, etc. In the framework of CSM these
doublets originate from the fact that in the vibrational limit the doublet components
are degenerate. The spacing of doublet levels is underestimated by CSM in Pt isotopes
and overestimated in ^{126}Xe and ^{130}Ba. According to the above comment, this suggests
that the chosen value for the deformation parameter d is smaller for Pt and larger
for Xe and Ba, than it should be. It is well known that the deformation status of

Fig. 6.13 The same as in
Fig. 6.12 but for the γ band
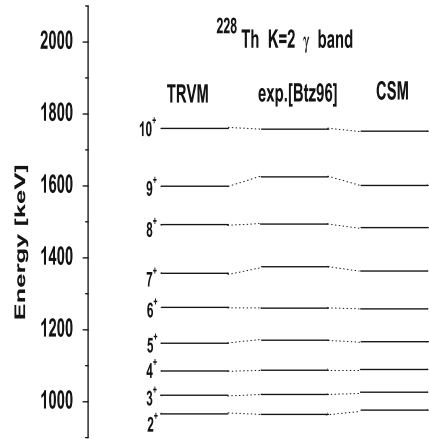
a nuclear system depends on the extent to which the open shell is filled up. Thus, in the isotopic chain of Gd, 4 isotopes ($^{152-156}$Gd) have a gamma stable structure while the remaining ones (^{150,158,160}Gd) are of gamma unstable type [RF05]. One notices that the crossing of gamma and beta bands takes place gradually, i.e. not all the states from the two bands cross each other respectively, for the same neutron number. Indeed, in ^{150}Gd, $E_{2^+_\beta} > E_{2^+_\gamma}$ while in ^{152,154}Gd this is reversed and become again valid for the heaviest two isotopes. As for the level 4^+, in the two bands for the first three isotopes 4^+_β is lower than 4^+_γ, while for the last three isotopes in the chain, the ordering is opposite. Of course, these level crossings are reflected in the inter-band transition probabilities connecting the two bands.

6.5.2 Electric Transition Probabilities

Description of intra- as well as of inter-band transition probabilities is a decisive test for any nuclear structure model. The reason is that these quantities are very sensitive to the detail structure of the wave functions. Therefore a viability certificate for CSM is given by the quality of the transition probability description.

From the many applications performed on this issue we selected those for ^{190}Pt, ^{192}Pt, ^{154}Gd, ^{126}Xe, ^{130}Ba, ^{228}Th which are representatives for gamma unstable, gamma stable and triaxial rotors behaving nuclei, respectively. The results for the three sets of isotopes are collected in Tables 6.1, 6.2 and 6.3, respectively. For gamma unstable and triaxial rotor nuclei a transition operator involving the harmonic (q_0) and the boson number non-conserving (q_2) terms (see Eq. (6.1.13)) is considered, while for Gd isotope the full three parameter formula has been used.

We note that a reasonable agreement with the experimental data is obtained by fixing the ratio q_2/q_0 so that a particular branching ratio, specified in Table 6.1, is

Table 6.1 Experimental and predicted values for some BE2 value ratios are given

$\frac{B(E2;I\to I')}{B(E2;J\to J')}10^2$	^{190}Pt				^{192}Pt			
	Exp.	Th.			Exp.	Th.		
		$q_2/q_0 = 0.44$	$q_2 = 0$	$d \to 0$		$q_2/q_0 = 0.44$	$q_2 = 0$	$d \to 0$
$\frac{2_\gamma^+ \to 0_g^+}{2_\gamma^+ \to 2_g^+}$	1.24	0.86	0.19	0	0.51	0.88	0.78	0
$\frac{3_\gamma^+ \to 2_g^+}{3_\gamma^+ \to 2_\gamma^+}$	1.8	1.8[a]	0.035	0	0.76	0.34	0.21	0
$\frac{3_\gamma^+ \to 4_g^+}{3_\gamma^+ \to 2_\gamma^+}$	49	36.2	30.2	40	26	25	24	40
$\frac{0_\beta^+ \to 2_g^+}{0_\beta^+ \to 2_\gamma^+}$	11	13.7	2.4	4.5	3.8	3.8[a]	2.2	4.5
$\frac{2_\beta^+ \to 0_g^+}{2_\beta^+ \to 0_\beta^+}$	0.2	0.05	0	0	0.022	0.0015	0	0
$\frac{2_\beta^+ \to 4_g^+}{2_\beta^+ \to 0_\beta^+}$	4.2	4.69	1.2	5.7	≤ 2.8	2.5	1.04	5.7

Data are taken from Ref. [FING72]. The vibrational limit ($d \to 0$) corresponds to the harmonic expression of the transition operator except for the transitions between beta and ground band states where the anharmonic component was used. The columns two and three correspond to the deformation d fitted from energy analysis, i.e. 0.6 for ^{190}Pt and 0.8 for ^{192}Pt. The two parameters version ($q_1 = 0$) of the transition operator was used
[a] Indicates the data which are fitted by fixing the ratio q_2/q_0

reproduced. One notices that the ratio $(2_\beta^+ \to 4_g^+)/(2_\beta^+ \to 0_\beta^+)$ is very sensitive to changing the strength of the anharmonic part of the transition operator. It is worth mentioning that the "large" ratios listed in Table 6.1 are fairly well described even at the level of vibrational limit. By comparing the results of column two and columns three and four, one may distinguish between the contribution due to the deformation and the anharmonic transition operator which, as a matter of fact, are forbidden within the vibrational approach. We calculated also the in-band transitions. Thus, the ratio $B(E2; 4_g^+ \to 2_g^+)/B(E2; 2_g^+ \to 0_g^+)$ for ^{192}Pt is 1.95 in the present calculation, while the IBA gives 10/7 for the limit of an infinite number of d- and s-bosons. This is to be compared with the experimental value 1.7. The IBA value is reached by the asymptotic value of this ratio expressed immediately by means of Eq. (6.2.28).

Considering only energies and B(E2) ratios the CSM is invariant to the transformation

$$d \to -d, \ A_4 \to -A_4, \ q_2 \to -q_2. \qquad (6.5.1)$$

Due to this feature, the sign of d and hence the sign of $Q(2_g^+)$ is not determined. We, arbitrarily, take d to be positive which results in having a negative value for the quadrupole moments of the 2_g^+ in ^{190,192}Pt. However, the relative signs predicted by CSM for the states 2_g^+, 4_g^+ and 2_γ^+ in the two nuclei mentioned above were observed experimentally [Bak] for the isotope ^{194}Pt.

Table 6.2 Branching ratios for gamma and beta bands of ^{154}Gd, predicted by the CSM, are compared with the experimental data taken from [GHK83]

^{154}Gd	Exp.	Th.		^{154}Gd	Exp.	Th.	
		$q_0 = 38.337$ $q_1 = 0$ $q_2 = 0$	$q_0 = 16.965$ $q_1 = 51.54$ $q_2 = 7.699$			$q_0 = 38.337$ $q_1 = 0$ $q_2 = 0$	$q_0 = 16.965$ $q_1 = 51.54$ $q_2 = 7.699$
$\frac{2_\gamma^+ \to 0_g^+}{2_\gamma^+ \to 2_g^+}$	0.468	0.509	0.500	$\frac{2_\beta^+ \to 0_g^+}{2_\beta^+ \to 2_g^+}$	0.123	0.0	0.555
$\frac{2_\gamma^+ \to 4_g^+}{2_\gamma^+ \to 2_g^+}$	0.144	0.087	0.120	$\frac{2_\beta^+ \to 4_g^+}{2_\beta^+ \to 2_g^+}$	2.76	13.234	2.192
$\frac{3_\gamma^+ \to 2_g^+}{3_\gamma^+ \to 4_g^+}$	1.006	1.302	1.117	$\frac{4_\beta^+ \to 2_g^+}{4_\beta^+ \to 4_g^+}$	0.086	0.0012	0.603
$\frac{4_\gamma^+ \to 2_g^+}{4_\gamma^+ \to 4_g^+}$	0.148	0.159	0.154	$\frac{4_\beta^+ \to 6_g^+}{4_\beta^+ \to 4_g^+}$	2.63	2.561	1.934
$\frac{4_\gamma^+ \to 6_g^+}{4_\gamma^+ \to 4_g^+}$	0.27	0.185	0.344	$\frac{6_\beta^+ \to 4_g^+}{6_\beta^+ \to 6_g^+}$	0.08	0.007	0.467
$\frac{5_\gamma^+ \to 4_g^+}{5_\gamma^+ \to 6_g^+}$	0.744	0.66	0.503	$\frac{2_\beta^+ \to 0_g^+}{2_\beta^+ \to 0_\beta^+}$	0.008	0.0	0.0019
$\frac{6_\gamma^+ \to 4_g^+}{6_\gamma^+ \to 6_g^+}$	0.081	0.081	0.073	$\frac{4_\beta^+ \to 2_g^+}{4_\beta^+ \to 2_\beta^+}$	0.0026	0.0	0.0014
$\frac{2_\gamma^+ \to 2_\beta^+}{2_\gamma^+ \to 0_\beta^+}$	2.5	1.212	0.874	$\frac{6_\beta^+ \to 4_g^+}{6_\beta^+ \to 4_\beta^+}$	0.0024	0.0	0.0011
$\frac{2_\gamma^+ \to 0_\beta^+}{2_\gamma^+ \to 0_g^+}$	0.4	1.193	1.802	$\frac{8_\beta^+ \to 6_g^+}{8_\beta^+ \to 6_\beta^+}$	0.006	0.0	0.0008
$\frac{2_\gamma^+ \to 2_\beta^+}{2_\gamma^+ \to 2_g^+}$	1.00	0.737	0.788	$\frac{10_\beta^+ \to 8_g^+}{10_\beta^+ \to 8_\beta^+}$	0.010	0.0	0.0016

The parameters q involved in the transition operator are given in units of $e.fm^2$

For ^{154}Gd we considered alternatively a harmonic and a three parameter transition operator. The three parameters were obtained by fitting the B(E2) values for the transitions $2_g^+ \to 0_g^+$, $2_\gamma^+ \to 0_g^+$ and $2_\gamma^+ \to 2_g^+$.

As seen in Table 6.2, the branching ratios are reasonably well described. We also calculated the in-band B(E2) values. The calculated reduced probabilities for the E2 transitions $J_i^+ \to (J-2)_i^+$ are very close to the experimental values. Concerning the inter-band transitions, good description is obtained for gamma to ground band transitions and $J_\beta^+ \to (J-2)_g^+$. However, large discrepancies are obtained for the transitions $J_\beta^+ \to (J+2)_g^+$ and $J_\beta^+ \to J_g^+$ although their relative values are well described. Similar discrepancies for these transitions are obtained also with the IBA formalism, as shown by Girit et al. [GHK83]. In this reference the reported ratios $(2_\gamma^+ \to 0_\beta^+)/(2_\gamma^+ \to 0_g^+)$ and $(2_\gamma^+ \to 2_\beta^+)/(2_\gamma^+ \to 2_g^+)$ are unreasonably large which in fact conflicts the band structure for the gamma band.

Table 6.3 B(E2) branching ratios for ^{126}Xe and ^{130}Ba predicted by the CSM (second column) are compared with the corresponding experimental data (first column)

$I_i \rightarrow I_f$	^{126}Xe Exp. [SEIF93]	Th.	$I_i \rightarrow I_f$	^{130}Ba Exp. [Kch]	Th.	$I_i \rightarrow I_f$	^{128}Th Exp. [Btz96]	Th.
$2_2^+ \rightarrow 0_1^+$	1.5 ± 0.4	1.5	$2_2^+ \rightarrow 0_1^+$	6.2 ± 0.7	6.2	$2_2^+ \rightarrow 0_1^+$	45(3)	45
2_1^+	100.0	100.0	2_1^+	100.0	100.0	2_1^+	100.0	100.0
$3_1^+ \rightarrow 2_2^+$	100.0	100.0	$3_1^+ \rightarrow 2_2^+$	100.0	100.0	4_1^+	3.1(3)	6.4
4_1^+	34.0^{+10}_{-14}	13	4_1^+	22.0 ± 3.0	23	$3_1^+ \rightarrow 2_1^+$	100.0	100.0
2_1^+	$2.0^{+0.6}_{-1.7}$	1.25	2_1^+	4.5 ± 0.6	9.0	4_1^+	67(6)	80
$4_2^+ \rightarrow 2_2^+$	100.0	100.0	$4_2^+ \rightarrow 2_2^+$	100.0	100.0	$4_2^+ \rightarrow 2_1^+$	15.0(1.2)	3.25
4_1^+	76.0 ± 22.0	76	4_1^+	54.10 ± 10.0	181	4_1^+	100.0	100.0
2_1^+	0.4 ± 0.1	5.5	2_1^+	2.3 ± 0.4	0.29	6_1^+	6.2(1.4)	1.73
$0_2^+ \rightarrow 2_2^+$	100.0	100.0	$0_2^+ \rightarrow 2_2^+$	100.0	100.0	$5_1^+ \rightarrow 4_1^+$	100.0	100.0
2_1^+	7.7 ± 2.2	1.1	2_1^+	3.3 ± 0.2	2.2	6_1^+	142(32)	169
$2_3^+ \rightarrow 0_2^+$	100.0	100.0	$2_3^+ \rightarrow 0_2^+$	100.0	100.0	$2_3^+ \rightarrow 0_1^+$	41(10)	59
2_2^+	2.2 ± 1.0	3.14	2_2^+	21.0 ± 4.0	20.13	2_1^+	100.0	100.0
4_1^+	2.0 ± 0.8	0.21	4_1^+	2.7 ± 0.5	1.49	4_1^+	420(60)	187
2_1^+	0.14 ± 0.06	0.18	2_1^+	3.3 ± 0.6	0.005	$4_3^+ \rightarrow 4_1^+$	100.0	100.0
0_1^+	0.13 ± 0.04	0.04	0_1^+	0.017 ± 0.003	0.016	6_1^+	470(240)	149
3_1^+	67.0 ± 22.0	20	3_1^+	–	59			
$5_1^+ \rightarrow 6_1^+$	75 ± 23	25	$4_3^+ \rightarrow 2_2^+$	2.9(5)	0.56			
4_2^+	76 ± 21	84	3_1^+	97(17)	17			
3_1^+	100.0	100.0	4_2^+	100.0	100.0			

(continued)

Table 6.3 (continued)

$I_i \to I_f$	126Xe		$I_i \to I_f$	130Ba		$I_i \to I_f$	128Th	
	Exp. [SEIF93]	Th.		Exp. [Kch]	Th.		Exp. [Btz96]	Th.
4_1^+	2.9 ± 0.8	0.15	4_1^+	3.4(6)	0.47			
$6_2^+ \to 6_1^+$	34^{+15}_{-25}	64	2_1^+	0.30(6)	0.07			
4_2^+	100.0	100.0						
4_1^+	0.49 ± 0.15	9.99						
$7_1^+ \to 6_2^+$	40 ± 26	31						
5_1^+	100.0	100.0						

Trying to correct the discrepancies mentioned above, a new version for the CSM was formulated in Ref. [RASA86], where a two boson excitation of the coherent state is chosen as generating function for the beta band. The new CSM, called CSM2, is able to describe not only the branching ratios but also the absolute B(E2) values for the inter-band beta to ground and gamma to beta transitions. It is still an open question whether the CSM itself is able to remove the advertised discrepancy by choosing a more appropriate anharmonic term in the expression of the transition operator.

Now let us turn our attention to the triaxial rotor like nuclei. Generally speaking, such nuclei are not easy to be described since K is no longer a good quantum number. However, within the CSM, K is not a good quantum number anyway, the question is whether the superposition of the K-components is the appropriate one to simulate the data. As seen in Table 6.3, this seems to be the case provided by CSM.

The question is why this simple model can account for such a big amount of features. The answer to this question is readily obtained if we look carefully at the wave function structure in the intrinsic frame of reference.

Results presented in this section were obtained by using the exact matrix elements involved in energy and transition probability calculations. In the following section we shall discuss the results obtained with approximate formulas for energies and reduced transition matrix elements.

6.6   Applications of Compact Formulas

The analytical expressions for energies and transition probabilities presented in the previous sections were applied to 42 nuclei from which 18 are considered to be near vibrational while 24 are well deformed. The results are compared with the data available for both energies and reduced transition probabilities. We divide this section into two parts one devoted to energies and one to e.m. transitions. The reason is that we aim at pointing out the change in the spectrum structure and separately in the behavior of the transition probabilities when one passes from a near vibrational to a deformed regime.

6.6.1 Energies

Energies for near vibrational nuclei were calculated with Eqs. (6.2.10–6.2.13). The parameters involved were calculated by a least square procedure. The results are listed in Table 6.4. Therein we also give the root mean square for the deviations of the calculated excitation energies from the corresponding experimental data, denoted by χ, the total number of states in the three bands, the ratio $E_{4_1^+}/E_{2_1^+}$ and the nuclear deformation β_2. The said ratio indicates how far we are from the vibrational limit which is 2. Another measure of this departure is of course the deformation parameter

d. For nuclei close to a spherical shape, d is under-unity, while for a transitional nucleus d may become larger than unity. Since the energies are power series of $x(=d^2)$ it is necessary to comment on the convergence of such series. A detailed study of this issue was presented in Ref. [RBF10], where it was shown that the convergence radius of the series associated to the overlap integral $I_J^{(0)}$ is larger than unity. As a matter of fact this property allows us to consider the nuclei in Table 6.4 with d larger than unity but smaller than the convergence radius found in Ref. [RBF10] as belonging to the class of near vibrational isotopes (Figs. 6.6, 6.10, 6.11, 6.12 and 6.13).

Excitation energies in ground, beta and gamma bands are presented in Figs. 6.14, 6.15 and 6.16 as function of angular momentum. The case of ^{152}Gd is included in Fig. 6.15 where the other even isotopes of Gd are presented. In Fig. 6.14 we notice that for ^{188,190,192}Os, ^{190,194,196}Pt and ^{186}Hg the three bands are well separated and evolve almost parallel with each other. All the said nuclei are gamma unstable since the band gamma is less excited than the band beta. In ^{102}Pd and ^{126}Xe the excited bands cross each other and they become gamma stable after the crossing point. In ^{182}Pt and ^{186}Pt the excited bands are close to each other, this feature being associated with the $SU(3)$ symmetry. We notice that in ^{154}Dy the excited bands and ground band are close to each other, which reflects the existence of a very flat potential in the β and the γ variables. A peculiar structure of the three bands is seen for ^{186}Hg where the beta band crosses the ground band becoming yrast state from $J = 4$. As shown in Fig. 6.15, ^{152}Gd is a gamma stable nucleus. The results concerning the fitted parameters for the well deformed nuclei are given in Tables 6.4, 6.5 and 6.6. Results for Gd isotopes are given separately in Table 6.5 and Fig. 6.15. Except for ^{154}Gd, which seems to be the critical nucleus in the phase transition from SU(5) to SU(3) symmetry [RF05], all isotopes from Table 6.5 are characterized by values of d close to the rotational limit which is 3.3. In Fig. 6.15 one sees that the first three isotopes exhibit the features of a gamma stable nucleus, while the heaviest two isotopes are gamma unstable nuclei. In ^{158}Gd, the excited bands have the states of even angular momentum degenerate, which results in exhibiting a SU(3) symmetry. For high odd angular momenta in gamma band of ^{154}Gd and ^{156}Gd the moment of inertia becomes different from that of even angular momentum states. This is caused by the series truncation, which does not assures the expansion convergence in this particular region of J.

Fitted parameters for some transuranic nuclei are given in Table 6.6, while the calculated energies are compared with the available corresponding data in Fig. 6.16. Except for ^{228,230}Th, which exhibit a triaxial shape [RBUG11], the listed nuclei have a ratio $E_{4_1^+}/E_{2_1^+}$ close to the rotational limit. In Table 6.6 one noticess the accuracy for the theoretical description. Except for ^{128}Th, ^{232}U and ^{240}Pu, where the two excited bands are only slightly split apart, for other nuclei the excited bands relative position reclaim on ideal SU(3) symmetry.

In Table 6.7 the fitted parameters for some deformed rare earth nuclei are presented. The energy ratios of the ground band states 4^+ and 2^+ ranges from 2.9 to 3.3. The lowest values 2.929, 3.009, 3.022 suggest that the nuclei to which they are

Table 6.4 The fitted parameters, d, A_1, A_2, A_3, A_4, A_5 determining the ground, γ and β energies in the limit of small d, i.e. near vibrational regime, for 13 nuclei

Nucleus	$E_{4_1^+}/E_{2_1^+}$	d	A_1 (keV)	A_2 (keV)	A_3 (keV)	A_4 (keV)	A_5 (keV)	χ (keV)	Number of states
^{102}Pd [FJ98]	2.293	1.45899	31.38296	8.58408	−48.05379	0	0	29.29906	11
^{126}Xe [KK02]	2.424	0.67610	16.98803	13.13610	−90.02417	−93.79735	0	37.42684	15
^{152}Gd [Art96]	2.194	1.51491	22.18661	2.18499	47.49858	77.67379	34.40286	33.04687	20
^{154}Dy [RH98]	2.233	1.53241	20.91108	3.36512	15.08504	51.90471	133.94467	44.59838	30
^{188}Os [S02]	3.083	1.62319	12.52609	9.63624	0	−9.81638	0	27.74638	13
^{190}Os [S03]	2.934	1.59990	11.27512	12.45678	0	0	163.08491	11.93490	14
^{192}Os [BAG98]	2.820	1.61011	10.53492	13.70670	0	0	263.51135	40.11629	16
^{182}Pt [SiFi95]	2.705	1.69634	17.19040	3.67131	115.45535	99.68881	−11.03489	38.35839	24
^{186}Pt [BAG03]	2.560	1.67744	17.34034	4.29899	109.10067	98.17453	−17.85114	35.31432	18
^{190}Pt [S03]	2.492	0.74815	12.23722	11.16625	0	−3.45036	0	54.24460	12
^{194}Pt [BS96]	2.470	0.83137	11.49716	15.25325	−89.44485	−109.08323	0	27.23740	11
^{196}Pt [CGT88]	2.465	0.95083	13.08631	15.24711	0	−11.04808	0	57.96742	13
^{186}Hg [BAG03]	2.665	0.92388	20.30171	4.24561	−138.41747	−16.77953	1063.07400	53.10842	24

Also, we give the r.m.s. for the deviations of the calculated and experimental energies, denoted by χ, the total number of states in the considered three bands, the ratio $E_{4_1^+}/E_{2_1^+}$ and the nuclear deformation β_2 [LRR99]. The fist column lists the nuclei and the reference from where the experimental data are taken
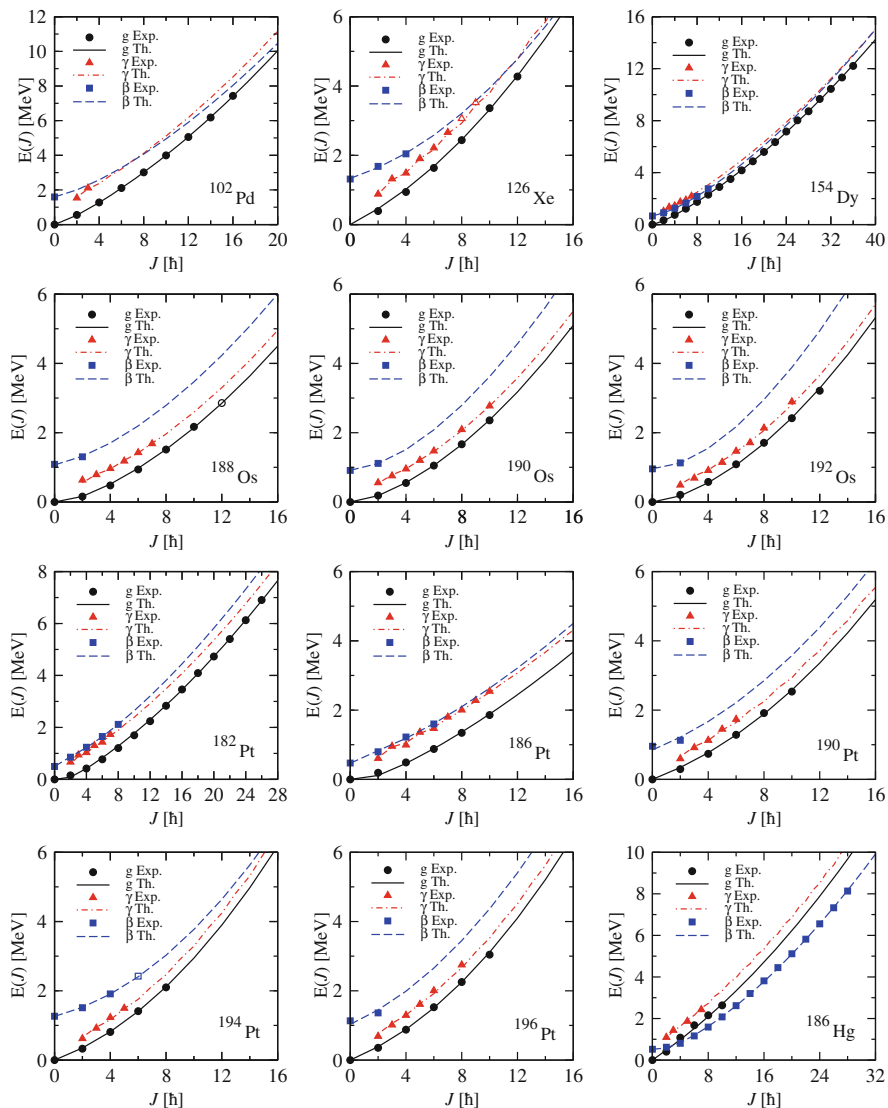
Fig. 6.14 Energy spectra of ground, γ and β bands described by means of vibrational formulas for nuclei belonging to different nuclear phases. Open symbols denote uncertain or with possible band assignment experimental points, which were not taken into account in the fitting procedure. Experimental data are taken from [FJ98, KK02, RH98, S02, S03, BAG98, SiFi95, BAG03, BS96, CGT88]

assigned ^{150}Nd, ^{152}Sm and ^{178}Os, satisfy the X(5) symmetry. Four nuclei, ^{176}Hf, ^{182,186}W and ^{186}Os, have the signature of triaxial nuclei. The remaining nuclei have the above mentioned ratio close to 3.3, i.e. they belong to the rotational behaving nuclei. The plots in Fig. 6.17 show that for some nuclei like ^{152}Sm, ^{172}Yb and ^{186}W,
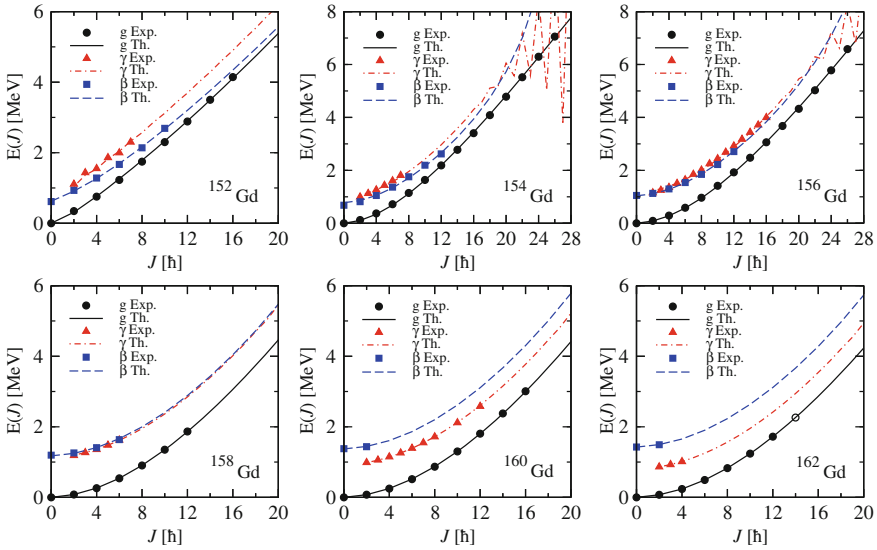
Fig. 6.15 The isotopic chain of Gd. First nucleus is treated like a near vibrational one, later ones are deformed nuclei described by means of asymptotic regime formulas with 4 parameters. Open symbols denote uncertain or with possible band assignment experimental points, which were not taken into account in the fitting procedure. Experimental data are taken from [Art96, RH98, Rei03, Hel04, Rei96, HR99]

the excited bands do not intersect each other. In ^{162}Dy the intersection is associated to the transition from the gamma unstable to the gamma stable behavior, while in ^{150}Nd the transition is, by contrary, from gamma stable to gamma unstable regime. For describing the complex structure of the three bands the five parameters formulas are used. Exception is for ^{164}Dy where the set of three parameters formulas is used. The reduced number of the necessary parameters is explained by the fact that here the beta band is missing (Table 6.7).

In Fig. 6.18, where the parameter d is plotted vs the quadrupole deformation, we see that results corresponding to the three classes of nuclei distinguished by the ratio E_{4^+}/E_{2^+}, are grouped around three straight lines, respectively.

6.6.2 E2 Transition Probabilities

For each considered nucleus the two parameters defining the quadrupole transition operator were determined by a least square fit of the experimental available data. As mentioned before, for the near vibrational limit the matrix elements of the transition operator $Q_{2\mu}$ were expanded as a power series of d from which we kept the terms non-depending on d and the next leading order terms which are in most cases linear
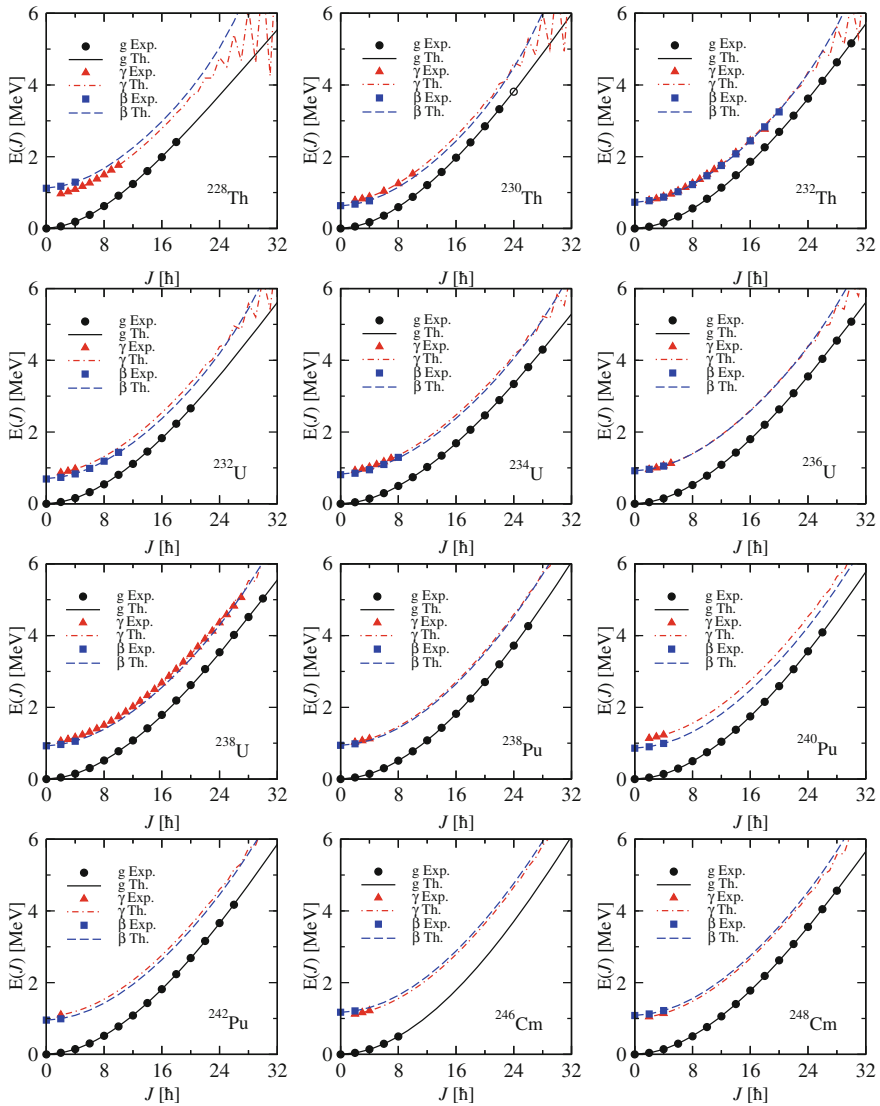
Fig. 6.16 Energy spectra of ground, γ and β bands described by means of asymptotic formulas with 4 parameters for $SU(3)$ nuclei from transuranic region. ^{228}Th and ^{230}Th are possible candidates for triaxial nuclei. Open symbols denote uncertain or with possible band assignment experimental points, which were not taken into account in the fitting procedure. Experimental data are taken form [ART97, GRO98, AKO93, Schm91, AKO94, Sch91, CH02, ChSi04, Akov02, Akov99]

Table 6.5 The same as in Table 6.4 but for the Gd isotopic chain

Nucleus	E_{4^+}/E_{2^+}	d	A_1 (keV)	A_2 (keV)	A_3 (keV)	χ (keV)	Number of states
^{154}Gd [RH98]	3.015	2.72583	18.68743	5.43251	-18.89754	38.51726	25
^{156}Gd [Rei03]	3.239	3.08725	22.03879	3.84937	-15.81253	31.48198	35
^{158}Gd [HR99]	3.288	3.30765	21.45168	4.67653	-10.95906	10.07559	15
^{160}Gd [Rei96]	3.302	3.31382	17.40521	5.69801	-1.72684	7.01074	19
^{162}Gd [Hel04]	3.291	3.28976	15.19002	5.83600	2.43502	1.04853	11

in d. All matrix elements needed for describing the experimental situation were analytically expressed. The B(E2) values are obtained by squaring the reduced matrix elements obtained as explained before. For near vibrational nuclei the results are collected in Tables 6.8, 6.9, 6.10 and 6.11 where, for comparison, the corresponding experimental data are listed. We note that the limit $d \to 0$ provides similar results as the linear expansion in d for the transition operator. However, there are transitions which are forbidden in the vibrational limit but are described quantitatively well by the linear expansion of $Q_{2\mu}$. We notice that, for the branching ratios given in Table 6.11, the results provided by the vibrational limit are in better agreement with the experimental data than those corresponding to a linear expansion of the transition operator. Moreover, some of the theoretical branching ratios are parameter independent. The agreement between the vibrational limit results and experimental data is especially good for ^{190}Pt which is considered to satisfy the $O(6)$ symmetry.

The B(E2) values for the well deformed nuclei considered here, have been calculated using the asymptotic expressions for the matrix elements given by Eqs. (6.3.21) and (6.3.22). The results are listed in Tables 6.12, 6.13, 6.14 and 6.15. As seen in these tables, a very good agreement between the results of calculations and the corresponding experimental data is obtained. A special mention is deserved by ^{156}Gd, ^{158}Gd, ^{152}Sm and ^{232}Th where 25, 23, 22 and 20 B(E2) values are available respectively, and an excellent agreement is obtained. Also for ^{172}Yb, ^{182}W and ^{186}Os, 17, 18 and 17 transitions respectively, are known and all of them are nicely described by the CSM formalism.

It is worth mentioning that the list of nuclei considered here includes isotopes of various "nuclear phases" with specific symmetries like gamma stable, gamma unstable, triaxial shape, deformed axial symmetric nuclei showing a SU(3) symmetry, and the critical nuclei satisfying the symmetries $E(5)$ (^{102}Pd) and $X(5)$ (^{152}Sm, ^{154}Gd) respectively. In the isotopic chain of $^{152-162}$Gd, two phase transitions take place namely from SU(5) to SU(3) with the critical nucleus ^{154}Gd and from SU(3) to O(6), i.e. to a gamma unstable shape, the critical nucleus being ^{160}Gd [RF05]. The properties of all these nuclei can be described fairly well by CSM. Since the analytical formulas employed in this section are easy to handle and moreover they are positively tested, the results presented above recommend the CSM as a powerful and realistic nuclear model.

Table 6.6 The same as in Table I but for other nuclei

Nucleus	E_{4^+}/E_{2^+}	d	A_1 (keV)	A_2 (keV)	A_3 (keV)	χ (keV)	Number of states
^{228}Th [ART97, GRO98]	3.235	3.20609	17.94631	1.58239	−7.03770	8.61377	21
^{230}Th [AKO93]	3.273	3.21904	13.85032	2.82743	−9.72828	4.42896	20
^{232}Th [Schm91]	3.284	3.37319	14.20081	2.53605	−7.87469	22.76356	40
^{232}U [Schm91]	3.291	3.44137	15.73529	2.17430	−10.14916	5.28270	19
^{234}U [AKO94]	3.296	3.66457	17.08527	1.73226	−9.05098	8.89688	25
^{236}U [Sch91]	3.304	3.61576	17.51131	1.92143	−8.44386	2.28183	22
^{238}U [CH02]	3.303	3.74042	19.38859	1.60137	−10.11735	26.83668	44
^{238}Pu [CH02]	3.311	3.96825	18.78524	2.38340	−8.40586	1.03977	18
^{240}Pu [ChSi04]	3.309	4.06356	20.88751	1.83394	−11.17675	3.34091	19
^{242}Pu [Akov02]	3.307	3.87399	20.15834	1.86784	−10.08071	2.90317	16
^{246}Cm [Akov99]	3.314	4.17501	20.61062	2.28038	−7.00481	1.34909	9
^{248}Cm [MATU95]	3.309	3.78738	19.18411	1.77579	−7.55677	4.11945	19

Table 6.7 The same as in Table I but for strongly deformed nuclei from the rare earth region

Nucleus	E_{4+}/E_{2+}	d	A_1 (keV)	A_2 (keV)	A_3 (keV)	A_4 (keV)	χ (keV)	Number of states
^{150}Nd [MATU95]	2.929	2.56790	19.49601	3.98450	−317.74302	−218.00288	21.85874	14
^{152}Sm [Art96]	3.009	2.69296	21.30931	4.03488	−20.22711	4.04777	47.24281	24
^{162}Dy [HR99]	3.294	3.09941	15.51332	6.30447	157.11712	113.15065	14.18735	28
^{164}Dy [SI01]	3.301	3.05374	13.15152	6.08637	0.0	0.0	4.60156	20
^{166}Er [SHU92]	3.289	2.83539	13.80805	5.81240	89.40226	60.78307	5.90918	23
^{172}Yb [SI95]	3.305	3.69655	26.79492	4.83027	34.86006	36.41885	24.74324	20
^{174}Yb [BRJU99]	3.310	3.78841	29.85375	4.05312	−8.45732	4.17396	2.82653	17
^{176}Hf [BRJU98]	3.284	3.20357	25.26813	4.06412	33.53111	37.14456	28.12626	22
^{182}W [SiFi95]	3.291	3.20632	21.88739	7.37645	−125.28004	−81.67164	9.13062	15
^{186}W [BAG03]	3.234	2.58620	12.34463	11.44538	−79.27311	−56.40554	15.05515	18
^{178}Os [BR94]	3.022	2.45573	16.62605	5.68882	−189.91058	−125.86003	37.91601	16
^{186}Os [BAG03]	3.165	2.37861	13.52361	10.41550	121.91976	91.28338	32.58668	25
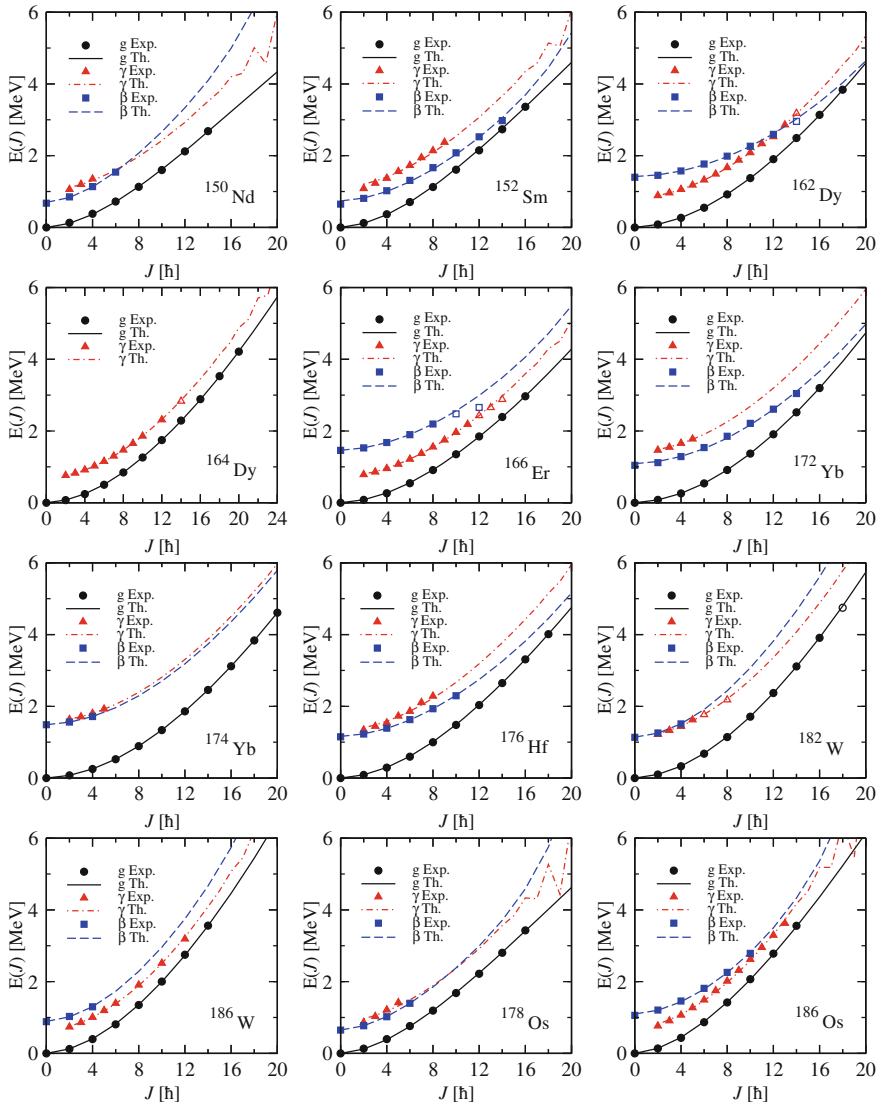
Fig. 6.17 Energy spectra of ground, γ and β bands described by means of asymptotic formulas with 5 parameters for strongly deformed nuclei from the rare earth region. Open symbols denote uncertain experimental points or probable band assignment, and were not taken into account in the fitting procedure. Experimental data are taken from [SiFi95, BAG03, MATU95, Art96, HR99, SI01, SHU92, SI95, BRJU99, BRJU98, BR94]

Table 6.8 B(E2) transition probabilities for near vibrational nuclei ^{102}Pd [FJ98], ^{154}Dy [RH98] and ^{152}Gd [Art96]

^{102}Pd				^{154}Dy				^{152}Gd			
B(E2) [W.u.]	Exp.	Th.	Th.	B(E2) [W.u.]	Exp.	Th.	Th.	B(E2) [W.u.]	Exp.	Th.	Th.
$J_i^\pi \to J_f^\pi$		$d \to 0$	Series of d	$J_i^\pi \to J_f^\pi$		$d \to 0$	Series of d	$J_i^\pi \to J_f^\pi$		$d \to 0$	Series of d
$2_g^+ \to 0_g^+$	32.6	18.27	20.69	$2_g^+ \to 0_g^+$	97	37.20	21.02	$2_g^+ \to 0_g^+$	73	60.88	76.00
$4_g^+ \to 2_g^+$	50.9	36.53	43.63	$4_g^+ \to 2_g^+$	157	74.40	164.89	$4_g^+ \to 2_g^+$	134	121.76	140.00
$2_\gamma^+ \to 2_g^+$	15	36.53	24.84	$6_g^+ \to 4_g^+$	199	111.60	194.50	$6_g^+ \to 4_g^+$	200	182.65	217.23
$2_\gamma^+ \to 0_g^+$	4.2	4.2	20.09	$8_g^+ \to 6_g^+$	220	148.80	197.30	$2_\beta^+ \to 0_\beta^+$	(42)	97.41	24.09
				$10_g^+ \to 8_g^+$	180	186.00	193.21	$0_\beta^+ \to 2_g^+$	180	180	58.61
				$12_g^+ \to 10_g^+$	170	223.20	191.74	$2_\beta^+ \to 0_g^+$	(0.31)	0	6.50
				$14_g^+ \to 12_g^+$	200	260.40	194.49	$2_\beta^+ \to 2_g^+$	(16.9)	0	61.05
								$2_\beta^+ \to 4_g^+$	[36]	81.00	41.16
d		0	1.45898	d		0	1.51491	d		0	1.53241
$q_h [(W.u.)^{\frac{1}{2}}]$		4.27391	5.78673	$q_h [(W.u.)^{\frac{1}{2}}]$		6.09923	94.8482	$q_h [(W.u.)^{\frac{1}{2}}]$		7.80268	2.19266
$q_{anh} [(W.u.)^{\frac{1}{2}}]$		1.44928	0.52039	$q_{anh} [(W.u.)^{\frac{1}{2}}]$		0	48.8486	$q_{anh} [(W.u.)^{\frac{1}{2}}]$		5.47727	6.41363

Values in square braces were not taken into account for the fitting procedure

Table 6.9 B(E2) transition probabilities for near vibrational nuclei ^{188}Os [S02], ^{190}Os [S03] and ^{192}Os [BAG98]

^{188}Os

B(E2) [W.u.] $J_i^\pi \to J_f^\pi$	Exp.	Th. $d \to 0$	Th. Series of d
$2_g^+ \to 0_g^+$	79	28.72	27.10
$4_g^+ \to 2_g^+$	133	57.44	56.46
$6_g^+ \to 4_g^+$	(138)	86.15	85.79
$8_g^+ \to 6_g^+$	[161]	114.87	114.71
$10_g^+ \to 8_g^+$	[188]	143.59	143.57
$4_\gamma^+ \to 2_\gamma^+$	47	45.13	40.19
$6_\gamma^+ \to 4_\gamma^+$	[70]	78.32	74.56
$4_\gamma^+ \to 3_\gamma^+$	[320]	0	198.11
$2_\gamma^+ \to 0_g^+$	5.0	0.79	10.88
$2_\gamma^+ \to 2_g^+$	16	57.44	83.29
$2_\gamma^+ \to 4_g^+$	[34]	0	14.31
$4_\gamma^+ \to 2_g^+$	1.29	1.25	0.20
$4_\gamma^+ \to 4_g^+$	19	41.03	41.52
$4_\gamma^+ \to 6_g^+$	[16]	0	22.06
$6_\gamma^+ \to 4_g^+$	[0.21]	1.70	0.01
$0_\beta^+ \to 2_g^+$	0.95	2.38	0.88
$0_\beta^+ \to 2_\gamma^+$	(4.3)	86.15	64.43
d		0	1.62319
$q_h\,[(W.u.)^{\frac{1}{2}}]$		5.35888	5.02388
$q_{anh}\,[(W.u.)^{\frac{1}{2}}]$		0.62933	−0.35919

^{190}Os

B(E2) [W.u.] $J_i^\pi \to J_f^\pi$	Exp.	Th. $d \to 0$	Th. Series of d
$2_g^+ \to 0_g^+$	71.9	30.10	22.86
$4_g^+ \to 2_g^+$	105	60.20	46.67
$6_g^+ \to 4_g^+$	113	90.30	70.89
$8_g^+ \to 6_g^+$	137	120.40	94.97
$10_g^+ \to 8_g^+$	[120]	150.50	119.15
$4_\gamma^+ \to 2_\gamma^+$	53	47.30	19.25
$6_\gamma^+ \to 4_\gamma^+$	[65]	82.09	40.05
$8_\gamma^+ \to 6_\gamma^+$	[61]	114.38	60.73
$4_\gamma^+ \to 3_\gamma^+$	65	0	112.28
$2_\gamma^+ \to 0_g^+$	5.9	1.09	3.81
$2_\gamma^+ \to 2_g^+$	33	60.2	95.13
$4_\gamma^+ \to 2_g^+$	0.68	1.71	0.07
$4_\gamma^+ \to 4_g^+$	30	43.00	31.97
$6_\gamma^+ \to 4_g^+$	[6]	0	9.50
$6_\gamma^+ \to 6_g^+$	[31]	38.31	19.10
$0_\beta^+ \to 2_g^+$	2.2	3.26	1.33
$0_\beta^+ \to 2_\gamma^+$	(23)	90.30	29.56
d		0	1.59990
$q_h\,[(W.u.)^{\frac{1}{2}}]$		5.4863	3.85134
$q_{anh}\,[(W.u.)^{\frac{1}{2}}]$		0.737623	−0.71724

^{192}Os

B(E2) [W.u.] $J_i^\pi \to J_f^\pi$	Exp.	Th. $d \to 0$	Th. Series of d
$2_g^+ \to 0_g^+$	64.4^{+7}_{-8}	23.80	23.85
$4_g^+ \to 2_g^+$	75.6	47.60	49.94
$6_g^+ \to 4_g^+$	100^{+5}_{-3}	71.40	75.72
$8_g^+ \to 6_g^+$	115	95.20	101.10
$10_g^+ \to 8_g^+$	105^{+9}_{-25}	119.00	126.41
$4_\gamma^+ \to 2_\gamma^+$	(45.3^{+14}_{-18})	37.40	41.19
$6_\gamma^+ \to 4_\gamma^+$	(52^{+3}_{-6})	64.91	74.41
$8_\gamma^+ \to 6_\gamma^+$	(48^{+7}_{-6})	90.44	105.58
$2_\gamma^+ \to 0_g^+$	5.62^{+21}_{-12}	1.73	11.56
$2_\gamma^+ \to 2_g^+$	46.0^{+26}_{-12}	47.60	65.22
$4_\gamma^+ \to 2_g^+$	(0.2876^{+25}_{-34})	2.75	0.42
$4_\gamma^+ \to 4_g^+$	30.9^{+37}_{-18}	34.00	37.45
$6_\gamma^+ \to 6_g^+$	$[26.0^{+55}_{-21}]$	30.29	29.79
$0_\beta^+ \to 2_g^+$	[0.60]	5.25	0.61
$0_\beta^+ \to 2_\gamma^+$	$[30.4^{+30}_{-23}]$	71.40	66.92
d		0	1.61011
$q_h\,[(W.u.)^{\frac{1}{2}}]$		4.87841	4.96308
$q_{anh}\,[(W.u.)^{\frac{1}{2}}]$		0.93545	−0.20690

Values in square braces were not taken into account for the fitting procedure

Table 6.10 B(E2) transition probabilities for near vibrational nuclei ^{194}Pt [BS96], ^{196}Pt [CGT88] and ^{186}Hg [BAG03]

^{194}Pt				^{196}Pt				^{186}Hg			
B(E2) [W.u.]	Exp.	Th.	Th.	B(E2) [W.u.]	Exp.	Th.	Th.	B(E2) [W.u.]	Exp.	Th.	Th.
$J_i^\pi \to J_f^\pi$		$d \to 0$	Series of d	$J_i^\pi \to J_f^\pi$		$d \to 0$	Series of d	$J_i^\pi \to J_f^\pi$		$d \to 0$	Series of d
$2_g^+ \to 0_g^+$	49.3	27.22	25.56	$2_g^+ \to 0_g^+$	40.57	16.23	30.47	$2_g^+ \to 0_g^+$	44	55.44	57.05
$4_g^+ \to 2_g^+$	85	54.45	53.10	$4_g^+ \to 2_g^+$	59.9	32.47	61.57	$2_\beta^+ \to 0_\beta^+$	[400]	88.71	295.27
$6_g^+ \to 4_g^+$	67	81.67	79.20	$6_g^+ \to 4_g^+$	[73]	48.70	92.57	$4_\beta^+ \to 2_\beta^+$	[200]	152.47	286.29
$8_g^+ \to 6_g^+$	50	108.90	105.89	$8_g^+ \to 6_g^+$	[78]	64.93	124.39	$6_\beta^+ \to 4_\beta^+$	290	211.69	261.19
$4_\gamma^+ \to 2_\gamma^+$	22	42.78	52.31	$4_\gamma^+ \to 2_\gamma^+$	[29]	25.51	19.46	$8_\beta^+ \to 6_\beta^+$	≈ 210	269.30	239.40
$2_\gamma^+ \to 0_g^+$	0.28	40.23	6.85	$2_\gamma^+ \to 0_g^+$	49	44.27	41.44	$4_\beta^+ \to 2_g^+$	80	0	3.38
$2_\gamma^+ \to 2_g^+$	89	54.45	50.43	$2_\gamma^+ \to 2_g^+$	[5]	25.97	39.80				
$4_\gamma^+ \to 2_g^+$	[0.22]	63.22	0.70	$4_\gamma^+ \to 2_g^+$	0.0158	0.65	0.04				
$4_\gamma^+ \to 4_g^+$	[20]	38.89	37.74	$4_\gamma^+ \to 4_g^+$	[0.56]	1.02	2.18				
$6_\gamma^+ \to 4_g^+$	134	120.68	1.53	$6_\gamma^+ \to 4_g^+$	0.48	1.39	4.08				
$0_\beta^+ \to 2_g^+$	135	81.67	89.62	$0_\beta^+ \to 2_g^+$	2.8	1.94	13.81				
$0_\beta^+ \to 2_\gamma^+$				$2_\beta^+ \to 0_g^+$	[0.0025]	0	0.05				
				$2_\beta^+ \to 4_g^+$	[0.13]	2.43	6.39				
				$0_\beta^+ \to 2_\gamma^+$	18	48.70	29.80				
d		0	0.83137	d		0	0.95083	d		0	0.92388
$q_h [(W.u.)^{\frac{1}{2}}]$		5.21769	5.46832	$q_h [(W.u.)^{\frac{1}{2}}]$		4.02904	4.13681	$q_h [(W.u.)^{\frac{1}{2}}]$		7.44606	34.2497
$q_{anh} [(W.u.)^{\frac{1}{2}}]$		4.48486	0.09065	$q_{anh} [(W.u.)^{\frac{1}{2}}]$		0.56888	−1.43127	$q_{anh} [(W.u.)^{\frac{1}{2}}]$		0	35.7881

Values in square braces were not taken into account for the fitting procedure

Table 6.11 Branching ratios for near vibrational nuclei ^{126}Xe [KK02], ^{182}Pt [SiF195], ^{186}Pt [BAG03] and ^{190}Pt [FING72]

^{126}Xe $\frac{B(E2;I\to I')}{B(E2;J\to J')}\times10^{-2}$	Exp.	Th. $d\to0$	Th. Series of d	^{182}Pt $\frac{B(E2;I\to I')}{B(E2;J\to J')}$	Exp.	Th. $d\to0$	Th. Series of d	^{186}Pt $\frac{B(E2;I\to I')}{B(E2;J\to J')}\times10^{-2}$	Exp.	Th. $d\to0$	Th. Series of d	^{190}Pt $\frac{B(E2;I\to I')}{B(E2;J\to J')}\times10^{-2}$	Exp.	Th. $d\to0$	Th. Series of d
$\frac{2^+_\gamma\to0^+_g}{2^+_\gamma\to2^+_g}$	1.38	1.63	2.96	$\frac{2^+_\beta\to2^+_g}{2^+_\beta\to0^+_g}$	0.24	0	11.52	$\frac{2^+_\gamma\to0^+_g}{2^+_\gamma\to2^+_g}$	9.31	9.31	34.05	$\frac{2^+_\gamma\to0^+_g}{2^+_\gamma\to2^+_g}$	1.24	2.86	4.80
$\frac{0^+_\beta\to2^+_g}{0^+_\beta\to2^+_\gamma}$	9.27	3.25	9.25	$\frac{2^+_\gamma\to2^+_g}{2^+_\gamma\to0^+_g}$	<4.94	4.94	12.67	$\frac{2^+_\beta\to0^+_g}{2^+_\beta\to0^+_\beta}$	7.59	0	≈0	$\frac{3^+_\gamma\to4^+_g}{3^+_\gamma\to2^+_\gamma}$	49	40[a]	20.28
$\frac{3^+_\gamma\to4^+_g}{3^+_\gamma\to2^+_\gamma}$	85.60	40[a]	20.34					$\frac{2^+_\beta\to0^+_g}{2^+_\beta\to4^+_g}$	11.06	0	0.03	$\frac{3^+_\gamma\to2^+_g}{3^+_\gamma\to2^+_\gamma}$	1.8	5.73	11.83
$\frac{3^+_\gamma\to2^+_g}{3^+_\gamma\to2^+_\gamma}$	2.29	3.25	7.50					$\frac{4^+_\gamma\to4^+_g}{4^+_\gamma\to2^+_\gamma}$	42.03	90.91[a]	73.44	$\frac{0^+_\beta\to2^+_g}{0^+_\beta\to2^+_\gamma}$	11	16.20	2.63
$\frac{4^+_\gamma\to4^+_g}{4^+_\gamma\to2^+_\gamma}$	86.33	90.91[a]	93.98					$\frac{4^+_\beta\to2^+_g}{4^+_\beta\to2^+_\beta}$	2.61	0	≈0	$\frac{2^+_\beta\to0^+_g}{2^+_\beta\to0^+_\beta}$	0.2	0	≈0
$\frac{4^+_\gamma\to2^+_g}{4^+_\gamma\to2^+_\gamma}$	1.09	3.25	0.18									$\frac{2^+_\beta\to4^+_g}{2^+_\beta\to0^+_\beta}$	4.2	4.83	4.13
$\frac{5^+_\gamma\to4^+_g}{5^+_\gamma\to3^+_\gamma}$	94.04	45.45[a]	46.20												
$\frac{5^+_\gamma\to4^+_g}{5^+_\gamma\to3^+_\gamma}$	3.76	4.64	1.79												
$\frac{6^+_\gamma\to6^+_g}{6^+_\gamma\to4^+_\gamma}$	86.19	46.67[a]	41.16												
$\frac{6^+_\gamma\to4^+_g}{6^+_\gamma\to4^+_\gamma}$	0.63	2.55	0.45												
d		0	0.67610	d		0	1.69634	d		0	1.67744	d		0	0.74815
q_{anh}/q_h		0.12749	−0.10137	q_{anh}/q_h		0.450	0.60093	q_{anh}/q_h		0.30512	0.00418	q_{anh}/q_h		0.16922	−0.07169

[a] Do not depend on any parameters

Table 6.12 B(E2) transition probabilities in the asymptotic limit for deformed Gd nuclei

B(E2) tr. prob	^{154}Gd		^{156}Gd		^{158}Gd		^{160}Gd	
$J_i^\pi \to J_f^\pi$	Exp.	Th.	Exp.	Th.	Exp.	Th.	Exp.	Th.
$2_g^+ \to 0_g^+$	157	161.4021	187	181.9295	198	200.4643	201.2	200.5707
$4_g^+ \to 2_g^+$	245	230.5744	263	259.8993	289	286.3776		
$6_g^+ \to 4_g^+$	285	253.9543	295	286.2527				
$8_g^+ \to 6_g^+$	[312]	265.8387	320	299.6486	[330]	330.1765		
$10_g^+ \to 8_g^+$			314	307.7755	340	339.1314		
$12_g^+ \to 10_g^+$			300	313.2351	[310]	345.1473		
$2_\beta^+ \to 0_\beta^+$	97	161.4021	[52]	181.9295				
$4_\beta^+ \to 2_\beta^+$			280	259.8993	[455]	286.3776		
$4_\gamma^+ \to 2_\gamma^+$					[113]	119.3240		
$5_\gamma^+ \to 3_\gamma^+$			100_{-1}^{+3}	173.6600				
$0_\beta^+ \to 2_g^+$	52	46.2919	8	7.4675	1.1652	2.2242		
$2_\beta^+ \to 0_g^+$	0.86	9.2584	0.63	1.4935	0.31	0.4448		
$2_\beta^+ \to 2_g^+$	6.7	13.2263	3.3	2.1336	0.079	0.6355		
$2_\beta^+ \to 4_g^+$	19.6	23.8073	4.1	3.8404	1.39	1.1439		
$4_\beta^+ \to 2_g^+$			1.3	2.1336	1.32	0.6355		
$4_\beta^+ \to 4_g^+$					0.37	0.5777		
$4_\beta^+ \to 6_g^+$			2.1	3.3943	3.16	1.0110		
$2_\gamma^+ \to 0_g^+$	5.7	10.8613	4.68	9.5440	3.4	9.1615	3.80	9.1323
$2_\gamma^+ \to 2_g^+$	12.3	15.5162	7.24	13.6343	6.0	13.0879	7.1	13.0461
$2_\gamma^+ \to 4_g^+$	1.72	0.7758	0.77	0.6817	(0.27)	0.6544	0.72	0.6523
$3_\gamma^+ \to 2_g^+$			7.3	17.0428	3.5	16.3599		
$3_\gamma^+ \to 4_g^+$			5.1	6.8171	1.77	6.5439		
$4_\gamma^+ \to 2_g^+$			1.8	5.6809	1.13	5.4533		
$4_\gamma^+ \to 4_g^+$			10	16.7329	7.31	16.0624		
$4_\gamma^+ \to 6_g^+$					[0.949]	1.3881		
$5_\gamma^+ \to 4_g^+$			8_{-8}^{+16}	15.1836				
$5_\gamma^+ \to 6_g^+$			11_{-11}^{+23}	8.6763				
$2_\gamma^+ \to 0_\beta^+$	[1.21]	0.1270						
$4_\gamma^+ \to 2_\beta^+$			[4.3]	0.0664				
$4_\beta^+ \to 2_\gamma^+$					[12.8]	0.0043		
d	2.72583		3.08725		3.30765		3.31382	
$q_h\,[(W.u.)^{\frac{1}{2}}]$	5.21088		4.88466		4.78579		4.77815	
$q_{anh}\,[(W.u.)^{\frac{1}{2}}]$	5.60468		2.25107		1.22853		0	

Values in square brackets were not taken into account for the fitting procedure. Experimental data are taken from [Art96, RH98, Rei03, Hel04, Rei96, HR99]
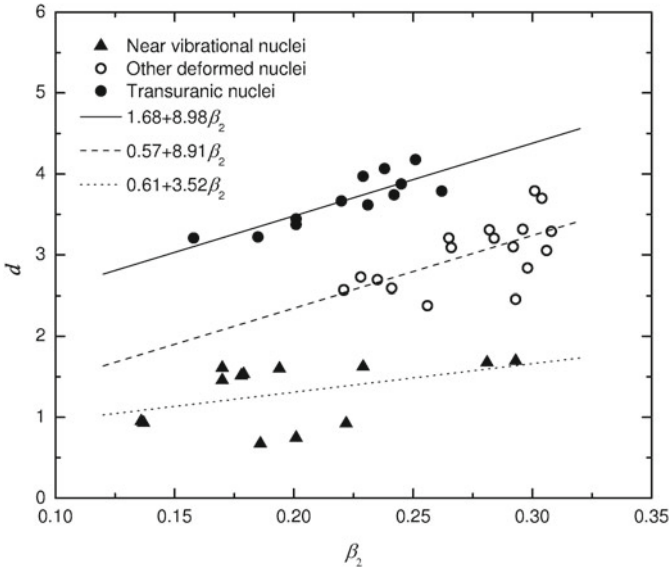
Fig. 6.18 The deformation parameter d as function of the nuclear deformation β_2 taken from Ref. [LRR99]

6.6.3 Conclusions

In Sect. 6.6 we considered the CSM approach for two extremes of small and large deformations, respectively. Thus, the matrix elements of the model Hamiltonian as well as of the E2 transition operator between the angular momentum projected states modeling the members of the ground, beta and gamma bands, are alternatively expanded in power series of $x(=d^2)$ and $1/x$. As a result the excitation energies in the three bands are expressed analytically as ratios of polynomials in x and $1/x$ respectively, with the coefficients depending on angular momentum. Concerning the matrix elements of the E2 transition operator, for small deformation they are, with a few exceptions, linear functions in d, the expansion coefficients being rational functions of the angular momentum. In the large deformation regime the whole angular dependence of the mentioned matrix elements is contained by a Clebsch Gordan coefficient which is accompanied by a factor depending on d for intraband and independent of deformation for interband transitions.

This simple description was used to describe the available data for 42 nuclei exhibiting various symmetries like SU(5), O(6), SU(3), triaxial shapes. The results are in good agreement with the corresponding experimental data for both excitation energies for the three bands and the transition probabilities. Note that for all symmetries mentioned above we use a sole Hamiltonian and a sole set of projected states. The distinct features of each symmetry are obtained by a specific deformation parameter and structure coefficients. Changing the nucleus under consideration, the

Table 6.13 B(E2) transition probabilities in the asymptotic limit for few deformed transuranic nuclei which have absolute experimental values also for inter-band transitions

B(E2) tr. prob	^{230}Th				^{238}U		^{238}Pu	
$J_i^\pi \to J_f^\pi$	Exp.	Th.	Exp.	Th.	Exp.	Th.	Exp.	Th.
$2_g^+ \to 0_g^+$	192	185.3438	198	223.2176	281	280.2843	285	285
$4_g^+ \to 2_g^+$	261	264.7768	286	318.8822				
$6_g^+ \to 4_g^+$			327	351.2164				
$8_g^+ \to 6_g^+$			343	367.6524	$[404_{-47}^{+67}]$	400.4061		
$10_g^+ \to 8_g^+$			361	377.6237	$[480_{-48}^{+61}]$	474.1651		
$12_g^+ \to 10_g^+$			370	384.3224	[500]	482.5765		
$14_g^+ \to 12_g^+$			390	389.1341	[491]	488.6182		
$16_g^+ \to 14_g^+$			390	392.7582				
$18_g^+ \to 16_g^+$			440	395.5863	[480]	496.7200		
$20_g^+ \to 18_g^+$			360	397.8550	[460]	499.5687		
$22_g^+ \to 20_g^+$			420	399.7152	[490]	501.9044		
$24_g^+ \to 22_g^+$			240	401.2682				
$26_g^+ \to 24_g^+$			350	402.5844				
$28_g^+ \to 26_g^+$			705	403.7141				
$2_\beta^+ \to 0_g^+$	[1.1]	1.1223	2.3	1.0374	[0.38]	0.7	[3.9]	1.5595
$2_\beta^+ \to 2_g^+$			≈0	1.4820	1.0	1.0		
$2_\beta^+ \to 4_g^+$	[3.8]	2.8859	[≈3.]	2.6676	[3.3]	1.8	[3.1]	4.0102
$2_\gamma^+ \to 0_g^+$	3.0	8.9506	3.0	9.8088	3.04	10.0168		
$2_\gamma^+ \to 2_g^+$	5.4	12.7866	7.1	14.0126	5.3	14.3097		
$2_\gamma^+ \to 4_g^+$	[0.35]	0.6393	≈0	0.7006	0.33	0.7155		
d	3.21904		3.37319		3.74042		3.96825	
$q_h\,[(W.u.)^{\frac{1}{2}}]$	4.73039		4.95197		5.00419		4.75640	
$q_{anh}\,[(W.u.)^{\frac{1}{2}}]$	1.95136		2.25107		1.54111		2.30027	

Values in square brackets were not taken into account for the fitting procedure. Only for ^{230}Th and ^{238}Pu the uncertain β-ground transition probabilities were used in order to fix the q_{anh} parameter. Experimental data are taken from [AKO93, Schm91, CH02]

coefficients are not changing chaotically but they obey a certain rule expressed by their dependence on $A + (N - Z)/2$ (see Ref. [RB14]). In fact this is a measure of the predictability power of the CSM approach. As shown for the Gd isotopes, CSM describes not only the nuclei corresponding to a certain symmetry but also those corresponding to the transition between them including the critical nucleus.

Comparing CSM with the Liquid Drop Model (LDM), one may say that CSM is a highly anharmonic model while LDM has a harmonic structure. However, as mentioned before, in the large deformation situation the CSM wave functions are similar to those characterizing LDM in the strong coupling limit. Another successful anharmonic model was proposed by Gneus and Greiner but that uses a large number of parameters and moreover the quadrupole conjugate momenta contribute to the

Table 6.14 B(E2) transition probabilities in the asymptotic limit for lightest rare earth nuclei

B(E2) tr. prob	^{150}Nd		^{152}Sm		^{162}Dy		^{164}Dy		^{166}Er	
$J_i^\pi \rightarrow J_f^\pi$	Exp.	Th.	Exp.	Th.	Exp.	Th.	Exp.	Th.	Exp.	Th.
$2_g^+ \rightarrow 0_g^+$	[115]	131.9577	144	183.2375	199	192.5001	209	198.8182	214	219.0829
$4_g^+ \rightarrow 2_g^+$	[175]	188.5110	209	261.7679	288	275.0002	272	284.0207	311	312.9756
$6_g^+ \rightarrow 4_g^+$	[212]	207.6258	245	288.3108	300	302.8848	325	312.8259	347	344.9756
$8_g^+ \rightarrow 6_g^+$	[236]	217.3421	285	301.8030	[347]	317.0590	310	327.4653	365	360.8425
$10_g^+ \rightarrow 8_g^+$			320	309.9883	[350]	325.6581	354	336.3466	371	370.6290
$12_g^+ \rightarrow 10_g^+$					320	331.4350	356	342.3132	376	377.2037
$14_g^+ \rightarrow 12_g^+$					330	335.5845	326	346.5988		
$2_\beta^+ \rightarrow 0_\beta^+$			[520]	183.2375						
$4_\beta^+ \rightarrow 2_\beta^+$			≈400	261.7679						
$4_\gamma^+ \rightarrow 2_\gamma^+$			[50]	109.0700						
$0_\beta^+ \rightarrow 2_g^+$	[0.0428]	8.9884	32.7	28.2136						
$2_\beta^+ \rightarrow 0_g^+$	[0.51]	1.7977	0.92	5.6427						
$2_\beta^+ \rightarrow 2_g^+$	[7.1]	2.5681	5.5	8.0610						
$2_\beta^+ \rightarrow 4_g^+$	[20]	4.6226	(19.0)	14.5098						
$4_\beta^+ \rightarrow 2_g^+$			≈1.0	8.0610						
$4_\beta^+ \rightarrow 4_g^+$			≈9.0	7.3282						
$4_\beta^+ \rightarrow 6_g^+$			(≈6.0)	12.8243						

(continued)

Table 6.14 (continued)

B(E2) tr. prob	150Nd		152Sm		162Dy		164Dy		166Er	
$J_i^\pi \to J_f^\pi$	Exp.	Th.	Exp.	Th.	Exp.	Th.	Exp.	Th.	Exp.	Th.
$2_\gamma^+ \to 0_g^+$	[3.0]	9.7248	3.62	12.8838	[0.0241]	8.9188	4.0	10.6601	5.5	12.6207
$2_\gamma^+ \to 2_g^+$	[5.7]	13.8926	9.3	18.4054	≈ 0	12.7411	8.0	15.2288	9.7	18.0296
$2_\gamma^+ \to 4_g^+$	[1.7]	0.6946	(0.78)	0.9203	[0.00330]	0.6371	0.96	0.7614	0.67	0.9015
$4_\gamma^+ \to 2_g^+$			0.59	7.6689						
$4_\gamma^+ \to 4_g^+$			5.5	22.5885						
$4_\gamma^+ \to 6_g^+$			[1.2]	1.9521						
$4_\gamma^+ \to 2_\beta^+$			[0.18]	0.0897						
d	2.60473		2.66667		3.28509		3.05374		2.94610	
$q_h\,[(W.u.)^{\frac{1}{2}}]$	4.93072		5.67534		4.72197		5.16240		5.61710	
$q_{anh}\,[(W.u.)^{\frac{1}{2}}]$	2.46967		4.37549		0		0		0	

Values in square brackets were not taken into account for the fitting procedure. The uncertain transition probabilities were used for 150Nd in the fitting procedure. Experimental data are taken from [MATU95, Art96, HR99, SI01, SHU92]

Table 6.15 B(E2) transition probabilities in the asymptotic limit for heaviest rare earth nuclei

B(E2) tr. prob	^{172}Yb		^{174}Yb		^{176}Hf		^{182}W		^{182}W		^{186}Os	
$J_i^\pi \to J_f^\pi$	Exp.	Th.	Exp.	Th.	Exp.	Th.	Exp.	Th.	Exp.	Th.	Exp.	Th.
$2_g^+ \to 0_g^+$	212	226.1302	201	214.4049	183	182.7660	137	119.5874	111	100.9240	92.3	94.6028
$4_g^+ \to 2_g^+$	301	323.0431	280	306.2927			196	170.8392	144	144.1772	134	135.1469
$6_g^+ \to 4_g^+$	320	355.7992	370	337.3503			200	188.1620	187	158.7966	184	148.8506
$8_g^+ \to 6_g^+$	400	372.4497	[388]	353.1374			209	196.9675	178	166.2278	174	155.8164
$10_g^+ \to 8_g^+$	375	382.5510	[335]	362.7150			203	202.3095	151_{-45}^{+15}	170.7362	190	160.0424
$12_g^+ \to 10_g^+$	(400)	389.3372	[369]	369.1493			191	205.8983	189_{-56}^{+20}	173.7649	170	162.8814
$14_g^+ \to 12_g^+$	(394_{-45}^{+60})	394.2116	[320]	373.7709			(170)	208.4761	138	175.9404		
$16_g^+ \to 14_g^+$							[204]	210.4177				
$18_g^+ \to 16_g^+$							[250]	211.9329				
$2_\beta^+ \to 0_\beta^+$							[200]	119.5874				
$4_\gamma^+ \to 2_\gamma^+$											72	56.3112
$6_\gamma^+ \to 4_\gamma^+$											119	111.1418
$8_\gamma^+ \to 6_\gamma^+$											79	134.1532
$10_\gamma^+ \to 8_\gamma^+$											89	146.0535
$0_\beta^+ \to 2_g^+$	[3.6]	4.0387	$[1.4_{-5}^{+11}]$	1.4								

(continued)

Table 6.15 (continued)

B(E2) tr. prob	^{172}Yb		^{174}Yb		^{176}Hf		^{182}W		^{182}W		^{186}Os	
$J_i^\pi \to J_f^\pi$	Exp.	Th.	Exp.	Th.	Exp.	Th.	Exp.	Th.	Exp.	Th.	Exp.	Th.
$2^+_\beta \to 0^+_g$	0.24	0.8077			1.0	2.0568	0.91	0.6483				
$2^+_\beta \to 2^+_g$	0.79	1.1539					0.63	0.9262				
$2^+_\beta \to 4^+_g$	2.5	2.0770			5.7	5.2890	1.73	1.6672				
$2^+_\gamma \to 0^+_g$	1.33	8.2744			4.1	8.9042	3.40	5.8162	4.63	7.5447	10.1	8.3604
$2^+_\gamma \to 2^+_g$			2.5	10.6707			6.74	8.3089	10.1	10.7781	23.5	11.9435
$2^+_\gamma \to 4^+_g$	(0.129)	0.5910					0.0339	0.4154			[1.2]	0.5972
$4^+_\gamma \to 2^+_g$	7	4.9252					2.35	3.4620			3.2	4.9764
$4^+_\gamma \to 4^+_g$	13	14.5070					10.4	10.1973			24.7	14.6579
$6^+_\gamma \to 4^+_g$											1.27	4.0925
$6^+_\gamma \to 6^+_g$											18.5	15.2008
$2^+_\gamma \to 0^+_\beta$	[2.42]	1.3344										
$2^+_\gamma \to 2^+_\beta$	[3.4]	1.9064										
d	3.69655		3.78841		3.20357		3.20632		2.58620		2.37861	
$q_h\,[(W.u.)^{\frac{1}{2}}]$	4.54818		4.32131		4.71811		3.81321		4.34301		4.57177	
$q_{anh}\,[(W.u.)^{\frac{1}{2}}]$	1.65546		0.97468		2.64170		1.48316		0		0	

Values in square brackets were not taken into account for the fitting procedure. Experimental data are taken from [SiFi95, BAG03, SI95, BRJU99, BRJU98, BR94]

Hamiltonian only through the quadratic terms. Moreover, energies are obtained by diagonalization procedure in a spherical basis which may encounter convergence difficulties for large deformations. By contrast, the CSM projects states of good angular momentum from a coherent state and two orthogonal polynomial excitations and consequently it is especially realistic for the well deformed nuclei. This feature is actually confirmed by the application shown in the last two sections were the transuranic nuclei spectra are obtained with high accuracy.

CSM accounts for features which are complementary to those described by IBA. Indeed, CSM's Hamiltonian is not a boson number conserving Hamiltonian. Moreover, while IBA uses a space of states with limited number of bosons, CSM states covers the whole boson space since they are projected from infinite series of bosons. Due to this feature the IBA approach is concerned with the description of low lying states with angular momentum not exceeding 12^+ and with a moderate deformation. By contrast, CSM works quite well for high spin states (in Figs. 6.14 and 6.16 energies for states with $J \leq 32$ are shown). CSM was applied for the description of the triaxial nuclei [MRF98] and the results were compared with those obtained within the Vibration Rotation Model [FaGr62]. Recently, a more extensive study of triaxial nuclei with CSM has been performed [RBUG11] and the results were compared with those produced by a solvable model.

Chapter 7
Pear Shaped Nuclei

7.1 CSM Extension for Pear Shaped Nuclei

The field of negative parity states is of about the same age as the one dealing with the positive parity states. The pioneering papers in this domain appeared already in the beginning of the fifties [ASP53, SAP55] of the last century and were based on high resolution alpha spectroscopy measurements. The states were identified as $1^-, 3^-, 5^-$ through angular correlations and conversion coefficients analysis, as well as by measuring the E1 branching ratio for the first state to 0^+ and 2^+.

The interest in the field of negative parity states increased considerably when first suggestions for octupole deformed nuclei appeared. Indeed, in Refs. [CH79, CH80] Chassman predicted parity doublets for several odd mass isotopes of Ac, Th and Pa. About the same time Moller and Nix [MN81] suggested that some even-even isotopes of Ra might have an octupole deformed ground band. Their calculations showed that the binding energy of these nuclei gains about 2 MeV, when an octupole deformation term is included in the mean field.

The nuclear surface exhibiting both quadrupole and octupole static deformation has the equation

$$R(\Omega) = R_0(1 + \beta_2 Y_{20} + \beta_3 Y_{30}), \qquad (7.1.1)$$

and looks as shown in Fig. 7.1.

The difficulty in the experimental study of pear shaped nuclei, is a missing observable which might be interpreted as a measure for the octupole deformation. Therefore some indirect information about this variable should be found. Along the time, several signatures were assigned to the octupole deformation: (a) The low position of the state 1^- heading the band 0^- is an indication that, as function of the octupole deformation, the potential energy has a flat minimum; (b) The parity alternating structure in ground and the low 0^- bands suggests that the two bands may be viewed as being projected from a sole deformed intrinsic state, exhibiting both quadrupole and octupole deformations; (c) A nuclear surface with quadrupole and octupole deformations

$$\beta_2 = 0 \qquad \beta_2 = 0.2 \qquad \beta_2 = 0.6$$

$\beta_3 = 0.2$

$\beta_3 = 0.6$
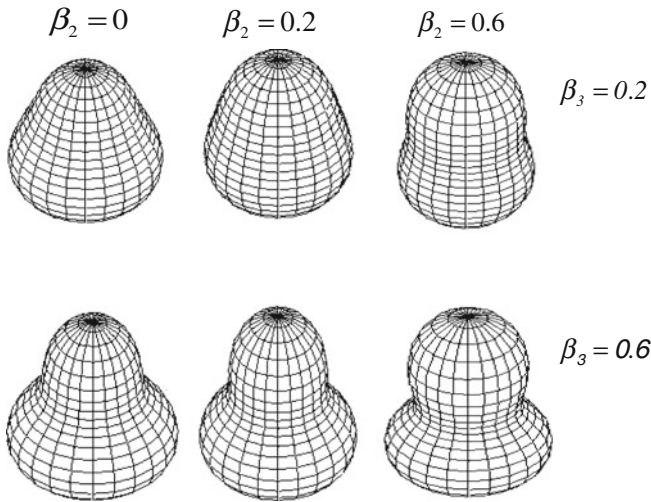
Fig. 7.1 Nuclear surfaces corresponding to different static quadrupole and octupole deformations

might have the center of charge in a different position than the center of mass, which results in having a dipole moment which, in interaction with an external electromagnetic field, may excite the state 1^- from the ground state, with a large probability.

It is clear that a nuclear surface with a static octupole deformation does not have a space reflection symmetry. On the other hand one knows that whenever a symmetry is spontaneously broken, a new phase is set up for the considered system. In this respect a pear shaped nucleus means a new nuclear phase, with specific properties. Therefore, any theory addressing this issue has to point out the new properties which are specific to the new nuclear phase. If the intrinsic ground state does not have a good reflection symmetry it sounds reasonable to assume that intrinsic gamma and beta bands also have this property. Then, instead of using ψ_γ and ψ_β as model states of the two bands, as shown in Eq. (6.1.1), we propose now to choose the functions Ψ_γ and Ψ_β respectively, which involves both the quadrupole and octupole deformations.

Thus, in this chapter the CSM is extended by assuming for the intrinsic states associated to the ground, beta and gamma bands also an octupole deformation. The new formalism is conventionally called the Extended Coherent State Model (ECSM). From each such a state, one projects simultaneously the parity and angular momentum and consequently two bands of opposite parities are obtained. We want to see whether there are any fingerprints of octupole deformation in the excited bands, $\beta^\pm$, $\gamma^\pm$.

The octupole deformation is described by means of an axially symmetric coherent state for the octupole bosons $b^\dagger_{30}$. Thus, the intrinsic states for the ground, beta and gamma bands are:

$$\Psi_g = e^{f(b_{30}^\dagger - b_{30})} e^{d(b_{20}^\dagger - b_{20})} |0\rangle_{(3)} |0\rangle_{(2)}, \quad \Psi_\beta = \Omega_\beta^\dagger \Psi_g, \quad \Psi_\gamma = \Omega_\gamma^\dagger \Psi_g. \qquad (7.1.2)$$

The notation $|0\rangle_{(k)}$ stands for the vacuum state of the 2^k-pole boson operators. Note that any of these states is a mixture of positive and negative parity components. Therefore, they don't have good reflection symmetry. Due to this feature, the new extension of the CSM formalism has to project out not only the angular momentum but also the parity from each intrinsic state. The double projection is performed in two steps. First, one projects the components of good parity from which the component of good angular momentum are determined:

$$\Psi_g^{(\pm)} = e^{-\frac{y_3 + y_2}{2}} \begin{pmatrix} \cosh(f b_{30}^+) \\ \sinh(f b_{30}^+) \end{pmatrix} e^{d b_{20}^+} |0\rangle_3 |0\rangle_2$$

$$\Psi_i^{(\pm)} = \Omega_i^+ \Psi_g^{(\pm)}, \quad i = \beta, \gamma, \quad y_2 = d^2, \quad y_3 = f^2,$$

$$\varphi_{JM}^{(i,k)} = \mathcal{N}_J^{(i,k)} P_{MK_i}^J \Psi_i^{(k)}, \quad K_i = 2\delta_{i,\gamma}, \quad k = \pm; \ i = g, \beta, \gamma,$$

$$J = (\delta_{i,g} + \delta_{i,\beta})(even\delta_{k,+} + odd\delta_{k,-}) + \delta_{i,\gamma} J (1 - \delta_{J,0} - \delta_{J,1}). \qquad (7.1.3)$$

The normalization factors have the expressions:

$$\left(N_J^{(g,k)} \right)^{-2} = e^{-\frac{1}{2}(2y_3 + 3y_2)} (2J + 1) \mathcal{I}_{(g,J)}^{(k)} (y_2, y_3), \quad y_2 = d^2, \quad y_3 = f^2,$$

where the overlap integrals defined by:

$$\mathcal{I}_J^{(\pm)} = \int_0^1 P_J(x) \begin{pmatrix} \cosh(f^2 P_2(x)) \\ \sinh(f^2 P_2(x)) \end{pmatrix} dx, \qquad (7.1.4)$$

with $P_J(x)$ denoting the Legendre Polynomial of rank J, can be analytically calculated:

$$\mathcal{I}_{(g,J)}^{(k)} = (3y_3)^J \sum_{p=p_{min}}^{\infty} \sum_{l=0}^{l_{Max}} \left(\frac{y_3^2}{4} \right)^{p-l} (9)^p \left(\frac{5}{27} \right)^l (-)^{l+J}$$

$$\times \frac{(p+J)!(2p+J)! F(-l, 2p - 3l + J + 1; \frac{9}{10} y_2)}{l! p! (2p - 3l + J)!(2p + 2J + 1)!}, \quad k = \pm.$$

Here $F(a, b; x)$ denotes the degenerate hypergeometric function. The summation indices are defined by:

$$p_{min} = \delta_{J,1}, \quad l_{max} = \left[\frac{2p + J}{3}\right], \quad \text{if } J \neq 1,$$

$$l_{max} = min\left\{p - 1, \left[\frac{2p + 1}{3}\right]\right\}, \quad \text{if } J = 1.$$

Alternatively, the projected states can be written in a tensorial form as:

$$\varphi_{JM}^{(i,k)} = \mathcal{N}_J^{(g,k)} \sum_{J_2, J_3} (N_{J_3}^{(k)} N_{J_2}^{(g)})^{-1} C_{0\ \ 0\ \ 0}^{J_3\ \ J_2\ \ J} [\Psi_{J_3}^{(k)} \phi_{J_2}^{(i)}]_{JM}; \quad k = \pm, \quad i = g, \beta, \gamma.$$

where

$$\Psi_{J_3}^{(k)} = N_{J_3}^{(k)} P_{M0}^J e^{f(b_{30}^\dagger - b_{30})} |0\rangle_3, \tag{7.1.5}$$

while $\phi_{J_2}^{(i)}$ is the i-band projected state ($i = g, \beta, \gamma$) (of positive parity) defined in the previous chapter within the CSM.

Using this factorization and the results of the previous chapter it becomes obvious that matrix elements for any function of quadrupole bosons can be expressed as simple functions of overlap integrals:

$$I_J^{(0)} = \int_0^1 P_J(x) e^{d^2 P_2(x)} dx, \tag{7.1.6}$$

and $I_J^{(1)}$, which is the first derivative of $I_J^{(0)}$ with respect to $y_2(=d^2)$.

Since for large values of the deformation parameter d, the projected states $\phi_{JM}^{(i)}$, with $i = g, \beta, \gamma$ behave like a Wigner function, with a definite quantum number "K", they describe rotational bands with $K = 0, 0, 2$, respectively. Analogously, the octupole states $\Psi_{JM}^{(\pm)}$ describe rotational bands having $K = 0$. Consequently, four of the six bands defined above have $K = 0$, while the remaining two are $K = 2$ bands. In order to stress on the parity partnership, we use the suggestive notations $g^\pm, \beta^\pm, \gamma^\pm$ for the six bands. Each pair of bands is expected to give rise to an alternating parity sequence as it happens in the case of ground and $K^\pi = 0^-$ bands, i.e. the $g^\pm$ pair. The set $\{\varphi_{JM}^{(i,k)}\}_{i,k;J,M}$, with $i = g, \beta, \gamma$ and $k = \pm$ is orthogonal. Note that for $f = 0$ only the positive parity states $\varphi_{J_3 M_3}^{(+)}$ are well defined. However, the limits for "f" going to zero exist both for $k = +$ and $k = -$, and the following relation holds:

$$\lim_{f \to 0} \varphi_{JM}^{(i,+)} = \varphi_{JM}^{(i)}.$$

Thus, the formalism proposed yields the CSM in the limit of $f \to 0$.

Keeping the spirit of the CSM, an effective boson Hamiltonian is studied in the restricted collective space generated by the six sets of projected states. Note that from each of the three intrinsic states, one generates by projection two sets of states,

one of positive and one of negative parity. When the octupole deformation goes to zero, the resulting states are just those characterizing the CSM model. We know already the effective quadrupole boson Hamiltonian in this limit. When the quadrupole deformation is going to zero the system exhibits vibrations around an octupole deformed equilibrium shape. We consider for the octupole Hamiltonian a harmonic structure, since the non-harmonic octupole terms can be simulated by the quadrupole anharmonicities. As for the coupling between quadrupole and octupole bosons, we suppose that this can be described by a product between the octupole boson number operator, $\hat{N}_3$, and the quadrupole boson anharmonic terms which are involved in the CSM Hamiltonian. Also, two scalar terms depending on the angular momenta carried by the quadrupole (J_2) and octupole bosons (J_3) respectively, are included. Thus, the model Hamiltonian has the expression:

$$H = H'_2 + \mathcal{B}_1 \hat{N}_3 (22\hat{N}_2 + 5\Omega^\dagger_{\beta'}\Omega_{\beta'}) + \mathcal{B}_2 \hat{N}_3 \Omega^\dagger_\beta \Omega_\beta$$
$$+ \mathcal{B}_3 \hat{N}_3 + \mathcal{A}_{(J23)}\mathbf{J_2J_3} + \mathcal{A}_\mathbf{J}\mathbf{J^2}. \tag{7.1.7}$$

Here H'_2 denotes the CSM Hamiltonian for quadrupole bosons from which one ignores the A_4, A_5 and A_2 terms. The reason is that for quadrupole well deformed nuclei the first two terms mentioned above, which affect only the beta band energies, are not necessary in order to obtain a good description of energy levels in the beta band. Concerning the third one, this is contained in the $\hat{\mathbf{J}}^2$ term, the angular momentum carried by the composite system of quadrupole and octupole bosons. As shown in Ref. [RRF97], the term $\mathbf{J_2}.\mathbf{J_3}$ is necessary in order to explain the low position of the state 1^- in the even-even Ra isotopes. Indeed, this term is attractive in the state 1^-, while for higher angular momenta is repulsive. It is noteworthy that all terms involved in Eq. (7.1.7), have a microscopic interpretation. Indeed, they can be obtained in a boson expansion formalism from a microscopic Hamiltonian involving quadrupole-quadrupole plus octupole-octupole two body interaction [RCSS73]. In the quoted reference, the fermion operators are written as polynomial expansions of quadrupole and octupole quasiparticle-random phase approximation (QRPA) boson operators.

The Hamiltonian given by Eq. (7.1.7) has vanishing matrix elements between any beta band state and a state belonging either to ground or to gamma bands. Therefore, the energies in the six bands are obtained as: (a) Expectation values if the state J^π belongs to the β^π band. The same is valid for the odd J states from the γ^+ band and even J states for the γ^- band. (b) Eigenvalues of a 2×2 matrix associated to each even (odd) value of J^+ (J^-) if this state belongs to one of the bands g^+ and γ^+ (g^- and γ^-) . The eigenstates of the model Hamiltonian in the restricted collective space of mixed quadrupole and octupole boson product states were used to calculate the intra-band E2 transition probabilities as well as the B(E1) and B(E3) values for the transitions connecting the negative parity and positive parity bands. Special emphasis was put on the E1 transitions between states belonging to the parity partner bands. The $E\lambda$ transition operators are considered in the lowest order in the quadrupole and octupole bosons:

$$Q_{\lambda\mu} = q_\lambda(b^{\dagger}_{\lambda\mu} + (-)^\mu b_{\lambda,-\mu}), \quad \lambda = 2, 3.$$

$$T^{(h)}_{1\mu} = q_1 \sum_{\mu_2,\mu_3} C^{3\ 2\ 1}_{\mu_3\ \mu_2\ \mu}(b^{\dagger}_{3\mu_3} + (-)^\mu b_{3,-\mu_3})(b^{\dagger}_{2\mu_2} + (-)^\mu b_{2,-\mu_2}) \quad (7.1.8)$$

The dipole transition operator is accompanied by an upper index "(h)" which suggests that both the quadrupole and octupole factor operators are linear in bosons, and therefore only the harmonic contribution of the respective degrees of freedom are considered. However, in order to describe the B(E1) values for the transitions connecting the g^- and g^+ bands , especially for states lying in the region where the static octupole deformation is settled, the harmonic dipole transition operator is to be amended with anharmonic terms. Thus, one can alternatively use the following expressions:

$$T^{(I)}_{1\mu} = T^{(h)}_{1\mu} + q_I \left\{ \left[b^{\dagger}_3(JJ)_2\right]_{1\mu} + \left[(JJ)_2 b_{\tilde{3}}\right]_{1\mu} \right\},$$

$$T^{(II)}_{1\mu} = T^{(h)}_{1\mu} + q_{II} \left\{ \left[b^{\dagger}_3(J_3 J_2)_2\right]_{1\mu} + \left[(J_2 J_3)_2 b_{\tilde{3}}\right]_{1\mu} \right\}. \quad (7.1.9)$$

The formalism described above has been applied to seven even-even nuclei for which there are available data concerning the bands under consideration [RIF02]. These nuclei are: ^{158}Gd, ^{172}Yb, ^{218}Ra, ^{226}Ra, ^{232}Th, ^{238}U, ^{238}Pu. Among these nuclei, there are two, ^{218}Ra and ^{226}Ra, which are known to have octupole deformation. The negative parity states in the remaining nuclei have a vibrational character. Including them in this study, had the goal to prove the capacity of this model to describe the octupole deformation in the vanishing limit which results in providing an unified picture for spherical and octupole deformed nuclei. In what follows, we shall describe separately the results for energies and e.m. transition probabilities.

7.1.1 Energies

The energies in the six bands depend on two deformation parameters, d and f and six structure coefficients involved in the model Hamiltonian (7.1.7), $\mathcal{A}_1$, $\mathcal{A}_2$, $\mathcal{A}_J$, $\mathcal{A}_{(J23)}$, $\mathcal{B}_1$, $\mathcal{B}_3$. In order to preserve the notations used in the publications devoted to this issue, we re-denoted the coefficients A_1, A_3 from Chap. 6 (see Eq. (6.1.9)), by $\mathcal{A}_1$, $\mathcal{A}_2$ respectively. Note that the parameter $\mathcal{B}_2$ is missing from the list. The accompanying term affects only the β^- energies. Therefore, the $\mathcal{B}_2$ coefficient may be determined by fitting one experimental energy from this band. However, for the nuclei considered here, there are no data for the negative parity beta band. This is the reason we omitted $\mathcal{B}_2$ from our calculations. The remaining parameters were fixed by a least square fit of the available data. The parameters yielded by the fitting procedure vary smoothly from one nucleus to another. In this respect one could say that they are not independent parameters. Indeed, the quadrupole deformation parameter is

Fig. 7.2 The quadrupole deformation parameter d, yielded by the fitting procedure, versus the experimental value for the deformation β
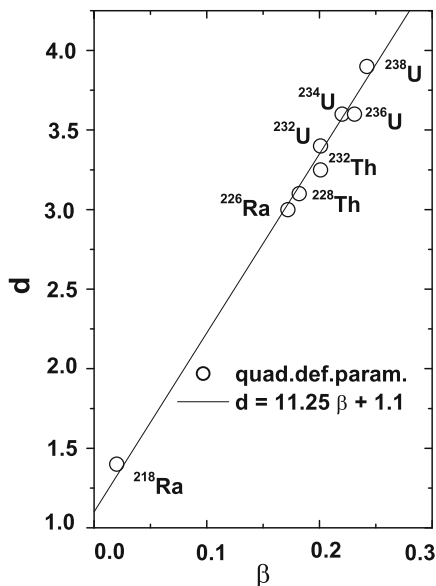
depending linearly on the nuclear deformation β (see Eq. (6.4.23)). This is confirmed in Fig. 7.2, where the parameter d shows a linear dependence on the experimental deformation, β. In Ref. [RI03], one showed that the octupole deformation parameter f exhibits also a linear dependence on the static octupole deformation:

$$k_3 \beta_3^{(0)} = f \sqrt{2} \left(1 + \frac{12 \mathcal{A}_J}{\mathcal{B}_3 + 22 d^2 \mathcal{B}_1} \right). \tag{7.1.10}$$

However, as we already mentioned, there is no measurable observable that could confer $\beta_3^{(0)}$ an experimental value. In other words, there is no operator whose expected value is proportional to f. This equation can however be used to define, theoretically, a static octupole deformation $\beta_3^{(0)}$. In Fig. 7.3 one gives the structure coefficients $\mathcal{A}$ and $\mathcal{B}$ as a function of A-0.5(N-Z). In order to have a better presentation for the isotopes of the same atomic mass number, A, we introduced an isospin asymmetry in the abscissa variable.

Thus, if one wants to study a nucleus not included in these plots, with a given (A,Z) and quadrupole deformation β_0, Figs. 7.2 and 7.3 allow us to determine all structure coefficients and the quadrupole deformation parameter d. As concerns the octupole deformation parameter f, this remains, still, a free parameter.

To save the space in Fig. 7.4 we give only the results of energy levels for the bands $g^{(\pm)}$ in three isotopes. Excitation energies of the three pairs of bands in ^{226}Ra are presented in a different form in Fig. 7.5. To have an idea about the volume of experimental data which are explained by the present model, we mention the case of
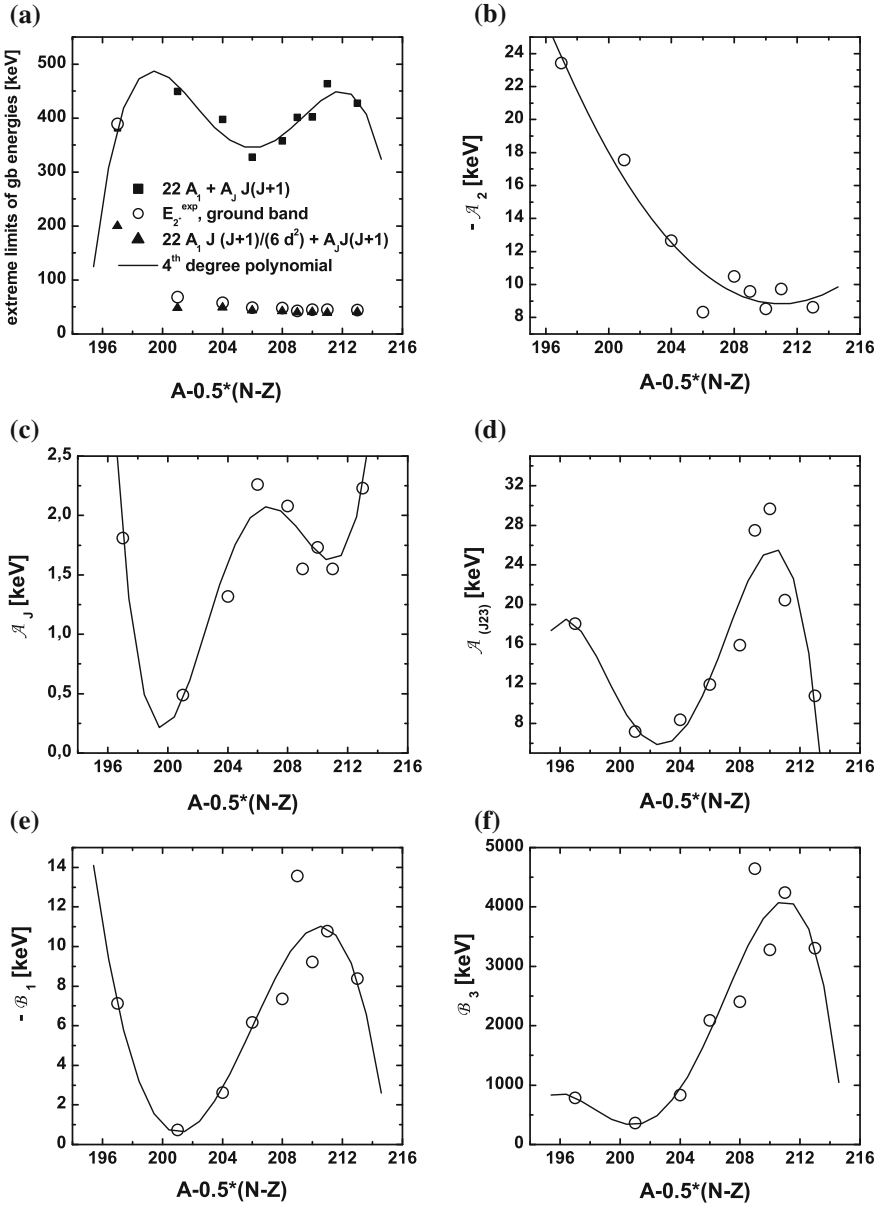
Fig. 7.3 The structure coefficients defining the model Hamiltonian by Eq. (7.1.7) are interpolated by a fourth order polynomial in A-(N-Z)/2 (panel **c–f**). Exception is for $-\mathcal{A}_2$ where a second order polynomial is used (panel **b**). The parameter $\mathcal{A}_1$ is interpreted in panel (**a**). Indeed, there we give the vibrational (*full square*) and rotational limits for the energy of the state 2_g^+. The experimental value is represented by *open circles*
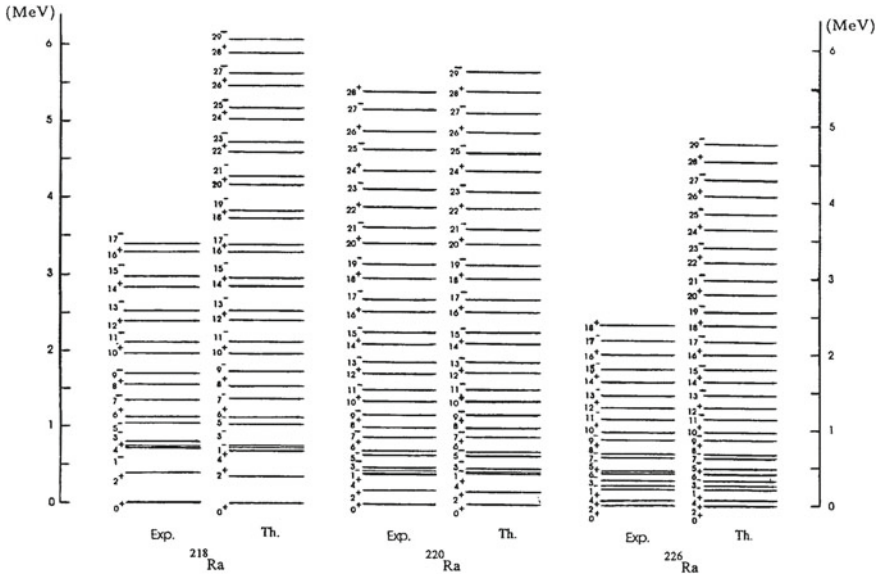
Fig. 7.4 Experimental and calculated energies for the $g^\pm$ bands in ^{218,220,226}Ra (see Ref. [RRF97])
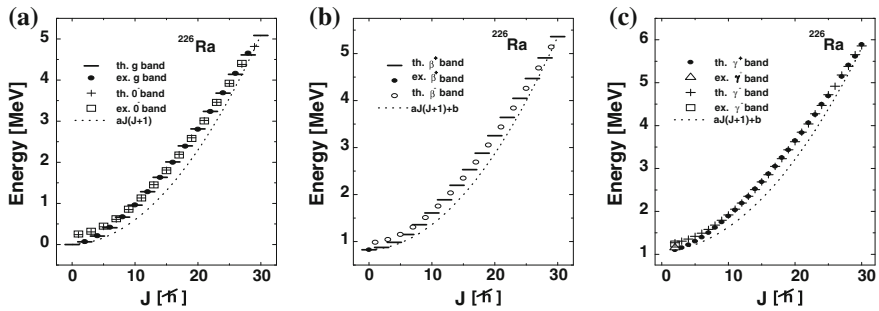
Fig. 7.5 Experimental and calculated energies for the bands $g^\pm, \beta^\pm, \gamma^\pm$ for ^{226}Ra

^{232}Th, where there are 55 experimental excitation energies which are described by the theoretical results with a very good accuracy.

In order to judge the quality of the agreement between the calculated energies and the corresponding experimental data, the dynamic moment of inertia ($\mathcal{J}_J^{(2)}$) was represented as function of the rotational frequency (ω) [RIF02] in several nuclei:

$$\hbar\omega_I = \frac{dE}{dI} \approx \frac{1}{2}(E_I - E_{I-2}), \ \mathcal{J}^{(2)}/\hbar^2 = \left(\frac{d\omega}{dI}\right)^{-1} \approx 2/(\omega_I - \omega_{I-2}). \quad (7.1.11)$$

For all considered nuclei, the agreement is very good. When the points for two parity partner bands are on the same curve in the above mentioned plot, one says that the

static octupole deformation is installed for the angular momenta where such a picture is valid. Concrete calculations show that this is the case for ^{226}Ra and ^{158}Gd. It is worth mentioning that the coordinates $(\omega, \mathcal{J}^{(2)})$ are not suitable for the ^{218}Ra case, since in the low part of the ground band, the energy spacing is almost constant which results in having very large values for the dynamic moment of inertia. This is consistent with the fact that the quadrupole deformation parameter for this isotope, is small. Under these circumstances, for this case we plotted the angular momentum versus the rotational frequency. This is shown in Fig. 7.6, for the three pairs of parity partner bands. Note that the plot referring to the two ground bands in ^{218}Ra, exhibits a back-bending at $J^\pi = 16^+$. Moreover, the positive parity band has also a forward bending at $J^\pi = 22^+$. The experimental energy plot indicates that an earlier back bending is taking place at $J = 10^+$, although there is only one point to support two successive sharp changes in the slope of the angular momentum function. According to the microscopic formalisms, the non-regular angular momentum dependence of the yrast state energies is due to a successive crossing of several bands of different nature, i.e., 0,2,4 quasiparticle bands. Moreover, since the alignment of the quasiparticle angular momentum is made to an almost spherical core, the intra-band E2 transitions are quite weak and therefore the set of states seen in ^{218}Ra can, only by an abuse of language, be organized in rotational bands. Since our predictions interpolate quite well the experimental curve we can state that the effects mentioned above are simulated by the competition between various terms of the model Hamiltonian.

The presence of octupole deformation is usually judged from the plot of the energy displacement function:

$$\delta E(J^-) = E(J^-) - \frac{(J+1)E((J-1)^+) + JE((J+1)^+)}{2J+1}, \qquad (7.1.12)$$

where $E(J^\pi)$ is the energy of the state of angular momentum J and parity π. If the partner bands, in a certain interval of angular momentum, have a $J(J+1)$ behavior and moreover they have similar moments of inertia, the displacement function vanishes in the chosen interval. It can be checked that this expression is proportional to the difference of the discrete first order derivatives of energy in the union of the parity partner bands, i.e. the common band, and in the positive parity band, with respect to J(J + 1). Therefore, the zeros of the displacement function are customarily considered as angular momenta for the states with static octupole deformation. Plotting this function for the nuclei listed in the beginning of this section, we identified the places where these nuclei might have octupole deformation.

In the ground band this might be a sequence of several states or just one state. Several nuclei show no zero for the displacement function. Concerning the excited partner bands, one observes that they have octupole deformation at different angular momenta than the ground band. For example, for ^{232}Th the displacement function of beta band cancels earlier (at 13^-) than that associated to gamma band (23^-) which at its turn vanishes before the ground band displacement energy function does. In this case, which is common to several nuclei from the list, the mentioned zeros are not degenerate. In our opinion these states are suspected to be fed with large probabilities
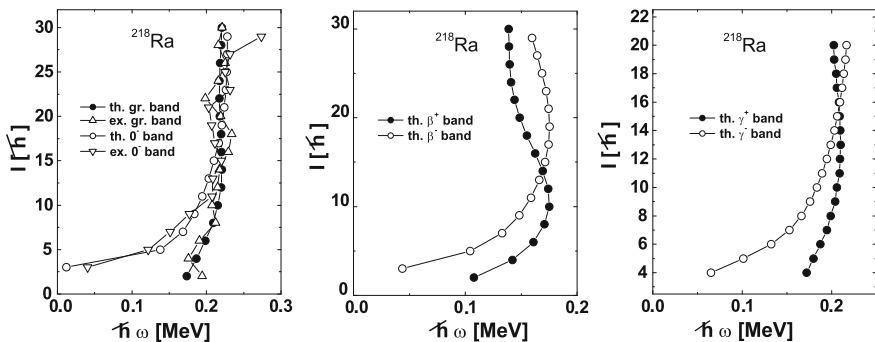
Fig. 7.6 The angular momentum is plotted versus the rotational frequency for the ground, 0^- (*left panel*), $\beta^\pm$, and $\gamma^\pm$ (*middle and right panels*) bands of ^{218}Ra. The experimental data for positive and negative parity states are represented by *up* and *down open triangles*, respectively

due to the E1 inter-band transition. As for gamma bands of ^{226}Ra, they form a single band starting with 9^- and the two bands of definite parity separate from each others, at 13^-. On the common curve, the states $J^\pm$ form a parity doublet. This is an excellent example supporting the statement that parity doublets may exist also in even-even nuclei.

The arguments given for the displacement function work for the case when energy exhibits a linear $J(J + 1)$ dependence. However, in all cases considered in our analysis, energies in the three pairs of parity partner bands deviate largely from the $J(J + 1)$ rule. Therefore, a more appropriate displacement function is:

$$\Delta E_{1,\gamma}(I) = \frac{1}{16}\Big[6E_{1,\gamma}(I) - 4E_{1,\gamma}(I - 1) - 4E_{1,\gamma}(I + 1)$$
$$+ E_{1,\gamma}(I - 2) + E_{1,\gamma}(I + 2)\Big], \text{ with } E_{1,\gamma} = E(I + 1) - E(I).$$
(7.1.13)

This function is proportional to the difference of the fourth order discrete derivatives of the parity partner bands energies, with respect to the angular momentum. Therefore, this function is vanishing if energies in the partner bands are quartic polynomials of J and moreover the highest rank terms of the two polynomials have the same coefficients. The parities associated to the angular momentum involved in the above equation are as follows: The states with angular momentum $(I \pm 2)$ have the same parity while the states $(I \pm 1)$ are of opposite parity as compared with the state I. This is true for the ground and beta bands. As for the gamma bands, this rule also holds but we have two chains depending whether the first state $(I - 2)$, in Eq. (7.1.13) is 2^+ or 2^-. In order to save the space, we give here only one figure, namely the one referring to ^{226}Ra (Fig. 7.7). It is worth noticing that the new displacement energy function has a beat pattern as a function of J, which might be due to a periodical dependence on J, of the energy fourth order derivatives. The results for other nuclei may be summarized as follows: For gamma bands, we found a node in the new dis-
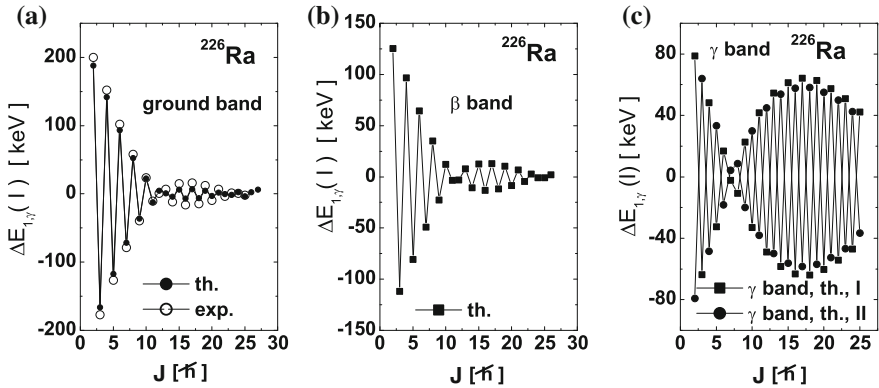
Fig. 7.7 The new displacement function given by Eq. (7.1.13) for ground (**a**), beta (**b**) and gamma (**c**) bands is represented as function of angular momentum. For gamma bands the label I is used when the state $2_\gamma^\dagger$ is the lowest angular momentum state involved in Eq. (7.1.13) while II corresponds to the calculations using 2_γ^- as the first in the chain. Experimental data were taken from Refs. [CO99, HJW93, AKO93]

placement energy function for all isotopes excepting ^{218}Ra. There are cases where the static octupole deformations appear in all three pairs of bands. Such examples are ^{226}Ra and ^{228}Th. The plot for ^{238}Pu shows nodes in the ground and gamma bands but not in beta band, while ^{232}Th has octupole deformation for a certain angular momentum in beta band and a different J in the gamma band, but is unstable against octupole deformation for any $J \leq 30$, in the ground band. In U isotopes, the only band where the octupole deformation may set on is the gamma band.

7.1.2 Electric Transition Probabilities

Using the transition operators given by Eqs. (7.1.8) and (7.1.9) we calculated the E1, E2 and E3 values in the six rotational bands and the results were compared with the corresponding experimental data. Here we comment on the results for the electric dipole transitions from states belonging to the 0^- band to the positive parity states of the ground band. We chose, for illustration the case of ^{226}Ra, where relevant data exist. Thus, in Table 7.1 we list the branching ratios

$$R_J = \frac{B(E1; J^- \to (J+1)^+)}{B(E1; J^- \to (J-1)^+)}. \tag{7.1.14}$$

We note the good quality of the agreement with the experimental data, especially for the results obtained with the transition operator $T^{(II)}$. As we have already mentioned, due to the rod effect concerning the charge distribution, the pear shaped nuclei are

Table 7.1 The branching ratios for the E1 transition probabilities between the states of g^- and those of g^+, as defined by Eq. (7.1.14), obtained with three transition operators, $T^{(h)}$ (second column), $T^{(I)}$ (third column) and $T^{(h)}$ (fourth column), defined by Eq. (7.1.9) are compared with the corresponding experimental data (first column) [CO99, SM95, CO97, HJW93, AKO93] for ^{226}Ra

J^π	Exp.	Th., h	Th., I	Th., II
1^-	1.85 ± 1.20	1.84	1.98	1.85
3^-	0.87 ± 0.35	1.12	1.31	0.95
7^-	1.79 ± 1.59	0.86	1.12	0.99
9^-	1.27 ± 0.68	0.83	1.10	1.13
11^-	1.12 ± 0.79	0.83	1.10	1.26
13^-	1.06 ± 0.68	0.85	1.11	1.35

The results shown in the third and fourth columns, are obtained with $q_I/q_1 = -0.16$, and $q_{II}/q_1 = -1.4$, respectively. Both cases use $q_1 = 10^{-2}$ e fm

expected to be excited with a large probability, by a dipole E1 operator. Therefore, in the case of ^{226}Ra where, according to Fig. 7.7, the octupole static deformation is set on at 13^-, one expects a jump of the reduced matrix elements for this value of the angular momentum.

These matrix elements are plotted in Fig. 7.8 as a function of angular momentum and compared with the experimental data from Refs. [CO99, HJW93, AKO93]. One sees that $T_{1\mu}^{(II)}$ yields results which agree with the data except for the fact that the transitions $14^\dagger \to 13^-$, $13^- \to 12^\dagger$ are underestimated. The oscillating behavior shown by the experimental data in the range of $1 \leq J \leq 7$ is nicely reproduced by these calculations. Note that data for I = 13, 14 and I = 11, 12 are equal to each other, respectively. In the calculations with $T^{(II)}$, the degeneracy appears at I = 9, 10 and a quasi-degeneracy at I = 7,8 and I = 11,12. By contrast, $T_{1\mu}^{(I)}$ produces such doublet structure for $3 \leq I \leq 13$, the consecutive doublets being separated by gaps which are increasing with J.

Before closing this subsection, we would like to make a short comment about the structure of the anharmonic dipole operators $T_{1\mu}^{(I)}$ and $T_{1\mu}^{(II)}$. It is well known that the magnetic dipole transition is determined by the current and spin distribution, while the electric one, by the charge distribution in the finite nuclei. This confers the M1 operator a linear dependence on the orbital angular momentum and spin operators. As for the electric transitions one cannot construct a dipole operator as linear superposition of angular momenta carried by the quadrupole and octupole bosons alone, since the resulting operator would be of positive parity. In order to have a negative parity operator, as a E1 operator should be, one has to multiply the angular momentum with one octupole boson. Moreover, in order to get the required multipolarities, one should consider a quadratic monomial of angular momentum.

The angular momentum dependence of the reduced matrix elements of dipole transition operators were studied also within the IBA [ZK01] and some microscopic formalisms [HHZ89, SS91, GER98]. The IBA paper uses for the transition operator

Fig. 7.8 The reduced matrix
elements for three distinct
transition operators: T^h(*up
triangle*), $T^{(I)}$(*open circles*),
$T^{(II)}$(*full square*) and
experimental values (*black
circles*). The units are
$q_1 = 10^{-2}$ efm. Strengths
are as in Table 7.1
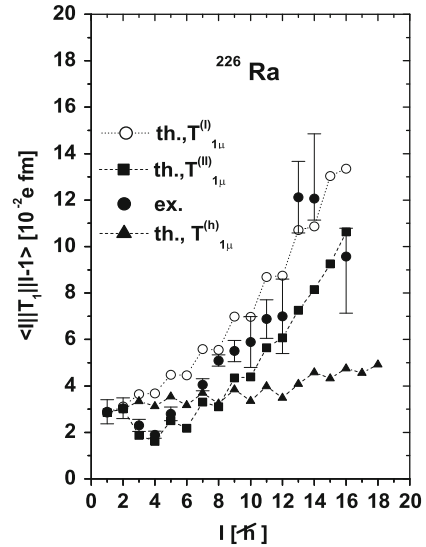
a three parameter expression. Despite this, the results for $2 \leq I \leq 7$ are largely
overestimated, while those for I $=$ 13, 14 are largely underestimated. In order to
improve the agreement with the data, the microscopic formalisms supplemented the
dipole operator with a corrective term of octupole type. The improvement refers
however to the low J values but the discrepancy in the regions of the m.e. jump still
persists. To complete the information about octupole states in nuclei, I advise the
reader to consult the comprehensive review papers on this issue [SGR88, BN96,
FRA01].

To conclude this section, one may say that the present extension of CSM is describ-
ing in a realistic fashion the spectra and the electric transitions of nuclei exhibiting
static octupole deformation.

7.1.3 The Dipole Bands

As already mentioned the formalism described above is known under the name of
extended coherent state model (ECSM). Here, the ECSM will be further extended
by considering the dipole parity partner bands [RRF09]. The difficulty encountered
when the restricted collective space is enlarged consists in finding an intrinsic state
which is orthogonal on the previously defined model states, before as well as after
angular momentum projection. The second step is to correct the model Hamiltonian
by a term so that the resulting Hamiltonian is effective in the extended space of
projected states. A possible solution for the intrinsic state generating the dipole
bands is:

$$\Psi^{(1,\pm)} = \Omega_3^\dagger b_{31}^\dagger \Psi_g^{(\pm)}, \quad \Omega_3^\dagger = [b_3^\dagger b_3^\dagger]_0 + \frac{f^2}{\sqrt{7}}. \tag{7.1.15}$$

From these states, two sets of angular momentum projected states are obtained, which are hereafter denoted by $\varphi_{JM}^{(1,\pm)}$. These states are weakly coupled to the states of other bands by the $\mathcal{B}_1$ and $\mathcal{B}_3$ terms. Moreover, these terms give large contribution to the diagonal matrix elements involving the projected dipole states. Aiming at describing quantitatively the properties of the dipole states, two terms are added to the model Hamiltonian:

$$\Delta H = \mathcal{C}_1 \Omega_3^\dagger \Omega_3 + \mathcal{C}_2 \Omega_3^\dagger \hat{N}_2 \Omega_3. \tag{7.1.16}$$

The new terms affect only the diagonal m.e. of the dipole states. $\mathcal{C}_2$ is determined so that the corresponding contribution to a particular state (say 2^-) cancels the one coming from the $\mathcal{B}_1$ term. $\mathcal{C}_1$ is determined so that the measured excitation energy of the state 1^- is reproduced. The contribution of the $\mathcal{B}_1$ and $\mathcal{B}_3$ terms to the off-diagonal matrix elements characterizing the dipole states amounts to few keV.

Thus, the final Hamiltonian to be used for describing simultaneously four positive and four negative bands, is:

$$\begin{aligned}
H = {} & \mathcal{A}_1(22\hat{N}_2 + 5\Omega_{\beta'}^\dagger \Omega_{\beta'}) + \mathcal{A}_2 \Omega_\beta^\dagger \Omega_\beta + \mathcal{A}_J \mathbf{J}^2 \\
& + \mathcal{B}_3 \hat{N}_3 + \mathcal{B}_1 \hat{N}_3 (22\hat{N}_2 + 5\Omega_{\beta'}^\dagger \Omega_{\beta'}) + \mathcal{A}_{(J23)} \mathbf{J_2 J_3} \\
& + \mathcal{C}_1 \Omega_3^\dagger \Omega_3 + \mathcal{C}_2 \Omega_3^\dagger \hat{N}_2 \Omega_3.
\end{aligned} \tag{7.1.17}$$

The items which were of interest for the three pairs of parity partner bands are also considered for the dipole bands. A special feature related to the dipole bands consists of: (a) Whether for these bands the magnetic or electric properties are prevailing; (b) Note that the two sets of bosons, of quadrupole and octupole type, carry separately an angular momentum. The question is what the angle between the two angular momenta is and how this is affected by rotation. The angle between the angular momenta $\mathbf{J_2}$ and $\mathbf{J_3}$ has the expression (7.1.18); (c) Of course, it would be nice if some signatures for a static octupole deformation were found in the dipole bands.

$$cos\varphi = \frac{\langle \phi_{JM}^{(k)} | \mathbf{J_2 . J_3} | \phi_{JM}^{(k)} \rangle}{\sqrt{\langle \phi_{JM}^{(k)} | \hat{J}_2^2 | \phi_{JM}^{(k)} \rangle \langle \phi_{JM}^{(k)} | \hat{J}_3^2 | \phi_{JM}^{(k)} \rangle}}, \quad k = 1, \pm. \tag{7.1.18}$$

Due to the rod effect saying that the charge density is maximum in the region where the surface curvature is maximum, a system having octupole deformation may exhibit a non-vanishing dipole moment. Consequently, interacting with an electromagnetic field such system can be driven in a state characterized by large E1 rates. In this context one expects that the B(E1) value exhibits a jump at the angular momentum where the octupole deformation is set on. This feature is illustrated in Fig. 7.8 where the reduced matrix element for the transition $I \rightarrow (I-1)$ is represented as function

of angular momentum. One notes a fairly good agreement between theoretical and experimental data.

The results for the $K^\pi = 1^-$ band energies are presented in Fig. 7.9 for ^{172}Yb, where relevant data are available [HJW93]. In Fig. 7.9 the dynamic moment of inertia is plotted versus the angular momentum. In this figure one notices that the results corresponding to even and those corresponding to odd angular momenta are lying on separate smooth curves as if these sets of states belonged to two distinct bands. The remark is valid for both the positive and negative parity bands.

In order to see whether there are signatures of octupole deformation in the dipole bands, we show in Fig. 7.10 the energy displacement functions for the two dipole bands with $K^\pi = 1^\pm$. According to Fig. 7.10, the states of angular momentum equal to 18, 19 may have static octupole deformation. To obtain a definite conclusion about the static octupole deformation we have analyzed the E1 and M1 properties of these bands. The relative magnitude of branching ratios for the bands with $K^\pi = 1^+$ and $K^\pi = 1^-$ indicate that the magnetic transitions are stronger for the positive parity states while the E1 transitions prevail for negative parity states. Due to this fact we call the band $K^\pi = 1^+$ as *the magnetic band*, while the negative parity band

Fig. 7.9 The dynamic moment of inertia for the dipole bands of positive and negative parity corresponding to the calculated and experimental energies, respectively, is plotted as function of the angular momentum
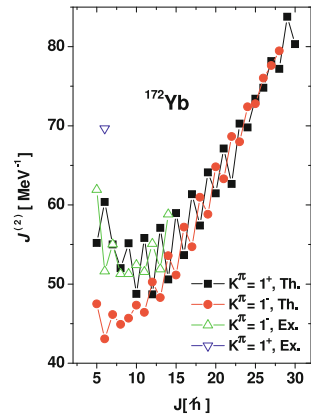
Fig. 7.10 The energy displacement functions δE (*left panel*) and ΔE (*right panel*), given in the text, are plotted as functions of J
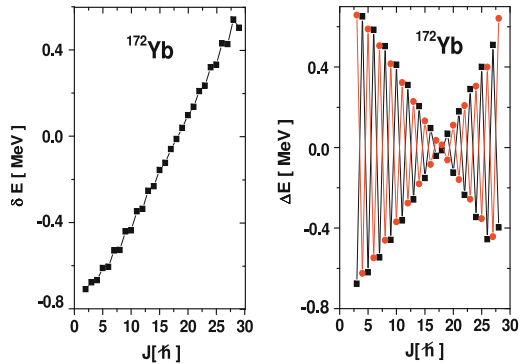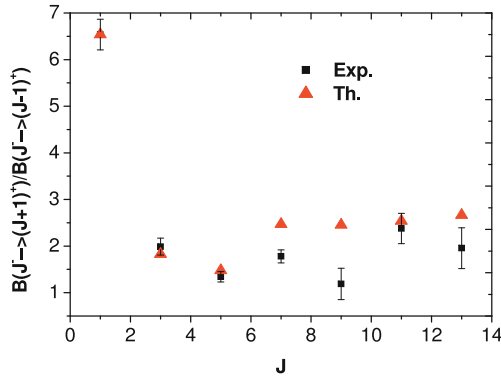
Fig. 7.11 The branching ratios characterizing the transitions of $K^\pi = 1^-$ states to the ground band states (*triangle*) are compared with the corresponding experimental data (*square*). The transition operator used is $T_{1\mu} = T_{1\mu}^h + T_{1\mu}^{anh}$, with the harmonic term defined in the text and $T_{1\mu}^{anh} = q_{anh}\left\{\left[b_3^\dagger\left(\hat{J}_3\hat{J}_2\right)_2\right]_{1\mu} + \left[\left(\hat{J}_3\hat{J}_2\right)_2 b_{\tilde{3}}\right]_{1\mu}\right\}$. All ratios correspond to the relative effective charge $q_{anh}/q_1 = -1.722$, where q_1 denotes the strength of the harmonic term

as *the electric band*. The branching ratios of the dipole states calculated within the formalism presented above are compared with the corresponding data in Fig. 7.11. In contrast to the case of $K^\pi = 0^-$ band, for the $K^\pi = 1^-$ band there is no jump in the behavior of the B(E1) value. However, the M1 branching ratio from the $K^\pi = 1^+$ to $K^\pi = 0^+$ get a jump for $J = 18, 19$, which are in fact the angular momenta where the energy displacement functions vanish. Due to this feature we consider the big value of the mentioned M1 branching ratio as a signature for the octupole deformation in the dipole bands.

Within ECSM, one can calculate the angle between the angular momenta carried by the quadrupole ($\mathbf{J_2}$) and octupole ($\mathbf{J_3}$) bosons respectively, for a state of total angular momentum $\mathbf{J}$. This angle is shown in Fig. 7.12 as function of the angular momentum for the states belonging to the four pairs of bands under study. Apart from small details, the features shown in Fig. 7.12 for ^{226}Ra are common to all other nuclei suspected to have octupole static deformation. For the dipole bands the angle has a saw-tooth structure. Here the angle characterizing the even and odd angular momenta stay on separate smooth curves suggesting once again that the two sets of states might form different bands. For the bands $g^\pm, \beta^\pm, \gamma^\pm$ the angle is decreasing up to a critical value after which is slightly increasing reaching a plateau at $\varphi = \pi/2$. The interpretation of this result is as follows. If the quadrupole bosons describe an ellipsoidal shape having the axis OZ as symmetry axis, the angular momentum $\mathbf{J_2}$ is oriented along an axis in the plane XOY, say OX, to which the maximum moment of inertia is associated. The octupole bosons describe a shape for which the moment of inertia corresponding to the axis OZ is maximum. Suppose now that a term describing the motion of a set of particles and a term describing their interaction with a phenomenological quadrupole-octupole core, are added to
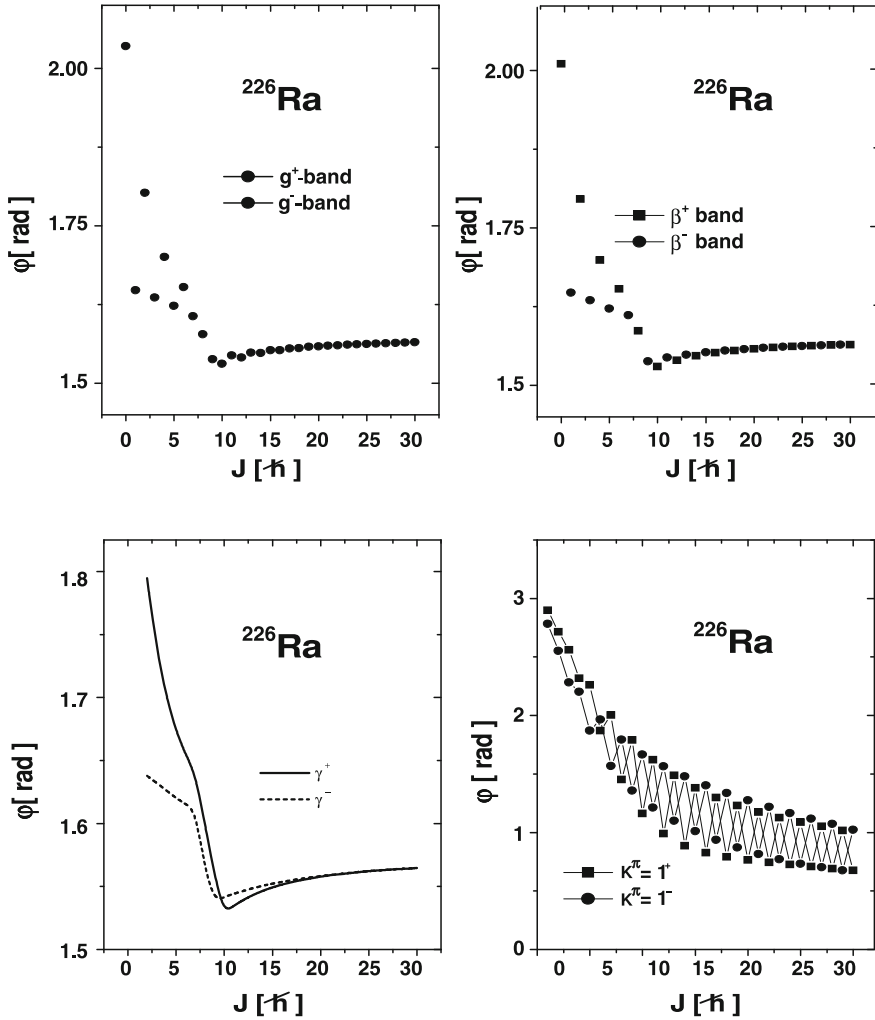
Fig. 7.12 The angle between the angular momenta carried by the quadrupole and octupole bosons respectively, in the states of $g^{\pm}$ (*upper left*), $\beta^{\pm}$ (*upper right*), $\gamma^{\pm}$ (*bottom left*) and dipole (*bottom right*) bands, versus angular momentum. Note that for g^+ and g^- one used the same symbol. However the angular momenta corresponding to the two sets of symbols are even and odd respectively

the model Hamiltonian (7.1.16). Depending on the strength of the interaction, the eigenstates of the resulting Hamiltonian may be characterized by a right or left trihedral ($\mathbf{j_F}$, $\mathbf{J_2}$, $\mathbf{J_3}$) with $\mathbf{j_F}$ denoting the angular momentum of the nucleons moving out the core. In case the two frames, right and left, define states of equal energies one says that the composite system exhibits a chiral symmetry. In this context we may say that the nuclear system excited in a high angular momentum state belonging

to either of the six bands $g^{\pm}$, $\beta^{\pm}$, $\gamma^{\pm}$, constitutes a precursor of a chiral symmetry system. Such a system will be studied in Chap. 10.

We raise the question whether the magnetic states described so far are related with the scissors mode [LOPA78]. The scissors mode describes the angular oscillations of the symmetry axes of proton and neutron systems. Here, we do not make any distinction between protons and neutrons, but we could say that we deal with two distinct entities, one described by the quadrupole and other by octupole bosons. The two systems rotate around axes which make an angle which was just described. By contrast to the scissors mode, where the angle between the symmetry axes is small, here the angle is large. Therefore, we could name the magnetic states described here as sheare states.

The final conclusion is that *the CSM and its extension is able to describe in a realistic fashion eight rotational bands, four of positive and four of negative parity.*

Chapter 8
Coupling of One, Two and Three Quasiparticles to a CSM Core

8.1 Coupling Quasiparticles to a CSM Core

8.1.1 Even-Even Systems

In Chap. 6, for some even-even isotopes of *Pt*, we attempted to interpret the high spin states of non-yrast type beyond 10^+, as beta like states. However, we saw that the position of the second 12^+ state is not well reproduced if we fit the energies from the upper part of the spectra. In fact this is a sign that the individual degrees of freedom play an important role there.

Here we present the results of Ref. [RLF83], where these states belong to a two quasiparticle-core band (2qp). The states of this band have a specific structure determined by the fact that one Cooper neutron-pair from the shell $i_{13/2}$ is broken and the resulting quasiparticles align their angular momentum, yielding a maximum J_2 value ($J_2^\pi = 12^+$) and moreover, the resulting angular momentum is aligned to the angular momentum of the core. Therefore, we consider a set of interacting spherical shell model particles coupled to a phenomenological core described in terms of quadrupole bosons by the CSM Hamiltonian. Outer particles interact among themselves through pairing and surface delta interactions. Hence, the Hamiltonian associated to the composite system of particles and core is:

$$H = H_{sp} + H_{pair} + H_{SDI} + H_{coup} + H_{coll}. \tag{8.1.1}$$

The first three terms describe the interacting particles and have the expressions:

$$H_{sp} = \sum (\epsilon_j - \lambda) c_{jm}^\dagger c_{jm},$$

$$H_{pair} = -\frac{G}{4} \sum_{j,j'} P_j P_{j'}^\dagger, \; P_j = \hat{j}(c_j^\dagger c_j^\dagger)_0, \hat{j} = \sqrt{2j+1}, \tag{8.1.2}$$

$$H_{SDI} = -4\pi G_1 \sum \frac{1}{2} \langle j_i m_i | Y_{\lambda\mu} | j_k m_k \rangle \langle j_l m_l | Y_{\lambda\mu}^* | j_s m_s \rangle c_{j_i m_i}^\dagger c_{j_l m_l}^\dagger c_{j_s m_s} c_{j_k m_k}.$$

The collective core is described by H_{coll} which is just the Hamiltonian used by the CSM formalism. Here we don't use the strength A_5 (see Eq. 6.1.11) in the fitting procedure of the data for the core. The coupling of particle system and the core is due to the term:

$$H_{coup} = M\omega^2 \sum_{J=0,2,4} \langle j||r^2 Y_J||j'\rangle \hat{j} \left[(c_j^\dagger c_{j'})_J T_J \right]_0, \text{ with}$$

$$T_{J\mu} = \chi \delta_{J,2} \alpha_{2\mu} + X_J (\alpha_2 \alpha_2)_{J\mu}. \tag{8.1.3}$$

In Ref. [RLF83], analytical formulas are obtained for the matrix elements of this Hamiltonian in the strong coupling as well as in the weak coupling regimes. Since here we deal with the Pt isotopes, which are only weakly deformed, we present only the latter version.

First, one treats the pairing Hamiltonian through the standard BCS formalism which defines the quasiparticle operators

$$d_{jm}^\dagger = u_j c_{jm}^\dagger - v_j c_{\widetilde{jm}}, \text{ with } c_{\widetilde{jm}} = (-)^{1+j-m} c_{j,-m}, u_j^2 + v_j^2 = 1. \tag{8.1.4}$$

In the quasiparticle representation, the model Hamiltonian becomes:

$$H_{lab} = H_{coll} + \sum e_j d_{jm}^\dagger d_{jm} + h_{coup}^{lab} + h_{SDI}^{lab}. \tag{8.1.5}$$

Here we used the label "lab", an abbreviation from laboratory, in order to distinguish between the present approach and the strong coupling formalism where the deformed single particle orbits requires a treatment in the intrinsic frame. In h_{SDI}^{lab} we did not include the quasiparticle number non-conserving terms. Also, we neglected the renormalization of H_{coll} due to the normal ordering of quasiparticles in the coupling term.

The quasiparticle-core Hamiltonian (8.1.5) was diagonalized in the basis $\{|C\rangle, |S, \tau\rangle_{int}\}$ with:

$$|C\rangle = \phi_{JM}^i \otimes |BCS\rangle, i = g, \beta, \gamma, J \leq 12,$$

$$|S, \tau\rangle \equiv |i\tau; J_1 J_2 IM\rangle = \frac{1}{\sqrt{2}} \left[\phi_{J_1}^i \otimes \left[d_{j_\tau}^\dagger d_{j_\tau}^\dagger \right]_{J_2} |BCS\rangle \right]_{I,M}, \tau = p, n; j_n = \frac{13}{2},$$

$$j_p = \frac{11}{2}, J_1 \leq \begin{cases} 10, & i = g \\ 6, & i = \gamma \\ 4, & i = \beta. \end{cases} \tag{8.1.6}$$

This way, one finds the amplitudes $f^{(i)}$ of the eigenstate:

$$|i, IM\rangle = \sum_C f_{(C)}^{(i)} |C\rangle + \sum_{S,\tau} f_{S,\tau}^{(i)} |S, \tau\rangle \tag{8.1.7}$$

which correspond to the eigenvalues $\epsilon_{i,I}$ ordered as:

$$\epsilon_{1,I} < \epsilon_{2,I} < \epsilon_{3,I} < \dots \tag{8.1.8}$$

Calculating the gyromagnetic factor of the states yielded by the diagonalization procedure, one gets information about whether the state is dominantly collective or a 2qp state. Denoting by g_F^τ and g_C the gyromagnetic factors for the 2-τ nucleons and the core systems respectively, the gyromagnetic factor for the composite system carrying an angular momentum $\mathbf{I}$ is defined by:

$$g_I \mathbf{I} = \mathbf{g_F^\tau J_2} + \mathbf{g_C J_1} \qquad (8.1.9)$$

The result for the gyromagnetic factor of the state $|i, IM\rangle$ (8.1.9) is:

$$g_I^{(k)} = g_C \sum_{i,J_1} (f_{i,J_1}^{(k)})^2 + \sum_{i,\tau,J_1,J_2} g_{I;J_1,J_2}^\tau (f_{(\tau i;J_1 J_2 I)}^{(k)})^2, \text{ with}$$

$$g_{I;J_1,J_2}^\tau = \frac{1}{2}\left[g_F^\tau + g_C + (g_F^\tau - g_C)\frac{J_2(J_2+1) - J_1(J_1+1)}{I(I+1)} \right]. \qquad (8.1.10)$$

The reduced E2 transition probabilities are calculated with the transition operator:

$$Q_{2\mu} = Q_{2\mu}^{coll} + Q_{2\mu}^{sp},$$

$$Q_{2\mu}^{coll} = q_0 \alpha_{2\mu} + q_2 (\alpha\alpha)_{2\mu},$$

$$Q_{2\mu}^{sp} = \sum_\tau e_{eff}^\tau \sum_{i,k} \frac{\hat{j}_i^\tau}{2} \langle j_i^\tau || r^2 Y_2 || j_k^\tau \rangle \left[(v_i v_k - u_i u_k)(d_i^\dagger d_k)_{2\mu} \right.$$

$$\left. + u_i v_k (-)^{l_k} ((d_l^\dagger d_k^\dagger)_{2\mu} + (-)^{j_i + j_k} (d_k d_i)_{2\mu}) \right]. \qquad (8.1.11)$$

The effective charge for protons and neutrons is taken equal to 1.5 and 0.5 , respectively. Using the Rose's convention [ROSE57], the B(E2) values for the transition $I_i \to I_f$ is defined by:

$$B(E2; I_i^+ \to I_{i'}'^+) = (\langle i, I||Q_2||i', I'\rangle)^2. \qquad (8.1.12)$$

The formalism presented above was applied to ^{188,190,192,194}Pt. Energies for ^{192}Pt are illustrated in Fig. 8.1.

Let us now analyze the effect of various terms involved in the model Hamiltonian on the energy spectrum. If in the coupling term the collective factor is restricted to the linear one, then the state 12^+ would be lower in energy than 10^+. This happens since the fully aligned 2qp state $[(\nu_{13/2})^2]_{12}$ is favored with respect to the partially aligned configuration $[(\nu_{13/2})^2]_{10}$. The interaction which restores the natural order for the two energies is the hexadecapole particle-core term. Indeed, this term affects mainly the states around 10^+ and leaves the states beyond 14^+, almost unchanged. The surface delta interaction affects in principal the diagonal matrix elements, decreasing them if $G_1 > 0$. This depression is large for small values of J_2 and small for large J_2. Since the major components of the yrast states beyond 10^+ have $J_2 = 12$, it is expected that all states are shifted down by more or less the same amount.

Fig. 8.1 The ground *left*, gamma *middle* and beta *right* energies predicted by the extended CSM in ^{192}Pt, are compared with experimental data. The structure coefficients and the deformation parameters, determined as explained in the text, are given in the figure legend. Experimental data are taken from Refs. [FING72, RBWW79, JNH77]

The BCS treatment was performed for the whole major shells of $i_{13/2}$ for neutrons and $h_{11/2}$ for protons. The resulting quasiparticle energies, in ^{192}Pt, are 1.485 and 1.305 MeV for neutrons and protons, respectively.

The CSM parameters d, A_1, A_2 for ^{192}Pt are kept the same as if the CSM was used alone to describe the low spin spectrum. Since the terms A_3 and A_4 are influencing only the beta state energies and moreover these states are also affected by the quasiparticle-core coupling, we modified them a bit and the actual values, which reproduces the first two energy levels in the beta band, are: $A_3 = -88.139$ keV, $A_4 = -108.906$ keV. The strengths for the coupling interaction have been fixed in the following way. The parameter $\chi/k\sqrt{2}$ is varied slightly around the value predicted by the liquid drop model. The coefficients X_0 and X_2 are taken equal to each other. Their common value and X_4 are chosen so that the energy difference $E_{12^+} - E_{10^+}$ lies close to the corresponding experimental data. Another point which is worth mentioning is the quenching of the 0 and 2 qp interaction due to the coupling term, by a factor of 0.2. By this quenching one prevents an over-counting of the collective effects of the 2qp operator, these being already included via the phenomenological quadrupole bosons. The parameters obtained for ^{192}Pt are listed in Fig. 8.1. The states beyond 10^+, have the aligned states $\left[(2\nu)_{J_2}|J_1^+\rangle\right]_{J_2+J_1}$ as a dominant component, where J_1^+ is a state from the CSM ground band. However, they have also components involving states of beta and gamma bands as collective factor states and the 2qp of proton types aligned to the angular momentum 10^+. The structure of wave functions in that region is reflected in the transition probabilities.

Table 8.1 Branching ratios for some low lying states

$10^2 \dfrac{B(E2;J\to J')}{B(E2;I\to I')}$	^{188}Pt		^{190}Pt		^{192}Pt		^{194}Pt	
	Exp.	Th.	Exp.	Th.	Exp.	Th.	Exp.	Th.
$\dfrac{2^+_\gamma \to 0^+_g}{2^+_\gamma \to 2_g}$	3.44	3.44	1.24	1.27	0.51	0.51	0.38	0.35
$\dfrac{3^+_\gamma \to 2^+_g}{3^+_\gamma \to 2_\gamma}$	4.5	5.24	1.8	1.67	0.76	0.44	0.5	0.35
$\dfrac{3^+_\gamma \to 4^+_g}{3^+_\gamma \to 2_\gamma}$		0.039	49	33.8	26	29.3		0.0013
$\dfrac{0^+_\beta \to 2^+_g}{0^+_\beta \to 2_\beta}$	≥ 11	12.23	11	5.06	3.8	3.7	7.9	3.7
$\dfrac{2^+_\beta \to 0^+_g}{2^+_\beta \to 0_\beta}$	0.83	0.014	0.02	0.002	0.022	6.5×10^{-4}		4.0×10^{-4}
$\dfrac{2^+_\beta \to 4^+_g}{2^+_\beta \to 0_\beta}$	19.0	7.4	4.2	4.4	≤ 2.8	0.83		1.68
$q_2/q_0 k\sqrt{2}$		0.114		0.064		0.008		0.012

Experimental data (Exp.) are taken from Ref. [FING72]. The parameter $q_0/k\sqrt{2}$ was fixed so that the experimental value of $B(E2; 2^\dagger \to 0^\dagger)$ [RBWW79] is reproduced

The results for transition probabilities are presented in Tables 8.1 and 8.2. The effective charge of the collective terms involved in the quadrupole transition operator, $q_0/k\sqrt{2}$ and $q_2/2k^2$, were adjusted as to reproduce the experimental data for the ratio $B(E2; 2^+_\gamma \to 2^+_g)$ and $B(E2; 2^+_g \to 0^+_g)$. The deformation parameter d for the four isotopes $^{188-194}$Pt is 0.9, 0.8, 0.8, 0.7, respectively. One should note that the big discrepancy between the experimental data and the CSM prediction for the ratio in the last row of Table 8.1 for ^{188}Pt, does not show up in ^{190}Pt. This discrepancy and differences appearing in the second last row are caused by the fact that the parameter d as well as the anharmonic term of the transition operator should be larger than they are.

The results for the gyromagnetic factor of the yrast states can be summarized as follows: It has a constant value equal to the $g_C = Z/A$ for $I \leq 8$ which reflects the fact the state have a pure collective nature. A discontinuity appears for $I = 10$ where g_I has the value -0.2 for ^{192}Pt and 0 for ^{190}Pt. For the second mentioned isotope the minimum value, -0.2, is reached for $I = 12$. For this angular momentum the gyromagnetic factor of ^{192}Pt keeps still equal to -0.2. Beyond 12^+, g_I is slowly increasing and at 18^+ vanishes. The negative values for g_I suggests that the leading component of the given state consists of two neutron quasiparticles aligned to the low lying collective states of the core. The higher states of the same angular momentum have also competitive components of 2 proton quasiparticles coupled to the states of the core. This is reflected in the value of the corresponding gyromagnetic factor, since the proton factor has a positive value. To give an example we mention the case of ^{192}Pt where the predictions for $g_I^{(i)}$ for the second and third 10^+ (i.e., $I = 10$, $i = 2, 3$) are 1.36 and $-0.19 \, \mu_N$, while the values for the second and third 12^+ are -0.19 and $1.11 \, \mu_N$, respectively.

Table 8.2 Experimental (Exp.) and predicted (Th.) B(E2) values for the transitions $(J \to (J-2))$ in the yrast band

$10^2 \dfrac{B(E2;J\to(J-2))}{B(E2;2_g^+\to0_g^+)}$	188Pt		190Pt		192Pt		194Pt	
	Exp.	Th.	Exp.	Th.	Exp.	Th.	Exp.	Th.
$4_g^+ \to 2_g^+$		1.81		1.89	$1.71 \pm 0.19^{[a]}$	1.94	$1.82 \pm 0.16^{[a]}$	1.96
$6_g^+ \to 4_g^+$		2.54		2.70	$1.43 \pm 0.6^{[a]}$	2.81	$1.56 \pm 0.53^{[f]}$	2.87
$8_g^+ \to 6_g^+$		3.15		3.40		3.62	$1.19 \pm 0.43^{[f]}$	3.73
$10_1^+ \to 8_g^+$		3.45		0.08	$(2. \pm 0.8) \times 10^{-2[d]}$	0.24×10^{-2}	$(4.2 \pm 1.3) \times 10^{-3[e]}$	0.83×10^{-3}
$12_1^+ \to 10_1^+$	$(2.32 \pm 1.05) \times 10^{-3[b]}$	1.73×10^{-3}	$0.21 \pm 0.08^{[c]}$	0.13	$0.71 \pm 0.15^{[b]}$	0.35		0.025
$14_1^+ \to 12_1^+$		0.80		0.97		0.93		1.05
$16_1^+ \to 14_1^+$		1.79		1.90		1.99		2.07
$18_1^+ \to 16_1^+$		2.52		2.68		2.84		2.95

[a] [JNH77]
[b] [RBWW79]
[c] [TMF78]
[d] [ROUL76]
[e] [JLF76]
[f] [GHK77]. The parameters involved in the transition operator are those listed in Table 8.1

8.1.2 Even-Odd Systems

The quasiparticle-core coupling Hamiltonian introduced in the previous subsection to study the states for an even-even system lying in the backbending region may also be used for studying the even-odd isotopes. Here we describe the results obtained by ignoring the SDI interaction. Its influence on the diagonal matrix elements is however simulated by a correction of the quasiparticle energies. In Ref. [RS87], this Hamiltonian was treated in both the intrinsic and laboratory reference frames. Numerical results are obtained, however, in the laboratory frame, where the diagonalization basis is defined by a subspace of the quasiparticle core-states due to the restrictions: (a) one considers only the one and three quasiparticle states; (b) the states of the core are the projected states used by the CSM to describe the ground, β and γ bands:

$$|i, J_1 j; IM\rangle = \left[\phi^i_{J_1} \otimes d^\dagger_j |BCS\rangle\right]_{IM} \equiv |C, 1, IM\rangle,$$

$$|i, J_1; j, j^2(J_2)J_3; IM\rangle = \left[\phi^i_{J_1} \otimes |j, j^2(J_2)J_3\rangle\right]_{IM} \equiv |C, 3, IM\rangle,$$

$$i = g, \beta, \gamma. \tag{8.1.13}$$

The diagonalization procedure provides the eigenvalues

$$\epsilon_{1,I} < \epsilon_{2,I} < \epsilon_{3,I} < ... \tag{8.1.14}$$

and the corresponding eigenstates:

$$|i, IM\rangle = \sum_{C,1} \mathcal{C}^{i,I}_{C,1} |C, 1, IM\rangle + \sum_{C,3} \mathcal{C}^{i,I}_{C,3} |C, 3, IM\rangle \tag{8.1.15}$$

The electric quadrupole and magnetic dipole transition operators connecting the eigenstates of the model Hamiltonian, have the same expressions as in the previous subsection. Therefore, the B(E2) and B(M1) values are defined as:

$$B(E2; kI \to k'I') = |\langle kI||Q_2||k'I'\rangle|^2,$$

$$B(M1; kI \to k'I') = |\langle kI||M_1||k'I'\rangle|^2. \tag{8.1.16}$$

Results for the E2 and M1 strengths are given in Table 8.3. With these quantities one may calculate the mixing ratios for the E2 and M1 transitions:

$$\delta = 8.78 \times 10^{-4}(E_{kI} - E_{k'I'})\frac{\langle kI||Q_2||k'I'\rangle}{\langle kI||M1||k'I'\rangle}. \tag{8.1.17}$$

Calculations were performed for ^{189}Pt, ^{191}Pt and ^{193}Pt. Results for energies in the heaviest isotope are shown in Fig. 8.2, where the experimental data available, taken from Refs. [PI75, BR78, ROT80, SAH77], are also given. For a better presentation we organized the data in $\Delta I = 2$ bands based on $j = \frac{13}{2}, \frac{11}{2}, \frac{9}{2}$, respectively. In all considered isotopes a back-bending appears in the yrast band for $I = \frac{33}{2}$. As results from our

Table 8.3 The B(E2) and B(M1) values for the transitions $I \to I - 2$ and $I \to I + 1$ respectively, predicted for some even-odd isotopes of Pt

I	$B(E2; I \to I - 2)(e^2 b^2)$			I	$B(M1; I \to I + 1)(e^2 fm^2 \times 10^{-2})$		
	^{189}Pt	^{191}Pt	^{193}Pt		^{189}Pt	^{191}Pt	^{193}Pt
17/2	0.101	0.135	0.075	9/2	0.126	0.159	0.133
21/2	0.041	0.162	0.058	11/2	0.204	0.298	0.233
25/2	0.628	0.530	0.475	13/2	0.001	0.001	0.001
29/2	2.464	1.597	1.469	15/2	0.122	0.144	0.118
15/2	0.087	0.071	0.045	17/2	0.140	0.103	0.109
19/2	0.143	0.175	0.085	19/2	0.073	0.166	0.135
23/2	1.152	0.821	0.754				
27/2	2.097	1.525	1.285				
31/2	2.248	1.801	1.379				

Fig. 8.2 The calculated energies (Th.) for the particle-core coupling Hamiltonian are compared with the corresponding experimental data (Exp.) for ^{193}Pt. Data are from Refs. [PI75, ROT80, SAH77, BR78]
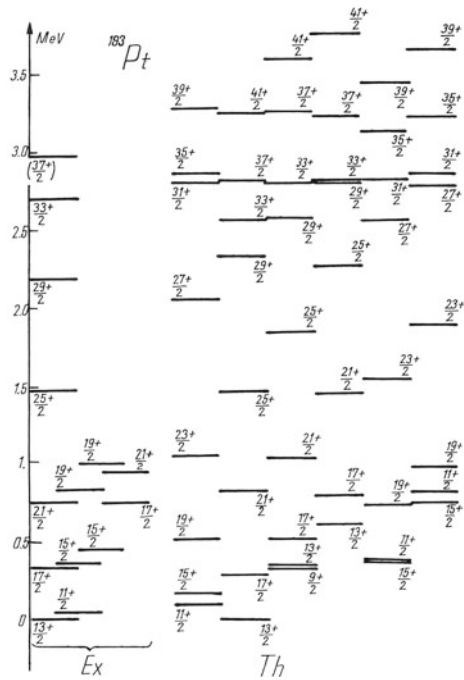
calculations, the maximum component of this state is $\phi_0^g |j^3 33/2\rangle$. Of course, to this state the particle-core component $\phi_0^g ((\pi h_{11/2}^2)_{10} \nu i_{13/2})_{33/2}$ could also contribute, but it was ignored since according to our estimation this is, indeed, small. On the other hand if one νqp would be coupled to the state $12^\dagger$, where the back-bending in the neighboring even-even isotope is taking place, one would expect that the state $37/2^+$ is the right place for the back-bending to show up. This proves that the back-bending in the even-odd system is caused by the intersection of 1 and three quasiparticle

bands. Indeed, the maximum angular momentum which one could meet in a three quasiparticle system is $33/2^+$. The first 2 bands headed by $11/2^+$ are bending at $I = 31/2^+$ while the bands which start with $9/2^+$ and $(13/2)^+_2$ respectively, have the back-bending at $29/2^+$. One notices the fact that the states where the intersection of 1qp and 3qp bands takes place, are almost degenerate. This degeneracy would not persist if the states $(2\pi h_{11/2} 1\nu i_{13/2})$ are included in the diagonalization basis. However, a staggering of the states mentioned above would still persist.

The strengths determining the electric and magnetic transitions operators respectively, are the same as for the even-even case. In order to account for the polarization effects which are not included here, the free gyromagnetic factor for neutron quasiparticles was quenched by a factor of 0.6. In Table 8.4 one sees that the quadrupole moment changes the sign at $11/2^+$ and again in the high spin region. Taking into account the structure of the core states in the intrinsic frame of reference, the change of sign for the quadrupole moment in a high spin state is determined by the oblate shape of the collective core in a state of a high angular momentum as we have seen in one previous chapter. The negative sign of the $11/2^+$ state is due the dominance character of the component having as collective factor state, the state 2^+_γ which, as we have shown earlier, has a quadrupole moment whose sign is different from the sign characterizing the quadrupole moments of the low lying states in the ground band. We note the large value of the mixing ratios for $I = 13/2^+$, which is caused by a small value for the corresponding B(M1) value.

Concerning the band structure, few additional words are necessary. Indeed, until now we artificially organized the energy levels in $\Delta I = 2$ bands starting with $I = 9/2$, 11/2, 13/2, respectively. The question is whether these sets of states are indeed bands in the traditional sense, i.e. the consecutive states of a given band are linked by strong E2 transitions.

Table 8.4 The electric quadrupole (Q_I) and magnetic dipole moments (μ_I) as well as the mixing ratios (δ) predicted for the states of some even-odd isotopes of Pt, are listed

I	Q_I(eb)			μ_I(efm)			δ		
	^{189}Pt	^{191}Pt	^{193}Pt	^{189}Pt	^{191}Pt	^{193}Pt	^{189}Pt	^{191}Pt	^{193}Pt
9/2	1.06	1.12	0.89	−0.165	−0.169	−0.168	−0.036	−0.030	−0.028
11/2	−0.24	−0.09	−0.06	−0.112	−0.117	−0.115	0.017	0.001	0.009
13/2	0.74	0.75	0.63	−0.107	−0.111	−0.110	−2.909	0.447	−18.12
15/2	1.64	1.28	1.26	−0.043	−0.048	−0.046	0.128	0.128	0.125
17/2	1.82	1.75	1.35	−0.008	−0.017	−0.014	0.171	0.278	0.228
19/2	0.71	0.75	0.61	0.045	0.038	0.037	−0.158	−0.089	−0.120
21/2	1.21	0.68	0.51	0.081	0.061	0.062			
23/2	0.43	0.24	−0.08	0.141	0.132	0.134			
25/2	0.15	−0.05	−0.32	0.149	0.142	0.142			
27/2	−1.17	−1.34	−2.15	0.276	0.260	0.280			
29/2	−0.82	−1.12	−1.64	0.252	0.241	0.247			
31/2	−1.73	−2.18	0.021	0.386	0.369	0.215			

According to the results listed in Table 8.3, this is true for the yrast bands headed by $I = 13/2$ and $I = 11/2$, respectively. However, the statement is not valid for other sets included in Fig. 8.2, due to the strong admixture of the excited band states which enhances the decay probability to the yrast line. We don't exclude the possibility of a finite band structure due to some band crossings below the angular momentum where the 1qp and 3qp bands intersect each other. Indeed, within the 1qp band one may distinguish three bands having as major collective state factor a state of the CSM bands, i.e. $\phi_{JM}^g \; \phi_{JM}^\beta$ or ϕ_{JM}^γ.

In Ref. [RS87], results for the gyromagnetic factor are also presented. They vary with angular momentum, in the following manner. It starts from a negative value (≈ -0.4) which corresponds to a neutron 1qp coupled to a collective state of low spin and therefore the contribution coming from g_F, which is negative, is dominant. The curve increases and reaches positive values for $I = 19/2$ from where high spins from the core are involved and therefore the effect due to the collective magnetic moments prevails. The gyromagnetic factor continues to increase up to $I = 31/2$ when a big fall down takes place for $I = 33/2$ where the values are -0.4 for ^{191,193}Pt and -0.8 for ^{189}Pt. Actually, for this spin the 1qp and 3qp bands cross each other. From this angular momentum the gyromagnetic factor is increasing again, which in fact reflects that the high spin collective states participate.

As a final conclusion, one may say that the present extension of the CSM formalism provides a consistent description of the spectroscopic properties of both the even-even and the even-odd nuclei.

8.1.3 Parity Partner Bands in Even-Odd Nuclei

We suppose that the rotational bands in even-odd nuclei may be described by a particle-core Hamiltonian:

$$H = H_{sp} + H_{core} + H_{pc}, \tag{8.1.18}$$

where H_{sp} is a spherical shell model Hamiltonian associated to the odd nucleon, while H_{core} is a phenomenological Hamiltonian which describes the collective motion of the core in terms of quadrupole and octupole bosons. This term is identical to that used [RRR06] in the previous chapter to describe eight rotational bands in even-even nuclei. The two subsystems interact with each other by H_{pc}, which has the following expression:

$$\begin{aligned}
H_{pc} = &-X_2 \sum_\mu r^2 Y_{2,-\mu}(-)^\mu \left(b_{2\mu}^\dagger + (-)^\mu b_{2,-\mu} \right) \\
&- X_3 \sum_\mu r^3 Y_{3,-\mu}(-)^\mu \left(b_{3\mu}^\dagger + (-)^\mu b_{3,-\mu} \right) + X_{jJ}\mathbf{jJ} + \mathbf{X_{I^2}I^2}.
\end{aligned} \tag{8.1.19}$$

The term $\mathbf{jJ}$ is similar to the spin-orbit interaction from the shell model and expresses the interaction between the angular momenta of the odd-particle and the core. In other words this term accounts for the interaction of the magnetic moments associated to the mentioned angular momenta. The last term is due to the rotational motion of the whole system, $\mathbf{I}$ denoting the total angular momentum of the particle-core system. The core states are described by eight sets of mutually orthogonal functions, obtained by projecting out the angular momentum and the parity from four quadrupole and octupole deformed functions: one is a product of two coherent states:

$$\Psi_g = e^{f(b_{30}^+ - b_{30})} e^{d(b_{20}^+ - b_{20})} |0\rangle_2 |0\rangle_3 \equiv \Psi_o \Psi_q |0\rangle_2 |0\rangle_3, \qquad (8.1.20)$$

while the remaining three are polynomial boson excitations of Ψ_g. The parameters d and f are real numbers and simulate the quadrupole and octupole deformations, respectively. The vacuum state for the k-pole boson, $k = 2, 3$, is denoted by $|0\rangle_k$.

   The particle-core interaction generates a deformation for the single particle trajectories. Indeed, averaging the model Hamiltonian with Ψ_g, one obtains a deformed single particle Hamiltonian, H_{mf} which plays the role of the mean field for the single particle motion:

$$H_{mf} = \mathcal{C} + H_{sp} - 2dX_2 r^2 Y_{20} - 2fX_3 r^3 Y_{30}, \qquad (8.1.21)$$

where $\mathcal{C}$ is a constant determined by the average of H_{core}. The Hamiltonian H_{mf} represents an extension of the Nilsson Hamiltonian by adding the octupole deformation term. In Ref. [RRR99] it was shown that in order to get the right deformation dependence of the single particle energies H_{mf} must be amended with a monopole-monopole interaction, $M\omega^2 r^2 \alpha_{00} Y_{00}$, where the monopole coordinate α_{00} is to be determined from the volume conservation restriction. This term has a constant contribution within a band. The constant value is, however, band dependent.

   In order to find the eigenvalues of the model Hamiltonian we follow several steps:

(1) In principle the single particle basis could be determined by diagonalizing H_{mf} amended with the monopole interaction. The product basis for particle and core may be further used to find the eigenvalues of H. Due to some technical difficulties in restoring the rotation and space reversal symmetries for the composite system wave function, this procedure is however tedious and therefore one prefers a simpler method. Thus, the single particle space consists of three spherical shell model states with angular momenta j_1, j_2, j_3. We suppose that j_1 and j_2 have the parity $\pi = +$, while j_3 has a negative parity $\pi = -$. Due to the quadrupole-quadrupole interaction the odd particle from the state j_1 can be promoted to j_2 and vice-verso. The octupole-octupole interaction connects the states j_1 and j_2 with j_3. Due to the above mentioned effects the spherical and space reversal symmetries of the single particle motion are broken. To be more specific, by diagonalizing H (8.1.18) in a projected spherical particle-core basis with the spherical single particle state factors mentioned above, the eigenstates could be written as a projected spherical particle-core state having as single particle state factor a function without rotation and parity good symmetries. Therefore, one could start with a coupled basis where the single particle state is a linear

combination of the spherical states, where the mixing coefficients are to be determined by a least square fitting procedure as to obtain an optimal description of the experimental excitation energies. Thus, instead of dealing with a spherical shell model state coupled to a deformed core without reflection symmetry, as the traditional particle-core approaches proceed, here the single particle orbits are lacking the spherical and space reversal symmetries and by this, their symmetry properties are consistent with those of the phenomenological core.

(2) We notice that Ψ_g is a sum of two states of different parities. This happens due to the specific structure of the octupole coherent state:

$$\Psi_o = \Psi_o^{(+)} + \Psi_o^{(-)}. \tag{8.1.22}$$

The states of a given angular momentum and positive parity can be obtained through projection from the intrinsic states:

$$|n_1 l_1 j_1 K\rangle \Psi_o^{(+)} \Psi_q, \quad |n_2 l_2 j_2 K\rangle \Psi_o^{(+)} \Psi_q, \quad |n_3 l_3 j_3 K\rangle \Psi_o^{(-)} \Psi_q. \tag{8.1.23}$$

The projected states of negative parity are obtained from the states:

$$|n_1 l_1 j_1 K\rangle \Psi_o^{(-)} \Psi_q, \quad |n_2 l_2 j_2 K\rangle \Psi_o^{(-)} \Psi_q, \quad |n_3 l_3 j_3 K\rangle \Psi_o^{(+)} \Psi_q. \tag{8.1.24}$$

The angular momentum and parity projected states are denoted by:

$$\varphi_{IM}^{(+)}(j_i K; d, f) = N_{i;IK}^{(+)} P_{MK}^I |n_i l_i j_i K\rangle \Psi_o^{(+)} \Psi_q \equiv N_{i;IK}^{(+)} \psi_{IM}^{(+)}(j_i K; d, f), i = 1, 2$$

$$\varphi_{IM}^{(+)}(j_3 K; d, f) = N_{3;IK}^{(+)} P_{MK}^I |n_3 l_3 j_3 K\rangle \Psi_o^{(-)} \Psi_q \equiv N_{3;IK}^{(+)} \psi_{IM}^{(+)}(j_3 K; d, f),$$

$$\varphi_{IM}^{(-)}(j_i K; d, f) = N_{i;IK}^{(-)} P_{MK}^I |n_i l_i j_i K\rangle \Psi_o^{(-)} \Psi_q \equiv N_{i;IK}^{(-)} \psi_{IM}^{(-)}(j_i K; d, f), i = 1, 2$$

$$\varphi_{IM}^{(-)}(j_3 K; d, f) = N_{3;IK}^{(-)} P_{MK}^I |n_3 l_3 j_3 K\rangle \Psi_o^{(+)} \Psi_q \equiv N_{3;IK}^{(-)} \psi_{IM}^{(-)}(j_3 K; d, f).$$
$$\tag{8.1.25}$$

The factors $N_{i,IK}^{(\pm)}$ assure that the projected states $\varphi^{(\pm)}$ are normalized to unity. Obviously, the unnormalized projected states are denoted by $\psi^{(\pm)}$. For the quantum number K we consider the lowest three values, i.e. $K = 1/2, 3/2, 5/2$. Note that the earlier particle-core approaches [RCD76, LEA82] restrict the single particle space to a single j, which results in eliminating the contribution of the octupole-octupole interaction.

(3) Note that for a given j_i, the projected states with different K are not orthogonal. Indeed, the overlap matrices:

$$A_{K,K'}^{(+)}(Ij_l; d,f) = \langle \psi_{IM}^{(+)}(j_lK; d,f) | \psi_{IM}^{(+)}(j_lK'; d,f) \rangle,$$

$$l = 1, 2, 3; \ K, K' = 1/2, 3/2, 5/2,$$

$$A_{K,K'}^{(-)}(Ij_l; d,f) = \langle \psi_{IM}^{(-)}(j_lK; d,f) | \psi_{IM}^{(-)}(j_lK'; d,f) \rangle,$$

$$l = 1, 2, 3; \ K, K' = 1/2, 3/2, 5/2, \tag{8.1.26}$$

are not diagonal. By diagonalizing the overlap matrices, one obtains the eigenvalues $a_{Ip}^{(\pm)}(j_l)$ and the corresponding eigenvectors $V_{IK}^{(\pm)}(j_l, p)$, with $K = 1/2$, $3/2, 5/2$ and $p = 1, 2, 3$. Then, the functions:

$$\Psi_{IM}^{(+)}(j_l, p; d,f) = N_{l;Ip}^{(+)} \sum_K V_{IK}^{(+)}(j_l, p) \psi_{IM}^{(+)}(j_lK; d,f),$$

$$\Psi_{IM}^{(-)}(j_l, p; d,f) = N_{l;Ip}^{(-)} \sum_K V_{IK}^{(-)}(j_l, p) \psi_{IM}^{(-)}(j_lK; d,f), \tag{8.1.27}$$

are mutually orthogonal. The norms are given by:

$$\left(N_{l;Ip}^{(\pm)} \right)^{-1} = \sqrt{a_{Ip}^{(\pm)}(j_l)}. \tag{8.1.28}$$

For each state, there is a term in the sum (8.1.27), which has a maximal weight. The corresponding quantum number K is conventionally assigned to the mixed state.

(4) In order to simulate the core deformation effect on the single particle motion, in some cases the projected states corresponding to different j must be mixed up.

$$\Phi_{IM}^{(+)}(p; d,f) = \sum_{l=1,2,3} \mathcal{A}_{pl}^{(+)} \Psi_{IM}^{(+)}(j_lp; d,f),$$

$$\Phi_{IM}^{(-)}(p; d,f) = \sum_{l=1,2,3} \mathcal{A}_{pl}^{(-)} \Psi_{IM}^{(-)}(j_lp; d,f). \tag{8.1.29}$$

The amplitudes $\mathcal{A}_{pl}^{(\pm)}$ can be obtained either by diagonalizing H_{mf} or, as we mentioned before, by a least square fitting procedure applied to the excitation energies.

The energies of the odd system are approximated by the average values of the model Hamiltonian corresponding to the projected states:

$$E_I^{(+)}(p; d,f) = \langle \Phi_{IM}^{(+)}(p; d,f) | H | \Phi_{IM}^{(+)}(p; d,f) \rangle,$$

$$E_I^{(-)}(p; d,f) = \langle \Phi_{IM}^{(-)}(p; d,f) | H | \Phi_{IM}^{(-)}(p; d,f) \rangle. \tag{8.1.30}$$

Note that due to the structure of the particle-core projected states, the energies for the odd system are determined by the coupling of the odd particle to the excited states of the core. This approach was applied for the description of the $K^\pi = 1/2^\pm$ bands.

However this procedure can be extended by including the $K \neq 0$ states in the space describing the deformed core.

8.1.4 The Description of the $K^\pi = \frac{3^\pm}{2}, \frac{5^\pm}{2}$ Bands

In principle the method presented in the previous subsection may work for the description of bands with the quantum number larger than $1/2$. However, the intrinsic reference frame for the odd system is determined by the deformed core and therefore one expects that this brings an important contribution to the quantum number K. To be more specific, we cannot expect that projecting out the good angular momentum from $|j5/2\rangle \otimes \Psi_g$ a realistic description of the $K = 5/2$ bands is obtained. Therefore, we assume that the $K^\pi = \frac{3^\pm}{2}, \frac{5^\pm}{2}$ bands are described by projecting out the angular momentum from a product state of a low K single particle state and the intrinsic gamma band state.

We recall that within CSM the states of the gamma band are obtained by projection from the intrinsic state:

$$\Psi_2^{(\gamma;\pm)} = \Omega_\gamma^\dagger \Psi_o^{(\pm)} \Psi_q \tag{8.1.31}$$

where the excitation operator for the gamma intrinsic state was defined before. The low index of Ψ in Eq. (8.1.31) is the K quantum number for the γ intrinsic state. Thus, a simultaneous description of the bands with $K = 1/2, 3/2, 5/2$ can be achieved with the projected states:

$$\varphi_{IM;1/2}^{(\pm)} = N_{I,1/2}^{(\pm)} \sum_J \left(N_J^{(g,\pm)}\right)^{-1} C_{1/2\,0\,1/2}^{j_1\,J\,I} \left[|n_1 l_1 j_1\rangle \otimes \varphi_J^{(g;\pm)}\right]_{IM},$$

$$\varphi_{IM;3/2}^{(\pm)} = N_{I,3/2}^{(\pm)} \sum_J \left(N_J^{(\gamma,\pm)}\right)^{-1} C_{-1/2\,2\,3/2}^{j_1\,J\,I} \left[|n_2 l_2 j_2\rangle \otimes \varphi_J^{(\gamma;\pm)}\right]_{IM},$$

$$\varphi_{IM;5/2}^{(\pm)} = N_{I,5/2}^{(\pm)} \sum_J \left(N_J^{(\gamma,\pm)}\right)^{-1} C_{1/2\,2\,5/2}^{j_1\,J\,I} \left[|n_3 l_3 j_3\rangle \otimes \varphi_J^{(\gamma,\pm)}\right]_{IM}. \tag{8.1.32}$$

In the above expressions the notation $N_J^{(i,\pm)}$, with $i = g, \gamma$ is used for the normalization factors of the projected states describing the ground and the gamma bands respectively, of the even-even core. Note that for each angular momentum I the above set of three projected states is orthogonal. The energies for the six bands with $K^\pi = 1/2^\pm, 3/2^\pm, 5/2^\pm$ are obtained by averaging the model Hamiltonian (8.1.18) with the projected states defined above.

$$E_{I,K}^{(\pm)} = \langle \varphi_{IM;K}^{(\pm)}|H|\varphi_{IM;K}^{(\pm)}\rangle, \quad K = 1/2, 3/2, 5/2. \tag{8.1.33}$$

The matrix elements of the particle core-interaction can be analytically calculated [RRF09].

8.1.5 Transition Probabilities

For some $K = 1/2$ bands data for the reduced $E1$ and $E2$ transition probabilities are available. They are given in terms of the branching ratios:

$$R_{I\pi} = \frac{B(E1; I^\pi \to (I-1)^{\pi'})}{B(E2; I^\pi \to (I-2)^\pi)}, \pi' \neq \pi \qquad (8.1.34)$$

The dipole and quadrupole transition operators are:

$$Q_{1\mu} = eq_1 \left((b_2^\dagger b_3^\dagger)_{1\mu} + (b_3 b_2)_{\widetilde{1\mu}} \right),$$
$$Q_{2\mu} = eQ_2 \left(b_{2\mu}^\dagger + (-)^\mu b_{2,-\mu} + ar^2 Y_{2\mu} \right). \qquad (8.1.35)$$

8.1.6 Numerical Results

Excitation energies for one positive and one negative parity bands with $K = \frac{1}{2}$, in three odd isotopes, ^{219}Ra, ^{237}U and ^{239}Pu, were calculated. The parameters defining H_{core}, as well as the deformation parameters d and f, are the same as for the eight rotational bands in the even-even neighboring isotopes. The single particle states are spherical shell model states with the appropriate parameters for the (N, Z) region of the considered isotopes [RiSh80]. Calculations correspond to the single particle states: $(j_1, j_2, j_3) = (2g_{7/2}, 2g_{9/2}, 1h_{9/2})$. In order to obtain the best agreement between the calculated excitation energies and the corresponding experimental data, in the expansion (8.1.29) a small admixture of the states $(j_1; j_3)$ and $(j_2; j_3)$ was considered: $|\mathcal{A}_{i,3}^{(+)}|^2$ and $|\mathcal{A}_{i,3}^{(-)}|^2$, are both equal to 0.001 for ^{219}Ra, while for ^{237}U and ^{239}Pu the amplitudes take the common values: $|\mathcal{A}_{i,3}^{(+)}|^2 = |\mathcal{A}_{i,3}^{(-)}|^2 = 0.04$. The mixing amplitude of the states (j_1, j_2) is negligible small. Energies (8.1.30) depend on the interaction strengths X_2, X_3, X_{jJ} and X_{I^2}. They were determined by fitting four particular energies in the two bands of different parities, i.e. $K^\pi = \frac{1}{2}^\pm$. The results of the fitting procedure are given in Table 8.5. Inserting them in Eq. (8.1.30),

Table 8.5 Parameters involved in the particle-core Hamiltonian obtained by fitting four excitation energies

Parameters	^{219}Ra	^{227}Ra	^{237}U	^{239}Pu
$X_2 b^2$ [keV]	22.714	-1.992	1.080	-2.515
$X_3 b^3$ [keV]	-8.823	169.511	2.227	4.937
X_{jJ} [keV]	-0.230	8.553	-5.817	-3.985
X_{I^2} [keV]	3.778	4.390	4.634	5.050

Here b denotes the oscillator length: $b = (\frac{\hbar}{M\omega})^{1/2}$; $\hbar\omega = 41A^{-1/3}$. The usual notations for nucleon mass (M) and atomic number (A) were used

the energies in the two bands with $K = 1/2$ are readily obtained.

$$E(I^{\pm}) = E_I^{(\pm)}(1; d, f) - E_{\frac{1}{2}}^{(+)}(1; d, f). \tag{8.1.36}$$

The theoretical results for excitation energies, given in Table 8.6 for ^{219}Ra, ^{237}U and ^{239}Pu and in Fig. 8.3 for ^{219}Ra, agree quite well with the corresponding experimental data. Our results suggest that the dominant K component is $K = 1/2$, while the dominant j component is $g_{9/2}$. Results of r.m.s. values for ^{219}Ra, ^{237}U and ^{239}Pu are 66.24 keV, 48.97 keV and 31.8 keV, respectively. In calculating the $r.m.s.$ value for ^{219}Ra we ignored the data for the states $53/2^{\pm}$ since the spin assignment is uncertain. It is interesting to mention that the spectra of ^{219}Ra were measured by two groups [COT87, Wi92] by the same reaction, ^{208}Pb(^{14}C, 3n)^{219}Ra. However, they assign for the ground state different angular momenta, $9/2^+$ [COT87] and $7/2^+$ [Wi92]. In our approach both assignments yield good description of the data. However, we made the option for $9/2^+$ since the corresponding results agree better with the experimental data than those obtained with the other ground state.

The case of ^{227}Ra was treated with the formalism presented in Sect. 8.1.4. The single particle basis is: $2g_{7/2}, 2g_{9/2}, 2f_{5/2}$. The first state coupled to the coherent state describing the unprojected ground state generates the parity partner bands
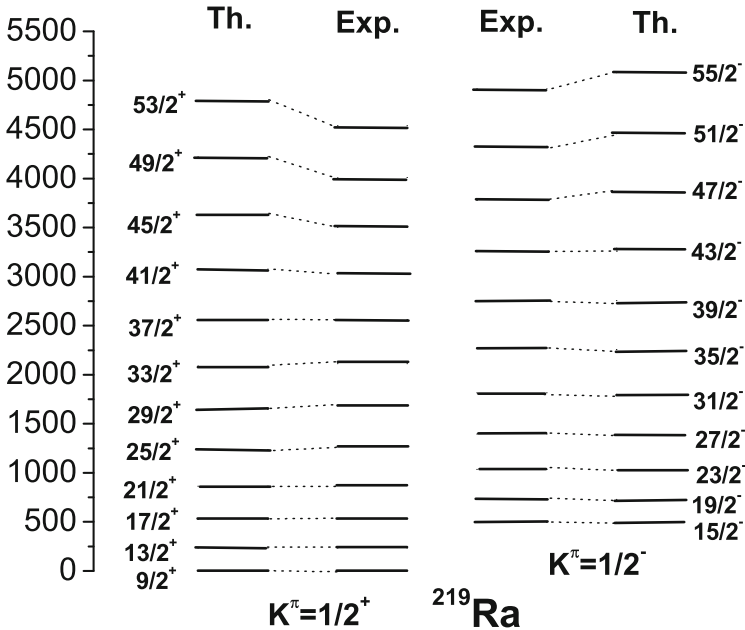

Fig. 8.3 Calculated (Th.) and experimental (Exp.) excitation energies for the $K^{\pi} = \frac{1}{2}^{\pm}$ bands in ^{219}Ra. The data were taken from Ref. [Wi92]

Table 8.6 Excitation energies in ^{219}Ra, ^{237}U and ^{239}Pu, for the bands characterized by $K^\pi = \frac{1}{2}^+$ and $K^\pi = \frac{1}{2}^-$, respectively, are given in keV

	^{219}Ra				^{237}U				^{239}Pu			
	$\pi = +$		$\pi = -$		$\pi = +$		$\pi = -$		$\pi = +$		$\pi = -$	
J	Exp.	Th.	Exp.	Th.	Exp.	Th.	Exp.	Th.	Exp.	Th.	Exp.	Th.
1/2					0.0	0.0		398.5	0.0	0.0	469.8	469.8
3/2					11.4	11.4		454.4	7.9	7.9	492.1	477.7
5/2					56.3	74.6		475.5	57.3	62.8	505.6	498.3
7/2					82.9	106.9		550.3	75.7	108.4	556.0	549.8
9/2	0.0	0.0			162.3	191.2		581.3	163.8	183.5	583.0	572.0
11/2	539.0	545.0			204.1	231.8		680.9	193.5	222.0	661.2	655.2
13/2	234.3	235.0	588.0	586.0	317.3	347.7	721.9	318.5	338.1	698.7	685.7	682.5
15/2	837.0	847.6	495.4	496.0	375.1	393.1	846.4	846.4	359.2	386.5	806.4	799.9
17/2	529.1	525.4	921.0	917.4	518.2	544.2	930.0	899.1	519.5	534.9	857.5	839.5
19/2	1229.0	1210.6	733.7	734.3	592.0	592.0	1027.5	1046.6	570.9	592.2	992.5	984.2
21/2	876.6	861.2	1309.0	1318.9	762.8	780.3	1131.0	1113.3	764.7	773.7	1058.1	1033.3
23/2	1622.0	1626.6	1035.6	1038.3	853.0	829.0	1250.7	1281.3	828.0	839.2	1219.4	1208.3
25/2	1271.6	1235.5	1722.0	1790.5	1048.7	1065.8	1376.1	1364.8	1053.1	1054.4	1300.9	1267.2
27/2	2022.0	2090.7	1393.6	1400.6	1155.1	1108.8	1515.7	1550.2	1127.8	1127.8	1487.4	1472.2
29/2	1684.7	1644.4	2137.0	2230.5	1372.2	1378.3	1662.3	1654.0	1381.5	1377.0	1584.9	1541.2
31/2	2444.0	2600.9	1815.6	1814.2	1494.1	1421.6	1821.8	1852.8	1467.8	1458.0	1795.4	1776.0
33/2	2113.4	2086.8	2552.0	2580.8	1729.2	1728.7	1987.7	1981.0	1748.5	1744.2	1908.9	1855.4
35/2			2272.1	2272.7	1868.2	1772.5	2166.5	2188.9	1847.0	1831.3	2143.4	2119.8
37/2	2563.6	2563.6	2987.0	3115.9	2117.2	2117.2	2349.7	2346.1	2152.2	2150.2	2272.0	2209.8
39/2			2750.8	2770.6	2272.2	2161.7	2547.5	2558.3	2263.0	2245.0	2529.4	2503.6

(continued)

Table 8.6 (continued)

J	^{219}Ra				^{237}U				^{239}Pu			
	$\pi = +$		$\pi = -$		$\pi = +$		$\pi = -$		$\pi = +$		$\pi = -$	
	Exp.	Th.	Exp.	Th.	Exp.	Th.	Exp.	Th.	Exp.	Th.	Exp.	Th.
41/2	3029.0	3076.7			2530.1	2544.1	2746.7	2749.4	2590.1	2597.9	2672.0	2604.4
43/2			3255.8	3303.4	2702.5	2589.4	2960.5	2960.5	2714.0	2700.5	2951.4	2927.5
45/2	3505.0	3627.9			2963.8	3009.5	3174.7	3191.3	3060.1	3087.5	3108.0	3039.3
47/2			3776.5	3867.8	3154.5	3055.6	3401.5	3395.3	3198.0	3198.0	3407.0	3395.3
49/2	4009.6	4218.7			3415.8	3513.7	3630.0	3671.7	3559.1	3619.1	3578.0	3514.4
51/2			4328.9	4462.5	3625.5	3560.5	3865.0	3862.4	3713.0	3737.0	3895.0	3895.8
53/2	4540.4	4759.2			3886.8	4057.8	4105.0	4190.9	4087.1	4194.0	4080.0	4029.9
55/2			4913.6	5044.1	4115.0	4104.8	4344.0	4350.0	4256.0	4319.8	4413.0	4436.7

The results of our calculations (Th.) are compared with the corresponding experimental data (Exp.) taken from Ref. [COT87, Wi92, ZH05]
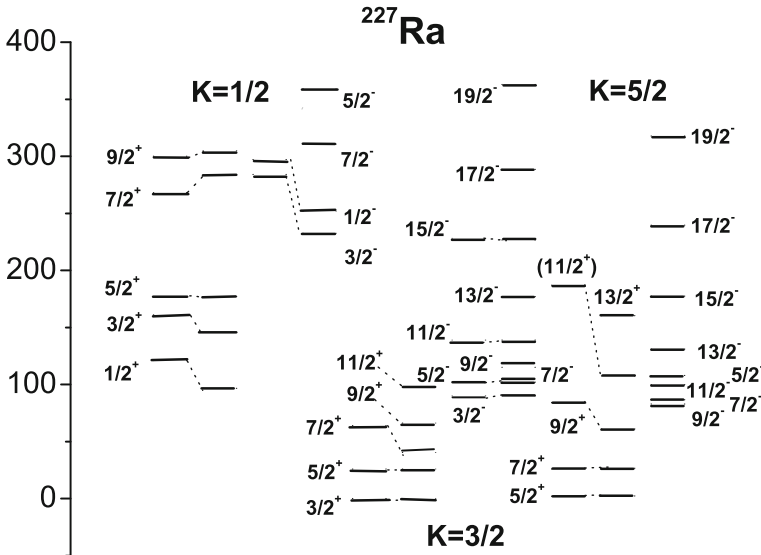
Fig. 8.4 Calculated *right column* and experimental *left column* excitation energies for the bands with $K^{\pi} = \frac{1}{2}^{\pm}, \frac{3}{2}^{\pm}, \frac{5}{2}^{\pm}$ in ^{227}Ra. The experimental data were taken from Refs. [LEA92, DZ95, Wi92]

$K^{\pi} = 1/2^{\pm}$. The bands $K^{\pi} = 3/2^{\pm}$ are obtained through projection from the product state $(2g_{9/2})\Psi_2^{(\gamma;\pm)}$, while the bands $K^{\pi} = 5/2^{\pm}$ originate from the intrinsic state $(2f_{5/2})\Psi_2^{(\gamma;\mp)}$. Concerning the bands characterized by $K^{\pi} = 1/2^{\pm}$ one could consider also the mixing of components with different K in the manner discussed in Sect. 8.1.3. However, numerical application suggests that such a mixing is not really necessary in order to obtain a realistic description of the available data. The calculated energies of the three bands in ^{227}Ra are compared with the corresponding experimental data in Fig. 8.4. In Fig. 8.4 we note that the present approach reproduces the experimental energies ordering in the band $K^{\pi} = 1/2^-$ band. The energy split of the states $3/2^-$, $1/2^-$ is nicely described although the doublet is shifted down by an amount of about 50 keV. In the band $5/2^+$ there exist an energy level which is tentatively assigned with $11/2^+$. Calculations suggest that this level could be assigned as $13/2^+$. No experimental data are available for the band $5/2^-$. In Fig. 8.4 we gave however the results also for this band. Note that the ordering for the lowest levels is not the natural one. However, starting with $13/2^-$ the normal ordering is restored.

Now we would like to comment on the parameters yielded by the fitting procedure, for the considered isotopes. Except for ^{237}U, where both quadrupole-quadrupole and octupole-octupole interactions are attractive, the two interactions have different characters for the rest of nuclei. In the first situation the λ ($= 2, 3$)-pole moments of the odd nucleon and of the collective core have different signs. In the remaining cases the two moments are of similar sign. We also remark the large strength for the $q_3.Q_3$ interaction in ^{227}Ra which is consistent with the fact the neighboring

even-even isotope exhibits a relatively large octupole deformation. Indeed, according to Refs. [RRF97, RIUF03] for this nucleus we have $f = 0.8$. The large value of the strength X_3 determines a large mixing amplitudes of the states $[g_{9/2}\Psi_g^{(+)}; f_{5/2}\Psi_g^{(-)}]$ as well as of the states $[g_{9/2}\Psi_g^{(-)}; f_{5/2}\Psi_g^{(+)}]$. Indeed, the value obtained for this amplitude is: $|A_{i,3}^{(+)}|^2 = |A_{i,3}^{(-)}|^2 = 0.07425$, $i = 1, 2$. Another distinctive feature for ^{227}Ra consists in the fact that the **jJ** interaction strength has a sign which is different from that associated to other nuclei. In fact the repulsive character of this interaction in ^{227}Ra is necessary in order to compensate the large attractive contribution of the q_3Q_3 interaction.

Further, we raised the question whether one could identify signatures for static octupole deformation in the two bands. To this goal, in Fig. 8.5, we plotted the energy displacement functions [RIUF03, RIO3, BON00] $\delta E(I)$, $\Delta E_{1,\gamma}(I)$, defined in the previous chapter, for ^{239}Pu. We choose this nucleus, since more data are available. The plot suggests that a static octupole deformation is possible for the states with angular momenta $I \geq \frac{51}{2}$, belonging to the two parity partner bands.
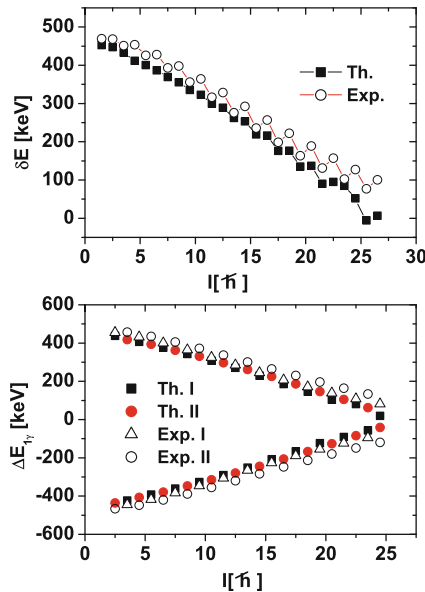

Fig. 8.5 The theoretical and experimental energy displacement functions $\delta E(I)$ and $\Delta E_{1,\gamma}(I)$ given by Eqs. (7.1.11) and (7.1.12) respectively, characterizing the isotope ^{239}Pu, are plotted as a function of the angular momentum I. Experimental data are taken from Ref. [ZH05]. In the lower panel, the theoretical and experimental $\Delta E_{1,\gamma}(I)$ corresponding to the states $I^\pi = \left(\frac{1}{2} + 2k\right)^+$ with k $= 1, 2, 3, \ldots$, are represented by the symbols *Th. I* and *Exp. I* respectively, while those associated with the negative parity states $I^\pi = \left(\frac{1}{2} + 2k\right)^-$ with k $= 1, 2, 3, \ldots$ bear the labels *Th. II* and *Exp. II*, respectively

Table 8.7 Experimental (Exp.) and calculated values of the ratio $B(E1)/B(E2)$ for the initial state J^π running from $19/2^-$ to $51/2^-$

| $J^\pi - J_{g.s.}$ | $\frac{B(E1;J\to(J-1))}{B(E2;J\to(J-2))} (10^{-6}\,\text{fm}^{-2})$ | | | |
	Exp.	Set I	Set II	Ref. [ZD93]
5^-	2.52(18)	2.52	2.52	1.195
6^+	1.12(08)	1.09	0.677	0.314
7^-	1.49(10)	3.97	3.284	1.318
8^+	1.23(16)	1.23	0.704	0.313
9^-	1.16(08)	4.56	3.194	1.442
10^+	2.77(64)	1.44	0.775	0.312
11^-	1.41(9)	4.59	2.829	1.567
12^+	3.68(26)	1.69	0.868	0.313
13^-	2.14(30)	4.39	2.448	1.691
14^+	1.96(14)	1.96	0.967	0.314
15^-	1.76(18)	4.11	2.131	1.814
16^+	1.06(17)	2.22	1.060	0.315
17^-	2.08(28)	3.84	1.887	1.936
18^+	3.34(48)	2.45	1.137	0.317
19^-	1.34(42)	3.62	1.704	2.057
20^+	2.38(44)	2.63	1.195	0.318
21^-	4.01(94)	3.44	1.568	2.177
Average	2.09(9)	2.97	1.7	1.072

For an easier writing the angular momenta are normalized to $J_{g.s.} = 9/2$. Experimental data are from Ref. [COT87]. Results are given in units of $10^{-6}\,\text{fm}^{-2}$. For comparison purposes we give the results of Ref. [ZD93] in the last column

Finally, we calculated the branching ratio R_J defined by Eq. (8.1.34), for ^{219}Ra. There are two parameters involved which were fixed so that two particular experimental data are reproduced. Choosing two distinct sets of data, one obtains the following parameters, respectively:

$$\text{set I}: \quad \frac{q_1}{q_2} = 18.377 \times 10^{-3}\text{fm}^{-1}, \quad ab^2 = -0.63616\,\text{fm}^2,$$

$$\text{set II}: \quad \frac{q_1}{q_2} = 11.310 \times 10^{-3}\text{fm}^{-1}, \quad ab^2 = -0.34422\,\text{fm}^2, \qquad (8.1.37)$$

where b denotes the oscillator strength characterizing the spherical shell model states for the odd nucleon, while a is the strength of the particle like transition operator (8.1.35). As shown in Table 8.7, the theoretical results agree reasonable well with the corresponding experimental data. Results show an oscillating behavior with maxima for the negative parity states. Note that some of the data are well described while others deviate from the data by a factor ranging from 2 to 3. In the fourth column of Table 8.7 we listed the results obtained in Ref. [ZD93] by a different model.

Comparison between the present formalism for even-odd nuclei and that of Ref. [BONA04], reveals the following features: (i) Having in mind the asymptotic behavior of the coherent states written in the intrinsic frame of reference [RKF83], one may anticipate that the wave function describing the odd system from Ref. [BONA04], might be recovered in the asymptotic limit of the present approach. Due to the fact that this formalism is associated to the laboratory reference frame, the Coriolis interaction does not show up explicitly. The split of the states of different parities is determined by the matrix elements of H_{pc}; (ii) Since the coherent states are axially symmetric functions, we don't account for the motion of the γ-like deformation. Again the two formalisms are on a par with each other; (iii) The approach of Ref. [BONA04] is of a strong coupling type and therefore K is a good quantum number, which is not the case in this approach. Indeed, we use the laboratory frame and the meaning of the quantum number K is given by the fact that the K-component of the projected function prevails over the components with $K' \neq K$; (iv) The Hamiltonian describing the odd system (8.1.18) involves a term H_{core} which describes in a realistic fashion the neighboring even-even system. By contrast, in Ref. [BONA04] the terms associated to the core are not appropriate for describing the complex structure of the even-even sub-system.

Before closing, we would like to add a few remarks about the possible development of the present formalism. Choosing for the core unprojected states, the generating states for the parity partner bands with $K^{\pi} = 0^{\pm}_{\beta}, 2^{\pm}_{\gamma}, 1^{\pm}$ states, otherwise keeping the same single particle basis for the odd nucleon, the present formalism can be extended to another four bands, two of positive and two of negative parity. Another noteworthy remark refers to the chiral symmetry [FRA01] for the composite particle and core system. Indeed, in Chap. 7 we showed that starting from a certain total angular momentum of the core, the angular momenta carried by the quadrupole ($\mathbf{J_2}$) and octupole ($\mathbf{J_3}$) bosons respectively, are perpendicular on each other. Naturally, we may ask ourselves whether there is a strength for the particle-core interaction such that the angular momentum of the odd particle becomes perpendicular to the plane ($\mathbf{J_2}, \mathbf{J_3}$). This would be a signature that the three component system exhibits a chiral symmetry.

As a final conclusion, one may say that the present CSM extension to odd nuclei can describe quite well the excitation energies in the parity partner bands with $K^{\pi} = \frac{1}{2}^{\pm}, \frac{3}{2}^{\pm}, \frac{5}{2}^{\pm}$.

Chapter 9
The Generalized Coherent State Model

9.1 CSM Extension to p-n Systems

The description of magnetic properties in nuclei has always been a central issue. The reason is that the two systems of protons and neutrons respond differently when they interact with an external electromagnetic field. Differences are due to the fact that by contrast to neutrons, protons are charged particles, the proton and neutron magnetic moments are different from each other and finally the protons and neutron numbers are also different. It was in 1965 that Greiner and his collaborators advanced the idea about different moments of inertia for proton and neutron systems [GR64] which should be reflected both in energies and magnetic transitions. This idea was further elaborated under the name of the two liquid drops model which has been used to describe the isovector 2^+ state [FA66] as well as the M1 properties [MGM75] of the rotational bands. Few years later a microscopic description of the magnetic dipole states was proposed by Gabrakov, Kuliev and Pyatov [GKP70], by using a deformed Woods Saxon mean field for the single particle motion. Shortly after, the same authors succeeded to eliminate the isoscalar spurious contributions to the magnetic mode [KP74]. Such dipole excitation was also studied by Rowe [SR77] within the potential vibrating method. The group which brought something essentially new in this field is that of Lo Iudice and Palumbo [IPF84]. They developed a phenomenological model, called Two Rotor Model (TRM), which assigns to the proton and neutron systems two rigid rotors, which are axially symmetric with different symmetry axes. The mode appears to be a vibrational mode of the angle between the two symmetry axes. This picture inspired the naming as "scissors mode". An essential property of the mode, predicted by TRM, is that it is excited due to the interaction of the nuclear convection current with the electromagnetic field. Although the predictions of the TRM for both energy and M1 probability to be excited, are much larger than the experimental data, obtained few years later, the big merit of this model s to predict a pure orbital mode, which is of collective nature, without involving the spin degrees of freedom. As a matter of fact, this feature was confirmed by all microscopic calculations. The field of collective M1 states was enormously stimulated by the group of Richter,

which identified the M1 state, for ^{156}Gd, in a high resolution (e, e') experiment at backward angles [BRS83]. The results for the excitation energy and the B(M1) value were confirmed by a nuclear resonance fluorescent experiment [BBD84]. Since then, many experiments have been performed and the number of nuclei known to exhibit a scissors mode was enlarged by many rear earth and actinides nuclei but also by some medium isotopes from the Ti region. Another phenomenological model aimed at describing the measured properties of 1^+ is the interacting boson model (IBA2). In this model, the M1 state is caused by breaking the F spin symmetry by a Majorana interaction of the proton-like and neutron-like bosons. The state energy is obtained by a suitable fixing of the interaction strength. Therefore IBA2 is not making predictions for the state energy but only for the M1 excitation probability from the ground state [IA81].

To obtain more detailed information about the literature devoted to this subject, we advise the reader to consult the review papers on this issue [RI90, IUD95, ZAW98].

Here we briefly describe how to extend the CSM so as to be able to account for the collective properties of the scissors mode [RFC87]. This extension is conventionally called "The generalized Coherent State Model" (GCSM). In contrast to the CSM, which uses only one boson for the composite system of protons and neutrons, within the GCSM the protons are described by proton-like bosons while the neutrons by neutron-like bosons. Since one has two quadrupole bosons instead of one, one expects from the beginning to have a more flexible model and to find a simpler solution satisfying the restrictions required by the CSM. The restricted collective space is defined for the three major bands, ground, beta and gamma, as well as for a band which is based on the isovector state 1^+. Orthogonality conditions are satisfied by the following six functions which generate by angular momentum projection, 6 rotational bands.

$$\phi_{JM}^{(g)} = N_J^{(g)} P_{M0}^J \psi_g, \quad \psi_g = exp[d(b_{p0}^\dagger + b_{n0}^\dagger) - d(b_{p0} + b_{n0})]|0\rangle,$$
$$\phi_{JM}^{(\beta)} = N_J^{(\beta)} P_{M0}^J \Omega_\beta \psi_g,$$
$$\phi_{JM}^{(\gamma)} = N_J^{(\gamma)} P_{M2}^J (b_{n2}^\dagger - b_{p2}^\dagger)\psi_g,$$
$$\tilde{\phi}_{JM}^{(\gamma)} = \tilde{N}_J^{(\gamma)} P_{M2}^J (\Omega_{\gamma,p,2}^\dagger + \Omega_{\gamma,n,2}^\dagger)\psi_g,$$
$$\phi_{JM}^{(1)} = N_J^{(1)} P_{M1}^J (b_n^\dagger b_p^\dagger)_{11}\psi_g,$$
$$\tilde{\phi}_{JM}^{(1)} = \tilde{N}_J^{(1)} P_{M1}^J (b_{n1}^\dagger - b_{p1}^\dagger)\Omega_\beta^\dagger\psi_g. \tag{9.1.1}$$

Here, the following notations were used:

$$\Omega_{\gamma,k,2}^\dagger = (b_k^\dagger b_k^\dagger)_{2,2} + d\sqrt{\frac{2}{7}}b_{k,2}^\dagger, \quad k = p, n,$$
$$\Omega_\beta^\dagger = \Omega_p^\dagger + \Omega_n^\dagger - 2\Omega_{pn}^\dagger,$$
$$\Omega_k^\dagger = (b_k^\dagger b_k^\dagger)_0 - \sqrt{\frac{1}{5}}d^2, \quad k = p, n,$$

$$\Omega^{\dagger}_{pn} = (b^{\dagger}_p b^{\dagger}_n)_0 - \sqrt{\frac{1}{5}} d^2. \tag{9.1.2}$$

Note that a priori we cannot select one of the two sets of states ϕ^{γ}_{JM} and $\tilde{\phi}^{\gamma}_{JM}$ for the gamma band, although one is symmetric and the other asymmetric against proton neutron permutation. The same is true for the two isovector candidates for the dipole states. The projected state norms have simple expressions in terms of the overlap integrals (6.1.15), after changing the variable d^2 by $\rho^2 = 2d^2$.

We seek now an effective Hamiltonian for which the projected states (9.1.1) are, at least in a good approximation, eigenstates in the restricted collective space. The simplest Hamiltonian fulfilling this condition is:

$$H = A_1(\hat{N}_p + \hat{N}_n) + A_2(\hat{N}_{pn} + \hat{N}_{np}) + \frac{\sqrt{5}}{2}(A_1 + A_2)(\Omega^{\dagger}_{pn} + \Omega_{np})$$
$$+ A_3(\Omega^{\dagger}_p \Omega_n + \Omega^{\dagger}_n \Omega_p - 2\Omega^{\dagger}_{pn}\Omega_{np}) + A_4 \hat{J}^2. \tag{9.1.3}$$

where the following new notations are introduced:

$$\hat{N}_{\tau} = \sum_m b^{\dagger}_{\tau m} b_{\tau m}, \quad \tau = p, n$$
$$\hat{N}_{pn} = \sum_m b^{\dagger}_{pm} b_{nm}, \quad \hat{N}_{np} = \hat{N}^{\dagger}_{pn}. \tag{9.1.4}$$

The Hamiltonian given by Eq. (9.1.3), has only one off-diagonal matrix element in the basis (9.1.1). That is $\langle \phi^{\beta}_{JM}|H|\tilde{\phi}^{(\gamma)}_{JM}\rangle$. However, our concrete calculations show that this affects the energies of β and $\tilde{\gamma}$ bands by an amount of few keV. Therefore, the excitation energies of the six bands are in a very good approximation, given by the diagonal element:

$$E^{(k)}_J = \langle \phi^{(k)}_{JM}|H|\phi^{(k)}_{JM}\rangle - \langle \phi^{(g)}_{00}|H|\phi^{(g)}_{00}\rangle, \quad k = g, \beta, \gamma, 1, \tilde{\gamma}, \tilde{1}. \tag{9.1.5}$$

It can be easily checked that the model Hamiltonian does not commute with the components of the F spin operator:

$$F_0 = \frac{1}{2}(\hat{N}_p - \hat{N}_n), \quad F_+ = \hat{N}_{pn}, \quad F_- = \hat{N}_{np}. \tag{9.1.6}$$

Hence, the eigenstates of H are F_0 mixed states. However, the expectation values of the F_0 operator on the projected model states are equal to zero. This is caused by the fact that the proton and neutron deformations are considered to be equal. In this case the states are of definite parity, with respect to the proton neutron permutation, which is consistent with the structure of the model Hamiltonian, this being invariant with respect to such a symmetry transformation. To conclude, by contrast to the IBA2

Hamiltonian, the GCSM Hamiltonian is not F spin invariant. Another difference to the IBA2, the most essential one, is that the GCSM Hamiltonian does not commute with the boson number operators. Due to this feature the coherent state approach proves to be the most adequate one to treat it.

Very useful information about the physics which can be touched by using the states $\phi_{JM}^{(1)}$ and $\tilde{\phi}_{JM}^{(1)}$ to describe the magnetic dipole mode, can be obtained from the asymptotic behavior of these states. Following the procedure in Chap. 6, one arrives at [RFC87]:

$$
\begin{aligned}
\phi_{JM}^{k} = N_J^{(k)} F^{(k)}(\beta_p, \beta_n, d; \theta) \theta G(\beta_p, \beta_n; \theta) \\
\times \left[\tilde{\beta}_p e^{-i\phi_{p,3}} + \tilde{\beta}_n e^{-i\phi_{n,3}}) D_{M1}^{J*}(\Omega_{int}) \right. \\
\left. + (\tilde{\beta}_p e^{i\phi_{p,3}} + \tilde{\beta}_n e^{i\phi_{n,3}})(-)^{J+1} D_{M,-1}^{J*}(\Omega_{int}) \right] \quad k = 1, \tilde{1}
\end{aligned}
$$

$$
G(\beta_p, \beta_n, d; \theta) = \frac{1}{\beta} e^{-[(d-\tilde{\beta}_p)^2 + (d-\tilde{\beta}_n)^2]} \frac{e^{-3d\beta\theta^2}}{2 - 3\theta^2},
$$

$$
F^{(1)}(\beta_p, \beta_n, d; \theta) = 1, \quad F^{(\tilde{1})}(\beta_p, \beta_n, d; \theta) = \frac{1}{\sqrt{10}} \left[(\tilde{\beta}_p - \tilde{\beta}_n)^2 + 12 \tilde{\beta}_p \tilde{\beta}_n \theta^2 - 7 \right],
$$

$$
\tilde{\beta}_\tau = k_\tau \beta_\tau, \quad \tau = p, n; \quad \beta = \frac{\tilde{\beta}_p + \tilde{\beta}_n}{\sqrt{2}}. \tag{9.1.7}
$$

A few comments on the asymptotic expressions are necessary. First, one notes that the expression for the states 1^+ and $\tilde{1}^+$ differ from each other by the factor $F^{(k)}$ which indicates that the state $\tilde{1}^+$ is higher in energy than 1^+, for large quadrupole deformation. Moreover, the function $\tilde{\phi}_{JM}^{(1)}$ is providing too small B(M1) values for the excitation of the mode from the ground state. This is the reason why from now on we consider $\phi_{JM}^{(1)}$ the privileged candidate for the low orbital collective M1 state. The angles $\phi_{\tau,3}$ with $\tau = p, n$ are related to the Eulerian angles associated to the proton and neutron systems Ω_τ through the transformation

$$
(\phi_{\tau,1}, \sigma\theta, \phi_{\tau,3}) \equiv \Omega_\tau^{-1} \Omega_{int}, \quad \sigma = \delta_{\tau,p} - \delta_{\tau,n}. \tag{9.1.8}
$$

This equation allows us to pass from the six Eulerian angles Ω_p, Ω_n to another six angles $\phi', \theta, \phi'', \Omega_{int}$ where Ω_{int} is associated to the intrinsic frame, while ϕ', ϕ'' are the two independent angles among $\phi_{\tau,1}, \phi_{\tau,3}$, which are nothing else but the first and the third angles of Ω_τ. If we set the azimuthal angles $\phi_{\tau,3}$ equal to zero and $\tilde{\beta}_p = \tilde{\beta}_n$ then, the resulting asymptotic function for 1^+ is just the wave function describing the scissors mode within the TRM. Due to this feature it becomes manifest that since the model function accounts for the motion of two more degrees of freedom, the GCSM is more flexible than the TRM in describing more complex situations.

9.1.1 The M1 and E2 Transitions

One weak point of the phenomenological models is that they use an expression for the transition operators which does not take care of the structure of the model Hamiltonian. Thus, the transition probabilities are influenced by the chosen Hamiltonian only by means of the wave functions. Here we attempt to relate the two operators, the transition operator and the Hamiltonian, by quantizing the classical counterpart of the dipole and quadrupole transition operators [RUD87, RD89].

$$T_{1M} = \frac{1}{c} \int j_1(qr) \mathbf{Y}_{l1}^{1M} \mathbf{J}_p d\mathbf{r},$$

$$Q_{2\mu} = \frac{5\sqrt{6}}{cq^2} \int \mathbf{J}_p . \mathbf{A}_{2\mu} d\mathbf{r}. \tag{9.1.9}$$

where q denotes the length of the wave vector of the e.m. field. The convection current of protons is denoted by $\mathbf{J}_p$, and can be expressed in terms of nuclear matter density ρ and velocity $\mathbf{v}$ by:

$$\mathbf{J}_p = \rho_p(r)\mathbf{v}. \tag{9.1.10}$$

The vector potential of the e.m. field is denoted by $\mathbf{A}_{2}\mu$, while $\mathbf{Y}_{l1}^{1M}$ stands for the vectorial spherical function. This expression reflects the interaction of the charged particles with the transversal electromagnetic field generated by the colliding electron. Also, the plane wave Born approximation has been adopted. The integrals involved are to be performed on the volume bordered by the nuclear surface:

$$R = R_0 \left[1 + \sum_\mu \alpha_{2\mu}^* Y_{2\mu} \right]. \tag{9.1.11}$$

The results are series of quadrupole coordinates, which after truncation at the second order for T_1 and third order for Q_2, look like:

$$T_{1M} = e \frac{\sqrt{10}}{2c} C_{\mu\mu_1 M}^{2\ 2\ 1} (\dot{\alpha}_{p\mu} \alpha_{p\mu_1} + \alpha_{p\mu} \dot{\alpha}_{p\mu}) j_1(q R_0) \mathcal{A}$$

$$\equiv e F_{1M}(\alpha, \dot{\alpha}) j_1(q R_0), \quad \mathcal{A} = \sqrt{\frac{3}{8\pi}} \frac{3Z R_0}{8\pi c\hbar k_p^2},$$

$$Q_{2\mu} = \frac{3Z e R_0^2}{4\pi qc} \left[\dot{\alpha}_{p\mu} - \sqrt{\frac{35}{8\pi}} (\dot{\alpha}_p \alpha_p)_{2\mu} + \frac{5}{2\pi} (\dot{\alpha}_p (\alpha_p \alpha_p)_2)_{2\mu} \right]. \tag{9.1.12}$$

Here the symbol "•" stands for the time derivative, R_0 for the nuclear radius, taken equal to $1.2 A^{1/3}$, and j_1 is the Bessel function of rank 1. These expressions are further quantized by replacing the coordinates by the corresponding bosons and the time derivatives by:

$$\dot{\alpha}_{p\mu} = \frac{1}{i\hbar} \left[H, \alpha_{pk} \right]. \tag{9.1.13}$$

The boson expression for the dipole operator $\hat{T}$ is:

$$\hat{T}_{1k}(q) = e\mathcal{F}_{1,k}\, j_1(q\, R_0) \equiv e\hat{F}_{1k}^{mg}, \tag{9.1.14}$$

where we denoted by "e" the electron charge and by $\mathcal{F}_{1,k}$, the following expression:

$$
\begin{aligned}
\mathcal{F}_{1,k} = -\mathcal{A}\frac{i}{\hbar ck_p^2}\Bigg[& (A_1 + 6A_4)\hat{J}_{pk} + \frac{A_3}{5}\hat{J}_{nk} \\
& + \frac{\sqrt{10}}{4}(A_2 - A_1)\left((b_n^\dagger b_p^\dagger)_{1k} + (b_n^\dagger b_p)_{1k} + (b_p^\dagger b_n)_{1k} - (b_n b_p)_{1k} \right) \\
& + \sqrt{2}A_3\Bigg[-\frac{1}{\sqrt{10}}(\Omega_n^\dagger \hat{J}_{pk} + \hat{J}_{pk}\Omega_n) - \Omega_{pn}^\dagger (-(b_p^\dagger b_n)_{1k} + (b_n b_p)_{1k}) \\
& + ((b_n^\dagger b_p^\dagger)_{1k} + (b_n^\dagger b_p)_{1k})\Omega_{np} \Bigg]\Bigg].
\end{aligned}\tag{9.1.15}
$$

In the above equation, the angular momenta for protons and neutrons are denoted by:

$$\hat{J}_{\tau k} = \sqrt{10}(b_\tau^\dagger b_\tau)_{1k}, \ \ \tau = p, n, \ \ k = 0, \pm 1. \tag{9.1.16}$$

The dipole magnetic form-factor is defined as:

$$F_{mg}^{(1)}(q) = |\langle 0_g^+ || \hat{F}_1^{mg} ||1^+\rangle|^2, \tag{9.1.17}$$

while the B(M1) value for the transition $0_g^+ \to 1^+$, has the expression:

$$B(M1; 0_g^+ \to 1^+) = 2\left(\frac{M_p c}{\hbar}\right)^2 R_0^2 \mu_N^2 |\langle 0_g^+ || \mathcal{F}_1 ||1^+\rangle|^2. \tag{9.1.18}$$

It can be checked that the B(M1) value is related with the dipole form-factor considered in the photon point value of the transferred momentum, $q_f = E_{1+}/\hbar c$, by a very simple equation:

$$F_{mg}^{(1)}(q_f) = \frac{2}{9}q_f^2 B(M1; 0_g^+ \to 1^+). \tag{9.1.19}$$

It is to be noticed that, although the magnetization effect coming from the intrinsic magnetic moments is neglected, the equations of motion of the charged particles coordinates determine a contribution due to the neutron system. If one identifies the gyromagnetic factor for the τ system, as the coefficient of the corresponding angular momentum, one obtains:

$$\begin{pmatrix} g_p \\ g_n \end{pmatrix} = \frac{3ZR_0^2}{8\pi k_p^2} \frac{Mc^2}{(\hbar c)^2} \begin{pmatrix} A_1 + 6A_4 \\ \frac{1}{5}A_3 \end{pmatrix}. \tag{9.1.20}$$

Then their ratio acquires a very simple expression:

$$\frac{g_p}{g_n} = \frac{5(A_1 + 6A_4)}{A_3}. \tag{9.1.21}$$

This is, indeed, an important result of the GCSM. Numerical calculations predict for this ratio values close to 5 which is similar to the modulus of the ad-hoc value used by IBA2. In the present model, the gyromagnetic values of proton and neutron systems are determined exclusively by the proton-neutron interaction terms and do not account for the magnetic moments of constituents. We note that the M1 transition operator comprises not only a linear combination of the proton and neutron systems angular momenta but also proton-neutron interaction terms. Calculations indicate that the contribution of the latter terms to the M1 transition probability is negligible. Due to this reason, we considered only the terms which are linear in angular momenta.

Another specific feature for GCSM refers to the collective gyromagnetic factor g_c defined as:

$$g_p \hat{J}_{p,\mu} + g_n \hat{J}_{n,\mu} = g_c \hat{J}_\mu \tag{9.1.22}$$

where $\hat{J}_\mu$ denotes the total angular momentum components:

$$\hat{J}_\mu = \hat{J}_{p,\mu} + \hat{J}_{n,\mu} \tag{9.1.23}$$

Since the projected ground band states are symmetric with respect to the proton-neutron permutation, it results immediately that:

$$g_c = \frac{1}{2}(g_p + g_n). \tag{9.1.24}$$

Using the quantization procedure mentioned before, in connection with the electric quadrupole moment from Eq. (9.1.12), one obtains:

$$\hat{Q}_{2\mu} = \frac{1}{i\hbar cq} \Bigg\{ Q_s \Big[b_{p\mu}^\dagger + b_{n\mu}^\dagger - (-)^\mu b_{p,-\mu} - (-)^\mu b_{p,-\mu} \Big]$$

$$+ Q_{as} \Big[-b_{n\mu}^\dagger + b_{p\mu}^\dagger + (-)^\mu b_{n,-\mu} - (-)^\mu b_{p,-\mu}$$

$$+ \mathcal{C}((b_n^\dagger b_p)_{2\mu} - (b_p^\dagger b_n)_{2\mu})$$

$$+ \frac{15}{2\pi k_p^2}((b_p^\dagger b_p^\dagger b_p^\dagger)_{2\mu} - (b_p b_p b_p)_{2\mu}) \Big] \Bigg\}, \text{ where}$$

$$Q_s = (A_1 + A_2 + 12A_4)\mathcal{B}, \quad Q_{as} = (3A_1 - A_2 + 12A_4)\mathcal{B},$$

$$\mathcal{C} = \frac{1}{2k_p}\sqrt{\frac{35}{\pi}} \frac{A_2 - A_1}{3A_1 - A_2 + 12A_4}, \quad \mathcal{B} = \frac{3ZeR_0^2}{16\pi\sqrt{2}k_p}. \tag{9.1.25}$$

9.1.2 Numerical Results

Here we present few numerical applications of the GCSM. Energies of the states in the six bands are obtained, as we mentioned already before, as expectation values of the model Hamiltonian on the projected states. They are functions of the structure coefficients A_i, with $i = 1, 2, 3, 4$, and the deformation parameter $\rho = d\sqrt{2}$. These are fixed as follows. For a given value of ρ the parameters A_i are determined by fitting the excitation energies of the states $2_g^\dagger$, $10_g^\dagger$, $2_\gamma^\dagger$, $0_\beta^\dagger$. Since the excitation energies in the beta band are most sensitive to changing ρ, we fixed ρ so that an overall agreement for the beta band is obtained. In fitting the energy of $2_\gamma^\dagger$, we assigned to the gamma band the proton-neutron asymmetric projected state. The agreement between the calculated energies and the experimental values for ground, beta, gamma bands as well as for the M1 state $1^\dagger$ is very good. In order to save space we don't give here the results for energies.

Once the deformation parameter is fixed, the M1 transition operator is determined provided we know the parameter k_p relating the quadrupole coordinate with the boson operator. This parameter can be fixed in the following manner. In the asymptotic region of deformation, the energies of the ground band are given by:

$$E_J^g = \left[\frac{A_1 + A_2}{6\rho^2} + A_4\right] J(J+1). \tag{9.1.26}$$

On the other hand, for large deformation, the liquid drop model provides for ground band energies the expression:

$$E_J^{rot} = \hbar^2 \frac{J(J+1)}{6B\beta_0^2}, \quad B = \frac{3}{8\pi}MAR_0^2. \tag{9.1.27}$$

Identifying the two energies, one finds:

$$\beta_0^2 = \frac{\pi}{3.24}\frac{\hbar^2}{M}A^{-5/3}\left[\frac{A_1 + A_2}{6\rho^2} + A_4\right]^{-1}. \tag{9.1.28}$$

On the other hand, the common value of the proton and neutron systems deformation may be defined as the expectation value of the second order invariant in α coordinates, on the unprojected ground state:

$$\bar{\beta}_0^2 = \langle\psi_g| \sum_\mu \alpha_{p\mu}^* \alpha_{p\mu} |\psi_g\rangle. \tag{9.1.29}$$

Table 9.1 The theoretical values for B(M1;$0_g^\dagger \to 1^\dagger$) ($\mu_N^2$) (second column) are compared with the experimental data (first column) taken from Refs. [BO86, BKR84, BBD84, BBD84] (here the summed M1 is considered), [PA86, RICH85]

	B(M1;$0_g^\dagger \to 1^\dagger$)($\mu_N^2$)		
	Exp.	Th.	$k_p^2 = \frac{\rho^2}{\beta_0^2}$
^{154}Gd	0.9 ± 0.2[a]	1.102	16.252
^{156}Gd	1.3 ± 0.2[b]	2.101	14.339
	1.5 ± 0.2[c]		
^{158}Gd	2.3 ± 0.5[b]	2.314	17.369
	1.4 ± 0.3[d]		
^{160}Gd	2.3 ± 0.67[d]	2.101	19.218
^{154}Sm	0.8 ± 0.2[b]	2.581	13.874
^{164}Dy	3.65[e]		
	2.9 ± 0.5[e]	2.045	19.666
	1.5 ± 0.3[b]		
^{168}Er	0.9 ± 0.2[b]	1.802	23.887
^{174}Yb	0.8 ± 0.2[b]	2.605	24.815
^{232}Th	1.3 ± 0.2[a]	2.338	19.6
^{238}U	1.5[f]	4.501	17.842
	2.7 ± 0.6[a]		

In the third column the scaling factor k_p, calculated with Eq. (9.1.31), is given
[a] [BO86]
[b] [BKR84]
[c] [BBD84]
[d] [BBD84]
[e] [PA86]
[f] [RICH85]

Ignoring the spurious contribution due to the zero point motion one obtains:

$$k_p \bar{\beta}_0 = \rho. \qquad (9.1.30)$$

Equating the two β deformations obtained so far, one arrives at a simple expression for k_p:

$$k_p = \frac{\rho}{\beta_0}. \qquad (9.1.31)$$

By this, the M1 transition operator is completely determined, which results in having a free parameter description for the M1 properties. In Table 9.1 we compare the predictions of the GCSM for the B(M1) values, with the corresponding data, in several nuclei. Using Eq. (9.1.17) and the same scale factor k_p as in Table 9.1, we plotted the M1 form-factor as a function of the effective momentum transfer

$$q_{eff} = q + \frac{3Z\alpha}{R_0} \sin \frac{1}{2}\phi, \tag{9.1.32}$$

and compared it with the existent data for ^{156}Gd, ^{232}Th and ^{238}U, which are determined by the normalized differential cross section for the (e, e′) process, through the equation:

$$|F_{mg}^{(1)}|_{exp}^2 = \frac{Z^2}{4\pi}(\frac{1}{2} + tg^2\frac{1}{2}\phi)^{-1}\left(\frac{d\sigma}{d\Omega}\right)\bigg/\left(\frac{d\sigma}{d\Omega}\right)_{Mott}. \tag{9.1.33}$$

The effective transfer momentum takes care of the screening effect due to the electron cloud of the target. The correction added to the actual momentum q depends on the nuclear charge Z and nuclear radius. α stands for the fine structure constant, while ϕ is the scattering angle in the (e, e′) process. The curves are determined by the Bessel function $j_1(qR_0)$ squared and have the following common features. They have a maximum at about $q_{eff} = 0.5(\text{fm}^{-1})$. They have however different heights and widths. Although the form-factor is evaluated in the plane wave Born approximation, the agreement with the experimental data is good for ^{156}Gd and ^{238}U and satisfactory for ^{232}Th in the region of $q_{eff} \geq 0.5$. However, large deviations are noticed for smaller transferred momenta which reclaims that a distorted plane wave approximation is necessary, in this interval (Fig. 9.1).

Let us now focus our attention on the B(E2) values. They were calculated by means of the transition operator defined by Eq. (9.1.25). Although the factor Q_s and Q_{as} have explicit expressions in terms of the structure coefficients entering the model Hamiltonian, they were considered as fitting parameters. Thus, they were fixed by fitting the experimental B(E2) values for the transitions $2_g^\dagger \rightarrow 0_g^\dagger$ and $4_\beta^\dagger \rightarrow 2_g^\dagger$, respectively. Here we present the results obtained for ^{154}Gd, for which the fitting procedure yields:
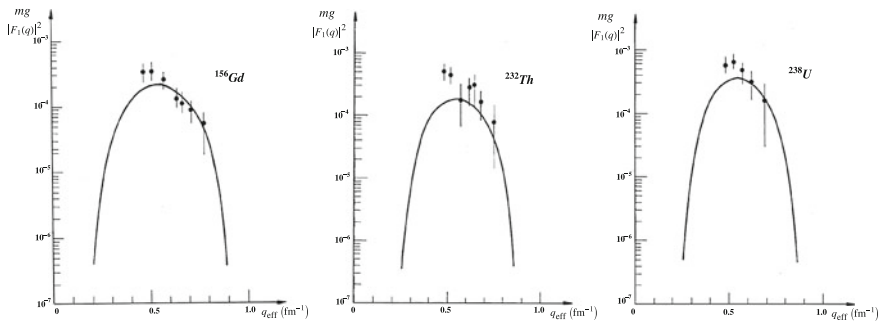

Fig. 9.1 The M1 form-factor for the (e, e′) scattering in ^{156}Gd, ^{232}Th and ^{238}U is calculated within the plane wave Born approximation and plotted as function of the effective transferred momentum. Calculating the form-factor we considered only the matrix element $\langle 0_g||\hat{J}_p||1^+\rangle$. The experimental data are taken from Ref. [Rich87]. The parameters ρ and A_i are those obtained by fitting the energies

$$Q_s = 40.219e.fm^2\,\text{MeV}, \quad Q_{as} = 22.82e.fm^2\,\text{MeV} \tag{9.1.34}$$

With the transition operator $Q_{2\mu}$ determined in this manner, we calculated some in-band transitions for ground and beta bands and the branching ratios for the lowest states in ground, beta and gamma bands. The theoretical results are compared with the corresponding data as well as with the predictions of the IBA2 model, in Table 9.2.

Inspecting Tables 9.1 and 9.2, one may conclude that the GCSM is able to describe realistically both the electric and magnetic properties of nuclei. It is also noteworthy that the GCSM, in contrast to other phenomenological models, is free of any fitting parameters when one calculates the energy and excitation probability of the scissors mode. Indeed, the parameters A_i are all fixed by fitting some selected energies in the ground, beta and gamma bands, while the deformation parameter ρ is chosen so that an overall agreement in beta band, which is the most sensitive band of ρ, is obtained. A detailed comparison of the GCSM with the TRM, IBA2, and proton-neutron deformation (NPD) model can be found in Ref. [IRD93].

9.2 Deformation Properties of the M1 Mode

A decisive light was shed on the question whether the scissors mode is a collective phenomenon or not, when Richter and his collaborators [RRW91] showed that the summed M1 strength for even isotopes of Sm depends quadratically on the quadrupole nuclear deformation. Later on it was found out that this holds also for Nd isotopic chain. This finding suggests moreover that there must be a linear interdependence of the B(M1) and B(E2) values [CBH87], i.e. the ratio of the two quantities is a constant in an isotopic chain. Since then, many theoretical works have been devoted to this issue trying to get a deeper insight for the scissors mode [GMU91, HM91, ZZ91].

Here we give the basic arguments showing that the GCSM is able to account also for the deformation properties of the mode [IRD93]. Indeed, let us consider the analytical expressions for B(M1) as well as for B(E2) value.

$$B(M1; 0^\dagger \to 1^\dagger) = \frac{9}{40\pi}(g_p - g_n)^2 \rho^4 \left[1 + \frac{1}{10}\left(\frac{N_0^{(g)}}{N_2^{(g)}}\right)^2\right]^2 \left(\frac{N_1^{(1)}}{N_0^{(g)}}\right)^2 \mu_N^2,$$

$$B(E2; 0^\dagger \to 2^\dagger) = \left(\frac{3}{4\pi}\right)^2 e^2 Z^2 R_0^4 \beta(\rho)^2, \quad \text{where}$$

$$\beta(\rho) \equiv \langle \phi_0^{(g)} || \alpha_p || \phi_2^{(g)} \rangle = \frac{\sqrt{5}}{2}\frac{\rho}{k_p}\left(\frac{N_2^{(g)}}{N_0^{(g)}} + \frac{1}{5}\frac{N_0^{(g)}}{N_2^{(g)}}\right) \equiv \frac{F(\rho)}{k_p}. \tag{9.2.1}$$

The quantities $N_J^{(g)}$ and $N_J^{(1)}$ were previously defined, they are the normalization factors for the projected state J from the ground and dipole bands, respectively. They are functions of the overlap integral $I_J^{(0)}(\rho^2)$, defined by Eq. (6.1.18), and its derivatives. To evaluate the expressions of the M1 and E2 transition reduced

Table 9.2 Theoretical B(E2) values and branching ratios (second column) are compared with the corresponding experimental data (column 1) and the IBA2 predictions (third column), for ^{154}Gd

$I_k - I_{k'}$	$B(E2; I_k \to I_{k'})(10^2 e^2 fm^4)$			$I_k - I_{k'}$	$B(E2; I_k \to I_{k'})(10^2 e^2 fm^4)$		
$2_g - 0_g$	77.3	77.3	77.3	$4_\beta - 2_g$	0.35	0.3	0.3
$4_g - 2_g$	117.8	117.7	108.8	$4_\beta - 4_g$	3.8	0.42	1.62
$6_g - 4_g$	138.2	141.5	116.4	$4_\beta - 6_g$	12	3.19	0.2
$8_g - 6_g$	152.6	163.3	116.4	$6_\beta - 4_g$	0.27	0.33	0.5
$10_g - 8_g$	173.1	185.4	112.1	$2_\beta - 0_\beta$	49[a]	110.9	55.3
					82[b]		
$0_\beta - 2_g$	25.8	1.7	2.6	$4_\beta - 2_\beta$	122	168.4	78.9
$2_\beta - 2_g$	4.0	0.4	0.6	$6_\beta - 4_\beta$	111	201.6	85.4
$2_\beta - 4_g$	11.9	1.47	1.65				

$\dfrac{I_k-I_{k'}}{I_{1m}-I'_{1m'}}$	$\dfrac{B(E2;I_k \to I'_{k'})}{B(E2;I_{1m} \to I'_{1m'})}$			$\dfrac{I_k-I_{k'}}{I_{1m}-I'_{1m'}}$	$\dfrac{B(E2;I_k \to I'_{k'})}{B(E2;I_{1m} \to I'_{1m'})}$		
$\frac{4_g-2_g}{2_g-0_g}$	1.52	1.52	1.41	$\frac{4_\gamma-2_g}{4_\gamma-4_g}$	0.148	0.267	0.29
$\frac{6_g-4_g}{4_g-2_g}$	1.17	1.20	1.07	$\frac{4_\gamma-6_g}{4_\gamma-4_g}$	0.27	0.176	0.36
$\frac{8_g-6_g}{6_g-4_g}$	1.1	1,154	1.0	$\frac{5_\gamma-4_g}{5_\gamma-6_g}$	0.744	1.079	1.0
$\frac{10_g-8_g}{8_g-6_g}$	1.13	1.135	0.96	$\frac{6_\gamma-4_g}{6_\gamma-6_g}$	0.081	0.117	0.2
$\frac{2_\beta-0_g}{2_\beta-2_g}$	0.123	0.572	0.52	$\frac{2_\gamma-2_\beta}{2_\gamma-0_\beta}$	2.5[c],15.87[d]	4.529	3.6
$\frac{2_\beta-4_g}{2_\beta-2_g}$	2.76	3.664	2.85	$\frac{2_\gamma-0_\beta}{2_\gamma-0_g}$	0.14[d], 0.4[c]	2.214	8.1
$\frac{4_\beta-2_g}{4_\beta-4_g}$	0.086	0.722	0.17	$\frac{2_\gamma-2_\beta}{2_\gamma-2_g}$	1.00	2.801	18.5
$\frac{4_\beta-6_g}{4_\beta-4_g}$	2.63	7.668	3.12	$\frac{2_\beta-0_g}{2_\beta-0_\beta}$	0.008	0.0021	0.005
$\frac{6_\beta-4_g}{6_\beta-6_g}$	0.08	0.66	0.35	$\frac{4_\beta-2_g}{4_\beta-2_\beta}$	0.0025	0.0018	0.003
$\frac{2_\gamma-0_g}{2_\gamma-2_g}$	0.468	0.618	0.64	$\frac{6_\beta-4_g}{6_\beta-4_\beta}$	0.0024	0.0017	0.002
$\frac{2_\gamma-4_g}{2_\gamma-2_g}$	0.144	0.075	0.143	$\frac{8_\beta-6_g}{8_\beta-6_\beta}$	0.006	0.0016	0.001
$\frac{3_\gamma-2_g}{3_\gamma-4_g}$	1.006	1.810	1.0	$\frac{10_\beta-8_g}{10_\beta-8_\beta}$	0.010	0.017	0.0

The GCSM predictions are due to Eq. (9.1.25) with Q_s and Q_{as} fixed as explained in the text. Experimental data are from Refs.
[a] [DI83, GHK83]
[b] [RNW71]
[c] [VBT69]
[d] [ZFL71]

probabilities for large deformation, we need the asymptotic expression of the norms ratios involved in Eq. (9.2.1). These can be derived with the help of the asymptotic expressions given in Chap. 6.

$$\frac{N_0^{(g)}}{N_2^{(g)}} \approx \sqrt{5}\left(1 - \frac{1}{2\rho^2}\right),$$

$$\left(\frac{N_1^{(1)}}{N_0^{(g)}}\right)^2 \approx \frac{20}{9\rho^2}\left(1 - \frac{2}{\rho^2}\right). \tag{9.2.2}$$

Using these results in connection to Eq. (9.2.1), one finds:

$$\beta(\rho) \approx \frac{\rho}{k_p}. \tag{9.2.3}$$

Keeping only the leading term, the reduced transition probabilities are then readily obtained:

$$B_{rot}(M1; 0^\dagger \to 1^\dagger) = \frac{9}{8\pi}(g_p - g_n)^2\rho^2\mu_N^2,$$

$$B_{rot}(E2; 0^\dagger \to 2^\dagger) = \left(\frac{3}{4\pi}\right)^2 e^2 Z^2 R_0^4 \frac{\rho^2}{k_p^2}. \tag{9.2.4}$$

From these equations it results that both transition probabilities depend quadratically on ρ which results in having a proportionality relationship between them:

$$B_{rot}(M1; 0^\dagger \to 1^\dagger) = 2\pi \frac{k_p^2}{Z^2 R_0^4} \frac{(g_p - g_n)^2}{e^2} B_{rot}(E2; 0^\dagger \to 2^\dagger)\mu_N^2. \tag{9.2.5}$$

In the near vibrational limit, i.e. ρ-small, the norms ratios and the reduced matrix element of alpha have, in the leading order the expressions:

$$\frac{N_0^{(g)}}{N_2^{(g)}} \approx \rho; \quad \left(\frac{N_1^{(1)}}{N_0^{(g)}}\right)^2 \approx 1 - \frac{7}{100}\rho^2,$$

$$\beta(\rho) \approx \frac{\sqrt{5}}{2k_p}(1 + \frac{1}{5}\rho^2). \tag{9.2.6}$$

Hence, in the regime of small deformation the M1 and E2 strengths are:

$$B_{vib}(M1; 0^\dagger \to 1^\dagger) \approx \frac{9}{40\pi}(g_p - g_n)^2\rho^4\mu_N^2,$$

$$B_{vib}(E2; 0^\dagger \to 2^\dagger) \approx \left(\frac{3}{4\pi}\right)^2 e^2 Z^2 R_0^4 \frac{5}{4k_p^2}\left(1 + \frac{1}{5}\rho^2\right)^2. \tag{9.2.7}$$

It is noteworthy that the two transitions strengths are not proportional to each other in the vibrational regime. Indeed, the M1 strength is vanishing in the limit $\rho \to 0$ while the E2 strength tends to a non-zero value which is caused by the zero point

shape fluctuations around the equilibrium configuration which are dominant when the nuclear shape approaches the spherical shape.

In order to obtain the explicit dependence of the M1 strength on deformation, we need to know how to relate the parameter ρ on the nuclear deformation β. The experimental value of β is defined by the equation:

$$B_{exp}(E2; 0^\dagger \rightarrow 2^\dagger) = \left(\frac{3}{4\pi}\right)^2 e^2 Z^2 R_0^4 \beta^2. \tag{9.2.8}$$

Comparing this relation with (9.2.1), one finds that

$$\beta(\rho) = \beta. \tag{9.2.9}$$

In virtue of (9.2.3), in the rotational regime we have:

$$\rho \approx k_p \beta. \tag{9.2.10}$$

In the vibrational limit, the function $\beta(\rho)$ consists of two terms

$$\beta(\rho) = \beta_0 + \beta, \tag{9.2.11}$$

one is ρ independent while the other one is depending quadratically on ρ. The experimental β will be identified with the latter term:

$$\beta_0 = \frac{\sqrt{5}}{2k_p}, \quad \beta = \beta(\rho) - \beta_0 \approx \frac{1}{2\sqrt{5}k_p}\rho^2. \tag{9.2.12}$$

Having the relations between the β and ρ deformations, one can express the M1 strength characterizing the two extreme regimes as function of β:

$$B_{rot}(M1) \uparrow \approx \frac{9}{8\pi}k_p^2 \beta^2 (g_p - g_n)^2 \mu_N^2,$$

$$B_{vib}(M1) \uparrow \approx \frac{9}{2\pi}k_p^2 \beta^2 (g_p - g_n)^2 \mu_N^2, \tag{9.2.13}$$

The M1 strength is therefore linear in β^2 in both rotational and vibrational limits. The slopes, however, are different in the two cases.

To conclude, one may say that the GCSM is able to account also for the deformation properties of the scissors mode. It is worth mentioning that the microscopic formalisms devoted to the interpretation of the scissors mode are using deformed single particle basis and inherently they are confronted to the elimination of spurious components of isoscalar nature. Since the GCSM uses states of definite angular momentum, such difficulties due to the spurious states contamination are not met.

Chapter 10
Two Applications of GCSM

10.1 Chiral Symmetry in Even-Even Nuclei

10.1.1 Introduction

The rotational spectra appear to be a reflection of a spontaneous rotational symmetry breaking when the nuclear system acquires a static nuclear deformation. The fundamental nuclear properties like nuclear shape, the nuclear mass and charge distribution inside the nucleus, electric and magnetic moments, collective spectra may be evidenced through the system interaction with an electromagnetic field. The two components of the field, electric and magnetic, are used to explore the properties of electric and magnetic nature, respectively. At the end of last century, the scissors like states [LOPA78, FPI84] as well as the spin-flip excitations [ZAW98] were widely treated by various groups. Some of them were based on phenomenological assumptions, while the other ones on microscopic considerations. The scissors like excitations are excited in (e, e′) experiments at backward angles and expected at an energy of about 2–3 MeV, while the spin-flip excitations are seen in (p, p′) experiments at forward angles and are located at about 5–10 MeV. The scissors mode describes the angular oscillation of proton against neutron system and the total strength is proportional to the nuclear deformation squared which reflects the collective character of the excitation. The subject has been reviewed by several authors [IUD95, ZAW98].

Since the total M1 strength of the $M1$ mode is proportional to the nuclear deformation squared, it was believed that the magnetic collective properties are in general associated with deformed systems. This is not true due to the magnetic dipole bands, where the ratio between the moment of inertia and the B(E2) value for exciting the first 2^+ from the ground state 0^+, $\mathcal{I}^{(2)}/B(E2)$, takes large values, of the order of $100\,(\mathrm{eb})^{-2}\mathrm{MeV}^{-1}$. These large values can be justified by a large transverse magnetic dipole moment (perpendicular to the total angular momentum) which induces dipole magnetic transitions, but almost no charge quadrupole moment [FRA01]. Indeed, there are several experimental data showing that the dipole bands have large values

for $B(M1) \sim 3-6\,\mu_N^2$ and very small values of $B(E2) \sim 0.1\,(\text{eb})^2$ (see for example Ref. [JEN99]). The states are different from the scissors mode, they being rather of a shears character. A system with a large transverse magnetic dipole moment which was studied in many publications, may consist of a triaxial core to which a proton prolate and a neutron oblate hole orbital are coupled. The interaction of particle and hole like orbitals is repulsive, which keeps the two orbits apart from each other. In this way the orthogonal angular momenta carried by the proton particles and neutron holes are favored. The maximal transverse dipole momentum is achieved, for example, when $\mathbf{j}_p$ is oriented along the small axis of the core, $\mathbf{j}_n$ along the long axis and the core rotates around the intermediate axis. Suppose the three orthogonal angular momenta form a right trihedral frame. If the Hamiltonian describing the interacting system of protons, neutrons and the triaxial core is invariant to the transformation which changes the orientation of one of the three angular momenta, i.e. the right trihedral frame is transformed to a left type, one says that the system exhibits a chiral symmetry. As always, such symmetry is identified when it is broken and consequently to the two trihedrals correspond distinct energies, otherwise close to each other. Thus, a signature for a chiral symmetry characterizing a triaxial system is the existence of two $\Delta I = 1$ bands which are close in energies. Increasing the total angular momentum the gradual alignment of $\mathbf{j}_p$ and $\mathbf{j}_n$ to the total $\mathbf{J}$ takes place and a magnetic band is developed.

The question which may arise is whether the picture of the three angular momenta system, carried by a phenomenological core, a prolate and an oblate single particle orbitals, with respect to which the chiral symmetry is defined, is unique for determining states connected with large M1 transitions. Note that the nuclear system which accommodates the chiral frame is odd-odd.

Here we attempt another chiral system consisting of one phenomenological core with two components, one for protons and one for neutrons, and two quasiparticles whose total angular momentum is oriented along the symmetry axis of the core due to the particle-core interaction. We investigate whether states of total angular momentum $\mathbf{I}$, where the three components mentioned above carry angular momenta, $\mathbf{J}_p, \mathbf{J}_n, \mathbf{J}_F$, which are mutually orthogonal, may exist. If such configuration exists, it is optimal for defining large transverse magnetic moment inducing large M1 transitions.

Since this scenario is based on the GCSM, a few useful features are worth recalling. The GCSM seems to be the only phenomenological model which treats simultaneously the M1 and E2 properties. Indeed, in Refs. [RUD87, RD89] the ground, beta and gamma bands are considered together with a $K^\pi = 1^+$ band built on the top of the scissor mode 1^+. By contrast to other phenomenological and microscopic models, which treat the scissors mode in the intrinsic reference frame, here one deals with states of good angular momentum and, therefore, there is no need to restore the rotational symmetry. As shown in Ref. [IRD93] the GCSM provides for the total M1 strength an expression which is proportional to the nuclear deformation squared (see Chap. 9). Consequently, the M1 strength of 1^+ and the B(E2) value for 2^+ are proportional to each other, although the first quantity is determined by the convection current while the second one by the static charge distribution. One weak

point of most phenomenological models is that they use expressions for transition operators which are not consistent with the structure of the model Hamiltonian. Thus, the transition probabilities are influenced by the chosen Hamiltonian only through the wave functions. By contradistinction, in Refs. [RUD87, RD89] the E2 transition operator, as well as the M1 form-factor, are derived analytically, by using the equation of motion of the collective coordinates determined by the model Hamiltonian. This way a consistent description of electric and magnetic properties of many nuclei was attained.

10.1.2 Proton and Neutron Bosons Angular Momenta

Note that Ψ_g, the wave function describing the ground state of the p-n system in the intrinsic frame of references, can be written in a factorized form:

$$\Psi_g \equiv \Psi_p \Psi_n, \tag{10.1.1}$$

where the factor functions are:

$$\Psi_p = exp[d_p b_{p0}^\dagger - d_p b_{p0}]|0\rangle_p, \quad \Psi_n = exp[d_n b_{n0}^\dagger - d_n b_{n0}]|0\rangle_n. \tag{10.1.2}$$

The τ functions, with $\tau = p, n$, are eigenstates of the z projection of the angular momentum and therefore can be expanded in the basis $|J_\tau 0\rangle$ defined by the eigenstates of $\mathbf{J}_\tau^2, J_{\tau 0}$:

$$\Psi_\tau = \sum_{J_\tau} C_{J_\tau} |J_\tau 0\rangle, \tau = p, n. \tag{10.1.3}$$

Denoting by

$$\varphi_{J_\tau M_\tau}^{(g)} = N_{J_\tau}^{(g)} P_{M_\tau 0}^{J_\tau} \Psi_\tau, \tag{10.1.4}$$

the angular momentum projected state associated to Ψ_τ and then inserting the expression (10.1.3) in the right hand side of (10.1.4), one finds that the expansion coefficients C_{J_τ} are related with the projected state norms, by:

$$C_{J_\tau} = \left(N_{J_\tau}^{(g)} \right)^{-1}. \tag{10.1.5}$$

Here $N_{J_p}^{(g)}$ and $N_{J_n}^{(g)}$ denote the norms of the angular momentum projected states associated to Ψ_p and Ψ_n, respectively. These have been analytically expressed in Ref. [CR74].

The above analysis can be easily extended to the intrinsic ground state describing the composite proton-neutron system:

$$\Psi_g = \Psi_p\Psi_n = \sum_{J_p,J_n=even} C_{J_p}|J_p0\rangle C_{J_n}|J_n0\rangle = \sum_{J_p,J_n,J} C_{J_p}C_{J_n}C_0^{J_p\ J_n\ J}{}_0\ {}_0|J,0\rangle.$$

$$(10.1.6)$$

The angular momentum projected state is defined by:

$$\phi_{JM}^{(g)} = N_J^{(g)}P_{M0}^J\Psi_g = N_J^{(g)}\sum_{J_pJ_n} C_{J_p}C_{J_n}C_0^{J_p\ J_n\ J}{}_0\ {}_0|J,M\rangle$$

$$= N_J^{(g)}\sum_{J_pJ_n}\left(N_{J_p}^{(g)}\right)^{-1}\left(N_{J_n}^{(g)}\right)^{-1}C_0^{J_p\ J_n\ J}{}_0\ {}_0\left[\varphi_{J_p}^{(g)}\varphi_{J_n}^{(g)}\right]_{JM},\quad(10.1.7)$$

with the norm:

$$\left(N_J^{(g)}\right)^{-2} = \sum_{J_p,J_n}\left(N_{J_p}^{(g)}\right)^{-2}\left(N_{J_n}^{(g)}\right)^{-2}\left(C_0^{J_p\ J_n\ J}{}_0\ {}_0\right)^2.\qquad(10.1.8)$$

In the above equations the standard notation for the Clebsch-Gordan coefficients has been used.

The average value of the angular momentum carried by the proton bosons is given by:

$$\langle\phi_{JM}^{(g)}|\hat{\mathbf{J}}_p^2|\phi_{JM}^{(g)}\rangle = \left(N_J^{(g)}\right)^2\sum_{J_p,J_n}\left(N_{J_p}^{(g)}\right)^{-2}\left(N_{J_n}^{(g)}\right)^{-2}J_p(J_p+1)\left(C_0^{J_p\ J_n\ J}{}_0\ {}_0\right)^2$$

$$\equiv \tilde{J}_{pJ}^{(g)}(\tilde{J}_{pJ}^{(g)}+1).\qquad(10.1.9)$$

Similarly, one calculates the average angular momentum carried by the neutron bosons, $\tilde{J}_{nJ}^{(g)}$. The two angular momenta, $\tilde{J}_{pJ}^{(g)}$, $\tilde{J}_{nJ}^{(g)}$, define the relative angle obeying the equation:

$$\cos(\mathbf{J}_p,\mathbf{J}_n)_J^{(g)} = \frac{J(J+1)-\tilde{J}_{pJ}^{(g)}(\tilde{J}_{pJ}^{(g)}+1)-\tilde{J}_{nJ}^{(g)}(\tilde{J}_{nJ}^{(g)}+1)}{2\sqrt{\tilde{J}_{pJ}^{(g)}(\tilde{J}_{pJ}^{(g)}+1)\tilde{J}_{nJ}^{(g)}(\tilde{J}_{nJ}^{(g)}+1)}}.\qquad(10.1.10)$$

Let us now consider the angular momentum projection of following dipole excitation of the intrinsic ground state

$$\phi_{JM}^{(1)} = N_J^{(1)}P_{M1}^J(b_n^\dagger b_p^\dagger)_{11}\Psi_g$$

$$= N_J^{(1)}\sum_{J'=even}\left(N_{J'}^{(g)}\right)^{-1}C_0^{J'\ 1\ J}{}_1\ {}_1\left[\left(b_n^\dagger b_p^\dagger\right)_1\varphi_{J'}^{(g)}\right]_{JM},\qquad(10.1.11)$$

with the norm having the expression:

$$\left(N_J^{(1)}\right)^{-2} = \sum_{J'=even} \left(N_{J'}^{(g)}\right)^{-2} \left(C_0^{J'\,1\,J}\right)^2.$$

(10.1.12)

It is worth calculating the separate contributions of proton and neutron bosons to building up the total angular momentum of a chosen magnetic dipole state. The effective angular momentum $\tilde{J}_{p,J}^{(1)}$ is defined as:

$$\tilde{J}_{p;J}^{(1)}(\tilde{J}_{p;J}^{(1)} + 1) = \langle \phi_{JM}^{(1)} | \hat{\mathbf{J}}_p^2 | \phi_{JM}^{(1)} \rangle$$

$$= 6 + \left(N_J^{(1)}\right)^2 \sum_{J_p, J_n, J'} \left(N_{J_p}^{(g)}\right)^{-2} \left(N_{J_n}^{(g)}\right)^{-2}$$

$$\times J_p(J_p + 1) \left(C_0^{J_p\,J_n\,J'}\right)^2 \left(C_0^{J'\,1\,J}\right)^2.$$

(10.1.13)

Since the ground state is symmetric with respect to the p-n permutation, one expects that the effective neutron angular momentum defined by averaging the operator $\hat{J}_{n;J}^2$ with the ground state projected function is equal to the effective proton angular momentum, i.e.

$$\tilde{J}_{n;J}^{(1)} = \tilde{J}_{p;J}^{(1)}.$$

(10.1.14)

Denoting the ground state angular momentum by

$$\mathbf{J}_{pn} = \mathbf{J}_p + \mathbf{J}_n,$$

(10.1.15)

then for the average value one obtains:

$$\tilde{J}_{pn;J}^{(1)}(\tilde{J}_{pn;J}^{(1)} + 1) \equiv \langle \phi_{JM}^{(1)} | \hat{\mathbf{J}}_{pn}^2 | \phi_{JM}^{(1)} \rangle$$

$$= \left(N_J^{(1)}\right)^2 \sum_{J''} \left(N_{J''}^{(g)}\right)^{-2} \left(C_0^{J''\,1\,J}\right)^2 \left(J''(J'' + 1) + 12\right).$$

(10.1.16)

Squaring Eq. (10.1.15) and averaging the result with the dipole projected state J, one can calculate the angle between the angular momenta $\mathbf{J}_p$ and $\mathbf{J}_n$:

$$\cos(\mathbf{J}_p, \mathbf{J}_n)_J^{(1)} = \frac{\tilde{J}_{pn;J}^{(1)}(\tilde{J}_{pn;J}^{(1)} + 1) - \tilde{J}_{p;J}^{(1)}(\tilde{J}_{p;J}^{(1)} + 1) - \tilde{J}_{n;J}^{(1)}(\tilde{J}_{n;J}^{(1)} + 1)}{2\sqrt{\tilde{J}_{p;J}^{(1)}(\tilde{J}_{p;J}^{(1)} + 1)\tilde{J}_{n;J}^{(1)}(\tilde{J}_{n;J}^{(1)} + 1)}}.$$

(10.1.17)

10.1.3 A Possible Extension of the GCSM

Here we shall consider a particle-core interacting system described by the Hamiltonian:

$$
H = H_{GCSM} + \sum_{\alpha} \epsilon_a c_{\alpha}^{\dagger} c_{\alpha} - \frac{G}{4} P^{\dagger} P
$$

$$
- \sum_{\tau=p,n} X_{pc}^{(\tau)} \sum_{m} q_{2m} \left(b_{\tau,-m}^{\dagger} + (-)^m b_{\tau m} \right) (-)^m - X_{sS} \mathbf{J}_F \cdot \mathbf{J}_c, \quad (10.1.18)
$$

with the notation for the particle quadrupole operator:

$$
q_{2m} = \sum_{a,b} Q_{a,b} \left(c_{j_a}^{\dagger} c_{j_b} \right)_{2m}, \quad Q_{a,b} = \frac{\hat{j_a}}{2} \langle j_a || r^2 Y_2 || j_b \rangle. \quad (10.1.19)
$$

Here H_{GCSM} denotes the phenomenological Hamiltonian described in previous chapter, associated to a proton and neutron bosonic core. The next two terms stand for a set of particles moving in a spherical shell model mean-field and interacting among themselves through pairing interaction. The low indices α denote the set of quantum numbers labeling the spherical single particle shell model states, i.e. $|\alpha\rangle = |nljm\rangle = |a, m\rangle$. The last two terms denoted hereafter as H_{pc} express the interaction between the satellite particles and the core through a quadrupole-quadrupole and a spin-spin force, respectively. The angular momenta carried by the core and particles are denoted by $\mathbf{J}_c (=\mathbf{J}_{pn})$ and $\mathbf{J}_F$, respectively. The mean field plus the pairing term is quasi-diagonalized by means of the Bogoliubov-Valatin transformation:

$$
a_{\alpha}^{\dagger} = U_a c_{\alpha}^{\dagger} - V_a s_{\alpha} c_{-\alpha}, \quad s_{\alpha} = (-)^{j_{\alpha} - m_{\alpha}},
$$

$$
a_{\alpha} = U_a c_{\alpha} - V_a s_{\alpha} c_{-\alpha}^{\dagger}, \quad (-\alpha) = (a, -m_{\alpha}). \quad (10.1.20)
$$

The free quasiparticle term is $\sum_{\alpha} E_a a_{\alpha}^{\dagger} a_{\alpha}$, while the qQ interaction preserves the above mentioned form, with the factor q_{2m} changed to:

$$
q_{2m} = \eta_{ab}^{(-)} \left(a_{j_a}^{\dagger} a_{j_b} \right)_{2m} + \xi_{ab}^{(+)} \left((a_{j_a}^{\dagger} a_{j_b}^{\dagger})_{2m} - (a_{j_a} a_{j_b})_{2m} \right), \quad \text{where}
$$

$$
\eta_{ab}^{(-)} = \frac{1}{2} Q_{ab} \left(U_a U_b - V_a V_b \right), \quad \xi_{ab}^{(+)} = \frac{1}{2} Q_{ab} \left(U_a V_b + V_a U_b \right). \quad (10.1.21)
$$

We restrict the single particle space to a single-j state where two particles are placed. In the space of the particle-core states we, therefore, consider the basis defined by:

$$|BCS\rangle \otimes \phi_{JM}^{(1)},$$

$$\Psi_{JI;M}^{(2qp;J1)} = N_{JI}^{(2qp;J1)} \sum_{J'} C_{J\,1\,J+1}^{J\,J'\,I} \left(N_{J'}^{(1)}\right)^{-1} \left[(a_j^\dagger a_j^\dagger)_J |BCS\rangle \otimes \phi_{J'}^{(1)}\right]_{IM},$$

(10.1.22)

where $|BCS\rangle$ denotes the quasiparticle vacuum, while $N_{JI}^{(2qp;J1)}$ is the norm given by

$$\left(N_{JI}^{(2qp;J1)}\right)^{-2} = \sum_{J'} 2 \left(N_{J'}^{(1)}\right)^{-2} \left(C_{J\,1\,J+1}^{J\,J'\,I}\right)^2.$$

(10.1.23)

Now, let us analyze the proton and neutron angular momentum composition for the two quasiparticle components of the particle-core basis. The effective angular momenta can be easily calculated:

$$\widetilde{J}_{\tau;JI}^{(1)}(\widetilde{J}_{\tau;JI}^{(1)} + 1) = \langle \Psi_{JI}^{(2qp;J1)} | \hat{J}_\tau^2 | \Psi_{JI}^{(2qp;J1)} \rangle$$

$$= \left(N_{JI}^{(2qp;J1)}\right)^2 \sum_{J'} 2 \left(C_{J\,1\,J+1}^{J\,J'\,I}\right)^2 \left(N_{J'}^{(1)}\right)^{-2} \widetilde{J}_{\tau;J'}^{(1)}(\widetilde{J}_{\tau;J'}^{(1)} + 1), \quad \tau = p, n,$$

$$\widetilde{J}_{pn;JI}^{(1)}(\widetilde{J}_{pn;JI}^{(1)} + 1) = \langle \Psi_{JI}^{(2qp;J1)} | (\hat{J}_p + \hat{J}_n)^2 | \Psi_{JI}^{(2qp;J1)} \rangle$$

$$= \left(N_{JI}^{(2qp;J1)}\right)^2 \sum_{J'} 2 \left(C_{J\,1\,J+1}^{J\,J'\,I}\right)^2 \left(N_{J'}^{(1)}\right)^{-2} \widetilde{J}_{pn;J'}^{(1)}(\widetilde{J}_{pn;J'}^{(1)} + 1).$$

(10.1.24)

The angle between proton and neutron angular momenta can be obtained from the equation:

$$\cos(\mathbf{J}_p, \mathbf{J}_n)_{JI}^{(1)} = \frac{\widetilde{J}_{pn;JI}^{(1)}(\widetilde{J}_{pn;JI}^{(1)} + 1) - \widetilde{J}_{p;JI}^{(1)}(\widetilde{J}_{p;JI}^{(1)} + 1) - \widetilde{J}_{n;JI}^{(1)}(\widetilde{J}_{n;JI}^{(1)} + 1)}{2\sqrt{\widetilde{J}_{p;JI}^{(1)}(\widetilde{J}_{p;JI}^{(1)} + 1)\widetilde{J}_{n;JI}^{(1)}(\widetilde{J}_{n;JI}^{(1)} + 1)}}.$$

(10.1.25)

10.1.4 About the Chiral Symmetry

For the three bands considered above, ground, dipole and two quasiparticles-dipole core, the angular momentum composition is illustrated in Fig. 10.1. Therein, the notations $\langle J_\tau \rangle$ stay for $\widetilde{J}_{\tau J}^{(g)}$, $\widetilde{J}_{\tau;J}^{(1)}$ and $\widetilde{J}_{\tau;JI}^{(1)}$, respectively. Note that for ground band states, when the proton and the neutron deformations are equal and large, the two angular momenta are aligned to each other in states of high angular momentum.

Fig. 10.1 Proton and
neutron angular momentum
composition of the states
from the ground band (*upper
panel*), the pure
phenomenological dipole
band (*middle panel*) and the
two quasiparticle-dipole
band (*bottom panel*). The
curves with the symbols of
full circles and *triangle up*
respectively, in the *upper*
and *middle panels*,
correspond to $d_p = 0.2$ and
$d_n = 2.4$, respectively
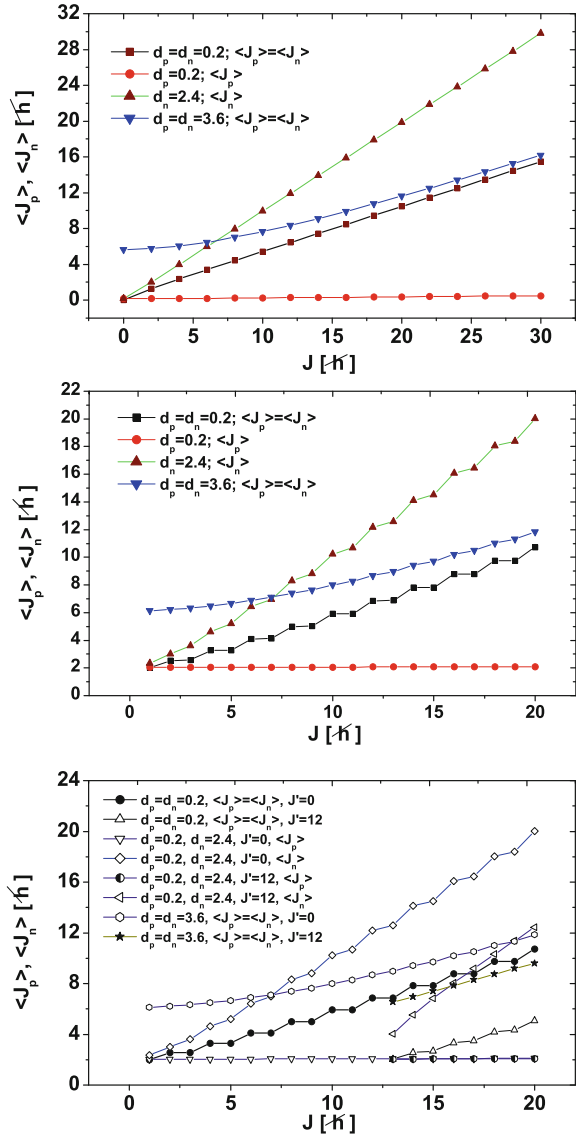
Indeed, as seen from the upper panel for large J we have $J \approx 2\langle J_p \rangle$. If the two
deformations are very different then, by far, the largest contribution is brought by
the most deformed system, the weakly deformed subsystem bringing an almost van-
ishing average angular momentum. As for the pure phenomenological dipole band,
represented in the middle panel of Fig. 10.1, we note an even-odd staggering for
small and moderate deformation. Such a structure is washed out for large deforma-
tion. These features are met also for the case of two quasiparticle-core dipole states

when the two quasiparticles total angular momentum is equal to zero. Due to the large K quantum number of the two quasiparticle components, when the angular momentum carried by the two quasiparticles is equal to 12, the dipole band starts with the angular momentum 13.

The two quasiparticle-core dipole state components of the particle-core basis involve three angular momenta, $\mathbf{J}_p$, $\mathbf{J}_n$, and the quasiparticles total angular momentum denoted by $\mathbf{J}_F$, which, in certain states, could be mutually orthogonal. Under this circumstance, suppose that the vectors set $\mathbf{J}_p$, $\mathbf{J}_n$, $\mathbf{J}_F$ form a right trihedral.

The transformation which changes the orientation of one component of the set, i.e. the right trihedral goes to a left one, is conventionally called chiral. Obviously, any such a transformation may be written as a product of a rotation of angle π around the chosen trihedral axis and a space reversal transformation. Excepting the spin-spin term, the Hamiltonian introduced above is invariant to any chiral transformation. In fact, the chiral symmetry breaking mentioned above is generating the so called chiral bands characterized, first of all, by a large intra-band M1 transition probability. The goal of this section is to identify states $\Psi_{JI;M}^{(2qp;J1)}$ characterized by an orthogonal trihedral $(\mathbf{J}_p, \mathbf{J}_n, \mathbf{J}_F)$.

The angle between the angular momenta carried by protons and neutrons in a ground band projected state is represented as function of the angular momentum J for different sets of proton and neutron deformations, in Fig. 10.2. Irrespective of the deformations magnitude, for $J = 0$, the angular momenta $\mathbf{J}_p$ and $\mathbf{J}_n$ are anti-aligned. For $J = 2$ the angle jumps down to 90° and 98° when both deformations are small or one is small while the other one only moderately small, respectively. Increasing the angular momentum, the angle characterizing the system of small deformations is smoothly decreasing, approaching the aligned picture for very large angular momentum. By contrast, when the proton and neutron deformations are very different, the angle is smoothly but slowly decreasing keeping close to 90°. In the case of equal and large proton and neutron deformations, the angle is continuously decreasing, the rotation gradually aligning the two angular momenta, $\mathbf{J}_p$ and $\mathbf{J}_n$.

Fig. 10.2 The angle between $\mathbf{J}_p$ and $\mathbf{J}_n$ within the ground-band states $\phi_{JM}^{(g)}$ for three sets of deformations (d_p, d_n)
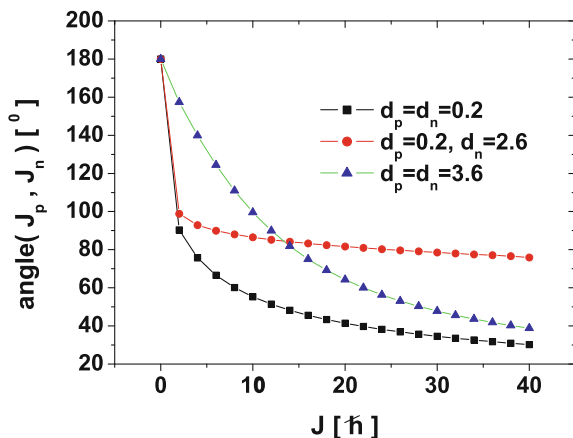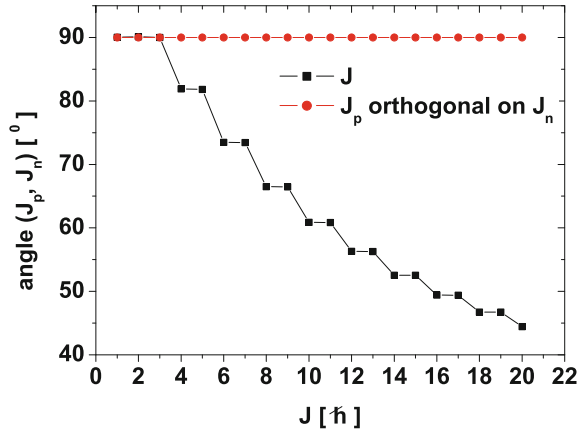
Fig. 10.3 The angle
between $\mathbf{J}_p$ and $\mathbf{J}_n$ within
the boson dipole state $\phi_{JM}^{(1)}$.
$d = 0.2$

The relative angle of the proton and neutron angular momenta in the pure boson
dipole state $\varphi_{JM}^{(1)}$ is presented in Fig. 10.3. One notices that the angle is 90° in the
first three dipole states of angular momenta 1, 2 and 3. Increasing the total spin,
the corresponding angles decrease monotonically. A step structure for the states J
and $J + 1$ with J-even shows up. We recall that in the previous applications of
the GCSM [RFC87], the unprojected state Ψ_g was considered for equal deformation
parameters for the proton and neutron systems. However, since the number of protons
and neutrons are different and, moreover, the two kinds of nucleons occupy different
shells, it is reasonable to suppose different deformation parameters for protons and
neutrons, respectively. The corresponding projected dipole states are denoted by
$\Phi_{JM}^{(1)}(d_p, d_n)$. For this situation, the dependence of the $(\mathbf{J}_p, \mathbf{J}_n)$ angle on the total
angular momentum is presented in Fig. 10.4.

When the deformation for protons is different from that of neutrons, the step
structure is washed out and the total angular momenta, where the relative angle is

Fig. 10.4 The angle
between $\mathbf{J}_p$ and $\mathbf{J}_n$ within
the boson dipole state
$\phi_{JM}^{(1)}(d_p, d_n)$. The
deformation parameters are
$d_p = 0.2$ and $d_n = 2.4$
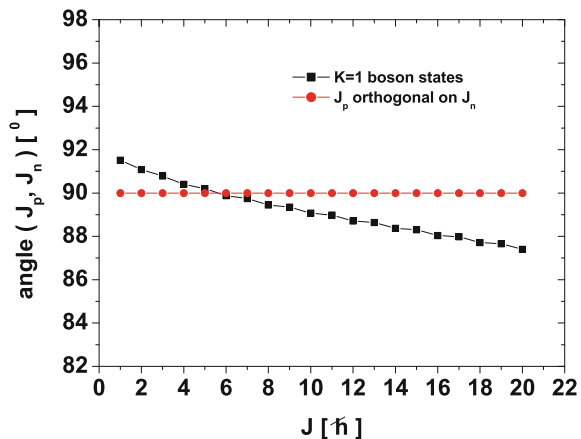
about 90°, are shifted to 5, 6 and 7. The angle decreases with angular momentum but with a much lower slope. Indeed, in the considered angular momentum interval the angle varies between 91.5° and 87°.

It is to be noticed that the angle of the proton and neutron angular momenta in the dipole states given in Figs. 10.3 and 10.4 is different from that characterizing the ground band states and shown in Fig. 10.2 for three sets of the proton and neutron deformation parameters, (d_p, d_n). Note that for the state 0^+, heading the ground band, the two angular momenta, $\mathbf{J}_p, \mathbf{J}_n$, are equal in magnitude, have the same direction but different orientation. This property holds irrespective of the deformation parameters d_p, d_n. From the value of 180°, the angle is decreasing when the total angular momentum is increased. When the proton and neutron deformations are equal, the angle tends to zero for J very large. The alignment is reached faster for small deformations than for large ones. If the deformations are different, namely one is small and the other moderately large, the angle is very slowly decreasing for $J \geq 2$, otherwise keeping close to 90°, reflecting the fact that for small deformation the rotational axis is almost indefinite. As for the dipole band, to build up the dipole state 1^+ one gets contribution not only from the ground band state 0^+, but also from the state 2^+ which results, for small deformations, an angle between proton and neutron angular momenta close to 90° (see Fig. 10.3). By contrast, when the deformation is large the above mentioned angle should be between 180° and 160° and, moreover, closer to one or another extreme depending on the rate of the mixture of the states 0_g^+ and 2_g^+ in the structure of the dipole state 1^+. According to this picture, the state 1^+ is not a typical scissors state, where the angle between the proton and neutron symmetry axes is very small, but rather a shears mode.

Let us see now how this picture modifies when we add to the boson dipole states the two quasiparticle state factor. As shown in Fig. 10.5, the case of common small deformation for protons and neutrons is similar to that in Fig. 10.3 where the two quasiparticle factor is missing. By contrast, here we have seven sets of states distinguished by the angular momentum J carried by the quasiparticle component. Otherwise, the

Fig. 10.5 The angle between $\mathbf{J}_p$ and $\mathbf{J}_n$ within the boson dipole state $\Psi_{JI;M}^{(2qp;J1)}(d)$. The deformation parameter d (see Eq. (10.1.22)) is equal to 0.2
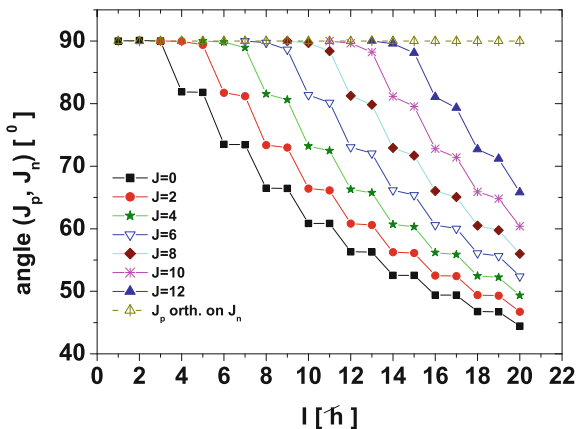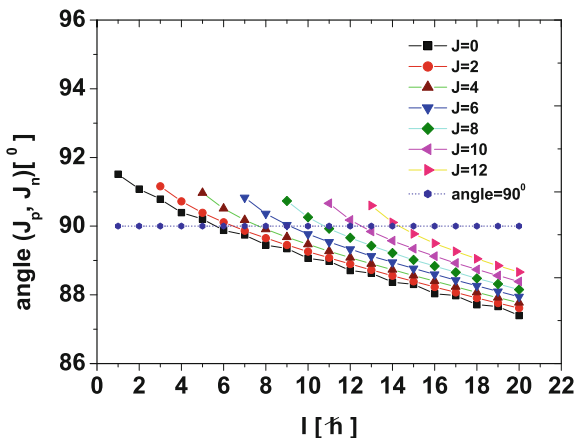
step function structure as well as the decreasing behavior as function of the total angular momentum, I, are preserved by any of the seven sets. The seven curves differ from each other by the angular moment I, where the protons and neutron angular momenta are orthogonal. Thus, for a given J (=0, 2, 4, ..., 12) the total angular momenta for which the proton-neutron angle is 90° are I = J + 1, J + 2, J + 3. The same remark holds also for Fig. 10.6, when compared with the situation in Fig. 10.4. Indeed, it seems that the larger the difference between proton and neutron deformations, the smaller the departure of the $(\mathbf{J}_p, \mathbf{J}_n)$ angle from 90° and the less pronounced the step structure of the angle I-dependence.

From Fig. 10.5 it is clear that for each value of the two quasiparticle angular momentum there are three states, the lowest angular momentum states being characterized by an orthogonal configuration $(\mathbf{J}_p, \mathbf{J}_n)$. Since the K quantum numbers for proton and neutron systems included in the core are small and, moreover, the total K being equal to unity, it is reasonable to suppose that $\mathbf{J}_p$ and $\mathbf{J}_n$ are both perpendicular to the intrinsic symmetry axis, that is OZ. The symmetry axis of the particle motion is determined by the mean field caused by the particle-core interaction of the qQ type. On the other hand, the quasiparticle angular momentum projection on the symmetry axis is, by construction, maximal. Therefore, $\mathbf{J}_F$ is oriented along the axis OZ, which results in having an orthogonal trihedral $(\mathbf{J}_p, \mathbf{J}_n, \mathbf{J}_F)$. Invoking the arguments of Ref. [FRA01], for such states a large transverse dipole moment is expected, which may induce a large M1 transition rate.

Finally, a short comment on the structure of the state with the quasiparticle factor state with angular momentum and projection $(J, 0)$:

$$\Psi_{JI;M}^{(2qp;01)} = \mathcal{N}_{JI}^{(2qp;01)} \sum_{J'} C_{0\ 1\ 1}^{J\ J'\ I} \left[(a_j^\dagger a_j^\dagger)_J \varphi_{J'}^{(1)} \right]_{IM} \left(N_{J'}^{(1)} \right)^{-1}. \qquad (10.1.26)$$

In such a state, the three angular momenta, $\mathbf{J}_p, \mathbf{J}_n, \mathbf{J}_F$ are in the same plane. Hence, one expects that the magnetic properties are different from those characterizing the

Fig. 10.7 The angle between $\mathbf{J}_p$ and $\mathbf{J}_n$ within the boson dipole state $\Psi_{JI;M}^{(2qp;01)}(d)$. The deformation parameter for protons is equal to that for neutrons and $d = 0.2$ (see Eq. (10.1.26))
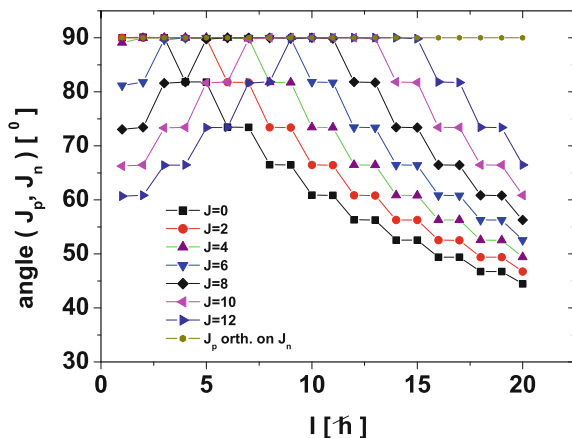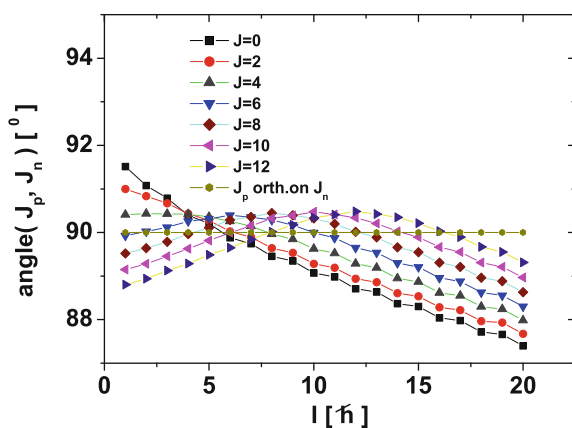

Fig. 10.8 The angle between $\mathbf{J}_p$ and $\mathbf{J}_n$ within the boson dipole state $\Psi_{JI;M}^{(2qp;01)}(d_p, d_n)$. The deformation parameters are $d_p = 0.2$ and $d_n = 2.4$

state where the mentioned vectors are mutually orthogonal. For comparison, these states are also considered in Figs. 10.7 and 10.8.

10.1.5 Magnetic Dipole Transitions

The magnetic moment of the phenomenological core is defined by:

$$\boldsymbol{\mu}_c = g_p \mathbf{J}_p + g_n \mathbf{J}_n \equiv g_c \mathbf{J}_{pn}, \tag{10.1.27}$$

where g_p, g_n and g_c denote the gyromagnetic factors for protons, neutrons and the core. Multiplying this with $\mathbf{J}_c = \mathbf{J}_{pn}$, and averaging the result with the function $\Psi_{JI;M}^{(2qp;J1)}$, one obtains an equation determining g_c:

$$g_{c;JI} = \frac{g_p + g_n}{2} + \frac{g_p - g_n}{2} \frac{\widetilde{J}^{(1)}_{p;JI}(\widetilde{J}^{(1)}_{p;JI} + 1) - \widetilde{J}^{(1)}_{n;JI}(\widetilde{J}^{(1)}_{n;JI} + 1)}{\widetilde{J}^{(1)}_{pn;JI}(\widetilde{J}^{(1)}_{pn;JI} + 1)}. \qquad (10.1.28)$$

Note that since the deformation parameters for proton and neutron are equal with each other, the average values of proton and neutron angular momenta are the same, $\widetilde{J}^{(1)}_p = \widetilde{J}^{(1)}_n$, which results in having a simple expression for the core gyromagnetic factor:

$$g_c = \frac{g_p + g_n}{2}. \qquad (10.1.29)$$

The expression (10.1.28) can be easily derived by writing first the core magnetic moment as a linear combination of the sum and the difference of proton and neutron angular momenta:

$$\boldsymbol{\mu_c} = \frac{g_p + g_n}{2}(\mathbf{J}_p + \mathbf{J}_n) + \frac{g_p - g_n}{2}(\mathbf{J}_p - \mathbf{J}_n). \qquad (10.1.30)$$

Since the scissors state, 1^+, is antisymmetric with respect to the proton-neutron permutation, while the ground state, 0^+, is symmetric, only the second term from the above equation contributes to the transition $0^+ \to 1^+$. This feature is not preserved when we treat the intra-band transitions of the chiral band, the states participating to the transition behaving similarly against the proton-neutron permutation.

Denoting by g_F the gyromagnetic factor for the two quasiparticle factor state and following a similar procedure as above we get for the whole system the following gyromagnetic factor:

$$g_{JI} = \frac{g_F + g_c}{2} + \frac{g_c - g_F}{2} \frac{\widetilde{J}^{(1)}_{pn;JI}(\widetilde{J}^{(1)}_{pn;JI} + 1) - J(J + 1)}{I(I + 1)}. \qquad (10.1.31)$$

We note that both gyromagnetic factors for the core and for the whole system depend on the angular momenta J and I.

In order to calculate the M1 transition probability we need the following reduced matrix elements:

$$\langle \Psi^{(2qp;J1)}_{JI} || J_F || \Psi^{(2qp;J1)}_{JI'} \rangle = 2\hat{I}' \hat{J} \sqrt{J(J + 1)} N^{(2qp;J1)}_{JI} N^{(2qp;J1)}_{JI'}$$

$$\times \sum_{J_1} \left(N^{(1)}_{J_1} \right)^{-2} \left(C^{J\ J_1\ I}_{J\ 1\ J+1} \right)^2 W(I'J_1 1J; JI),$$

$$(10.1.32)$$

$$\langle\Psi_{JI}^{(2qp;J1)}||g_p J_p + g_n J_n||\Psi_{JI'}^{(2qp;J1)}\rangle = N_{JI}^{(2qp;J1)} N_{JI'}^{(2qp;J1)} \hat{I}'\hat{I}$$

$$\times \sum_{J_1} C_{J\ 1\ J+1}^{J\ J_1\ I} C_{J\ 1\ J+1}^{J\ J_1\ I'} \left(N_{J_1}^{(1)}\right)^{-2} W(JJ_1 I1; I'J_1)$$

$$\times \left(g_p \sqrt{\tilde{J}_{p;J_1}(\tilde{J}_{p;J_1}+1)} + g_n \sqrt{\tilde{J}_{n;J_1}(\tilde{J}_{n;J_1}+1)}\right).$$

Using the previous results regarding the average value of $\hat{J}_\tau^2$, the last expression of the above equations, considered for the case $I' = I$, simplifies to:

$$\langle\Psi_{JI}^{(2qp;J1)}||g_p J_p + g_n J_n||\Psi_{JI}^{(2qp;J1)}\rangle = g_p\sqrt{\tilde{J}_{p;JI}(\tilde{J}_{p;JI}+1)} + g_n\sqrt{\tilde{J}_{n;JI}(\tilde{J}_{n;JI}+1)}.$$

$$(10.1.33)$$

The M1 transition operator is defined by:

$$M_{1,m} = \sqrt{\frac{3}{4\pi}}\mu_{1,m}. \qquad (10.1.34)$$

As shown in the previous chapter, the transition operator can be derived using the equations of motion for the quadrupole coordinates. This way some higher order boson corrective terms may be included.

From the above mentioned equations describing the magnetic moment, one notes that even in the second order in bosons, the gyromagnetic factors have components which multiply the proton-neutron dipole operators in addition to those accompanying the angular momenta $\hat{J}_p$ and $\hat{J}_n$. Although the present formalism is purely phenomenological and therefore the magnetic moments of neutrons are not included, due to the proton-neutron coupling terms involved in the model Hamiltonian, the neutron gyromagnetic factor is not vanishing.

Actually, restricting the expression for the transition operator to the angular momenta, the above equation provides analytical expressions for the proton and neutron system gyromagnetic factors. For illustration, in Table 10.1 we give the results for the reduced magnetic dipole transitions between two adjacent states from a two quasiparticle $(i_{13/2})^2$ band, for two sets of the deformation parameters. They are chosen such that to correspond to a near vibrational regime. We recall that a rotational picture is reached for a deformation parameter larger than 3 [CR74]. We note that for $J \geq 6$, where J denotes the quasiparticle total angular momentum, and system angular momentum I larger than 10, the transitions might be considered of collective nature. Although we truncated the angular momentum I to 20, from Table I it is conspicuous that the larger is I, the larger is the M1 strength.

Table 10.1 The BM1 values, given in units of μ_N^2, of the transitions $I \to (I-1)$ calculated with the wave functions $\Psi_{JI;M}^{(2q_P;J1)}$ given by Eq. (10.1.22), for two sets of deformation parameters (d_p, d_n) and the single particle orbital $i_{13/2}$

$I \to (I-1)$	$(d_p, d_n) = (1.0, 1.0)$							$(d_p, d_n) = (0.2, 2.4)$						
	J=0	2	4	6	8	10	12	J=0	2	4	6	8	10	12
1														
2	0.929							0.691						
3	0.720							0.535						
4	0.765	0.057						0.468	0.112					
5	0.669	0.158						0.409	0.248					
6	0.773	0.216						0.393	0.346	0.367				
7	0.704	0.287	0.169					0.361	0.415	0.786				
8	0.832	0.297	0.438	0.280				0.362	0.463	1.110	0.656			
9	0.773	0.358	0.648	0.722				0.340	0.500	1.353	1.402			
10	0.913	0.335	0.833	1.104	0.376			0.350	0.524	1.538	2.011	0.939		
11	0.858	0.400	0.950	1.437	0.979			0.333	0.547	1.679	2.491	2.014		
12	1.004	0.352	1.073	1.692	1.531	0.459		0.346	0.557	1.789	2.877	2.938	1.204	
13	0.951	0.427	1.131	1.921	2.023	1.206		0.332	0.575	1.876	3.184	3.681	2.593	
14	1.102	0.359	1.224	2.087	2.429	1.916	0.531	0.348	0.576	1.945	3.432	4.301	3.811	1.447
15	1.050	0.446	1.322	2.250	2.787	2.565	1.404	0.335	0.593	2.000	3.635	4.814	4.845	3.130
16	1.204	0.359	1.313	2.356	3.078	3.124	2.259	0.352	0.585	2.044	3.802	5.242	5.721	4.641
17	1.152	0.459	1.388	2.478	3.341	3.622	3.057	0.340	0.603	2.082	3.941	5.601	6.464	5.955
18	1.308	0.356	1.356	2.544	3.550	4.047	3.766	0.359	0.589	2.110	4.057	5.905	7.099	7.094
19	1.257	0.470	1.434	2.641	3.748	4.428	4.406	0.348	0.614	2.140	4.155	6.164	7.644	8.080
20	1.415	0.354	1.383	2.677	3.899	4.751	4.968	0.368	0.609	2.161	4.235	6.382	8.113	8.938

The magnetic dipole transition operator is determined by the following gyromagnetic factors: $g_F = 1.3527\,\mu_N$; $g_P = 0.666\,\mu_N$; $g_n = 0.133\,\mu_N$

10.1.6 Numerical Results and Discussions

The formalism described above was applied for ^{188,190}Os and ^{192}Pt. Unfortunately, there are no available data concerning the magnetic bands for even-even-nuclei. In choosing these nuclei we had in mind the fact that nuclei around $A = 190$ are gamma soft and a phase transition from prolate to oblate through a triaxial shape is expected to occur. Indeed, the signature for a triaxial rotor

$$E_{2_g^+} + E_{2_\gamma^+} = E_{3_\gamma^+}, \tag{10.1.35}$$

is satisfied with good accuracy by the chosen nuclei. Discrepancies for ^{188}Os, ^{190}Os and ^{192}Pt are 2, 11 and 8 keV, respectively.

We calculated first the excitation energies for the bands described by the angular momentum projected functions

$$\phi_{JM}^{(g)}|BCS\rangle, \phi_{JM}^{(\beta)}|BCS\rangle, \phi_{JM}^{(\gamma)}|BCS\rangle, \phi_{JM}^{(1)}|BCS\rangle, \widetilde{\phi}_{JM}^{(1)}|BCS\rangle, \Psi_{JI;M}^{(2qp;J1)}. \tag{10.1.36}$$

and the particle-core Hamiltonian H (10.1.18). The single particle space was restricted to the single proton shell $h_{11/2}$. Several parameters like the structure coefficients defining the model Hamiltonian and the deformation parameters are to be fixed. Since in the present application the proton and neutron deformations are equal, we need only one "global" deformation, $\rho = \sqrt{2}d$. For a given ρ we determine the parameters involved in H_{GCSM} by fitting the excitation energies in the ground, β and γ bands, through a least square procedure. ρ was then varied and fixed to that value which provides the minimal root mean square of the results deviations from the corresponding experimental data. Excitation energies of the phenomenological magnetic bands described by $\phi_{JM}^{(1)}$ and $\widetilde{\phi}_{JM}^{(1)}$ respectively, are free of any adjustable parameters. The strengths of the pairing and $Q.Q$ interaction for $j = 11/2$ were taken close to the values used in Ref. [RLF83], where spectra of some Pt even-even isotopes were interpreted with a particle-core Hamiltonian, the core being described by the Coherent State Model (CSM). Thus, the quasiparticle energy for ^{192}Pt is 1.25 MeV while for ^{188,190}Os this is 0.915 which is about the value yielded by a BCS treatment in the extended space of single particle states. Concerning the particle-core qQ interaction strength we fixed first the strength X'_{pc} defined by:

$$X'_{pc} = 6.5\eta_{\frac{11}{2}\frac{11}{2}}^{(-)} X_{pc}^{(p)}, \tag{10.1.37}$$

Since the considered outer particles are protons, the neutron particle-core coupling term is ineffective. Therefore we put $X_{pc}^{(n)} = 0$. The parameters mentioned above have the values listed in Table 10.2.

Table 10.2 The structure coefficients of the model Hamiltonian were determined by a least square procedure

$\rho = d\sqrt{2}$	A_1 (keV)	A_2 (keV)	A_3 (keV)	A_4 (keV)	X'_{pc} (keV)	X_{sS} (keV)	g_p (μ_N)	g_n (μ_N)	g_F (μ_N)	r.m.s. (keV)
^{188}Os	2.2	438.7	−93.8	−70.5	9.1	1.02	3.0	0.828	−0.028	1.289	16.93
^{190}Os	2.0	366.1	92.6	24.0	12.2	1.66	2.0	0.7915	0.0086	1.289	18.63
^{192}Pt	2.0	555.4	−25.4	−12.8	7.7	−23.4	1	0.666	0.133	1.289	

On the last column the r.m.s. values characterizing the deviation of the calculated and experimental energies are also given. The deformation parameter ρ is dimensionless. The parameter X'_{pc} is that defined by Eq. (10.1.37). As usual the spin gyromagnetic factor was quenched by a factor 0.75 in order to account for the influence of the proton excited states on the magnetic moment

Fig. 10.9 Experimental (Exp.) and calculated (Th.) excitation energies in ground, β and γ bands of ^{188}Os. Data are taken from [S02]

Fig. 10.10 The same as in Fig. 10.9 but for ^{190}Os with data from Ref. [S03]

Fig. 10.11 Experimental and calculated excitation energies in ground, β and γ bands for ^{192}Pt. They correspond to the fitted parameters listed in Table 10.2. The r.m.s. value of the deviation of the theoretical results and the corresponding experimental data is equal to 67 keV

Excitation energies calculated with these parameters are compared with the corresponding experimental data, in Figs. 10.9, 10.10, and 10.11. One notes a good agreement of results with the corresponding experimental data.

Unfortunately, there is no available data concerning the magnetic states. However, in Refs. [S02, S03] the states of 1304.82 and 1115.5 keV in ^{188}Os and ^{190}Os respectively (Figs. 10.12 and 10.13), perform a M1 decay to the ground band states. These states could tentatively be associated to the heading states of the two dipole bands
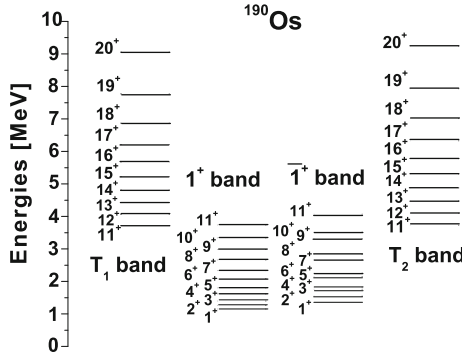
Fig. 10.12 The same as in Fig. 10.13 but for ^{190}Os. Here the dipole bands from the lower columns are described by $|1; JM\rangle$ and $|\bar{1}; JM\rangle$.
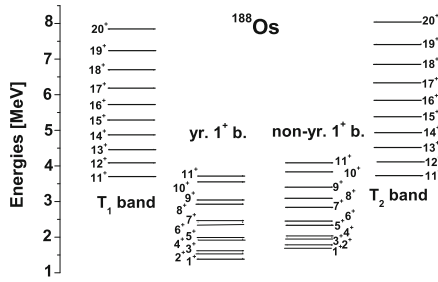
Fig. 10.13 Excitation energies for the yrast (*lower-left*) and non-yrast (*lower-right*) boson dipole states of ^{188}Os. The twin bands T_1 and T_2 are also shown

which are located at 1400 and 1538 keV, respectively. For ^{188}Os, the states $|1; JM\rangle$ are not in a natural order from $J \geq 6$. Indeed, the yrast states belong to the 1^+ band except the states with $J = 6, 8, 10$ which are of $\bar{1}^+$ type. Similarly, non-yrast states have a $\bar{1}^+$ character except the states of $J = 6, 8, 10$, which are of 1^+ type.

The results for the magnetic dipole bands of ^{192}Pt are plotted in Fig. 10.14. Excitation energies shown there are those from Table 10.3. The lower bands exhibit a pronounced doublet structure. Indeed, in the band 1^+ we notice the staggering $4^+, 5^+; 6^+, 7^+; 8^+, 9^+;$ etc., while in the band $\bar{1}^+$ the states are grouped in a different manner: $1^+, 2^+; 3^+, 4^+; 5^+, 6^+; 7^+, 8^+;$ etc. The first three states of the 1^+ band are close in energy, while in the band $\bar{1}^+$ the first two doublets have an unnatural spin ordering. The experimental data [BAG12] show two states of uncertain spin assignment which decay by M1 to $2_g^+, 2_\gamma^+$ and 0_g^+ and lie close to the band heads of the two dipole bands having the energies of 1.874 and 2.033 MeV respectively. According to the present calculations these states might have the spin 1 and 2 respectively, the mentioned energies being comparable with those associated to the first two states of the band 1^+. The lowest dipole states of magnetic nature are identified as having the energies 2.149 and 2.319 MeV respectively, which are not too far from the calculated energies of the states 1^+. In order to decide to which of the two experimental sets of
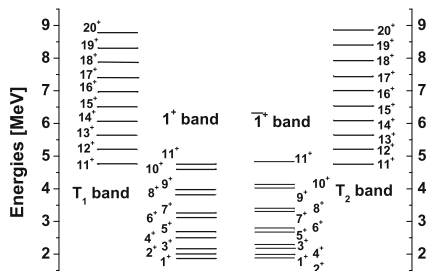
Fig. 10.14 The excitation energies for the dipole bands described by $\phi_{JM}^{(1)}$ (*left lower column*) and $\tilde{\phi}_{JM}^{(1)}$ (*right lower column*), respectively. The bands T_1 (*upper left column*) and T_2 (*upper right column*), conventionally called twin bands, are also shown. The T_1 and T_2 bands were obtained with $X'_{pc} = -0.023$ MeV and $X_{sS} = 0.001$ MeV for the *left column* and $X_{sS} = -0.001$ MeV for the *right column*

Table 10.3 Excitation energies, given in MeV, for the four magnetic bands denoted by 1^+, $\bar{1}^+$, T_1 and T_2 respectively, in ^{192}Pt

J^+	1^+-band	$\bar{1}^+$-band	T_1-band	T_2-band
1^+	1.874	2.010		
2^+	2.033	1.983		
3^+	2.183	2.291		
4^+	2.519	2.289		
5^+	2.676	2.763		
6^+	3.127	2.783		
7^+	3.287	3.364		
8^+	3.832	3.413		
9^+	3.994	4.065		
10^+	4.623	4.147		
11^+	4.785	4.852	4.757	4.765
12^+	5.492	4.969	5.201	5.218
13^+	5.651	5.718	5.638	5.662
14^+	6.436	5.868	6.073	6.106
15^+	6.589	6.655	6.512	6.553
16^+	7.450	6.840	6.957	7.008
17^+	7.596	7.661	7.409	7.469
18^+	8.535	7.881	7.868	7.938
19^+	8.670	8.735	8.330	8.410
20^+	9.689	8.989	8.788	8.878

The twin bands T_1 and T_2 have $K = 11$

data the results of these calculations could be associated, additional investigations are necessary from both theoretical and experimental sides.

The weak feature of the present formalism is that does not reproduce the right staggering in the γ band of ^{192}Pt. Actually, the experimental energy spacings in this band is almost constant up to the state 5^+, increases for 6^+ and then a smaller spacing for the pair of states $6^+, 7^+$ is recorded. Since one has only one staggering situation, one cannot conclude upon a staggering $(J^+, (J+1)^+)$ with J-even. It may happen that the state 6^+ does not really belong to the γ band. Thus, to draw a definite conclusion one needs data for excitation energies of the higher spin states. On the other hand the GCSM formalism [RFC87] predicts for small deformation a staggering $(3^+, 4^+)$; $(5^+, 6^+)$; $(7^+, 8^+)$, etc. while for large deformation the doublet structure is changed to $(2^+, 3^+)$; $(4^+, 5^+)$; $(6^+, 7^+)$, etc. The results shown in Fig. 10.11 are compatible with the first level clustering, which reflects the regime of a small deformation. Indeed, the energy spacings, given in keV, are: 224; 230; 289; 278; 349; 315; 402; 346. As seen in the list, except for the spacing $(3^+, 4^+)$ which is almost the same as $(2^+, 3^+)$, the rule for the doublet structure $(J^+, (J+1)^+)$ with J odd is obeyed. The bands T_1 and T_2, tentatively called twin bands, have some distinctive properties. First of all, both are $K = 11$ bands. The meaning of this statement will be commented in detail for ^{192}Pt. Since the unprojected state, generating the bands T_1 and T_2 through angular momentum projection, has $K = 11$, after projection the wave function is a superposition of different K components among which the one having $K = 11$ prevails over the others [CR74]. The magnetic nature of the bands T_1 and T_2 is confirmed by the large intraband M1 transitions, as shown in Figs. 10.15, 10.16 and 10.17. The energies of states of the same angular momentum are close to each other. Indeed, their difference ranges from 8 to 90 keV. It is worth
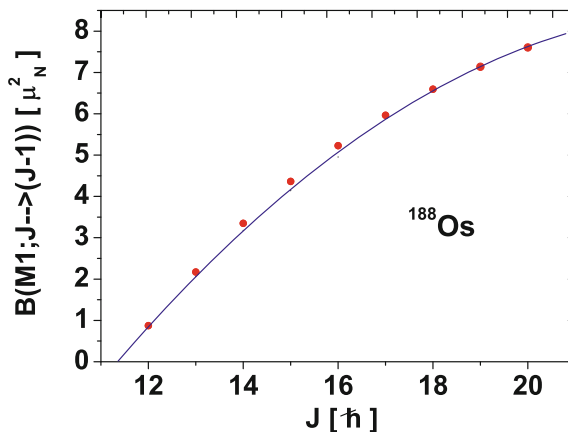
Fig. 10.15 The BM1 values associated with the dipole magnetic transitions between two consecutive levels in the T_1 band of ^{188}Os. The results are interpolated with a second rank polynomial (*full curve*). The gyromagnetic factors employed are $g_p = 0.828\,\mu_N$, $g_n = -0.028\,\mu_N$ and $g_F = 1.289\,\mu_N$
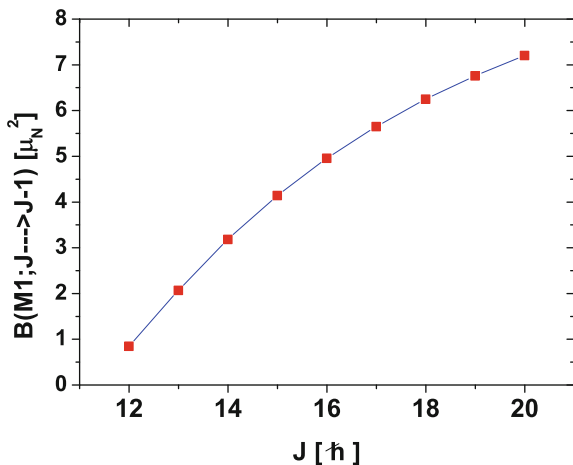
Fig. 10.16 The $B(M1)$ values associated with the dipole magnetic transitions between two consecutive energy levels of the T_1 band, in ^{192}Pt. The gyromagnetic factors employed in our calculations are: $\mu_p = 0.666\,\mu_N$, $\mu_n = 0.133\,\mu_N$ and $\mu_F = 1.289\,\mu_N$. As usual the spin gyromagnetic factor was quenched by a factor 0.75 in order to account for the influence of the proton excited states on the magnetic moment

Fig. 10.17 The magnetic dipole reduced probabilities within the two quasiparticle-core bands corresponding to the quasiparticle total angular momentum J. The gyromagnetic factors are the same as those used in Fig. 10.15
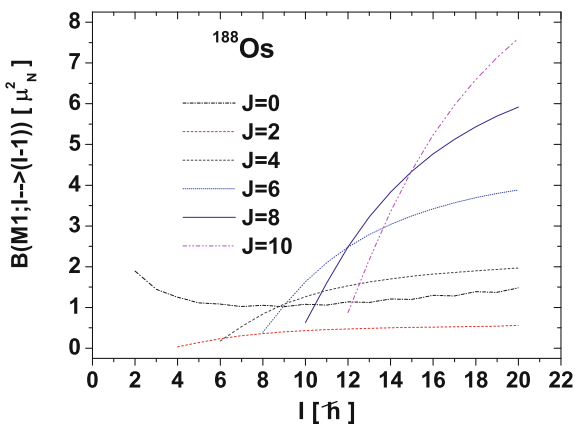
noting that energy spacing varies very little in the two twin bands. Indeed, in T_1 it goes from 435 keV reached for 13^+, to 462 keV met at 19^+. As for the T_2 band the minimum energy spacing is of 444 keV met for three states, 12^+, 13^+, 14^+, while the maximum spacing is 472 keV for 19^+. These spacings were plotted in Fig. 10.18 as function of angular momentum. The curves for the two twin bands are almost parallel to each other and behave as a polynomial in J, of rank three. These spacings are used to calculate the so called *signature energy staggering*, defined by:

$$S(J) = \frac{E(J) - E(J-1)}{2J}. \tag{10.1.38}$$
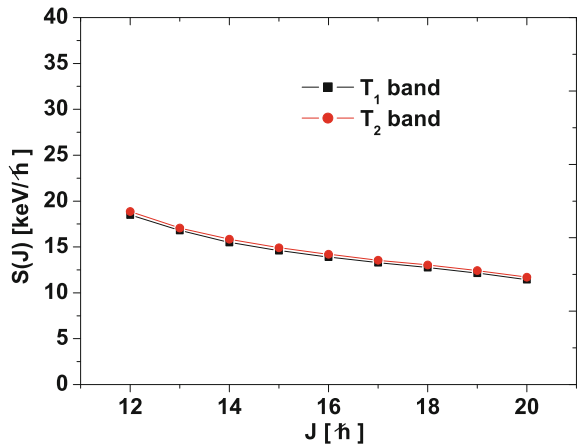
This function, plotted in Fig. 10.19, exhibits no staggering and is decreasing monoton-
ically and very slowly with J. Indeed, the e-cart of maximum and minimum value
is only of about 7 keV. For an ideal chiral band this parameter should be independ-
ent of J. Both twin bands intersect the lower dipole bands at the energy level 11^+.
Due to this feature we would expect that a backbending takes place at this angular
momentum. However, due to the doublet structure in the lower dipole bands it is
difficult to define consistently the moment of inertia for the $\Delta J = 1$ states. Despite
the mentioned encountered difficulties, the plot of the moment of inertia vs. the
rotational frequency squared starts with a backbending, continues with a forward
bending, from 14^+, and again a backbending from 19^+. This picture is common
for both twin bands. For illustration, in Fig. 10.20 we present the situation of the T_1
band. Denoting by $\mathcal{J}$, $E(J)$ and ω the double moment of inertia, the energy of the
state J^+ belonging to the T_1 band and the rotational frequency respectively, for the
chosen $\Delta J = 1$ band one gets:

Fig. 10.20 The double moment of inertia calculated for the angular momenta 12^+-20^+ with Eq. (10.1.39) are represented as function of the corresponding rotational frequency given by (10.1.40)
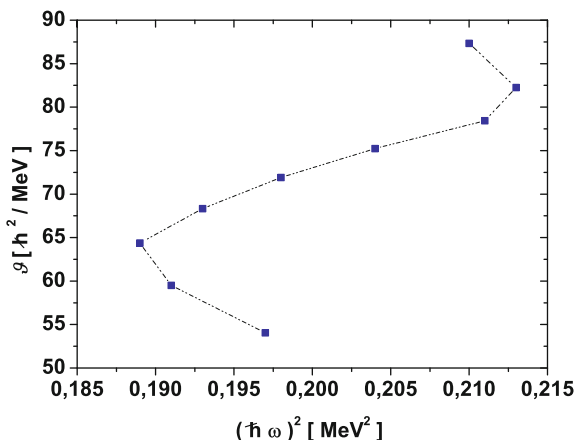
$$\mathcal{J} = \frac{2(J+1)}{E(J+1) - E(J)}, \tag{10.1.39}$$

$$\hbar\omega = E(J+1) - E(J). \tag{10.1.40}$$

In Fig. 10.20 we see that, indeed, the moment of inertia exhibits a double backbending when is represented as function of the rotational frequency squared. If we consider also the energy levels of the band 1^+ before its crossing with the band T_1 the graph of Fig. 10.20 would be continued to the left side by a saw teeth like curve.

For ^{188,190}Os the gyromagnetic factor were calculated in the following manner. Considering for the core's magnetic moment the classical definition, one obtains an analytical expression involving the quadrupole coordinates and their first order time derivatives, which can be further calculated by means of the Heisenberg equation. Finally, writing the result in terms of quadrupole boson operators and identifying the factors multiplying the proton and neutron angular momenta with the gyromagnetic factors of proton and neutrons, one obtains:

$$\begin{pmatrix} g_p \\ g_n \end{pmatrix} = \frac{3ZR_0^2}{8\pi k_p^2} \frac{Mc^2}{(\hbar c)^2} \begin{pmatrix} A_1 + 6A_4 \\ \frac{1}{5}A_3 \end{pmatrix}, \tag{10.1.41}$$

where Z and R_0 denote the nuclear charge and radius, while M and c are the proton mass and the light velocity. k_p is a parameter defining the canonical transformation relating the coordinate and conjugate momenta with the quadrupole bosons, while A_1, A_3, A_4 are the structure coefficients involved in H_{GCSM}. Since within the GCSM the core gyromagnetic factor is

$$g_c = \frac{1}{2}(g_p + g_n), \tag{10.1.42}$$

we may identify it with the liquid drop value, Z/A, and consequently the canonicity coefficient acquires the expression:

$$k_p^2 = \frac{3}{16\pi} A R_0^2 \frac{Mc^2}{(\hbar c)^2} \left(A_1 + 6A_4 + \frac{1}{5}A_3 \right). \tag{10.1.43}$$

Inserting this in Eq. (10.1.41), the gyromagnetic factors are readily obtained. This procedure was used for ^{188,190}Os with the results from Table 10.2.

With the expression for the transition operator just determined, the B(M1) value for the transitions $1^+ \rightarrow 0_g^+$ and $1^+ \rightarrow 2_g^+$ can be calculated. The results are $0.2772\,\mu_N^2$, $0.0139\,\mu_N^2$ for ^{188}Os and $0.1752\,\mu_N^2$, $0.0085\,\mu_N^2$ for ^{190}Os. As a matter of fact, this proves that the chiral bands T_1 and T_2 are of different nature than the low lying scissors mode. Indeed, the first are essentially determined by the moment of inertia dependence on the angular momentum, while the second by the nuclear deformation.

The gyromagnetic factors for the collective core of ^{192}Pt, denoted by g_p and g_n, were determined from equations predicted by the GCSM model,

$$g_c = \frac{g_p + g_n}{2}, \quad g_n = \frac{1}{5}g_p, \tag{10.1.44}$$

and taking $g_c = \frac{Z}{A}$.

Finally, the M1 transition probabilities were calculated with the Eqs. (10.1.32) and (10.1.33). The results are represented in Fig. 10.15 for ^{188}Os and Fig. 10.16 for ^{192}Pt as a function of J. The J dependence seems to be quadratic, the $B(M1)$ value increasing from $0.847\,\mu_N^2$ (J = 12) to $7.204\,\mu_N^2$ (J = 20). Note that in the present calculations one considered the term of the model Hamiltonian breaking the chiral symmetry only for energies and not for the corresponding wave functions. This feature leads to the fact that the two partner bands are described by identical functions which results in having the same B(M1) values for both.

Note that the bands T_1 and T_2 correspond to two reference frames of the three angular momenta $\mathbf{J}_F, \mathbf{J}_p, \mathbf{J}_n$ which are related by a chiral transformation which changes the sign of $\mathbf{J}_F$. The matrix elements of the X_{sS} term in the two reference frames differ from each other by sign. Therefore, for one band, T_1, the interaction sS is attractive while for the other band, T_2, repulsive. However, there are another two chiral transformations which change the signs of $\mathbf{J}_p$ and $\mathbf{J}_n$, respectively, of the right handed frame associated to the band T_1. Each of the corresponding bands is therefore a partner band for T_1. The additional bands will be denoted hereafter by T_3 and T_4 respectively. They are also partner bands for T_2 since their frames, are obtainable from that defining T_2, by rotations around the axes $\mathbf{J}_n$ and $\mathbf{J}_p$ respectively with an angle equal to π. However, the sS interaction is not invariant to the mentioned transformation which results that the bands T_2 and $T_{3,4}$ are different from each other. Note that each of the π rotations, mentioned above, is a product of two chiral transformations and therefore a chiral transformation. It is worth noting that the T_3 and T_4 transformations break not only the chiral symmetry but also the p-n permutation symmetry of the core.

Indeed, the transformed spin-spin interaction is of negative parity with respect to the p-n permutation. This is the reason why the average of this interaction with the two quasiparticle-core dipole state is vanishing. Therefore the bands corresponding to the frames T_3 and T_4 are degenerate, the common energy split being exclusively determined by the sS interaction which is nonvanishing for the T_1 and T_2 bands. If we enlarge the space by adding the states of two quasiparticles-core ground band type, these states are linked with the two quasiparticle-core dipole states by means of the T_3 (or T_4) transformed spin-spin interaction. By diagonalization, one obtains two bands each member state being a linear combination of the two states from the basis. The band of states whose dominant component is a two quasiparticle-core dipole state, is of magnetic nature. Concluding, there are four chiral bands among which two are degenerate, which have a negative parity with respect to the p-n permutation of the core. In addition there are two bands of mixed parity from which only one exhibits magnetic properties.

The chiral symmetry has been intensively studied for odd-odd and odd-even nuclei around A = 130 [PET96, SI05] and A = 100[VFK04]. Recently, the investigation has been extended also to some heavy nuclei with $A \approx 190$ [BAL04]. The first interpretation of the twin bands in terms of a spontaneous chiral symmetry breaking was given by Frauendorf [FRA97], while the first measurement was reported in Ref. [PET96]. Several approaches devoted to the chiral bands description have been proposed. Among these, the particle-asymmetric rotor (PAR) model is the most popular. It is interesting to mention that PAR was much earlier developed, both analytically and numerically, in Refs. [TF75, TF76, TOF76, TYF77].

The experimental systematics established the criteria upon which one could decide whether a pair of bands might be considered of a chiral nature. Briefly, these are: (1) The partner bands are almost degenerate; (2) The energy staggering parameter must be angular momentum independent; (3) The staggering behavior of the ratio $B(M1)/B(E2)$ and $B(M1)_{in}/B(M1)_{out}$, where $B(M1)_{in}$ and $B(M1)_{out}$ denote the intra-band and inter-band reduced M1 transition probabilities for the partner bands. In Ref. [PET06] it was shown that these criteria are necessary but sometimes not sufficient, the partner bands corresponding to nuclear shapes which are not close to each other.

Note that this procedure is based on angular momentum projection from proton-neutron boson coherent states. In general, the used boson Hamiltonians are invariant to the rotation transformation and therefore treated with basis states of good angular momentum. This procedure has the advantage, over the other boson formalisms, of not having redundant components caused by using different sets of Euler angles for proton and neutron bosons, respectively.

The present description exhibits some specific features. While the previous formalisms were focused mainly on the odd-odd nuclei, only few publications refering also to even-odd [MUK07] and even-even isotopes [LU09], the presented approach concerns the even-even systems and is based on a new concept. While within the other approaches there are only two magnetic bands related by a chiral transformation, here one found four magnetic bands with definite p-n symmetry of the core and one with mixed symmetry having this property. Two of the bands with unique

Fig. 10.21 The four frames
are related by a chiral
transformation. The
spin-spin interaction
corresponding to each
thriedral is also mentioned.
They generate the bands T_i
with i = 1, 2, 3, 4,
respectively
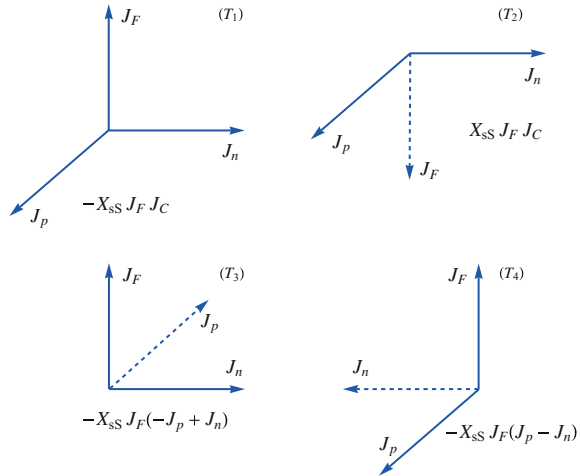
symmetry are degenerated. Note that there are two symmetries broken, that of p-n
permutation and the chiral one. These distinct frames defined by a certain relative
orientation of the three angular momenta are suggestively presented in Fig. 10.21.

10.2 Monopole Charge Properties Within the GCSM

10.2.1 Introduction

One body transition density operators play an important role in the microscopic
description of various properties showing up in nuclear systems. For example, the
charge density operator matrix elements corresponding to the ground state of a spher-
ical system can be determined, with high precision, in elastic electron scattering,
which results in having precious information about the spatial charge distribution.
Similarly, the matrix elements between the ground state and excited states within the
ground band might provide information about the nuclear shape [CO76]. Indeed, in
an electron scattering experiment at large momentum transfer the radial dependence
of the charge distribution can be directly measured. Combining this result with other
information on electromagnetic interaction in the considered nuclei, in the reference
quoted above more refined statements on the deformed shapes could be made.

The structure of the spectra in deformed nuclei requires the use of a deformed
mean field. The final state describing an interacting many body system is a deformed
state and therefore its use for the description of the transition probabilities requires
the projection of the components with good angular momentum. In particular, in
order to account for the contribution of the tensorial components of the charge den-
sity, the many body ground state built up with deformed single particle states must be

projected over the angular momentum [ZANE77]. There is no doubt that projection is
of paramount importance for transitional and deformed nuclei. However, the correc-
tion brought by projection to the results obtained in the intrinsic frame depends on the
observable under consideration [VIL66, MOY86]. For example, averaging a model
Hamiltonian on an intrinsic ground state yields the system energy while averaging
it on angular momentum projected states, a whole band of energy levels is obtained.
For instance, describing the collective magnetic dipole state with a deformed single
particle basis one obtains $K = 1$ states which are abusively called 1^+ states. To
our knowledge there is no rigorous proof that the admixture with the components of
angular momentum 2 is negligible. Another example we want to comment upon is
that of the rotational bands which are considered to be a set of states characterized
by the same quantum number K. However, in the laboratory frame of reference, K
is not a good quantum number and the meaning of a K-state is actually a state with
a dominant K-component. The effect of projection is felt by the operator matrix
elements. There are cases of operators whose matrix elements are affected very little
by the the angular momentum projection of the intrinsic states. The simplest case
is the one when the operator is just a C-number constant. Its matrix elements in the
unprojected and projected states are equal to each other. At first glance, that would
suggest that other operators insensitive to projecting the angular momentum from
the intrinsic wave function, would be scalar operators. Of course, that is not true and
an example is the boson number operator in a phenomenological picture.

One issue of the present section is to study the scalar part of the charge density
operator within the generalized coherent state model (GCSM). Thus, we shall con-
sider the matrix element of the charge density operator, truncated at its scalar term,
on the unprojected ground state and alternatively on the projected $J^\pi = 0^+$ state.
We also raise the question of how different are these matrix elements from those cor-
responding to a high angular momentum projected state. All matrix elements quoted
above are studied as function of nuclear deformation.

Another scalar operator which is considered here is the E0 transition operator. The
monopole transition is often used to characterize various states of angular momentum
equal to zero. Thus, in Ref. [SGEC98] the monopole transition $0_\beta^+ \to 0_g^+$ strength
was expressed in terms of the mixing coefficient of the two states characterized by
different deformations but lying close to each other in energy. In this way the transi-
tion strength may provide the mixing coefficient for the two states. In ^{158}Gd several
0^+ states were seen in a (p,t) experiment [LES02]. These states have been micro-
scopically interpreted within a projected shell model and, alternatively, within the
quasiparticle-phonon model [ISS04]. The authors of Ref. [ISS04] calculated the E2
strength for the transition from the ground state to the first 2^+ state, the E0 strength
for the transition from the excited 0^+ states to the ground state, and the two-nucleon
spectroscopic amplitudes. The experimental strengths for E0 and E2 transitions are
concentrated in one and two states respectively, while the theoretical results [ISS04]
show a large fragmentation of the two transition strengths. The experimental spec-
troscopic amplitudes indicate that two states are mainly populated which contrasts
the theoretical result where the amplitude is fragmented among several states. From

the analysis of Ref. [ISS04] it seems that the E0 strength is a signature only for one excited 0^+ state, as it was in fact considered in Ref. [SGEC98].

10.2.2 The Charge Density

Suppose that the nuclear charge is distributed uniformly inside the nuclear surface:

$$R(\theta, \varphi) = R_0 \left(1 + \sum_{\lambda=0,2;\mu} \alpha^*_{\lambda\mu} Y_{\lambda\mu} \right) \equiv R_0 + \Delta R. \qquad (10.2.1)$$

with $\alpha_{\lambda\mu}$ denoting the quadrupole collective coordinates. The charge density has the expression:

$$\rho(r, \theta, \varphi) = \rho_0 H \left[R(\theta, \varphi) - r \right], \qquad (10.2.2)$$

where H denotes the Heaviside function, while ρ_0 is the constant density corresponding to a sphere of radius $R_0 = 1.2A^{1/3} fm$. Expanding the charge density around the surface corresponding to vanishing quadrupole coordinates, one obtains:

$$\rho(r, \theta, \varphi) = \rho_0 \left[H(R_0 - r) + \Delta R \delta(R_0 - r) - \frac{1}{2} (\Delta R)^2 \delta'(R_0 - r) + \cdots \right] \quad (10.2.3)$$

In momentum space the charge density can be written as a sum of tensor operators of various ranks. For example the term of rank λ and projection μ reads:

$$\rho_{\lambda\mu}(q) = C \int r^2 j_\lambda(qr) \left(\int \rho(r, \theta, \varphi) Y_{\lambda\mu} d\Omega \right) dr. \qquad (10.2.4)$$

Here j_λ is the spherical Bessel function of first kind. The transfer momentum, during the scattering process with a charged particle, is denoted by q. C is a normalization factor which might be chosen such that for $q = 0$ the density ρ_0 is obtained. Here we choose $C = 1$, which means that in momentum space we deal with the total charge instead of charge density.

Let us consider first the scalar term involved in the expression of the charge density. The volume conservation restriction yields a relation between the monopole and quadrupole coordinates:

$$\alpha_{00} = -\frac{1}{\sqrt{4\pi}} \sum_\mu |\alpha_{2\mu}|^2, \qquad (10.2.5)$$

As for the scalar charge density, one obtains:

$$\rho_{00}(q) = \frac{3Ze}{qR_0} j_1(qR_0) - \frac{3}{8\pi} ZeqR_0 j_1(qR_0) \sum_\mu |\alpha_{2\mu}|^2, \qquad (10.2.6)$$

Quantizing the quadrupole collective coordinate, we can define the transition mono-
pole operator, $\hat{\rho}_{00}$. The elastic monopole form-factor is obtained as the expectation
value of $\hat{\rho}_{00}$ on the ground state wave function in the collective space. Here we con-
sider alternatively the unprojected ground state and the projected states describing
the J-members of the ground band. In order to calculate the expectation values of the
monopole charge density operator in the states mentioned above we have to express
the coordinates in terms of boson operators through the canonical transformation:

$$\hat{\alpha}_{2\mu} = \frac{1}{k_p \sqrt{2}} \left(b_{p\mu}^{\dagger} + (-)^{\mu} b_{p-\mu} \right), \quad \hat{\pi}_{2\mu} = \frac{i k_p}{\sqrt{2}} \left((-)^{\mu} b_{p-\mu}^{\dagger} - b_{p\mu} \right). \quad (10.2.7)$$

The transformation relating the coordinates and conjugate momenta with the boson
operators $b_{p\mu}^{\dagger}, b_{p\mu}$, is determined up to a multiplicative constant, k_p. This is at our
disposal and will be fixed in several alternative ways described along this section.
The results for the average values, corresponding to the unprojected ground state and
J-projected states within the GCSM, are:

$$\langle \psi_g | \sum_{\mu} |\hat{\alpha}_{2\mu}|^2 | \psi_g \rangle = \frac{1}{k_p^2} \left(d^2 + \frac{5}{2} \right),$$

$$\langle \phi_{JM}^g | \sum_{\mu} |\hat{\alpha}_{2\mu}|^2 | \phi_{JM}^g \rangle = \frac{1}{k_p^2} \left(\frac{d^2}{2} + \frac{5}{2} \right) + \frac{d^2}{2k_p^2} \frac{I_J^{(1)}(d^2)}{I_J^{(0)}(d^2)}, \quad (10.2.8)$$

with

$$I_J^{(0)}(y) = \int_0^1 P_J(x) e^{y P_2(x)} dx, \quad I_J^{(1)}(y) = \frac{\partial I_J^{(0)}(y)}{\partial y}, \quad y = d^2, \quad d = \sqrt{2} d_p.$$

$$(10.2.9)$$

In the above expressions $P_J(x)$ denotes the Legendre polynomial of rank J. Denoting
by:

$$A(q) = \frac{3Ze}{qR_0} j_1(qR_0), \quad C(q) = -\frac{3}{8\pi} Zeq R_0 j_1(qR_0), \quad (10.2.10)$$

the matrix elements of the charge operator read:

$$\langle \psi_g | \hat{\rho}_{00}(q) | \psi_g \rangle = A(q) + \frac{1}{k_p^2} \left(d^2 + \frac{5}{2} \right) C(q), \quad (10.2.11)$$

$$\langle \phi_{JM}^{(g)} | \hat{\rho}_{00}(q) | \phi_{JM}^{(g)} \rangle = A(q) + C(q) \left[\frac{1}{2k_p^2} \left(d^2 + 5 \right) + \frac{d^2}{2k_p^2} \frac{I_J^{(1)}(d^2)}{I_J^{(0)}(d^2)} \right]. \quad (10.2.12)$$

These expressions correspond to Ze times the elastic form factor in the intrinsic and laboratory frame, respectively. In what follows we refer to them as total charge Q. In a previous chapter, simple expressions for the extreme regimes of near spherical and rotational behaviors have been obtained for the overlap integrals involved in the above equation. The results for the case of $J = 0$ state are:

$$\langle\phi_{00}^{(g)}|\sum_{\mu}|\hat{\alpha}_{2\mu}|^2|\phi_{00}^{(g)}\rangle = \frac{1}{2k_p^2}\left[\frac{d^4}{5} + d^2 + 5\right], \qquad d = \text{small (d} \leq 1),$$

$$\langle\phi_{00}^{(g)}|\sum_{\mu}|\hat{\alpha}_{2\mu}|^2|\phi_{00}^{(g)}\rangle = \frac{1}{k_p^2}\left[d^2 + 2 - \frac{2}{9}\frac{1}{d^2}\right], \qquad d = \text{large (d} \geq 3). \quad (10.2.13)$$

We recall that for well deformed nuclei, d is typically greater than three. In the low momentum regime ($qR_0 \ll 1$), the expression (10.2.6) is much simplified:

$$\rho_{00}(q) = Ze\left[1 - \frac{1}{10}\left(qR_0\right)^2 - \frac{1}{8\pi}\left(qR_0\right)^2\sum_{\mu}|\alpha_{2\mu}|^2\right]. \qquad (10.2.14)$$

Let us turn our attention to the quadrupole component of the charge density. Following the same procedure as in the case of the monopole component, we obtain:

$$\rho_{2\mu} = \int r^2 j_2(qr)\left[\int \rho(r, \theta, \varphi)Y_{2\mu}d\Omega\right]dr = \rho_0 R_0^3 j_2(qR_0)\alpha_{2\mu}. \qquad (10.2.15)$$

Under the restriction $qR_0 \ll 1$, the result is:

$$\rho_{2\mu} = \frac{3Ze}{40\pi}\left(qR_0\right)^2\alpha_{2\mu}. \qquad (10.2.16)$$

To conclude, in the second order expansion in the surface coordinates, the charge density is:

$$\rho_{\mu}(q) = \frac{3Ze}{qR_0}j_1(qR_0) - \frac{3}{8\pi}Ze(qR_0)j_1(qR_0)\sum_{\mu}|\alpha_{2\mu}|^2$$

$$+ \frac{3Ze}{4\pi}j_2(qR_0)\alpha_{2\mu}. \qquad (10.2.17)$$

Thus, ρ is expressed as a second order polynomial in α:

$$\rho_{\mu}(q) = A(q) + B(q)\alpha_{2\mu} + C(q)\sum_{\mu}|\alpha_{2\mu}|^2, \qquad (10.2.18)$$

with the coefficients depending on the transferred momentum, defined by Eq. (10.2.10) and:

$$B(q) = \frac{3Ze}{4\pi} j_2(qR_0).$$ (10.2.19)

In the intrinsic reference frame the expression becomes:

$$\rho_\mu(q) = A(q) + B(q)\left(\delta_{\mu,0}\beta\cos\gamma + (\delta_{\mu,2} + \delta_{\mu,-2})\frac{\beta\sin\gamma}{\sqrt{2}}\right) + C(q)\beta^2.$$
(10.2.20)

We notice that the surface of constant charge density is of an ellipsoidal form which is consistent with the liquid drop shape. Coupling a particle to such a core, the single particle motion would be determined by a quadrupole deformed mean field. In the boson representation, defined above, one obtains:

$$\hat{\rho}_\mu(q) = A(q) + \frac{5C(q)}{2k_p^2} + \frac{B(q)}{k_p\sqrt{2}}\left(b_{p\mu}^\dagger + (-)^\mu b_{p,-\mu}\right)$$
$$+ \frac{C(q)}{k_p^2}\hat{N}_p + \frac{C(q)}{2k_p^2}\left(b_{p\mu}^\dagger b_{p,-\mu}^\dagger + b_{p,-\mu}b_{p\mu}\right)(-)^\mu, \quad (10.2.21)$$

where $\hat{N}_p$ denotes the proton boson number operator. The boson term $\left(b_{p\mu}^\dagger b_{p-\mu}^\dagger + b_{p-\mu}b_{p\mu}\right)(-)^\mu$ has diagonal matrix elements in ground and beta bands much larger than the off-diagonal one. Moreover, the matrix elements do not depend on the angular momenta of the states involved. For this reason we shall replace it by its average value, which is equal to $2d_p^2$. Under these circumstances the zero component of the charge density operator becomes:

$$\hat{\rho}_0(q) = \mathcal{T} + \frac{B}{k_p\sqrt{2}}\left(b_{p0}^\dagger + b_{p0}\right) + \frac{C}{k_p^2}\hat{N}_p.$$ (10.2.22)

where

$$\mathcal{T} = A + \frac{C}{2k_p^2}(d^2 + 5).$$ (10.2.23)

Acting with this boson operator on the unprojected ground state, one obtains:

$$\hat{\rho}_0(q)\psi_g = \left[\left(\mathcal{T} + \frac{B}{\sqrt{2}k_p}d_p\right) + \left(\frac{B}{\sqrt{2}k_p} + \frac{Cd_p}{k_p^2}\right)b_{p0}^\dagger\right]\psi_g.$$ (10.2.24)

We recall the fact that the canonical transformation relating the quadrupole coordinate and conjugate momenta with the boson operators is determined up to a multiplicative constant which was denoted by k_p. Taking for this constant the value

$$k_p = -\frac{C}{B}d,$$ (10.2.25)

the unprojected ground state becomes eigenfunction for the boson operator $\hat{\rho}$:

$$\hat{\rho}_0(q)\psi_g = \left(A + \frac{B^2}{2C}\frac{5}{d^2}\right)\psi_g. \tag{10.2.26}$$

Considering the low momentum expansion for the coefficients A, B and C this equation becomes:

$$\hat{\rho}_0(q)\psi_g = Ze\left[1 - \frac{(qR_0)^2}{10}\left(1 + \frac{1}{2\pi d^2}\right)\right]\psi_g. \tag{10.2.27}$$

Thus, the parameter k_p has a very simple expression:

$$k_p = \frac{5}{2}d \tag{10.2.28}$$

Alternatively, the canonicity parameter could be determined in the following way. The stability condition for the average value of $\hat{\rho}$ on the unprojected ground state, against the variation of d provides the following equation for the deformation parameter d.

$$2Cd + k_pB = 0. \tag{10.2.29}$$

However, in our previous investigations d was fixed by fitting some energies in the ground band. We could keep those values for d and use Eq. (10.2.29) to determine k_p. We notice that the value of k_p obtained this way is twice as much as the one given by Eq. (10.2.25). In this case, the low momentum regime provides $k_p = 5d$.

At this stage it is worth recalling the way the canonicity parameter k_p was fixed within the GCSM model when the M1 and E2 properties were investigated. In the asymptotic regime, i.e. d large, the ground band energies can be expressed as [RUD87]:

$$E_J^g = \left[\frac{A_1 + A_2}{6d^2} + A_4\right]J(J+1). \tag{10.2.30}$$

Equating this expression with that given by the liquid drop model, one finds an equation relating the nuclear deformation with the parameter ρ:

$$\beta_0^2 = \frac{\pi}{3.24}\frac{\hbar^2}{M_N}A^{-5/3}\left[\frac{A_1 + A_2}{6d^2} + A_4\right]^{-1}. \tag{10.2.31}$$

Identifying this deformation with the average value of the second order invariant in α's coordinates and subtracting the zero point motion contribution one finds:

$$k_p = \frac{d}{\beta_0}. \tag{10.2.32}$$

Table 10.4 The values for the k_p/d ratio calculated in two alternative ways: (a) according to Eq. (10.2.31), as in Ref. [RUD87]

	^{152}Gd	^{154}Gd	^{156}Gd	^{158}Gd	^{160}Gd	^{154}Sm	^{164}Dy	^{168}Er	^{174}Yb	^{232}Th	^{238}U
β_0^{-1}	1.471	1.320	1.176	1.158	1.146	1.129	1.140	1.242	1.261	1.247	1.142
k_p/d	1.406	1.393	1.381	1.368	1.355	1.394	1.329	1.303	1.264	0.864	0.820

In this case the ratio is equal to β_0^{-1}, given by Eq. (10.2.31), and the resulting values are given in the first row; (b) the ratio is given by Eq. (10.2.25) for a transfer momentum $q = 0.54\,\text{fm}^{-1}$. The corresponding values are listed in the second row

In Table 10.4, the values of β_0^{-1} are compared with those of k_p/d given by Eq. (10.2.25). We notice that the two sets of data are quite close to each other.

10.2.3 Electric Monopole Transition

The scattering process where the colliding particle may be inside the target nucleus involves longitudinal momenta associated to the Coulomb field [BOH98]:

$$\mathcal{M}(C\lambda, \mu) = \int \rho(\mathbf{r}) f_\lambda Y_{\lambda\mu}(\theta, \varphi) d\tau, \tag{10.2.33}$$

where f_λ is a function depending on the radial motion of the particle inside nucleus. If the monopole Coulomb momentum is expanded in powers of r, then the lowest order term giving rise to an intrinsic transition is proportional to r^2. Therefore, the monopole operator responsible for the transition with $\lambda\pi = 0+$ is:

$$m(E0) = \int \rho(\mathbf{r}) r^2 d\tau. \tag{10.2.34}$$

where ρ denotes the electric charge density. Expanding ρ in terms of the liquid drop coordinates $\alpha_{2\mu}$, we obtain:

$$m(E0) = \rho_0 R_0^5 \left(\frac{4\pi}{5} + \sqrt{4\pi}\alpha_{00} + 2\sum_\mu |\alpha_{2\mu}|^2 \right). \tag{10.2.35}$$

Using the volume conservation condition for the monopole coordinate α_{00}, the final result for the monopole moment is:

$$m(E0) = \frac{3}{5} Ze R_0^2 \left[1 + \frac{5}{4\pi} \sum_\mu |\alpha_{2\mu}|^2 \right]. \tag{10.2.36}$$

The matrix element of this operator gives the amplitude for the transition probability between the involved state. In particular for the transition $J_\beta^+ \to J_g^+$ we obtain:

$$\rho(E0) \equiv \langle \phi_{JM}^{(\beta)} | m(E0) | \phi_{JM}^{(g)} \rangle = \frac{3\sqrt{5} Z e R_0^2}{8\sqrt{2} \pi k_p^2}. \tag{10.2.37}$$

Note that the amplitude for the monopole transition is not depending on the state angular momentum. Moreover, the same expression is obtained if the projected states are replaced by the unprojected ground and beta states, respectively.

In nuclei which exhibit shape coexistence, calculations of $E0$ transitions could provide a test for the mixing amplitudes of states with different deformations, defining the ground state [SGEC98]. For these cases, $\rho(E0)$ can be expressed in terms of the mixing coefficient λ and the difference between the r.m.s. associated to the states involved in the E0 transition, i.e. the beta state 0_β^+ and the ground state 0_g^+.

In what follows we shall show how the shape coexistence may be investigated within the GCSM approach. First we show that the monopole transition can be expressed in terms of r.m.s. radii of beta and ground bands. Indeed, using Eq. (10.2.36) for $m(E0)$ the r.m.s radii of the states from ground and beta bands are defined as:

$$\langle r^2 \rangle_J^g = \frac{3}{5} Z e R_0^2 \left[1 + \frac{5}{4\pi} \langle \phi_{JM}^{(g)} | \sum_\mu |\alpha_{2\mu}|^2 | \phi_{JM}^{(g)} \rangle \right],$$

$$\langle r^2 \rangle_J^\beta = \frac{3}{5} Z e R_0^2 \left[1 + \frac{5}{4\pi} \langle \phi_{JM}^{(\beta)} | \sum_\mu |\alpha_{2\mu}|^2 | \phi_{JM}^{(\beta)} \rangle \right], \tag{10.2.38}$$

Note that dividing the above expressions by Z, one obtains the charge radii in the states of angular momentum J. Both matrix elements involved in Eq. (10.2.38) can be expressed by the expectation value of the boson number operator $\hat{N}$, in the state J^+ from the ground band:

$$\langle r^2 \rangle_J^g = \frac{3}{5} Z e R_0^2 \left[1 + \frac{5}{8\pi k_p^2} \left(d^2 + 5 + 2\langle \phi_{JM}^{(g)} | \hat{N} | \phi_{JM}^{(g)} \rangle \right) \right],$$

$$\langle r^2 \rangle_J^\beta = \frac{3}{5} Z e R_0^2 \left[1 + \frac{5}{4\pi k_p^2} \left(d^2 + 7 + 2\langle \phi_{JM}^{(g)} | \hat{N} | \phi_{JM}^{(g)} \rangle \right) \right], \tag{10.2.39}$$

From these relations we obtain that the difference of the beta and the ground band r.m.s. does not depend on the angular momentum J. Moreover, the said difference is related to $\rho(E0)$ by a very simple equation:

$$\rho(E0) = \sqrt{\frac{5}{8}} \left(\langle r^2 \rangle_0^\beta - \langle r^2 \rangle_0^g \right). \tag{10.2.40}$$

In a previous chapter we saw that each projected state is a superposition of components with different quantum numbers K. However, the prevailing component has $K = 0$ for ground and beta bands and $K = 2$ for gamma band. Thus, the model is quite flexible for studying the band mixing. The question is whether the present formalism can be extended for studying the interaction between states of the same angular momenta and K. Indeed, GCSM can be used to describe the collective properties of both gamma stable, where $E_{0_\beta^+} < E_{2_\gamma^+}$, and gamma unstable nuclei when the ordering of the head states of beta and gamma bands is opposite to the one mentioned above. For the gamma stable nuclei there are cases where the state 0_β^+ is low in energy. An attempting interpretation for such a situation assumes that this state belongs to the second well of the potential energy in the β variable, while the ground state is located in the well with a less deformed minimum. In what follows we shall show that our model is able to account for this kind of shape coexistence. Indeed, if the potential barrier is not high one can expect that the system is tunneling from one well to another and therefore is reasonable to assume that the real ground state is in fact a linear combination of the states 0_g^+ and 0_β^+. To simplify the notations, the projected states with angular momentum zero from the ground and beta bands are hereafter denoted by $|0_g^+\rangle$ and $|0_\beta^+\rangle$, respectively. Adding to the model Hamiltonian a term which couples the states from ground and beta bands than the new Hamiltonian yields new eigenstates with angular momentum equal to zero:

$$|0\rangle_I = \sqrt{\lambda}|0_g^+\rangle + \sqrt{1-\lambda}|0_\beta^+\rangle,$$
$$|0\rangle_{II} = -\sqrt{1-\lambda}|0_g^+\rangle + \sqrt{\lambda}|0_\beta^+\rangle. \qquad (10.2.41)$$

Using the above results, one can calculate the amplitude of the $E0$ transition, relating the new states, i.e. $0_{II} \rightarrow 0_I$. The final results is:

$$\rho_{I,II}(E0) = \left[\sqrt{\lambda(1-\lambda)} + (2\lambda-1)\sqrt{\frac{5}{8}}\right]\left(\langle r^2\rangle_0^\beta - \langle r^2\rangle_0^g\right). \qquad (10.2.42)$$

Replacing $\rho_{II,I}(E0)$ by the corresponding experimental value, the relation (10.2.41) becomes an equation for the mixing coefficient λ. In conclusion, due to Eq. (10.2.41) the GCSM can provide information about the shape coexistence.

10.2.4 Numerical Results

Our numerical studies refer to the scalar term of the charge density as well as to the monopole transition from $0_\beta^+ \rightarrow 0_g^+$. In both cases one intends to draw a definite conclusion about the effect of projection on these quantities. Also, one investigates how the projection effect depends on the nuclear deformation.

Fig. 10.22 The total charges of ^{154}Gd in the ground band states with J = 0, 2, 4, 20, respectively, are plotted as function of the nuclear deformation for $qR_0 = 0.2$ (panel **a**) and $qR_0 = 1.2$ (panel **b**). The results for unprojected ground state are almost the same as for the projected $J = 0$ state and therefore is not plotted here. These calculations correspond to k_p given by Eq. (10.2.25)
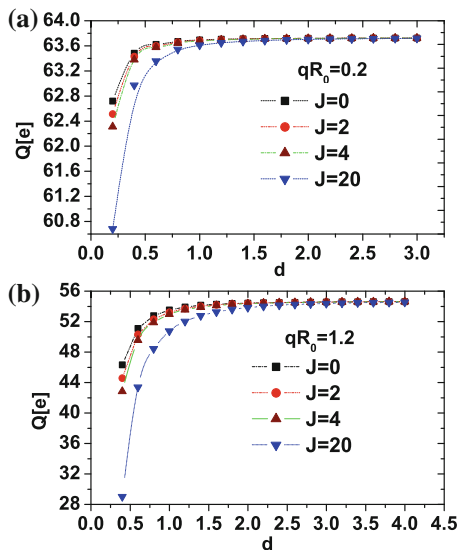
The matrix elements of the scalar part of the charge operator in the intrinsic and laboratory frame are given by Eqs. (10.2.11) and (10.2.12), respectively. The latter gives the q dependent charge of the system in the state J^+ of the ground band given by angular momentum projected state $\phi_{JM}^{(g)}$, while the former expresses the q dependent charge of the intrinsic ground state. In Fig. 10.22, the charge is represented as function of the deformation parameter d for $qR_0 = 0.2$ and $qR_0 = 1.2$ respectively. Calculations were made with R_0 corresponding to ^{154}Gd. For both qR_0 values, the charge of the system in the projected $J = 0$ state and in the unprojected ground state are indistinguishable. As one increases the angular momentum, the effect of projection is larger, particularly at smaller d values. The projection effect is vanishing for $d \geq 2$. In the limit of $d \rightarrow 0$, the matrix elements (10.2.12) exhibits the behavior given by:

$$\langle \phi_{JM}^{(g)} | \hat{\rho} | \phi_{JM}^{(g)} \rangle = A(q) - C(q) - \frac{J}{4d^2} B(q). \qquad (10.2.43)$$

Due to this feature, for small deformations a large fall down of the curves corresponding to $J = 20$ in Fig. 10.22, is obtained. For $d > 2$ the charges corresponding to the unprojected and the $J = 0, 2, 4, 20$ projected states, are about the same. The common value of Q is very close to the value 64, which is the nuclear charge of ^{154}Gd. Also, the deformation parameter of ^{154}Gd, determined in Ref. [RUD87] to be 3.0545, lies on the saturation plateau. Actually, this feature confirms that for deformed systems the strong coupling limit holds. The fact that for $qR_0 = 0.2$ the charge is close to the value 64 corresponds to the well-known fact that the form factor is close to one when $q \ll 1/R_0$, and that is consistent with the assumption of fast convergence of the expansion of the charge density in terms of the quadrupole

Fig. 10.23 The total charge of ^{156}Gd is plotted as function of the nuclear deformation for $qR_0 = 0.2$ (panel **a**) and $qR_0 = 1.2$ (panel **b**). The results for unprojected ground state cannot be distinguished from those corresponding to the projected $J = 0$ state
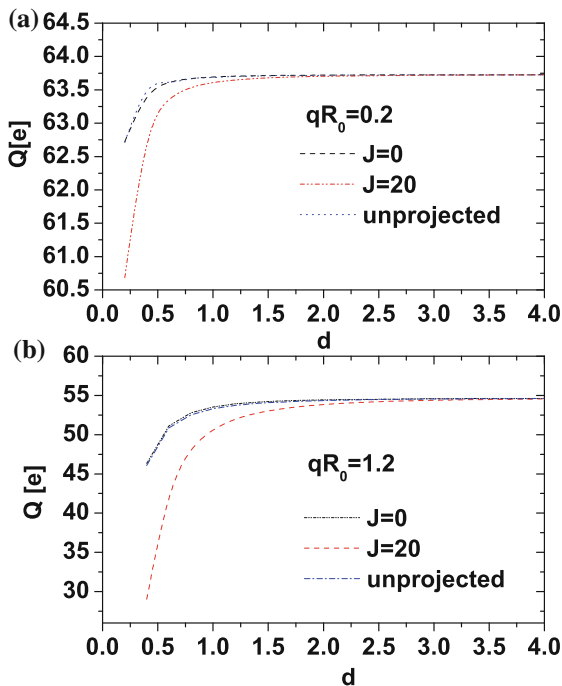
collective coordinates. A screening of charge for small deformation and large angular momentum is noticed. According to Fig. 10.22b, for large qR_0 the screening shows up also for unprojected as well as for projected ground state. Moreover, for small deformation the deviation of the charge in the state with $J = 20$ is substantially different from that corresponding to the ground state.

Similar features are seen in Fig. 10.23 where the charge is calculated for R_0 corresponding to ^{156}Gd with, according to Ref. [RUD87], the deformation parameter equal to 3.2195. Here only the results for $J = 0$ and $J = 20$ as well as for the unprojected ground state are shown although the latter are practically the same as for the projected 0^+ state. The screening effect for high transferred momentum, mentioned for ^{154}Gd, is less pronounced for ^{156}Gd, as indicated by Fig. 10.23b.

In conclusion, the projection operation does not affect the scalar q dependent charge of deformed systems in the ground state.

We note from Eqs. (10.2.11) and (10.2.12) that the total charge is determined by summing two distinct terms, one depending exclusively on the transferred momentum, that is denoted by $A(q)$, and a term which is a product of two factors depending on q and d, respectively. One may ask oneself what is the relative contribution of these terms to the total charge for non-vanishing q values. We answered this question by studying the ratios $Q/A(q)$ as function of qR_0 for two values of the deformation parameter d. Thus, in Fig. 10.24 we see that the term depending on deformation may affect the charge of the ground state at most by 15% for $qR_0 = 2$. In the state with
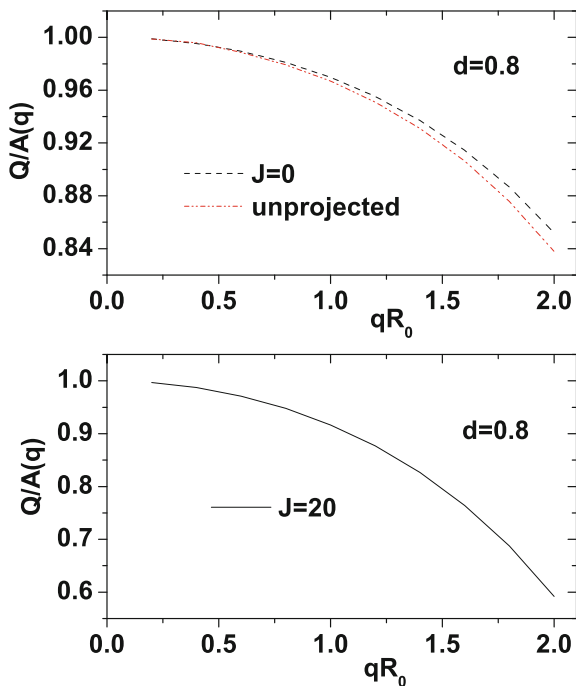
$J = 20$ and the quoted value of qR_0 the deformation relative contribution is of 40 %. For large nuclear deformation, d $= 3.2195$, the relative contribution of the deformation is ranging from zero to 5 % when qR_0 is increased from 0 to 2 (Fig. 10.25).

As already shown in the previous sections, the matrix elements of the charge density and monopole transition operator depend on the parameter k_p. This parameter is proportional to the deformation parameter d. In Fig. 10.26 we represent k_p/d as a function of the product qR_0, where R_0 stands for the nuclear radius. In the interval $(0, 2)$ for qR_0, the ratio is slowly decreasing from 2.5 to 2.2. Therefore, the value 2.5 obtained for k_p/d in the low momentum regime could be considered as a reasonable approximation for the whole interval considered in Fig. 10.22.

Now let us focus our attention on the monopole transition $0^+_\beta \to 0^+_g$. The transition amplitude was calculated with Eq. (10.2.37). We notice that the monopole transition operator $m(E0)$ has an expression identical with that supplied by the liquid drop model. However, the wave functions are specific to the GCSM and they may describe the spherical and deformed nuclei in a unified fashion. Another feature which is specific to our description is the canonicity parameter k_p defining the equations which relate the coordinates and conjugate momenta to the boson operators. Within the liquid drop model in its original form the canonicity parameter is chosen such that the boson Hamiltonian does not contain a term like $\sum_\mu (-)^\mu \left(b^\dagger_{2\mu} b^\dagger_{2-\mu} + b_{2-\mu} b_{2\mu} \right)$. This idea is not applicable to GCSM, since the starting Hamiltonian is anharmonic and, moreover, is already considered in the boson picture. Here we present the results

Fig. 10.25 The same as in
Fig. 10.24 but for d = 3.2195
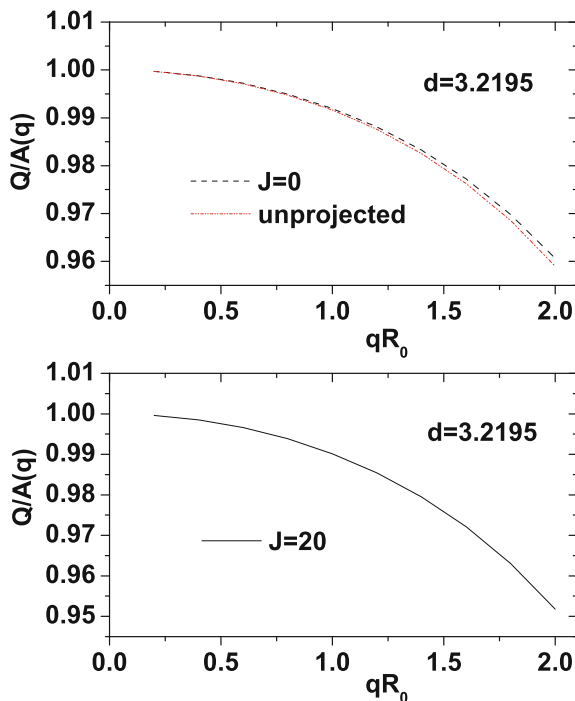
Fig. 10.26 The ratio k_p/d
with k_p given by
Eq. (10.2.25), is plotted as
function of qR_0. The curve
corresponds to a deformation
parameter $d = 3.2195$
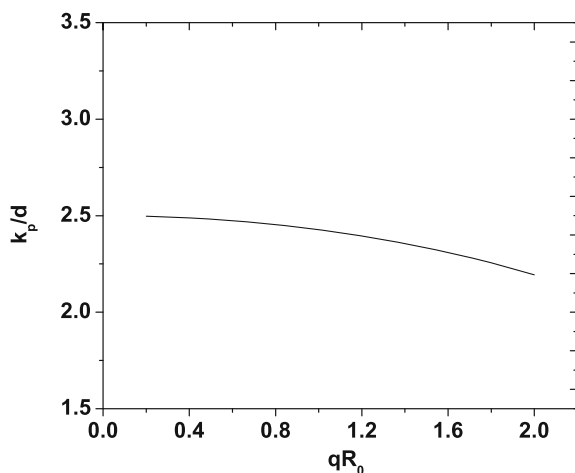
obtained by fixing k_p in three different ways: (a) From the minimum condition
for the charge density and the low momentum transfer restriction. This provides a
simple expression for $k_p(=5d)$; (b) Requiring that the unprojected ground state is
an eigenstate of the scalar part of the charge density operator. Note the fact that
this condition is fulfilled automatically in microscopic models where a many body

Table 10.5 The monopole transition amplitudes predicted by Eq. (10.2.37) are compared with the experimental data taken from Refs. [LKH82, ISS04, WZCH99, GAR01, GAC01, KISP05, WIM08]

	$\rho(E0)[e.\,\text{fm}^2]$			
	Th., $k_p = \frac{5}{2}d$	Exp.	Th., $k_p = 5d$	Th., k_p from Ref. [RUD87]
^{152}Gd	9.105	10.23 ± 1.15^a	2.276	26.284
^{154}Gd	8.574	11.749 ± 0.101^a	2.143	30.765
^{156}Gd	7.784	7.469 ± 0.071^a	1.946	35.170
^{158}Gd	6.286	5.487 ± 0.465^b	1.571	29.282
^{160}Gd	5.606		1.401	26.688
^{154}Sm	7.116	12.818 ± 2.551^e	1.779	34.912
^{164}Dy	5.804		1.451	27.341
^{168}Er	5.820	$1.24 \pm 0.51^{b,f}$	1.455	23.567
^{174}Yb	6.083	$<1.85\ ^e$	1.521	23.906
^{232}Th	11.731	13.646 ± 4.88^b	2.933	47.142
^{238}U	11.228	5.502 ± 0.05^c	2.807	53.847
		23.2 ± 2.262^c		

Equation (10.2.37) have been used alternatively for k_p for which the charge density operator admits the unprojected ground state as eigenfunction (first column) and for k_p which were used in Ref. [?] to describe the M1 and E2 properties of the nuclei listed in this Table

[a] [LKH82]
[b] [ISS04, WZCH99]
[c] [GAC01]
[d] [KISP05]
[e] [WIM08]
[f] [GAR01]

Slater determinant is eigenstate of the charge density operator. For a low momentum regime, the mentioned condition provides $k_p = \frac{5}{2}d$; (c) As in Ref. [RUD87] i.e., $k_p = \frac{d}{\beta_0}$, with β_0 fixed by equating the expressions of the asymptotic energies in the ground band and that of the liquid drop model in the large deformation regime. The results of our calculations obtained with the three versions of fixing k_p are given in Table 10.5. The predictions are compared with the available experimental data for ten nuclei. Notice that the data from the quoted references were transformed by multiplying them with the factor R_0^2.

By inspection of Table 10.5, we notice that except for the cases of ^{168}Er and ^{174}Yb all the other data are reasonably well described by choosing $k_p = \frac{5}{2}d$. For ^{168}Er and ^{174}Yb, it seems that the version which provides $k_p = 5d$ yields a good agreement with the corresponding experimental data. Using the parameter k_p from Ref. [RUD87], which corresponds to a consistent description of the E2 and M1 properties, one obtains $\rho(E0)$ values which exceed the experimental data by a factor ranging from 2.6 to 5.

These discrepancies could be attributed to the fact that the collective coordinates respond differently to the interaction with longitudinal and transverse components of

the electromagnetic external field, respectively. The former components may determine a E0 excitation while the latter one, can excite the nuclei through, for example, a $E2$ transition. The fact that different k_p are needed to reproduce E2 and E0 properties suggests that these are independent features. In other words the E0 properties are not determined by the E2 ones and this perhaps expresses the need to introduce the monopole bosons.

According to Table 10.4, the values of k_p provided by the procedure labeled by (c) infer a large transfer momentum, while those defined by (a) and (b) are obtained under the low momentum restriction. We would like to mention that the model Hamiltonian used by GCSM is a fourth order boson Hamiltonian, while the charge density expansion in collective quadrupole coordinates is truncated at second order. This lack of consistency might be another source for the discrepancy between the values of k_p obtained here and those given in Ref. [RUD87].

Note that the set of nuclei considered involves a chain of even isotopes of Gd. Along this chain the shape undertakes a transition from a spherical to a deformed one. The critical point of this transition is met in ^{154}Gd [CLCR04]. In the group theory language the transition takes place between nuclei with SU(5) symmetry and nuclei having SU(3) symmetry. It was suggested that the critical point corresponds to an unknown symmetry called X(5) symmetry [IA01]. This shape transition was also studied within the GCSM formalism in Ref. [RF05]. Here we raised the question whether this shape transition is reflected in a specific manner by the behavior of the E0 transition amplitude. To explore this feature we plotted the predicted as well as the experimental $\rho(E0)$ values as function of $A^{2/3}$, in Fig. 10.27. Note that the experimental results exhibit, indeed, a maximum for A = 154. The theoretical results were interpolated by a fourth order polynomial which presents an inflexion point for the critical value of A. Thus, we may say that the shape transition is reflected by the fact that an inflexion point shows up in the behavior of the transition amplitude.

Fig. 10.27 The predicted values of $\rho(E0)$ for some even isotopes of Gd, are represented as function of $A^{2/3}$. For comparison the experimental results are also given
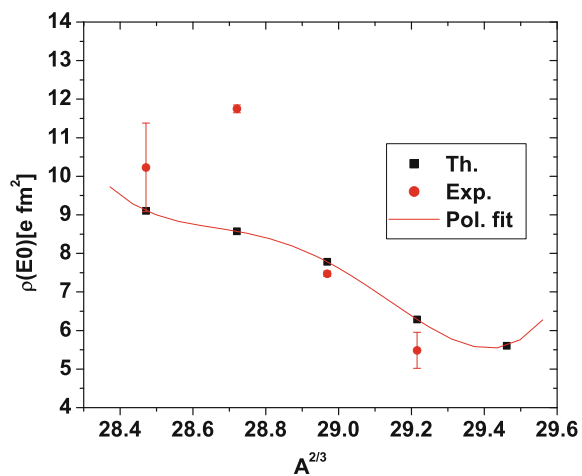
Summarizing, the GCSM is used to study the ground state band charge density as well as the E0 transitions from 0^+_β to 0^+_g. The influence of the nuclear deformation and of angular momentum projection on the charge density is investigated. The monopole transition amplitude was calculated for ten nuclei. The results are compared with some previous theoretical studies and with the available experimental data. Our results concerning angular momentum projection are consistent with those of previous microscopic calculations for the ground state density. The calculations for the E0 transitions agree quite well with the experimental data. Issues like how the shape transitions or shape coexistence are reflected in the $\rho(E0)$ behavior are also addressed.

Chapter 11
Boson States Basis

11.1 Eigenstates for a Harmonic Hamiltonian

Let us consider the Hamiltonian associated to a harmonic liquid drop:

$$H = \frac{1}{2} \sum_{m=-2}^{2} (-1)^m \left(\pi^m \pi^{-m} + \alpha_m \alpha_{-m} \right), \tag{11.1.1}$$

The chosen units system is that where the mass parameter, oscillator strength and the Plank constant $\hbar$ are equal to 1. The quadrupole coordinate and momenta obey the conditions:

$$\alpha_m^* = (-1)^m \alpha_{-m}, \quad \pi^m = -i \frac{\partial}{\partial \alpha_m}, \quad -2 \le m \le 2. \tag{11.1.2}$$

Let V be the linear manifold of quintuplets, $\alpha = (\alpha_{-2}, \alpha_{-1}, \alpha_0, \alpha_1, \alpha_2)$ with components satisfying the above mentioned conditions. These conditions together with the one asserting that α is a tensor of rank 2 are assured by the fact the nuclear radius is a real quantity.

The orthogonal group R_5 is defined as the set of linear transformations on V which leaves the following quadratic form invariant:

$$I_2(\alpha) = \sum_{m=-2}^{2} (-1)^m \alpha_m \alpha_{-m} = \beta^2, \quad \beta \ge 0. \tag{11.1.3}$$

Note that R_5 is a symmetry group for H. Let us denote by R_3' the subgroup of R_5 formed of all transformations given by the matrices $D^2(\Omega)$ for the irreducible representations (IR) of the ternary orthogonal group R_3, with the angular momentum equal to 2. Transformations from R_3' leave invariant not only I_2 but also:

$$I_3(\alpha) = \alpha_0^3 - 3\alpha_{-1}\alpha_0\alpha_1 - 6\alpha_{-2}\alpha_0\alpha_2$$
$$+ \frac{3}{2}\sqrt{6}\left(\alpha_{-1}^2\alpha_2 + \alpha_1^2\alpha_{-2}\right) = \beta^3\cos 3\gamma. \qquad (11.1.4)$$

The tensor α can be expressed in terms of intrinsic coordinates and the Euler angles as:

$$\alpha_m = \beta\left\{\cos\gamma D_{m0}^{2*}(\Omega) + \sqrt{\frac{1}{2}}\sin\gamma\left[D_{m2}^{2*}(\Omega) + D_{m-2}^{2*}(\Omega)\right]\right\}, \qquad (11.1.5)$$

where Ω stands for the Euler angles defining the rotation which brings the laboratory reference frame to the body fixed (intrinsic) frame whose axes are oriented along the principal axes of the inertial ellipsoid.

It is worth mentioning that the transformation $(\beta, \gamma, \Omega) \rightarrow \alpha$ is not biunivoc. Indeed, for a given α of V there is a set of points (β, γ, Ω) which satisfy Eq. 11.1.5, which define an orbit of the octahedral symmetry group of the nuclear surface.

Consider the Fock space S where the eigenfunctions of H is complete. Vectors from S are complex functions defined on V, quadratic integrable with respect to the measure on V, defined as:

$$d^5\alpha = \frac{3}{2\pi^2}d\alpha_0\Pi_{m=1}^2(d\,\Re\alpha_m d\,\Im\alpha_m) = \frac{3}{4\pi^2}\beta^4|\sin 3\gamma|d\beta d\gamma d\Omega, \qquad (11.1.6)$$

where $d\Omega$ is the Haar measure on the group R_3. Note that if the scalar product in S is defined in terms of intrinsic variables β, γ, Ω in the intervals $[0, \infty)$; $[0, 2\pi]$; $[0, 2\pi] \times [0, \pi] \times [0, 2\pi]$, then the result should be divided by 24, the order of the octahedral group. In building up the eigenfunctions one uses the tensors of rank 2 and 3, defined by:

$$Y_2(\alpha) = 2\sqrt{2}\alpha_2\alpha_0 - \sqrt{3}\alpha_1^2,$$
$$Y_3(\alpha) = 2\alpha_{-1}\alpha_2^2 - \sqrt{6}\alpha_0\alpha_1\alpha_2 + \alpha_1^3. \qquad (11.1.7)$$

In the intrinsic frame, the Hamiltonian H looks like:

$$H = \frac{1}{2}\left(-\beta^{-4}\frac{\partial}{\partial\beta}\beta^4\frac{\partial}{\partial\beta} + \beta^{-2}\Lambda^2 + \beta^2\right), \qquad (11.1.8)$$

where

$$\hat{\Lambda}^2 = -(\sin 3\gamma)^{-1}\frac{\partial}{\partial\gamma}\sin 3\gamma\frac{\partial}{\partial\gamma} + \sum_{k=1}^3\left[4\sin^2(\gamma - \frac{2}{3}\pi k)\right]^{-1}L_k^2. \qquad (11.1.9)$$

is the square of the Casimir operator of the group R_5. We denoted by L_k the angular momentum components in the intrinsic frame.

The coordinate α and its conjugate momentum can be expressed in terms of the boson operators:

$$b_m^\dagger = \frac{1}{\sqrt{2}}\left(\alpha_m - (-1)^m \frac{\partial}{\partial \alpha_{-m}}\right),$$

$$b_m = \frac{1}{\sqrt{2}}\left((-1)^m \alpha_{-m} + \frac{\partial}{\partial \alpha_m}\right). \qquad (11.1.10)$$

The spectrum of H is $n + \frac{5}{2}$ with n denoting the number of bosons in the eigenfunction, while that of Λ^2 has also a simple form as function of the seniority quantum number λ, i.e. $\lambda(\lambda + 3)$. This defines the number of bosons which are not paired to an angular momentum equal to zero.

The above statements result from the relations which connect the boson number operator $\hat{N}$ to the Hamiltonian and the Casimir operator Λ^2:

$$\hat{N} = \sum_{m=-2}^{2} b_m^\dagger b_m = H - \frac{5}{2},$$

$$\hat{\Lambda}^2 = \hat{N}(\hat{N} + 3) - 5(b^\dagger b^\dagger)_0 (bb)_0. \qquad (11.1.11)$$

Hamiltonian H is invariant to the rotations R_3 generated by the angular momentum components in the laboratory reference frame:

$$\hat{J}_0 = \sum_{m=-2}^{2} m\alpha \frac{\partial}{\partial \alpha_m},$$

$$\hat{J}_+ = 2\left(\alpha_2 \frac{\partial}{\partial \alpha_1} + \alpha_{-1} \frac{\partial}{\partial \alpha_{-2}}\right) + \sqrt{6}\left(\alpha_1 \frac{\partial}{\partial \alpha_0} + \alpha_0 \frac{\partial}{\partial \alpha_{-1}}\right),$$

$$\hat{J}_- = 2\left(\alpha_1 \frac{\partial}{\partial \alpha_2} + \alpha_{-2} \frac{\partial}{\partial \alpha_{-1}}\right) + \sqrt{6}\left(\alpha_0 \frac{\partial}{\partial \alpha_1} + \alpha_{-1} \frac{\partial}{\partial \alpha_0}\right) \qquad (11.1.12)$$

In conclusion, H commutes with the operators $\hat{N}$ and $\hat{\Lambda}^2$, $\hat{J}^2$, $\hat{J}_0$ and consequently its eigenfunction can be indexed by the quantum numbers which are eigenvalues of the mentioned operators. On the other hand the above operators are Casimir operators for the groups $SU(5)$, R_5, R_3 and R_2, respectively. This fact suggests that the eigenfunctions of H can be classified according to the reduction chain of the symmetry group $U(5)$: $U(5) \supset SU(5) \supset R_5 \supset R_3 \supset R_2$. Having in mind that there might be several irreducible representations (IR) for R_3 which correspond to the same IR of R_5, an additional index, p, is necessary to distinguish the IR of R_3. This is called as degeneracy quantum number. We mention that there is no intermediary group between R_5 and R_3 whose Casimir operator may distinguish the degenerate states of R_3. This is the reason why the quantum number p is referred to as *the missing quantum number*. Therefore the eigenfunctions of H classified according to the

above mentioned scheme are denoted by: $|n \lambda p I M\rangle$. In Refs. [GRC78, RCG78] these functions were analytically expressed alternatively as function of the coordinates α, the intrinsic frame coordinates β, γ, Ω and the quadrupole bosons $b_m^\dagger$. Moreover, the matrix elements of any interaction expressed as polynomial of the alpha coordinates are also analytically given.

In what follows we shall sketch the procedure used in the mentioned references, for deriving the analytical expressions for the eigenfunctions of H.

Aiming at this goal we consider the form (11.1.8) and the associated eigenvalue equation. Using the variable separation method one obtains that β is separated and the corresponding differential operator has analytical solution. Since there is no Casimir operator for the missing quantum number the separation of γ and Ω is not possible.

Therefore the variable separation method leads to the following form of the wave function:

$$|n\lambda p I M\rangle = F_{n\lambda}(\beta) \sum_{\substack{0 \le K \le I \\ K=even}} G_{\lambda p I K} \left[D_{MK}^{I*}(\Omega) + (-1)^I D_{M-K}^{I*}(\Omega) \right]. \quad (11.1.13)$$

where

$$F_{n\lambda} = \left[2(\frac{1}{2}(n-\lambda))! \right]^{\frac{1}{2}} \left[\Gamma(\frac{1}{2}(n+\lambda+5)) \right]^{-\frac{1}{2}} \beta^\lambda L_{\frac{1}{2}(n-\lambda)}^{\lambda+\frac{3}{2}}(\beta^2) exp(-\frac{1}{2}\beta^2). \quad (11.1.14)$$

$L_{\frac{1}{2}(n-\lambda)}^{\lambda+\frac{3}{2}}(\beta^2)$ denotes the Laguerre polynomials. Functions $F_{n\lambda}$ are orthonormal in the interval $[0, \infty)$ with the measure $\beta^4 d\beta$. Also the functions $\{[(2I+1)/8\pi^2]^{\frac{1}{2}} D_{MK}^I\}$ are orthonormal on R_3 with the measure $d\Omega$.

For what follows it is useful to introduce the notations:

$$F_{n\lambda} = (-1)^{\frac{1}{2}(n-\lambda)} \beta^\lambda \Phi_{n\lambda}(\beta),$$

$$Q_{\lambda p I M}(\alpha) = \beta^\lambda \sum_{\substack{0 \le K \le I \\ K=even}} G_{\lambda p I K}(\gamma)[D_{MK}^{I*}(\Omega) + (-1)^I D_{M-K}^{I*}(\Omega)]. \quad (11.1.15)$$

One can show that the new functions $Q_{\lambda p I M}$ obey the equations:

$$\hat{N}' Q_{\lambda p I M} = \lambda Q_{\lambda p I M}, \quad \Delta Q_{\lambda p I M} = 0, \quad (11.1.16)$$

where N' is the Euler operator and Δ the Laplace operator in 5D.

$$\hat{N}' = \sum_{m=-2}^{2} \alpha_m \frac{\partial}{\partial \alpha_m}, \quad \hat{\Delta} = \sum_{m=-2}^{2} (-1)^m \frac{\partial^2}{\partial \alpha_m \partial \alpha_{-m}}. \quad (11.1.17)$$

Equation (11.1.16) asserts that Q's are harmonic and homogeneous polynomials of degree λ. The Casimir operator Λ^2 can be expressed in terms of the Euler and Laplace operators:

$$\hat{\Lambda}^2 = \hat{N}'(\hat{N}' + 3) - \beta^2 \hat{\Delta}. \tag{11.1.18}$$

In Ref. [VIL68] it was proved that the solutions for the harmonic and homogeneous polynomials are:

$$Q_{\lambda p II} = E \left\{ \alpha_2^{-\lambda + I + 3p} \frac{\partial^q}{\partial \alpha_{-2}^q} [Q_{r, p+q}(\alpha)] \right\} \tag{11.1.19}$$

where the polynomials $Q_{r, p+q}$ are defined by:

$$Q_{r, p+q}(\alpha) = \frac{2^{-p-q-r}[2(p + q + r)]!}{(p + q)!(p + q + r)!} E \left\{ [Y_3(\alpha)]^r [I_3(\alpha)]^{p+q} \right\}. \tag{11.1.20}$$

The operator E is the projection operator of homogeneous polynomials onto the harmonic and homogeneous polynomials. Several restrictions and definitions have been used:

$$q = \lambda - \frac{1}{2}(I + 3r) - 3p, \quad r = \frac{1}{2}[1 - (-1)^I],$$

$$\lambda - I \leq 3p \leq \lambda - \frac{1}{2}(I + 3r). \tag{11.1.21}$$

The eigenfunctions of H, $|n\lambda p I M\rangle$, defined above as homogeneous and harmonic polynomials, form a complete set of functions. Using the recipe of projecting the homogeneous polynomials [VIL68], the polynomials Q may be written as linear combination of tensors of rank I with coefficients expressed as functions of the invariants I_2 and I_3.

$$Q_{\lambda p II}(\alpha) = \sum_{h=0}^{\frac{1}{2}(I - 3r)} P_{\lambda I p h}(I_2(\alpha), I_3(\alpha)) R_{Ih}(\alpha). \tag{11.1.22}$$

The factors involved in the sum have the expressions:

$$P_{\lambda I p h}(I_2(\alpha), I_3(\alpha)) = \sum_s {}_3F_2(\lambda - I - 3p, q + 1, q - h - 3sI; -\lambda - \frac{1}{2}, q - h + I; 1)$$

$$\times \frac{(-1)^s 2^{-p-3-\frac{1}{2}h}(-3)^h q!(3s)![2(p + q + r - s)]!}{h!(q - h)!s!(p + q + r - s)!(p + q - h - 2s)!(-q + h + 3s)!}$$

$$\times [I_2(\alpha)]^{-q+h+3s}[I_3(\alpha)]^{p+q-h-2s},$$

$$R_{Ih}(\alpha) = \alpha_2^{\frac{1}{2}(I - 3r) - h}[Y_2(\alpha)]^h [Y_3(\alpha)]^r \tag{11.1.23}$$

The symbol $_3F_2$ represents the generalized hypergeometric function. Further, Eq. (11.1.15) is used to identify the coefficients $G_\lambda pIK(\gamma)$. The final result is:

$$G_{\lambda pIK}(\gamma) = \sum_{h=0}^{\frac{1}{2}(I-3r)} (1+\delta_{K0})^{-1} T_{IKh}(\gamma) P_{\lambda pIh}(1, \cos 3\gamma), \qquad (11.1.24)$$

where $P_{\lambda pIh}(1, \cos 3\gamma)$ is obtained from Eq. (11.1.23) by replacing $I_2(\alpha) = 1$, $I_3(\alpha) = \cos 3\gamma$, while the factor T has the expression:

$$T_{IKh}(\gamma) = \left[\frac{(I+K)!(I-K)!}{(2I)!}\right]^{\frac{1}{2}} 2^{\frac{1}{4}(I+3r+6h)} 3^{\frac{1}{4}(I-r)} K^r h! \sum_{u=0}^{h} \sum_{v=0}^{[\frac{1}{4}(I-K-r-2u)]}$$

$$\times \frac{(\frac{1}{2}(I-3r)-u)!(-\frac{1}{12}\sqrt{3}\sin 3\gamma)^{r+u}(\cos\gamma)^{\frac{1}{2}(I-K-r)+h-2u-2v}(\frac{1}{6}\sqrt{3}\sin\gamma)^{\frac{1}{2}K-r-u+2v}}{u!v!(h-u)!(v+\frac{1}{2}K)!(\frac{1}{2}(I-K-r)-u-2v)!}.$$
$$(11.1.25)$$

Here the simbol $[x]$ was used for the integer part of x. Denoting by $\mu_{\lambda pI}$ the norm of function $|n\lambda pIM\rangle$ we have:

$$\mu_{\lambda pI}^{-2} = \langle n\lambda pIM|n\lambda pIM\rangle$$

$$= [2(2I+1)]^{-1} \sum_{\substack{0 \le K \le I \\ K=even}} (1+\delta_{K0}) \int_0^{2\pi} |\sin 3\gamma||G_{\lambda pIK}(\gamma)|^2 d\gamma. \quad (11.1.26)$$

In what follows we shall use the function of γ defined as:

$$\Psi_{\lambda pIK}(\gamma) = \mu_{\lambda pI} G_{\lambda pIK}. \qquad (11.1.27)$$

Having already the general expression for the function of γ, we shall give few results which are useful in concrete applications.

(A) A yrast state is characterized by the following relations: $n = \lambda = \frac{1}{2}(I + 3r)$, $p = 0$. In this case the function depending on γ has a simple expression:

$$\Psi_{\frac{1}{2}(I+3r),0,I,K}(\gamma) = 2^{\frac{1}{2}(I-r)+1} 3^{\frac{1}{4}(I-3r-2)} \pi^{-\frac{1}{4}} (1+\delta_{K0})^{-1} \left\{ \frac{(I+K)!(I-K)!\Gamma(\frac{1}{2}(I+5+3r))}{[(I+1)(I+2)]^r(2I)!(\frac{1}{2}(I-3r))} \right\}^{\frac{1}{2}}$$

$$\times (-K\sin 3\gamma)^r \sum_{v=0}^{[\frac{1}{4}(I-K-r)]} \frac{(\cos\gamma)^{\frac{1}{2}(I-K-3)-2v}(\frac{1}{6}\sqrt{3}\sin\gamma)^{\frac{1}{2}K-3+2v}}{v!(v+\frac{1}{2}K)!(\frac{1}{2}(I-K-r)-2v)!}.$$
$$(11.1.28)$$

(B) In the case of states with low angular momentum it is advantageous to express the functions $P_{\lambda pIh}$ in terms of Gegenbauer polynomials C_t^ν, defined by means of the generating function:

$$(1 - 2x \cos 3\gamma + x^2)^{-\nu} = \sum_{t=0}^{\infty} C_t^\nu (\cos 3\gamma) x^t. \tag{11.1.29}$$

The final result of expanding the functions P in terms of Gegenbauer polynomials is:

$$P_{\lambda pIh}(1, \cos 3\gamma) = \sum_s \frac{2^{q - \frac{1}{2}h} (\frac{1}{2}(I - 3r) - q)! \Gamma(\frac{1}{2} + r + s)}{h! \Gamma(\lambda + \frac{3}{2}) \Gamma(\frac{1}{2} + r)} C_{p+q+h-2s}^{\frac{1}{2}+r+s} (\cos(3\gamma))$$

$$\times \left[\sum_{k,u} \frac{(-1)^{s+k} 3^{s-u} (q+k)! \Gamma(\lambda - k + \frac{3}{2})}{k! u! (\frac{1}{2}(I - 3r) - q - k)! (q - s + k - 2u)! (2s - q - h + u - k)!} \right]. \tag{11.1.30}$$

Using this expression one obtains for the wave functions with the angular momentum $I = 0, 2, 3, 5$ compact expressions:

$$\Psi_{3(p+r),p,3r,2r}(\gamma) = \nu_{3r,p} (-\sin 3\gamma)^r C_p^{\frac{1}{2}+r} (\cos 3\gamma), \tag{11.1.31}$$

$$\Psi_{3p+3r+\rho,p,2+3r,2r}(\gamma) = 2^{\frac{1}{2}(r-1)} (-1)^{\rho-1} \nu_{2+3r,p} (-\sin 3\gamma)^r$$

$$\times \left[C_{p-\rho+1}^{\frac{3}{2}+r} (\cos 3\gamma) \cos \gamma - C_{p+\rho-2}^{\frac{3}{2}+r} (\cos 3\gamma) \cos 2\gamma \right]$$

$$\Psi_{3p+3r+\rho,p,2+3r,2+2r}(\gamma) = (-1)^{\rho-1} \nu_{2+3r,p} (-\sin 3\gamma)^r$$

$$\times \left[C_{p-\rho+1}^{\frac{3}{2}+r} (\cos 3\gamma) \sin \gamma + C_{p+\rho-2}^{\frac{3}{2}+r} (\cos 3\gamma) \sin 2\gamma \right].$$

The newly introduced indices take the values: $r = 0, 1, \quad \rho = 1, 2$. The factors ν are:

$$\nu_{0p} = \frac{1}{2} (2p+1)^{\frac{1}{2}}, \quad \nu_{3p} = \left[\frac{7(2p+3)}{2(p+1)(p+2)} \right]^{\frac{1}{2}},$$

$$\nu_{2p} = \left[\frac{2}{5}(p+1) \right]^{-\frac{1}{2}}, \quad \nu_{5p} = 3 \left[\frac{2}{11}(p+1)(p+2)(p+3) \right]^{-\frac{1}{2}}. \tag{11.1.32}$$

(C) These equations are very useful when one intends to calculate the reduced transition probabilities within the liquid drop model. Note that for such cases one needs to calculate two types of matrix elements: (a) m.e. of powers of $\cos \gamma$ and $\sin \gamma$ between functions Ψ with the expressions from above; (b) m.e. for the powers β^l. Such m.e. have also analytical expressions:

$$\int_0^\infty \Phi_{n'\lambda'}(\beta)\Phi_{n\lambda}(\beta)\beta^{\lambda+\lambda'+l+4}e^{-\beta^2}\,d\beta = (-1)^{\frac{1}{2}(n-\lambda)+\frac{1}{2}(n'-\lambda')}$$

$$\times \left[\frac{(\frac{1}{2}(n'-\lambda'))!\Gamma(\frac{1}{2}(n'+\lambda'+5))}{(\frac{1}{2}(n-\lambda))!\Gamma(\frac{1}{2}(n+\lambda+5))}\right]^{\frac{1}{2}}$$

$$\times \sum_m \frac{(-1)^m \Gamma\left(m+\frac{1}{2}(\lambda+\lambda'+l+3)+1\right)\Gamma\left(\frac{1}{2}(n-\lambda')-m-\frac{1}{4}l\right)}{m!(\frac{1}{2}(n'-\lambda')-m)!\Gamma\left(\lambda'+m+\frac{5}{2}\right)\Gamma\left(\frac{1}{2}(\lambda-\lambda')-m-\frac{1}{2}l\right)}.$$

$$(11.1.33)$$

With these, the necessary information to perform calculations with Hamiltonians derived from that of the liquid drop is complete. Readers who want to have some intermediate steps in deriving the above mentioned results are advised to consult Refs. [GRC78, RCG78]. Alternative solutions for the eigenfunctions of the liquid drop Hamiltonian may be also found in Refs.[CHMO76, CMW76]. The advantage of the formalism given here consists of that it provides m.e of compact and simple form. Indeed, as shown in [RCG78] they can be written as ratios of products, each factor being linear combination of the quantum numbers n, λ, p, I.

11.2 The Degeneracy of the Boson Basis

Quadrupole collective properties of nuclei can be described by diagonalizing a quadrupole boson Hamiltonian in the basis $|N_2 v_2 \alpha_2 I_2 M_2\rangle$ associated to the irreducible representation corresponding to the group reduction chain $SU(5) \supset R_5 \supset R_3 \supset R_2$. The quantum numbers N_2 (the number of quadrupole bosons), v_2 (seniority) and I_2 (angular momentum) are determined by the eigenvalues of the Casimir operators of the groups $SU(5)$, R_5 and R_3, respectively. The angular momentum projection on the axis z is denoted by M_2. Here, α_2 denotes the missing quantum number and labels the R_3 irreducible representations which are characterized by the same angular momentum I and belong to the same irreducible representation of R_5. The name suggests the absence of an intermediate group between R_5 and R_3 having a Casimir operator whose eigenvalues could distinguish the states of the same I_2 belonging to the same irreducible representation of R_5, v_2.

It is desirable to have an analytical solution for the number of distinct values acquired by α_2 for a fixed pair of v_2 and I_2, denoted by $d_{v_2}(I_2)$. Of course for each (v_2, I_2) one knows to calculate $d_{v_2}(I_2)$ numerically, as the number of solutions (p_2) for the double inequality:

$$v_2 - I_2 \le 3p_2 \le v_2 - \frac{1}{2}(I_2+3r_2), \quad r_2 = \frac{1}{2}\left[1-(-)^{I_2}\right]. \qquad (11.2.1)$$

Algorithms for calculating the multiplicity of the irreducible representations in the chain $SU(5) \supset R_5 \supset R_3 \supset R_2$, different from the one described here are presented in Refs. [KT71, SHI76, RGG82].

The character of an R_5 irreducible representation has the expression [WE26, WE46]

$$\chi_v(\varphi_1, \varphi_2) = \frac{\det(e^{(i\varphi_m K_n)} - e^{-(i\varphi_m K_n)})_{m,n=1,2}}{\det(e^{(i\varphi_m R_n)} - e^{-(i\varphi_m R_n)})_{m,n=1,2}}, \qquad (11.2.2)$$

where $\det(x_{m,n})_{m,n=1,2}$ denotes the determinant associated to the matrix $(x_{m,n})_{m,n=1,2}$. Let (R_1, R_2) be the sum of all positive roots for the group R_5, i.e. $(R_1, R_2) = (3/2, 1/2)$. The vector (K_1, K_2) is obtained by adding to (R_1, R_2) the highest weight (L_1, L_2) vector, which for the group R_5 is equal to $(v, 0)$. (φ_1, φ_2) is an arbitrary vector. The restriction of R_5 to R_3 can be achieved by setting:

$$\frac{\varphi_1}{2} = \varphi_2 \equiv \varphi. \qquad (11.2.3)$$

On the other hand the irreducible representation I of the group R_3 is characterized by the character:

$$\chi_I(\varphi) = \frac{\sin(I + \frac{1}{2})\varphi}{\sin\frac{1}{2}\varphi}. \qquad (11.2.4)$$

Let us consider the set $\mathcal{C}$ of conjugated elements of R_3. The complex functions defined on $\mathcal{C}$ can be organized as a Hilbert space $\mathcal{S}$ with the scalar product defined by:

$$(f, g) = \int_0^{2\pi} f^*(\varphi)g(\varphi)\rho(\varphi)d\varphi, \qquad (11.2.5)$$

where f and g are two elements of $\mathcal{S}$ and ρ denotes the Haar measure for R_3 [VIL68] whose expression is:

$$\rho(\varphi) = \frac{1}{\pi} \sin^2 \frac{\varphi}{2}. \qquad (11.2.6)$$

The set of functions $(\chi_I)_I$ is complete in $\mathcal{S}$ and therefore any function $\chi_v(\varphi)$ can be expanded as:

$$\chi_v(\varphi) = \sum_I d_v(I)\chi_I(\varphi) \qquad (11.2.7)$$

The expansion coefficient $d_v(I)$ is just the multiplicity of the representation (I) characterizing the (v) representation splitting. Taking into account that χ_I are orthonormal functions one obtains:

$$d_v(I) = \int_0^{2\pi} \chi_I^*(\varphi)\chi_v(\varphi)\rho(\varphi)d\varphi. \tag{11.2.8}$$

The final expression for χ_v can be written as a ratio of two determinants:

$$\chi_v(\varphi) = \frac{\Delta(v)}{\Delta(0)}, \text{ where}$$

$$\Delta(v) = \det\begin{pmatrix} e^{i\varphi(2v+3)} - e^{-i\varphi(2v+3)} & e^{i\varphi} - e^{-i\varphi} \\ e^{i\varphi(v+\frac{3}{2})} - e^{-i\varphi(v+\frac{3}{2})} & e^{i\frac{1}{2}\varphi} - e^{-i\frac{1}{2}\varphi} \end{pmatrix}. \tag{11.2.9}$$

Changing the variable $z = e^{i\varphi}$, $d_v(I)$ is expressed as a contour integral:

$$d_v(I) = \frac{i}{4\pi} \int_{|z|=1} \frac{1}{z^{2v+I+2}} \frac{(z^{v+1}-1)(z^{v+2}-1)(z^{2v+3}-1)(z^{2I+1}-1)}{(z^2-1)(z^3-1)} dz. \tag{11.2.10}$$

Further we perform the expansion

$$F_{k_1 k_2}(z) \equiv \frac{1}{(1-z^{k_1})(1-z^{k_2})} = \sum_{n=0}^{\infty} N_{k_1 k_2}(n)z^n. \tag{11.2.11}$$

The needed expansion coefficients were calculated in Ref. [GR04]:

$$N_{23}(n) = \left[\frac{n}{2}\right] - \left[\frac{n}{3}\right] + \chi\left(\frac{n}{3}\right),$$
$$N_{13}(n) = \left[\frac{n}{3}\right] + 1. \tag{11.2.12}$$

where [x] denotes the integer part of x.

The singular part of the integrand of Eq. (11.2.10) is:

$$G(z) = \frac{1}{z}\left(\frac{\theta(I-2v-5)}{z^{I-2v-5}} + \frac{\theta(2v-I)}{z^{2v-I}} - \frac{\theta(2v+I+1)}{z^{2v+I+1}}\right)F_{13}(z)$$
$$+ \frac{1}{z}\left(\frac{\theta(v+I)}{z^{v+I}} - \frac{\theta(v-I-1)}{z^{v-I-1}} - \frac{\theta(I-v-3)}{z^{v-I-3}}\right)F_{23}(z). \tag{11.2.13}$$

With these details the residuum for the function G is readily calculated and the final result for multiplicity is:

$$d_v(I) = P(I - 2v - 5) + P(2v - I) - P(2v + I + 1)$$
$$+ Q(v + I) - Q(v - I - 1) - Q(I - v - 3). \tag{11.2.14}$$

where the Q and P denote:

$$Q(n) = \frac{1}{2}\theta(n)N_{13}(n), \quad P(n) = \frac{1}{2}\theta(n)N_{23}(n). \tag{11.2.15}$$

$\theta(x)$ denotes the step function defined as: $\theta(x) = 1$, for $x \geq 0$ and $\theta(x) = 0$, for $x < 0$. The procedure can be extended to the degeneracy of the group R_{2l+1} caused by the reduction to R_3.

Since in many places along this book we deal also with octupole bosons we need to know the multiplicity for the reduction $R_{2l+1} \supset R_3$, with $l = 3$. The final expression of this degeneracy in the integral form can be written in unified fashion:

$$d_v^{(l)}(I) = \frac{i}{4\pi} \int_{|z|=1} \frac{\left(z^{2I+1} - 1\right)\left(z^{2v+2l-1} - 1\right)\prod_{k=1}^{2l-2}\left(z^{v+k} - 1\right)}{z^{lv+I+2}\prod_{k=1}^{2l-2}\left(z^{k+1} - 1\right)}\,dz, \tag{11.2.16}$$

with $l = 2$ for R_5 and $l = 3$ for R_7. The integral was analytically expressed in Ref. [GR04] also for the octupole case.

It can be proved that the above expression, for an arbitrary l, gives the multiplicity for the reduction $R_{2l+1} \supset R_3$. Moreover, even for the general case an analytical solution is possible [GR04].

Chapter 12
Unified Single Particle Basis

12.1 Projected Spherical Single Particle Basis

In the previous sections we used, in several contexts, the over-completeness property of a coherent state. This allowed us to project out a basis suitable to treat phenomenological boson Hamiltonians. Here we further exploit the salient feature of the coherent states to be a convenient source of generating a complete set of independent states. The inspiring paper for this project was that of Nilsson [NIL55] which defines a deformed single particle state as eigenstate of a mean field Hamiltonian which has a deformed shape similar to a deformed phenomenological core. This basis has been extensively used by very many authors to describe some microscopic properties of deformed nuclei. However, whenever one wants to describe a physical observable which is sensitive to changing the angular momentum, one has to project out the good angular momentum from the BCS or RPA many body ground state. This operation is not simple at all, and concerning the latter ground-state, only approximate solutions have been obtained so far.

Due to this feature we believe that any positive attempt aiming at avoiding such difficulties is welcome. We present here a single particle basis which might constitute an attempt of this type [RDI93, RGG01, REG02, REF04]. We start with a particle-core Hamiltonian:

$$\tilde{H} = H_{sm} + H_{core} - M\omega_0^2 r^2 \sum_{\lambda=0,2} \sum_{-\lambda \leq \mu \leq \lambda} \alpha_{\lambda\mu}^* Y_{\lambda\mu}. \qquad (12.1.1)$$

Here H_{sm} denotes a spherical shell model Hamiltonian, while H_{core} is a harmonic quadrupole boson Hamiltonian associated to a phenomenological core. The interaction of the two subsystems is accounted for by the third term of the above equation, written in terms of the shape coordinates $\alpha_{00}, \alpha_{2\mu}$. The quadrupole shape coordinates are related to the quadrupole boson operators by the canonical transformation

from Eq. (6.3.2). The monopole shape coordinate α_{00} is to be determined from the volume conservation condition. In a quantized form, the result is:

$$\alpha_{00} = -\frac{1}{2k^2\sqrt{\pi}} \left[5 + \sum_\mu \left(2b_\mu^\dagger b_\mu + (b_\mu^\dagger b_{-\mu}^\dagger + b_{-\mu}b_\mu)(-)^\mu \right) \right]. \qquad (12.1.2)$$

Averaging $\tilde{H}$ on the eigenstates of H_{sm}, hereafter denoted by $|nljm\rangle$, one obtains a deformed boson Hamiltonian whose ground state is described, in the harmonic limit, by a coherent state similar to ψ_g defined by Eq. (6.1.1). On the other hand, the average of $\tilde{H}$ on ψ_g is similar to the Nilsson Hamiltonian [NIL55].

$$H_{mf} = \langle \psi_g | H_{pc} | \psi_g \rangle = \omega_b d^2 + H_{sm} - \hbar\omega_0 r'^2 \left[\frac{\sqrt{2}d}{k} Y_{20} - \frac{1}{8\pi k^2}(5 + 4d^2) \right], \tag{12.1.3}$$

where the stretched coordinates are used, i.e., $r' = \frac{m\omega}{\hbar} r$. Further, extracting from the above Hamiltonian the zero point deformation energy

$$\lim_{d \to 0} (H_{mf} - H_{sm}) = \frac{5\hbar\omega_0 r'^2}{8\pi k^2}, \tag{12.1.4}$$

One arrives at a more recognizable form:

$$H_{mf} = \omega_b d^2 + H_{sm} - \hbar\omega_0 r'^2 \left(\frac{\sqrt{2}d}{k} Y_{20} - \frac{1}{2\pi k^2} d^2 \right). \tag{12.1.5}$$

We note that the deformed terms involved in the Nilsson model Hamiltonian and the mean field H_{mf} are identical provided the following equation holds:

$$\frac{d}{k} = \frac{\beta}{\sqrt{2}}. \tag{12.1.6}$$

One recovers the original Nilsson Hamiltonian [NIL55]:

$$H_{Nilsson}(\beta) = H_{sm} - \hbar\omega_0 r'^2 \beta Y_{20}. \tag{12.1.7}$$

if in (12.1.5) one ignores the constant terms i.e., those which are independent of the particle coordinates.

   Due to these properties, it is expected that the best trial functions to be used to generate, through projection, a spherical basis are:

$$\Psi_{nljm}^{pc} = |nljm\rangle \psi_g. \tag{12.1.8}$$

The upper index appearing in the l.h. side of the above equation, suggests that the product function is associated to the particle-core system. The projected states are obtained in the usual manner, by acting on these deformed states with the projection operator defined by Eq. (6.1.8). In general, the projected states corresponding to different m quantum numbers are not orthogonal. A certain subset of projected states is however, orthogonal:

$$\Phi_{nlj}^{IM}(d) = \mathcal{N}_{nlj}^{I}(d) P_{MI}^{I}[|nljI\rangle\psi_g]. \qquad (12.1.9)$$

These states can be written in a tensorial form as:

$$\Phi_{nlj}^{IM}(d) = \mathcal{N}_{nlj}^{I}(d) \sum_{J} C_{I\,0\,I}^{j\,J\,I} (N_J^g)^{-1} \left[|nlj\rangle\phi_J^g\right]_{IM}, \qquad (12.1.10)$$

with the normalization factor given by:

$$(\mathcal{N}_{nlj}^{I}(d))^{-2} = \sum_{J} \left(C_{I\,0\,I}^{j\,J\,I}\right)^2 (N_J^g)^{-2}. \qquad (12.1.11)$$

The projected states ϕ_J^g and their norms N_J^g are the same as in Eq. (6.1.7). Hence, they describe members of the ground band in the CSM.

The main properties of these projected spherical states (12.1.10) are: (a) They are orthogonal with respect to I and M quantum numbers. (b) Although the projected states are associated to the particle-core system, they can be used as a single particle basis. Indeed, when a matrix element of a particle-like operator is calculated, the integration on the core collective coordinates is performed first, which results in obtaining a final factorized expression: one factor carries the dependence on deformation and one is a spherical shell model matrix element. To be more specific, let us consider a one-body operator T_μ^k. Its reduced matrix element can be calculated and written in a factorized form:

$$\langle\Phi_{nlj}^{I}||T^k||\Phi_{n'l'j'}^{I'}\rangle = f_{nljI}^{n'l'j'I'}(d)\langle nlj||T^k||n'l'j'\rangle, \quad \text{with} \qquad (12.1.12)$$

$$f_{nljI}^{n'l'j'I'}(d) = \mathcal{N}_{nlj}^{I}(d)\mathcal{N}_{n'l'j'}^{I'}(d)\hat{j}\hat{I'} \sum_{J} C_{I\,0\,I}^{j\,J\,I} C_{I'\,0\,I'}^{j'\,J\,I'} W(jkJI'; j'I) \left(N_J^g\right)^{-2};$$

(c) The connection between the nuclear deformation and the parameter d entering the definition of the coherent state ψ_g is readily obtained by requiring that the strength of the particle-core quadrupole-quadrupole interaction be identical to the Nilsson deformed term of the mean field:

$$\frac{d}{k} = \sqrt{\frac{2\pi}{45}}(\Omega_\perp^2 - \Omega_z^2). \qquad (12.1.13)$$

Here $\Omega_\perp$ and Ω_z denote the frequencies of Nilsson's mean field related to the deformation $\delta = \sqrt{45/16\pi}\beta$ by:

$$\Omega_\perp = \left(\frac{2+\delta}{2-\delta}\right)^{1/3}, \ \ \Omega_z = \left(\frac{2+\delta}{2-\delta}\right)^{-2/3}. \tag{12.1.14}$$

Actually, expanding $\Omega_\perp$ and Ω_z in terms of δ and keeping only the first order, the Eq. (12.1.13) yields (12.1.6). The average of the particle-core Hamiltonian $H' = \tilde{H} - H_{core}$ on the projected spherical states, defined by Eq. (12.1.10), has the expression

$$\epsilon_{nlj}^I = \langle \Phi_{nlj}^{IM}(d)|H'|\Phi_{nlj}^{IM}(d)\rangle = \epsilon_{nlj} - \hbar\omega_0(N + \frac{3}{2})C_{I0I}^{j2j}C_{1/201/2}^{j2j}\frac{(\Omega_\perp^2 - \Omega_z^2)}{3}$$

$$+ \hbar\omega_0(N + \frac{3}{2})\left[1 + \frac{5}{2d^2} + \frac{\sum_J(C_{I-I0}^{jIJ})^2 I_J^{(1)}}{\sum_J(C_{I-I0}^{jIJ})^2 I_J^{(0)}}\right]\frac{(\Omega_\perp^2 - \Omega_z^2)}{90}. \tag{12.1.15}$$

Here we used the standard notation for the Clebsch Gordan coefficients $C_{m_1m_2m}^{j_1j_1j}$. $I_J^{(k)}$ are the overlap integrals defined in Eqs. (6.1.15 and 6.1.18).

Since the core contribution does not depend on the quantum numbers of the single particle energy level, it produces a shift for all energies and therefore is omitted in Eq. (12.1.15). The first term from (12.1.15) is, of course, the single particle energy for the spherical shell model state $|nljm\rangle$. Given the fact that the basis (12.1.8) recovers the spherical shell model basis in the vibrational limit, the corresponding single-particle energies (12.1.15) also have to reproduce the spherical shell model energy in the limit of $d \to 0$. However the limit

$$\lim_{d\to 0}\varepsilon_{nlj}^I = \varepsilon_{nlj} + \hbar\omega_0\left(N + \frac{3}{2}\right)\left[\frac{5}{2} + \frac{1}{2}\left(j - I + \frac{1}{2}\left(1 - (-)^{j-I}\right)\right)\right]\frac{1}{4\pi k^2}, \ \ j \neq I, \tag{12.1.16}$$

is different from ε_{nlj} by the $1/k^2$ term in the above equation which is actually a measure of the so called *zero point energy*. The deviation is very small due to the constant k whose usual value varies around 10. However, at high j orbitals the correction becomes sizable and a split of the energy correction over the quantum number I, shows up at vanishing deformation. In order to avoid this, one must normalize the single-particle energies (12.1.15) by extracting the zero point deformation energy given by the corrective term from (12.1.16). Thus, the normalized single-particle energies are expressed as

$$\epsilon_{nlj}^I = \epsilon_{nlj} - \hbar\omega_0(N + \frac{3}{2})C_{I0I}^{j2j}C_{1/201/2}^{j2j}\frac{(\Omega_\perp^2 - \Omega_z^2)}{3}$$

$$+ \hbar\omega_0(N + \frac{3}{2})\left[1 + \frac{\sum_J(C_{I-I0}^{jIJ})^2 I_J^{(1)}}{\sum_J(C_{I-I0}^{jIJ})^2 I_J^{(0)}}\right]\frac{(\Omega_\perp^2 - \Omega_z^2)}{90}$$

$$- \hbar\omega_0\left(N + \frac{3}{2}\right)\left[j - I + \frac{1}{2}\left(1 - (-)^{j-I}\right)\right]\frac{1}{8\pi k^2}. \tag{12.1.17}$$

According to our remark concerning the use of the projected spherical states for describing the single particle motion, the average values ϵ_{nlj}^{I} may be viewed as approximate expressions for the single particle energies in deformed Nilsson orbits. We may account for the deviations from the exact eigenvalues by considering, at a latter stage, the exact matrix elements of the two body interaction when a specific treatment of the many body system is applied. It is worth mentioning that the dependence of the new single particle energies on deformation is similar to that shown by the Nilsson model. This is clearly seen in Fig. 12.1, where the proton and neutron single particle energies are plotted as function of the deformation parameter d. Although the energy levels are similar to those of the Nilsson model, the quantum numbers in the two schemes are different. Indeed, here we generate from each j a multiplet of $(2j + 1)$ states as I, which plays the role of the Nilsson quantum number Ω, runs from 1/2 to j and moreover the energies corresponding to the quantum numbers K and $-$K are equal to each other. On the other hand, for a given I there are $2I + 1$ degenerate sub-states while the Nilsson states are only double degenerate. As explained in Ref. [RDI93], the redundancy problem can be solved by changing the normalization of the model functions:

$$\langle \Phi_\alpha^{IM} | \Phi_\alpha^{IM} \rangle = 1 \Longrightarrow \sum_M \langle \Phi_\alpha^{IM} | \Phi_\alpha^{IM} \rangle = 2. \qquad (12.1.18)$$
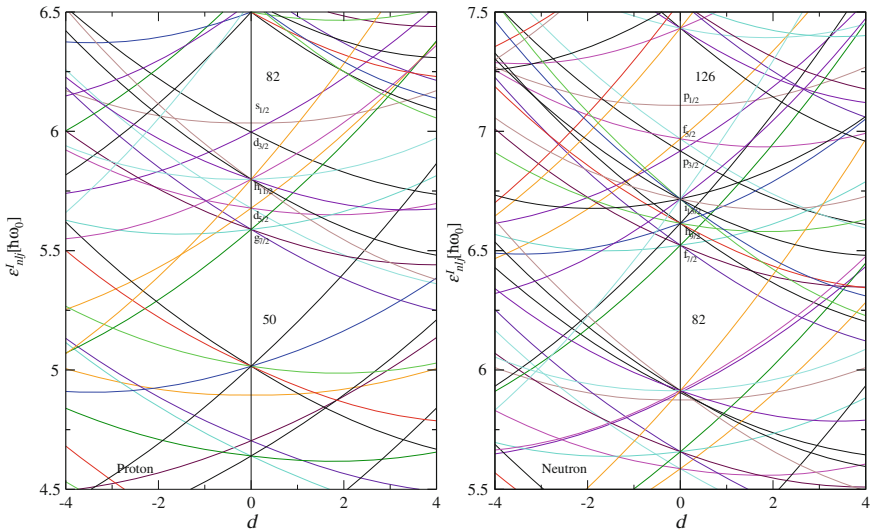

Fig. 12.1 Proton and neutron single-particle energies in the region of $N = 5$ and $N = 6$ shells respectively, given by Eq. (12.1.17) where the shell model parameters $\kappa = 0.0637$ and $\mu = 0.60$ for protons and $\mu = 0.42$ for neutrons were used. The canonical transformation constant is fixed to $k = 10$

Due to this weighting factor, the particle density function is providing the consistency result that the number of particles which can be distributed on the $(2I + 1)$ sub-states is at most 2, which agrees with the Nilsson model. Here α stands for a set of shell model quantum numbers nlj. Due to this normalization, the states $\Phi_{\alpha IM}$, used to calculate the matrix elements of a given operator, should be multiplied with the weighting factor $\sqrt{2/(2I + 1)}$.

The role of the core component is to induce a quadrupole deformation for the matrix elements of the operators acting on particle degrees of freedom, as shown by Eq. (12.1.12). Indeed, the factor f carries the dependence on the deformation parameter d, while the other factor is just the reduced matrix elements corresponding to the spherical shell model states. Thus, Eq. (12.1.12) can be viewed as a deformation transformation of the matrix elements in the spherical basis. In conclusion, due to the properties mentioned above, although these states are associated to a particle-core system, they can be used as a single particle basis. Therefore, one may think of a set of single particle states Ψ_α^{IM} which are eigenstates of an effective rotational invariant fermionic one-body Hamiltonian H_{eff}, with the corresponding energies given by Eq. (12.1.17).

$$H_{eff}\Psi_\alpha^{IM} = \epsilon_\alpha^I(d)\Psi_\alpha^{IM}. \tag{12.1.19}$$

This definition should be supplemented by the request that the matrix elements of any operator between states Ψ_α^{IM} and $\Psi_{\alpha'}^{I'M'}$ are equal to the matrix elements of the same operator between the corresponding shell model states multiplied with a deformation factor, given by Eq. (12.1.12). Due to these features, these states can be used as single particle basis to treat many body Hamiltonians which involve one-body operators which is actually the case when one deals with a many body Hamiltonian with a two body separable interaction. Thus, in a second quantization language, an arbitrary one body operator $\hat{V}_1$ can be written as:

$$\hat{V}_1 = \sum_{\alpha,I,M;\alpha',I'M'} \sqrt{\frac{2}{2I + 1}} \langle \Phi_\alpha^{IM}(d)|V|\Phi_{\alpha'}^{I'M'}(d)\rangle \sqrt{\frac{2}{2I' + 1}} c_{\alpha IM}^\dagger c_{\alpha' I'M'},$$
$$\text{with } \alpha = (\text{nlj}), \ \alpha' = (\text{n'l'j'}). \tag{12.1.20}$$

Let us analyze the procedure mentioned before from a different angle. As we stated already, averaging the particle-core Hamiltonian on the coherent state ψ_g, the Nilsson Hamiltonian for the single particle motion is obtained. Mathematically, the effect of this operation consists of projecting the particle-core space, $S_p \otimes S_b$, into the particle space S_p,

$$S_p \otimes S_b \rightarrow S_p. \tag{12.1.21}$$

Rotational symmetry is thereby broken. Our idea was to go back to $S_p \otimes S_b$ and restore the symmetry in that space and embed the elements specific to S_p into the particle-core space:

$$S_p \rightarrow S_p \otimes S_b,$$
$$T_\mu^k \rightarrow T_\mu^k \otimes I_b,$$
$$\langle j||T^k||j'\rangle \rightarrow \langle I||T^k \otimes 1_b||I'\rangle = f_{nljI}^{n'l'j'I'}(d)\langle j||T^k||j'\rangle. \quad (12.1.22)$$

where I_b stands for the unity operator in the boson space. The last equality shows that the net result of embedding the single particle space into the particle-core space is to quench the particle matrix elements through a deformation multiplicative factor.

To complete our arguments concerning the use of particle-core states in many body calculations, we have to clarify whether an equation similar to (12.1.12) is also valid for a two body interaction. The formal difficulty in understanding the use of the basis (12.1.9) for a many body system stems in the fact that according to the definition (12.1.9), to a n particle system one associates a product of n single particle spherical shell model states and a product of n core wave functions. Indeed, at a superficial glance that would overestimate the core contribution and the picture would be different from a more realistic situation when the given system is described by a product of n-spherical shell model states and a single core state which should be common to all particles moving around. In Appendix F, we prove that due to the specific properties of the coherent states, the two many body wave functions, one with several cores and one with a sole core, describe two equivalent physical systems. As a matter of fact with this proof, our arguments pleading for the use of the projected states from Eq. (12.1.9) as a single particle basis for deformed nuclei, are complete. It is clear now that the difficulties, mentioned at the beginning of this section, concerning the many body description of deformed nuclear systems are no longer standing up.

The single particle basis must satisfy a few tests required by the experimental information on the single particle features of the nuclei: (a) The nucleon density function should reflect the deformation dependence of the mean field; (b) The projected spherical single particle states must predict for the quadrupole moment of the first state 2^+ the sign suggested by experiment; (c) Using the basis states to calculate the binding energies, the right place of the magic numbers are to be found; (d) The right order of the shell filling may indicate which is the spin of the ground state in the odd nuclei; (e) The model should fix the algorithm of fixing the free parameters involved. In what follows such issues will be separately treated.

12.1.1 Nucleon Density Function

Another property of the spherical projected single-particle basis is the distribution of the nucleons on the states associated to the energies (12.1.17). The density operator corresponding to the projected spherical states can be written as:

$$\hat{\rho} = \sum_{nljIM} \frac{2}{2I+1} \left| \Phi_{nlj}^{IM}(d) \right|^2. \quad (12.1.23)$$

Using the tensorial form of the projected particle-core state (12.1.10), and replacing the product of the projected core states and their corresponding complex conjugates by their scalar product, one obtains:

$$\langle \hat{\rho} \rangle_{coll} = 2 \sum_{nljm>0} ||nljm\rangle|^2 , \qquad (12.1.24)$$

which is exactly the spherical shell model nucleon density. This result is also consistent with the nucleon density calculated with projected Nilsson single particle states. According to this expression the deformation depends on the degree of feeling the last shell under consideration. The question which might be raised is whether an explicit deformation dependence for nucleon density is possible.

Inspired by the fact that the deformation dependence of the mean field is obtained by averaging the particle-core Hamiltonian with the quadrupole boson coherent state (6.1.1), we extend the procedure to the nucleon density (12.1.23) with the result:

$$\langle \psi_g | \hat{\rho} | \psi_g \rangle = \sum_{nljIM} \frac{2}{2I+1} \left| \langle \psi_g | \Phi_{nlj}^{IM}(d) \rangle \right|^2 . \qquad (12.1.25)$$

Similarly, the wave function associated to the deformed single particle mean field might be viewed as the overlap of the projected spherical state with the core's coherent state:

$$\langle \psi_g | \Phi_{nlj}^{IM}(d) \rangle = \mathcal{N}_j^I \sum_J F_{JM}^{jI}(d) |nljM\rangle, \qquad (12.1.26)$$

where

$$F_{JM}^{jI}(d) = C_{I\,0\,I}^{j\,J\,I} C_{M\,0\,M}^{j\,J\,I} (N_J)^{-2} . \qquad (12.1.27)$$

A direct connection between the k-pole transition densities defined by the projected spherical single particle and the spherical shell model bases, can be obtained by using the second quantization form of a one body operator, which is a tensor of rank k and projection m with respect to the rotation transformations:

$$
\begin{aligned}
\hat{T}_{km} &= \sum \sqrt{\frac{2}{2I+1}} \langle \Phi_{nlj}^{IM} | \hat{T}_{km} | \Phi_{n'l'j'}^{I'M'} \rangle \sqrt{\frac{2}{2I'+1}} c_{\alpha IM}^\dagger c_{\alpha' I'M'} \\
&= \sum \frac{2}{\hat{I}\hat{I'}} \langle \Phi_{nlj}^{I} || \hat{T}_k || \Phi_{n'l'j'}^{I'} \rangle C_{M'mM}^{I'kI} c_{\alpha IM}^\dagger c_{\alpha' I'M'} \\
&= \sum_{\alpha I;\alpha' I'} \frac{2}{\hat{I}\hat{I'}} \langle \alpha I || \hat{T}_k || \alpha' I' \rangle \hat{\rho}_{km}^{ps}(\alpha I; \alpha' I') . \qquad (12.1.28)
\end{aligned}
$$

For the sake of simplicity we used the abbreviations and notations:

$$|\alpha IM\rangle = |\Phi_{nlj}^{IM}\rangle, \quad \alpha = (nlj), \quad \hat{I} = \sqrt{2I+1},$$

$$\hat{\rho}_{km}^{ps}(\alpha I; \alpha' I') = -\frac{\hat{I}}{\hat{k}}\left(c_{\alpha I}^{\dagger}c_{\widetilde{\alpha' I'}}\right)_{km}, \quad c_{\widetilde{\alpha IM}} = (-1)^{I-M}c_{\alpha I,-M}. \quad (12.1.29)$$

The upper index "ps" accompanying the density matrix indicate that it is associated to the "projected spherical" single particle basis. Changing the single particle basis to that of spherical shell model and following the same procedure one finds:

$$\hat{T}_{km} = \sum \langle nlj||\hat{T}_k||n'l'j'\rangle \hat{\rho}_{km}^{sm}(nlj; n'l'j'), \text{ with}$$

$$\hat{\rho}_{km}^{sm}(nlj; n'l'j') = -\frac{\hat{j}}{\hat{k}}\left(c_{nlj}^{\dagger}c_{\widetilde{n'l'j'}}\right)_{km}. \quad (12.1.30)$$

Using the equation relating the matrix elements within the projected spherical and the spherical shell model basis one obtains:

$$\hat{\rho}_{km}^{sm}(nlj; n'l'j') = \sum_{I,I'}\frac{2}{\hat{I}\hat{I}'}f_{jI;k}^{j'I'}(d)\hat{\rho}_{km}^{ps}(nljI; n'l'j'I'). \quad (12.1.31)$$

Taking into account the explicit expression of the norms $\mathcal{N}_j^I$ and the analytical form of the Racah coefficient with one vanishing index, it can be proved that for $k = 0$ the factor f is equal to unity:

$$f_{jI;0}^{j'I'}(d) = \delta_{I,I'}\delta_{j,j'}. \quad (12.1.32)$$

Consequently, we have:

$$\hat{\rho}_{00}^{sm}(nlj; nlj) = \sum_{I}\frac{2}{2I+1}\hat{\rho}_{00}^{ps}(nljI; nljI). \quad (12.1.33)$$

Going back to the definition of $\hat{\rho}$ in the two basis (12.1.29) and (12.1.30), by a direct and simple calculation one finds that Eqs. (12.1.33) and (12.1.24) are identical. For illustration, in Figs. 12.2 and 12.3 we represent the nucleon density as given by Eqs.(12.1.24), (12.1.25), respectively.

12.1.2 The Quadrupole Moment for the First 2^+

For what follows it is useful to study the quadrupole moment of the ground band state 2^+ within the projected spherical single particle basis. Let us derive the expression
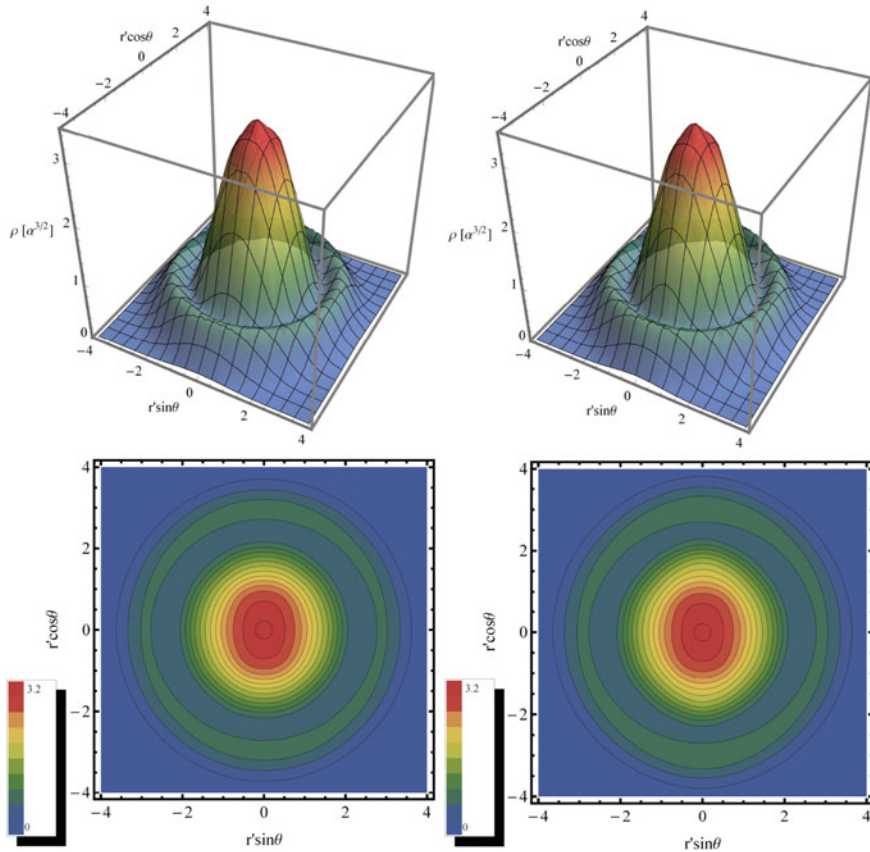
Fig. 12.2 Total nuclear density given by Eq. (12.1.24) is represented as function of $x = r' \sin \theta$ and $z = r' \cos \theta$ in units of $\alpha^{\frac{3}{2}}$ in 3D plots (*up*) and contour plots (*down*) for ^{150}Gd (*left*) and ^{156}Gd (*right*). In both cases the densities corresponding to two adjacent *curves* differ from each other by $0.21\alpha^{3/2}$

of the quadrupole moment within the GCSM. The liquid drop model (LDM) predicts for the quadrupole moment the expression:

$$Q_{2\mu} = \frac{3 Z e R_0^2}{4\pi} \left(\alpha_{2\mu} - \frac{10}{\sqrt{70\pi}} (\alpha_2 \alpha_2)_{2\mu} \right), \quad R_0 = 1.2 A^{1/3} fm. \qquad (12.1.34)$$

Within LDM the state 2^+ is a one phonon state, $b_{2\mu}^\dagger |0\rangle$, which yields for the quadrupole moment, with the standard definition, the expression:

$$\langle 22 | Q_{20} | 22 \rangle = -\frac{3 Z e R_0^2 \sqrt{5}}{7\pi k^2 \sqrt{\pi}}. \qquad (12.1.35)$$
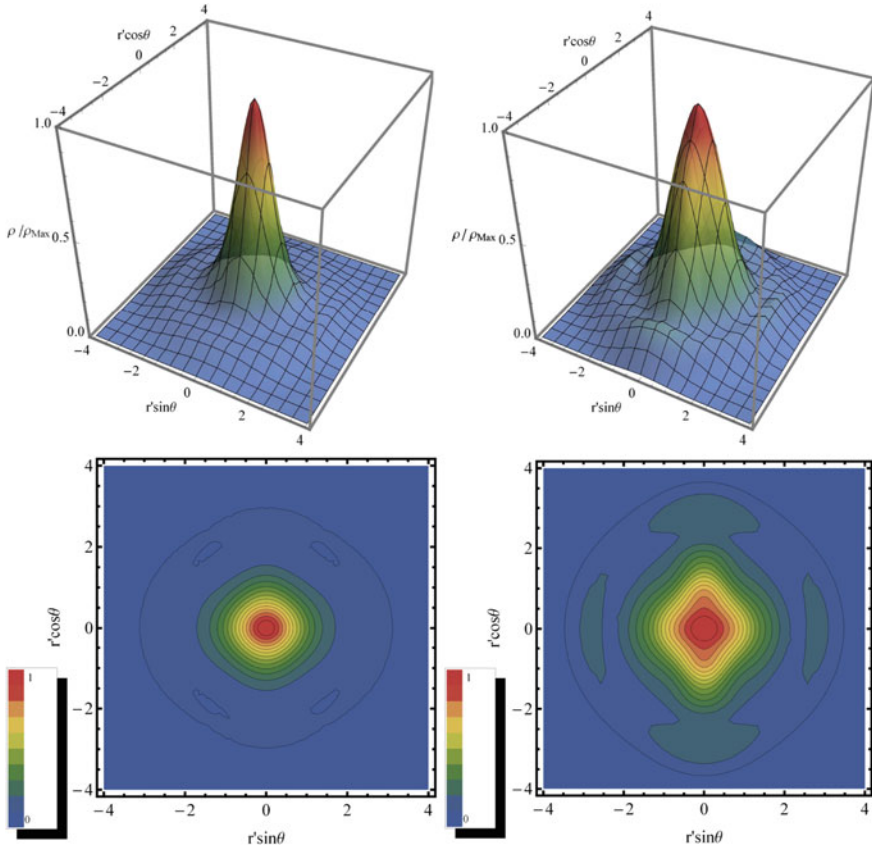
Fig. 12.3 Total nuclear density projected on the quadrupole boson coherent state defined by Eq. (12.1.25) and normalized to its maximum value is represented as function of $x = r' \sin \theta$ and $z = r' \cos \theta$ in 3D plots (*up*) and contour plots (*down*) for ^{150}Gd (*left*) and ^{156}Gd (*right*). Contour plots are made with a step of $0.062/\rho_{max}$

From here it results that for spherical nuclei the quadrupole moment is always negative. The GCSM defines the state 2^+ by the angular momentum projected state $\phi^g_{JM}(d_n, d_p)$ (see Eq. (9.1.1)) while the quadrupole moment, in the boson representation, is:

$$Q_{20} = \frac{3ZeR_0^2}{4\pi} \left[\frac{1}{k_p \sqrt{2}} \left(b^\dagger_{b0} + b_{p0} \right) - \frac{5}{k_p^2 \sqrt{70\pi}} \left((b^\dagger_p b^\dagger_p)_{20} + (b_p b_p)_{20} + (b^\dagger_p b_p)_{20} \right) \right].$$

$$(12.1.36)$$

Averaging this operator with the projected state mentioned above one obtains:

$$\langle \phi_{22}^g(d_n, d_p) | Q_{20} | \phi_{22}^g(d_n, d_p) \rangle = -\frac{3ZeR_0^2}{7\pi} \left[\frac{1}{\sqrt{2}} \frac{d_p}{k_p} + \frac{1}{7} \sqrt{\frac{5}{\pi}} \left(\frac{d_p}{k_p} \right)^2 \left(1 + \frac{I_2^{(1)}(\rho)}{I_2^{(0)}(\rho)} \right) \right].$$

$$(12.1.37)$$

As we shall see, this equation may be used for determining the ratio d_p/k_p and then the other parameters of the model, i.e. d_n and k_n.

12.1.3 Shell Filling Order: Magic Numbers and the Spin of Odd System Ground State

Another issue addressed in this section regards the ability of the model proposed to describe the shell filling and how that compares with what we know from the Nilsson model. To this goal we calculated the second order binding energy difference

$$\Delta E_{Tot} = -\frac{3}{16} \left[2E(N) - E(N+2) - E(N-2) \right], \qquad (12.1.38)$$

with $E(N)$ denoting the total sum of proton and neutron single particle energies for a nucleus with N neutrons. This quantity is plotted for the isotopic chains of Cd and Te in Fig. 12.4. We notice that both models show two major peaks corresponding to the magic number 82 and the shell filling at $N = 68$ for Cd and $N = 70$ for Te. The distributions of peaks for Te isotopes obtained with the projected spherical single particle basis (PSSPB) and Nilsson model respectively, are similar. Some differences appear in the case of Cd's. In the case of Nilsson plot there is a peak for $N = 76$ which is missing in the case of PSSPB. On the other hand the plot with PSSPB exhibits a peak for $N = 56$ which is missing in the case of the plot made with the Nilsson model. The major peak at $N = 70$ for Nilsson model is shifted to $N = 68$ for our method.

The order of the shell filling is, of course, depending on the quadrupole deformation. A test for this feature is to identify the levels around the last occupied one and compare their spin with the experimental value for the ground state spin, in an even-odd nucleus. The results are compared with the data for a few odd nuclei in Table 12.1. Among the identified angular momenta for the last and the second last occupied as well as for the first unoccupied levels one finds the angular momenta characterizing the ground state according to the experimental data. The reason we listed all three spins is that in the region of the Fermi sea, the level density is high and a small uncertainty in determining the deformation may change the position of the level crossing and thus the filling order. Moreover, our estimation does not take into consideration the effect of the residual interaction which may also shift the position of the Fermi level. We note that the agreement is reasonably good suggesting that
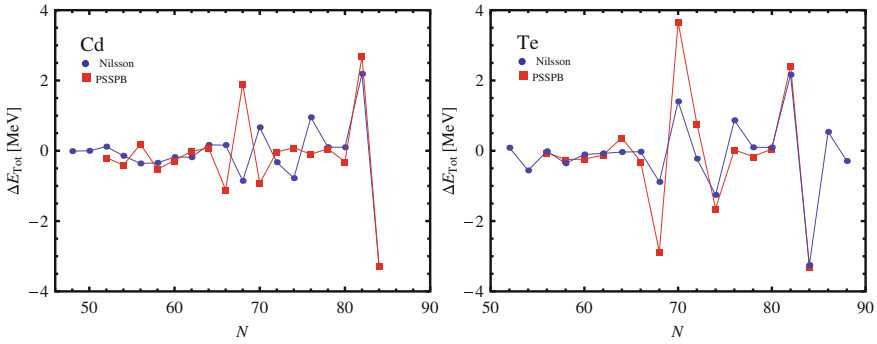
Fig. 12.4 The binding energy second order difference, ΔE_{Tot} for the isotopes of Cd (*left panel*) and Te (*right panel*) is represented as function of the number of neutrons, N. For Nilsson model calculations, we included also the $\Delta N = 2$ matrix elements with $N_{cutoff} = 10$

the ground state has the spin of the first unoccupied level for ^{155}Gd, ^{167}Er, ^{177}Hf, ^{179}Hf and that of the second last occupied state for ^{187}Os, ^{189}Os, ^{157}Gd.

12.1.4 The Model Parameters

Besides the nuclear shell model parameters, the projected single particle basis involves another two, namely the deformation parameter d and the constant k entering the canonical transformation relating the quadrupole coordinates with the boson operator. When some tuning properties which are isospin dependent are concerned, the single particle projected basis for protons and neutrons should be different and consequently different parameters d and k are to be used. The isospin dependence of these parameters is underlined by using different notations for them, when they are involved in the equation for protons, d_p and k_p, and neutrons, d_n and k_n, respectively. The algorithm of fixing these parameters is defined by several steps: (a) By equating the theoretical result for the ratio of excitation energies of the ground band levels 2^+ and 4^+, denoted by $R_{4/2}$, to the experimental value, one obtains a relation determining the global deformation $\rho(=d\sqrt{2})$ (see the chapter about the GCSM); (b) Inserting d in Eq. (12.1.6) the parameter k is readily obtained; (c) From the expression of the $B(E2)$ value associated to the transition $0^+ \rightarrow 2^+$ the parameter k_p is obtained; (d) Using again Eq. (12.1.6) corresponding to the proton system, the deformation parameter d_p is calculated; (e) From the equation defining $\rho = (d_p^2 + d_n^2)^{1/2}$, one determines d_n; (f) The Eq. (12.1.6) for neutrons finally determines k_n.

This procedure was applied to 194 isotopes and the resulting parameters were collected in several tables. For 186 isotopes, the quadrupole deformation involved in Eq. (12.1.6) is taken from Ref. [MNMS95]. For the remaining eight isotopes the quadrupole deformation from Ref. [MNMS95] provides a wrong sign for the

Table 12.1 With the nuclear deformation β taken for Ref. [MNM95] and the deformation parameters as well as the canonicity constants determined as discussed in the text we determined the quantum numbers $[N l j I]$ of the last occupied (Locc), the second last occupied (Slocc) and the first unoccupied (Funocc) neutron states of several even-odd isotopes

Nucleus	β_2	ρ	d	k	d_p	k_p	d_n	k_n	Locc	Slocc	Funocc	I_{Exp}
^{155}Gd	0.252	2.939	2.078	12.4534	1.951	11.6878	2.199	13.1745	$[66\frac{13}{2}\frac{1}{2}]$	$[55\frac{9}{2}\frac{3}{2}]$	$[66\frac{13}{2}\frac{3}{2}]$	$\frac{3}{2}$
^{157}Gd	0.271	3.161	2.235	12.5011	2.088	11.6810	2.373	13.2707	$[66\frac{13}{2}\frac{1}{2}]$	$[55\frac{9}{2}\frac{3}{2}]$	$[66\frac{13}{2}\frac{5}{2}]$	$\frac{3}{2}$
^{167}Er	0.294	3.697	2.614	13.5377	2.430	12.5842	2.786	14.4282	$[53\frac{7}{2}\frac{5}{2}]$	$[55\frac{9}{2}\frac{5}{2}]$	$[66\frac{13}{2}\frac{7}{2}]$	$\frac{7}{2}$
^{177}Hf	0.277	3.403	2.406	13.1820	2.245	12.2975	2.557	14.0107	$[53\frac{5}{2}\frac{1}{2}]$	$[51\frac{3}{2}\frac{1}{2}]$	$[55\frac{9}{2}\frac{7}{2}]$	$\frac{7}{2}$
^{179}Hf	0.278	3.415	2.415	13.1845	2.252	12.2973	2.567	14.0157	$[55\frac{9}{2}\frac{7}{2}]$	$[53\frac{5}{2}\frac{1}{2}]$	$[66\frac{13}{2}\frac{9}{2}]$	$\frac{9}{2}$
^{187}Os	0.212	2.588	1.830	12.9232	1.735	12.2539	1.920	13.5595	$[53\frac{7}{2}\frac{7}{2}]$	$[53\frac{5}{2}\frac{1}{2}]$	$[55\frac{9}{2}\frac{9}{2}]$	$\frac{1}{2}$
^{189}Os	0.183	2.234	1.580	12.8377	1.514	12.3051	1.643	13.3491	$[55\frac{9}{2}\frac{9}{2}]$	$[53\frac{5}{2}\frac{1}{2}]$	$[66\frac{13}{2}\frac{11}{2}]$	$\frac{1}{2}$

Presuming that the Fermi sea is close to one of the mentioned states we can get information upon the spin of the ground state of the odd system whose experimental values (see [RiSh80] p. 78) are listed in the last column. Indeed, in the region of the last occupied state the level density is high which results that the odd nucleon position is sensitive to the residual interaction

quadrupole moment of the lowest state 2^+. In order to correct this drawback, one slightly changed the procedure of fixing the involved parameters. Indeed, for three isotopes, ^{74}Ge, ^{74}Se and ^{76}Se, one inserted for β the corresponding experimental values from Refs.[TAM82, SF06, MOO93], otherwise kept the same algorithm as before. As for the last five nuclides, ^{72}Ge, ^{116}Cd, ^{122,124,126}Te, for which the nuclear deformations are also not experimentally known, the fitting procedure is as follows: (a) Inserting ρ, fixed by fitting the ratio $R_{4/2}$, in the defining equation of Q_2 (12.1.37), this becomes an equation for d_p/k_p; (b) Considering Eq. (12.1.6) for protons with the ratio d_p/k_p just determined, one obtains an equation for β; (c) Knowing ρ, one calculates d and from (12.1.6), k; (d) With d and d_p, the deformation d_n is readily obtained; (e) Again, the Eq. (12.1.6) for neutrons determines k_n. This way the signs of 50 experimental values for Q_2 [ST05] are reproduced.

The results concerning the canonicity parameters k, k_p and k_n for the 194 isotopes can be interpolated by linear functions of the atomic mass number A.

$$k = 0.0513471 \cdot A + 4.28957, \quad rms = 2.59477, \qquad (12.1.39)$$

$$k_p = 0.0488292 \cdot A + 4.61187, \quad rms = 2.71376, \qquad (12.1.40)$$

$$k_n = 0.0538922 \cdot A + 3.80843, \quad rms = 3.17185. \qquad (12.1.41)$$

The projected spherical basis, presented here, was successfully used to describe some deformed atomic clusters [RGG01], the M1 scissors-like mode for even Sm isotopes [REG02] and the Gamow-Teller amplitude for single and double beta decay processes [REF04]. For the sake of saving space, these applications will not be presented here.

To conclude, the coherent state approach is very useful not only for accounting for some phenomenological properties of complex nuclei, but also for providing an unified description of spherical and deformed nuclei by means of a projected spherical single particle basis.

Chapter 13
Boson Hamiltonians

13.1 Semiclassical Study of Some Fourth Order Boson Hamiltonians

13.1.1 TDVP for a Fourth Order Boson Hamiltonian

We consider a fourth order quadrupole boson Hamiltonian

$$
\begin{aligned}
H = {} & A_{11}(b^+b)_0 + \{A_{30}(b^+b^+b^+)_0 + A_{21}(b^+b^+b)_0 \\
& + \sum_{J=0,2,4} A_{31}^{(J)}[(b^+b^+)_J(b^+b)_J]_0 \\
& + \sum_{J=0,2,4} A_{40}^{(J)}[(b^+b^+)_J(b^+b^+)_J]_0 + h.c.\} \\
& + \sum_{J=0,2,4} A_{22}^{(J)}[(b^+b^+)_J(bb)_J]_0
\end{aligned}
\tag{13.1.1}
$$

This Hamiltonian has been used by several authors to describe the low lying collective states of positive parity. The quadrupole bosons b_μ^+, $(-2 \le \mu \le 2)$ are of phenomenological type. For example they could be associated to the small and harmonic oscillations of nuclear surface around a spherical equilibrium shape. Throughout this section the index "2" specifying the angular momentum carried by the quadrupole bosons is omitted. It is worth mentioning that among the invariants of fourth order comprised by the model Hamiltonian only five are linearly independent. Consequently, the forth order terms could be rewritten so that only five parameters appear in the new version.

The eigenvalues of H can be obtained by a diagonalisation procedure using the basis $|Nv\alpha IM\rangle$ with N the number of bosons, v the seniority, α the "missing"

quantum number, I the angular momentum and M its projection on z-axis. Here the spectral properties of H will be studied within a time dependent formalism. Such treatment may give information not only about the static properties but also about the time evolution of the nuclear system.

Thus, we consider the variational equation

$$\delta \int_0^t \langle\psi|H - i\hbar\frac{\partial}{\partial t'}|\psi\rangle dt' = 0. \tag{13.1.2}$$

The solutions of this equations satisfy the time dependent Schrödinger equation provided the variational states $|\psi\rangle$ span the whole Hilbert space. Here we confine the boson space to the subspace generated by the states

$$|\psi\rangle = exp[z_0 b_0^+ - z_0^* b_0 + z_2(b_2^+ + b_{-2}^+) - z_2^*(b_2 + b_{-2})]|0\rangle \tag{13.1.3}$$

where z_μ $(\mu = 0, 2)$ are complex functions of time and z_μ^* denote the corresponding complex conjugate functions. $|0\rangle$ stands for the vacuum state of the quadrupole bosons.

The wave function $|\psi\rangle$ is a coherent state with respect to the boson operators b_0^+, $b_{\pm 2}^+$. By means of the boson operators b_μ^+, b_μ one can define the collective coordinates and their conjugate momenta:

$$\alpha_\mu = \frac{1}{\sqrt{2k}}(b_\mu^+ + (-1)^\mu b_{-\mu}); \quad \pi_\mu = \frac{ik}{\sqrt{2}}((-1)^\mu b_{-\mu}^+ - b_\mu), \quad \mu = 0, \pm 2 \tag{13.1.4}$$

up to a real constant k.

Note that by Eq. (13.1.2), to the quantum mechanical eigenvalue problem of H, a set of classical equations for a point $M(t)$ in the phase space $\{(z_0, z_0^*, z_2, z_2^*)\}$ is associated. Knowing the position of M at a certain value for t, say t_0, the Eq. (13.1.2) determine $M(t)$ for any $t \geq t_0$. The set $\{M(t)\}_{t \geq t_0}$ defines the classical trajectories. Some of these trajectories can be quantized [KaGr79]. If H is restricted to its harmonic term the semiclassical spectrum coincide up to an additive constant to the corresponding quantal one.

The functions $|\psi\rangle$ form an overcomplete set in the boson space. This stems from that no vector component is missing in the expansion of $|\psi\rangle$ in the basis $|Nv\alpha IM\rangle$. Therefore, to some extent the variational function $|\psi\rangle$ is able to account for some properties of H in the whole boson space. Due to these features one hopes that choosing a coherent state as trial function, the requantized system approximate reasonably well the initial one.

Now let us denote by u_μ, v_μ the real and imaginary components of z_μ, respectively. Their time dependence is determined by solving the classical equations of motion yielded by (13.1.2):

$$\dot{u}_0 = \frac{1}{2}\frac{\partial \mathcal{H}}{\partial v_0}; \quad \dot{v}_0 = -\frac{1}{2}\frac{\partial \mathcal{H}}{\partial u_0}$$

$$\dot{u}_2 = \frac{1}{4}\frac{\partial \mathcal{H}}{\partial v_2}; \quad \dot{v}_2 = -\frac{1}{4}\frac{\partial \mathcal{H}}{\partial u_2}$$

(13.1.5)

where "$\bullet$" denotes the time derivative operation and $\mathcal{H}$ is the expected value of H (13.1.1)

$$\begin{aligned}
\mathcal{H}(u_0, v_0, u_2, v_2) \equiv \langle \psi \mid H \mid \psi \rangle &= A(u_0^2 + v_0^2 + 2u_2^2 + 2v_2^2) \\
&+ 2Bu_0(6u_2^2 - u_0^2) + 2C(2u_0v_2^2 \\
&+ 4v_0u_2v_2 - u_0v_0^2) + D(u_0^2 + 2u_2^2)^2 \\
&+ E(u_0v_0 + 2u_2v_2)^2 + F(u_0v_2 - u_2v_0)^2 \\
&+ G(v_0^2 + 2v_2^2)^2.
\end{aligned}$$

(13.1.6)

The factors $A, B, C, \ldots, G$ are determined by the coefficients involved in the model Hamiltonian. Hereafter the units convention $\hbar = 1$ is adopted.

Note that, since the trial wave function was subject to the restriction defined by $z_2 = z_{-2}$, the number of parameters characterizing the fourth order terms is equal to four and not to five as suggested by the Eq. (13.1.1).

In deriving (13.1.5) from (13.1.2) the expression for the density of classical action was needed:

$$s(t) \equiv \langle \psi \mid i\frac{\partial}{\partial t} \mid \psi \rangle = i[u_0\dot{v}_0 - v_0\dot{u}_0 + 2(u_2\dot{v}_2 - v_2\dot{u}_2)] \qquad (13.1.7)$$

It can be easily checked that $\mathcal{H}$ is constant in time for u_0, v_0, u_2, v_2 satisfying the Eq. (13.1.5).

$$\mathcal{H}(u_0, v_0, u_2, v_2) = E. \qquad (13.1.8)$$

The classical equations of motion (13.1.5) are highly nonlinear. Therefore, only numerical solutions are possible. However, there are closed and periodic orbits surrounding closely a given minimum point of the energy surface which can be approximated reasonably well by the solutions of the linearized equations of motion with respect to that minimum. Finding such solutions is certainly much easier than integrating the coupled differential equations. This class of orbits will be analyzed in the following subsection.

13.1.2 Stationary Points of $\mathcal{H}$

To find the periodic and harmonic states we have to find first the stationary points of $\mathcal{H}$ by solving the equations:

$$\dot{u}_\mu = 0, \quad \dot{v}_\mu = 0, \quad \mu = 0, 2. \tag{13.1.9}$$

and then to depict the minima. There are seven solutions for the Eq. (13.1.9), provided the coefficients of the model Hamiltonian satisfy the inequality:

$$9B^2 - 8AD \geq 0 \tag{13.1.10}$$

All of them have vanishing values for the v components: $\overset{\circ}{v}_0 = \overset{\circ}{v}_2 = 0$.

Three of the stationary points have $\overset{\circ}{u}_2 = 0$. The values of $\overset{\circ}{u}_0$ distinguishing between these three stationary points, hereafter denoted by S, D_1, E_1, are

$$\overset{\circ}{u}_0(S) = 0, \quad \overset{\circ}{u}_0(D_1) = (3B + X)/4D, \quad \overset{\circ}{u}_0(E_1) = (3B - X)/4D, \tag{13.1.11}$$

where the following notation was used: $X = (9B^2 - 8AD)^{\frac{1}{2}}$. The other four points are denoted by D_2, D_3, E_2, E_3 respectively, and have the coordinates $(\overset{\circ}{u}_0, \overset{\circ}{u}_2)$ given by:

$$(D_2; D_3; E_2; E_3) = ((X_0, Y_0); (X_0, -Y_0); (X_1, Y_0); (X_1, -Y_0)) \tag{13.1.12}$$

with

$$\begin{pmatrix} X_0 \\ X_1 \end{pmatrix} = \frac{-3B \mp X}{8D}, \quad Y_0 = \sqrt{\frac{3}{2}} \overset{\circ}{u}_0 \tag{13.1.13}$$

The points S, D_k, E_k (k = 1, 2, 3) are represented in Fig. 13.1a for $B > 0$ and in Fig. 13.1b for $B < 0$. The nature of the stationary points is found by analyzing the
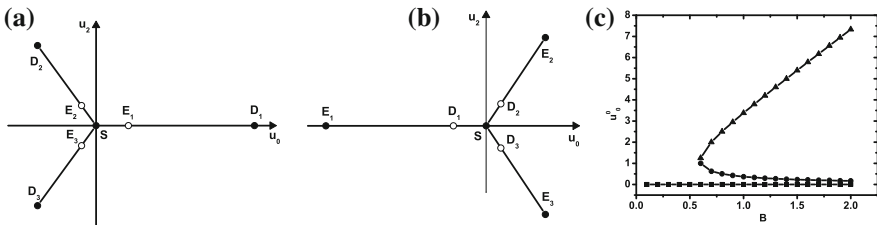

Fig. 13.1 **a** Stationary points of the energy surface for $B > 0$. *Black circles* correspond to minima while *open circles* to saddle ponts; **b** The same as in a, but for $B < 0$; **c** The stationary coordinate $\overset{\circ}{u}_0$ as function of B for $D = 0.4, A = 1, C = E = F = 0$ (in units of MeV). One distinguishes three branches (see the comment from the text)

sign of the Hessian function associated to $\mathcal{H}$. The results are as follows: For $B > 0$, the point S and D_k are minima for $\mathcal{H}$, while E_k are saddle points. When $B < 0$, the minima are in S and E_k, while D_k are saddle points for $\mathcal{H}$. Replacing the coordinates z_μ, z_μ^* by the values which produce the minima D_k ($B > 0$), the variational state become $|\psi(D_k)\rangle$ with k $= 1, 2, 3$. These states describe the static ground state of our system. Any two of these three wave functions can be related by a rotation transformation. Indeed, it can be checked that the following equations hold:

$$| \psi(D_2)\rangle = R(0, \frac{\pi}{2}, 0) \, | \, \psi(D_1)\rangle, \quad | \, \psi(D_3)\rangle = R(\frac{\pi}{2}, \frac{\pi}{2}, 0) \, | \, \psi(D_1)\rangle, \quad (13.1.14)$$

where

$$| \psi(D_1)\rangle = exp[\overset{\circ}{u}_0(D_1)(b_0^+ - b_0)] \, | \, 0\rangle, \qquad (13.1.15)$$

and $\overset{\circ}{u}_0(D_1)$ denotes the coordinate u_0 for D_1 which is given by (13.1.11). In virtue of these relations and the fact that H is a scalar for rotations, it results that the ground state is degenerate. Indeed, for $B > 0$ we have

$$\mathcal{H}(D_1) \ = \ \mathcal{H}(D_2) \ = \ \mathcal{H}(D_3) \qquad (13.1.16)$$

Parametrizing the average values of the quadrupole coordinate as:

$$\langle\psi|\alpha_0|\psi\rangle = \beta \cos\gamma, \quad \langle\psi|\alpha_{\pm2}|\psi\rangle = \frac{1}{\sqrt{2}}\beta \sin\gamma, \qquad (13.1.17)$$

one obtains the relation between the coordinates u_0 and $u_{\pm2}$ and the classical deformations β and γ:

$$u_0 = \frac{k}{\sqrt{2}}\beta \cos\gamma; \quad u_2 = \frac{k}{2}\beta \sin\gamma \qquad (13.1.18)$$

It is worth mentioning what is the shape of the nuclear system for the stationary points of $\mathcal{H}$. This can be obtained either from Eq. (13.1.8) or by evaluating the invariants β^2 and $\beta^3 \cos 3\gamma$:

$$I_2 \equiv \beta^2 = (\frac{\sqrt{2}}{k})^2(u_0^2 + 2u_2^2), \ I_3 \equiv \beta^3 \cos 3\gamma = (\frac{\sqrt{2}}{k})^3 u_0(u_0^2 - 6u_2^2). \ (13.1.19)$$

Inserting the coordinates of the stationary points into the Eq. (13.1.19) it results:

$$I_2(S) = I_3(S) = 0 \qquad (13.1.20)$$

As for the other points the values of the invariants are:

$$I_2(D_n) = \frac{8}{k^2}X_0^2, \;\; I_3(D_n) = -\frac{16\sqrt{2}}{k^3}X_0^3,$$

$$I_2(E_n) = \frac{8}{k^2}X_1^2, \;\; I_3(E_n) = -\frac{16\sqrt{2}}{k^3}X_1^3; \;\; n = 1, 2, 3 \qquad (13.1.21)$$

where X_0, X_1 are defined by (13.1.13). One can prove that:

$$sign\, I_3 = sign\, B \text{ for any of } D_n, E_n, \; n = 1, 2, 3. \qquad (13.1.22)$$

Therefore for $B > 0$ the nuclear system exhibits a prolate, while for $B < 0$ cor-
responds to an oblate axially symmetric shape. In order to obtain a triaxial ground
state, the model Hamiltonian should comprise boson monomials of order higher than
four. The stationary coordinate $\overset{\circ}{u}_0$ (according to the previous analysis there are three
values: 0, $(3B - X)/4D$, $(3B + X)/4D$) this is plotted in Fig. 13.1c as function of
B for $D = 2/5$ and $A = 1$. There are three branches in this plot: (i) $u_0 = 0$ for any
value of B; as we have already seen this abscissa axis correspond to the minimum
point of the type S; (ii) From the compatibility condition (13.1.10) it results that the
lower limit for B is $\sqrt{8AD}/3$. For this value of B, there is only one stationary point
(minimum) for $\mathcal{H}$; (iii) For larger values of B there are two stationary points different
from zero. One is a minimum, while the other one is a saddle point.

For a particular set of parameters (in units of MeV)

$$A = 1, \;\; B = 0.8, \;\; D = 0.4, \;\; C = E = F = 0 \qquad (13.1.23)$$

the cuts of the potential energy surface for $u_2 = 0$ and $u_0 = 2.5$ are given in Fig. 13.2a,
b respectively. In order to stress the sensitivity of the u_2 potential energy on the fixed
value of u_0 we give it in Fig. 13.2c, d for $u_0 = 0$ and $u_0 = -1.25$, respectively.

13.1.3 The RPA Like Equations

For what follows it is convenient to use the phase space coordinates:

$$U_k = 2^{\frac{k+2}{4}}u_k, \;\; V_k = 2^{\frac{k+2}{4}}v_k; \;\; k = 0, 2 \qquad (13.1.24)$$

Written in terms of these coordinates the energy function has the stationary points
$(\overset{\circ}{U}_k, \overset{\circ}{V}_k)$. Denoting by (q_k, p_k) the deviation of the current point from the "mini-
mum"

$$q_k = U_k - \overset{\circ}{U}_k, \;\; p_k = V_k - \overset{\circ}{V}_k \qquad (13.1.25)$$

the classical equations for q_k and p_k are:

(a)

(b)

(c)

(d)
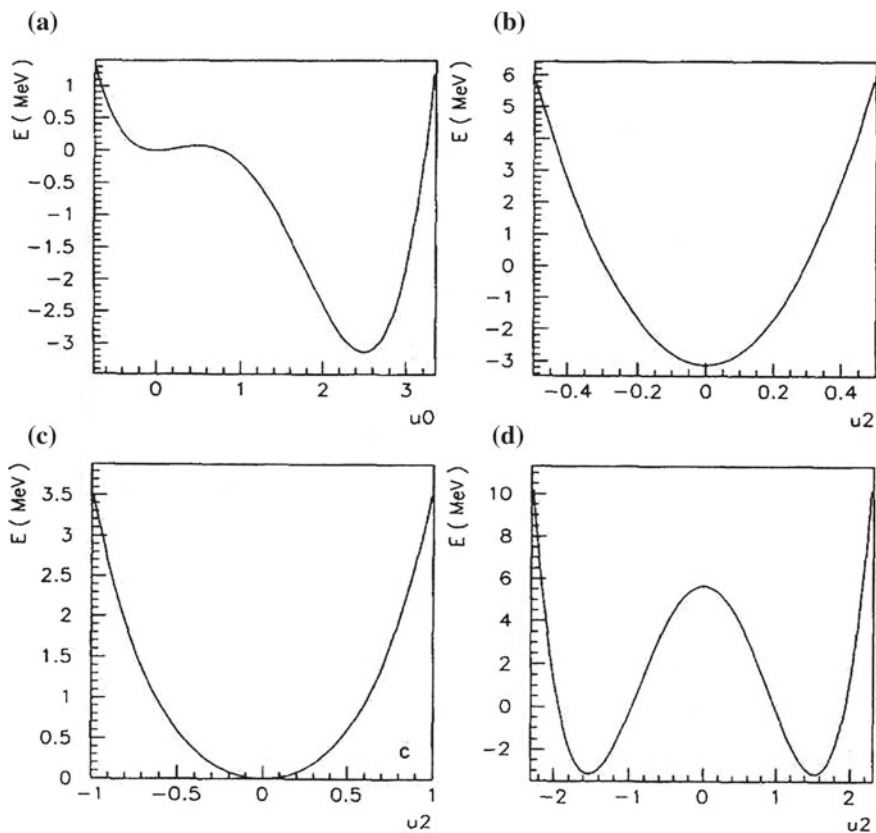
Fig. 13.2 The cuts of the equipotential energy obtained with the parameters A $= 1$, B $= 0.8$, D $= 0.4$, C $=$ E $=$ F $= 0$ (in units of MeV) with the planes: $u_2 = 0$ **(a)**, $u_0 = 2.5$ **(b)**, $u_0 = 0$ **(c)** and $u_0 = -1.25$ **(d)**

$$\dot{q}_k = \{q_k, \mathcal{H}\}; \quad \dot{p}_k = \{p_k, \mathcal{H}\} \qquad (13.1.26)$$

where $\{ \, , \, \}$ denotes the Poisson bracket. Keeping only the linear terms in q_k, p_k in the r.h.s. of (13.1.26), one obtains

$$\dot{q}_k = \sum_{m=0,2} A_{km} p_m; \quad \dot{p}_k = \sum_{m=0,2} B_{km} q_m \qquad (13.1.27)$$

where the matrices A and B have simple expressions in terms of the structure coefficients. Consider now the complex conjugate variables a_k^*, a_k with

$$a_k^* = \frac{q_k - i p_k}{\sqrt{2}} \qquad (13.1.28)$$

Using the coordinates a_k^*, a_k, the normal mode coordinate is defined by:

$$C^* = \sum_{k=0,2} (R_k a_k^* - S_k a_k) \qquad (13.1.29)$$

where the amplitudes R_k and S_k are determined so that the following equations are obeyed:

$$\{C^*, \mathcal{H}\} = i\omega C^*, \quad \{C^*, C\} = i \qquad (13.1.30)$$

From Eqs. (13.1.29) and (13.1.30) it results the RPA equations:

$$\begin{pmatrix} \frac{A-B}{2} & -\frac{A+B}{2} \\ \frac{A+B}{2} & -\frac{A-B}{2} \end{pmatrix} \begin{pmatrix} R \\ S \end{pmatrix} = \omega \begin{pmatrix} R \\ S \end{pmatrix} \qquad (13.1.31)$$

The compatibility condition for this homogeneous system of equations yields the dispersion equation for ω:

$$\omega^4 + \mathcal{B}\omega^2 + \mathcal{C} = 0 \qquad (13.1.32)$$

with

$$\mathcal{B} = \sum_{i,k=0,2} A_{ik} B_{ki}; \quad \mathcal{C} = (A_{00} A_{22} - A_{20} A_{02})(B_{00} B_{22} - B_{20} B_{02}) \qquad (13.1.33)$$

The amplitudes R_k, S_k are determined by Eq. (13.1.31) up to a multiplicative constant which is determined by the second Eq. (13.1.30), which yields:

$$\sum_{k=0,2} (R_k^2 - S_k^2) = 1. \qquad (13.1.34)$$

For the two sets of degenerate minima (one prolate and one oblate) the results for energy and amplitudes are particularly simple.

If the parameters involved in the model Hamiltonian (13.1.1) are such that $\mathcal{C} = 0$, the Eq. (13.1.32) admits $\omega = 0$ as solution. On the other hand the appearance of a vanishing energy is a signature for a phase transition. Here the transitions might be from spherical to axially deformed prolate shape, when $\omega_0 = 0$, and from prolate to an oblate deformed shape for $\omega_2 = 0$.

The equation $\mathcal{C} = 0$ determines four separatrices in the parameter space bordering two different "phases". Their equations are:

$$A - 6B\beta_0 + 6D\beta_0^2 = 0, \quad A - 2C\beta_0 + E\beta_0^2 = 0,$$

$$A + 6B\beta_0 + 2D\beta_0^2 = 0, \quad A + 2C\beta_0 + \frac{1}{2}F\beta_0^2 = 0. \qquad (13.1.35)$$

It is worth commenting on that the energies dependence on the coefficients C, E, and F multiplying the terms coupling the coordinates and momenta. These of course may influence the distribution as well as the nature of stationary points. Ignoring the coordinates-momenta coupling terms the situation becomes more transparent. Indeed, the separatrices become:

$$D = 0, \quad B = \pm\frac{2}{3}\sqrt{2AD}.$$

For $D > 0$, the branch corresponding to the sign $+$ delimits spherical and prolate shapes, while the curve determined by the sign $-$ borders the spherical and oblate phases.

Under these circumstances, the situation $\omega_2 = 0$ cannot be reached with the Hamiltonian (13.1.1) where the second order term $(b^+b^+ + bb)$ is missing. Including this term, one could approach the prolate—oblate transition through a gamma unstable regime.

Note that the Eq. (13.1.30) is equivalent to the differential equation:

$$\overset{\bullet}{C}^* = i\,\omega\,C^* \qquad (13.1.36)$$

which has the solution

$$C^* = K^*e^{i\omega t} \qquad (13.1.37)$$

where K^* is a complex number $K^* = |\,K^*\,|\,e^{i\varphi}$ which may be fixed by requiring that some "initial" conditions are fulfilled. The quantization procedure imposes a restriction to the classical action and this allows us to fix $|\,K^*\,|$ but not φ [RCGP84]. However, the classical energy does not depend on φ and therefore the quantization condition fully determines the energies. Keeping still the classical picture, it is instructive to get an image about how the nuclear system moves when accommodating one of the RPA state. To this aim we shall successively consider the oscillations around the minimum points D_1, D_2, D_3 which are visualized in Fig. 13.1a for a prolate shape. For the sake of simplicity we consider the case with $C = E = F = 0$. To begin with, let us start with D_1. For $\overset{\circ}{u}_2 = 0$ the RPA equations have a block structure. Indeed, for the state of energy ω_0 the amplitudes R_0, S_0 can analytically be calculated, while R_2, S_2 are equal to zero. Conversely, for the state of energy ω_2 the amplitudes R_0, S_0 are vanishing, while R_2, S_2 are not. Reversing the RPA transformation (13.1.29), one can express the canonical variables a_k^*, a_k in terms of

the normal mode variables. This way the time dependence of the coordinates u_k, v_k are readily obtained.

Denoting by $u_l^{(k)}$ the coordinates u_l corresponding to the RPA state of energy ω_k one obtains the following result:

$$u_l^{(k)} = \overset{\circ}{u}_l + \delta_{ln}(\frac{A}{\omega_n 2^{\frac{n}{2}}})^{\frac{1}{2}} \mid K_n^* \mid \cos(\omega_n t + \varphi_n); \quad l, n = 0, 2 \qquad (13.1.38)$$

Parameterizing the nuclear radius by the classical coordinates α_μ (13.1.4) with $k = \sqrt{2}$,

$$R = R_0(1 + \sum \alpha_\mu Y_{2\mu}^*) \qquad (13.1.39)$$

the deviation of the nuclear radius corresponding to the nth axis of the intrinsic frame of reference, from the constant value R_0 is:

$$\Delta R_n = (\frac{5}{4\pi})^{\frac{1}{2}} R_0 \beta \cos(\gamma - \frac{2\pi}{3} n), \quad n = 1, 2, 3 \qquad (13.1.40)$$

By means of Eq. (13.1.18), these quantities can be easily expressed in terms of the phase space coordinates u_0, u_2:

$$\Delta R_n = (\frac{5}{4\pi})^{\frac{1}{2}} R_0 [\frac{1}{2}(-u_0 + \sqrt{3}u_2)\delta_{n1} + \frac{1}{2}(-u_0 - \sqrt{3}u_2)\delta_{n2} + u_0\delta_{n3}] \quad (13.1.41)$$

Inserting (13.1.38) in (13.1.40), the result for the state of energy ω_0 is:

$$\Delta R_1 = \Delta R_2 = -\frac{1}{2}\Delta R_3,$$

$$\Delta R_3 = (\frac{5}{4\pi})^{\frac{1}{2}} R_0 [\overset{\circ}{u}_0 + (\frac{A}{\omega_0})^{\frac{1}{2}} \mid K_0^* \mid \cos(\omega_0 t + \varphi_0)] \qquad (13.1.42)$$

while for the RPA state corresponding to ω_2, one obtains:

$$\begin{pmatrix} \Delta R_1 \\ \Delta R_2 \end{pmatrix} = \frac{1}{2}(\frac{5}{4\pi})^{\frac{1}{2}} R_0 [-\overset{\circ}{u}_0 \pm \sqrt{3}(\overset{\circ}{u}_2 + (\frac{A}{2\omega_2})^{\frac{1}{2}} \mid K_2^* \mid \cos(\omega_2 t + \varphi_2))]$$

$$\Delta R_3 = (\frac{5}{4\pi})^{\frac{1}{2}} R_0 \overset{\circ}{u}_0 \qquad (13.1.43)$$

The Eqs. (13.1.42) and (13.1.43) comprise the signatures of the two RPA solutions. The first solution is a β-like vibration, since gamma is constantly equal to zero, while β exhibits a harmonic motion around a static value. The nuclear system oscillates along the 3rd axes with the pulsation ω_0. The amplitudes of the oscillations along the 1st and 2nd axes are half of that corresponding to the oscillation along the 3rd axes. We also notice on that the radii R_1 and R_2 oscillate in phase with respect to each other but out of phase with respect to the radius R_3.

As for the other RPA solution (ω_2), both the β and γ variables are functions of time. However, the radius R_3 is a constant of time. The radii R_1 and R_2 oscillate with opposite phase but with equal frequencies. This equatorial motion of the nuclear system is conventionally called gamma vibration. It is worth noting that for harmonic spherical limit (only A is different from zero) the beta and gamma vibrations loose the above mentioned meaning. Indeed, their energies become equal and they describe quadrupole oscillations around a spherical shape.

Consider now the motion around the points D_2 and D_3 from Fig. 13.1 which are characterized by $\mathring{u}_2 = +\sqrt{\frac{3}{2}}\mathring{u}_0$ and $\mathring{u}_2 = -\sqrt{\frac{3}{2}}\mathring{u}_0$ respectively. To express the quantities ΔR_k as functions of time, one has first to reverse the RPA transformation (13.1.29) and then use the connection with the coordinates u_0 and u_2. The final expressions for ΔR_k are:

$$\Delta R_1 = -\frac{1}{2}(\frac{5}{4\pi})^{\frac{1}{2}} R_0[\mathring{u}_0 - \sqrt{3}\mathring{u}_2 + \frac{1}{2}\sqrt{\frac{21}{2}}\sqrt{\frac{A}{\omega_2}} \mid K_2^* \mid \cos(\omega_2 t + \varphi_2)],$$

$$\Delta R_2 = -\frac{1}{2}(\frac{5}{4\pi})^{\frac{1}{2}} R_0[\mathring{u}_0 + \sqrt{3}\mathring{u}_2 + \frac{1}{2}\sqrt{\frac{5}{2}}\sqrt{\frac{A}{\omega_0}} \mid K_0^* \mid \cos(\omega_0 t + \varphi_0)]$$

$$\Delta R_3 = (\frac{5}{4\pi})^{\frac{1}{2}} R_0[\mathring{u}_0 + \frac{1}{4}\sqrt{\frac{5}{2}}\sqrt{\frac{A}{\omega_0}} \mid K_0^* \mid \cos(\omega_0 t + \varphi_0)]$$

$$+ \frac{1}{4}\sqrt{\frac{21}{2}}\sqrt{\frac{A}{\omega_2}} \mid K_2^* \mid \cos(\omega_2 t + \varphi_2)]. \qquad (13.1.44)$$

In conclusion, for a ground state which is not axially symmetric the axes 1 and 2 vibrate with the definite frequencies ω_2 and ω_0, respectively. Concerning the third axis, its motion is determined by a constructive interference of two vibrations of frequency ω_0 and ω_2, respectively. Also it is worth noting that this radius oscillates in antiphase with the radii R_1 and R_2.

13.1.4 Large Amplitude Motion

The results of the previous subsection were based on the linearization procedure applied to the classical equations of motion. Solving the linearized equations one finds classical periodic orbits which might be quantized. On the other hand, for a given set of initial conditions the exact solutions of the classical equations of motion can be obtained by numerical methods. Note that, since the energy is a constant of motion one has to specify only three initial coordinates, the fourth one being determined by requiring that the point belongs to the energy surface. If the orbit lies close to the minimum point of the energy surface, it may be approximated by that corresponding to the linearized equations of motion. The latter orbits might be

quantized through the Bohr-Sommerfeld procedure. If the closed orbit is lying far away from the minimum point, the linearization method does not work and we are faced with the quantization of a large amplitude motion. Along the time, several solutions for such a quantization procedure have been proposed. Here we mention only those procedures which have a direct connection to this study. According to Kan and Griffin [KaGr79] , the gauge invariant and periodic orbits are quantized by imposing the following restriction to the associated action:

$$\int_0^T s(t')dt' = 2n\pi \tag{13.1.45}$$

where $s(t)$ is given by Eq. (13.1.7) and T denotes the period of the orbit under consideration. Another method was proposed by Cambiaggio et al. in Ref. [CAM93]. Therein, the authors study the Fourier spectrum of the action:

$$S(t) = \int_0^t s(t')dt' \tag{13.1.46}$$

As mentioned above, there is a family of classical orbits depending continuously on the energy E. For a given value of E one calculates the Fourier spectrum of $S(t)$. One selects that value of E which satisfies the following consistency condition: the first peak in the Fourier spectrum has an abscissa equal to $E - E_0$, where E_0 is the minimum value of the classical energy. Let us denote the selected energy by E_1. The process is continued for $E > E_1$ and the next quantized energy is depicted when the consistency condition, i.e. the first peak appears at an energy equal to $E_2 - E_1$, is obeyed, etc. It is worth noting that the action $S(t)$ and its time derivative $s(t)$ have their peaks located at equal energies. Due to this feature, the above procedure may be also applied to the time derivative $s(t)$. For the sake of simplicity we shall adopt the latter version. This will be applied to find the quantum states lying in the second well of the potential energy shown in the Fig. 13.2a and in the well from Fig. 13.2b, respectively.

The classical orbits corresponding to the two potential energies are fully determined once the phase space coordinates characterizing the system at the initial time, $t = 0$, are specified. Thus, we consider the orbits emerging from the points

$$P_1 = (2.5, 0, \bar{v}_0, 0), \quad P_2 = (2.5, 0, 0, \bar{v}_2) \tag{13.1.47}$$

where $\bar{v}_0$ and $\bar{v}_2$ are determined by requiring that P_1 and P_2 belong to the surface given by the Eq. (13.1.8). Conventionally, a point in the phase space is specified by its coordinates, i.e. (u_0, u_2, v_0, v_2). The minimum values of the potential energies shown in Fig. 13.2a, b are equal. The common value is:

$$E_0 = -3.125 \, \text{MeV} \tag{13.1.48}$$

One can check that the trajectories comprising P_1 are of a beta type, while those passing through P_2 have a gamma character. The first three beta states fulfilling the consistency conditions for the quantization procedure have the excitation energies

$$e_1 = 1.72, \quad e_2 = 3.02, \quad e_3 = 4.00 \, (\text{MeV}) \tag{13.1.49}$$

It is worth mentioning that this procedure predicts an excitation energy which is twice as much as the energy of gamma vibration. This reflects the degeneracy of the vibrations along the axes u_2 and u_{-2}. Indeed, identifying u_2 and u_{-2} the fundamental frequencies defining the Fourier spectrum for $s(t)$ are doubled. Due to this fact in the Fourier spectrum shown in Fig. 13.4d the peak corresponding to the first gamma vibration appears at 8.14 MeV. The lower peak at about 2 MeV corresponds to the vibrational beta state, induced by an anharmonic coupling.

In order to see how the nuclear shape changes when the excitation energy is increased, some additional details about the structure of the states are necessary. To begin with, we consider first two beta states, namely those lying at 1.72 and 4 MeV. The Fourier spectra of the corresponding action density are shown in Fig. 13.3a, b, respectively. In the Fig. 13.3a one sees three peaks having the energies $e_1, 2e_1, 3e_1$, respectively. The second and third peaks correspond to two and three beta phonon states, respectively. To conclude, due to the anharmonic terms of the model Hamiltonian, the first excited state is a mixture of one (this is the dominant component), two and three phonon states.

As shown in Fig. 13.3b, the state lying at 4 MeV has a more complex structure. Indeed, this state is about 1 MeV above the previous state which lies close the first minimum of the potential energy (see Fig. 13.2a). Consequently the classical orbit surrounds both minima and therefore a larger number of components contribute in building up the state. In other words, the state is determined by the interference of two oscillations having different reference energies. This feature is revealed by Fig. 13.3d, showing the time dependence of $s(t)$ given by Eq. (13.1.7). By contrast, Fig. 13.3c shows a sole frequency characterizing the first beta state.

The shape variables β, γ behave differently in the two states considered above. While for the first state, i.e. that of energy equal to 1.72 MeV, the beta deformation is a periodic function of time (describing a harmonic oscillation of β around its static value), as shown in Fig. 13.3e for the third state, which has the excitation energy of about 4 MeV, the beta variable exhibits two components describing the oscillations around a spherical and a deformed equilibrium shape, respectively. The latter behavior is shown in Fig. 13.3f. The beta vibration character of the first state is also confirmed by the plot Fig. 13.3g showing the time dependence of gamma. The gamma deformation is constantly equal to its static value. Therefore the prolate shape with axial symmetry is preserved in time. The time evolution of the deformation γ in the state lying at 4 MeV, is shown in Fig. 13.3h. The nuclear shape changes suddenly from prolate to oblate and after a while comes back to the initial shape which is preserved for another interval of time. The average value of gamma is $\pi/6$. This is
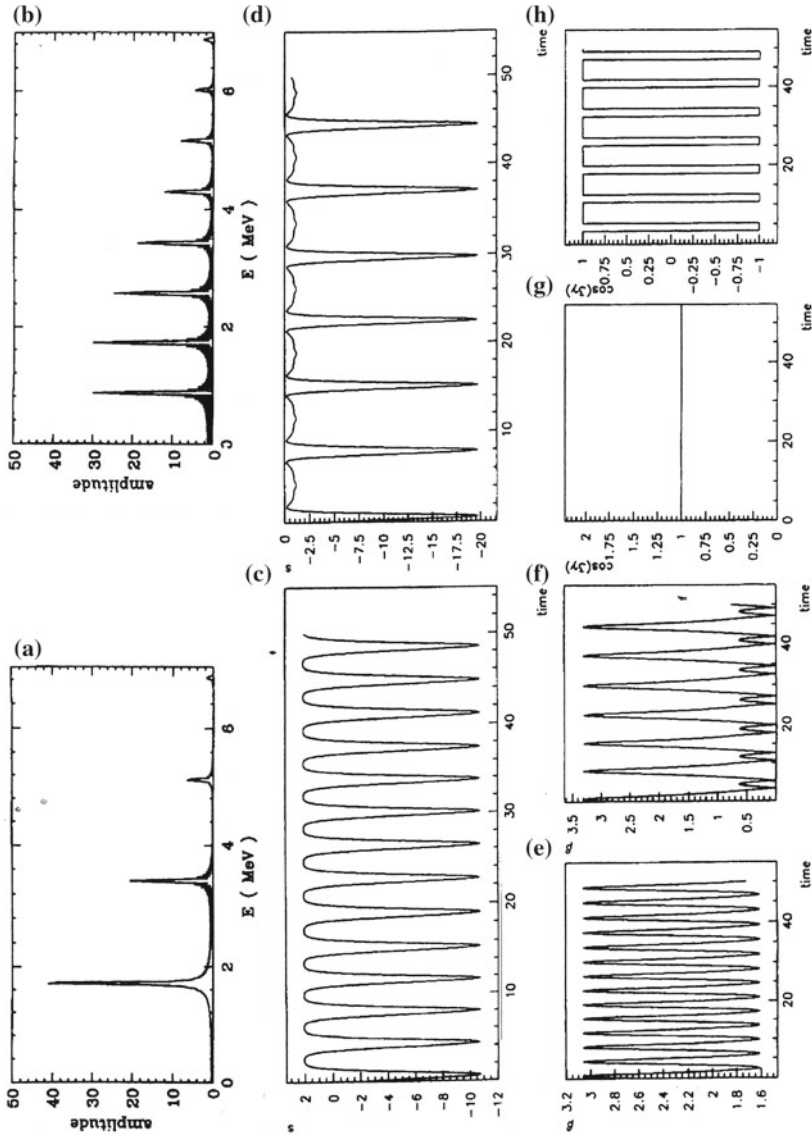
Fig. 13.3 **a** Fourier spectrum of the action density for the first quantized beta-like state. The consistency condition is fullfiled at the excitation energy $e_1 = 1.72\,\mathrm{MeV}$. The parameters involved in the model Hamiltonian are the same as in Fig. 13.2a. **b** The same as in (**a**) but for the third quantized beta-like state. The consistency condition is fulfilled for $e_3 = 4.00\,\mathrm{MeV}$; the energy is normalized to the ground state energy. **c** The time dependence of the action density for the first quantized beta state. **d** The same as in (**c**) but for the third quantized beta state. **e** The time dependence of the deformation parameter β for the first quantized beta state. **f** The same as in (**e**) but for third quantized beta state. **g** The time dependence of the papameter $\cos 3\gamma$ for the first quantized beta state. **h** The same as in (**g**) but for the third quantized beta state

a typical case of large amplitude motion pointing to the coexistence of two different shapes.

As for the potential well from Fig. 13.2b, one finds two quantum states of gamma type, whose excitation energies are 4.07 and 7.82 MeV, respectively. It is worth noting that, although these states lie above the saddle point ($u_2 = 0$) having the excitation energy equal to 3.075 MeV (see Fig. 13.2a), due to the initial conditions, the corresponding trajectories do not reach this point. This happens since the kinetic energy within a period is not large enough to exceed the deep of the u_0–potential well.

Let us focus our attention on the first excited gamma like state lying inside the potential energy shown in Fig. 13.2b. In this state the beta and gamma degrees of freedom are coupled together. However, we keep calling the state as gamma vibrational state in virtue of the geometrical interpretation referring to the time dependence of the nuclear ellipsoidal axes. As we have already seen, there are two frequencies which are contributing both to $\cos 3\gamma$ and β variables. This is again shown in Fig. 13.4a, b, where the time dependencies of β and $\cos 3\gamma$ are plotted, respectively. The complex structure of the shape coordinates yields the action time derivative $s(t)$ which is shown in Fig. 13.4c. Its Fourier spectrum is plotted in Fig. 13.4e. Since the two frequencies are commensurable the classical orbit is a closed curve. This feature is pictured in Fig. 13.4d, where the trajectory starting from P_2 with $\bar{v}_2$ satisfying the equation $\mathcal{H} = 0.95$ is plotted. One sees that the curve is located in a finite domain $(u_0, u_2) \in [2.17, 2, 52] \otimes [-0.36, 0.36]$ which is consistent with the above mentioned property concerning the confinement inside the second well of the potential Fig. 13.2a.

The last case considered here is that of the trajectory starting from P_2 lying on the surface with energy E = 5 MeV (we recall that the second quantized energy is of 4.70 MeV). The solutions $u_0(t)$, $u_2(t)$ of the classical equations of motion with the initial conditions mentioned above, do not have any periodic structure. They are plotted in Figs. 13.5a and 13.5b as functions of time. Collecting the points $\{(u_0(t), u_2(t))\}_t$ one obtains the trajectory from Fig. 13.5c, which encircles all minima presented in Fig. 13.1a (the points S, D_1, D_2, D_3). The corresponding Fourier spectrum for the derivative of the action $s(t)$, shown in Fig. 13.5d, is given in Fig. 13.5e and does not exhibit a discrete structure. Therefore such orbits cannot be quantized.

13.1.5 Summary and Conclusions

Here we summarize the main achievements for the large amplitude motion. We solved numerically the equations of motion and showed the time dependence of the shape variables β and $\cos 3\gamma$, as well as the Fourier spectrum for the time derivative of the classical action. If the "consistency" condition is satisfied one can extract the quantized energy from the Fourier spectrum. The corresponding quantum state is a mixture of states with higher energies. In the case of beta states, these higher energies
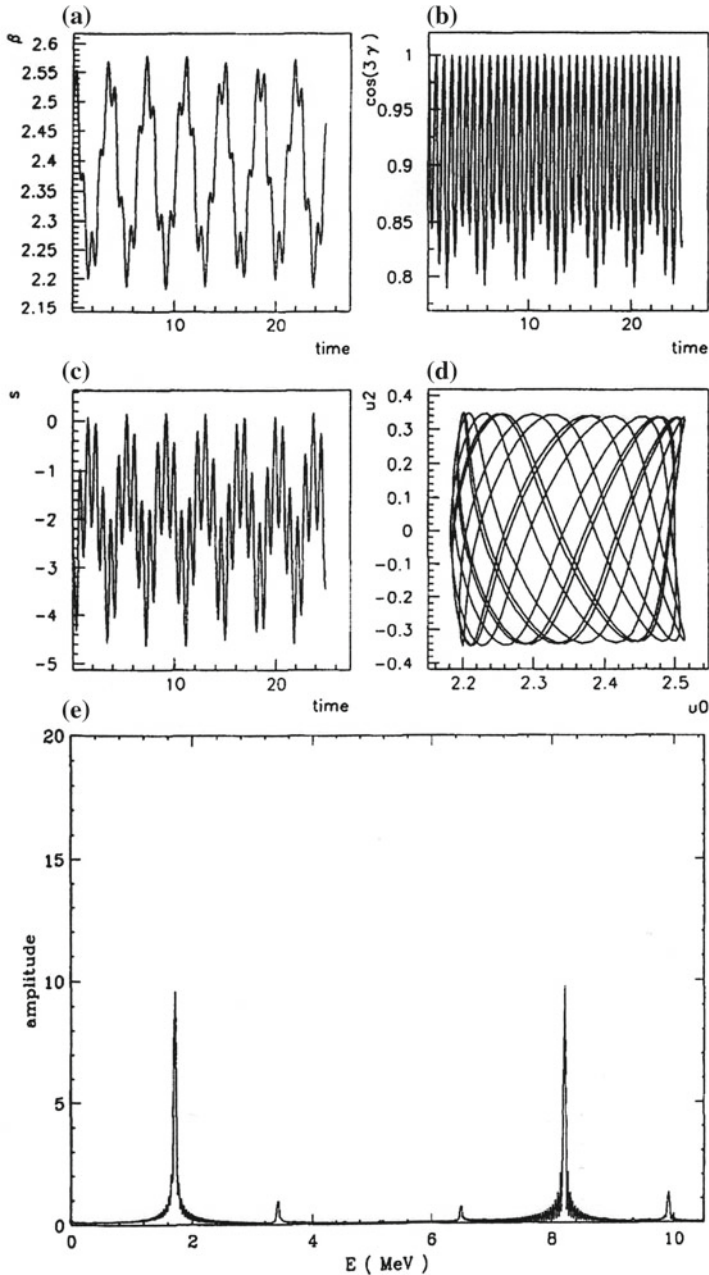
Fig. 13.4 **a** The time dependence of the deformation β for the first quantized gamma state. The consistency condition is achieved for $e_1 = 4.07$ MeV. The parameters defining the Hamiltonian are those from Fig. 13.2a. **b** The time dependence of the parameter $\cos 3\gamma$ for the first quantized gamma state. **c** The time dependence of the action density for the first quandized gamma state. **d** The classical trajectory corresponding to the first quantized gamma state, in the plane (u_0, u_2). **e** Fourier spectrum of the action density given in (**c**)
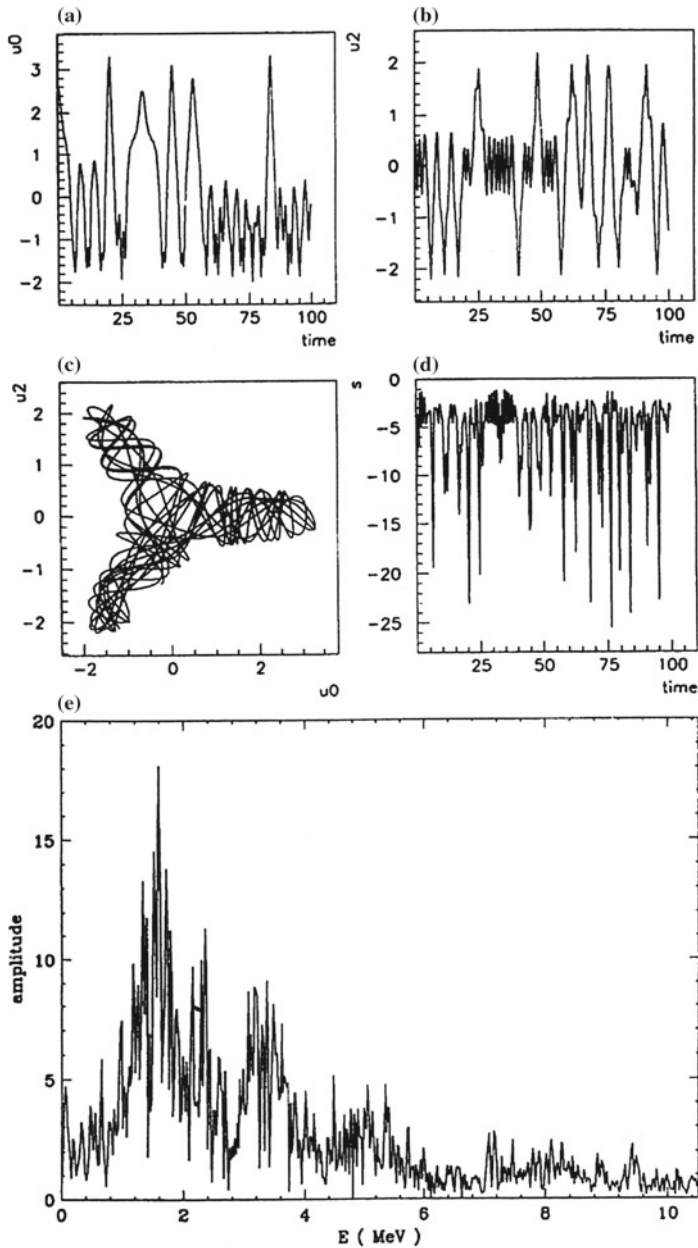
Fig. 13.5   a The time dependence of the coordinate u_0 for the first gamma-like trajectory at the energy $E = 5\,\mathrm{MeV}$. The parameters defining the Hamiltonian are those from Fig. 13.2a. **b** The same as in (**a**) but for the coordinate u_2. **c** The open classical trajectory of a gamma type motion in the plane (u_0, u_2). The time evolutions of the coordinates u_0, u_2 are given in (**a**) and (**b**), respectively. **d** The time dependence for the action density corresponding to the trajectory shown in (**c**). **e** Fourier spectrum of the action density for the trajectory given in (**c**)

are multiple of the lowest energy, while in the case of gamma states there are two fundamental frequencies associated with oscillations of the first and second nuclear radii, respectively. The orbits are closed and periodical. Also, a case of high energy ($\mathcal{H} = 5$) is considered. The corresponding orbit is surrounding all minima points and is not a closed one. Obviously, such kind of orbits cannot be quantized. All results described above, were obtained using for the parameters defining the Hamiltonian (13.1.1) the following values: A = 1, B = 0.8, D = 0.4, C = E = F = G = 0. These parameters determine the energies of the harmonic beta and gamma states: $\omega_0 = 2$. and $\omega_2 = 4.23$ MeV. Within the harmonic approximation (RPA) the next two excited beta states have the energies equal to 4 and 6 MeV, respectively. The energies of the first three states of the harmonic picture should be compared with the values 1.72, 3.02, 4. MeV, which are predicted by the Fourier spectrum analysis. The difference in the two sets is caused by the higher RPA contributions in the latter states. The one and two phonon gamma states have the energies equal to 4.23 and 8.46 MeV, respectively, while the first peaks in the Fourier spectrum of the gamma like trajectories are located at 4.07 and 7.82 MeV. By comparing the two sets of energies one may conclude that including the "RPA-boson" correlations the energies are decreased. Also, the anharmonicities affect beta like states to a larger extent than the states of gamma type.

Of course, a legitimate question is how well does the quantized energies for the "large amplitude" trajectories approximate the exact ones which could be obtained by diagonalizing the quantal Hamiltonian (13.1.1). To answer this question we invoke the results of Ref. [CAM93] where such a comparison is made in connection with a solvable model Hamiltonian. Indeed, for the cases where the Fourier spectrum has a discrete structure, the quantized spectrum approximate fairly well the exact one. For the complementary cases the diagonalization procedure applied to the quantal Hamiltonian is slowly convergent and therefore a special treatment is required from both quantal and classical sides.

13.2 Solvable Sixth Order Boson Hamiltonians

13.2.1 A Sextic Boson Hamiltonian

Here we shall treat semi-classically the following sixth order quadrupole boson Hamiltonian

$$H = A_1 \sum_{\mu} b_{\mu}^{\dagger} b_{\mu} + A_2 \sum_{\mu} \left(b_{\mu}^{\dagger} b_{-\mu}^{\dagger} + b_{-\mu} b_{\mu} \right) (-)^{\mu} + A_4 \hat{P}^2 + A_6 \hat{P}^3, \quad (13.2.1)$$

where $b_{\mu}^{\dagger}$ (b_{μ}) with $-2 \leq \mu \leq 2$, denotes the creation (annihilation) quadrupole boson operator and

$$\hat{P} = \frac{1}{2} \sum_{\mu} \left(b_{\mu}^{\dagger} + (-)^{\mu} b_{-\mu} \right) \left(b_{-\mu}^{\dagger} + (-)^{\mu} b_{\mu} \right) (-)^{\mu}. \tag{13.2.2}$$

Obviously, the model Hamiltonian does not commute with the boson number operator

$$\hat{N} = \sum_{\mu} b_{\mu}^{\dagger} b_{\mu}. \tag{13.2.3}$$

As in the previous section we are interested in solving the time dependent variational principle (TDVP) equations

$$\delta \int_{0}^{t} \langle \Psi | \left(H - i\hbar \frac{\partial}{\partial t'} \right) | \Psi \rangle dt' = 0. \tag{13.2.4}$$

with the variational state $|\Psi\rangle$ given by:

$$|\Psi\rangle = \exp \left[z_0 b_0^{\dagger} - z_0^* b_0 + z_2 (b_2^{\dagger} + b_{-2}^{\dagger}) - z_2^* (b_2 + b_{-2}) \right] |0\rangle. \tag{13.2.5}$$

The boson vacuum state is denoted by $|0\rangle$. The function $|\Psi\rangle$ depends on the complex parameters z_0, z_2 and their complex conjugates z_0^*, z_2^*. These parameters play the role of classical phase space coordinates whose equations of motion are provided by the TDVP equations. The function $|\Psi\rangle$ is a good candidate for the trial function, given the fact that H does not conserve the number of bosons. Note that the trial function is a mixture of components of different angular momenta which results in obtaining an intrinsic frame for the boson system. Also, the trial function is a mixture of components which are eigenstates of the z-component of the angular momentum. The corresponding eigenvalues for such components are conventionally called K quantum numbers. From Eq. (13.2.5) it results that Ψ is a mixture of even K components. As proved in Refs. [GRC78, RCG78], the coherent state $|\Psi\rangle$ may generate, through projection, the full SU(5) basis $|Nv\alpha JM\rangle$ with N- the number of bosons, v the seniority, α the missing quantum number, J and M the angular momentum and its projection on z-axis. From the trial function only the $K = even$ components of good angular momentum can be projected. The meaning of K quantum number in the projection formalism was commented in Ref. [RCGD82]. Indeed, the projected state with fixed K is actually a linear combination of components with different K', the projection of angular momentum on the z-axis of the intrinsic frame defined as in the framework of the liquid drop model. However, for large deformation the component with $K' = K$ prevails. To conclude, the quantum number K is related with an intermediate intrinsic frame where the function $|\Psi\rangle$ (13.2.5) has only $K = even$ components, while K' is defined within the real intrinsic frame defined by the principal axes of the moment of inertia.

Then, the variational principle equation yields the following equations:

$$\frac{\partial \mathcal{H}}{\partial z_0} = -i\hbar \overset{\bullet}{z_0^*}, \quad \frac{\partial \mathcal{H}}{\partial z_0^*} = i\hbar \overset{\bullet}{z_0}$$

$$\frac{\partial \mathcal{H}}{\partial z_2} = -2i\hbar \overset{\bullet}{z_2^*}, \quad \frac{\partial \mathcal{H}}{\partial z_2^*} = 2i\hbar \overset{\bullet}{z_2}. \tag{13.2.6}$$

Here the symbol "$\bullet$" denotes the time derivative operation. It is convenient to have the classical equations of motion in a canonical form. In order to reach this goal we perform the following change of variables

$$q_i = 2^{(k+2)/4}\mathbf{Re}(z_k), \quad p_i = \hbar 2^{(k+2)/4}\mathbf{Im}(z_k), \quad k = 0, 2, \quad i = \frac{k+2}{2}. \tag{13.2.7}$$

Up to an additive constant, $\frac{35}{4}A_4 + \frac{315}{8}A_6$, the classical energy function, defined as the average value of the model Hamiltonian with the coherent state $|\Psi\rangle$, has the expression:

$$\mathcal{H} \equiv \langle\Psi|H|\Psi\rangle = \frac{A'}{2\hbar^2}(p_1^2 + p_2^2) + \frac{A}{2}(q_1^2 + q_2^2) + \frac{D}{4}(q_1^2 + q_2^2)^2 + \frac{F}{6}(q_1^2 + q_2^2)^3, \tag{13.2.8}$$

where the following notations were used:

$$A' = A_1 - 2A_2, \quad A = A_1 + A_2 + 14A_4 + \frac{189}{2}A_6,$$

$$D = 4A_4 + 54A_6, \quad F = 6A_6. \tag{13.2.9}$$

The new variables obey the equations:

$$\frac{\partial \mathcal{H}}{\partial q_k} = -\overset{\bullet}{p_k}, \quad \frac{\partial \mathcal{H}}{\partial p_k} = \overset{\bullet}{q_k}, \quad k = 1, 2 \tag{13.2.10}$$

The sign minus in the first Eq. (13.2.10) suggests that p_k and q_k play the role of classical generalized momenta and coordinates, respectively. In terms of bosons, the conjugate coordinates have the expression:

$$\alpha_0 = \frac{1}{\sqrt{2}}(b_0^\dagger + b_0), \quad \pi_0 = \frac{\hbar}{i\sqrt{2}}(b_0 - b_0^\dagger),$$

$$\alpha_2 = \frac{1}{2}(b_2^\dagger + b_{-2}^\dagger + b_2 + b_{-2}), \quad \pi_2 = \frac{\hbar}{i2}(b_2 + b_{-2} - b_2^\dagger - b_{-2}^\dagger) \tag{13.2.11}$$

The phase space coordinates are given by:

$$q_k = \langle \Psi | \alpha_i | \Psi \rangle,$$
$$p_k = \langle \Psi | \pi_i | \Psi \rangle, \ \ k = 1, 2; \ \ i = 1 + (-1)^k. \qquad (13.2.12)$$

The nice feature of the classical energy function $\mathcal{H}$ consists of the fact that it does not contain powers of momenta higher than two, although we started with a high order boson Hamiltonian.

It is worth mentioning that similar time dependent approaches are also used for treating many body systems, when for example a Hartree Fock or an RPA approximation [RiSh80, RCGP84] is performed.

13.2.2 The Classical Description

From Eq. (13.2.10), the momenta can be expressed as the coordinate time derivative:

$$p_k = \frac{\hbar^2}{A'} \dot{q}_k, \ \ k = 1, 2. \qquad (13.2.13)$$

The classical energy expressed in terms of the polar coordinates (r, θ) associated to the plane (q_1, q_2), and their time derivatives looks like:

$$\mathcal{H} = \frac{\hbar^2}{2A'} (\dot{r}^2 + r^2 \dot{\theta}^2) + V(r), \qquad (13.2.14)$$

where $V(r)$ is the potential energy:

$$V(r) = \frac{1}{2} A r^2 + \frac{1}{4} D r^4 + \frac{1}{6} F r^6. \qquad (13.2.15)$$

For $r > 0$, depending on the coefficients involved, the potential energy function exhibits either two or no extreme points. In the first situation, the ordering of the maximum and minimum points is decided by the relative signs of the defining coefficients A, D and F. Here we study the case $A > 0$, $D < 0$, $F > 0$, $D^2 > 4AF$, which defines a potential having first a maximum and then a minimum. The other ordering situation is also interesting but will be not considered here. Since $V(r)$ depends only on even powers of r, $r = 0$ is an extreme point. For example for the coefficients A, D, F satisfying the ordering relations mentioned above, $r = 0$ is a minimum point.

For illustrative purposes we assume some concrete values for the structure coefficients involved, satisfying the sign restrictions mentioned above:

$$A = 3 \text{ MeV}, \quad D = -0.4 \text{ MeV}, \quad F = 0.01 \text{ MeV}, \quad A' = 0.0025 \text{ MeV}. \quad (13.2.16)$$

There are two constants of the motion, the energy:

$$\mathcal{H} = E, \quad (13.2.17)$$

and the third component of the angular momentum,

$$\mathcal{L}_3 \equiv \frac{1}{2}(q_1 p_2 - q_2 p_1) = \frac{\hbar^2}{2A'} r^2 \dot{\theta}. \quad (13.2.18)$$

For the sake of completeness we give also the expressions of the other two components of angular momentum:

$$\mathcal{L}_1 = \frac{1}{4}[\hbar(q_1^2 - q_2^2) + \frac{1}{\hbar}(p_1^2 - p_2^2)], \quad \mathcal{L}_2 = \frac{1}{2}[\hbar q_1 q_2 + \frac{1}{\hbar} p_1 p_2]. \quad (13.2.19)$$

These components generate a classical $SU_c(2)$ algebra with the multiplication operation:

$$\{\mathcal{L}_i, \mathcal{L}_k\} = \epsilon_{ikj}\mathcal{L}_j, \quad (13.2.20)$$

where $\{,\}$ denotes the Poisson brackets and ϵ_{ikj} the antisymmetric unit tensor. $\mathcal{L}_i$ might be obtained as average values on $|\Psi\rangle$ (13.2.5) of angular momentum components operators $\hat{L}_i$ acting on a boson space [RPB03] and defined in Chap. 3.

These boson operators generate a boson $SU_b(2)$ algebra. The correspondence $\frac{1}{i\hbar}[,] \rightarrow \{,\}$ achieves a homeomorphism of the two algebras mentioned above, $SU_c(2)$ abd $SU_b(2)$. Since the operators $\frac{b_2 + b_{-2}}{\sqrt{2}}$ and $\frac{b_2^\dagger + b_{-2}^\dagger}{\sqrt{2}}$ satisfy boson commutation relations, Eq. (3.4.17) represent the Schwinger boson representation of the angular momentum components acting in a fictitious space [Schw65].

The boson algebra defined above is different from the $SU_q(2)$ algebra of the angular momentum components carried by the quadrupole boson operators in the laboratory frame:

$$\mathbf{J}_\mu = \sqrt{10}\hbar \left(b^\dagger b\right)_{1\mu} \quad (13.2.21)$$

Indeed, with respect to the associated $SU_q(2)$ group, the bosons $b_{2\mu}^\dagger$ are tensors of rank 2 and projection μ. The tensor character of the quadrupole bosons with respect to the $SU_b(2)$ algebra is decided by their commutation relations with the generators $\hat{L}_k$. Thus, one finds that $b_0^\dagger$ and $\frac{b_2^\dagger + b_{-2}^\dagger}{\sqrt{2}}$ are the components $\frac{1}{2}$ and $-\frac{1}{2}$ respectively, of a tensor of rank $\frac{1}{2}$ with respect to the rotations around a set of axes $(1', 2', 3')$ obtained from $(1, 2, 3)$ through the transformation: $1 \rightarrow 3'$, $2 \rightarrow 1'$, $3 \rightarrow 2'$. Indeed, it can

be checked that the operators $\frac{\hat{L}_2 - i\hat{L}_3}{\sqrt{2}}, -\frac{\hat{L}_2 + i\hat{L}_3}{\sqrt{2}}, \hat{L}_1$ are the components $-1, +1, 0$ respectively, of a tensor of rank one with respect to the group $SU_b(2)$.

Due to Eq. (3.4.17), the operator $\hat{L}_3$ does not commute with $\mathbf{J}^2$ and consequently an eigenstate of $\hat{L}_3$ is a mixture of components of different angular momenta. We stress on the fact that the operators $\hat{L}_k$ generate rotations in a fictitious space. Moreover, they are different from the components of angular momentum in the intrinsic frame as defined within the liquid drop model. Three differences between the two momenta are to be noticed: (i) they obey different commutation relations; (ii) the intrinsic angular momentum describes the motion of the Euler angles, while the angular momentum considered here is defined by means of the intrinsic coordinates and their corresponding conjugate momenta; (iii) the intrinsic angular momentum length is the same as that of angular momentum in the laboratory frame. However, for the angular momentum $\hat{L}_k$ such an equality holds neither in the quantum mechanical picture nor for their classical images. Indeed, by a direct calculation one finds:

$$\langle \Psi | \hat{J}^2 | \Psi \rangle = 6\hbar^2 \left(|z_0|^2 + 2|z_2|^2 \right),$$

$$\langle \Psi | \hat{L}^2 | \Psi \rangle = \frac{\hbar^2}{4} \left[\left(|z_0|^2 + 2|z_2|^2 \right)^2 + 3 \left(|z_0|^2 + 2|z_2|^2 \right) \right]. \quad (13.2.22)$$

From these equations one derives an equation relating the averages of $\hat{J}^2$ and $\hat{L}^2$.

$$\langle \Psi | \hat{J}^2 | \Psi \rangle = -9 + 12\sqrt{\frac{9}{16} + \langle \Psi | \hat{L}^2 | \Psi \rangle},$$

$$\langle \Psi | \hat{L}^2 | \Psi \rangle = \frac{1}{144} \left[\langle \Psi | \hat{J}^2 | \Psi \rangle \right]^2 + \frac{1}{8} \langle \Psi | \hat{J}^2 | \Psi \rangle,$$

$$\hbar^2 \sum_{k=1}^{3} \mathcal{L}_k^2 = \frac{1}{144} \left[\langle \Psi | \hat{J}^2 | \Psi \rangle \right]^2. \quad (13.2.23)$$

This equation constitutes a proof for the assertion made above.

Therefore, classifying the states describing the intrinsic degrees of freedom by the quantum numbers associated to the $\hat{L}^2$ and $\hat{L}_3$ operators is a point of view which is different from all known boson formalisms. However, here $\langle \Psi | \hat{L}^2 | \Psi \rangle$ is not a constant of motion for the classical system which is a consequence of the fact that $\langle \Psi | \mathbf{J}^2 | \Psi \rangle$ is not either, despite the fact that in the laboratory frame the model Hamiltonian is a scalar operator with respect to the rotation group. Actually, this happens since the trial function has not good symmetry with respect to rotations. This implication does not hold in general. For example the BCS function breaks the gauge invariance and on the other hand the average of the particle number operator is a constant of motion for the classical system. However, an example of a sixth order boson Hamiltonian which together with the trial function Ψ define a classical system which admits both $\mathcal{L}_3$ and $\mathcal{L}^2$ as prime integrals, will be analyzed in one of the next subsections. In that case in the laboratory frame the $SU(2) \otimes SU(2)$ symmetry can be used to classify

the nuclear states, one group factor being associated to the dynamic deformations β and γ, while the other one to the motion of the Euler angles.

In order to avoid the confusion generated by the use of a common name for the $\hat{L}_\mu$ and $\mathbf{J}_\mu$ operators we shall conventionally call $\hat{L}_\mu$ as the components of the pseudo-momentum of the quadrupole intrinsic coordinates. Moreover, to simplify the nomenclature, hereafter we shall refer to $\hat{L}$ as to intrinsic pseudo-momentum. We notice that the variable θ is analogous to the dynamic γ deformation in the liquid drop model. Due to this analogy the intrinsic pseudo-momentum might be also called as the γ angular momentum.

The trial function $|\Psi\rangle$ is a superposition of components with odd number of bosons and components with even number. Obviously, the first components are mixture of intrinsic pseudo-momenta equal to half-integer multiple of $\hbar$ while the second type of components comprise only intrinsic pseudo-momenta which are integer multiples of $\hbar$. It results that from Ψ one may project both components with L_3 equal to $k\hbar$, k=integer and components with L_3 equal to $\frac{2k+1}{2}\hbar$, k=integer. One expects therefore that the third component of the classical intrinsic pseudo-momentum can take both sets of values mentioned above.

From the classical equation of motion it results that $\dot{\mathcal{L}}_3 = 0$ and consequently, the equation $\mathcal{L}_3 = const.$ holds. Actually, this equation is implied by the conservation law equation $[H, \hat{L}_3] = 0$, which takes place in the quantal picture. The classical system has two constants of motion, $\mathcal{H}$ and $\mathcal{L}_3$, and two degrees of freedom, r and θ. Therefore, the system is fully integrable and, consequently, analytical solutions for trajectories are expected to be possible.

Note that $\frac{\hbar^2}{A'}$ plays the role of the mass, m_0, of a classical non-relativistic particle moving in a central force field. The classical energy may be viewed as a counterpart of a microscopic Hamiltonian including a two body monopole-monopole interaction. In that case the coordinate r signifies the classical image of a collective microscopic coordinate [ReiSc82]. It is worth noting that the function $\mathcal{L}_3$ is actually half of the angular momentum component describing the rotation around an axis perpendicular to the plane spanned by the q_1, q_2 coordinates.

$$\bar{\mathcal{L}}_3 = q_1 p_2 - q_2 p_1. \tag{13.2.24}$$

Eliminating the angular variable in Eq. (13.2.14) one obtains:

$$\frac{\hbar^2}{2A'}\dot{r}^2 + V_{eff}(r) = E, \tag{13.2.25}$$

where $V_{eff}(r)$ is the effective potential energy given by:

$$V_{eff}(r) = \frac{A'\bar{\mathcal{L}}_3^2}{2\hbar^2 r^2} + V(r). \tag{13.2.26}$$

The constant of motion $\mathcal{L}_3$ depends on the initial conditions determining the classical trajectory $(q_1(t), q_2(t), p_1(t), p_2(t))$.

Before fixing the constant of motion, some additional comments are necessary. Since the operators $\hat{L}_\mu$ act in the boson space spanned by the operators $b_0^\dagger$ and $(b_2^\dagger + b_{-2}^\dagger)/\sqrt{2}$, which behave like spinors, one may say that they generate a SU(2) group. On the other hand we have seen that $\bar{\mathcal{L}}_3$ describe a rotation around an axis perpendicular on the plane of the (q_1, q_2) coordinates. Extending the plane to a three dimensional space (q_1, q_2, q_3) with q_3 the coordinate corresponding to the axis perpendicular to the plane (q_1, q_2), one could assert that $\mathcal{L}_k$ generates an SO(3) group describing the rotation in the specified three dimensional space. Since the angular momentum associated to these rotations takes values which are integer multiples of $\hbar$, we fix the constant of motion by the quantization restriction:

$$\mathcal{L}_3 = \frac{L}{2}\hbar, \quad L = 0, 1, 2, ... \quad (13.2.27)$$

Here we treat only the trajectories corresponding to the even values of L which results in confining our considerations to the quantization condition:

$$\mathcal{L}_3 = L\hbar, \quad L = 0, 1, 2, ... \quad (13.2.28)$$

The trajectories corresponding to half integer values of L in Eq. (13.2.28) can be treated in a similar manner. In principle, the values of L from Eq. (13.2.28) should be upper bounded by the angular momentum $\mathcal{L}$ length. However, $\mathcal{L}^2$ is not a constant of motion and therefore such limitation for L does not exist. Replacing $\bar{\mathcal{L}}_3$ by its quantized expression, the effective potential becomes:

$$V_{eff}(L; r) = \frac{2A'L^2}{r^2} + V(r). \quad (13.2.29)$$

This is a generalization of the Davidson potential [Dav32] since contains additional fourth and sixth powers of the coordinate r. For $L < 59$, $V_{eff}(L; r)$ exhibits a two minima shape. For the critical value $L = 59$, the minimum of the left well gets unified with the maximum of V_{eff} which results in arising an inflection point. For $L = 25$ and the set of parameters specified by Eq. (13.2.16), $V_{eff}(L; r)$ was plotted as function of r, in Fig. 13.6. The deep of the two wells depends on intrinsic pseudo-momentum in a different fashion. Indeed, while the first minimum exhibits a strong L dependence the second one is only slightly depending on L. This feature is shown in Fig. 13.7. From there we see that the difference between the maximum and the first minimum values of V_{eff} is decreasing with L and is vanishing at L equal about 59, where the two extremes become an inflection point.

From the equations of motion for $x = r^2$ and θ, one obtains:

$$dt = \frac{\hbar}{2}\sqrt{\frac{3}{A'F}}\frac{dx}{\sqrt{P_4(x; E, L)}}, \quad d\theta = L\sqrt{\frac{3}{A'F}}\frac{dx}{x\sqrt{P_4(x; E, L)}}, \quad (13.2.30)$$

Fig. 13.6 The effective
potential with the
coefficients A', A, D, F
specified in Eq. 13.2.16, is
plotted as function of r for
$L = 25$ with L the
pseudo-angular momentum
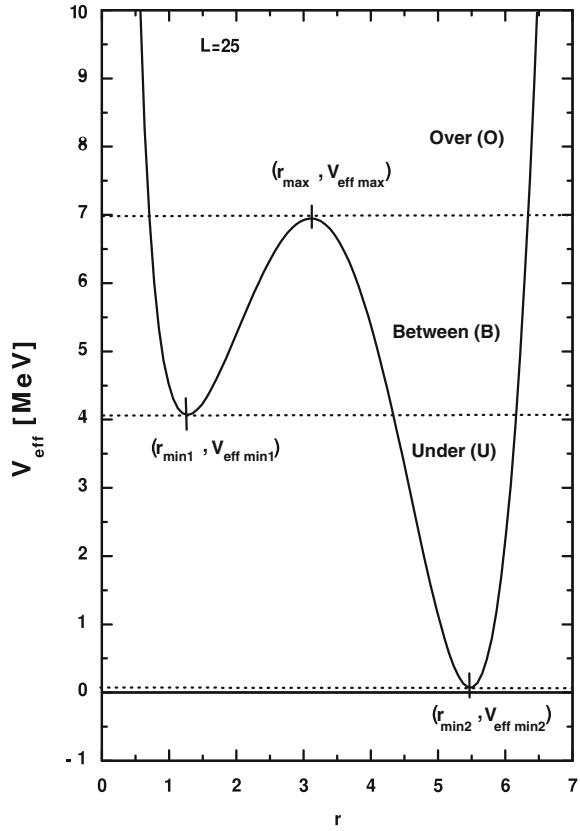
where

$$P_4(x; E, L) = -x^4 - \alpha x^3 - \beta x^2 - \gamma(E)\, x - \delta(L),$$

$$\alpha = \frac{3D}{2F} < 0, \quad \beta = \frac{3A}{F} > 0, \quad \gamma(E) = -\frac{6E}{F} < 0, \quad \delta(L) = 12\frac{A'L^2}{F} > 0.$$

$$(13.2.31)$$

For any $L < 59$ there are three energy domains defined as follows (see Fig. 13.6 for the case $L = 25$):

$$(a) \quad \text{UNDER, for } E \in [V_{eff\ min\,2}(L), V_{eff\ min\,1}(L)],$$

$$(b) \quad \text{BETWEEN, for } E \in [V_{eff\ min\,1}(L), V_{eff\ max}(L)], \qquad (13.2.32)$$

$$(c) \quad \text{OVER, for } E \in [V_{eff\ max}(L), +\infty).$$

The labels for the three intervals will be hereafter abbreviated by U, B and O respectively, whenever one wants to mention the fact that a given observable characterizes a
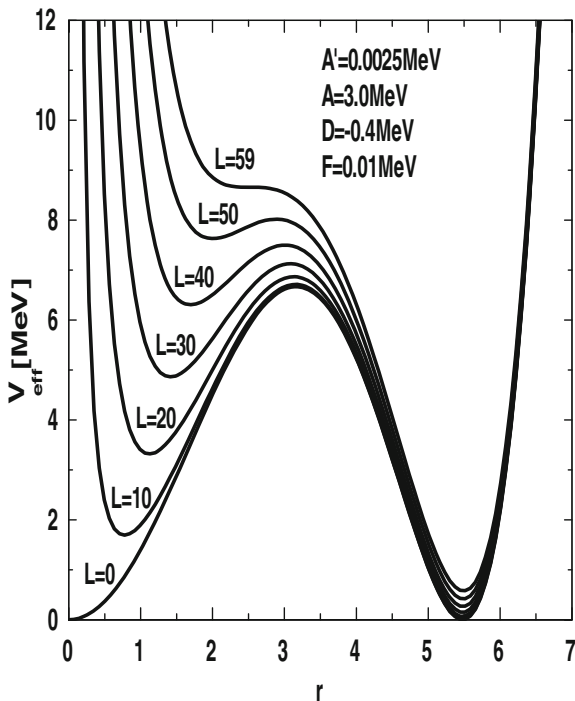
certain energy region. The system motion is allowed only for the values of "x" where
the polynomial P acquires positive values. Such allowed intervals are depicted sep-
arately for each of the energy regions U, B and O.

13.2.3 Results for an "U" Energy

In the energy interval U, the motion is possible only in the right well (see Fig. 13.6).
Indeed, inside U, the equation

$$P_4(x; E, L) = 0, \qquad (13.2.33)$$

has two real

$$x_1 = a(E, L), \quad x_2 = b(E, L), \quad x_1 > x_2, \qquad (13.2.34)$$

and two complex conjugate solutions:

$$x_3 = u(E, L) + i v(E, L) = x_4^*, \qquad (13.2.35)$$

Writing the polynomial $P_4(x; E, L)$ in the form

$$P_4(x; E, L) = -\prod_{k=1}^{4}(x - x_k), \tag{13.2.36}$$

it is clear that $P_4(x; E, L) \geq 0$ for $x \in [x_2, x_1]$.

For what follows it is useful to introduce the equation

$$v^2\lambda^2 + (ab - (a + b)u + (u^2 + v^2))\lambda - \frac{1}{4}(a - b)^2 = 0. \tag{13.2.37}$$

whose solutions are conventionally denoted by $\lambda_{1,2}(E, L)$ $(\lambda_2 > \lambda_1)$. We notice that the first Eq. (13.2.30) provides the time as function of the radial coordinate r. The analytical result for this sunction is given in Appendix H. By an inversion operation one obtains r as a function of time. Inserting this in the second Eq. (13.2.30) and integrating the resulting equation, one obtains θ as function of time. The two functions of time, r and θ, are periodic. However, their periods are different from each other. Moreover, they are not commensurable, which results in having open trajectories. Here we give details about the description of the motion of r, the calculations for the θ variable being performed by following similar steps.

For r, the period of the motion, $T_U(E, L)$, i.e. twice the time elapsed between two successive passages through the turning points situated at $r_{\min} = \sqrt{b(E, L)}$ and $r_{\max} = \sqrt{a(E, L)}$, is given by the equation [PBM81, WW50, GrRy65]

$$T_U(E, L) = \pi\hbar\sqrt{\frac{3}{A'F}} \frac{1}{\sqrt[4]{\Delta_U(E, L)}} \, _2F_1(\frac{1}{2}, \frac{1}{2}; 1; k_U^2(E, L)), \tag{13.2.38}$$

where

$$\Delta_U(E, L) = (ab - (a + b)u + (u^2 + v^2))^2 + (a - b)^2v^2, \tag{13.2.39}$$

with a, b, u and v depending on the energy E and the quantum number L as shown in Eqs. (13.2.35) and (13.2.36). $_2F_1(a, b; c; z)$ is the Gauss hypergeometric function and

$$k_U^2(E, L) = \frac{\lambda_2(E, L)}{\lambda_2(E, L) - \lambda_1(E, L)}. \tag{13.2.40}$$

The classical action corresponding to the degree of freedom r, written in units of $2\pi\hbar$ is given by the following integral:

$$I_U(E, L) = \frac{1}{2\pi\hbar} \int_{V_{eff\,\min2}(L)}^{E} T_U(w, L)dw. \tag{13.2.41}$$

13.2.4 Results for a "B" Energy

Similarly, in the case B, the zeros of the polynomial $P_4(x; E, L)$, are positive numbers denoted by

$$x_1 = a(E, L), \quad x_2 = b(E, L), \tag{13.2.42}$$
$$x_3 = c(E, L), \quad x_4 = d(E, L),$$

and ordered as follows

$$x_1 > x_2 > x_3 > x_4. \tag{13.2.43}$$

The solution for t as a function of r is given in Appendix H. The periods in both wells, left and right, are equal to each other. Indeed, one can prove that the two periods have a common expression:

$$T_{\text{B}}(E, L) = \pi\hbar \sqrt{\frac{3}{A'F}} \frac{1}{\sqrt{(a(E, L) - c(E, L))(b(E, L) - d(E, L))}}$$
$$_2F_1(\frac{1}{2}, \frac{1}{2}; 1; k_B^2(E, L)), \tag{13.2.44}$$

where

$$k_B^2(E, L) = \frac{(a(E, L) - b(E, L))(c(E, L) - d(E, L))}{(a(E, L) - c(E, L))(b(E, L) - d(E, L))}. \tag{13.2.45}$$

Since the hypergeometric function has a simple pole in $k = 1$ the period diverges when the energy approaches $V_{\text{eff max}}(L)$ from below. If we calculate the period for $E = V_{\text{eff max}}(L)$, the same divergence is obtained.

For the left well, the integral action given in units of $2\pi\hbar$ is equal to that formulated for the right well but restricted to the corresponding energy interval:

$$I_{\text{left}}(E, L) = I_B(E, L) = \frac{1}{2\pi\hbar} \int_{V_{\text{eff min1}}(L)}^{E} T_B(w, L)dw. \tag{13.2.46}$$

The action for a trajectory of energy E lying in the right well consists of two terms:

$$I_{\text{right}}(E, L) = I_U(V_{\text{eff min1}}(L), L) + I_B(E, L). \tag{13.2.47}$$

It turns out that $I_U(V_{eff\,min1}(L), L)$ is an integer number, namely

$$I_U(V_{eff\,min1}(L), L) = \frac{1}{2\pi\hbar} \int\limits_{V_{eff\,min2}(L)}^{V_{eff\,min1}(L)} T_U(w, L)dw = L. \qquad (13.2.48)$$

This equation was numerically checked in Ref. [RAU06] and seems to be a consequence of the restriction for the constant of motion $\mathcal{L}_3$, i.e. $\mathcal{L}_3 = L\hbar$. If we change this to $\mathcal{L}_3 = \frac{L}{2}\hbar$ the r.h.s. of the above equation would be $L/2$ and, moreover, the equation would be satisfied only for even values of L. The nice feature of our quantization procedure is that it produces degenerate quantal states in the two wells which in fact is consistent with what one obtains by solving the one dimensional stationary Schrödinger equation associated to the potential V_{eff}. Indeed, if E is an eigenvalue in the interval $[V_{eff\,min1}, V_{eff\,max}]$ then there are two independent solutions: for one solution the square of the wave function modulus is centered in the first well, while for another solution the system is localized in the second well. The initial condition is decisive for the system to choose one state or another. By contrast, the Schrödinger equation for the case $\mathcal{L}_3 = \frac{L}{2}\hbar$ with $L = odd$ yields non-degenerate states whose probability distributions are centered either on one or on another well.

Note that the classical trajectory in a well is taking care of the presence of the trajectory in the other well and thereby the tunneling effect is already included. If the two states are determined by the potential restricted to a single well respectively, then the final states are to be determined by switching on the interaction between the two states caused by the barrier separating the two wells. If the states energy is far away from the maximum value of the effective potential one expects that the two solutions are not interacting with each other. If this condition is not fulfilled the tunneling effect produces a shift of energies in the two wells. Since the two wells are centered in different r, one expects the shifts of the corresponding levels are different from each other. The difference of energies in the two wells and the time interval necessary for tunneling from one well to the other obey the uncertainty principle inequality. Of course, we should keep in mind that we deal with the intrinsic degrees of freedom which are fully decoupled from the rotational motion. Whether this degeneracy persists when the rotational degrees of freedom are switched on, i.e. the system is considered in the laboratory frame, is an issue to be studied in one of the next subsections. Deconspiring the result obtained there, we just mention that, indeed, such degeneracy persists, the degenerate states being characterized by the same seniority quantum number and different angular momenta. However, neither seniority nor the angular momentum are constants of motion for the intrinsic motion of the system considered so far. Indeed, considering the Casimir operator of the group O(5), defining the seniority quantum number,

$$\hat{\Lambda}^2 = \hat{N}(\hat{N} + 3) - 5\left(b^\dagger b^\dagger\right)_{00} (bb)_{00}, \qquad (13.2.49)$$

and averaging it on the trial function one obtains:

$$\langle\Psi|\hat{\Lambda}^2|\Psi\rangle = 2\left(q_1^2 + q_2^2 + \frac{1}{\hbar^2}\left(p_1^2 + p_2^2\right)\right) + \frac{1}{\hbar^2}\left(q_1 p_2 - q_2 p_1\right)^2, \quad (13.2.50)$$

One can check that this quantity is not a constant of motion although seniority is a good quantum number for the starting boson Hamiltonian. Therefore, the degeneracy in the intrinsic frame is caused by a different symmetry. As we mentioned before, the Hamilton function is invariant against changing $\mathcal{L}_3 \to -\mathcal{L}_3$ or equivalently against changing the axis 1 with the axis 2 and axis 2 by axis 1. Whether the degeneracy seen for the states in the two wells, when $\mathcal{L}_3 = L\hbar$, is caused by the symmetry mentioned above is still an open question.

Thus, the final expression for the integral action for a trajectory from the right well is

$$I_{\text{right}}(E, L) = L + I_{\text{left}}(E, L). \quad (13.2.51)$$

We notice that $k_B^2(E, L) < 1$ for $E < V_{\text{eff max}}(L)$, but $k_B^2(V_{\text{eff max}}(L), L) = 1$.

13.2.5 Results for an "O" Energy

The case (c) called "OVER" is similar to the case "UNDER". The only change to be done in the formulae pertaining to case U is the mere replacement $b(E, L) \to d(E, L)$ required by the conventional designations of the zeros of the polynomial P_4. Thus, the roots of $P_4(x; E, L)$, are

$$x_1 = a(E, L), \ x_2 = u(E, L) + iv(E, L) = x_3^*, \ x_4 = d(E, L), \quad (13.2.52)$$

with $x_1 > x_4$. (See also the notations for case (b) BETWEEN, when all roots are real and positive.)

Correspondingly, we denote by $\lambda_{1,2}(E, L)$ ($\lambda_2 > \lambda_1$) the solutions of the equation

$$v^2\lambda^2 + (ad - (a+d)u + u^2 + v^2)\lambda - \frac{1}{4}(a-d)^2 = 0. \quad (13.2.53)$$

For a chosen energy in the interval O, the first Eq. (13.2.30) has the analytical solution given in Appendix H.

The period of the motion of the coordinate r, $T_O(E, L)$, i.e. twice the time elapsed between two successive passages through the turning points situated at $r_{\min} = \sqrt{d(E, L)}$ and $r_{\max} = \sqrt{a(E, L)}$, is given by the equation

$$T_O(E, L) = \pi\hbar\sqrt{\frac{3}{A'F}}\frac{1}{\sqrt[4]{\Delta_O(E, L)}} \, {}_2F_1(\frac{1}{2}, \frac{1}{2}; 1; k_O^2(E, L)), \quad (13.2.54)$$

where

$$k_O^2(E, L) = \frac{\lambda_2(E, L)}{\lambda_2(E, L) - \lambda_1(E, L)}. \tag{13.2.55}$$

and $\Delta_O(E, L)$ is the discriminant of Eq. (13.2.53). When the energy approaches $V_{eff\,max}(L)$ from above, $\lambda_2 \to \infty$, and $k_O^2 \to 1$. Thus, the period of the motion diverges also when the energy approaches $V_{eff\,max}(L)$ from above.

The integral action for the case O is:

$$I_O(E, L) = I_{\text{right}}(V_{eff\,max}(L), L) + \frac{1}{2\pi\hbar} \int\limits_{V_{eff\,max}(L)}^{E} T_O(w, L)dw. \tag{13.2.56}$$

13.2.6 The Virtual Motion Under the Hump

The region shown in Fig. 13.6 under the hump is forbidden for the classical motion of r. Indeed, there the energy is smaller than V_{eff} which results in having a negative kinetic energy as required by Eq. (13.2.25). Note that for this situation, the integral (13.2.30) provides imaginary values for time, i.e., $\tau = it$. It is interesting to notice that by changing the time variable t by $-i\tau$ the resulting equation can be again integrated since the corresponding effective potential is now $-V_{eff}$ while the energy becomes -E. Trajectories in the well $-V_{eff}$ are conventionally called virtual. They are periodic curves in the new variable τ. Moreover, this period may be connected with the tunneling time through the hump, for the associated quantum system [ReiSc82, Ne85, LaMa94].

The period of the motion in the well $-V_{eff}(L; r)$, or in the hump of $V_{eff}(L; r)$, is given by

$$T_{\text{virt}}(E, L) = \pi\hbar\sqrt{\frac{3}{A'F}} \frac{1}{\sqrt{(a(E, L) - c(E, L))(b(E, L) - d(E, L))}}$$
$$_2F_1(\frac{1}{2}, \frac{1}{2}; 1; k_V^2(E, L)), \tag{13.2.57}$$

where

$$k_V^2(E, L) = \frac{(b(E, L) - c(E, L))(a(E, L) - d(E, L))}{(a(E, L) - c(E, L))(b(E, L) - d(E, L))}. \tag{13.2.58}$$

The integral action for the inverse of the hump potential is obtained in an analogous way with the procedure described before. The final result is:

$$I_{\text{virt}}(E, L) = \frac{1}{2\pi\hbar} \int\limits_{E}^{V_{\textit{eff} \, \max}(L)} T_{\text{virt}}(w, L)dw. \qquad (13.2.59)$$

13.2.7 Numerical Application

Here we give information about trajectories and the semiclassical spectrum corresponding to the coefficients (13.2.16). The shape of trajectories depends on the chosen value of energy. Here we consider a pair of trajectories corresponding to an energy lying close to the maximum value of the effective potential, Fig. 13.6. One trajectory is lying in the left well, while the other one in the right well. The two trajectories are quite different. Indeed, as shown in Fig. 13.8, upper left panel, in the left well r is running most of the distance $\sqrt{x_4} - \sqrt{x_3}$ in a very short time, then spends a large interval of time to reach the value $\sqrt{x_3}$ and to depart from it. Finally, r is coming quickly back to the value $\sqrt{x_4}$. The angle θ undertakes a jump of 2.5 *rad* before ending a period of motion. As for the right well, the r curve corresponding to E close to $V_{\textit{eff} \, \max}$ is different from the one commented above. Indeed, Fig. 13.8, upper right panel, shows that r stays longer close to the value $\sqrt{x_2}$ and a very short time in the neighborhood of $\sqrt{x_1}$. On the other hand, θ changes the speed around the half of period which is at variance with the behavior of the trajectory from the left well.

From Fig. 13.8 we see that after an interval of two periods of r, 2T, the variable θ covers about 11 *rad* in the left well, lower left panel, and only 5 *rad* in the right well, as shown in the lower right panel. This suggests that the trajectory $r = r(\theta)$ is not closed.

The two trajectories, lying in the left and right well respectively, correspond to E $= 6.984326$ MeV and are presented in Fig. 13.9.

As shown there, the inner and outer trajectories are almost tangent to each other. When the energy value is far from $V_{\textit{eff},\max}$ ($=6.98433$) there is an unreachable region, due to the hump. Such a situation is presented in Fig. 13.10 for E $= 6$ MeV and L $= 25$.

The periods of trajectories lying close to the maximum value of $V_{\textit{eff}}$ are much larger than those staying far from the top of the hump. As a matter of fact, the period of r has a discontinuity for $E = V_{\textit{eff} \, \max}$, which is pictorially shown in Fig. 13.11. Such a discontinuous behavior suggests that $V_{\textit{eff} \, \max}$ is a critical point of a phase transition. In one phase, for a given energy, the system may follow one of two r trajectories of equal periods, depending on the initial conditions, while in the second phase only one trajectory is possible.

Other two properties of the period are worth mentioning. From Fig. 13.11 it is clear that the curve does not start from zero. That means that the limit of period,
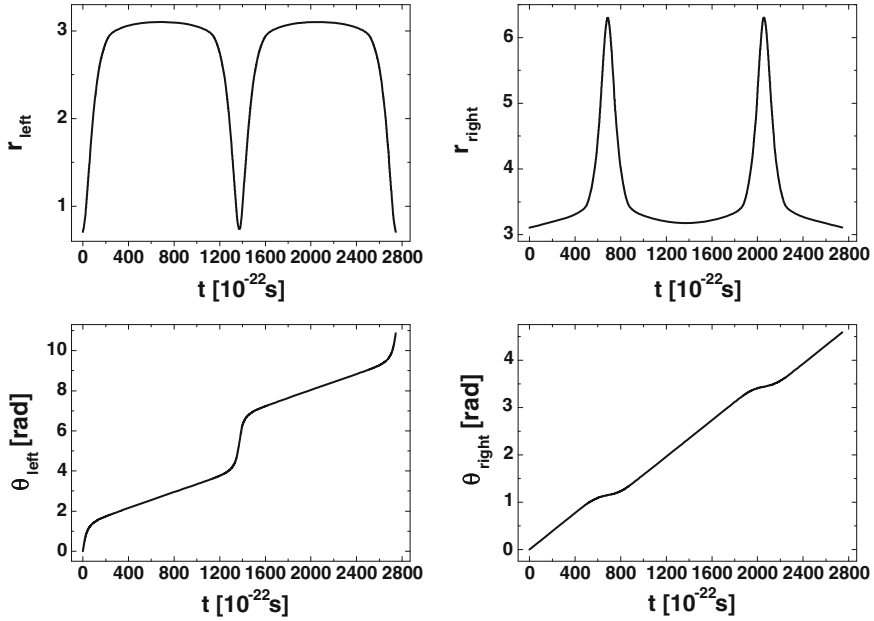
Fig. 13.8 The trajectories $r(t)$ (adimensional) and $\theta(t)$ (in units of *rad*) for the *left* and *right* wells, $E = 6.984326$ MeV and $L = 25$, where L has the meaning specified by Eq. (13.2.28)

Fig. 13.9 The trajectories $r(\theta)$ (adimensional) are represented in the coordinates $q_1 = r\cos(\theta)$ and $q_2 = r\sin(\theta)$ for $L = 25$ and $E = 6.984326$ MeV. The curves in both the *left* (the *inner curve*) and *right* (the *outer curve*) wells are given
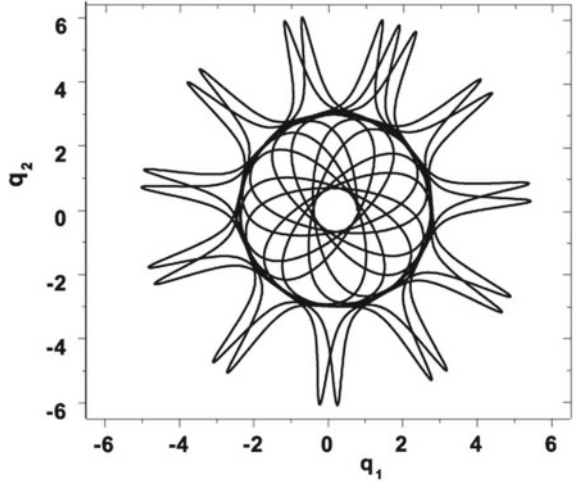
when the energy tends to $V_{eff\,min2}$, is a non-vanishing finite value T_{min2}. Also when $E \to V_{eff\,min1}$, the period is a non-vanishing quantity, T_{min1}. On the other hand when the energy is equal to the minimum value of the effective potential the trajectories of r are reduced to one of the stationary points $r(t) = r_{0,1}$, $r(t) = r_{0,2}$ which are

Fig. 13.10 The trajectories
$r(\theta)$ (adimensional) are
represented in the
coordinates $q_1 = r\cos(\theta)$
and $q_2 = r\sin(\theta)$ for L=25
and E=6 MeV. The curves
in both the *left* (the *inner
curve*) and *right* (the *outer
curve*) wells are given
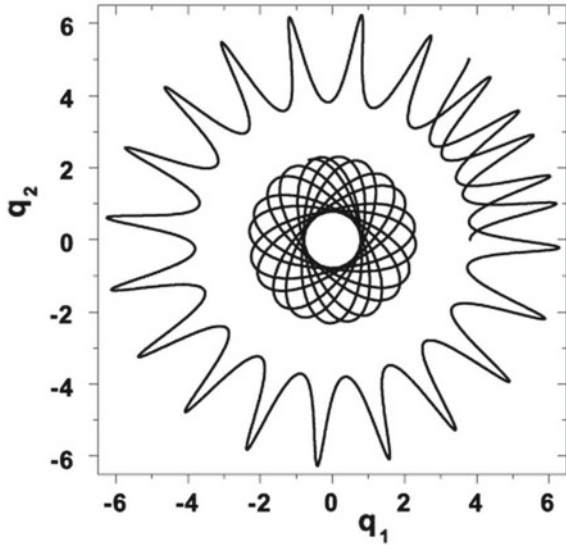
Fig. 13.11 The trajectory
periods in the *left* well of the
region B as well as in the
region O are plotted as
function of energy
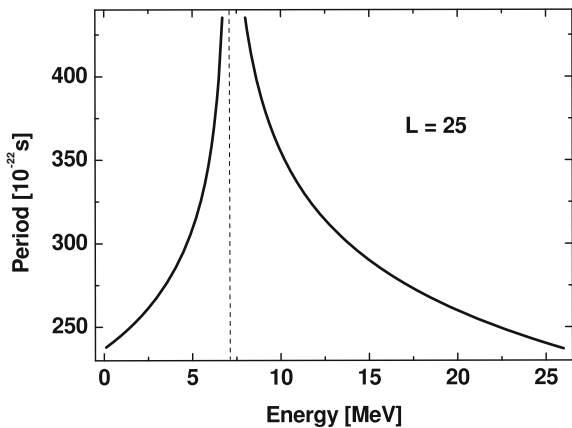
characterized by a vanishing period. The results reflect the fact that the periods T_U
and T_B given by Eqs. (13.2.39) and (13.2.45) respectively, are singular for energies
equal to $V_{eff\,min2}$ and $V_{eff\,min1}$, respectively. In order to restore the continuity feature
of the two periods one has to admit that the energy cannot reach the extreme values
of V_{eff} where the kinetic energy would be equal to zero, but there is a limiting energy
in each of the two wells, E_{01}, E_{02} determined by the period limits mentioned above.
As a matter of fact, this is a nice classical display for the zero point motion appearing
in the quantum mechanical picture.

13.3 Quantization of Periodic Trajectories

We note that $\mathcal{H}$ does not depend on θ but only on its conjugate momentum. Consequently, there is a constant of motion $\mathcal{L}_3$ which is discretized by the constraint (13.2.28). The remaining variable r and its conjugate momentum p_r are both involved in the classical Hamiltonian. Moreover, r performs a periodical motion. Consequently, its motion can be quantized by a constraint for the classical action similar to the Bohr-Sommerfeld condition, corrected with the zero point motion term. This condition will be applied separately for each region specified in Fig. 13.6. Thus, in the energy region called "UNDER", the quantization equation

$$I_{\mathrm{U}}(E, L) = n_1 + \frac{1}{2}, \qquad (13.3.1)$$

gives the energy levels $E_{\mathrm{under}}(L, n_1)$ situated in the right well below $V_{\mathit{eff}\,\mathrm{min}\,1}(L)$. Let us denote by E_0 the solution of Eq. (13.3.2) for $n_1 = 0$ and by E_{01} and E_{02} the energies of the first quantized states (of n = 0) in the two wells respectively. It is remarkable that the following equation holds:

$$E_{01} = V_{\mathit{eff}\,\mathrm{min}\,1}(L) + E_{02}, n_1 = L. \qquad (13.3.2)$$

This equation says that $V_{\mathit{eff}\,\mathrm{min}\,1}(L) + E_{02}$ is a quantal level in both left and right wells. Moreover, below this energy, in the right well there are another L levels. The quantization condition in the left and right wells of the region "BETWEEN", reads

$$I_{\mathrm{left}}(E, L) = n_2 + \frac{1}{2}, \quad I_{\mathrm{right}}(E, L) = n_1 + \frac{1}{2}, \qquad (13.3.3)$$

These equations determine the same energy levels in both wells

$$E_{\mathrm{left}}(L, n_2) = E_{\mathrm{right}}(L, n_1), \qquad (13.3.4)$$

where $n_1 = n_2 + L$. The spectrum in the region "OVER" is obtained by solving the equation provided by the quantization condition

$$I_{\mathrm{O}}(E, L) = n_3 + \frac{1}{2}. \qquad (13.3.5)$$

The virtual quantum states lying in the potential $-V_{\mathit{eff}}$ are obtained from

$$I_{\mathrm{virt}}(E, L) = n_4 + \frac{1}{2}. \qquad (13.3.6)$$

Having the integral action for the forbidden energy region, one can calculate the transmission coefficient through the potential barrier. Indeed, according to the WKB (Wentzel-Kramer-Brillouin) approximation, the transmission coefficient through the

hump is given by the equation:

$$D(E, L) \approx \exp(-2\pi I_{\mathrm{virt}}(E, L)). \tag{13.3.7}$$

13.3.1 Numerical Results

Solving the above equations of E, one finds the semiclassical spectrum of the system. It is instructive to see how many quantum states with energy less than $V_{\mathit{eff\,max}}$ accommodate in each of the two wells. The number of states is presented in Figs. 13.12 and 13.13 as a function of angular momentum for the left and right well, respectively. Note that for some L, the number of states is the same as for the L+1 case.

Fig. 13.12 The number of states from the *left* well are given as function of L (13.2.28)
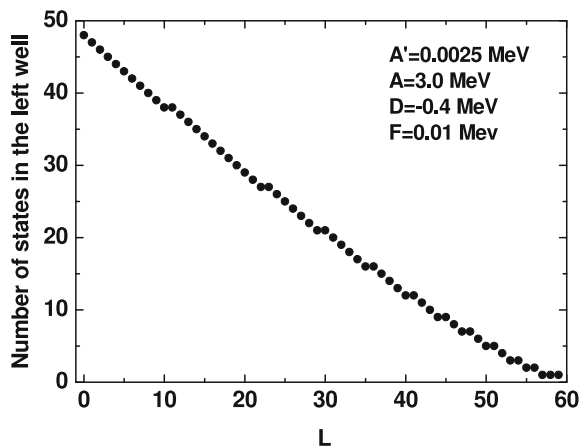
Fig. 13.13 The number of states in the *right* well is plotted as function of L (13.2.28)
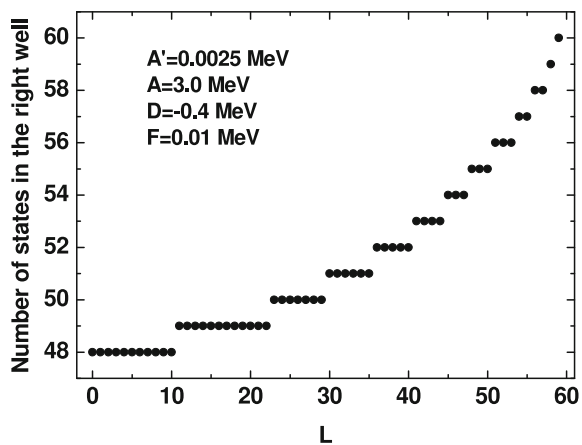
Fig. 13.14 The energy levels of the $L = 0$, $L = 1$ and $L = 2$ bands from the *left* well. Energy levels are labeled by n
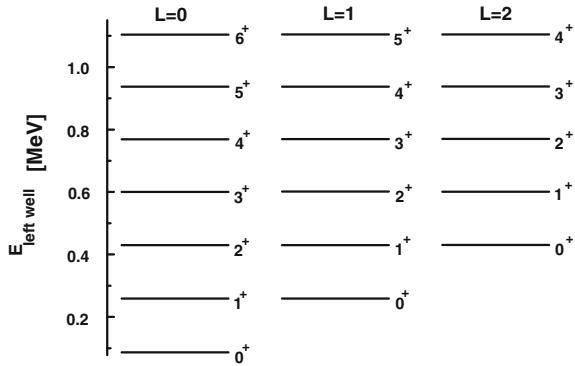
Fig. 13.15 The energy levels in the $L = 0$, $L = 1$ and $L = 2$ bands obtained in the *right* well. Energy levels are labeled by n
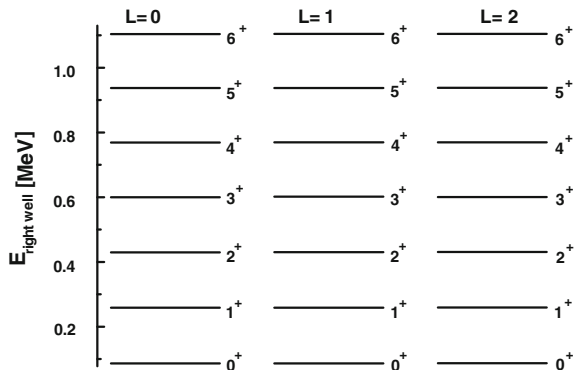
The quantal states are tentatively organized in rotational bands in Figs. 13.14 and 13.15, in a full analogy with the standard definition of the lowest bands within the liquid drop model. Indeed, each energy level is labeled by two quantum numbers, L and n. We have two options to organize the energy levels in columns. One is to choose n as column index and the second one when L is the column label. The first one is apparently more attractive because then we would have a $\Delta L = 1$ sequence which looks similar to some rotational bands in the laboratory frame. The second one is also a good option since L here is the third component of $\mathcal{L}$ and therefore would play the role of a K quantum number. In order to decide which one corresponds to the standard definition of a band one has to analyze the reduced transition probabilities between consecutive states of a band. Here we make the option for the second version having in mind the following arguments. If we consider a lowest order boson expression for the E2 transition operator, T^{ha}, this cannot relate states characterized by $L = integer$, since it is a tensor of rank $\frac{1}{2}$. Let us consider now as anharmonic term a scalar operator with respect to the group generated by $\hat{L}_k$ with k $= 1, 2, 3$:

$$T^{anh} = q_{anh} \left[2b_0^\dagger b_0 + \left(b_2^\dagger + b_{-2}^\dagger \right) (b_2 + b_{-2}) \right]. \tag{13.3.8}$$

Obviously, this can relate states of equal L. Therefore, when the transition operator has the expression $T^{ha} + T^{anha}$ the bands are decoupled from each other. If the rotational symmetry is restored, then on the top of each member of the above defined bands, one could build a full band. A similar situation may be met in the case of $L = half\ integer$.

In contradistinction to what happens for real trajectories, the integral action for the virtual states, is a decreasing function of energy. Also, the number of states from $-V_{eff}$ is a decreasing function of intrinsic pseudo-momentum.

Energy levels for the virtual states do not coincide with energy levels corresponding to real states of left and right well. The differences in energy and the period of virtual states satisfy the uncertainty relations.

Let us consider the transmission coefficients corresponding to the virtual state of highest energy, i.e., the first one under the hump. These are calculated within the WKB approximation by making use of Eq. (13.3.7), for a given value of the intrinsic pseudo-momentum. The results are given in Figs. 13.16 and 13.17. It is worth mentioning the discontinuity of D(E, L) given by Eq. (13.3.7) for some values of L. Indeed, going from the values 10, 22, 29, 35, 40, 44, 47, 50, 53, 55 to 11, 24, 30, 36, 41, 45, 48, 51, 54, 56 respectively, one achieves a very big jump in magnitude for the transmission coefficient. These discontinuities correspond to the jumps in the number of states in terms of L.

Note that the transmission coefficients depend exponentially on the energy distance of the first virtual state and $V_{eff\,max}$.

Fig. 13.16 The transmission coefficient calculated with Eq. (13.3.7) is plotted as function of L given by Eq. (13.2.28)
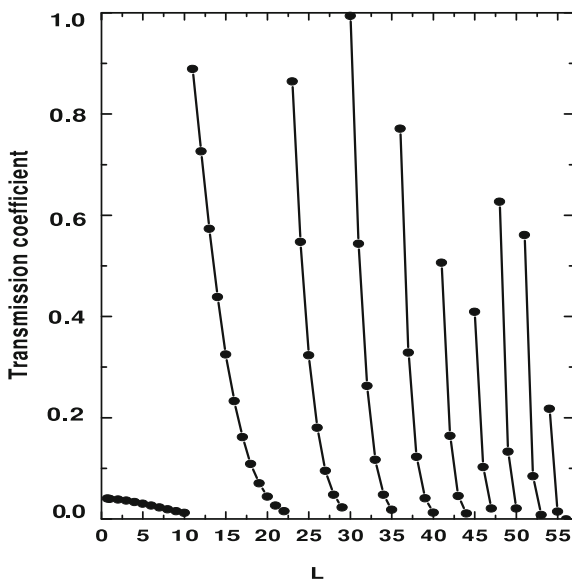
Fig. 13.17 The transmission coefficient (adimensional) defined by Eq. (13.3.7) is plotted versus $\Delta E_{max-first}$ the excitation energy (given in units of keV) of the first virtual state
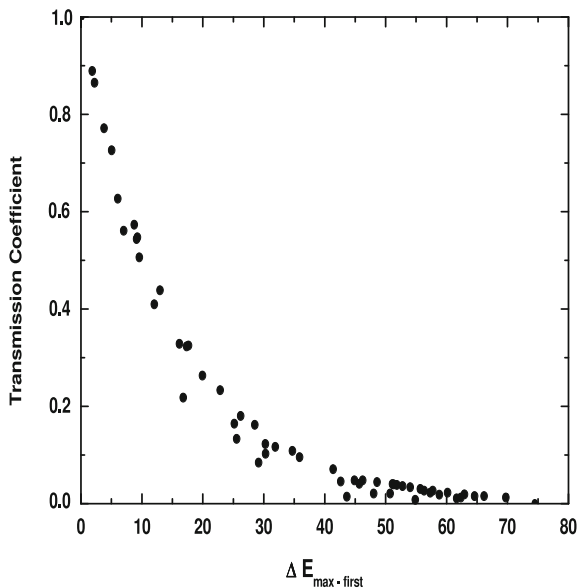
13.3.2 Another Boson Hamiltonian

Here we spend few words about another sixth order quadrupole boson Hamiltonian which exhibits some distinct properties:

$$H_2 = \epsilon \sum_{\mu} b_{\mu}^{\dagger} b_{\mu} + \sum_{J=0,2,4} C_J \left[(b^{\dagger} b^{\dagger})_J (bb)_J) \right]_0 + F(b^{\dagger} b^{\dagger})_0 \hat{N}(bb)_0. \quad (13.3.9)$$

$\hat{N}$ denotes the quadrupole boson number operator. Using the same notations as in the previous subsections, the average of H_2 on $|\Psi\rangle$ has the expression:

$$\mathcal{H}_2 = \frac{A}{2} \left(q_1^2 + q_2^2 + \frac{1}{\hbar^2}(p_1^2 + p_2^2) \right) + \frac{B}{4} \left(q_1^2 + q_2^2 + \frac{1}{\hbar^2}(p_1^2 + p_2^2) \right)^2$$

$$+ \frac{C}{8\hbar^2}(q_1 p_2 - q_2 p_1)^2 + \frac{F}{10} \left[\frac{1}{4} \left(q_1^2 + q_2^2 + \frac{1}{\hbar^2}(p_1^2 + p_2^2) \right)^2 \right.$$

$$\left. - \frac{1}{\hbar^2}(q_1 p_2 - q_2 p_1)^2 \right] \left(q_1^2 + q_2^2 + \frac{1}{\hbar^2}(p_1^2 + p_2^2) \right). \quad (13.3.10)$$

where A, B, C have simple expressions in terms of C_J with $J = 0, 2, 4$. Note that the classical energy involves terms which are quartic or even sextic in momenta as

well as terms coupling the coordinates and momenta. These two features are missing in the classical Hamiltonian treated above. Also, one can prove that both $\mathcal{L}^2$ and $\mathcal{L}_3$ are constants of motion. We recall that in the case treated in the previous subsection only $\mathcal{L}_3$ had this property. Taking the two constants equal to $\hbar^2 L(L+1)$ and $\hbar M$ respectively, the energy becomes a function of the quantum numbers L and M:

$$E_{LM} = 2A\sqrt{L(L+1)} + 4BL(L+1) + \frac{C}{2}M^2$$
$$+ F\frac{8}{5}\sqrt{L(L+1)}\left[L(L+1) - M^2\right]. \tag{13.3.11}$$

This energy is associated to the motion of the intrinsic degrees of freedom. Supposing that these degrees of freedom are only weakly coupled to the Euler angles, then the total energy may be written as:

$$E_{JLM} = E_{LM} + \delta J(J+1). \tag{13.3.12}$$

where J denotes the angular momentum in the laboratory frame while δ has a simple expression in terms of the structure coefficients ϵ and C_J with $J = 0, 2, 4$. On the other hand, the ground band energies can be obtained by averaging H on the states $\{|N v \alpha J M\rangle\}$ with $N = v = \frac{J}{2}$. The same energies are obtained if in Eq. (13.3.11) one substitutes:

$$2\sqrt{L(L+1)} \rightarrow \frac{J}{2}, \quad M = 0. \tag{13.3.13}$$

Thus, energies of the ground band are given by the following equation:

$$E_J = A\frac{J}{2} + B\frac{J^2}{4} + \delta J(J+1) + \frac{F}{5}\frac{J^3}{8}$$
$$\equiv A_1 J + B_1 J^2 + C_1 J^3. \tag{13.3.14}$$

The three parameters formula describes a large number of experimental ground band energies with high accuracy [RAU06].

Alternatively, the quantal energy for the intrinsic motion can be obtained by quantizing the anharmonic plane oscillator and the third component of the intrinsic pseudo-momentum. In this case the result is:

$$E_{n,M} = A(n+1) + B(n+1)^2 + \frac{C}{2}M^2 + \frac{F}{5}\left[(n+1)^3 - 4(n+1)M^2\right]. \tag{13.3.15}$$

Neglecting the zero point energy terms and taking $M = \sqrt{L(L+1)}$ one obtains:

$$E_{n,L} = A_1 n - B_1 n^2 + C_1 L(L+1) + \frac{F}{5}\left(n^3 - 4nL(L+1)\right) \tag{13.3.16}$$

Fig. 13.18 Excitation
energies of the $J^\pi = 0^+$
states described
semi-classically, panel **a**, and
by eigenvalues of the model
Hamiltonian, corresponding
to the seniority $v = 0$, panel
b, and $v = 3$, panel **c**
respectively, are compared
with the experimental data
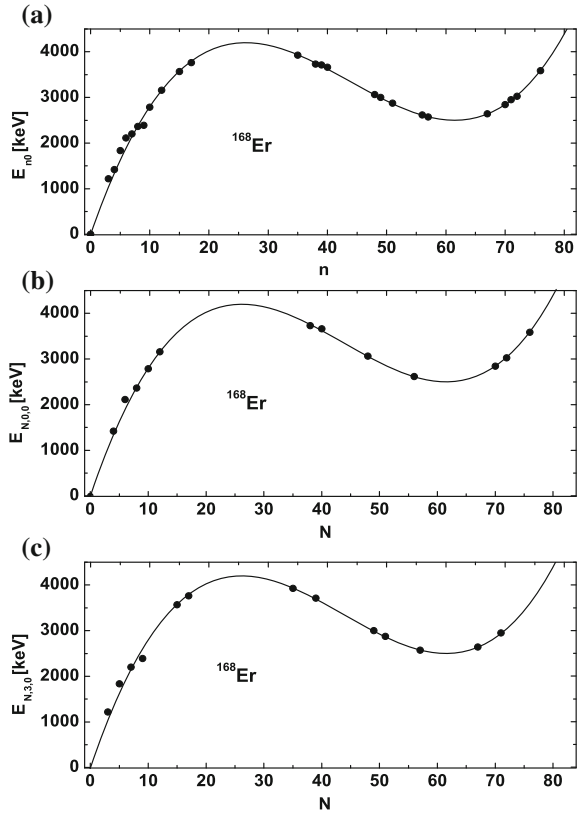
with evident notations for the coefficients A_1, B_1, C_1. From the above equation one
sees that the sixth order term brings two types of corrections, one depending on n^3
and one depending on the product $nL(L+1)$. Equation (13.3.16), involving four free
parameters, seems to be very useful to describe in a realistic fashion the excitation
energies of states having the same angular momentum. Using the analytical formulas
provided by the classical and quantal treatments respectively, a good description of
the monopole and quadrupole multiplets, identified experimentally in Ref. [Buc06],
for ^{168}Er was possible. Results are given in Figs. 13.18 and 13.19.

13.3.3 Summary and Conclusions

Here we treated, semiclassically, two boson Hamiltonians of sixth order. Concerning
the first Hamiltonian the results are as follows. In terms of polar coordinates (r, θ),
the classical equations of motion have a canonical form. There are two constants

Fig. 13.19 Excitation energies of the $J^\pi = 2^+$ states, described semi-classically, panel **a**, and by eigenvalues of the model Hamiltonian, corresponding to the seniority $v = 1$, panel **b** and $v = 2$, panel **c**, respectively, are compared with the experimental data
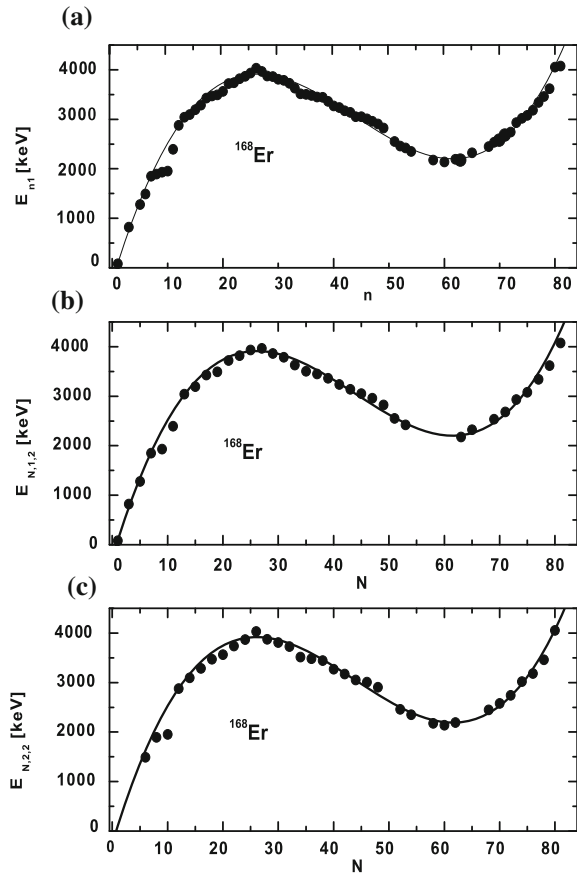
of motion and therefore the system is fully integrable. The reduced classical phase space is one dimensional, the independent degree of freedom being the radius r. For a suitable set of the structure coefficients, the effective potential involved in the classical energy function has a two minima shape. Note that the kinetic energy is separated from the potential. The differential equation in r can easily be integrated. The trajectories $r(t)$ are periodic. Fixing the constant of motion $\mathcal{L}_3$, the equation of motion for θ can also be analytically solved. The corresponding solution $\theta(t)$ is also a periodical function of time. The periods of $r(t)$ and $\theta(t)$ are different from each other. Moreover, they are incommensurable and therefore the trajectory $r(\theta)$ is not closed. The emphasis is put mainly on the $r(t)$ trajectories. There are three distinct energy regions, labeled by U, B and O, where the $r(t)$ trajectories have distinct behaviors. Indeed, for a given energy E and a given value of L in the region U there is only one periodic trajectory, in B the are two trajectories of equal periods while in O again there is only one periodic trajectory.

The period magnitude depends on energy. It is an increasing function for $E <$ $V_{eff\,max}$ and is singular at the interval end, while for the complementary region the period decreases when the energy is increased. This feature suggests that $E = V_{eff\,max}$ is a critical point where the system undertakes a phase transition. Moreover, the periods in B and U have finite nonvanishing values when the energy tends to $V_{eff\,min1}$ and $V_{eff\,min2}$ respectively. In a quantal picture this is equivalent to saying that these limiting values cannot define touchable states and therefore a zero point motion corresponds to a finite relative energy with respect to the potential energy minima.

Although the trajectories $r(t)$ have a complex structure which is far from that of a periodic harmonic function, they can be quantized by a constraint for the integral action similar to the Bohr-Sommerfeld quantization condition. This way one obtains a semi-classical spectrum for each of the regions U, B and O. Choosing the constraint (13.2.28) for $\mathcal{L}_3$ in the region U there are $L + 1$ states, while in B an equal number of states in the left and right wells, respectively. The states in B are tentatively organized in rotational bands keeping close to the conventional definition adopted by the liquid drop model. Each energy level is labeled by two quantum numbers (L, n), one being used as band label (L) while the other one to distinguish the levels of the same band. The bands in the right well are very little excited. Thus, the bands are almost identical concerning the energy spacings.

The tunneling phenomenon from the left to the right well through the separating barrier was also studied. A special attention is paid to the first virtual state under the hump. It is noteworthy that there are several values for the intrinsic pseudo-momentum L where the transmission coefficients, evaluated within the WKB approach, exhibit a spectacular increase in magnitude. It is interesting to see whether this result has some relevance for alpha or heavy cluster emission where the tunneling takes place from a bound state to an unbound state. Represented as a function of the energy distance between the chosen state and $V_{eff\,max}$, the transmission coefficient is an exponentially decreasing function.

The other Hamiltonian has a more complex structure, involving quartic and sextic terms in momenta and terms coupling the coordinates and moments. Such a Hamiltonian was treated both semiclassically and quantum mechanically. In both cases one obtains analytical formulas for energies. These were used to describe quantitatively the excitation energies of the monopole and quadrupole multiplets respectively, in ^{168}Er.

Chapter 14
Comparison of CSM with Some Other Models

14.1 Solvable Models and Hamiltonian Symmetries

14.1.1 Introduction

It has been noticed that a given nuclear phase may be associated to a certain symmetry. Hence, its properties may be described with the help of the irreducible representation of the respective symmetry group. Thus, the gamma unstable nuclei can be described by the $O(6)$ symmetry [WIJE56], the symmetric rotor by the $SU(3)$ symmetry and the spherical vibrator by the $U(5)$ symmetry. The gamma triaxial nuclei are characterized by the invariance symmetry group $D2$ [DF58] of the rigid triaxial rotor Hamiltonian. Thus, even in the 50's of the last century, the symmetry properties were greatly appreciated. However, a big push forward was brought by the interacting boson approximation (IBA) [AI76, ArIa76, IAAR87], which succeeded to describe the basic properties of a large number of nuclei in terms of the symmetries associated to a system of quadrupole (d) and monopole (s) bosons which generate a $U(6)$ algebra. The three limiting symmetries $U(5)$, $O(6)$, $SU(3)$ are dynamic symmetries for $U(6)$. Moreover, for each of these symmetries a specific group reduction chain provides the quantum numbers characterizing the states, which are suitable for a certain region of nuclei. For nuclei lying close to the region characterized by a certain symmetry, the perturbative corrections are to be included.

In Ref. [CAIA81], a new classification scheme was proposed, all nuclei being distributed on the legs of a symmetry triangle. The vertices of this triangle symbolize the $U(5)$ (vibrator), $O(6)$ (gamma soft) and $SU(3)$ (symmetric rotor), while the legs of the triangle denote the transitional region. The properties of nuclei lying far from vertices are difficult to explain since the states have some characteristics of one vertex while some others are easy to describe by using the adjacent symmetry. The transition from one phase to another reaches a critical point depending on the specific parametrization as well as on the transition type [RB98, RO04, TRO05]. In Refs. [GIKI80, DI83], it has been proved that on the $U(5) - O(6)$ transition leg there

exists a critical point for a second order phase transition, while the $U(5) - SU(3)$ leg has a first order phase transition. Later on it was found that some nuclei are falling inside the Casten's triangle.

Recently, Iachello [Iac00, IA01] pointed out that these critical points correspond to distinct symmetries, namely $E(5)$ and $X(5)$ (not known yet), respectively. For the critical value of an ordering parameter, energies are given by the zeros of a Bessel function of half integer and irrational indices, respectively. The description of low lying states in terms of Bessel functions was used first by Jean and Willet [WIJE56], but the interesting feature saying that this is a critical picture in a phase transition and defines a new symmetry was, indeed, advanced first in Ref. [Iac00].

Representatives for the two symmetries have been experimentally identified. To give an example, the relevant data for ^{134}Ba [CAZA00] and ^{152}Sm [ZAM86] suggest that they are close to the $E(5)$ and $X(5)$ symmetries, respectively. Another candidate for E(5) symmetry, proposed by Zamfir et al. [ZZ90] is ^{102}Pd. A systematic search for $E(5)$ behavior in nuclei was reported in Ref. [CLCR04].

Shortly after the pioneering papers concerning critical point symmetries appeared, some other attempts were performed, using other potentials like Coulomb, Kratzer [FOVI03] and Davidson potentials [BONA04]. These potentials yield also Schrödinger solvable equations and the corresponding results may be interpreted in terms of symmetry groups. In Ref. [RGF05] the hypothesis advanced was that the critical point in a phase transition is state dependent. The test with a hybrid model was made for ^{134}Ba and ^{104}Ru.

The departure from the gamma unstable picture was treated by several authors whose contributions are reviewed by Fortunato in Ref. [FO05]. The difficulty in treating the gamma degree of freedom consists in the fact that this is coupled to the rotational degrees of freedom. A full solution for the Bohr-Mottelson Hamiltonian including an explicit treatment of gamma deformation can be found in Refs. [GRC78, RCG78]. Therein, the gamma unstable and the rotor Hamiltonian were also separately treated. A more complete study of the rotor Hamiltonian and the distinct phases associated to a tilted moving rotor is given in Ref. [GRC98]. Distinct solutions, expressed in laboratory frame shape coordinates, were reported in Refs. [CHMO76, CMW76, SR77]. The gamma dependent part of the wave function was found as a solution to a specific differential equation in Ref. [BE59].

Finding the γ depending part of the wave function becomes even more complicated when we add to the liquid drop Hamiltonian a potential depending on β and γ at a time. To simplify the starting problem related to the inclusion of γ, one uses model potentials which are sums of a β term, $V(\beta)$, and a factorized $\beta - \gamma$ term $U(\gamma)/\beta^2$. This way the nice feature for the beta variable to be decoupled from the remaining four variables, specific to the harmonic liquid drop, is preserved. In the next step, the potential in gamma is expanded around $\gamma = 0$ or $\gamma = \frac{\pi}{6}$. In the first case, if only the singular term is retained one obtains the infinite square well model described by Bessel functions in γ. If the γ^2 term is added to this term, the Laguerre functions are the eigenstates of the approximated γ depending Hamiltonian, which results in defining the so called X(5) approach.

Note that any approximation applied to the γ-Hamiltonian modifies automatically the differential equation for β. Indeed, the centrifugal term $\tau(\tau + 3)/\beta^2$ disappears but another one is expected to show up from the $\beta-\gamma$ coupling, after some approximations are performed.

The drawback of these approximations is that the resulting functions are not periodic, as the starting Hamiltonian. Moreover, they are orthonormalized on unbound intervals, although the underlying equation was derived under the condition of $|\gamma|$ small. Moreover, the scalar product of the resulting functions is not defined with the integration measure $|\sin 3\gamma| d\gamma$ as in the liquid drop model. Under these circumstances it happens that the approximated Hamiltonian in γ loses its hermiticity.

Here we shall describe some solvable approaches where the said drawbacks are removed.

14.1.2 The Starting Hamiltonian

Written in the intrinsic frame of reference, the original Bohr-Mottelson Hamiltonian has the expression:

$$H = -\frac{\hbar^2}{2B}\left[\frac{1}{\beta^4}\frac{\partial}{\partial\beta}\beta^4\frac{\partial}{\partial\beta} + \frac{1}{\beta^2 \sin 3\gamma}\frac{\partial}{\partial\gamma}\sin 3\gamma\frac{\partial}{\partial\gamma}\right.$$

$$\left. -\frac{1}{4\beta^2}\sum_{k=1,2,3}\frac{Q_k^2}{\sin^2(\gamma - \frac{2}{3}\pi k)}\right] + V(\beta, \gamma), \qquad (14.1.1)$$

where the dynamic deformation variables are denoted by β and γ, while the intrinsic angular momentum components by Q_k, with $k = 1, 2, 3$. Within the liquid drop model (LDM) the potential energy depends quadratically on β. Here we assume that the potential energy depends on both deformation variables, beta and gamma. Without exception, the solvable models proposed for a simultaneous description of β and γ variables, adopt the variable separation methods. Two situations are to be distinguished:

(a) If the potential energy term is depending on deformation variables in a separable manner:

$$V(\beta, \gamma) = V(\beta) + U(\gamma), \qquad (14.1.2)$$

and some additional assumptions are adopted, the eigenvalue equation associated to H (14.1.1) can be separated in two parts, one equation describing the beta variable and the other one the gamma deformation and the Euler angles $\Omega = (\theta_1, \theta_2, \theta_3)$. Indeed, in this case the separation of variables, achieved by various models, is based on two approximations [CA04, BLMPY07]: (i) restriction to small values of γ, i.e. $|\gamma| \ll 1$; (ii) replacing the factor $1/\beta^2$ by $1/\langle\beta^2\rangle$ in the terms involved in the equation

for γ. The diagonalization of the Bohr-Mottelson Hamiltonian shows that the first approximation is valid for large γ stiffness while the second one for small γ stiffness [BLMPY07].

(b) A complete separation of equations for the two variables, β and γ is possible if we choose the potential

$$V(\beta, \gamma) = V(\beta) + U(\gamma)/\beta^2. \qquad (14.1.3)$$

This way the approximation consisting of replacing β^2 by $\langle \beta^2 \rangle$ is avoided but the restriction to the case $|\gamma| \ll 1$ is still kept. Thus, the theory involves one parameter which is the γ stiffness which affects the excitation energies in both the beta and gamma bands.

In what follows the two equations, for β and γ, will be considered separately.

14.1.3 The Treatment of the β Hamiltonian

The solvable models for β, presented here, have been used by E(5) formalisms, which ignore the potential in γ. Considering the potential in γ, of course, the picture for β is changed. However, as we shall see later on, it is very easy to derive analytically the energies and wave functions associated to β from the corresponding results of the E(5) descriptions. Actually, this is the motivation for reviewing, here, the beta solvable models.

The equation in β is:

$$\left[-\frac{1}{\beta^4} \frac{\partial}{\partial \beta} \beta^4 \frac{\partial}{\partial \beta} + \frac{\Lambda}{\beta^2} + u(\beta) \right] f(\beta) = \epsilon f(\beta), \qquad (14.1.4)$$

where Λ is the eigenvalue of the Casimir operator of the $SO(5)$ group. This is related to the seniority quantum number τ, by $\Lambda = \tau(\tau + 3)$. The 'reduced' potential $u(\beta)$ and energy ϵ are defined as:

$$E = \frac{\hbar^2}{2B} \epsilon, \quad V = \frac{\hbar^2}{2B} u. \qquad (14.1.5)$$

where E denotes the eigenvalue of the Hamiltonian H corresponding to the potential $V(\beta)$. Here we mention the most used potentials for β:

14.1.3.1 The case of $u(\beta) = \beta^2$

A full description of the eigenstates of the Bohr-Mottelson Hamiltonian satisfying the symmetry $U(5) \supset SO(5) \supset SO(3) \supset SO(2)$, may be found in Refs. [GRC78, RCG78] and Chap. 11 of this book. In particular, the solution of the radial Eq. (14.1.4)

with $u(\beta) = \beta^2$ is easily obtained by bringing first Eq. (14.1.4) to the standard Schrödinger form by changing the function f to ψ by:

$$\psi(\beta) = \beta^2 f(\beta). \tag{14.1.6}$$

The equation obeyed by the new function ψ is:

$$\frac{d^2\psi}{d\beta^2} + \left[\epsilon - \beta^2 - \frac{(\tau+1)(\tau+2)}{\beta^2}\right]\psi = 0. \tag{14.1.7}$$

This equation is analytically solvable. The solution is:

$$\psi_{n\tau}(\beta) = \sqrt{\frac{2(n!)}{\Gamma(n+\tau+5/2)}}\, L_n^{\tau+3/2}(\beta^2)\beta^{\tau+2}\exp(-\beta^2/2), \tag{14.1.8}$$

$$\epsilon_n = 2n + \tau + 5/2, \quad n = 0,\,1,\,2,\,\ldots;\quad \tau = 0, 1, 2, 3, \ldots \tag{14.1.9}$$

where L_n^ν denotes the generalized Laguerre polynomials. The number of polynomial nodes is denoted by n and is related to the number of the quadrupole bosons (N) in the state, by: $N = 2n + \tau$. Consequently, the initial Eq. (14.1.4) has the solution

$$f_{n\tau} = \beta^{-2}\psi_{n\tau}. \tag{14.1.10}$$

The spectrum, given by Eq. (14.1.9), may be also obtained by using the unitary representation of the $SU(1, 1)$ group with the Bargman index $k = (\tau + 5/2)/2$. Indeed, the standard generators for $SU(1, 1)$ are:

$$K_0 = \frac{1}{4}H_0, \quad K_\pm = \frac{1}{4}\left[\frac{(\tau+1)(\tau+2)}{\beta^2} - (\beta \pm \frac{d}{d\beta})^2\right], \tag{14.1.11}$$

where

$$H_0 = -\frac{d^2}{d\beta^2} + \beta^2 + \frac{(\tau+1)(\tau+2)}{\beta^2},$$

$$H_0\psi_n = \epsilon_n\psi_n. \tag{14.1.12}$$

H_0 obeys the following equations:

$$\left[K_-, K_+\right] = -\frac{1}{2}H_0, \quad \left[K_\pm, H_0\right] = \pm 4K_\pm. \tag{14.1.13}$$

14.1.3.2 Davidson's Potential

Another potential in β which yields a solvable model is due to Davidson [Dav32]:

$$u(\beta) = \beta^2 + \frac{\beta_0^4}{\beta^2}. \tag{14.1.14}$$

This potential was used by several authors in different contexts [EEP86, SR77, BONA04]. For example, the potential was used by Bonatsos et al. [BLMPY07], to describe the dynamic deformation variable β. For this potential the above Eqs. (2.6–2.10) hold for τ replaced [BONA04] by

$$\tau' = -\frac{3}{2} + \left[\left(\tau + \frac{3}{2} \right)^2 + \beta_0^4 \right]^{1/2}. \tag{14.1.15}$$

In particular, the excitation energies have the expressions:

$$E_{n,\tau} = 2n + 1 + \left[\left(\tau + \frac{3}{2} \right)^2 + \beta_0^4 \right]^{1/2}. \tag{14.1.16}$$

The factor β_0^4 is considered to be a free parameter which is to be determined variationally for each angular momentum, as suggested in Ref. [BONA04]:

$$\frac{d^2 R_L^{(g)}}{d\beta_0^2} = 0, \tag{14.1.17}$$

where R denotes the ratio of the excitation energy of the ground band state L^+ and the excitation energy of the state 2_g^+.

14.1.3.3 Five Dimensional Infinite Well

Now, let us turn our attention to the situation considered by Iachello in Ref. [Iac00], where the potential term associated to the spherical to gamma unstable shape transition is so flat that it can be mocked up as an infinity square well:

$$u(\beta) = \begin{cases} 0, & \beta \le \beta_w, \\ \infty, & \beta > \beta_w. \end{cases} \tag{14.1.18}$$

A more convenient form for the equation in β, is obtained through the function transformation:

$$\varphi(\beta) = \beta^{3/2} f(\beta), \tag{14.1.19}$$

The equation for φ is

$$\frac{d^2\varphi}{d\beta^2} + \frac{1}{\beta}\frac{d\varphi}{d\beta} + \left[\epsilon - u(\beta) - \frac{(\tau + 3/2)^2}{\beta^2}\right]\varphi = 0. \tag{14.1.20}$$

Changing the variable β to z by

$$z = k\beta, \quad k = \sqrt{\epsilon} \tag{14.1.21}$$

and denoting with $\widetilde{\varphi}(z) = \varphi(\beta)$ the function of the new variable, one arrives at:

$$\frac{d^2\widetilde{\varphi}}{dz^2} + \frac{1}{z}\frac{d\widetilde{\varphi}}{dz} + \left[1 - \frac{(\tau + 3/2)^2}{z^2}\right]\widetilde{\varphi} = 0. \tag{14.1.22}$$

This equation is analytically solvable, the solutions being the Bessel functions of half integer order, $J_{\tau+3/2}(z)$. Since for $\beta > \beta_w$ the function $\widetilde{\varphi}$ is equal to zero, the continuity condition requires that the solution inside the well must vanish for the value of β equal to β_w. This, in fact, yields a quantized form for the eigenvalue E. Indeed, let $x_{\xi,\tau}$ be the zeros of the Bessel function J_ν:

$$J_{\tau+3/2}(x_{\xi,\tau}) = 0, \quad \xi = 1, 2, \ldots; \quad \tau = 0, 1, 2, \ldots \tag{14.1.23}$$

Then, due to the substitution introduced in Eqs. (14.1.21) and (14.1.5) one obtains:

$$E_{\xi,\tau} = \frac{\hbar^2}{2B}k_{\xi,\tau}^2, \quad k_{\xi,\tau} = \frac{x_{\xi,\tau}}{\beta_w}. \tag{14.1.24}$$

To conclude, the differential equation for the beta deformation corresponding to an infinite well potential provides the energy spectrum given by Eq. (14.1.24) and the wave functions:

$$f_{\xi,\tau} = C_{\xi,\tau}\beta^{-3/2}J_{\tau+3/2}\left(\frac{x_{\xi,\tau}}{\beta_w}\beta\right), \tag{14.1.25}$$

where $C_{\xi,\tau}$ is a normalization factor.

It is worth noticing that the spectra corresponding to E(5) and Davidson potentials become directly comparable by establishing the formal correspondence $n = \xi - 1$.

14.1.4 The Sextic Oscillator with a Centrifugal Barrier

The Hamiltonian of the sextic oscillator with a centrifugal barrier has the expression [LA04, LA10]:

$$H_x = -\frac{\partial^2}{\partial x^2} + \frac{\left(2s - \frac{1}{2}\right)\left(2s - \frac{3}{2}\right)}{x^2} + [b^2 - 4a(s + \frac{1}{2} + M)]x^2 + 2abx^4 + a^2 x^6, \tag{14.1.26}$$

where $x \in [0, \infty)$. The classical counterpart of H_x was studied in Ref. [RAU06]. Analytical solutions for the classical trajectories were found, and then quantized. Also, we note that for the particular value $a = 0$ the sextic potential becomes the Davidson potential [Dav32]. Here we use the quantal form of the equation of motion and show that they yield also analytical solutions. To be concrete, the eigenvalue equation associated to (14.1.26) is quasi-exactly solvable for any value of b. Indeed, for any given non-negative integer M, it has $M + 1$ solutions which can be found algebraically. This can be easily verified if we consider the Schrödinger equation

$$H_x \psi(x) = E \psi(x) \tag{14.1.27}$$

and take as an appropriate *ansatz* the function

$$\psi_n(x) = P_n(x^2) x^{2s - \frac{1}{2}} e^{-\frac{ax^4}{4} - \frac{bx^2}{2}}, \quad n = 0, 1, 2, \ldots \tag{14.1.28}$$

where $P_n(x^2)$ is a polynomial in x^2 of degree n. Indeed, substituting (14.1.28) in (14.1.27) and eliminating the common factor, we obtain an equation for the $P_n(x^2)$

$$Q P_n(x^2) = E P_n(x^2), \tag{14.1.29}$$

with

$$Q = -\left(\frac{\partial^2}{\partial x^2} + \frac{4s - 1}{x} \frac{\partial}{\partial x}\right) + 2b\left(x\frac{\partial}{\partial x} + 2s\right) + 2ax^2\left(x\frac{\partial}{\partial x} - 2M\right). \tag{14.1.30}$$

Now, let us assume that M is a non-negative integer: $M = 0, 1, 2, \ldots$. In this case the differential spectral Eq. (14.1.29) can easily be transformed into an algebraic form. The action of the Q-operator (14.1.30) on $P_n(x^2)$ gives again a polynomial in x^2 at the same order. Considering the coefficients of the polynomial $P_n(x^2)$ as components of an $(M+1)$-vector, one can treat (14.1.29) as an $(M+1)$-dimensional spectral matrix equation. This means that the initial Schrödinger equation (14.1.27) has at least $M + 1$ solutions of the form (14.1.28) and thus can be interpreted as a quasi-exactly solvable equation of order $M + 1$.

If in Eq. (14.1.4) one makes the change of function $f(\beta) = \beta^{-2}\varphi(\beta)$ one gets

$$\left[-\frac{\partial^2}{\partial\beta^2} + \frac{L(L+1)+2}{\beta^2} + v_1(\beta) \right] \varphi(\beta) = \varepsilon_\beta \varphi(\beta). \qquad (14.1.31)$$

We choose $v_1(\beta)$ such that Eq. (14.1.31) becomes the equation for a sextic oscillator potential with a centrifugal barrier. Indeed, this is achieved with the identifications

$$x = \beta, \quad E = \varepsilon_\beta, \quad \left(2s - \frac{1}{2}\right)\left(2s - \frac{3}{2}\right) = L(L+1) \quad \Rightarrow \quad s = \frac{L}{2} + \frac{3}{4}, \qquad (14.1.32)$$

$$v_1(\beta) = (b^2 - 4ac)\beta^2 + 2ab\beta^4 + a^2\beta^6, \quad c = \frac{L}{2} + \frac{5}{4} + M.$$

This identification was possible after adding the term $-2/\beta^2$ to the equation for β (14.1.4) and $2/\langle\beta^2\rangle$ to that of γ (14.1.57). This way the final centrifugal term in Eq. (14.1.31) will be $L(L+1)/\beta^2$. This trick assures a rational form for s.

Suppose we fixed the constant parameters a and b. Then, the potential depends on c which, in its turn, depends on L and M. It is desirable that the potential is independent on angular momentum, i.e. c is a constant. Due to the equation relating c and L

$$L = 2c - \frac{5}{2} - 2M, \qquad (14.1.33)$$

this infers a certain dependence of L on M. Indeed, in order to keep c constant it is necessary that increasing/decreasing M by one unit should take place at a time with decreasing/increasing L by two units. So we get two constant values for c, one for L-even and other for L-odd

$$(M, L) : (k, 0); (k-1, 2); (k-2, 4); (k-3, 6) \ldots \Rightarrow c = k + \frac{5}{4} \equiv c^+ \quad (L\text{-even}), \qquad (14.1.34)$$

$$(M, L) : (k, 1); (k-1, 3); (k-2, 5); (k-3, 7) \ldots \Rightarrow c = k + \frac{7}{4} \equiv c^- \quad (L\text{-odd}). \qquad (14.1.35)$$

The final form of the potential will be

$$v_1^\pi(\beta) = (b^2 - 4ac^\pi)\beta^2 + 2ab\beta^4 + a^2\beta^6 + u_0^\pi, \quad (\pi \equiv \pm), \qquad (14.1.36)$$

where u_0^π are constants which will be fixed such that the minima $(\beta_{min}^\pi > 0)$ of the two potentials $v_1^+(\beta)$ and $v_1^-(\beta)$ have the same energy. The extremal points can be obtained from the first derivative of the potential

$$\frac{\partial v_1^\pi(\beta)}{\partial \beta}\Big|_{\beta=\beta_0^\pi} = 0 \Rightarrow (\beta_0^\pi)^2 = 0 \quad \text{and} \quad (\beta_0^\pi)^2 = \frac{1}{3a}\left[-2b \pm \sqrt{b^2 + 12ac^\pi}\right].$$

$$(14.1.37)$$

For $\beta_{\min} = 0$ we have $u_0^+ = u_0^-$. When $\beta_{\min} > 0$ we can set $u_0^+ = 0$ and from the condition $v_1^-(\beta_0^-) - v_1^+(\beta_0^+) = 0$ we get

$$u_0^- = (b^2 - 4ac^+)(\beta_0^+)^2 - (b^2 - 4ac^-)(\beta_0^-)^2 + 2ab[(\beta_0^+)^4 - (\beta_0^-)^4]$$
$$+ a^2[(\beta_0^+)^6 - (\beta_0^-)^6].$$

$$(14.1.38)$$

The shape of the potential $v_1^\pi(\beta)$ depends on the signs of $b^2 - 4ac^\pi$ and b. When $b > 2\sqrt{ac^\pi}$, the potential has a minimum at $\beta = 0$ and it increases monotonously with β. When $-2\sqrt{ac^\pi} < b < 2\sqrt{ac^\pi}$, a minimum shows up at $\beta > 0$, while for $b < -2\sqrt{ac^\pi}$, the potential has a maximum and a minimum.

The excitation energies for the β equation are easily obtained using Eqs. (14.1.5) and (14.1.32).

$$E_\beta(n_\beta, L) = \frac{\hbar^2}{2B}\left[4bs(L) + \lambda_{n_\beta}^{(M)}(L) + u_0^\pi\right], \quad n_\beta = 0, 1, 2, \ldots, M. \quad (14.1.39)$$

The notation $\lambda_{n_\beta}^{(M)}$ is used for the eigenvalue corresponding to the eigenvector determining the coefficients defining the polynomial $P_n(x^2)$. Functions in the β variable are given by the Eq. (14.1.28) replacing x with β

$$\varphi_{n_\beta,L}^{(M)}(\beta) = N_{n_\beta,L} P_{n_\beta,L}^{(M)}(\beta^2)\beta^{2s-\frac{1}{2}}e^{-\frac{a}{4}\beta^4 - \frac{b}{2}\beta^2}, \quad n_\beta = 0, 1, 2, \ldots M, \quad (14.1.40)$$

where $N_{n_\beta,L}$ are the normalization constants.

Note that in all treatments mentioned above, no potential in γ is considered. Due to this fact the spectra and wave functions are labeled by the seniority quantum number τ. This feature does not hold when we switch on the γ-depending potential and, moreover, impose variable separability by approximating the terms depending on γ.

14.1.5 The Description of γ Degree of Freedom

Let us consider the Hamiltonian

$$H = -\frac{1}{\sin 3\gamma}\frac{\partial}{\partial \gamma}\sin 3\gamma\frac{\partial}{\partial \gamma} + U(\gamma) + W(\gamma, Q), \quad (14.1.41)$$

where U is a periodic function in γ with the period equal to 2π and

$$W(\gamma, Q) = \frac{1}{4} \sum_{k=1}^{3} \frac{1}{\sin^2\left(\gamma - \frac{2\pi}{3}k\right)} Q_k^2 \qquad (14.1.42)$$

with Q_k denoting the components of the intrinsic angular momentum.

Any approximation for the potential, by expanding it in power series of γ, alters the periodic behavior of the eigenfunction. Moreover, the approximating Hamiltonian loses its hermiticity with respect to the scalar product defined with the measure for the gamma variable, $|\sin(3\gamma)|d\gamma$.

We illustrate this by considering the case of a more complex potential

$$U = u_1 \cos(3\gamma) + u_2 \cos^2(3\gamma). \qquad (14.1.43)$$

Performing the change of function $\varphi = \sqrt{|\sin(3\gamma)|}\psi$, the eigenvalue equation $H\psi = E\psi$, becomes $\tilde{H}\varphi = 0$, with

$$\tilde{H} = \frac{\partial^2}{\partial\gamma^2} + \frac{9}{4}\left[1 + \frac{1}{\sin^2(3\gamma)}\right] - U - W + E. \qquad (14.1.44)$$

We shall consider two situations:

A. *Suppose that* $|\gamma| \ll 1$. Expanding the terms in γ in power series up to the fourth order, one obtains:

$$U_4 = u_1 + u_2 - 9\gamma^2 \left(\frac{u_1}{2} + u_2\right) + 27\gamma^4 \left(\frac{u_1}{8} + u_2\right),$$

$$W_4 = \frac{1}{3}\left(1 + 2\gamma^2 + \frac{26\gamma^4}{9}\right)\left(Q_1^2 + Q_2^2\right)$$

$$+ \frac{2\sqrt{3}\gamma}{9}\left(1 + 2\gamma^2\right)\left(Q_2^2 - Q_1^2\right)$$

$$+ \frac{1}{4}\left(\frac{1}{\gamma^2} + \frac{1}{3} + \frac{\gamma^2}{15} + \frac{2\gamma^4}{189}\right)Q_3^2. \qquad (14.1.45)$$

The low index of U and W suggests that the expansions in γ were truncated at the fourth order. Note that due to the term W, the equations of motion for the variable γ and Euler angles are coupled together. Such a coupling term can in principle be handled as we did for the harmonic liquid drop in Ref. [GRC78, RCG78]. Here, we separate the equation for γ by averaging W_4 with an eigenfunction for the intrinsic angular momentum squared. The final result for H_4 is:

$$H_4 = \frac{\partial^2}{\partial\gamma^2} + \frac{1}{4\gamma^2}\left(1 - \langle Q_3^2\rangle\right) + h_0 + h_2\gamma^2 + h_4\gamma^4$$

$$+ \frac{2\sqrt{3}\gamma}{9}\left(1 + 2\gamma^2\right)\langle Q_2^2 - Q_1^2\rangle,$$

$$h_0 = E - \frac{1}{3}L(L+1) + \frac{1}{4}\left\langle Q_3^2 \right\rangle - (u_0 + u_1 + u_2) + \frac{15}{2},$$

$$h_2 = -\frac{2}{3}L(L+1) - \frac{13}{20}\left\langle Q_3^2 \right\rangle + \frac{9}{2}u_1 + 9u_2 + \frac{27}{20},$$

$$h_4 = -\frac{26}{27}L(L+1) - \frac{121}{126}\left\langle Q_3^2 \right\rangle - \frac{27}{8}u_1 - 27u_2 + \frac{27}{14}. \qquad (14.1.46)$$

where L denotes the angular momentum. If the average is made with the Wigner function D_{MK}^L, important simplifications are obtained since the following relations hold:

$$\left\langle Q_2^2 - Q_1^2 \right\rangle = 0, \quad \left\langle Q_3^2 \right\rangle = K^2 \qquad (14.1.47)$$

Actually, this is the situation considered here. Note that H_4 contains a singular term in γ, at $\gamma = 0$, coming from the term coupling the intrinsic variable γ with the Euler angles. One could get rid of such a coupling term by starting with a potential in gamma containing a singular term which cancels the contribution produced by the W term. Thus, the new potential would be

$$U' = U + \frac{9K^2}{4\sin^2(3\gamma)}. \qquad (14.1.48)$$

The corresponding fourth order expansion for the Hamiltonian is:

$$H_4' = \frac{\partial^2}{\partial\gamma^2} + \frac{1}{4\gamma^2} + h_0' + h_2'\gamma^2 + h_4'\gamma^4, \qquad (14.1.49)$$

$$h_0' = h_0 + K^2, \quad h_2' = h_2 + \frac{27}{20}K^2, \quad h_4' = h_4 + \frac{27}{14}K^2.$$

Some remarks concerning the equation $H_4'\varphi = 0$ are worth mentioning:

(i) If in this equation one ignores the γ^4 term, the resulting equation has the Laguerre functions as solutions and moreover the Hamiltonian exhibits the $X(5)$ features.

(ii) Note also that the Hamiltonian coefficients are different from those of Ref. [FO05]. The difference is caused by the fact that here, the expansion is complete.

(iii) Taking in the expanded potential $u_1 = u_2 = 0$ and ignoring, for γ small, the term $\frac{27}{20}K^2\gamma^2$, the resulting potential is that of an infinite square well which was treated by Iachello in Ref. [IA01]. The solutions are, of course, the Bessel functions of half integer indices.

(iv) Irrespective of the potential in γ, in the regime of $|\gamma|$ small a term proportional to γ^2 shows up due to the rotational Hamiltonian W. Therefore, even when the potential is taken as an infinite square well, of the form $1/\gamma^2$, the equation describing the γ variable admits a Laguerre function as solution and not, as might be expected, a Bessel function of semi-integer index. Amazingly, the potential in γ is also of Davidson type.

(v) None of the mentioned solutions is periodic.

(vi) Also, the approximated Hamiltonians are not Hermitian in the Hilbert space of functions in gamma with the integration measure as introduced by the liquid drop model, i.e. $|\sin 3\gamma| d\gamma$.

B. The case $|\gamma - \pi/6| \ll 1$. Using the fourth order expansion in $y = |\gamma - \pi/6|$, one obtains a Hamiltonian similar to that given by Eq. (14.1.50):

$$H_4' = \frac{\partial}{\partial \gamma^2} + h_2' \gamma^2 + h_4' \gamma^4 + 2\sqrt{3} y \left(1 + \frac{22\sqrt{3}}{3} y^2 \right) \langle Q_3^2 - Q_2^2 \rangle. \quad (14.1.50)$$

If $\langle Q_3^2 - Q_2^2 \rangle = 0$ and, moreover, one ignores the term in γ^4 the resulting equation in γ describes a harmonic oscillator. Again the eigenfunctions, i.e. the Hermite functions, are orthogonal on an unbound interval of γ, and not on $[0, 2\pi]$.

14.1.6 An Exact Solution Which Preserves Periodicity and Hermiticity

In order to remove the drawbacks mentioned above, we try first to avoid making approximations. Thus, let us consider the Hamiltonian given by Eq. (14.1.41) where instead of U we consider U' as defined by Eq. (14.1.48), and ignore for a moment W. Changing the variable $x = \cos 3\gamma$, the eigenvalue equation associated to this Hamiltonian, $HS = ES$, becomes:

$$\left(1 - x^2\right) \frac{d^2 S}{d x^2} - 2x \frac{dS}{d x} + \left(\frac{1}{9}(E - u_1 x - u_2 x^2) - \frac{K^2}{4(1-x^2)} \right) S = 0. \quad (14.1.51)$$

Note that we denoted the eigenfunction by S which suggests that the differential Eq. (14.1.51) is obeyed by a spheroidal function. If $u_1 = u_2 = K = 0$, the solution of this equation is the Legendre polynomial P_n, while $E = 9n(n+1)$. This case was considered in Ref. [FO05]. This function may be used to approximate the solution of the original liquid drop model. For other particular choices of the coefficients u_1, u_2 defining the potential in gamma, the solution is readily obtained if one compares the above equation with that characterizing the spheroidal oblate functions [ABST72]

$$\left(1 - x^2\right) \frac{d^2 S_{nm}}{d x^2} - 2x \frac{dS_{nm}}{d x} + \left(\lambda_{nm} - c^2 x^2 - \frac{m^2}{1-x^2} \right) S_{nm} = 0. \quad (14.1.52)$$

The prolate case is reached by changing $c \to ic$.

For $c = 0$, the solutions of Eq. (14.1.52) are the associated Legendre functions P_n^m. For $c \neq 0$, S_{nm}, with m, n integers and $n \geq m \geq 0$, are linear series of these functions.

In the case $u_1 = 0$, the solution of Eq. (14.1.51) is identified as being the spheroidal function while the energy is simply related to λ_{nm}:

$$m = \frac{K}{2}, \quad c^2 = \frac{u_2}{9}, \quad \lambda_{nm} = \frac{1}{9}E_{nm}. \tag{14.1.53}$$

Here E_{nm} denotes the eigenvalue E corresponding to the quantum numbers n and m. For $|c|$ small the energies E_{nm} exhibits the asymptotic expansion

$$\begin{aligned}
E_{nm} \approx 9n(n+1) &- \frac{2\left(n(n+1)+m^2-1\right)}{(2n-1)(2n+3)}u_2 \\
&+ \frac{1}{18}\frac{\left[(n-1)^2-m^2\right](n^2-m^2)}{(2n-3)(2n-1)^3(2n+1)}u_2^2 \\
&- \frac{1}{18}\frac{\left[(n+1)^2-m^2\right]\left[(n+2)^2-m^2\right]}{(2n+1)(2n+3)^3(2n+5)}u_2^2.
\end{aligned} \tag{14.1.54}$$

Eq. (14.1.54) considered for a fixed m but various n, defines a band. Similar expansions may be derived for $|c|$ large.

$$\begin{aligned}
E_{nm} &\approx -u_2 + 3q\sqrt{u_2} + 9\left(m^2 - \frac{q^2+5}{8}\right) - \frac{27q}{64\sqrt{u_2}}(11 + q^2 - 32m^2), \\
q &= 2(n-m) + 1
\end{aligned} \tag{14.1.55}$$

We notice that the spectrum has a rotational behavior for small c, due to the term $n(n+1)$, while for large values of c it has an oscillator feature, the energy depending linearly on n.

If one needs the expansion up to the $1/c^2$ terms, the results for the first few energies are:

$$\begin{aligned}
E_{11} &= 9\left(\frac{1}{4} - c^2 + c + \frac{5}{16c} + \frac{33}{64c^2}\right), \\
E_{21} &= 9\left(-\frac{3}{4} - c^2 + 3c + \frac{9}{16c} + \frac{135}{64c^2}\right), \\
E_{22} &= 9\left(\frac{13}{4} - c^2 + c + \frac{29}{16c} + \frac{177}{64c^2}\right), \\
E_{31} &= 9\left(-\frac{11}{4} - c^2 + 5c - \frac{5}{16c} + \frac{219}{64c^2}\right), \\
E_{32} &= 9\left(\frac{9}{4} - c^2 + 3c + \frac{81}{16c} + \frac{855}{64c^2}\right), \\
E_{33} &= 9\left(\frac{33}{4} - c^2 + c + \frac{69}{16c} + \frac{417}{64c^2}\right).
\end{aligned} \tag{14.1.56}$$

Fig. 14.1 The spheroidal energies $E'_{nm} = \lambda_{nm} = E_{nm}/9$, for $0 \le m \le n \le 3$ are plotted as functions of $c = \sqrt{u_2}/3$
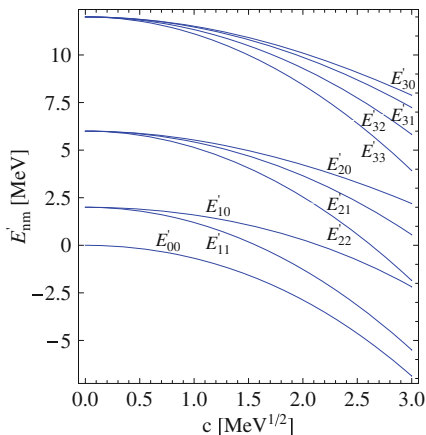
It is worth spending a few words on Fig. 14.1, where the energies correspond to the spheroidal functions with the parameters specified by Eq. (14.1.54). Indeed, for $c \to 0$ one notices some multiplet degeneracy which suggests a symmetry with respect to K, i.e. a rotation invariance of states of a given n. Increasing c, the split in energy is similar to that in Nilsson [NIL55] model when the energy is Ω dependent. The difference is that, while in Nilsson model each deformed state is a superposition of states with different angular momentum, here the multiplet members are characterized by the same n. In this respect, the feature shown in Fig. 14.1 is similar to the one obtained with a spherical projected single particle basis [RDI93]. In the region of large c, for a given large n the set of states of different m seem to form a band. On the other hand, for a fixed m the set of states with different n is a band of equidistant energy levels.

14.1.7 Mathieu Equation

Expanding the γ dependent term $W(\gamma, \Omega)$ in power series around $\gamma_0 = \frac{\pi}{6}$ and then averaging the result with the Wigner function D^L_{MR}, the common eigenfunctions of Q^2, Q_1 and L_z (the angular momentum projection on the third axis of the laboratory frame), leads to the equation in gamma variable:

$$\left[-\frac{1}{\sin 3\gamma} \frac{\partial}{\partial \gamma} \sin 3\gamma \frac{\partial}{\partial \gamma} - \frac{3}{4} R^2 + \left(10L(L+1) - \frac{39}{4} R^2 \right) \left(\gamma - \frac{\pi}{6} \right)^2 \right.$$
$$\left. + v_2(\gamma) \right] \phi(\gamma) = \tilde{\varepsilon}_\gamma \phi(\gamma), \tag{14.1.57}$$

where the following notations are used:

$$v_2(\gamma) = \frac{2B}{\hbar^2} V_2(\gamma), \quad \tilde{\varepsilon}_\gamma = \langle \beta^2 \rangle \frac{2B}{\hbar^2} E_\gamma. \tag{14.1.58}$$

Further, we change the function

$$\phi(\gamma) = \frac{\mathcal{M}(3\gamma)}{\sqrt{|\sin 3\gamma|}}. \tag{14.1.59}$$

The equation for the new function is:

$$\left[\frac{\partial^2}{\partial \gamma^2} + \left(\tilde{\varepsilon}_\gamma + \frac{1}{4} + \frac{3}{4} R^2 \right) + \frac{9}{4 \sin^2 3\gamma} - \left(10 L(L+1) - \frac{39}{4} R^2 \right) \left(\gamma - \frac{\pi}{6} \right)^2 \right.$$
$$\left. - v_2(\gamma) \right] \mathcal{M}(3\gamma) = 0. \tag{14.1.60}$$

The potential in γ is chosen to exhibit a minimum at $\gamma_0 = \pi/6$:

$$v_2(\gamma) = \mu \cos^2 3\gamma. \tag{14.1.61}$$

Making the Taylor expansions around the minimum value of the gamma potential:

$$\frac{9}{4 \sin^2 3\gamma} \sim \frac{9}{4} + \frac{81}{4} \left(\gamma - \frac{\pi}{6} \right)^2, \quad \mu \cos^2 3\gamma \sim 9\mu \left(\gamma - \frac{\pi}{6} \right)^2, \tag{14.1.62}$$

the equation for the variable γ becomes:

$$\left[\frac{\partial^2}{\partial \gamma^2} + \left(\tilde{\varepsilon}_\gamma + \frac{3}{4} R^2 + \frac{5}{2} \right) \right.$$
$$\left. - \left(10 L(L+1) - \frac{39}{4} R^2 + 9\mu - \frac{81}{4} \right) \left(\gamma - \frac{\pi}{6} \right)^2 \right] \mathcal{M}(3\gamma) = 0. \tag{14.1.63}$$

Using again in (14.1.63) the approximation

$$\left(\gamma - \frac{\pi}{6} \right)^2 = \frac{1}{9} \cos^2 3\gamma, \tag{14.1.64}$$

and making the change of variable $y = 3\gamma$, we obtain

$$\left[\frac{\partial^2}{\partial y^2} + \frac{1}{9} \left(\tilde{\varepsilon}_\gamma + \frac{3}{4} R^2 + \frac{5}{2} \right) \right.$$
$$\left. - \frac{1}{9} \left(\frac{10}{9} L(L+1) - \frac{13}{12} R^2 + \mu - \frac{9}{4} \right) \cos^2 y \right] \mathcal{M}(y) = 0. \tag{14.1.65}$$

This can be written in a compact form as:

$$\left(\frac{\partial^2}{\partial y^2} + a - 2q \cos 2y\right) \mathcal{M}(y) = 0, \tag{14.1.66}$$

where

$$q = \frac{1}{36}\left(\frac{10}{9}L(L+1) - \frac{13}{12}R^2 + \mu - \frac{9}{4}\right), \quad a = \frac{1}{9}\left(\bar{\varepsilon}_\gamma + \frac{3}{4}R^2 + \frac{5}{2}\right) - 2q. \tag{14.1.67}$$

Eq. (14.1.66) is just the well-known Mathieu equation. For $q \neq 0$ the Mathieu functions are periodic in γ only for a certain set of values of a, called characteristic values. These are denoted by c_n^+ for even and c_n^- for odd functions, respectively. In the plane (a, q), the characteristics curves $c_n^\pm$ separate the stability regions, shown in Fig. 14.2 by gray color, from the non-stability ones, indicated by white color in the quoted figure. For $q = 0$ the equalities $c_n^\pm(0) = n^2$ hold. By means of Eq. (14.1.68) the characteristic values determine the energy E.

$$E_\gamma(n_\gamma, L, R) = \frac{\hbar^2}{2B}\frac{1}{\langle \beta^2 \rangle}\left[9a_{n_\gamma}(L, R) + 18q(L, R)\right.$$
$$\left. -\frac{3}{4}R^2 - \frac{5}{2}\right], \quad n_\gamma = 0, 1, 2, \ldots. \tag{14.1.68}$$

The orthonormalization restriction for the Mathieu functions is

$$\int_0^{2\pi} \mathcal{M}_n(y)\mathcal{M}_m(y)dy = \pi\delta_{nm}. \tag{14.1.69}$$

Fig. 14.2 The characteristic curves $c_n^\pm$ are plotted as functions of q for several values of n
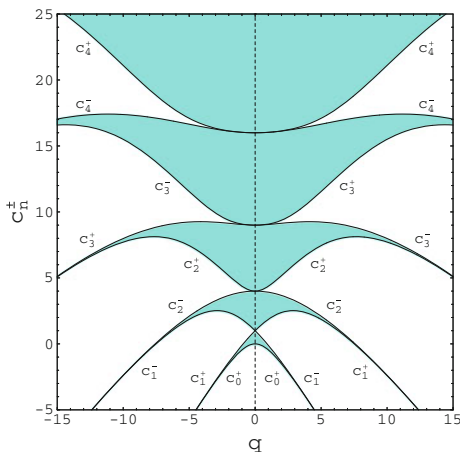
The total energy for the system is obtained by summing the energies given by the Eqs. (14.1.39) and (14.1.68)

$$E(n_\beta, n_\gamma, L, R) = E_0 + E_\beta(n_\beta, L) + E_\gamma(n_\gamma, L, R) \qquad (14.1.70)$$

Once the wave functions are determined by solving the corresponding eigenvalue equations, we can proceed to calculating the electric transition probabilities. The reduced E2 transition probabilities were calculated by using alternatively a harmonic, $T^{(h)}$, and an anharmonic transition operator, $T_{2\mu}^{(anh)}$, having the expressions:

$$T_{2\mu}^{(h)} = t\beta \left(\cos\gamma D_{\mu 0}^2 + \frac{\sin\gamma}{\sqrt{2}} (D_{\mu 2}^2 + D_{\mu,-2}^2) \right),$$

$$T_{2\mu}^{(anh)} = t_1\beta \left(\cos\gamma D_{\mu 0}^2 + \frac{\sin\gamma}{\sqrt{2}} (D_{\mu 2}^2 + D_{\mu,-2}^2) \right)$$

$$+ t_2 \sqrt{\frac{2}{7}} \beta^2 \left(-\cos 2\gamma D_{\mu 0}^2 + \frac{\sin 2\gamma}{\sqrt{2}} (D_{\mu 2}^2 + D_{\mu,-2}^2) \right) \quad (14.1.71)$$

The strengths t, t_1 and t_2 are free parameters which are fixed by fitting one and two particular $B(E2)$ values, respectively. Due to the structure of the wave functions specified above, the matrix elements between the states involved in a given transition are factorized into matrix elements of the transition operators factors depending on β, γ and the Euler angles, respectively.

To summarize, so far we have used a form of the potential in β and γ variables which yields separable equations for the two deformations. Several potentials in β were described, which yield a fully solvable equation. Similarly, two potentials in the γ deformation were presented, which yield solvable equations for spheroidal and Mathieu functions, respectively. Any combination of one solvable equation in β and one solvable equation in γ define a solvable approach. Thus one obtains Infinite Square Well and Spheroidal (ISWS), Davidson and Spheroidal (DSA), Sextic and Spheroidal (SSA), Infinite Square well and Mathieu (ISWM), Davidson and Mathieu (DMA), Sextic and Mathiew (SMA) approach. Each of these methods was applied for several nuclei and the results were compared with both the experimental data and CSM. Some selected applications are presented below.

Concerning the methods which treat the γ variable with spheroidal functions we present as an example the nucleus ^{150}Nd, which exhibits the so called $X(5)$ symmetry. The parameters defining the excitation energies and the E2 transition probabilities were fitted by the least square method. For each model $\langle \beta^2 \rangle$ was taken constant, namely the average values of the expected values in various states from the ground band. The fitted parameters are given in Table 14.1. The corresponding results for energies and B(E2) values are given in Tables 14.2 and 14.3, respectively.

As representatives for the SMA formalism we chose three isotopes ^{228,230}Th and ^{182}W. The Triaxial Vibration Rotation Model (TRVM) [MFK97], predicts for ^{228}Th $\gamma^\circ = 13^\circ$. Thus, this isotope is closer to an axial symmetric shape than to a triaxial one. A similar situation is expected also for ^{130}Th. Under such circumstances, one

Table 14.1 The parameters determining the excitation energies as well as those involved in the transition operator are listed for ^{150}Nd

^{150}Nd	X(5)	ISWA	DSA	SSA	CSM	
B_1 (keV)	17.77	14.68			A_1 (keV)	19.219
X (keV)	966.50				A_2 (keV)	3.467
E (keV)			369.5	0.75	A_3 (keV)	−658.299
F (keV)		28.88	26.48	3.87	A_4 (keV)	−491.884
u_1		−152.35	−168.78	−3877.84	A_5 (keV)	−438.394
u_2		0.0	0.0	0.0	d	2.42
β_0			1.71		$q_1[W.u.]^{1/2}$	0.527
a				2636.48	$q_2[W.u.]^{1/2}$	−4.916
b				88.	$q_3[W.u.]^{1/2}$	6.344
$t_1\ [W.u.]^{1/2}$	1.03	538.99	154.70	1754.26		
$t_2\ [W.u.]^{1/2}$	0.49	−387.08	−25.31	−6698.41		

Table 14.2 Energies calculated within various models are compared with experimental data for ^{150}Nd. Data are taken from Ref. [MATU95]

^{150}Nd	Exp	X(5)	ISWA	DSA	SSA	CSM
2_g^+	130	124	121	124	111	130
4_g^+	381	361	358	384	348	386
6_g^+	720	675	682	738	683	734
8_g^+	1,130	1,054	1,084	1,158	1,098	1,149
10_g^+	1,599	1,494	1,560	1,625	1,580	1,618
12_g^+	2,119	1,993	2,106	2,129	2,118	2,133
14_g^+	2,683	2,549	2,722	2,664	2,707	2,688
0_β^+	675	702	580	739	630	675
2_β^+	851	926	783	863	822	852
4_β^+	1,138	1,328	1,157	1,123	1,158	1,167
6_β^+	1,541	1,833	1,639	1,477	1,590	1,541
8_β^+		2,415	2,209	1,897	2,095	1,931
10_β^+		3,067	2,859	2,364	2,661	2,319
2_γ^+	1,062	1,091	1,087	1,076	1,091	1,101
3_γ^+	1,201	1,198	1,197	1,195	1,197	1,191
4_γ^+	1,353	1,327	1,333	1,345	1,328	1,310
5_γ^+		1,476	1,491	1,518	1,474	1,448
6_γ^+		1,641	1,671	1,713	1,663	1,615
7_γ^+		1,823	1,872	1,924	1,838	1,790
8_γ^+		2,020	2,093	2,151	2,079	1,998
9_γ^+		2,233	2,334	2,390	2,276	2,201
10_γ^+		2,461	2,594	2,641	2,561	2,445
r.m.s. (keV)		114	48	28	29	20

Table 14.3 Results obtained with several approaches for ^{150}Nd are compared with the corresponding experimental data taken from Ref. [KR02]

B(E2)(W.u.)	Exp	X(5)	ISWA	DSA	SSA	CSM
$2_g^+ \to 0_g^+$	115_{-2}^{+2}	107	104	92	116	81
$4_g^+ \to 2_g^+$	182_{-2}^{+2}	169	168	144	177	160
$6_g^+ \to 4_g^+$	210_{-2}^{+2}	212	210	183	211	222
$8_g^+ \to 6_g^+$	278_{-25}^{+25}	243	243	224	240	278
$10_g^+ \to 8_g^+$	204_{-12}^{+12}	269	269	268	266	330
$2_\beta^+ \to 0_\beta^+$	114_{-23}^{+23}	85	83	130	86	116
$4_\beta^+ \to 2_\beta^+$	170_{-51}^{+51}	128	125	194	144	165
$0_\beta^+ \to 2_g^+$	39_{-2}^{+2}	67	73	51	37	41.2
$2_\beta^+ \to 0_g^+$	$1.2_{-0.2}^{+0.2}$	2.1	2.9	3.1	1.6	5.2
$2_\beta^+ \to 2_g^+$	9_{-2}^{+2}	10	10	9	6	9
$2_\beta^+ \to 4_g^+$	17_{-3}^{+3}	39	42	40	26	26
$4_\beta^+ \to 2_g^+$	$0.12_{-0.02}^{+0.02}$	1.07	1.61	1.64	0.57	5.6
$4_\beta^+ \to 4_g^+$	7_{-1}^{+1}	6	8	8	5	7.2
$4_\beta^+ \to 6_g^+$	70_{-13}^{+13}	30	33	46	26	26
$2_\gamma^+ \to 0_g^+$	$3_{-0.8}^{+0.8}$	2.4	8	9.8	5.1	16.3
$2_\gamma^+ \to 2_g^+$	$5.4_{-1.7}^{+1.7}$	3.6	11.9	14.3	7.3	5.4
$2_\gamma^+ \to 4_g^+$	$2.6_{-2.0}^{+2.0}$	0.2	0.6	0.7	0.4	0.74
$4_\gamma^+ \to 2_g^+$	$0.9_{-0.3}^{+0.3}$	1.6	5	6.1	3	28.6
$4_\gamma^+ \to 4_g^+$	$3.9_{-1.2}^{+1.2}$	5.3	15.5	18.9	9	9.6

may ask why considering these nuclei as samples of triaxiality. The reason is as follows. It is well known the fact that the most distinctive signature of the triaxial rigid rotor is the equation relating the energies of three particular states:

$$E_{2_1^+} + E_{2_2^+} = E_{3_1^+}. \tag{14.1.72}$$

Actually this equation is only approximately obeyed by the considered nuclei. Indeed, denoting by ΔE the modulus of the difference between the left and right hand side of the said relation, the experimental data for the two nuclei lead to the values:

$$\Delta E = 4\text{keV}; \ 8\text{keV}; \ 10\text{keV} \tag{14.1.73}$$

for ^{228}Th, ^{230}Th and ^{182}W, respectively. Clearly, these deviations indicate that, indeed, these isotopes are close an ideal triaxial rotor. As a matter of fact, this is a good reason to use the $\gamma = 30°$ as reference picture. Deviations from this static situation were considered by a Taylor expansion. It is worth mentioning that the Th isotopes considered here, were found [BLMPY05, LB06] to be located in the region with octupole vibration, as opposed to octupole deformation, the border between the two regions located at ^{224}Th or ^{226}Th [BLMPY05, LB06, BB08]. One may say that

the Th isotopes may be used to study not only the transition from gamma unstable to triaxial shapes but also the one from octupole deformed to octupole vibrational nuclei. It is an open question whether a quadrupole triaxial shape may favor the onset of the static octupole deformation.

The parameters involved in the expressions of energies as well as of the electric reduced quadrupole transition probabilities were determined by a fitting procedure with the results listed in Table 14.4. The calculated excitation energies with the SMA and CSM approaches are compared with the experimental data in Fig. 14.3 for ^{228}Th, Fig. 14.4 for ^{230}Th and Fig. 14.5 for ^{182}W.

From these figures we may conclude that the SMA procedure provides a reasonable quantitative description of the experimental data. Moreover, the two theoretical methods considered, SMA and CSM, yield agreements with the data of similar quality with a slight advantage for the CSM.

In Refs. [ZACA91, MBZC07] one considers the level staggering in the γ band as a sensitive signature for triaxiality. The doublet structure is reflected in the saw-teeth shape of the function:

$$S(J) = \frac{[E(J) - E(J-1)] - [E(J-1) - E(J-2)]}{E(2_g^+)} \qquad (14.1.74)$$

where $E(J)$ stands for the energy of the state J^+ belonging to the γ band. It is worth noting that $S(J)$ is proportional to the discrete second derivative of $E(J)$ with respect to J. In order to see whether this signature is revealed also by SMA and CSM approaches, we plotted in Figs. 14.6 and 14.7 the function $S(J)$ for the nuclei ^{228,230}Th. We notice a very weak staggering for ^{228}Th. For ^{230}Th there are not enough relevant data while the two formalisms, *SMA* and *CSM* show a well pronounced and almost no staggering, respectively. We note that the oscillation amplitude of $S(J)$ is increasing with J. As mentioned already before, the transition to a triaxial regime in *CSM* is determined by anharmonicities and quadrupole deformation. Within the *SMA*, which describes the deformations β and γ in the intrinsic frame, the triaxial shape is assumed from the beginning when a potential with a minimum in $\gamma_0 = \frac{\pi}{6}$ is chosen and the rotational term is expanded in powers of γ around $\gamma = \frac{\pi}{6}$. Actually this is reflected in Figs. 14.6 and 14.7 which suggests an excess of staggering predicted by SMA. It is interesting to notice that while Eq. (14.1.73) recommends ^{228}Th as exhibiting a triaxial shape from Fig. 14.6 we see that experimental data as well as the *CSM* indicate that these nuclei show only a quite weak staggering. Due to this feature some people have doubts that the staggering in the γ band would represent a signature for triaxiality.

Table 14.4 The parameters $\hbar^2/2B$, a, b, $\frac{1}{\langle\beta^2\rangle}$, μ involved in the energy expression provided by SMA (14.1.70), are given for ^{228}Th, ^{230}Th and ^{182}W

Nucleus	$\frac{\hbar^2}{2B}$ (keV)	a	b	$1/\langle\beta^2\rangle$	μ	t_1	t_2	d	A_1 (keV)	A_2 (keV)	A_3 (keV)	q_1	q_2
^{228}Th	1.147	1323.661	−41.9	2.439	2,936	t_1	$3.371\,t_1$	3.14	17.731	15.122	−7.021	15.927	−1.132
^{230}Th	0.467	3041.51	100.	2.59	9,093	136	1822.4	3.16	13.904	2.650	−10.00	$0.961[W.u.]^{1/2}$	−1.255
^{182}W	0.477	11508.56	95	3.457	12772.6	158.48	4.736.037	3.22	21.54	7.470	−12.29	$3.756[W.u.]^{1/2}$	−0.175

Also we give the values for the parameters t_1 and t_2 (in units of $[W.u.]^{1/2}$), defining the transition operator used by SMA (14.1.71). On the last six columns we give the parameters determining the CSM excitation energies, d, A_1, A_2, A_3, and the specific E2 transition operator i.e., q_1 and q_2 in units of eb for ^{228}Th and $[W.u.]^{1/2}$ for ^{230}Th and ^{182}W

Fig. 14.3 Excitation energies for ground β and γ band states calculated with SMA and CSM are compared with the corresponding experimental data for ^{228}Th. Experimental data are from Ref. [GRO98]

g band

18^+ 2463 2408 2417

16^+ 1997 1988 2001 γ band

10^+ 1825 1763 1755

14^+ 1571 1600 1610
9^+ 1627 1628 1611
8^+ 1521 1497 1485 β band

7^+ 1365 1380 1365
6^+ 1271 1270 1262 4^+ 1304 1290 1283
12^+ 1189 1239 1248
5^+ 1157 1175 1169 2^+ 1167 1176 1170
4^+ 1078 1091 1091 0^+ 1105 1120 1120
3^+ 1007 1023 1027   SMA Exp. CSM
10^+ 855 912 918
2^+ 945 969 979
                SMA Exp. CSM

8^+ 570 623 626

6^+ 339 378 380 ^{228}Th

4^+ 166 187 187

2^+ 52 58 58
0^+ 0 0 0
SMA Exp. CSM

Fig. 14.4 Excitation energies for ground β and γ band states calculated with SMA and CSM are compared with the corresponding experimental data for ^{230}Th. Experimental data are from Ref. [AKO93]

g band

24^+ 3849 3812 3837

22^+ 3331 3325 3325

20^+ 2840 2850 2840 ^{230}Th

18^+ 2377 2398 2384

16^+ 1945 1972 1956 γ band

14^+ 1547 1573 1560 10^+ 1575 1520 1532
9^+ 1400 1390
8^+ 1288 1251 1266 β band
12^+ 1184 1208 1199 7^+ 1145 1149
6^+ 1048 1040 1048
5^+ 941 884 884 4^+ 812 770 785
10^+ 860 880 874 4^+ 863 826 823
3^+ 793 826 823
2^+ 737 781 776 2^+ 662 678 680
8^+ 580 594 591   SMA Exp. CSM 0^+ 593 635 635
                                                                SMA Exp. CSM

6^+ 349 357 356

4^+ 171 174 174

2^+ 53 53 53
0^+ 0 0 0
SMA Exp. CSM

Fig. 14.5 Excitation energies for ground, beta and gamma bands in ^{182}W, obtained with SMA and CSM formalism respectively, are compared with the corresponding experimental data taken from Ref. [SING10]

Fig. 14.6 Staggering function for ^{228}Th

Fig. 14.7 Staggering function for ^{230}Th

14.1.8 A Possible Relationship of the SMA and the CSM

The applications considered above point the fact that SMA and CSM describe the data of the considered nuclei equally well. This amazing feature raises the question *why that happens?*

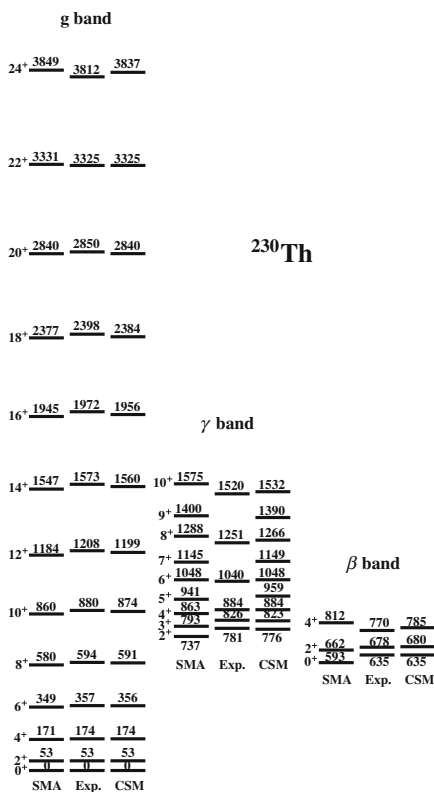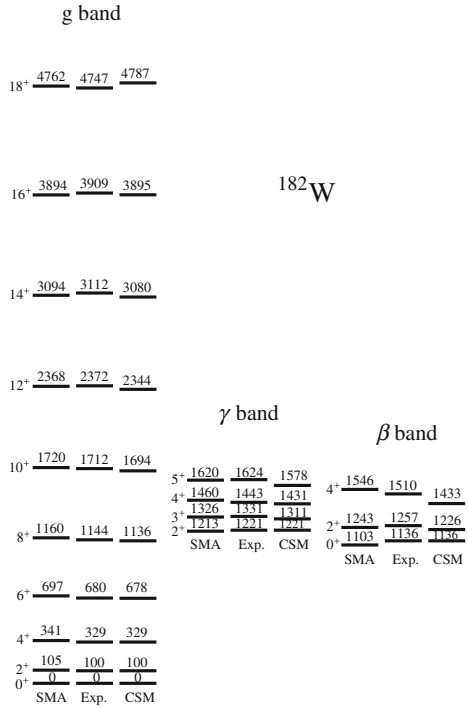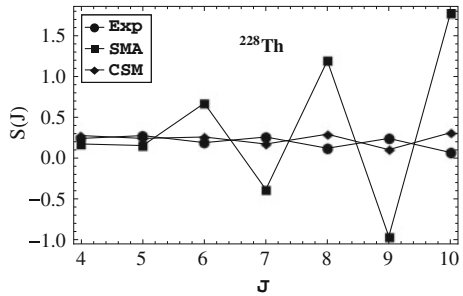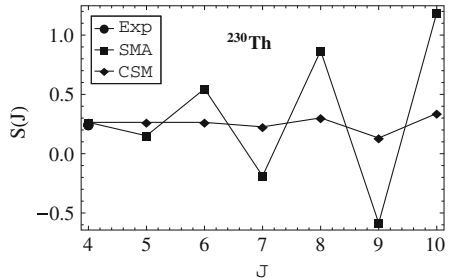Aiming at answering this question, we study the classical properties emerging from CSM, by dequantizing the specific boson Hamiltonian used by CSM, considering its average with the coherent state:

$$|\psi\rangle = \exp\left[z_0 b_0^\dagger + z_2 b_2^\dagger + z_{-2} b_{-2}^\dagger - z_0^* b_0 - z_2^* b_2 - z_{-2}^* b_{-2} \right] |0\rangle, \quad (14.1.75)$$

where z_k, z_k^* with $k = 0, \pm 2$ are complex numbers depending on time. As usual $|0\rangle$ denotes the vacuum state for the quadrupole bosons. The classical Hamilton function associated to the CSM's model Hamiltonian is:

$$
\begin{aligned}
\mathcal{H} \equiv \langle \psi | H | \psi \rangle &= 2(11A_1 + 3A_2)\left(|z_0|^2 + |z_2|^2 + |z_{-2}|^2 \right) \\
&+ A_1 \left(2z_2^* z_{-2}^* + z_0^{*2} - d^2 \right)\left(2z_2 z_{-2} + z_0^2 - d^2 \right) \\
&+ \frac{A_3}{70}\left[2\left(6z_0^* z_2^* z_{-2}^* - z_0^{*3} \right) + 3d\left(2z_2^* z_{-2}^* + z_0^{*2} \right) - d^3 \right] \\
&\times \left[2\left(6z_0 z_2 z_{-2} - z_0^3 \right) + 3d\left(2z_2 z_{-2} + z_0^2 \right) - d^3 \right].
\end{aligned}
\quad (14.1.76)
$$

The equations of motion described by the classical coordinates z_0, $z_\pm$ and their complex conjugates z_0^*, $z_\pm^*$ are obtained from the variational principle of the minimum action:

$$\delta \int_0^t \langle \psi | H - i\hbar \frac{\partial}{\partial t'} | \psi \rangle dt' = 0. \quad (14.1.77)$$

The variational principle yields the classical equations:

$$\frac{\partial H}{\partial z_k} = -i \, \dot{z}_k^*, \quad \frac{\partial H}{\partial z_k^*} = i \, \dot{z}_k, \quad k = 0, \pm 2. \quad (14.1.78)$$

These equations support the interpretation of z_k, with $k = 0, \pm 2$, as classical phase space coordinates and of z_k^* as the corresponding conjugate momenta. With the complex coordinates we may define the canonical conjugate coordinates:

$$Q_k = \frac{z_{-k} + z_k^*}{\sqrt{2}}, \quad P_k = \frac{z_k - z_{-k}^*}{i\sqrt{2}} \quad k = 0, \pm 2. \quad (14.1.79)$$

which, evidently, obey the equations:

$$\{Q_0, P_0\} = 1, \quad \{Q_{\pm 2}, P_{\pm 2}\} = 1,$$

$$\{Q_k, \mathcal{H}\} = \dot{Q}_k, \quad \{P_k, \mathcal{H}\} = \dot{P}_k, \ k = 0, \pm 2. \tag{14.1.80}$$

The Poisson brackets are defined in terms of the pairs $(Q_k, P_k), k = 0, \pm 2$. Thus, for the coordinates z_k, z_k^* we have: $\{z_k, z_k^*\} = -i$.

In what follows we shall study the Hamilton function $\mathcal{H}$ in the subspace defined by $z_2 = z_{-2}$, where we use the canonical coordinates defined by:

$$q_0 = Q_0, \quad p_0 = P_0, \quad q_2 = \frac{Q_2 + Q_{-2}}{2}, \quad p_2 = \frac{P_2 + P_{-2}}{2i} \tag{14.1.81}$$

These coordinates are related to the real and imaginary part of the complex variable z_k by the following equations:

$$q_0 = \sqrt{2} u_0, \quad p_0 = \sqrt{2} v_0, \quad q_2 = 2 u_2, \quad p_2 = 2 v_2,$$

$$u_0 = Re\ z_0, \quad v_0 = Im\ z_0, \quad u_2 = Re\ z_2, \quad v_2 = Im\ z_2. \tag{14.1.82}$$

In the expression of $\mathcal{H}$ we adopt the following approximation and coordinate transformations: (i) we neglect the terms non-quadratic in momenta as well as the terms coupling the coordinate with momenta; (ii) we take care of the restriction $z_2 = z_{-2}$ by introducing the new canonical coordinates q_0; p_0 and q_2; p_2; (iii) for the new coordinates we use the polar form:

$$q_0 = r \cos \gamma, \quad q_2 = r \sin \gamma \tag{14.1.83}$$

In this way $\mathcal{H}$ is a sum of the kinetic and potential energies:

$$\mathcal{H} = (11 A_1 + 3 A_2 + A_1 d^2 + \frac{3}{70} d^2 A_3)(p_0^2 + p_2^2) + V(r, \gamma),$$

$$V(r, \gamma) = A_1 d^4 + \frac{A_3}{70} d^6 + r^2 \left[(11 A_1 + 3 A_2) - \frac{d^2}{2} A_1 - \frac{3 A_3}{70} d^4 - \frac{d^2}{2} A_1 \cos(2\gamma) \right]$$

$$+ \frac{A_3 \sqrt{2}}{70} d^3 r^3 \cos(3\gamma) + \left(\frac{A_1}{4} + \frac{9 A_3}{280} d^2 \right) r^4 - \frac{3 A_3 d}{70\sqrt{2}} r^5 \cos(3\gamma)$$

$$+ \frac{A_3}{280} r^6 (\cos(6\gamma) + 1). \tag{14.1.84}$$

In order to obtain a separable equation for the variables r and γ we approximate $V(r, \gamma)$ by a sum of two potentials one depending only on r, $(V_1(r))$, and the other one only on γ, $(V_2(\gamma))$. The $V_1(r)$ potential is obtained by summing the terms depending exclusively on r and the coupling terms for which the γ depending factors were taken in the minimum point of $V_2(\gamma)$, i.e. $\frac{\pi}{6}$. The term denoted by $V_2(\gamma)$ is obtained from

the coupling term proportional to $\cos(6\gamma)$, with the factor depending on r considered in the minimum point of $V_1(r)$, denoted by r_0. The approximated potential will be denoted by $U(r, \gamma)$.

$$U(r, \gamma) \approx V_1(r) + V_2(\gamma),$$

$$V_1(r) = A_1 d^4 + \frac{A_3}{70} d^6 + r^2 \left[(11A_1 + 3A_2) - \frac{3A_1}{4} d^2 - \frac{3A_3}{70} d^4 \right]$$

$$+ \left(\frac{A_1}{4} + \frac{27}{280} d^2 \right) r^4 + \frac{A_3}{280} r^6,$$

$$V_2(\gamma) = \frac{A_3}{280} r_0^6 \cos(6\gamma). \tag{14.1.85}$$

In Fig. 14.8 we plotted the approximated $V(r, \gamma)$ for values of the parameters, d, A_1, A_2, A_3 close to those listed in Table 14.4 for ^{182}W. Indeed, the parameters in Table 14.4 were slightly modified such that the exact potential $V(r, \gamma)$ reaches the minimum value in the same point $(r_0, \pi/6)$ as the approximated one, $U(r, \gamma)$. The difference between the contour plot as well as the potential section for the exact $(V(r, \gamma))$ and approximated potential $(U(r, \gamma))$ are essentially small.

The classical Hamilton function becomes:

$$\mathcal{H} = (11A_1 + 3A_2 + A_1 d^2 + \frac{3}{70} d^2 A_3)(p_0^2 + p_2^2) + U(r, \gamma). \tag{14.1.86}$$
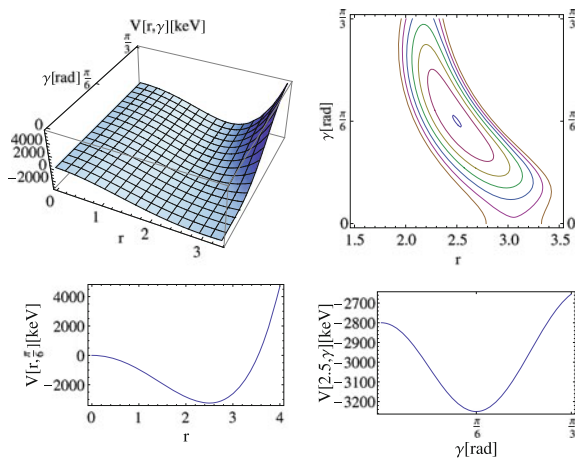
Fig. 14.8 The potential $V(r, \gamma)$ is plotted as function of the r and γ for ^{182}W (*left panel*). The parameters involved are given in Table 14.4. The minimum is reached in $(r_0, \gamma_0) = (2.5, \frac{\pi}{6})$. Equipotential curves separated by 50 keV, surrounding the minimum value of the potential are given in the *upper right panel*. $V_{min} = -3250.92\,keV$. Two sections $\gamma = \frac{\pi}{6}$ and $r_0 = 2.5$ are presented in the *lower panels*

This can be quantized by replacing the sum of the momenta squared by the Laplace operator written in polar coordinates:

$$\hat{H} = -(11A_1 + 3A_2 + A_1 d^2 + \frac{3}{70} d^2 A_3) \left(\frac{1}{r} \frac{\partial}{\partial r} + \frac{\partial^2}{\partial r^2} + \frac{1}{r^2} \frac{\partial^2}{\partial \gamma^2} \right) + V_1(r) + V_2(\gamma).$$

(14.1.87)

It is convenient to introduce the notation:

$$\mathcal{F} = (11A_1 + 3A_2 + A_1 d^2 + \frac{3}{70} d^2 A_3).$$

(14.1.88)

The Schrödinger equation:

$$\hat{H} \Psi(r, \gamma) = E \Psi(r, \gamma),$$

(14.1.89)

for the trial function:

$$\Psi(r, \gamma) = \psi_1(r) e^{iK\gamma} \psi_2(\gamma),$$

(14.1.90)

is separated:

$$\left[-\mathcal{F} \left(\frac{1}{r} \frac{\partial}{\partial r} + \frac{\partial^2}{\partial r^2} - \frac{K^2}{r^2} \right) + V_1(r) \right] \psi_1(r) e^{iK\gamma} = E^{(1)} \psi_1(r) e^{iK\gamma},$$

$$\left[-\mathcal{F} \left(\frac{2iK}{r_0^2} \frac{\partial}{\partial \gamma} + \frac{1}{r_0^2} \frac{\partial^2}{\partial \gamma^2} \right) + V_2(\gamma) \right] \psi_2(\gamma) = E^{(2)} \psi_2(\gamma).$$

(14.1.91)

In what follows we shall show that the first Eq. (14.1.91) leads to a Schrödinger equation for a sextic potential plus a centrifugal term while the second equation provides a differential equation obeyed by the Mathieu function.

Indeed, dividing both sides of the first Eq. (14.1.91) by $\mathcal{F}$ and denoting by

$$u_1(r) = V_1(r)/\mathcal{F}, \quad \varepsilon_r = E^{(1)}/\mathcal{F}$$

(14.1.92)

the equation in the variable r becomes:

$$\left[-\frac{\partial^2}{\partial r^2} - \frac{1}{r} \frac{\partial}{\partial r} + \frac{K^2}{r^2} + u_1(r) \right] \psi_1(r) = \varepsilon_r \psi_1(r).$$

(14.1.93)

Changing the function

$$\psi_1(r) = r^{-\frac{1}{2}} \phi(r),$$

(14.1.94)

the equation for the new function is

$$\left[-\frac{\partial^2}{\partial r^2} + \frac{K^2 - \frac{1}{4}}{r^2} + u_1(r) \right] \phi(r) = \varepsilon_r \phi(r),$$

(14.1.95)

which is nothing else but the Schrödinger equation for a sextic potential plus a centrifugal term.

Now let us turn our attention to the second equation in (14.1.91). Multiplying it by $r_0^2/\mathcal{F}$ and denoting by:

$$\mu = \frac{A_3}{\mathcal{F}280}r_0^8, \quad \varepsilon_\gamma = \frac{r_0^2 E^{(2)}}{\mathcal{F}}, \tag{14.1.96}$$

one obtains:

$$\left[-\frac{\partial^2}{\partial\gamma^2} - 2iK\frac{\partial}{\partial\gamma} + \mu\cos 6\gamma\right]\psi_2(\gamma) = \varepsilon_\gamma\psi_2(\gamma). \tag{14.1.97}$$

With the change of function:

$$\psi_2(\gamma) = e^{-iK\gamma}M(3\gamma), \tag{14.1.98}$$

we obtain:

$$\left[\frac{\partial^2}{\partial\gamma^2} + \varepsilon_\gamma + K^2 - \mu\cos 6\gamma\right]M(3\gamma) = 0. \tag{14.1.99}$$

Changing now the variable γ to $y = 3\gamma$ the equation for the Mathieu function is readily obtained:

$$\left[\frac{\partial^2}{\partial y^2} + a - 2q\cos 2y\right]M(y) = 0, \tag{14.1.100}$$

where the following notations were used:

$$a = \frac{1}{9}(\varepsilon_\gamma + K^2), \quad 2q = \frac{\mu}{9}. \tag{14.1.101}$$

Before closing this section we would like to comment on the relation of the variable r and the dynamic nuclear deformation β. Aiming at this goal, let us consider the canonical transformation relating the quadrupole conjugate coordinates and the boson operators:

$$\hat{\alpha}_{2\mu} = \frac{1}{k\sqrt{2}}\left(b_{2\mu}^\dagger + (-)^\mu b_{2,-\mu}\right), \quad \hat{\pi}_{2\mu} = \frac{ik}{\sqrt{2}}\left(b_{2,-\mu}^\dagger(-)^\mu - b_{2\mu}\right). \tag{14.1.102}$$

Note that the canonical transformation from above is determined up to a multiplicative factor k. Averaging these equations with the coherent state ψ (14.1.75) one obtains that the coordinates Q_μ and P_μ introduced above are related with the quadrupole operators by:

$$Q_\mu = \langle\psi|k\hat{\alpha}_{2\mu}|\psi\rangle, \quad P_\mu = \langle\psi|\frac{1}{k}\hat{\pi}_{2\mu}|\psi\rangle. \tag{14.1.103}$$

Identifying the averages of $\hat{\alpha}_{2\mu}$, with the quadrupole coordinates in the intrinsic reference frame we obtain [RBD95]:

$$Q_0 = ka_{20} = k\beta\cos\gamma, \quad Q_{\pm2} = \frac{k\beta}{\sqrt{2}}\sin\gamma. \qquad (14.1.104)$$

In the restricted classical phase space the canonical coordinates are:

$$q_0 = k\beta\cos\gamma, \quad q_2 = k\beta\sin\gamma. \qquad (14.1.105)$$

From here it results:

$$r = k\beta \qquad (14.1.106)$$

Using this simple relation in connection with the differential equation in r, one obtains the Shrödinger equation for sextic potential plus centrifugal term in the variable β.

$$\left[-\frac{\partial^2}{\partial\beta^2} + \frac{K^2 - \frac{1}{4}}{\beta^2} + k^2 u_1(k\beta) \right]\phi(k\beta) = \varepsilon_\beta\phi(k\beta) \qquad (14.1.107)$$

In concluding this section, we may say that while in Ref. [RBUG11] the sextic potential for β and the γ potential, yielding the equation for the Mathieu function, were introduced as an ad-hoc choice, here they are derived in a natural manner from the CSM formalism. Moreover, the variable separation is based on two approximations suggested by the classical picture: (i) the non-quadratic terms in momenta are ignored and (ii) the coupling of coordinates and momenta are vanishing due to the local character of the classical phenomenological forces.

14.2 Lipas's Projection Method

The CSM model states for the ground band are identical to those introduced by P.O. Lipas and his collaborators in a series of papers which started with Ref. [LS69] where the model was formulated in great details and [HHL70] where a short application was presented. The Hamiltonian used there was a harmonic one. The initial version of the CSM treated, indeed, the ground band [RD76] with the same generating function but with a highly anharmonic Hamiltonian. The extensions of the two models to three interacting bands are essentially different both in terms of the model states and the Hamiltonian. Also, in many respects the philosophical viewpoints are entirely at odds. Moreover, while the projection method (PM) extension (EPM) limits itself to a simultaneous description of the ground, beta and gamma bands, the CSM was

developed extensively in several directions described in the previous chapters in a comprehensive but not exhaustive manner. Due to the said common features it is fair to devote some space to the PM description.

To sketch the context in which the PM approach appeared, note first that the big merit of the liquid drop model (LDM) is that it offers a reasonable description of spherical and well deformed nuclei. The prediction, somewhat confirmed by experimental data, was that spherical nuclei have equidistant spectrum while the deformed nuclei exhibit rotational bands. However, between the two limiting classes there are transitional (from spherical to well deformed) nuclei whose properties cannot be accounted for by none of the two extreme pictures. The drop from LDM oscillates around a spherical shape and therefore it is difficult to describe nuclei with static deformation. Moreover, for transitional nuclei there are properties which are mainly attributed to anharmonicities. Therefore, both experimental data and principle problems required corrections for LDM, along this line.

P.O. Lipas and his collaborators attempted to build up a model which treats the static deformation and anharmonicities in the simplest possible manner. The quadrupole coordinates defining the nuclear surface are defined in the standard way

$$R(\theta, \phi) = R_0[1 + \sum_m a_m^* Y_{2m}].\tag{14.2.1}$$

The LDM supposes that in the intrinsic frame of reference $a_{\pm 1} = 0$, $a_2 = a_{-2}$. Due to these restrictions, the intrinsic coordinates are not the components of a tensor of rank 2. This property is recovered once the restrictions mentioned above are released. Thus, the intrinsic frame in the PM is different from the standard one defined by the LDM. The LDM Hamiltonian is rotationally invariant while that used by the PM is not. The symmetry is broken in two ways: (a) one assumes that a_0 has a static value β; (b) The inertial as well the stiffness parameters are m-dependent i.e., the drop is anisotropic.

Hence, the drop considered by the PM is described by the deformed Hamiltonian:

$$h = \frac{1}{2}\sum_m B_m|\dot{a}_m|^2 + \frac{1}{2}\sum_m C_m|a_m|^2 + \frac{1}{2}(a_0 - \beta)^2.\tag{14.2.2}$$

The quantization of this Hamiltonian is achieved by Writing it in terms of the quadrupole bosons defined by the canonical transformation:

$$a_\mu = \frac{1}{k\sqrt{2}}(b_\mu^\dagger + (-)^\mu b_{-\mu}), \quad \pi_\mu = \frac{ik}{\sqrt{2}}((-)^\mu b_{-\mu}^\dagger - b_\mu) = B_\mu \dot{a}_\mu.\tag{14.2.3}$$

The said transformation is determined up to a constant k which is determined such that the cross term $b_0^\dagger b_0^\dagger + b_0 b_0$ has a vanishing coefficient. The quantized Hamiltonian looks like:

$$
h = \hbar\omega \left[(b_0^\dagger b_0 + \frac{1}{2}) - d(b_0^\dagger + b_0) + d^2 \right]
$$

$$
+ \hbar\omega \left[\sum_{m \neq 0} f_m ((b_m^\dagger b_m + \frac{1}{2}) + \sum_{m \neq 0} (b_m^\dagger b_{-m}^\dagger (-)^m + b_{-m} b_m (-)^m) \right], \quad (14.2.4)
$$

where

$$
f_m = \frac{1}{2} \left(\frac{B_0}{B_m} + \frac{C_m}{C_0} \right), \quad g_m = \frac{1}{4} \left(-\frac{B_0}{B_m} + \frac{C_m}{C_0} \right),
$$

$$
\hbar\omega = \sqrt{\frac{C_0}{B_0}}, \quad d = \frac{1}{\sqrt{2}} k\beta, \quad k = (B_0 C_0)^{1/4}. \quad (14.2.5)
$$

The first term, the one corresponding to the zeroth component of the boson operator, admits the coherent state as eigenfunction, while the second one can be diagonalized through the Bogoliubov-Valatin transformation for each $m \neq 0$. Thus, the boson Hamiltonian (14.2.4) is fully solvable and defines a deformed basis which is to be used for treating complex rotationally invariant Hamiltonians, in the laboratory frame. In this respect the intrinsic Hamiltonian plays a similar role as the mean field does for the particle motion.

The chosen invariant Hamiltonian is a harmonic one and the energy is defined by its average with the coherent state. Energy depends on a scaling parameter c_1 and the deformation parameter d. The model is tested numerically for the ground band energies of ^{152}Gd and ^{152}Sm where the known levels, at that time, were up to 8^+ in ^{152}Gd and 12^+ for ^{152}Sm. The calculated energy spacing is less than the experimental one and the deviation is an increasing function of the angular momentum. The agreement is however qualitatively good, although the parameters were fixed by fitting the lowest two energies.

The projected states defined by PM were used in Ref. [RD76] in connection with a complex anharmonic Hamiltonian for many nuclei where data are available up to high spin states. In the quoted reference and [RGB77] the authors obtained analytical expressions for the overlap integrals which facilitated very much the numerical application. The agreement obtained was overall very good. Moreover, the calculations were extended for two bands, the ground and beta, in Ref. [Ra76, RB76]. These two publications are, in fact, precursors of the CSM.

The authors of the PM, extended the formalism by including the excited bands, β and γ. Thus, the projected states for ground, beta and gamma bands are:

$$
|g_0\rangle = P_{M0}^2 |\tilde{0}\rangle, \quad |\beta_0\rangle = P_{M0}^2 (b_0^\dagger - d)|\tilde{0}\rangle, \quad |\gamma_0\rangle = P_{M2}^2 b_2^\dagger |\tilde{0}\rangle. \quad (14.2.6)
$$

Note that the projected model states are not mutually orthogonal. The state overlaps go to zero when $d \to \infty$ and to 1 for $d \to 0$. This infers that at least for the transitional region the orthogonalization through the Gram-Schmidt procedure is necessary. The order of orthogonalization is chosen such that the link between the vibrational and rotational spectrum be consistent with the Sheline-Sakai scheme. This way the obtained orthogonal basis states are:

$$|g\rangle = |g_0\rangle, \quad |\gamma\rangle = N_\gamma(1 - |g\rangle\langle g|)|\gamma_0\rangle, \quad |\beta\rangle = N_\beta(1 - |g\rangle\langle g| - |\gamma\rangle\langle\gamma|)|\beta_0\rangle.$$
(14.2.7)

Since the main purpose is to qualitatively study the low lying spectra of the transitional nuclei, the rotationally invariant Hamiltonian used for the description in the laboratory frame is, again, proportional to the boson number operator, i.e. of the form $c_1\hat{N}$. Energies are defined by averaging the model Hamiltonian with the orthogonalized boson states. Results were as follows: (a) The right sign for the experimental spectroscopic quadrupole moment is reproduced; (b) Although there are only two adjustable parameters, the energy scaling parameter c_1 and the deformation parameter, the low lying spectra of ^{114}Cd and ^{152}Sm are reasonably well described; (c) The calculated quadrupole moment of the first state 2^+ in ^{114}Cd is close to the corresponding experimental data.

Aiming at improving the agreement with the data, the intrinsic function for the ground band was taken as the ground state of the whole intrinsic Hamiltonian, i.e. including also the anisotropic terms:

$$|\tilde{0}\rangle = exp(db_0^\dagger + A_1 b_1^\dagger b_{-1}^\dagger + A_2 b_2^\dagger b_{-2}^\dagger)|0\rangle$$
(14.2.8)

We see that the new function contains two additional factors which are coherent states for the $SU(1)$ groups acting on the dipole and quadrupole degrees of freedom, respectively. These states where fully described in one of previous chapters. Actually, they are vacuum states for the Bogoliubov-Valatin transformed bosons. The excited states were defined by acting on the newly defined ground state with the operators:

$$\tilde{b}_0^\dagger = b_0^\dagger - d, \quad \tilde{b}_m^\dagger = b_m^\dagger - A_{|m|}b_{-m}, \quad m \neq 0.$$
(14.2.9)

From this point the same path as for the isotropic case was followed. That is the states were orthogonalized and then the average values with the orthogonal states were calculated. The agreement with experiment was improved, having 4 free parameters instead of 2, but not to such extent that the efforts are justified.

The full description of the CSM was published in 1981,1982 and 1983 [RCGD81, RCGD82, RS83], with the main results presented in Chap. 6.

From 1985 to 1987, several publications [SuLi185, SuLi285, Su87] formulated a refinement of the extended projection method (EPM) which significantly improved the quantitative results obtained before. Here, we describe the main ingredients of the new version of the EPM.

The authors gave up the orthogonalization process of the deformed basis for the ground, β and γ bands. Instead, the model Hamiltonian, which is of fourth order in the quadrupole bosons, is diagonalized in the non-orthogonal basis. The generalized eigenvalue problem provides an orthogonal set of eigenstates which, in fact, are the optimal orthogonal Schmidt basis. Concerning the Hamiltonian, this is at the beginning considered to be the most general fourth order Hamiltonian constructed by imposing some restrictions as hermiticity, rotational and time reversal invariance. Since the formalism is purely phenomenological, one ignores the underlying microscopic boson expansion many body Hamiltonian and thus the structure coefficients (multiplying the monomials B_{mn}, with m denoting the number of operators $b^\dagger$ while n the number of annihilation boson operators b, involved) are taken as free parameters. There are nine parameters in total. The number of parameters is too big and should be diminished by requiring additional criteria to be fulfilled. First, one notices that several high order terms have no other effect on the matrix elements than renormalizing the m.e. of the second order boson terms, in the asymptotic limit. Due to this feature we ignore them. The numerical analysis indicates that some third order terms bring a negligible correction on the matrix elements. Also, from the fourth order terms one keeps only one, the rest being either negligible or not independent terms. Thus, the starting Hamiltonian:

$$H = \sum_{m,n=0,1,2} c_{mn} B_{mn}, \quad \text{with} \quad B_{11} = b^\dagger \cdot \bar{b} = N$$

$$B_{20} = b^\dagger \cdot b^\dagger + \bar{b} \cdot \bar{b}, \quad B_{21} = [b^\dagger b^\dagger]_2 \cdot \bar{b} + h.c.$$

$$B_{30} = [b^\dagger b^\dagger]_2 \cdot b^\dagger + h.c., \quad B_{40} = (b^\dagger b^\dagger)^2 + h.c.,$$

$$B_{31} = b^\dagger \; b^\dagger b^\dagger \cdot \bar{b} + h.c., \quad B_{22}^{(L)} = [b^\dagger b^\dagger]_L \cdot [\bar{b}\bar{b}]_L, \quad L = 0, 2, 4. \quad (14.2.10)$$

is contracted to an effective Hamiltonian:

$$H = c_0 N + c_1 B_{20} + c_2 B_{21}' + c_3 B_{22}^{(2)'}, \quad \text{where}$$

$$B_{21}' = -\sqrt{\frac{7}{8}}\frac{1}{d} B_{21} - N, \quad B_{22}^{(2)'} = \frac{7}{2d^2} B_{22}^{(2)} + \sqrt{\frac{7}{8}}\frac{1}{d} B_{21} + N. \quad (14.2.11)$$

To calculate all matrix elements involved, one has to calculate numerically 11 overlap integrals. Information about the boson expansion convergence of H was obtained by successive fits using the second-order (3 parameters), third order (4 parameters) and fourth order (5 parameters) expansion of the laboratory frame Hamiltonian. Thus, the results for the isotopic chains of Sm, Gd, Yb and Er show that the parameters c_0 and c_1 obtained with the three and four parameters version do not differ too much from each other, but they are significantly different when the fifth parameter is added. On the other hand, the parameters c_2 and c_3 obtained by the fitting procedure within the four and five parameters version, respectively, are not far away from each other. Thus, it is not clear how big the corrections to c_0 and c_1 are when terms of order higher than 4 are added.

The transition probabilities were studied with a transition operator which is linear in the quadrupole bosons:

$$T^{(E2)} = e^*(b^\dagger + \bar{b}). \tag{14.2.12}$$

The effective charge e^* was fixed by fitting the experimental reduced transition probability $B(E2; 2_g \to 0_g)$. Numerical results were compared with those obtained by other methods, like rotation-vibration model (RVM) [FaGr62], the dynamic pairing-plus-quadrupole model (DPPQ) [Ku67], boson expansion technique (BET) [KT72] as well as with the experimental data. For Sm isotopes the agreement with experimental data appraised by means of the rms values of deviations is better than that corresponding to the IBA method. Also, the spectroscopic quadrupole moments of Sm isotopes are excellently described. The theoretical results are closer to the experimental data than those yielded by IBA as well as by BET.

The transition rates are very sensitive to the wave function structure. For example, if transition probabilities are calculated with the states (14.2.6) and alternatively with the states yielded by the diagonalization procedure, the results are dramatically different. Anharmonic effects may be included either by considering higher order terms in the expression of the transition operator or by considering anharmonic terms in the model Hamiltonian and, consequently, the wave functions are correspondingly modified. In Ref. [SuLi185] the latter option is adopted. For illustration, the results for the ratios:

$$R_1 = \frac{B(E2; 2_\gamma \to 0_g)}{B(E2; 2_\beta \to 0_g)}, \quad R_2 = \frac{B(E2; 2_\gamma \to 0_\beta)}{B(E2; 2_\beta \to 0_g)}. \tag{14.2.13}$$

calculated with the wave functions obtained when only the harmonic term is included in H and alternatively with all anharmonic terms added are shown in Table 14.5. From there we may conclude that indeed, the anharmonicities play a crucial role for a quantitative description of the transition rates:

Comparison of the EPM results with the IBA predictions for even-even isotopes of Sm was presented also in Refs. [SuLi285, Su87] and concluded that EPM does better for many of the data.

Note that since 1987 there has not been any publication on the EPM. Moreover, all existing applications refer mainly to the low lying states and even these only for few isotopes.

On the contrary, CSM was widely used (about 194 nuclei were studied) and its extensions explain in a realistic fashion a large variety of collective phenomena in

Table 14.5 Ratios R_1 and R_2 calculated with harmonic (h) and full anharmonic (ah) Hamiltonian

Ratios	^{146}Sm (d ≈ 1.5)		^{150}Sm (d ≈ 2.5)	
	h	ah	h	ah
R_1	4	400	60,000	1
R_2	0.03	3,000	40,000	10

spherical, transitional and well deformed nuclei. Moreover, the high and very high angular momentum states are accessible.

Before closing this section we would like to mention a few features of the CSM which contrast the EPM: (i) The model spaces for intrinsic and projected states for the two models are different. Indeed, within the CSM the states are orthogonal before and after projection and the latter ones have a structure in the extreme limits of vanishing and large deformation parameter, which are consistent with the Sheline-Sakai scheme. The beta states include excitations of third order in bosons while those from gamma band states with two phonons; (ii) The model Hamiltonian is by construction effective, i.e. it leaves the beta states uncoupled to the states from the ground and gamma bands. Moreover, it includes high anharmonicities, in the three parameter version (which works pretty well for a large number of nuclei) being of sixth order in bosons, while the five parameters version is of eight order in bosons; (iii) An important achievement of the CSM is the existence of analytical formulas for both excitation energies and transition probabilities in the near vibrational and rotational regions. It seems that the expressions obtained can be used also for the transitional nuclei; (iv) The CSM extensions to the description of the proton and neutron systems, of the negative parity states, of the even-odd nuclei and even of the chiral spectra in even-even nuclei, cover a huge variety of collective features in nuclei; (v) The ability of coherent states to generate single particle and boson basis were intensively exploited; (vi) Due to the semiclassical properties of the coherent state manifested by that it minimizes the uncertainty relations of quadrupole coordinates and their conjugate momenta, the classical features of highly anharmonic Hamiltonians could be studied. On this line the exact classical solution for a sixth order boson Hamiltonian was presented. Solutions for the quantization of the classical trajectories were also described.

In view of the above mentioned properties, one could assert that CSM represents one of the most versatile collective model able to describe states of high spin in transitional and well deformed nuclei, covering various classes of nuclei characterized by specific symmetries or in other words, nuclear phases.

14.3 Rotation Vibration Model

The quadrupole degrees of freedom have been intensively used by phenomenological models to interpret the data for energies and electromagnetic transitions of collective states. In the pioneering model of Bohr and Mottelson [BM53] (**L**iquid **D**rop **M**odel = LDM) some collective properties are treated in terms of quadrupole shape coordinates describing small oscillations of the nuclear surface around a spherical equilibrium shape.

The harmonic motion of the liquid drop and the restriction to a spherical shape for the ground state are severe limitations of this approach. The first improvement of

the LDM was obtained in the rotation-vibration model (RVM) [FaGr62] in which the deviation of the shape coordinates from their static values is considered and by this an axially symmetric deformed shape is described. Here we give the main ingredients of RVM. The nuclear surface is described by five quadrupole coordinates which are complex functions of time:

$$R = R_0(1 + \sum_\mu \alpha_{2\mu}^*(t)Y_{2\mu}), \quad \alpha_{2\mu}^* = (-1)^\mu \alpha_{2,-\mu}. \tag{14.3.1}$$

The intrinsic frame is obtained from the laboratory one by a rotation of Euler angle $\Omega = (\theta_1, \theta_2, \theta_3)$ defining the frame of principal axes of inertia ellipsoid. Correspondingly, by rotating the quadrupole coordinates $\alpha_{2\mu}$ which form a tensor of rank 2, one obtains a set of coordinate characterizing the system in the intrinsic reference frame:

$$a_{2\mu} = \sum_\nu D_{\nu\mu}^{2*}\alpha_{2\nu}. \tag{14.3.2}$$

By contrast to the Bohr-Mottelson model which assumes $a_{22} = a_{2,-2}$, $a_{21} = a_{2,-1} = 0$ and moreover, the nonvanishing coordinates are parametrized as:

$$a_{20} = \beta \cos \gamma, \quad a_{22} = a_{2,-2} = \frac{\beta}{\sqrt{2}} \sin \gamma \tag{14.3.3}$$

the RVM uses the intrinsic coordinates $a_{20}, a_{22}(= a_{2,-2})$ to study the classical and quantized Hamiltonian. Thus instead of quantizing the classical Hamiltonian by writing the Laplace operator in the curvilinear space spanned by the dynamic (β, γ) deformations, where the volume element of intrinsic variables is $\beta^4 |\sin 3\gamma| d\beta d\gamma$ the quantization is achieved in the Euclidean space of a_{20}, a_{22} with the volume element equal to $da_{20}da_{22}$. To simplify the notations from now on we shall omit the low index 2 specifying the rank of the shape coordinate. Thus, the classical Hamiltonian of the liquid drop written in terms of intrinsic coordinates reads:

$$H = \sum_k \frac{I_k^2}{2\mathcal{J}_k(a_\mu)} + \frac{1}{2}B \sum_\nu \dot{a}_\nu^* \dot{a}_\nu + V(a_\nu), \tag{14.3.4}$$

with B denoting the mass parameter and $V(a_\nu)$ the potential energy of surface oscillations:

$$V(a_\nu) = \frac{1}{2}C_0 a_0^2 + \frac{1}{2}C_2(a_2^2 + a_{-2}^2), \tag{14.3.5}$$

where C_0, C_2 stand for the elasticity parameters. The symbols I_k, $\mathcal{J}_k$ stand for the kth component of the intrinsic angular momentum and the moment of inertia relative to the axis k, respectively.

Suppose now that the nuclear surface has an axially deformed static shape, i.e. the time dependence of the coordinates is of the form:

$$a_0(t) = \beta_0 + a_0'(t), \quad a_{\pm2} = 0 + a_{\pm2}'(t), \quad |\frac{a_\nu'}{\beta_0}| \ll 1, \quad \nu = 0, \pm2. \quad (14.3.6)$$

Considering the deviations from the static values small, one can expand the reciprocal moment of inertia in terms of the coordinate relative deviations from the static values, i.e. a_ν'/β_0. In the next step the kinetic energy is quantized by the replacements:

$$B\dot{a}_0 = -i\hbar\frac{\partial}{\partial a_0'}, \quad B\sqrt{2}\dot{a}_2' = -i\hbar\frac{\partial}{\sqrt{2}\partial a_2'}. \quad (14.3.7)$$

The quantized Hamiltonian is:

$$H \equiv T + V = T_R + T_V + T_{RV} + V_{a_0a_2}(a_0', a_2'),$$

$$T_R = \frac{\hat{I}^2 - \hat{I}_3^2}{2\mathcal{J}_0} + \frac{\hat{I}_3^2}{16Ba_2^2}, \quad \mathcal{J}_0 = 3B\beta_0^2,$$

$$T_V = -\frac{\hbar^2}{2B}\left(\frac{\partial^2}{\partial a_0'^2} + \frac{1}{2}\frac{\partial^2}{\partial a_2'^2}\right)$$

$$T_{RV} = \frac{\hat{I}^2 - \hat{I}_3^2}{2\mathcal{J}_0}\left[2\frac{a_2'^2}{\beta_0^2} - 2\frac{a_0'}{\beta_0} + 3\frac{a_0'^2}{\beta_0^2}\right]$$

$$- \frac{\hat{I}_+^2 + \hat{I}_-^2}{2\mathcal{J}_0}\left[-\sqrt{6}\frac{a_0'a_2'}{\beta_0^2} + \frac{1}{3}\sqrt{6}\frac{a_2'}{\beta_0}\right] + 2\epsilon\frac{a_0'}{\beta_0}, \quad \epsilon = \frac{\hbar^2}{\mathcal{J}_0},$$

$$V_{a_0a_2}(a_0', a_2') = \frac{1}{2}C_0a_0'^2 + C_2a_2'^2. \quad (14.3.8)$$

The basis states for treating the rotation-vibration term T_{RV} is defined by the eigenstates of the unperturbed operator:

$$H_0 = T_R + T_V + V_{a_0a_2}(a_0', a_2'). \quad (14.3.9)$$

The function with a proper symmetry against the change $a_2' \to -a_2'$ is:

$$|IK, n_2n_0\rangle = \left(\frac{2I+1}{16\pi^2}\frac{1}{1+\delta_{K,0}}\right)^{1/2}(D_{MK}^I + (-)^I D_{M-K}^I)$$

$$\times\left(\frac{\lambda^{\frac{1}{2}K+1}\Gamma(\frac{1}{2}K+1+n_2)}{n_2!}\right)^{\frac{1}{2}}\left(\Gamma(\frac{1}{2}K+1)\right)^{-1}|a_2'|^{\frac{1}{2}}(a_2')^{\frac{1}{2}K}e^{-\frac{1}{2}\lambda a_2'^2}$$

$$\times_1F_1(-n_2, \frac{1}{2}K+1; \lambda a_2'^2)\frac{1}{(n_0!)^{\frac{1}{2}}}\underbrace{\hat{\beta}_0\hat{\beta}_0\dots\hat{\beta}_0}_{n_0\ times}|0\rangle,$$

$$E^{IK}_{n_2,n_0} = (n_0 + \frac{1}{2})E_\beta + (2n_2 + \frac{1}{2}K + 1)E_\gamma + (I(I+1) - K^2)\frac{1}{2}\epsilon,$$

$$I = \begin{cases} 0, 2, 4, \dots & \text{for } K = 0 \\ K, K+1, \dots & \text{for } K \neq 0 \end{cases}, \quad n_0, n_2 = 0, 1, 2, \dots,$$

where

$$E_\beta = \hbar \left(\frac{C_0}{B}\right)^{\frac{1}{2}} = \hbar\omega_0, \quad E_\gamma = \hbar \left(\frac{C_2}{B}\right)^{\frac{1}{2}} = \hbar\omega_2, \quad \epsilon = \frac{\hbar^2}{3B\beta_0^2},$$

(14.3.10)

$$a'_0 = \sqrt{\frac{\hbar}{2B\omega_0}}(\hat{\beta}_0 + \hat{\beta}_0^+), \quad \dot{a}'_0 = -i\omega_0 \sqrt{\frac{\hbar}{2B\omega_0}}(\hat{\beta}_0 - \hat{\beta}_0^+), \quad \lambda = \frac{2E_\gamma}{3\epsilon\beta_0^2}.$$

The eigenvalues of H can be obtained by diagonalizing it in the basis defined above. Note that the matrix elements of the rotation-vibration term in this basis can be analytically calculated. The model authors made a systematic of spectra in different regions of the nuclear chart by choosing for each angular momentum 13 states $|IK, n_2 n_0\rangle$ with $K \leq 6$ and $n_0 + n_2 \leq 2$. The wave functions are used for describing the reduced E2 transition probabilities. The transition operator is also expanded in power series around the deformation static values. The final expression is:

$$T_{2\mu} = \frac{3Z}{4\pi} R_0^2 \left[D^2_{\mu 0} \left(\beta_0 (1 + \frac{2}{7} \left(\frac{5}{\pi}\right)^{\frac{1}{2}} \beta_0) \right) + D^2_{\mu 0} a'_0 \left(1 + \frac{4}{7} \left(\frac{5}{\pi}\right)^{\frac{1}{2}} \beta_0 \right) \right.$$
$$+ D^2_{\mu 0} \frac{2}{7} \left(\frac{5}{\pi}\right)^{\frac{1}{2}} (a'^2_0 - 2a'^2_2) + (D^2_{\mu 2} + D^2_{\mu -2}) \left(\left(1 - \frac{4}{7} \left(\frac{5}{\pi}\right)^{\frac{1}{2}} \beta_0\right) a'_2 \right.$$
$$\left. \left. - \frac{4}{7} \left(\frac{5}{\pi}\right)^{\frac{1}{2}} a'_0 a'_2 \right) \right].$$

(14.3.11)

With the Rose convention for the reduced matrix elements, the B(E2) transitions are readily obtained:

$$B(E2; I_i \rightarrow I_f) = |\langle I_i ||T_2|| I_f \rangle|^2.$$

(14.3.12)

The RVM has been successfully applied to a large number of nuclei, including the even-even isotopes of Sm, Gd, Dy, Er, Yb, Hf, W, Os, Th, U, Pu. The agreement with experimental data was good for both excitation energies in the ground, beta and gamma bands and the E0, E2 and E4 reduced transition probabilities. The parameters of the RVM are the reciprocal moment of inertia ϵ, and the vibrational energies E_β and E_γ. They were fixed by fitting the data concerning the excitation energies of the first 2^+ state and the head states of the beta and gamma bands. However, some systematic deviations from the experimental data are to be noted. They were interpreted in terms of the Coriolis anti-pairing (CAP)[MoVa60] and blocking of the

states above the Fermi sea in excited states. The corrections due to these effects were accounted for in a phenomenological way and thus, the agreement with the data was improved.

14.3.1 Comparison of the RVM and the CSM

In this subsection we shall prove that the RVM energies for the ground beta and gamma bands can be analytically derived within a semiclassical treatment of the CSM Hamiltonian [MRF98]:

$$H = A_1 \left(22\hat{N} + 5\Omega^\dagger_{\beta'}\Omega_{\beta'} \right) + A_2 \hat{I}^2 + A_3 \Omega^\dagger_\beta \Omega_\beta. \tag{14.3.13}$$

We recall that $\hat{N}$ and $\hat{I}^2$ denote the quadrupole boson number and total angular momentum squared operators, respectively. Here the notations from Chap. 6 are used:

$$\Omega^\dagger_{\beta'} = \left[b^\dagger_2 \times b^\dagger_2 \right]^0 - \frac{d^2}{\sqrt{5}}, \tag{14.3.14}$$

$$\Omega^\dagger_\beta = \left[b^\dagger_2 \times b^\dagger_2 \times b^\dagger_2 \right]^0 + \frac{3d}{\sqrt{14}} \left[b^\dagger_2 \times b^\dagger_2 \right]^0 - \frac{d^3}{\sqrt{70}}, \tag{14.3.15}$$

where $b^\dagger_{2\mu}$ ($-2 \le \mu \le 2$) are the components of the quadrupole boson operator.

The classical motion of an axially non-symmetric shape can be studied by the associated energy function:

$$\mathcal{H} = \langle \Psi | \hat{H} | \Psi \rangle, \tag{14.3.16}$$

where

$$|\Psi\rangle = exp(z_0 b^\dagger_{20} + z_2 b^\dagger_{22} + z_{-2} b^\dagger_{2-2} - z^\star_0 b_{20} - z^\star_2 b_{22} - z^\star_{-2} b_{2-2})|0\rangle, \tag{14.3.17}$$

and $\hat{H}$ is given by (14.3.13). The vacuum state for the quadrupole bosons is denoted by $|0\rangle$. The coefficients $z_0, z_2, z_{-2}, z^\star_0, z^\star_2, z^\star_{-2}$ are complex functions of time and define the classical phase space coordinates. By direct calculation one finds:

$$\begin{aligned}
\mathcal{H} = {}& 2 \left(11A_1 + 3A_2 \right) \left(z_0 z^\star_0 + z_2 z^\star_2 + z_{-2} z^\star_{-2} \right) \\
& + A_1 \left(z_0^2 + 2z_2 z_{-2} - d^2 \right) \left(z^{\star\,2}_0 + 2z^\star_2 z^\star_{-2} - d^2 \right) \\
& + \frac{A_3}{70} \left[2 \left(6z_0 z_2 z_{-2} - z_0^3 \right) + 3d \left(z_0^2 + 2z_2 z_{-2} \right) - d^3 \right] \\
& \times \left[2 \left(6z^\star_0 z^\star_2 z^\star_{-2} - z^{\star\,3}_0 \right) + 3d \left(z^{\star\,2}_0 + 2z^\star_2 z^\star_{-2} \right) - d^3 \right].
\end{aligned} \tag{14.3.18}$$

The motion of the phase space coordinates is governed by the equations provided by the variational principle[1]

$$\delta \int_0^t \langle \Psi | (H - i \frac{\partial}{\partial t'}) | \Psi \rangle dt' = 0. \tag{14.3.19}$$

The results are:

$$\{z_k, \mathcal{H}\} = i\dot{z}_k, \quad \{z_k^\star, \mathcal{H}\} = i\dot{z}_k^\star, \quad \{z_k, z_{k'}^\star\} = -i\delta_{kk'}, \tag{14.3.20}$$

where the Poisson bracket is defined with respect to the canonically conjugate variables $(u_k, v_k) = (\sqrt{2}Re(z_k), \sqrt{2}Im(z_k))$. Stationary points of the phase coordinates motion are also stationary points for the surface of constant energy:

$$\mathcal{H}(z_0, z_0^\star, z_2, z_2^\star, z_{-2}, z_{-2}^\star) = E \tag{14.3.21}$$

Suppose now that this surface exhibits a minimum point $(z_0, z_2) = (u_0, u_2)$ with u_0 and u_2 being real numbers. The existence of such a minimum is proved in Ref. [RBD95]. Since we want to mention here some classical features which do not depend on whether this minimum is axially symmetric or not we consider the simplifying case of $u_2 = 0$. Expanding $\mathcal{H}$ around the minimum point and keeping only the quadratic terms in the deviations z_k', $z_k^\star{}'$, one obtains:

$$\mathcal{H} = \mathcal{H}_0 + \mathcal{H}_\beta + \mathcal{H}_\gamma. \tag{14.3.22}$$

where $\mathcal{H}_0$ is a constant term (not depending on coordinates) and

$$\mathcal{H}_\beta = B_1 z_0' z_0^\star{}' + B_2 \left(z_0'^2 + (z_0^\star{}')^2 \right), \tag{14.3.23}$$

$$\mathcal{H}_\gamma = G_1 \left(z_2' z_2^\star{}' + z_{-2}' z_{-2}^\star{}' \right) + G_2 \left(z_2' z_{-2}' + z_2^\star{}' z_{-2}^\star{}' \right), \tag{14.3.24}$$

The coefficients B_1, B_2, G_1 and G_2 have the following expressions:

$$G_1 = 22A_1 + 6A_2,$$
$$G_2 = 2A_1(u_0^2 - d^2) - \frac{3A_3}{35}(d + 2u_0)(u_0 - d)(2u_0 - du_0 - d^2),$$
$$B_1 = 22A_1 + 6A_2 + 4A_1 u_0^2 + \frac{18}{35}A_3 u_0^2 (d - u_0)^2,$$
$$B_2 = A_1(u_0^2 - d^2) - \frac{3A_3}{70}(d - 2u_0)(u_0 - d)(2u_0 - du_0 - d^2). \tag{14.3.25}$$

---

[1] We use the units $\hbar = c = 1$.

Note that at the level of quadratic approximation there is no $\beta - \gamma$ coupling term. The classical motion can be quantized as follows. One defines first a new set of coordinates:

$$Q_2 = \frac{1}{\sqrt{2}}(z_2^\star + z_{-2}), \quad Q_{-2} = \frac{1}{\sqrt{2}}(z_{-2}^\star + z_2), \quad Q_0 = \frac{1}{\sqrt{2}}(z_0^\star + z_0), \quad (14.3.26)$$

$$P_2 = \frac{i}{\sqrt{2}}(z_{-2}^\star - z_2), \quad P_{-2} = \frac{i}{\sqrt{2}}(z_2^\star - z_{-2}), \quad P_0 = \frac{i}{\sqrt{2}}(z_0^* - z_0). \quad (14.3.27)$$

The Poisson brackets of these coordinates can be easily calculated and the result reflects their canonically conjugate character:

$$\{Q_k, P_{k'}\} = \delta_{kk'}, \quad k = 0, \pm 2. \quad (14.3.28)$$

For small deviations from the minimum point, it is useful to introduce the parametrization:

$$Q_{\pm 2} = \sqrt{2}\gamma e^{\pm 2i\phi} \equiv \sqrt{2}q_{\pm 2} \quad (14.3.29)$$

Let us consider as coordinate operators $\hat{Q}_k$, and the corresponding momenta defined by:

$$\hat{P}_{\pm 2} = -\frac{i}{\sqrt{2}}\frac{\partial}{\partial q_{\pm 2}}, \quad \hat{P}_0 = -i\frac{\partial}{\partial Q_0} \quad (14.3.30)$$

Indeed, one can easily check that

$$\left[\hat{Q}_{\pm 2}, \hat{P}_{\pm 2}\right] = i, \quad \left[\hat{Q}_0, \hat{P}_0\right] = i, \quad (14.3.31)$$

The transformation $(Q_k, P_k) \to (\hat{Q}_k, \hat{P}_k)$ with $k = 0, \pm 2$ is usually called canonical quantization. Quantized Hamiltonians are obtained by writing $\mathcal{H}_\beta$ and $\mathcal{H}_\gamma$ in terms of $(Q_{\pm 2}, P_{\pm 2})$ and then making the above mentioned replacements. The latter transformation is made after putting the mixed Q and P terms in a symmetrized form. The final results are:

$$\hat{H}_\gamma = -\frac{1}{4}(G_1 - G_2)\left(\frac{\partial^2}{\partial\gamma^2} + \frac{1}{\gamma}\frac{\partial}{\partial\gamma} + \frac{1}{4\gamma^2}\frac{\partial^2}{\partial\phi^2}\right) + (G_1 + G_2)\gamma^2 \quad (14.3.32)$$

$$\hat{H}_\beta = -\frac{1}{2}(B_1 - 2B_2)\frac{\partial^2}{\partial Q_0^2} + \frac{1}{2}(B_1 + 2B_2)Q_0^2 \quad (14.3.33)$$

Note that H_γ describes a plane oscillator in terms of the polar coordinates $(\gamma, 2\phi)$. The spectra which are obtained with the above two operators, H_β and H_γ, are:

$$E_N^{(\gamma)} = \omega_\gamma(N + 1), \quad N = 2n + \frac{1}{2}|K|, \quad n = 0, 1, 2, \ldots \quad |K| = 0, 2, 4, \ldots$$

(14.3.34)

$$E_n^{(\beta)} = \omega_\beta(n + \frac{1}{2}), \quad n = 0, 1, 2, \ldots$$

(14.3.35)

where

$$\omega_\gamma = \left(G_1^2 - G_2^2\right)^{1/2}, \quad \omega_\beta = \left(B_1^2 - 4B_2^2\right)^{1/2}$$

(14.3.36)

Inspecting the expressions of the coefficients G and B, one sees that G_1 and B_1 are mainly given by the $\hat{N}$ term of the model Hamiltonian. Indeed, the coefficient A_2 accompanying $\hat{I}^2$ is usually small. Therefore, the γ and β harmonic frequencies are decreased by anharmonicities. Although we discuss the simplest case, the γ degree of freedom could not be entirely decoupled from the rotational coordinate ϕ. This seems to be a general feature for the liquid drop model. The Hamiltonian $\hat{H}_\beta + \hat{H}_\gamma$ is similar to the unperturbed part of the RVM. Moreover, the semiclassical spectrum obtained above is identical with the one provided by the vibrational part of the unperturbed Hamiltonian. Concerning the coupling terms, here only one is reproduced. The reason is that by restricting the coherent state to the $b_{20}^\dagger, b_{22}^\dagger, b_{2-2}^\dagger$ bosons, the motion of two Euler angles is not taken into account. We notice the fact that, since the CSM is a boson formalism, it includes powers of momenta larger than two, which contrasts the RVM where only terms quadratic in momenta are involved.

The CSM uses a highly anharmonic Hamiltonian and the projected states are superpositions of all K quantum numbers. This results in generating some important effects for high spin states. By contradistinction, RVM uses a harmonic vibrational Hamiltonian and a diagonalization basis subject to the restriction $K \leq 6$. On the other hand, in order to adapt the CSM to higher excited bands would require a great amount of additional effort. The effect of anharmonicities on the γ and β vibrational energies was analyzed in detail in Ref. [RBD95].

14.3.2 The Triaxial Rotation Vibration Model

In the Ba and Xe region there are experimental data which cannot be described by the RVM, the deviations being caused by the restriction to the axially symmetric equilibrium shape. In Ref. [MFK97] the mentioned restriction is released and the agreement with experimental data was improved.

We consider, again, the classical Hamiltonian associated to a harmonic liquid drop. Now we suppose that the equilibrium shape is an asymmetric ellipsoid. Therefore the stationary point of the energy surface is achieved in (β, a_2) with both coordinates

different from zero. The coordinates time dependence is carried by their deviations
from the static values:

$$a_0(t) = \beta_0 + a_0'(t), \quad a_2(t) = a_2 + a_2'(t). \tag{14.3.37}$$

The new dynamical coordinates are supposed to be small comparing them to the static
deformations. In this case we may expand the model Hamiltonian up the second order
in a_0'/β_0 and a_2'/a_2. After quantization, the Hamiltonian splits up into several terms
which can be written as:

$$H \equiv T + V = T_{rot} + T_{vib} + T_{rotvib} + V_{\beta_0 a_2}(a_0', a_2'), \tag{14.3.38}$$

where the following notations were used:

$$T_{rot} = \frac{\hat{\mathbf{I}}^2 - \hat{I}_3^2}{2I_0} + \frac{\hat{I}_3^2}{16Ba_2^2}, \quad T_{vib} = -\frac{\hbar^2}{2B}(\frac{\partial^2}{\partial a_0'^2} + \frac{1}{2}\frac{\partial^2}{\partial a_2'^2}),$$

$$T_{rotvib} = \frac{\hat{\mathbf{I}}^2 - \hat{I}_3^2}{2I_0} f_0(\beta_0, a_2, a_0', a_2') + \frac{\hat{I}_+^2 + \hat{I}_-^2}{2I_0} f_1(\beta_0, a_2, a_0', a_2')$$

$$+ \frac{\hat{I}_3^2}{16Ba_2^2} f_2(a_2, a_2') + 2\epsilon\frac{a_0'}{\beta_0}, \tag{14.3.39}$$

$$V_{\beta_0 a_2}(a_0', a_2') = \frac{1}{2}C_0 a_0'^2 + C_2 a_2'^2.$$

The expansion coefficients f_0, f_1, and f_2, have the expressions:

$$f_0 = -2\frac{a_0'}{\beta_0} + 3\frac{a_0'^2}{\beta_0^2} + \frac{2}{\beta_0^2}(a_2^2 + 2a_2 a_2' + a_2'^2),$$

$$f_1 = \frac{1}{3}\sqrt{6}\frac{1}{\beta_0}(a_2 + a_2') - \sqrt{6}\frac{1}{\beta_0^2}a_0'(a_2 + a_2'),$$

$$f_2 = -2\frac{a_2'}{a_2} + 3\frac{a_2'^2}{a_2^2}. \tag{14.3.40}$$

We mention that the notations introduced in the subsection devoted to the RVM are
preserved. The eigenstates of the unperturbed Hamiltonian

$$H_0 = T_{rot} + T_{vib} + V_{\beta_0 a_2}, \tag{14.3.41}$$

are taken as diagonalization basis for the coupling Hamiltonian. A basis state
$|IK, n_2 n_0\rangle$ is labeled by the total angular momentum (I), its projection on the intrin-
sic z-axis (K) and by the number of phonons for the β (n_0) and γ (n_2) vibrations. For
$K = 0$, the angular momentum I takes only even values, whereas for $K = 2, 4, 6, \ldots$

all values $I > K$ are allowed. The basis is restricted to quantum numbers $K \leq 6$ and $n_2 + n_0 \leq 2$.

The TRVM has four parameters. These are the vibration energies $E_\beta(=\hbar\sqrt{\frac{C_0}{B}})$ and $E_\gamma(=\hbar\sqrt{\frac{C_2}{B}})$, the inverse moment of inertia ϵ and the ratio a_2/β_0 of the static deformations. To these four parameters, we add the Lipas's parameter α_L [HoLi68], which corrects the incomplete description of the variation of the moment of inertia due to the restriction of the diagonalization space. The Lipas's parameter relates the excitation energies E_0, obtained by diagonalizing the model Hamiltonian, with the energies E which are to be compared with the data:

$$E = E_0/(1 + \alpha_L E_0). \tag{14.3.42}$$

The Lipas's parameter influences only the energies, but not the wave functions.

The transition probabilities can be readily obtained once we have determined the initial and final states as well as the transition operator. In Ref. [MFK97] a compact expression for the transition operator $m(E2, \mu)$ was obtained. This is given by:

$$
\begin{aligned}
m(E2, \mu) = \frac{3Z}{4\pi} R_0^2 \Bigg[& \mathcal{D}_{\mu 0}^2 \left(\beta_0 \left(1 + \frac{2}{7} \left(\frac{5}{\pi} \right)^{\frac{1}{2}} \beta_0 \right) \right) + \mathcal{D}_{\mu 0}^2 a_0' \left(1 + \frac{4}{7} \left(\frac{5}{\pi} \right)^{\frac{1}{2}} \beta_0 \right) \\
& + \mathcal{D}_{\mu 0}^2 \frac{2}{7} \left(\frac{5}{\pi} \right)^{\frac{1}{2}} (a_0'^2 - 2(a_2 + a_2')^2) \\
& + (\mathcal{D}_{\mu 2}^2 + \mathcal{D}_{\mu -2}^2) \left(\left(1 - \frac{4}{7} \left(\frac{5}{\pi} \right)^{\frac{1}{2}} \beta_0 \right) (a_2 + a_2') \right. \\
& \left. - \frac{4}{7} \left(\frac{5}{\pi} \right)^{\frac{1}{2}} a_0'(a_2 + a_2') \right) \Bigg]
\end{aligned}
\tag{14.3.43}
$$

We use standard notations for the nucleus charge (Ze), nuclear radius (R_0) and Wigner's functions ($\mathcal{D}_{MK}^2$). The transition operator depends on both the static and the dynamical deformations. It contains not only terms which are linear in a_0' and a_2' but also quadratic and constant terms. While the latter terms are caused by the deformation effects due to the expansion around the static values, the former terms reflect an anharmonic structure for the E2 transition.

For illustration purposes, the TRVM was applied for ^{126}Xe, ^{130}Ba and ^{228}Th which are considered to be of triaxial shape, and results were compared with those obtained in the framework of CSM. The fitted parameters characterizing the TRVM and CSM, respectively, are listed in Table 14.6.

Energies corresponding to these parameters are represented in Fig. 14.9 for ^{126}Xe and ^{130}Ba where, the experimental data and the results of the IBA (interacting boson approximation) are also given for comparison purposes. The results for the CSM have been already given in Chap. 6, Figs. 6.10–6.13. The predictions of the TRVM for ^{228}Th are also given in the last quoted figure. Results obtained with the CSM

Table 14.6 Parameters used by the TRVM (the first 5) and the CSM (the last 5) for ^{126}Xe, ^{130}Ba and ^{228}Th. Their significance is explained in the text

	^{126}Xe	^{130}Ba	^{228}Th
E_β (keV)	1,769	1,168	1,120
E_γ (keV)	1,314	1,179	645
ϵ (keV)	81.3	80.5	17.54
a_{20}/β_0	0.333	0.329	0.1585
α_L (keV^{-1})	10^{-4}	10^{-4}	10^{-4}
d	1.46	1.32	3.14
A_1 (keV)	14.325	15.783	17.731
A_2 (keV)	19.211	12.377	1.512
A_3 (keV)	14.411	-0.423	-7.021
q_2/q_0	-0.119	0.073	-0.071
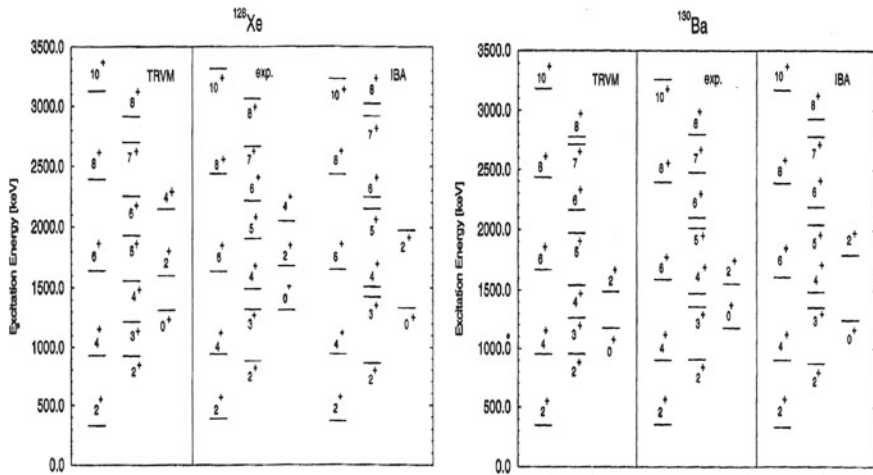
Fig. 14.9 The experimental (exp.), the TRVM and IBA predictions for the excitation energies in the ground, β and γ bands in ^{126}Xe and ^{130}Ba. Data are from Ref. [Kch]

and the TRVM for the β bands are collected in Table 14.7. The calculated B(E2) branching ratios are listed in Table 14.8. Considering the data in Tables 6.3 and 14.8 one can judge the quality of the agreement between the TRVM predictions and the corresponding experimental data. Note that the CSM accounts for non-axial properties by means of anharmonicities included. From the analysis presented in this section as well as in Chap. 6 for the three considered nuclei, one may conclude that the two formalisms, TRVM and CSM, yield similar agreement with the data concerning both the energies and the B(E2) values. In Fig. 14.9 one sees that the TRVM describes the experimental data better than IBA, although the two models use the same number of parameters.

Table 14.7 Experimental (first column) and predicted excitation energies (in units of keV) of the 0_2^+ band given by the TRVM (second column) and the CSM (third column)

	^{126}Xe			^{130}Ba			^{228}Th		
	Exp.	TRVM	CSM	Exp.	TRVM	CSM	Exp.	TRVM	CSM
0^+	1,314	1,314	1,314	1,179	1,179	1,179	1,120	1,120	1,120
2^+	1,679	1,600	1,670	1,557	1,490	1,523	1,176	1,173	1,170
4^+	2,042	2,150	2,254		2,053	2,017	1,290	1,292	1,283
6^+		2,758	3,025		2,644	2,635		1,468	1,454
8^+		2,917	3,968		3,196	3,365		1,690	1,679
10^+		3,518	5,074		3,947	4,200		1,946	1,949

Table 14.8 B(E2) branching ratios for ^{126}Xe , ^{130}Ba and ^{228}Th in the triaxial Rot-Vib Model (TRVM). Data were taken from Refs. [Kch, Btz96] and shown in Table 6.3

$I_i \to I_f$	^{126}Xe	$I_i \to I_f$	^{130}Ba	$I_i \to I_f$	^{228}Th
$2_2^+ \to 0_1^+$	8.7	$2_2^+ \to 0_1^+$	4.5	$2_3^+ \to 0_1^+$	54
2_1^+	100.0	2_1^+	100.0	2_1^+	100.0
				4_1^+	6.1
$3_1^+ \to 2_2^+$	100.0	$3_1^+ \to 2_2^+$	100.0	$3_1^+ \to 2_1^+$	100.0
4_1^+	24	4_1^+	16	4_1^+	62
2_1^+	4.4	2_1^+	2.6		
$4_2^+ \to 2_2^+$	100.0	$4_2^+ \to 2_2^+$	100.0	$4_4^+ \to 2_1^+$	15.1
4_1^+	66	4_1^+	57	4_1^+	100
2_1^+	1.5	2_1^+	2.75	6_1^+	8.84
$0_2^+ \to 2_2^+$	100.0	$0_2^+ \to 2_2^+$	100.0	$5_1^+ \to 4_1^+$	100.0
2_1^+	1.1	2_1^+	3.0	6_1^+	112
$2_3^+ \to 0_2^+$	100.0	$2_3^+ \to 0_2^+$	100.0	$2_5^+ \to 0_1^+$	65
2_2^+	0.8	2_2^+	0.04	2_1^+	100
4_1^+	0.04	4_1^+	0.11	4_1^+	267
2_1^+	0.01	2_1^+	0.06		
0_1^+	0.01	0_1^+	0.04		
3_1^+	20	3_1^+	18		
$5_1^+ \to 6_1^+$	43	$4_3^+ \to 2_2^+$	670	$4_5^+ \to 4_1^+$	100
4_2^+	83	3_1^+	214	6_1^+	362
3_1^+	100.0	4_2^+	100.0		
4_1^+	0.8	4_1^+	7.2		
$6_2^+ \to 6_1^+$	22	2_1^+	23.3		
4_2^+	100.0				
4_1^+	1.3				
$7_1^+ \to 6_2^+$	22				
5_1^+	100.0				

14.4 The Generalized Collective Model

As already mentioned, the liquid drop model has the merit of describing nuclei of spherical shape or well deformed but is fully unusable for the transitional cases, where specific properties like gamma soft, triaxial deformation, isomeric states show up. For example, even for near spherical nuclei the triplet $0^+, 2^+, 4^+$ is not degenerate. Therefore, the presence of anharmonic terms in the model Hamiltonian is necessary. How to choose anharmonicities such that the continuous emergence of rotational bands from the multi-phonon degenerate states be described? Moreover, due to the development of accelerator and detector devices a huge amount of data regarding states of high and very high spins are available.

The first anharmonic model was proposed by Gneuss and Greiner (GGM) [GMG69, GG71] which used a Hamiltonian of sixth order in the quadrupole coordinate, $\alpha_{2\mu}$, and second order in the conjugate momenta, $\pi_{2\mu}$, including a linear coupling with coordinates. The terms which do not depend on momenta define the potential energy. This is chosen as a polynomial in the invariants of second and third order in $\alpha_{2\mu}$. The Hamiltonian involves two mass and six stiffness parameters which are to be determined by minimizing the χ^2 associated to eight experimental data and corresponding theoretical values obtained either through diagonalization if the energies are concerned or by calculating the transition probabilities with the resulting wave functions. The most difficult step in applying this model is to write the matrix elements in the collective "mathematical" basis defined by Hecht [H65]. In the intrinsic frame the potential energy looks like:

$$V(\beta, \gamma) = C_2\beta^2 + C_3\beta^3 \cos(3\gamma) + C_4\beta^4$$
$$+ C_5\beta^5 \cos(3\gamma) + C_6\beta^6 \cos^2(3\gamma) + D_6\beta^6. \qquad (14.4.1)$$

Note that the invariance to the octaedral group requires the symmetry of $V(\beta, \gamma)$ to the transformation:

$$\gamma \to -\gamma, \quad \gamma \to \gamma + \frac{2\pi}{3}. \qquad (14.4.2)$$

Also, the rotational invariance implies that the potential and mass parameters do not depend on the Euler angles. Once the six stiffness and the two mass parameters are determined by fitting some data, the remaining of experimental information regarding energies and transition probabilities are predictions of the model. Moreover, the potential energy surface (PES) in the β and γ dynamic deformations can be represented as a contour plot. This way one may say that to the low lying spectrum and transitions connecting its members one associates a PES. Conversely, the shape and characteristics of the PES reflect some fundamental properties of nuclei. Is the number of parameters large enough to describe the principal collective properties of nuclei? For example, the properties of a minimum in the potential ($\beta - \gamma$ location, depth and the curvature in the β and γ direction) require 5 parameters. The sixth parameter may be used to calculate details about one ground-state minimum but in

order to describe two minima there is not enough freedom for fixing details. The GGM was however very useful in describing nuclei intermediate between spherical vibrator, deformed rotor and triaxial nuclei. The PES associated to the intermediate nuclei reflect the smooth evolution of the transitions between the limiting situations. What are the elements of nuclear structure which are directly connected with the PES? They are: minima are assigned to the ground state or isomeric state, stiffness determines vibrational excitation energies, while barriers hinder transitions, etc.

In contrast to some earlier calculations where the bands β and γ are not interacting and therefore the head states energies can be freely moved at the desired values, the GGM takes properly into account the $\beta - \gamma$ interaction in the γ soft potential bringing the γ band at a low lying energy and consequently one can assert, for example, that Os isotopes are asymmetric nuclei.

Another interesting result refers to oblate and prolate nuclei whose PES are mirror images with respect to the $\gamma = 30°$ axis. These nuclei have identical spectrum and in the first order in α, the same transition probabilities and mean square radii. Also, the quadrupole moments are equal in magnitude but of different sign.

For the PES exhibiting two minima, one could determine the membership of an energy level to one or another minimum by calculating either the quadrupole moments or the mean square radii, knowing the fact that for less deformed minimum these quantities are smaller. Thus, the PES for ^{112}Cd and ^{114}Cd suggest that close to the triplet $0^+, 2^+, 4^+$ which belongs to the spherical minimum, there are deformed states located in the second minimum. It is noteworthy that the GGM explains, by means of a PES with two minima, the striking experimental result for ^{72}Ge and ^{98}Mo saying that the first excited state is 0^+. For the said nuclei the zero point energy is quite high, which results in having even low lying excited states at energies larger than the height of the barrier separating the two minima. Their wave functions will be spread over both wells. These states of mixed symmetries cannot be organized in rotational bands.

Another category of nuclei considered in Ref. [GG71] is that of Te, Xe, and Ba. The corresponding PES indicate that they are asymmetric nuclei with some specific features: The excited state 0^+ is missing from the region of the vibrational triplet. Instead, the state 3^+ shows up. Another property reflected by the PES is the large softness in the γ direction which determines a small difference between the ground state minimum and the oblate minimum. Actually, the spectra associated to each of the mentioned nuclei are essentially influenced by the relative position of the two minima. An interesting result which is worth mentioning is that concerning the first excited band in ^{174}Hf. Indeed, this is not the β band, as expected, but the ground state band belonging to the oblate minimum. This is attested by the sign of the quadrupole moments of the ground state and β bands.

As for the kinetic energy parameters, they do not have a transparent physical meaning. However, the numerical analysis showed that the parameter of the harmonic term stretches or compresses the spectrum, depending on whether enlarged or diminished, but it does not change the sequence order. On the contrary, the anharmonic term changes the level ordering (only because of it one could obtain the state

2^+ belonging to the triplet on the first place) and even the bands order. Also, the convergence of the numerical procedure is sensitive to the variation of the anharmonic term.

It should be mentioned that there is no reason, except for simplicity, for choosing in the kinetic energy only quadratic terms in momenta. Why choose the kinetic energy in second order in momenta and the potential energy of sixth order? One may argue that classical mechanic requires such dependence. However, this contrasts the requirement that the Hamiltonian is invariant to the transformation which changes α with π and vice-versa. Also, it should be invariant to the canonical transformations which mix the coordinates with momenta. On the other hand if one uses a boson Hamiltonian involving anharmonicities, the associated Hamiltonian in coordinate and momenta would comprise terms quartic and sextic in momenta, which suggests that the GGM misses the effects produced by high anharmonicities in momenta.

The GGM was to some extent improved by other collaborators of Greiner, by extending its flexibility such that the description of states of very high spin is possible. The new version, called the generalized collective model (GCM) [HSMG80, HMG81], is based essentially on the same principles as the GGM but involving several technical new features: (i) The diagonalization basis is a physical one, labeled by the quantum numbers $|N v \alpha J M\rangle$, obtained analytically by three groups [CHMO76, CMW76, GRC78]. The model authors preferred the basis of Chacon and Moshinski since the matrix elements of the used Hamiltonian are obtainable in a convenient form for their codes. (ii) The kinetic energy has three terms (not two as in the GGM), two of them coupling momenta with coordinates. (iii) The potential energy generalizes the one used in the GGM including many additional terms:

$$V(\beta, \gamma) = \sum_{\rho, \mu} V_{\rho\mu} \beta^\rho (\cos 3\gamma)^\mu, \quad 2 \le \rho \le 6, \quad 0 \le \mu \le 4. \qquad (14.4.3)$$

Actually, not all of the expansion coefficients are used in practical applications. The ones employed in calculations correspond to the indices in the Table 14.9. (iv) Adding to the stiffness parameters, whose indices are listed in the Table 14.9, the three mass parameters, one obtains that the GCM uses 20 parameters, whereas the GGM involves only 8. In concrete applications, these parameters were fixed by fitting the data about some low lying energy levels, reduced E2 transition probabilities and quadrupole moments. (v) It is important to notice that while the potential $V(\beta, \gamma)$ of the GGM is obtained from a low order polynomial expansion in the second and third order invariants in the quadrupole coordinates, the GCM includes terms which do not correspond to monomials of the said invariants.

Table 14.9 The indices defining the stiffness parameters given in Eq. (14.4.3)

μ	0	1	2	3	4
ρ	2, 3, 4, 5, 6	2, 3, 4, 5	2, 3, 4, 6	2, 3	2, 3

This model has been successfully applied to the isotopic chains of Pt, Os and W and the specific features are interpreted in terms of the PES. For example the Pt isotopes show a transition from the γ soft, nearly triaxial nucleus $^{196}_{78}$Pt to the nearly γ-unstable nuclei $^{188}_{78}$Pt and $^{190}_{78}$Pt. $^{186}_{78}$Pt exhibits two minima, one at the prolate and one at the oblate axis. The same is observed for $^{184}_{76}$Os. Increasing the neutron number, the oblate minimum disappears while the prolate minimum develops to a γ-soft, nearly triaxial minimum in $^{192}_{76}$Os. Two minima are also noticed in the PES of $^{184}_{74}$W and $^{186}_{74}$W, but only one in $^{180}_{74}$Pt and $^{182}_{74}$Pt. Special attention must be paid to the last two isotopes where, because of few available data, the PES is not uniquely determined.

The said isotopes with two minima in the PES exhibits a backbending structure in the yrast band and this is due to the crossing of the lowest bands in the two minima. This picture is achieved by the "catch up" of the ground state band due to the bands in the second minimum lying on the oblate axis. It is worth mentioning that this backbending is different from that caused by crossing of the ground band with a two quasiparticle-core band. Indeed, for some Pt isotopes there are several states 10^+ and several 12^+ which are of two quasiparticle nature. Moreover, the first 12^+ is heading a $(\nu i_{13/2})^2$ qp band which can be explained only in the framework of a prticle-core coupling picture [RLF83].

The GCM was also applied to $^{238}_{92}$U, where energies in the ground band are known up to spin 30^+ and a few states in the side bands β and γ. Unfortunately, only very few data are known about the transition probabilities. This is the reason why for this case only 18 parameters were used. The existent data are fairly well explained. However, there are experimental suggestions of a secondary minimum at very high deformation on the prolate axis [UF79]. For such situation the model is inadequate. Indeed, for two minima corresponding to very different deformations, the model encounters difficulties concerning the states convergence. The convergence is very bad even when 30 phonons are included in the basis. This situation proves that the properties of very deformed nuclei cannot be described by using a basis of spherical bosons. This is the point where the CSM seems to be a better option for describing the deformed nuclei.

Since the GCM and GGM use in fact the same fundamental ingredients, the difference regarding only some technical details, the unified name of the two models as *the Gneus-Greiner model* is more appropriate.

14.4.1 Comparison with the CSM

The CSM and GGM are two phenomenological models which address similar issues. However, the followed paths are different and, because of their capacities to simulate the realm, the two models are not similar to a certain extent. First of all, the CSM uses a boson Hamiltonian while within the GGM the collective Hamiltonian depends in a specific way on coordinates and momenta. In this respect the CSM includes effects coming from the higher order terms in momenta. The essential difference between the

two formalisms consists in the bases used to treat the chosen Hamiltonian. For a given angular momentum, the CSM basis consists of angular momentum projected states (which, by construction, are orthogonal), from a coherent state and two orthogonal polynomial excitations of it. The criteria for selecting the unprojected states ensure a connection between the vibrational and rotational spectra according to the empirical rule of Sheline-Sakai [Sh60, Sa76]. The model Hamiltonian fulfills the invariance conditions (rotation, hermiticity, time reversal) and, moreover, is effective in the three dimensional basis, meaning that the β band is decoupled from the ground and γ bands. Although the projected states are eigenfunctions of the angular momentum squared and its projection on z-axis, they depend on a deformation parameter. This makes the basis suitable for treating the well deformed nuclei contrasting the GGM, which confronts with convergence difficulties when applied to very deformed nuclei. Both are recovering the traditional models, as the liquid drop, triaxial rotator, the model for gamma unstable nuclei, as limiting cases. Also, they describe the transition between these extreme pictures.

Another difference between the two models is that, while the GGM uses 20 parameters and a huge boson bases, the CSM has, in its simplified version, 4 parameters (and in the full version 6), and a three dimensional basis. Despite the reduced dimension, each basis member is an infinite series of bosons and, because of that, effects coming from the whole boson space are included. The situation looks as if a very complicated boson Hamiltonian was diagonalized in the whole boson space and then from the resulting eigenfunctions only those corresponding to the lowest three eigenvalues were depicted. Subsequently, an effective Hamiltonian is treated in the reduced collective space. In this respect, the CSM is easier to handle and its predictability power is larger than that of GGM. Concerning the PES structure, we have already compared the results of CSM for ^{190}Pt and ^{182}W with those of Kumar and Baranger model [KB68], which, to some extent, is the microscopic counterpart of the GGM (see Chap. 6), and the exactly solvable model called SMA (see the first section of this chapter), respectively. We concluded that the compared models are consistent with each other at least in what regards the corresponding PES.

14.5 Interacting Boson Approximation

One central issue of the many body theories is to project out a set of coordinates to be used for describing the collective properties of nuclei. This was actually the goal of the Interacting Boson Approximation (IBA) [AI76, ArIa76] which supposed that nucleons of the next closed major shell, if that is less of half filled or the nucleon holes for the shells which are more than half-filled, are pairwise coupled to angular momentum zero and two. The paired nucleons or holes are considered to behave like monopole (s) or quadrupole bosons ($d_\mu^\dagger$, with $-2 \leq \mu \leq 2$). Despite their boson character the total number of bosons is restricted to half of the total number of particles/holes in the next filled major shell. To give an example, consider the case of $^{152}_{64}$Gd$_{92}$. The next closed shell for protons (neutrons) is 50 (80) resulting in a total

of 14+12 valence nucleons. Therefore, this isotope possesses a total of 13 bosons. If we denote by n_s and n_d the number of bosons of type s and d, respectively, the restriction $n_s + n_d = N$ with N the total number of nucleons divided by 2 in the open shells must be fulfilled by any physical state yielded by diagonalizing a model Hamiltonian.

The boson components $\hat{s}$ and $\hat{d}_\mu$ with $-2 \leq \mu \leq 2$ define a 6 dimensional space. The unitary transformations acting on this space form a group called $U(6)$ whose generators are the 36 operators: $\hat{d}^\dagger_\mu \hat{d}_\nu$, $\hat{d}^\dagger_\mu \hat{s}$, $\hat{s}^\dagger \hat{d}_\mu$, $\hat{s}^\dagger \hat{s}$. For pragmatic reasons, it is more convenient to use instead the basis defined as angular momentum coupled products:

$$\left[\hat{s}^\dagger \times \hat{s}\right]^0, \quad \left[\hat{d}^\dagger \times \hat{s}\right]^2_\mu, \quad \left[\hat{s}^\dagger \times \hat{\tilde{d}}\right]^2_\mu, \quad \left[\hat{d}^\dagger \times \hat{\tilde{d}}\right]^0$$

$$\left[\hat{d}^\dagger \times \hat{\tilde{d}}\right]^1_\mu, \quad \left[\hat{d}^\dagger \times \hat{\tilde{d}}\right]^2_\mu, \quad \left[\hat{d}^\dagger \times \hat{\tilde{d}}\right]^3_\mu, \quad \left[\hat{d}^\dagger \times \hat{\tilde{d}}\right]^4_\mu. \qquad (14.5.1)$$

With the help of the 36 generators of the $U(6)$ group one builds the most general invariant, with respect to rotations, which is of fourth order in bosons. Considering now the restriction regarding the total number of bosons and recoupling the terms involved, the final expression of the Hamiltonian looks more transparent:

$$\hat{H} = \epsilon'' \hat{n}_d + a_0 \hat{P}^\dagger \hat{P} + a_1 \hat{L}^2 + a_2 \hat{Q}^2 + a_3 \hat{T}^2 + a_4 \hat{T}^2_4. \qquad (14.5.2)$$

Here the following tensors of rank 0, 1, ..., 4 are involved:

$$\hat{P} = \frac{1}{2} \left(\left[\hat{\tilde{d}} \times \hat{\tilde{d}}\right]^0 - \hat{s}\hat{s} \right),$$

$$\hat{T}_l = \left[\hat{d}^\dagger \times \hat{\tilde{d}}\right]^l, \quad l = 0, \ldots, 4,$$

$$\hat{L}_\mu = \sqrt{10}\,\hat{T}_{1\mu}, \quad \hat{Q}_{2\mu} = \left(\hat{d}^\dagger_\mu \hat{s} + \hat{s}^\dagger \hat{\tilde{d}}_\mu\right) - \frac{\sqrt{7}}{2}\hat{T}_{2\mu}. \qquad (14.5.3)$$

To find the eigenvalues of this Hamiltonian, one could diagonalize it in a certain basis defined by the Casimir operators of the intermediary groups of a certain reduction chain of the maximal symmetry group of H, that is $U(6)$. A piece of this chain should be $O(3) \supset O(2)$, in order to assure the presence, among the basis quantum numbers, of the angular momentum and its projection on z-axis. The groups of the chain are generated by subsets of operators (14.5.1) which form a closed Lie algebra. There are three possible chains obeying the said requirements:

$$\begin{aligned}
\mathbf{A}: \quad & U(6) \supset U(5) \supset O(5) \supset O(3) \supset O(2), \\
\mathbf{B}: \quad & U(6) \supset SU(3) \supset O(3) \supset O(2), \\
\mathbf{C}: \quad & U(6) \supset O(6) \supset O(5) \supset O(3) \supset O(2). \qquad (14.5.4)
\end{aligned}$$

The operators which generate the smaller groups are:

$$\mathbf{O(6)}: \quad \hat{L}_\mu, \quad \left[\hat{d}^\dagger \times \hat{\tilde{d}}\right]_\mu^3, \quad \left[\hat{d}^\dagger \times \hat{s}\right]_\mu^2 - \left[\hat{s}^\dagger \times \hat{\tilde{d}}\right]_\mu^2,$$

$$\mathbf{U(5)}: \quad \left[\hat{d}^\dagger \times \hat{\tilde{d}}\right]_M^L, \quad L = 0, 1, \ldots, 4,$$

$$\mathbf{O(5)}: \quad \left[\hat{d}^\dagger \times \hat{\tilde{d}}\right]_M^L, \quad L = 1, 3,$$

$$\mathbf{SU(3)}: \quad \hat{L}_\mu, \quad \hat{Q}_\mu,$$

$$\mathbf{O(3)}: \quad \left[\hat{d}^\dagger \times \hat{\tilde{d}}\right]_M^1, \quad \mathbf{O(2)}: \quad \left[\hat{d}^\dagger \times \hat{\tilde{d}}\right]_0^1, \tag{14.5.5}$$

The Casimir operators of the groups listed in (14.5.4) are given in Table 14.10. where the generators of $O(5)$ and $O(6)$ are:

$$\mathbf{O(5)}: \quad \hat{\Lambda}_{\mu\nu} = \hat{d}_\mu^\dagger \hat{\tilde{d}}_\nu - \hat{d}_\nu^\dagger \hat{\tilde{d}}_\mu,$$

$$\mathbf{O(6)}: \quad \hat{\tilde{\Lambda}}_{\mu,\nu} = \hat{\Lambda}_{\mu\nu}, \quad \hat{d}_\mu^\dagger \hat{s} - \hat{s}^\dagger \hat{\tilde{d}}_\nu. \tag{14.5.6}$$

Throughout this book we used the standard notation, $\hat{\tilde{b}}_\mu$, for the second rank tensor $(-)^\mu \hat{b}_{-\mu}$. With the above generators, one defines the Casimirs:

$$\hat{\tilde{\Lambda}}^2 = \frac{1}{2} \sum_{\mu\nu} \hat{\tilde{\Lambda}}_{\mu\nu} \hat{\tilde{\Lambda}}_{\mu\nu}^\dagger, \quad \hat{\Lambda}^2 = \frac{1}{2} \sum_{\mu\nu} \hat{\Lambda}_{\mu\nu} \hat{\Lambda}_{\mu\nu}^\dagger. \tag{14.5.7}$$

whose eigenvalues are $\bar{\lambda}(\bar{\lambda} + 4)$ and $\lambda(\lambda + 3)$. The quantum numbers $\bar{\lambda}$ and λ are called the generalized seniority and seniority, respectively. The basis defined by the three reduction chains is listed in Table 14.11. The quantum numbers belong to the intervals:

Table 14.10 The Casimir operators (CO) their eigenvalues (EIG) and corresponding quantum numbers (QN) for the groups involved in the chains (14.5.4)

Group	U(6)	O(6)	U(5)	O(5)	SU(3)	O(3)	O(2)
CO	$\hat{N}$	$\hat{\tilde{\Lambda}}^2$	$\hat{n}_d$	$\hat{\Lambda}^2$	$\hat{C}^2$	$\hat{L}^2$	$\hat{L}_z$
EIG	N	$\bar{\lambda}(\bar{\lambda}+4)$	n_d	$\lambda(\lambda+3)$	$l^2 + lm + m^2 + 3(l+m)$	L(L+1)	M
QN	N	$\bar{\lambda}$	n_d	λ	(l,m)	L	M

Table 14.11 The states labeled by the quantum numbers corresponding to the three group reduction chains

Reduction chain	A	B	C
Basis state	$|N n_d \lambda \tau L M\rangle$	$|N(l, m)KLM\rangle$	$|N \bar{\lambda} \lambda \tau L M\rangle$

$$\bar{\lambda} = N, N-2, N-4, \ldots, 1 \quad \text{or} \quad 0,$$
$$\lambda = \bar{\lambda}, \bar{\lambda}-1, \ldots, 0, \quad \text{or} \quad \lambda = n_d, n_d-2, n_d-4, \ldots, 1 \quad \text{or} \quad 0,$$
$$(l, m) = (2N, 0), (2N-4, 2), \ldots (2N-6, 0), (2N-10, 2), \ldots,$$
$$(2N-12, 0), (2N-16, 2), \ldots . \tag{14.5.8}$$

Since the steps from $O(5)$ to $O(3)$ and $SU(3)$ to $O(3)$ are not decomposable, i.e. there are several irreducible representations (irrep) of $O(3)$ which correspond to a single irrep of $O(5)$ and several irrep of $O(3)$ appear in the same irrep of $SU(3)$. To count the degenerate states from $O(5) \supset O(3)$ one uses a "missing" quantum number τ (which might be the number of d-boson triplet coupled to zero angular momentum) and *Elliot's quantum number*, K. For the chain **B**, K and L run as follows:

$$K = \min(l, m), \min(l, m) - 2, \ldots, 1 \quad \text{or} \quad 0$$
$$\text{For} \quad K = 0, \quad L = \max(l, m), \max(l, m) - 2, \ldots, 1 \quad \text{or} \quad 0,$$
$$\text{For} \quad K \neq 0, \quad L = K, K+1, K+2, \ldots, K + \max(l, m). \tag{14.5.9}$$

In order to solve the Schrödinger equation associated to (14.5.2) we have to expand its eigenstate in the basis defined by one of the above group reduction chains. This would be a numerical solution. Alternatively, we could impose some restrictions on the defining coefficients such that the resulting Hamiltonian is diagonal in a chosen basis. To this end we have to express the components of the initial Hamiltonian, those written in terms of the invariant monomials in the bosons $\hat{s}$ and $\hat{d}$, in terms of the Casimir operators discussed before. This is fully achievable and the final form would be close but not identical to the multipole expansion (14.5.2). In order to get a diagonal form for H one has to set all coefficients equal to zero except for those accompanying the Casimir operators associated to the chosen reduction chain. Thus, one obtains three Hamiltonians which have analytical eigenvalues:

$$\hat{H}_{IBA}^A = \epsilon \hat{n}_d + C_{n_d} \hat{n}_d^2 + C_\lambda \hat{\Lambda}^2 + C_L \hat{L}^2,$$
$$E_{n_d \lambda L}^A = \epsilon n_d + C_{n_d} n_d^2 + C_\lambda \lambda(\lambda+3) + C_L L(L+1),$$
$$\hat{H}_{IBA}^B = C_Q \hat{Q}^2 + C_L \hat{L}^2 = \frac{1}{2} C_Q \hat{C}^2 + \left(C_L - \frac{3}{8} C_Q\right) \hat{L}^2,$$
$$E_{lmL}^B = \frac{C_Q}{2} \left[l^2 + m^2 + lm + 3(l + m) \right] + \left(C_L - \frac{3C_Q}{8} \right) L(L+1),$$
$$\hat{H}_{IBA}^C = C_{\bar{\lambda}} \hat{\bar{\Lambda}}^2 + C_\lambda \hat{\Lambda}^2 + C_L \hat{L}^2 \,,$$
$$E_{\bar{\lambda}\lambda L}^C = C_{\bar{\lambda}} \bar{\lambda}(\bar{\lambda}+4) + C_\lambda \lambda(\lambda+3) + C_L L(L+1). \tag{14.5.10}$$

The spectrum defined by $E_{n_d \lambda L}^A$ is referred to as *the vibrational limit* since its leading term is identical with the harmonic term from the geometrical model the difference being that within *IBA*, $n_d \leq N$, whereas in the latter case the boson number might be

infinite. The set of energies E_{lmL}^{B} defines the *rotational limit* since it contains the rotor like term $L(L+1)$. Finally, the set $E_{\lambda\lambda L}^{C}$ is similar to that for γ-unstable nuclei in the geometrical model and for this reason is called *the γ-unstable limit*. The signature of this kind of nuclei is that the energy of 2_2^+ is lower than that of the state 0_2^+. If the Hamiltonian H_{IBA} can be projected onto one of those in (14.5.10), one says that it exhibits a *dynamical symmetry*. Note that none of the Hamiltonians mentioned above involves the O(2) Casimir, L_z, since that would break the rotational symmetry.

In order to calculate the reduced transition probabilities we need the expressions of transitions operators, $\hat{T}_{LM}^{i}$, with "i" taking the values E and M for electric and magnetic transitions, respectively. They are listed below:

$$\hat{T}_{2M}^{E} = \beta_2 \left(\left[\hat{d}^\dagger \times \hat{\tilde{s}} \right]_M^2 \right) + \gamma_2 \left[\hat{d}^\dagger \times \hat{\tilde{d}} \right]_M^2,$$

$$\hat{T}_{00}^{E} = \alpha_0 \left[\hat{s}^\dagger \times \hat{\tilde{s}} \right]^0, \quad \hat{T}_{4M}^{E} = \gamma_4 \left[\hat{d}^\dagger \times \hat{\tilde{d}} \right]_M^4,$$

$$\hat{T}_{1M}^{M} = \gamma_1 \left[\hat{d}^\dagger \times \hat{\tilde{d}} \right]_M^1, \quad \hat{T}_{3M}^{M} = \gamma_1 \left[\hat{d}^\dagger \times \hat{\tilde{d}} \right]_M^3, \tag{14.5.11}$$

Note that $\hat{T}_{1M}^{M}$ is proportional to the angular momentum and therefore is diagonal in any of the bases labeled by **A**, **B**, **C** respectively, and consequently it does not cause any transition. Therefore, the above expression must be supplemented by higher order terms of the form:

$$\left[\left[\hat{d}^\dagger \times \hat{\tilde{s}} \right]^2 \times \left[\hat{d}^\dagger \times \hat{\tilde{d}} \right]^1 \right]_M^1 \quad \text{or} \quad \left[\left[\hat{d}^\dagger \times \hat{\tilde{d}} \right]^2 \times \left[\hat{d}^\dagger \times \hat{\tilde{d}} \right]^1 \right]_M^1. \tag{14.5.12}$$

This model was successfully used to interpret the main collective properties in low lying spectra of large number of nuclei. Certainly, in order to broaden the scope, several extension have been proposed along the time. To distinguish the approach described before from its extensions people refer to it as IBA1.

In order to save space here we do not give details about the other versions and restrict ourself to enumerating them:

• **IBA2**: This formalism makes a distinction between the s and d bosons associated to protons and those of neutrons [Ar77]. The Hamiltonian is a sum of three terms, two associated to protons and neutrons respectively and one describing the interaction of the two components. The interaction contains the so-called Majorana interaction:

$$\hat{M} = \lambda\sqrt{5} \left[(\hat{s}_\nu^\dagger \hat{d}_\pi^\dagger - \hat{s}_\pi^\dagger \hat{d}_\nu^\dagger) \times (\hat{s}_\nu \hat{\tilde{d}}_\pi - \hat{s}_\pi \hat{\tilde{d}}_\nu) \right]^0$$

$$+ \sum_{L=1,3} \xi_L \sqrt{2L+1} \left[\left[\hat{d}_\nu^\dagger \times \hat{d}_\pi^\dagger \right]^L \times \left[\hat{\tilde{d}}_\nu \times \hat{\tilde{d}}_\pi \right]^L \right]^0. \tag{14.5.13}$$

Notice that this term involves three new parameters. This interaction has the property that pushes up the $p - n$ antisymmetric states and leaves the symmetric one unaffected. This feature is exploited in order to fit the energy of the scissors mode 1^+. In this respect, IBA2 cannot predict the energy of 1^+.

- **sdg-IBA**: This approach uses an additional boson comparing it with IBA1, that is the boson g carrying the angular momentum 4. Also, it relaxes the restriction for the total number of bosons N, which is considered now as a free parameter. This way the model can be applied also to high spin states.

- **sdf-IBA**: In this version of IBA, a new boson shows up, namely the boson f of angular momentum three. This makes applications to negative parity bands possible.

- **IBFM**: Is a core-plus particle model, with the core described by IBA1. The approach is meant to describe the even-odd nuclei.

Finally, we mention that IBA1 has a microscopic counterpart which was earlier formulated by Jolos and his collaborators [Jol74, Ja74, Jol75]. Indeed, a $SU(6)$ algebra is constructed microscopically by boson expanding the quadrupole two quasiparticle operators within a Holstein Primakoff formalism. The Lie algebra is closed by retaining in the commutators algebra only the collective quadrupole operators and neglecting the noncollective terms in the expansion. Thus, the quasiparticle operators $A_{2\mu}^\dagger$ and the quadrupole density operators $B_{2\mu}^\dagger$ are represented by 36 boson operators

$$b_{2\mu}^\dagger (N - \hat{N})^{1/2}, (N - \hat{N})^{1/2} b_{2\mu}, b_{2\mu}^\dagger b_{2\nu}, \tag{14.5.14}$$

where $b_2^\dagger$ is the collective quadrupole phonon operator, $\hat{N}$ the phonon number operator, while N is an expansion cut-off factor. Replacing the square root factors by the s bosons, one obtains the phenomenological $U(6)$ algebra used by IBA1. Implementing the above boson expansion terms in the starting microscopic Hamiltonian one obtains the Holstein-Primakoff boson representation of the initial many body fermionic Hamiltonian. This approach is called the truncated quadrupole-phonon model (TQPM). If the expansion coefficients are replaced with phenomenological parameters, the results obtained in all limiting symmetries ($SU(3)$, $SU(5)$, $O(5)$ ...) are the same in both models.

14.5.1 Comparison with the CSM

The CSM does not uses the boson $\hat{s}$. The Hamiltonian is defined in terms of quadrupole bosons and is effective in a restricted collective space projected over the angular momentum, from one coherent state and two polynomial excitations of it. The idea of effectiveness is common to both models. A two bosons coherent state can be written as linear combination of any of the bases **A**, **B**, **C** states, the result having the property that none of the components is missing. Due to this feature, the states used by the CSM generalizes the bases mentioned above.

Since the coherent state is a deformed function with a classical behavior and, moreover, an infinite series of bosons it is expected to be suitable for the description of deformed nuclei staying in a high spin state. This property contrasts IBA1 which uses a relatively small number of bosons due to the restriction concerning the total number and, consequently, it is not suitable for deformed nuclei and states of high spin. For example for ^{232}Th and ^{238}U where energies of states up to 32^+ in the ground, 20^+ in the β and 11^+ in the γ band are known, the CSM yields results impressively close to the data.

The property which mostly differentiates between the two approaches is that the CSM Hamiltonian does not commute with the boson number operator. The projected states are also combinations of components with different number of bosons. To cover the nuclei of different dynamic symmetries, the IBA1 uses a specific Hamiltonian while the CSM employs a sole Hamiltonian. The unifying feature of the CSM procedure is assured by the interaction of the bands ground and γ. Moreover, we have seen that even in the vibrational limit the states of the β band can be written as a specific excitation of the γ band. This is the reason why the transition between β and γ bands is stronger than between β and ground band. The latter aspect is shared also by IBA.

We have seen that CSM produces analytical expressions for both excitation energies and transition probabilities. For example, for the ratio characterizing the ground band in the asymptotic region one has:

$$\frac{B(E2; (J+2)^+ \to J^+)_g}{B(E2; J^+ \to (J-2)^+)_g} = \frac{(J+1)(J+2)(2J-1)(2J+1)}{J(J-1)(2J+3)(2J+5)}. \qquad (14.5.15)$$

Specializing this expression for $J = 2$ one obtains:

$$\frac{B(E2; 4^+ \to 2^+)_g}{B(E2; 2^+ \to 0^+)_g} = \frac{10}{7} \qquad (14.5.16)$$

This result coincides with that predicted by IBA1 in the limit $O(6)$ with $N \to \infty$. In this limit the IBA1 predicts [MtV79]:

$$\frac{B(E2; (J+2)_g^+ \to J_g^+)}{B(E2; 2_g^+ \to 0_g^+)} = \frac{5}{2}\frac{J+2}{J+5}, \quad \frac{B(E2; (J)_\gamma^+ \to J_g^+)}{B(E2; 2_g^+ \to 0_g^+)} = \frac{10(J+1)}{J+5}. \qquad (14.5.17)$$

The first equation considered for $J = 2$, indeed, leads to a ratio equal to 10/7.

It is interesting to specify the CSM predictions for the above ratios in the vibrational limit, having in mind that they do not depend on the nuclear deformation. Using the results of Chap. 6 for the vibrational limit one obtains:

$$\frac{B(E2; (J+2)_g^+ \to J_g^+)}{B(E2; 2_g^+ \to 0_g^+)} = \frac{J+2}{2}, \quad \frac{B(E2; (J)_\gamma^+ \to J_g^+)}{B(E2; 2_g^+ \to 0_g^+)} = 2(J+1). \qquad (14.5.18)$$

Comparing these results with the corresponding ones given by IBA1 one remarks a difference of a factor $5/(J + 5)$ in both cases.

It is worth mentioning that, in the regime of large deformation, the CSM results for transition probabilities agree with the Alaga's rule. On the other hand, the reduced transition probabilities predicted by IBA1 do not obey the said rule. This is explained by the fact that the restriction of the total number of bosons prevents reaching the asymptotic regime of deformation.

Concerning the extension called IBA2, this must be compared with the GCSM. We recall that GCSM describes in an unified fashion the bands of electric nature, such as the ground, β and γ bands, and the magnetic band built on the dipole scissors mode 1^+. The model contains the two rotors and two drops models as limiting cases. Moreover, it is one of the very few formalisms which predict analytic expressions of the M1 strength which depends quadratically on the nuclear deformation.

In its turn, the IBA2 introduces the Majorana interaction in order to get the right energy of the scissors state. Also, IBA2 does not predict the quadratic dependence of the M1 strength on the nuclear deformation.

The CSM has no correspondent version to the sdg-IBA. The reason is simple: due to the fact that the basis states are infinite series of bosons, there is no need for a boson g.

The CSM extension to pear-shaped nuclei corresponds to the sdf-IBA. In this context we recall that the CSM extension which includes the octupole degrees of freedom is able to describe simultaneously 8 rotational bands, four of positive and four of negative parity. Again, the description includes states of very high angular momentum. Moreover, signatures for static octupole deformations are pointed out not only in the ground but also in excited bands. On the other hand, the sdf-IBA is not describing the high spin states and due to this fact misses the states where the static octupole deformation is set on.

The extension to the even-odd nuclei called IBMF also has a correspondent within the CSM. The first application which coupled a CSM core to a system of particles interacting among themselves by pairing and surface delta forces, concerned some even-even isotopes of Pt, where the existence of several states 10^+ and 12^+ was described by the intersection of the ground collective band with a 2qp band of neutron type and 2qp of proton type. Later on, the formalism was extended to even odd nuclei where the 1qp-core and 3qp-core bands were studied.

Recently, a new extension for the even-odd nuclei was formulated [RRF14] where the description of the core includes the octupole degrees of freedom, while the single particle space contains two shells of positive parity and one of negative parity. As a result, six rotational bands were obtained, three of positive and three of negative parity.

As mentioned already several times, using the language of symmetries, the nuclei have been classified such that they are placed on the sides of a triangle having in the vertexes the symmetries of $SU(5)$, $SU(3)$ and $O(6)$. Later on, it was pointed out that even inside the triangle border, one may find some nuclei. The nuclei staying on a leg of triangle exhibit properties associated to the phase transition between the adjacent vortexes. Moreover, the critical points for these transitions are also characterized by

special symmetries, like $E(5)$, $X(5)$ (unknown yet), $Z(5)$ (unknown yet). In Chap. 6 we showed that the CSM is able to describe not only the nuclei corresponding to the said vertex symmetries but also the transitions between them including the critical nuclei.

As a general conclusion one may say that the IBA together with its extensions are able to account for the collective features of low lying states of moderate spin and nuclear deformation. Due to its simplicity, it became very popular especially among experimentalists who are extensively using the available codes to interpret their measurements.

On the other hand, the CSM is a complete boson approach which is based on a different philosophy from IBA and tries to get a general view upon the nuclear properties of states with spin ranging from low up to very high values and nuclei belonging to all three categories, spherical, deformed and transitional. Having the coherent state as principal ingredient, the model describes very well the classical properties of nuclei.

Chapter 15
Conclusions

15.1 Summary and Conclusions

Here we summarize by giving a unitary view of the material presented in the previous chapters. We start by presenting some arguments which may answer the question **Why use the coherent states?** Since the coherent state was first used by Glauber for a system of photons, a lot of progress has been made to extend the concept to other systems with various goals. The ground state properties of a many body system is often described by coherent state as in the BCS theory, the random phase approximation (RPA) or the time dependent Hartree-Fock (TDHF) formalisms. In general, the dequantization procedure defined by a time dependent variational equation is most reliable when the trial function is of a coherent type. Indeed, only in this case quantizing back the classical trajectories the resulting spectrum might be close to that associated with the initial many-body Hamiltonian. Such a treatment can be applied also to quadrupole boson Hamiltonians. Indeed, as we showed in this book, the classical trajectories of complicated boson Hamiltonians of fourth and sixth order in bosons can be analytically expressed. The corresponding periodic trajectories which surround closely the minima points as well as those of large amplitude could be quantized. The motion in a double well potential and the tunneling process through the potential barrier were also considered.

The over-complete property of a coherent state allows for accounting the dynamics causing the collective motion. Indeed, by expanding the coherent state in a Hilbert space basis, no expansion coefficient is missing. Due to this property, for a quadrupole boson Hamiltonian contributions in the whole boson space are included, which is not the case when a diagonalization procedure is adopted. The useful consequence of the said property is the role of the coherent state as generating function for a basis of states in the considered Hilbert space. Several bases have been generated by projection from a coherent state having either a phenomenological or a microscopic structure. In this context we mention the SU(5), the SU(1,1) boson basis and the O(5) basis projected out from a generalized BCS function. It is well known that the interaction of particles with the core breaks the rotational symmetry manifested in

the structure of the mean-field. This property is exploited by defining a projected spherical single particle basis.

Here we deal with quadrupole boson Hamiltonians and therefore we use an axially symmetric coherent state defined by the quadrupole boson, b_{20}^+ and b_{20}, and simple polynomial excitations of it. It is generally accepted that the nuclear system behaves more or less classically in a state of high angular momentum. This fact recommends the coherent states as an efficient tool for treating the high spin states. Indeed, it is well known that the coherent states minimize the Heisenberg uncertainty relations, which in fact reflects a classical character. However, the coherent state breaks several symmetries among which the most important are the rotational and the gauge ones. The question is whether restoring these symmetries, the classical properties are preserved or not. This feature is studied in chapter two for the mentioned symmetries and two pairs of conjugate coordinates: the quadrupole coordinate and its conjugate momentum and the boson number operator and the conjugate phase.

Studying a second order boson Hamiltonian within a time dependent variational formalism with a quadrupole coherent state as a trial function, and a constraint, the corresponding classical equation is exactly solvable, which results in having a closed formula for the ground band energies, which generalizes the result of Holmberg and Lipas. In the classical picture, the kinetic and potential energies are naturally separated. The potential is just the Davidson potential. Alternatively, the energy can be obtained with the angular momentum projected state, i.e. within an approach of variation after projection. An analytical formula for energies is obtained, which is similar to that resulting in a semi-classical treatment. The two very simple formulas have been applied to 44 nuclei covering regions characterized by different dynamic symmetries or, in other words, belonging to various known nuclear phases. In all cases one obtains very good agreement with the experimental data.

The coherent state description (CSM): Being encouraged by the results obtained for the ground band, we extended these ideas to three interacting bands, ground, beta and gamma. We started with an axially symmetric coherent state as a model state of the ground band in the intrinsic frame and two polynomial excitations of that, which are associated to the beta and gamma band. The excitations were chosen such that the three states are orthogonal before and after angular momentum projection. The three sets of projected states have very attractive properties: (1) they depend on a real parameter which simulates the nuclear deformation. (2) when the deformation is going to zero the functions for the ground band tend to the highest seniority states $|\frac{J}{2}\frac{J}{2}0JM\rangle$, while those for gamma and beta bands go to the second and third highest seniority states, respectively. When the deformation is large the projected wave functions are identical with those provided by the liquid drop model. Moreover, the continuous link between the two sets of wave functions, in vibrational and rotational limits, is the same as the correspondence established empirically by Sheline and Sakai. Within the restricted boson space of projected states we considered an effective boson Hamiltonian, which yields maximally decoupled bands. For a given J, the energies for beta band and gamma band states of odd angular momentum are taken to be the corresponding average values while the states of ground band and gamma band of even angular momenta are obtained by diagonalizing a 2×2 matrix. Energies

and quadrupole transition probabilities are given in an analytical form, which in the vibrational as well as rotational limits become very simple. This model is called the Coherent State Model (CSM) and was applied to a huge number of nuclei belonging to different symmetry regions. Salient features are analytically pointed out within both the laboratory and intrinsic frame.

Several Extension of CSM: The CSM was subject to several extensions:

(1) A particle-core Hamiltonian with the core described by the CSM was considered in particle-core space to describe the properties caused by the crossing of the ground, beta and gamma bands with a two quasiparticle-core band where the particle-like angular momentum is aligned to the collective one leading to several backbendings. The model was applied to the Pt region where several states 12^+ were seen. In a similar spirit we described the one and three quasiparticle bands in even odd nuclei.

(2) We attached to the quadrupole bosons an isospin quantum number distinguishing the proton-like from the neuron-like bosons. The formalism obtained following a similar path and arguments as for CSM was conventionally called the Generalized Coherent State Model (GCSM). This new approach describes simultaneously the major bands, ground, beta and gamma, and one band built on the top of the scissors state 1^+. We proved analytically that the GCSM predicts for the total M1 strength of exciting 1^+ from the ground state 0^+, a quadratic dependence on the nuclear deformation, which in fact confirms the collective character of the mode. Based on semi-classical calculations we derived an analytical expression for the gyromagnetic factor of neutrons which corrects the M1 transition operator towards improving the agreement with the data. The GCSM was the first approach extended to describe the scissors modes in the even-odd nuclei, predictions being later on confirmed by experiment.

(3) Recently, the GCSM Hamiltonian has been amended by a mean field, a pairing and a particle-core term consisting of a quadrupole-quadrupole and a spin-spin interaction. The collective magnetic dipole band is crossed by four two quasiparticle magnetic bands which have a chiral character. The chiral symmetry is broken by the spin-spin term in four distinct ways, which results in having four twin bands. I just mention that this is the first formalism which treats the twin bands in even-even nuclei.

(4) The CSM may be easily extended to the negative parity states if the unprojected state of ground band is replaced by a product function of two coherent states, one of quadrupole and one of octupole type. This way the unprojected ground state violates not only the rotational symmetry but also the space reflection symmetry. Therefore, in the laboratory frame we have to restore not only the rotational symmetry but also the parity. This way, instead of three bands described by the CSM we have three pairs of parity bands. The space was enlarged by adding two dipole parity partner bands. We kept the principles governing the CSM in constructing the generating functions for independent bands and the effective Hamiltonian. Thus, the extension provides a realistic description of eight rotational bands, four of positive and four of negative parity. The properties of these bands have been studied in several publications. Excitation energies of these bands as well as B(E2), B(E1) and B(E3) values have been described for a large number of nuclei.

(5) Adding an odd particle to the Hamiltonian used at (4), we extended the description to the odd nuclei. Here we describe realistically six rotational bands, three of positive and three of negative parity bands. One points out that one pair of parity partner bands exhibits a chiral symmetry.

Projected spherical single particle basis: Averaging a particle core-Hamiltonian with a coherent state one obtains a deformed mean field which resembles the Nilsson Hamiltonian. On the other hand averaging the particle-core Hamiltonian with the spherical single particle wave function one obtains a boson Hamiltonian which admits the axially deformed quadrupole coherent states as eigenfunctions. This suggests that projecting out the good angular momentum from the product function of a spherical shell model state and an axially deformed quadrupole coherent state might be an efficient basis to treat the particle core-Hamiltonian. From the projected states we succeeded to select a basis. This basis can be used to treat particle-like Hamiltonians. Indeed, when the matrix element of a particle-like operator is calculated, first the boson factors are orthogonalized leading to a factor depending on nuclear deformation. In particular, the average of the particle-core Hamiltonian with an element of the projected spherical basis gives a set of single particle energies whose deformation dependence is similar to that of Nilsson model states. Moreover, when the deformation is going to zero the single particle energies go to those of spherical shell model. Therefore, the defined basis has the nice property that it recovers the shell model basis in the vibrational limit, while the Nilsson model energies are obtained when the deformation goes apart from zero. This feature allows us to treat in an unified fashion the spherical and deformed nuclei. This was tested by describing the scissors-like modes and the rate of the $2\nu\beta\beta$ decay. A systematic analysis including 190 nuclei from all regions of the nuclides periodic table, is presented in a recent publication [RB14].

Comparison with other models: A special chapter is devoted to the comparison of our methods and some phenomenological models which are very popular in the field of nuclear structure. (a) The first model used for comparison with the CSM is a phenomenological solvable model. Starting from the Bohr-Mottelson Hamiltonian written in the intrinsic coordinates supplemented with a specific potential term, by expanding the rotational and potential terms in series of the variable γ around its static values, $0°$ and $30°$, we obtained a separable form for the differential equations associated to the dynamic deformation variables, which are fully solvable. Thus, the equation in γ is satisfied by the spheroidal or Mathieu functions, depending whether the static value of γ is $0°$ or $30°$. Regarding the β variable, the equations used are alternatively those for a sextic oscillator potential with a centrifugal barrier included, an infinite square well or a Davidson potential. Solutions were used to describe the ground, beta and gamma bands energies and E2 transition probabilities for axially deformed and triaxial nuclei, respectively. The differences and similarities with the CSM were discussed in detail. The other models to which we referred in this book comparing them with the CSM are: (b) The liquid drop model. We didn't devote special space to this model since we used it in many places along the book; (c) The projection method of Lipas and Haapakoski; (d) The deformed liquid drop the model

of Greiner and Faessler; (e) The model of Gneuss and Greiner; (f) The Interacting Boson Approximation proposed by Arima and Iachello.

The book covers the essential features of a large variety of nuclear structure properties of both collective and microscopic nature. Most of the results are given in an analytical form, giving a deep insight of the considered phenomena. The detailed comparison with all existent nuclear structure models provides the readers a proper framework and, at the same time, the perspective of new developments. The book is very useful for young as well as for experienced researchers. Due to its self-content exposure, the book can be successfully read and used also by undergraduate students.

Appendices

Appendix A: Useful Mathematics Information

A.1.1 Elements of Group Theory

We say that a set $\{g_i\}$ is a group if it obeys the following restrictions:

(1) There is a multiplication operation "." with respect to which the set is closed, i.e. if g_i and g_j are group elements, then $g_i.g_j$ also belongs to the group;
(2) Multiplication is an associative operation: $g_i.(g_j.g_k) = (g_i.g_j).g_k$;
(3) There is a unity element **1**, with the property that for any g_i we have: $\mathbf{1}.g_i = g_i.\mathbf{1} = g_i$;
(4) For any group element g_i there is another group element denoted as g_i^{-1} with the property that $g_i.g_i^{-1} = g_i^{-1}.g_i = \mathbf{1}$.

The groups are of several types. A discrete group has a finite number of elements. An example is the group of transformations which leave a cristal invariant. Operations of space inversion, charge conjugation and temporal inversion constitute a special class of discrete groups. The continuous group is a group which depends continuously on a set of parameters. The simplest example is the group of orthogonal transformations in a plane, O(2). Such transformations preserve the distance between two arbitrary points. If one rotates the plane with the angle θ then a point which before rotation had the coordinates (x, y) will have after rotation the coordinates (x', y') which are related to the old coordinates by:

$$\begin{pmatrix} x' \\ y' \end{pmatrix} = \begin{pmatrix} \cos\theta & \sin\theta \\ -\sin\theta & \cos\theta \end{pmatrix}\begin{pmatrix} x \\ y \end{pmatrix}. \tag{A.1}$$

Denoting by $x^1 = x$ and $x^2 = y$, this equation becomes:

$$x^{k\prime} = O^{ki}x^i. \tag{A.2}$$

For small angles the above equations lead to:

$$\delta x^i = \theta \epsilon^{ij} x^j, \tag{A.3}$$

where ϵ^{ij} is the 2×2 antisymmetric matrix with $\epsilon^{12} = 1$. It is simple to prove that $O^{ij}(\theta)$ form a group. The restriction that these transformations preserve distances leads to:

$$x'^i x'^i = x^j \left\{ O^{ij} O^{ik} \right\} x^k = x^i x^j. \tag{A.4}$$

Hence,

$$O^{ij} O^{ik} = \delta^{jk}, \text{ or } O^T \mathbf{1} O = \mathbf{1}. \tag{A.5}$$

The unity matrix is called the group metric. Due to the above relation the group $O(2)$ is *the orthogonal group in two dimensions*. Also, due to the said properties, $O(2)$ is also called the group of the real and orthogonal matrices 2×2. One can prove that any element of $O(2)$ may be written as:

$$O(\theta) = e^{\theta \tau}, \tag{A.6}$$

where τ is the matrix:

$$\tau = \begin{pmatrix} 0 & 1 \\ -1 & 0 \end{pmatrix} \tag{A.7}$$

Indeed, expanding the exponential in power series one obtains:

$$e^{\theta \tau} = \cos \theta \mathbf{1} + \tau \sin \theta = \begin{pmatrix} \cos \theta & \sin \theta \\ -\sin \theta & \cos \theta \end{pmatrix} \tag{A.8}$$

Note that all elements are parametrized with a sole angle. For this reason one says that $O(2)$ is a group with a single parameter, i.e. it has the dimension 1. The orthogonality condition provides the equation for the determinant of the group element:

$$det \left(O O^T \right) = det O det O^T = (det O)^2 = 1, \Rightarrow det O = \pm 1 \tag{A.9}$$

The elements of $O(2)$ characterized by $det O = +1$ form a group, called $SO(2)$. Elements for which $det O = -1$ can be obtained by multiplying an element of $SO(2)$ with the matrix:

$$P = \begin{pmatrix} 1 & 0 \\ 0 & -1 \end{pmatrix} \tag{A.10}$$

P describes the parity transformation:

$$x \to x, \quad y \to -y. \tag{A.11}$$

Note that $P^2 = 1$ and thus P is a discrete group. In general, a group is uniquely defined by the multiplication rule. For the bidimensional matrices this is:

$$O^{ij}(\theta) O^{jk}(\theta) = O^{ik}(\theta). \tag{A.12}$$

Any matrix $D(\theta)$ (not necessarily orthogonal or of dimension 2) which has the multiplication rule:

$$D(\theta)D(\theta') = D(\theta + \theta'); \quad D(\theta) = D(\theta + 2\pi) \qquad (A.13)$$

is a representation of $O(2)$ since has the same multiplication rule.

The angular momentum operator in two dimensions is defined as:

$$L \equiv i\epsilon^{ij}\frac{\partial}{\partial x^j} = i(x^1\partial^2 - x^2\partial^1). \qquad (A.14)$$

This operator is the generator of a rotation around an axis perpendicular on the plane (x^1, x^2). Then, the operator

$$U(\theta) = e^{i\theta L} \qquad (A.15)$$

describes a rotation in plane and therefore is an element of $SO(2)$.

It is instructive to see how the scalar and vectorial fields transform when the coordinate system is rotated by $U(\theta)$, defined above.

Let $\Phi(x)$ be a scalar field. Under the action of an element of $SO(2)$, the field transforms like:

$$U(\theta)\Phi(x)U^{-1}(\theta) = \Phi(x') \qquad (A.16)$$

This equation might be proved by using the expansion:

$$e^A B e^{-A} = B + [A, B] + \frac{1}{2!}[A, [A, B]] + \frac{1}{3!}[A, [A, [A, B]]] + \dots \qquad (A.17)$$

and then identifying the Taylor series of $\Phi(x')$ around the point x.

A vectorial field $\Phi^i(x)$ transforms, against the $SO(2)$ action, as follows:

$$U(\theta)\Phi^i(x)U^{-1}(\theta) = O^{ij}(-\theta)\Phi^j(x') \qquad (A.18)$$

A.1.2 Representations of SU(2) and U(1)

If g_i is an element of the group G, then $D(g_i)$ is called the group representation if satisfying equation:

$$D(g_i)D(g_j) = D(g_ig_j) \qquad (A.19)$$

for any group element. A representation is irreducible if it can be written in a block-diagonal form:

$$D(g_i) = \begin{pmatrix} D_1(g_i) & 0 & 0 \\ 0 & D_2(g_i) & 0 \\ 0 & 0 & D_3(g_i) \end{pmatrix} \qquad (A.20)$$

where D_i are group representations of lower dimension.

A method of generating higher representations for O(2) is the vectors multiplication. For example if A^i and A^j are vectors then their product transforms as:

$$\left(A^{i'}B^{j'}\right) = \left[O^{i'i}(\theta)O^{j'j}(\theta)\right]\left(A^iB^j\right). \tag{A.21}$$

The matrix $O^{i'i}(\theta)O^{j'j}(\theta)$ constitutes a representation of the group $SO(2)$ since it has the same multiplication rule as $O(2)$, and the space where they act is of dimension 2×2. We shall call tensor the set which transforms, under the action of the group $O(2)$, as a product of vectors. In general a tensor $T^{ijk\cdots}$ transforms under the action of the group $O(2)$ elements as the product of a row of vectors:

$$\left(T'\right)^{i_1i_2\cdots} = O^{i_1j_1}O^{i_2j_2}...T^{j_1j_2\cdots} \tag{A.22}$$

Notice that the transformation of $T^{ijk\cdots}$ is identical with the transformation of the vector product $x^ix^jx^k....$ This product is a representation of O(2) since the matrix

$$O^{i_1,i_2..i_N;j_1,j_2..j_N} \equiv O^{i_1j_1}(\theta)O^{i_2,j_2}(\theta)...O^{i_N,j_N}(\theta), \tag{A.23}$$

has the same multiplication rule as O(2). In general, the tensors obtained through vector multiplication form reducible tensors. Forming suitable combinations, symmetric or antisymmetric, one can extract irreducible tensors. A simple way of constructing irreducible tensors is to use the constant tensors: δ^{ij}, ϵ^{ij}. Indeed, one can check that such tensors obey the equation:

$$\begin{aligned}\delta^{i'j'} &= O^{i'i}O^{j'j}\delta^{ij}, \\ \epsilon^{i'j'} &= O^{i'i}O^{j'j}\epsilon^{ij}\end{aligned} \tag{A.24}$$

The first equation expresses the orthogonality property for the matrix O, while the second one defines the determinant of the matrix O which is 1 if it belongs to SO(2). From these equations it results that the tensor δ^{ij} is invariant. Since ϵ^{ij} transforms as a tensor only if the determinant of O is one, it is called pseudovector. If O is a space inversion operator then the l.h.s. of the above equation is written as:

$$\begin{pmatrix}1 & 0 \\ 0 & -1\end{pmatrix}\begin{pmatrix}0 & 1 \\ -1 & 0\end{pmatrix}\begin{pmatrix}1 & 0 \\ 0 & -1\end{pmatrix} = -\begin{pmatrix}0 & 1 \\ -1 & 0\end{pmatrix} \tag{A.25}$$

To conclude, the pseudotensor ϵ changes the sign under the space inversion considered above. These two tensors can be used to construct symmetric and antisymmetric scalar forms, by multiplying two vectors:

$$A^i\delta^{ij}B^j = A^iB^i, \quad A^i\epsilon^{ij}B^j = A^1B^2 - A^2B^1. \tag{A.26}$$

To form irreducible representations of higher order, the following relations are necessary:

$$\epsilon^{ij}\epsilon^{kl} = \delta^{ik}\delta^{jl} - \delta^{il}\delta^{jk}, \quad \epsilon^{ij}\epsilon^{jk} = -\delta^{ik}. \tag{A.27}$$

Let us consider now the complex number $u = a + ib$ and suppose it transforms like:

$$u' = U(\theta)u = e^{i\theta}u \tag{A.28}$$

Obviously, U is a unitary transformation:

$$U \times U^\dagger = 1 \tag{A.29}$$

The action of U upon the complex number u becomes more evident if one uses its polar form:

$$u' = U(\theta)\rho e^{i\alpha} = \rho e^{i(\theta+\alpha)}. \tag{A.30}$$

Therefore, this transformation preserves the norm of the complex number and shifts the angle with θ. $U(\theta)$ can be looked at as a unitary matrix of dimension 1. The set of these is a group denoted by $U(1)$. The multiplication rule is:

$$e^{i\theta}e^{i\theta'} = e^{i(\theta+\theta')} \tag{A.31}$$

similar to that for the group $O(2)$ although the space where the two groups act is different. Indeed, the space of $U(1)$ is the uni-dimentional space of the complex numbers. One says that the two groups are isomorphic to each other.

$$SO(2) \sim U(1). \tag{A.32}$$

In other words, there is a one to one correspondence of the elements of the two groups

$$e^{\theta\tau} \leftrightarrow e^{i\theta}. \tag{A.33}$$

To explain the correspondence between O(2) and U(1), we consider two scalar fields which transform under SO(2) transformations of small angle as:

$$\delta\Phi^i = \theta\epsilon^{ij}\Phi^j \tag{A.34}$$

Let us consider now the complex field:

$$\Phi = \frac{1}{\sqrt{2}}(\Phi^1 + i\Phi^2). \tag{A.35}$$

Variation of Φ under the action of $U(1)$ for small angles is:

$$\delta\Phi = -i\theta\Phi. \tag{A.36}$$

This equation can be directly obtained from A.35. The product $\Phi^*\Phi$ is invariant against $U(1)$. On the other hand, for $O(2)$ the combination $\frac{1}{2}\Phi^i\Phi^i$ is invariant. However, the relation

$$\frac{1}{2}\Phi^i\Phi^i = \Phi^*\Phi. \tag{A.37}$$

holds. Therefore the two groups are isomorphic and have the same invariants. An important property of $O(2)$ consists of that it is Abelian, i.e. their elements commute with each other.

A.1.3 Representations of the Groups SO(3) and SU(2)

The group $O(3)$ is a non-abelian group which leaves invariant the distance in a three dimensional space. Matrices having this property are of dimension 3×3 and orthogonal. The orthogonality conditions reduce the number of independent matrix elements from 9 to 3. Any element from $O(3)$ can be written as an exponential of an antisymmetric matrix:

$$O = \exp\left(i \sum_{k=1}^{3} \theta^k \tau^k \right). \tag{A.38}$$

where τ^k are matrices with imaginary elements. There are only three independent 3×3 matrices, thus just the number of independent degrees of freedom. In conclusion, $O(3)$ is a Lie group parametrized with three angles. The antisymmetric matrices mentioned above are

$$\tau^1 = \tau^x = -i \begin{pmatrix} 0 & 0 & 0 \\ 0 & 0 & 1 \\ 0 & -1 & 0 \end{pmatrix}, \quad \tau^2 = \tau^y = -i \begin{pmatrix} 0 & 0 & -1 \\ 0 & 0 & 0 \\ 1 & 0 & 0 \end{pmatrix},$$

$$\tau^3 = \tau^z = -i \begin{pmatrix} 0 & 1 & 0 \\ -1 & 0 & 0 \\ 0 & 0 & 0 \end{pmatrix}. \tag{A.39}$$

Note that the above matrices can be expressed by means of the completely antisymmetric tensor ϵ^{ijk}:

$$(\tau^i)^{jk} = -i\epsilon^{ijk}, \tag{A.40}$$

where $\epsilon^{123} = 1$. The antisymmetric matrices satisfy the following commutation relations:

$$\left[\tau^i, \tau^j \right] = i\epsilon^{ijk} \tau^k. \tag{A.41}$$

The matrices τ which satisfy the above commutation relations define the Lie algebra $SO(2)$. Notice that an element of the group is obtained by exponentiating an algebra element. The constants ϵ^{ijk} involved in the commutation relations are called the structure constants of the Lie algebra. It is clear that specifying the structure constants, one determines both the algebra and the associated group. For small angles, the coordinates are shifted with the quantities:

$$\delta x^i = \epsilon^{ijk} \theta^k x^j. \tag{A.42}$$

As we proceeded for the case of $SO(2)$ we introduce the operators:

$$L^i \equiv i\epsilon^{ijk} x^j \partial^k. \tag{A.43}$$

One can show that these operators satisfy the same commutation relations as the matrices τ^i, which are specific for the $SO(3)$ algebra. Let us consider the operator:

$$U(\theta^k) = e^{i\theta^k L^k}.\tag{A.44}$$

Under the action of such operator the scalar and vectorial fields transform as follows:

$$\begin{aligned}
U(\theta^k)\Phi(x)U^{-1}(\theta^k) &= \Phi(x'),\\
U(\theta^k)\Phi^i(x)U^{-1}(\theta^k) &= (O^{-1})^{ij}(\theta^k)\Phi^j(x').
\end{aligned}\tag{A.45}$$

The irreducible representations of the tensor fields of higher orders can be extracted by using the constant tensors δ^{ij} and ϵ^{ijk}. For concrete calculations the following relations are useful:

$$\begin{aligned}
\epsilon^{ijk}\epsilon^{lmn} &= \delta^{il}\delta^{jm}\delta^{kn} - \delta^{il}\delta^{jn}\delta^{km} + \delta^{im}\delta^{jn}\delta^{kl}\\
&\quad - \delta^{im}\delta^{jl}\delta^{kn} + \delta^{in}\delta^{jl}\delta^{km} - \delta^{in}\delta^{jm}\delta^{kl},\\
\epsilon^{ijk}\epsilon^{klm} &= \delta^{il}\delta^{jm} - \delta^{im}\delta^{jl}
\end{aligned}\tag{A.46}$$

As in the case of the $O(2)$ group, here one could also establish the connection with a special unitary group. To this end consider the set of matrices 2×2 which are unitary and of determinant equal to 1. The unitarity condition plus the condition of having the determinant equal to one, reduces the number of independent matrix elements to: $8 - 4 - 1 = 3$. Any unitary matrix can be written as an exponential of a hermitian matrix:

$$U = e^{iH}\tag{A.47}$$

Taking into account that the unitary and special matrices can be parametrized by three parameters, then it is convenient to choose as hermitian matrices, the Pauli matrices and to represent an arbitrary element of $SU(2)$ in the form:

$$U = e^{i\theta^k \sigma^k/2},\tag{A.48}$$

where:

$$\sigma^x = \begin{pmatrix} 0 & 1 \\ 1 & 0 \end{pmatrix}, \quad \sigma^y = \begin{pmatrix} 0 & -i \\ i & 0 \end{pmatrix}, \quad \sigma^z = \begin{pmatrix} 1 & 0 \\ 0 & -1 \end{pmatrix},\tag{A.49}$$

The matrices σ^i obey the commutation relations:

$$\left[\frac{\sigma^i}{2}, \frac{\sigma^j}{2}\right] = i\epsilon^{ijk}\frac{\sigma^k}{2}.\tag{A.50}$$

These commutation relations are identical with those characterizing the $SO(3)$ algebra. Due to this reason one says the following isomorphism holds:

$$SO(3) \sim SU(2).\tag{A.51}$$

To make this correspondence explicit we notice that:

$$e^{i\sigma^j\theta^j/2} = \cos(\theta/2) + i(\sigma^k n^k)\sin(\theta/2), \qquad (A.52)$$

where $\theta^i = n^i\theta$ and $(n^i)^2 = 1$. It results:

$$e^{i\tau^j\theta^j} \leftrightarrow e^{i\sigma^j\theta^j/2} \qquad (A.53)$$

where the l.h.s. is an orthogonal 3×3 matrix while the r.h.s. contains a unitary complex 2×2 matrix. We just mention that the isomorphism is local. In general, the correspondence is one to two and not one to one. Although the matrices from the two sides act in different spaces, they have the same multiplication rules. This fact allows us to establish a relation between the vectors (x, y, z) and the matrices mentioned before. To establish this relation we introduce the notation:

$$h(x) = \boldsymbol{\sigma} \cdot \mathbf{x} = \begin{pmatrix} z & x - iy \\ x + iy & -z \end{pmatrix}. \qquad (A.54)$$

Then the SU(2) transformation

$$h' = UhU^{-1}, \qquad (A.55)$$

is equivalent with the SO(3) transformation:

$$\mathbf{x}' = \mathbf{O} \cdot \mathbf{x}. \qquad (A.56)$$

A.1.4 Representations of the Group SO(N)

Generalization to $O(N)$ is straightforward. $O(N)$ is the group which leaves invariant the distance $\sqrt{(x^i)^2}$. These transformations are rotations defined as follows:

$$x'^i = O^{ij}x^j. \qquad (A.57)$$

Alternatively, one could say that the group $O(N)$ is the set of the real and orthogonal matrices of dimension $N \times N$. The number of independent matrix elements is obtained by subtracting from the total number, the number of restrictions due to the orthogonality conditions.

$$N^2 - \frac{1}{2}N(N + 1) = \frac{1}{2}N(N - 1). \qquad (A.58)$$

This is just the number of N-dimensional antisymmetric matrices which are linearly independent. Any element of $O(N)$ can be written as exponential of an antisymmetric

matrix $O = e^A$. Therefore, we could choose the following parametrization:

$$O = exp \left(i \sum_{k=1}^{N(N-1)/2} \theta^k \tau^k \right),$$ (A.59)

where τ^i are antisymmetric matrices, linearly independent with imaginary elements. These are called the group generators, while θ^i are rotation angles or the group parameters. Finding the irreducible representations of the group $O(N)$ is a complicated operation due to the complex structure of the commutator equations. The closing relation of the elements product is proved by using the factorization theorem of Baker-Campbell-Hausdorff:

$$e^A e^B = e^{A+B+(1/2)[A,B]+\dots}$$ (A.60)

where by the symbol "..." we understand the multiple commutators. As the commutator of two antisymmetric matrices is an antisymmetric matrix, it results that the exponent from the r.h.s. is an element of $O(N)$. The antisymmetric matrices algebra is characterized by the commutation relations:

$$[\tau^i, \tau^j] = i f^{ijk} \tau^k.$$ (A.61)

where f^{ijk} are the structure constants of the group. The structure constant can be determined for any N if the generators for $O(N)$ are chosen to be τ^i:

$$[\tau^i, \tau^j] = i f^{ijk} \tau^k.$$ (A.62)

The commutators for these matrices can be easily calculated:

$$[M^{ij}, M^{lm}] = i(-\delta^{il} M^{jm} + \delta^{jl} M^{im} + \delta^{im} M^{jl} - \delta^{mj} M^{il})$$ (A.63)

To define the action of any element from $O(N)$ upon fields we need the operators:

$$L^{ij} \equiv i(x^i \partial^j - x^j \partial^i).$$ (A.64)

It can be proved that these operators exhibit commutation relations specific to $SO(N)$. Consider now the operator:

$$U(\theta^{kj}) = e^{i\theta^{kj} L^{kj}},$$ (A.65)

where θ^{ij} is an antisymmetric matrix. The structure constants f^{ijk} could be looked at as forming a representation of the algebra. If one defines:

$$(\tau^i)^{jk} = f^{ijk},$$ (A.66)

then, this is a representation of the $O(N)$ generators. It also results that f^{ijk} is a constant tensor as δ^{ij} is. For small angles the field transforms according to:

$$\delta \Phi^i = i\theta^a (\tau^a)_{ij} \Phi^j.$$ (A.67)

We recall that before we discussed about the isomorphisms: $O(2) \sim U(1)$ and $O(3) \sim SU(2)$. One could show that the following isomorphisms hold:

$$SO(4) \sim SU(2) \otimes SU(2); \quad SO(6) \sim SU(4). \tag{A.68}$$

One should mention that there is no other isomorphism between $SO(N)$ and $SU(M)$ besides those mentioed before. This can be proved by considering the number of the independent elements for the groups to be compared.

A.1.5 Irreducible Representations of D_2

The group D_2 is a subgroup of the rotation group R_3, its elements being rotations of angle π around the axes 1, 2, 3, respectively. There are 4 distinct elements: R_π^1, R_π^2, R_π^3, E, with E denoting the unity element, i.e., the identical rotation.

The irreducible representations of a group can be identified with the help of *characters*. We call *character* a function defined on the group having complex values:

$$\chi : G \to C.$$

It is worth enumerating some useful properties:

(1) χ associated to equivalent representations are equal;
(2) the identical transformation corresponds to the unity element;
(3) $\chi(E) = f$ - the dimension of the representation;
(4) the number of distinct irreducible representations of the group is equal to the number of equivalence classes in the group.

$$\sum_G \chi^{(\alpha)}(G) \chi^{(\beta)*}(G) = g \delta_{\alpha\beta},$$

$$\sum_G |\chi^{(\alpha)}(G)|^2 = g \text{ - the group order.}$$

If $f_1, f_2, \cdots, f_r$ are the dimensions of the irreducible representations, we have:

$$|f_1|^2 + |f_2|^2 + \cdots + |f_r|^2 = g.$$

In the particular case of the Abelian groups $(r = g)$, all irreducible representations are of dimension 1: $f_1 = f_2 = \cdots = f_r = 1$.

Generally speaking, the dimensions of the irreducible representations are divisors of the order of the group. For D_2, all representations are unidimensional and moreover, $\chi(G) = \pm 1$ if $G \neq E$. Consequently, the characters for D_2 are those

Table A.1 The characters defining the irreducible representations for D_2

D_2	E	R^1_π	R^2_π	R^3_π
A	1	1	1	1
B_1	1	-1	-1	1
B_2	1	-1	1	-1
B_3	1	1	-1	-1

from the Table A.1. The angular momentum components involved in the rigid rotor Hamiltonian behaves against the action of the D_2 elements as follows:

$$R^j_\pi I_j R^{j+}_\pi = I_j,$$

$$R^j_\pi I_k R^{j+}_\pi = -I_k; k \neq j, \quad k, j = 1, 2, 3,$$

$$R^j_\pi H_R R^{j+}_\pi = H_R.$$

It results that H_R is invariant to the action of any element of D_2. Also, one can show that D_2 is a subgroup of the octahedral group. Indeed, preserving the meaning of the transformations T_k used in Chap. 4, we have:

$$R^2_\pi = T_1; \quad R^3_\pi = (T_2)^2; \quad R^1_\pi = R^3_\pi R^2_\pi = (T_2)^2 T_1; \quad E = (T_1)^2. \tag{A.69}$$

A.1.6 Tensorial Operators

A particular set of Euler angles defines the rotation relating the laboratory and intrinsic reference frames (Fig. A.1). A set of $2k + 1$ operators T^k_κ, with $\kappa = -k, -k+1, , ..., k-1, k$, which at a rotation of Euler angles $\Omega = \alpha, \beta, \gamma$, transforms according the rule:

$$R(\Omega) T^k_\kappa R^{-1}(\Omega) = \sum_\kappa D^k_{\kappa'\kappa}(\Omega) T^k_{\kappa'}, \tag{A.70}$$

defines a tensor operator of rank k. An equivalent definition due to Racah consists of the commutation relations with the spherical components of the angular momentum, $J_{\pm 1}, J_0$:

$$\left[J_\mu, T^k_\mu \right] = (-1)^\mu [k(k+1)]^{1/2} C^{k \ 1 \ k}_{\kappa \pm \mu, \mp \mu \ \kappa} T^k_{\kappa \pm \mu}, \quad \mu = 0, \pm 1. \tag{A.71}$$

One can check that the spherical components of the angular momentum form a tensor of rank 1. Also, the eigenfunctions of the orbital angular momentum, Y_{lm}, behave as a tensor of rank l and projection m. The m.e. of a tensor operator between eigenfunctions of the angular momentum squared and its projection on z-axix, satisfy the Wigner-Eckart theorem asserting that they can be written in a factorized
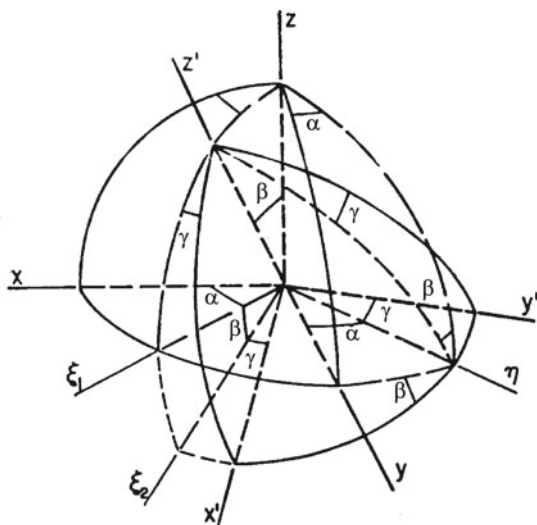
Fig. A.1 The Euler angles relating, by a rotation, the laboratory reference frame (x, y, z) and the intrinsic frame of coordinates (x', y', z'). ξ_1 and ξ_2 are intermediary axes between x and x' while η is an intermediary axis between y and y'

form, the entire angular momentum projections dependence being contained in a Clesch-Gordan coefficient. The other factor is conventionally called *the reduced matrix element*.

$$\langle j'm'|T_\kappa^k|jm\rangle = C_{m\ \kappa\ m'}^{j\ k\ j'}\langle j'||T^k||j\rangle. \tag{A.72}$$

Multiplying two tensors of ranks k_1 and k_2 respectively, one obtains a superposition of tensors of ranks k obeying $|k_1 - k_2| \le k \le k_1 + k_2$. Projecting a certain rank reads:

$$T_\kappa^k = \sum_{\kappa_1, \kappa_2} C_{\kappa_1\ \kappa_2\ \kappa}^{k_1\ k_2\ k} T_{\kappa_1}^{k_1} T_{\kappa_2}^{k_2}. \tag{A.73}$$

The scalar product of two operators of the same rank is by definition the product of rank 0.

$$\left[T^k(1)T^k(2)\right]_0^0 = \frac{1}{\hat{k}} \sum_\kappa (-1)^\kappa T_\kappa^k(1) T_{-\kappa}^k(2). \tag{A.74}$$

In concrete calculations it is useful to know the explicit expressions of the reduced matrix elements. Here are some examples:

$$\langle j'||J||j\rangle = [j(j+1)]^{1/2}\,\delta_{jj'},$$

$$\langle l_f||Y^l||l_i\rangle = \frac{1}{\sqrt{4\pi}}\frac{\hat{l}_i\hat{l}}{\hat{l}_f}C_{0\ 0\ 0}^{l_i\ l\ l_f},$$

$$\langle \tfrac{1}{2} lj \| Y^k(\Omega) \| \tfrac{1}{2} l'j' \rangle = (-1)^{j-j'} \sqrt{\frac{2k+1}{4\pi}} C^{j\ k\ j'}_{\frac{1}{2}\ 0\ \frac{1}{2}} \Big[1 + (-1)^{l+k+l'} \Big],$$

$$\langle j_1' j_2' j \| \big[T^k(1) T^k(2) \big]^0 \| j_1 j_2 j \rangle = \frac{\hat{j}_1' \hat{j}_2'}{\hat{k}} (-1)^{j_1' + j_2' - j} W(j_1 j_2 j_1' j_2'; jk)$$

$$\times \langle j_1' \| T^k(1) \| j_1 \rangle \langle j_2' \| T^k(2) \| j_2 \rangle. \qquad (A.75)$$

In the last equation, $W(a\ b\ c\ d; e\ f)$ stands for the Racah coefficient.

A.1.7 Matrix Representation of Rotations

The rotation of Euler angle $\Omega = (\alpha, \beta, \gamma)$ is defined by:

$$R(\Omega) = e^{-i\gamma J_{z'}} e^{-i\beta J_\eta} e^{-i\alpha J_z} = e^{-i\alpha J_z} e^{-i\beta J_y} e^{-i\gamma J_z}. \qquad (A.76)$$

The matrix elements of the rotation operator between two eigenfunctions of J^2 and J_z are known under the name of *Wigner functions*:

$$D^j_{m'm}(\Omega) = \langle jm' | R(\Omega) | jm \rangle. \qquad (A.77)$$

The action of a rotation operator on an eigenfunction of J^2 and J_z reads:

$$R(\Omega) | jm \rangle = \sum_{m'} D^j_{m'm}(\Omega) | jm' \rangle. \qquad (A.78)$$

The dependence on the three Euler angles is factorized as:

$$D^j_{m'm}(\Omega) = e^{-im'\alpha} d^j_{m'm}(\beta) e^{-im\gamma}. \qquad (A.79)$$

The reduced matrix $d^j_{m'm}(\beta)$ has the expression:

$$d^j_{m'm}(\beta) = \big[(j+m)!(j-m)!(j+m')!(j-m')! \big]^{1/2}$$

$$\times \sum_{\kappa} (-1)^\kappa \big[(j-m'-\kappa)!(j+m-\kappa)!(\kappa+m-m')!\kappa! \big]^{-1}$$

$$\times [\cos(\beta/2)]^{2j+m-m'-2\kappa} [-\sin(\beta/2)]^{m'-m+2\kappa}. \qquad (A.80)$$

The Wigner functions satisfy the relations:

$$\int d\Omega D^{j_1 *}_{\mu_1 m_1}(\Omega) D^{j_2}_{\mu_2 m_2}(\Omega) = \frac{8\pi^2}{2j_1 + 1} \delta_{j_1 j_2} \delta_{\mu_1 \mu_2} \delta_{m_1 m_2}. \qquad (A.81)$$

For the reduced matrix, the orthonormalization relation holds only for j:

$$\int\limits_0^\pi d_{\mu m}^j(\beta) d_{\mu m}^{j'}(\beta) \sin\beta d\beta = \frac{2}{2j+1}\delta_{jj'}. \qquad (A.82)$$

The harmonic functions and Legendre polynomials are particular cases of the rotation matrix:

$$D_{m0}^l(\alpha,\beta,0) = \sqrt{\frac{4\pi}{2l+1}} Y_{lm}^*(\beta,\alpha),$$

$$D_{00}^l(0,\beta,0) = P_l(\cos\beta). \qquad (A.83)$$

The reduced matrix satisfies the following symmetry relations:

$$d_{mm'}^{j*}(\beta) = d_{mm'}^j(\beta),$$

$$d_{m'm}^j(-\beta) = d_{mm'}^j(\beta),$$

$$d_{m'm}^j(-\beta) = (-1)^{m'-m} d_{m'm}^j(\beta),$$

$$d_{m'm}^j(\beta) = (-1)^{m'-m} d_{mm'}^j(\beta),$$

$$d_{m'm}^j(\beta) = d_{-m,-m'}^j(\beta),$$

$$d_{m'm}^j(\beta) = (-1)^{m'-m} d_{-m',-m}^j(\beta),$$

$$\frac{1}{2}\sum_j (2j+1) d_{m\mu}^j(\beta) d_{m\mu}^j(\beta) = \delta(\cos\beta - \cos\beta'). \qquad (A.84)$$

The symmetry relations of the Wigner functions which are frequently met are:

$$D_{m'm}^j(-\gamma,-\beta,-\alpha) = D_{mm'}^{j*}(\alpha,\beta,\gamma),$$

$$D_{m'm}^{j*}(\alpha,\beta,\gamma) = (-1)^{m'-m} D_{-m',-m}^j(\alpha,\beta,\gamma),$$

$$\sum_m D_{m'm}^{j*}(\Omega) D_{m''m}^j(\Omega) = \delta_{m',m''},$$

$$\sum_m D_{mm'}^{j*}(\Omega) D_{mm''}^j(\Omega) = \delta_{m',m''}. \qquad (A.85)$$

The product of two rotation matrices can be written as a linear combination of rotation matrices:

$$D_{\mu_1 m_1}^{j_1}(\Omega) D_{\mu_2 m_2}^{j_2}(\Omega) = \sum_j C_{\mu_1\ \mu_2\ \mu_1+\mu_2}^{j_1\ j_2\ j} C_{m_1\ m_2\ m_1+m_2}^{j_1\ j_2\ j} D_{\mu_1+\mu_2,m_1+m_2}^j(\Omega). \qquad (A.86)$$

This equation may be reversed with the result:

$$D^j_{\mu m}(\Omega) = \sum_{\mu_1 m_1} C^{j_1\,j_2\,j}_{\mu_1\mu-\mu_1\mu} C^{j_1\,j_2\,j}_{m_1 m-m_1 m} D^{j_1}_{\mu_1 m_1}(\Omega) D^{j_2}_{\mu-\mu_1 m-m_1}(\Omega). \qquad \text{(A.87)}$$

A.1.8 Angular Momenta Addition

Consider two independent subsystems characterized by angular momenta $\mathbf{J}_1$ and $\mathbf{J}_2$, respectively. The state of the whole system is described by the wave function:

$$|j_1 j_2 m_1 m_2\rangle = |j_1 m_1\rangle |j_2 m_2\rangle, \qquad \text{(A.88)}$$

where $|j_k m_k\rangle$ are eigenfunctions for J_k^2 and $J_{k,z}$, with $k = 1, 2$. The set of functions just defined is complete in the space describing the system with two components. Consider the total angular momentum:

$$\mathbf{J} = \mathbf{J}_1 + \mathbf{J}_2. \qquad \text{(A.89)}$$

Another set of operators which can define a complete set of functions is formed of J_1^2, J_2^2, J^2, J_z. The common eigenfunctions of these operators are: $|(j_1 j_2) jm\rangle$. Any function from this set can be written in an unique manner in the complete basis defined by Eq. (A.88).

$$\begin{aligned}
|(j_1 j_2) jm\rangle &= \sum_{m_1, m_2} \langle j_1 j_2 m_1 m_2 | (j_1 j_2) jm\rangle |j_1 j_2 m_1 m_2\rangle \\
&= \sum_{m_1, m_2} \langle j_1 j_2 m_1 m_2 | (j_1 j_2) jm\rangle |j_1 m_1\rangle |j_2 m_2\rangle. \qquad \text{(A.90)}
\end{aligned}$$

The coefficients of this expansion are called *the Clebsch-Gordan coefficients*. In the literature several notations are used. In this book the following notation was used:

$$C^{j_1\,j_2\,j}_{m_1\,m_2\,m} = \langle j_1 j_2 m_1 m_2 | (j_1 j_2) jm\rangle. \qquad \text{(A.91)}$$

In what follows we shall enumerate the properties of the Clebsch-Gordan coefficients:

(1) The matrix $\langle j_1 j_2 m_1 m_2 | (j_1 j_2) jm\rangle$ is unitary. Consequently the equation:

$$|(j_1 j_2) jm\rangle = \sum_{m_1, m_2} C^{j_1\,j_2\,j}_{m_1\,m_2\,m} |j_1 m_1\rangle |j_2 m_2\rangle, \qquad \text{(A.92)}$$

can be reversed:

$$|j_1 m_1\rangle |j_2 m_2\rangle = \sum_{j} C^{j_1\,j_2\,j}_{m_1\,m_2\,m} |(j_1 j_2) jm\rangle. \qquad \text{(A.93)}$$

(2) $C^{j_1\ j_2\ j}_{m_1\ m_2\ m} = 0$, if $m_1 + m_2 \neq m$. The coefficiet is vanishing if the involved agular momenta do not obey the triangle rule: $|j_1 - j_2| \leq j \leq (j_1 + j_2)$.

(3) Racah obtained an analytical expression for the Clebsch-Gordan coefficient:

$$C^{j_1\ j_2\ j}_{m_1\ m_2\ m} = \delta_{m_1+m_2,m} \left[\frac{(2j+1)(j_1+j_2-j)!(j_1-j_2+j)!(-j_1+j_2+j)!}{(j_1+j_2+j+1)!} \right]^{1/2}$$

$$\times \left[(j_1+m_1)!(j_1-m_1)!(j_2+m_2)!((j_2-m_2)!(j+m)!(j-m)! \right]^{1/2}$$

$$\times \sum_z (-1)^z \left[z!(j_1+j_2-j-z)!(j_1-m_1-z)!(j_2+m_2-z)! \right.$$

$$\times \left. (j-j_2+m_1+z)!(j-j_1-m_2+z)! \right]^{-1} . \tag{A.94}$$

(4) The orthogonality relations are::

$$\sum_{m_1,m_2} C^{j_1\ j_2\ j}_{m_1\ m_2\ m} C^{j_1\ j_2\ j'}_{m_1\ m_2\ m'} = \delta_{jj'}\delta_{mm'},$$

$$\sum_{j,m} C^{j_1\ j_2\ j}_{m_1\ m_2\ m} C^{j_1\ j_2\ j}_{m'_1\ m'_2\ m} = \delta_{m_1 m'_1}\delta_{m_2 m'_2}. \tag{A.95}$$

(5) Symmetry relations:

$$C^{j_1\ j_2\ j_3}_{m_1\ m_2\ m_3} = (-1)^{j_1+j_2-j_3} C^{j_1\ j_2\ j_3}_{-m_1,\ -m_2,\ -m_3}$$

$$= (-1)^{j_1+j_2-j_3} C^{j_2\ j_1\ j_3}_{m_2\ m_1\ m_3}$$

$$= (-1)^{j_1-m_1} \frac{\hat{j}_3}{\hat{j}_2} C^{j_1\ j_3\ j_2}_{m_1,\ -m_3,\ -m_2}$$

$$= (-1)^{j_2+m_2} \frac{\hat{j}_3}{\hat{j}_1} C^{j_3\ j_2\ j_1}_{-m_3,\ m_2,\ -m_1}, \quad \text{where } \hat{j} = \sqrt{2j+1}. \tag{A.96}$$

(6) Particular cases:

$$C^{j_1\ j_2\ j_3}_{0\ 0\ 0} = (-1)^{j+j_3} \left[\frac{(2j_3+1)(j_1+j_2-j_3)!(j_1+j_3-j_2)!(j_2+j_3-j_1)!}{(j_1+j_2+j_3+1)!} \right]^{1/2}$$

$$\times \frac{j!}{(j-j_1)!(j-j_2)!(j-j_3)!}. \tag{A.97}$$

Here we used the notation $j_1 + j_2 + j_3 = 2j$. If $j_1 + j_2 + j_3 = odd$, the coefficient is equal to zero.

$$C^{j_1 \ j_2 \ j_1+j_2}_{j_1 \ j_2 \ j_1+j_2} = 1,$$

$$C^{j_1 \ j_2 \ j_3}_{0 \ 0 \ 0} = 0, \text{ if } j_1 + j_2 + j_3 = \text{odd},$$

$$C^{j_1 \ 0 \ j_3}_{m_1 \ 0 \ m_3} = \delta_{j_1 j_3} \delta_{m_1 m_2}. \tag{A.98}$$

(7) Coefficients with small quantum numbers. Let us consider an electron with the orbital angular momentum equal to $1\hbar$. The total angular momentum might be any of j satisfying inequalities: $\frac{1}{2} \leq j \leq \frac{3}{2}$.

$$|jm\rangle = \sum_{m_l, \sigma} C^{1 \ \frac{1}{2} \ j}_{m_1 \ \sigma \ m} Y_{1m_1} \chi_{\frac{1}{2}\sigma}. \tag{A.99}$$

Clebsch-Gordan coefficients have simple expressions, the wave functions having the final form:

$$\psi_{\frac{1}{2}\frac{1}{2}} = -\sqrt{\frac{1}{3}} Y_{10}\chi_{\frac{1}{2}\frac{1}{2}} + \sqrt{\frac{2}{3}} Y_{11}\chi_{\frac{1}{2}-\frac{1}{2}},$$

$$\psi_{\frac{1}{2}-\frac{1}{2}} = -\sqrt{\frac{2}{3}} Y_{1-1}\chi_{\frac{1}{2}\frac{1}{2}} + \sqrt{\frac{1}{3}} Y_{10}\chi_{\frac{1}{2}-\frac{1}{2}},$$

$$\psi_{\frac{3}{2}\frac{3}{2}} = Y_{11}\chi_{\frac{1}{2}\frac{1}{2}},$$

$$\psi_{\frac{3}{2}\frac{1}{2}} = \sqrt{\frac{2}{3}} Y_{10}\chi_{\frac{1}{2}\frac{1}{2}} + \sqrt{\frac{1}{3}} Y_{11}\chi_{\frac{1}{2}-\frac{1}{2}},$$

$$\psi_{\frac{3}{2}-\frac{1}{2}} = -\sqrt{\frac{1}{3}} Y_{1-1}\chi_{\frac{1}{2}\frac{1}{2}} + \sqrt{\frac{2}{3}} Y_{10}\chi_{\frac{1}{2}-\frac{1}{2}},$$

$$\psi_{\frac{3}{2}-\frac{3}{2}} = Y_{1-1}\chi_{\frac{1}{2}-\frac{1}{2}}. \tag{A.100}$$

The coefficients for the wave function of angular momentum equal to 1 are given in Table A.2.

Consider now three angular momenta $\mathbf{j}_1, \mathbf{j}_2, \mathbf{j}_3$. Coupling them succesively, one can achieve a state of total angular momentum $\mathbf{j}$ in two distict ways:

$$\mathbf{j}_1 + \mathbf{j}_2 = \mathbf{j}_{12}, \quad \mathbf{j}_{12} + \mathbf{j}_3 = \mathbf{j},$$

$$\mathbf{j}_2 + \mathbf{j}_3 = \mathbf{j}_{23}, \quad \mathbf{j}_1 + \mathbf{j}_{23} = \mathbf{j}. \tag{A.101}$$

Table A.2 Expressions for $C^{\frac{1}{2} \ l \ j}_{m_s \ m_l \ m}$

	$m_s = \frac{1}{2}$	$m_s = -\frac{1}{2}$
$j = l + \frac{1}{2}$	$\sqrt{\frac{l+m+\frac{1}{2}}{2l+1}}$	$\sqrt{\frac{l-m+\frac{1}{2}}{2l+1}}$
$j = l - \frac{1}{2}$	$\sqrt{\frac{l-m+\frac{1}{2}}{2l+1}}$	$-\sqrt{\frac{l+m+\frac{1}{2}}{2l+1}}$

The state obtained with the first coupling scheme is:

$$|(j_1 j_2) j_{12} m_{12}\rangle = \sum_{m_1,m_2} C^{j_1\ j_2\ j_{12}}_{m_1\ m_2\ m_{12}} |j_1 m_1\rangle |j_2 m_2\rangle. \tag{A.102}$$

$$|[(j_1 j_2) j_{12}, j_3)] jm\rangle = \sum_{m_{12},m_3} C^{j_{12}\ j_3\ j}_{m_{12}m_3\ m} |(j_1 j_2) j_{12} m_{12}\rangle |j_3 m_3\rangle$$

$$= \sum_{\substack{m_1,m_2 \\ m_3,m_{12}}} C^{j_1\ j_2\ j_{12}}_{m_1\ m_2\ m_{12}} C^{j_{12}\ j_3\ j}_{m_{12}\ m_3\ m} |j_1 m_1\rangle |j_2 m_2\rangle |j_3 m_3\rangle. \tag{A.103}$$

Similarly, following the second coupling scheme the final state reads:

$$|[j_1, (j_2 j_3) j_{23}] jm\rangle = \sum_{\substack{m_1,m_2, \\ m_3,m_{23}}} C^{j_2\ j_3\ j_{23}}_{m_2\ m_3\ m_{23}} C^{j_1\ j_{23}\ j}_{m_1\ m_{23}\ m} |j_1 m_1\rangle |j_2 m_2\rangle |j_3 m_3\rangle. \tag{A.104}$$

The functions (A.102) and (A.104) represent two distinct bases connected by a unitary transformation:

$$|[(j_1 j_2) j_{12}, j_3)] jm\rangle = \sum_{j_{23}} \langle [j_1, (j_2 j_3) j_{23}] j | [(j_1 j_2) j_{12}, j_3] j\rangle | [j_1, (j_2 j_3) j_{23}] jm\rangle. \tag{A.105}$$

Further, the transformation coefficients can be written in the form:

$$\langle [j_1, (j_2 j_3) j_{23}] j | [(j_1 j_2) j_{12}, j_3] j\rangle = \hat{j}_{12} \hat{j}_{23} W(j_1 j_2 j j_3; j_{12} j_{23}), \tag{A.106}$$

where the factor $W(j_1 j_2 j j_3; j_{12} j_{23})$ is called *the Racah coefficient*. This can be expressed as a linear combination of products of four Clebsch-Gordan coefficients:

$$W(j_1 j_2 j j_3; j_{12} j_{23}) = \sum_{\substack{m_1,m_2,m_3, \\ m_{12},m_{23}}} C^{j_1\ j_2\ j_{12}}_{m_1\ m_2\ m_{12}} C^{j_{12}\ j_3\ j}_{m_{12}\ m_3\ m} C^{j_2\ j_3\ j_{23}}_{m_2\ m_3\ m_{23}} C^{j_1\ j_{23}\ j}_{m_1\ m_{23}\ m}$$

$$\times \frac{1}{\hat{j}_{12} \hat{j}_{23}}. \tag{A.107}$$

The Racah coefficients have the analytical expressions:

$$W(abcd; ef) = [(abe)] [(cde)] [(acf)] [(bdf)] \sum_{\kappa} (-1)^{a+b+c+d+\kappa} (\kappa + 1)!$$

$$\times [(a + b + c + d - \kappa)!(a + d + e + f - \kappa)!(b + c + e + f - \kappa)!]^{-1}$$

$$\times [(\kappa - a - b - e)!(\kappa - c - d - e)!(\kappa - a - c - f)!(\kappa - b - d - f)!]^{-1}, \tag{A.108}$$

where we denoted:

$$[(abc)] = \left[\frac{(a+b-c)!(a-b+c)!(-a+b+c)!}{(a+b+c+1)!} \right]^{1/2}. \qquad \text{(A.109)}$$

Using this expression one can prove the following symmetry relations:

$$W(abcd; ef) = W(badc; ef) = W(cdab; ef) = W(acbd; fe) \qquad \text{(A.110)}$$

$$= (-1)^{e+f-a-d} W(ebcf; ad) = (-1)^{e+f-b-c} W(aefd; bc).$$

If one argument is vanishing the coefficient has a simple expression:

$$W(abcd; 0f) = \delta_{ab}\delta_{cd}(-1)^{f-b-d} \frac{1}{\hat{b}\hat{d}}. \qquad \text{(A.111)}$$

The orthogonality relation is:

$$\sum_e (2e+1)(2f+1)W(abcd; ef)W(abcd; eg) = \delta_{fg}. \qquad \text{(A.112)}$$

The product of two Clebsch-Gordan coefficients having a common pair of indices, j, m, can be written as a linear combination of Racah coefficients:

$$C^{a\ b\ e}_{\alpha\ \beta\ \alpha+\beta} C^{e\ d\ c}_{\alpha+\beta,\ \delta,\ \alpha+\beta+\delta} = \sum_f \hat{e}\hat{f} C^{b\ d\ f}_{\beta,\ \delta,\ \beta+\delta} C^{a\ f\ c}_{\alpha,\ \beta+\delta,\ \alpha+\beta+\delta} W(abcd; ef). \qquad \text{(A.113)}$$

Appendix B: Overlaps and m.e. in CSM

The equations connecting the overlap integrals I_{02}^{J2}, $\mathcal{I}_J^{(k)}$ ($k = 2, 3, 4$) (see 6.1.15) and the basic integrals $I_J^{(0)}$, $I_J^{(1)}$ are as follows (details given in Ref. [RCGD82]:

$$I_{02}^{J2} = 2\sqrt{\frac{J(J+1)}{6(J-1)(J+2)}} \left\{ \frac{1-x}{x} I_J^{(0)} + I_J^{(1)} \right\}, \quad x = d^2,$$

$$\mathcal{I}_J^{(2)} = \left[\frac{1}{3} + \frac{2}{(J-1)(J+2)} \right] I_J^{(1)} + \frac{2}{x} \left[\frac{1+x}{3} + \frac{1-x}{(J-1)(J+2)} \right] I_J^{(0)}, \text{J} = \text{even}$$

$$\mathcal{I}_J^{(2)} = \frac{1}{2J+1} \left[(J-1)I_{J+1}^{(0)} + (J+2)I_{J-1}^{(0)} \right], \quad \text{J} = \text{odd}.$$

$$\mathcal{I}_J^{(3)} = 3Z_J - 2\mathcal{I}_J^{(2)}, \ \mathcal{I}_J^{(4)} = \frac{14}{3} \mathcal{I}_J^{(2)'} + \frac{10}{3} \mathcal{I}_J^{(2)} - 7Z_J,$$

$$Z_J = \frac{1}{2J+1}\left\{\left[J + \frac{(J+1)(J+2)}{6x}\right]I_{J-1}^{(0)} + \left[J+1 - \frac{J(J-1)}{6x}\right]I_{J+1}^{(0)}\right\}, J = \text{odd},$$

$$Z_J = \frac{2+x}{3x^2}I_J^{(0)} + \frac{2}{3}I_J^{(1)}, \quad J = \text{even}. \tag{B.1}$$

It is worth mentioning that the matrix element of any quadrupole boson monomial with the angular momentum projected states can be fully expressed in terms of the norms of the states involved. Then, due to the above equations the mentioned m.e. can be expressed in terms of $I_J^{(0)}$ and $I_J^{(1)}$.

In order to calculate the energies of the three bands, we need the m.e. of the terms involved in the model Hamiltonian, corresponding to the projected states basis. To this end we introduce the notations:

$$H_{20} = (b^+b^+)_0 + h.c, \quad H_{22} = (b^+b^+)_0(bb)_0. \tag{B.2}$$

Results for the nonvanishing m.e. are listed below:

$$\langle\varphi_{JM}^g|H_{20}|\varphi_{JM}^g\rangle = 2\sqrt{\frac{1}{5}}d^2, \tag{B.3}$$

$$\langle\varphi_{JM}^g|H_{20}|\varphi_{JM}^\beta\rangle = \frac{6d}{\sqrt{14}}\frac{N_J^\beta}{N_J^g},$$

$$\langle\varphi_{JM}^g|H_{20}|\varphi_{JM}^\gamma\rangle = 2\sqrt{\frac{2}{5}}d^2(2J+1)N_J^g N_J^\gamma e^{-d^2}I_{02}^{J2},$$

$$\langle\varphi_{JM}^\beta|H_{20}|\varphi_{JM}^\beta\rangle = 2\sqrt{\frac{1}{5}}d^2 + \frac{72}{5}\sqrt{\frac{1}{5}}d^2\left(\frac{N_J^\beta}{N_J^g}\right)^2,$$

$$\langle\varphi_{JM}^\beta|H_{20}|\varphi_{JM}^\gamma\rangle = \frac{6}{35}(2J+1)N_J^\beta N_J^\gamma e^{-d^2}\left[(7d+3d^3)I_{02}^{J2} + 4d^3 I_{02}^{J2'}\right],$$

$$\langle\varphi_{JM}^\gamma|H_{20}|\varphi_{JM}^\gamma\rangle = 2\sqrt{\frac{1}{5}}d^2 + \frac{24}{7}\sqrt{\frac{1}{5}}(2J+1)(N_J^\gamma)^2 e^{-d^2}d^2\mathcal{I}_J^{(2)}, \tag{B.4}$$

$$\langle\varphi_{JM}^g|H_{22}|\varphi_{JM}^g\rangle = \frac{1}{5}d^4,$$

$$\langle\varphi_{JM}^g|H_{22}|\varphi_{JM}^\beta\rangle = \frac{6d^3}{\sqrt{70}}\frac{N_J^\beta}{N_J^g},$$

$$\langle\varphi_{JM}^g|H_{22}|\varphi_{JM}^\gamma\rangle = \frac{2}{5}\sqrt{\frac{2}{7}}N_J^g N_J^\gamma e^{-d^2}d^4 I_{02}^{J2},$$

$$\langle \varphi^\gamma_{JM}|H_{22}|\varphi^\gamma_{JM}\rangle = \frac{1}{5}d^4 + \frac{8}{245}(2J+1)$$

$$\times (N^\gamma_J)^2 e^{-d^2}\left[(14d^2+25d^4)\mathcal{I}^{(2)}_J - 7d^4\mathcal{I}^{(3)}_J + 3d^4\mathcal{I}^{(4)}_J\right],$$

$$\langle \varphi^\gamma_{JM}|H_{22}|\varphi^\beta_{JM}\rangle = \frac{6}{35}\sqrt{\frac{1}{5}}(2J+1)N^\beta_J N^\gamma_J e^{-d^2}\left[(29d^3+3d^5)I^{J2}_{02} + 4d^5 I^{J2'}_{02}\right],$$

$$\langle \varphi^\beta_{JM}|H_{22}|\varphi^\beta_{JM}\rangle = \frac{1}{5}d^4 + \frac{18}{175}\left(\frac{N^\beta_J}{N^g_J}\right)^2$$

$$\times \left[44d^4 + 25d^2 + 4J(J+1) + (4d^2-12d^4)\frac{I^{(1)}_J}{I^{(0)}_J}\right]. \quad \text{(B.5)}$$

Here the symbol " ' " has the meaning of the first derivative with respect to x $(=d^2)$ Using these results one can check that $22\hat{N} + 5\Omega^+_{\beta'}\Omega_{\beta'}$ has vanishing m.e. between φ^β_{JM} and φ^i_{JM} with $i = g,\gamma$. The nonvanishing m.e. of the remaining operators ivolved in the CSM Hamiltonian are:

$$\langle \varphi^\beta_{JM}|\Omega^+_\beta\Omega_\beta|\varphi^\beta_{JM}\rangle = \frac{54}{1225}\left(\frac{N^\beta_J}{N^g_J}\right)^2$$

$$\times \left\{\frac{2450}{3} + 350d^2 + \frac{369}{2}d^4 + \frac{147}{2}J(J+1) + (833d^2+357d^4)\frac{I^{(1)}_J}{I^{(0)}_J}\right\},$$

$$\text{(B.6)}$$

$$\langle \varphi^\beta_{JM}|\Omega^+_\beta\Omega^2_{\beta'} + h.c.|\varphi^\beta_{JM}\rangle = \frac{96}{5}\sqrt{\frac{1}{70}}d$$

$$\times \left[\frac{1}{2}d^2 - \langle \varphi^\beta_{JM}|\hat{N}|\varphi^\beta_{JM}\rangle - 18\left(\frac{N^\beta_J}{N^g_J}\right)^2\left(1 + \frac{d^2}{7} + \frac{3}{5}d^2\frac{I^{(1)}_J}{I^{(0)}_J}\right)\right],$$

$$\text{(B.7)}$$

$$\langle \varphi^\beta_{JM}|\Omega^{+2}_{\beta'}\Omega^2_{\beta'}|\varphi^\beta_{JM}\rangle = \frac{288}{875}d^2\left(\frac{N^\beta_J}{N^g_J}\right)^2$$

$$\times \left[3d^4 + J(J+1) - 2(d^2+1)d^2\frac{I^{(1)}_J}{I^{(0)}_J}\right]. \quad \text{(B.8)}$$

Appendix C: Near Vibrational Expansion

The coefficients of the near vibrational energy expansions have the expressions:

$$\sum_{k=0}^{3} A_{J,k}^{(g)} x^k = \frac{J}{2} + \frac{J}{2(2J+3)}x + \frac{9}{2}\frac{(J+1)(J+2)}{(2J+3)^2(2J+5)}x^2$$

$$+ \frac{27}{2}\frac{(J+1)(J+2)}{(2J+3)^3(2J+5)(2J+7)}x^3,$$

$$\sum_{k=0}^{3} Q_{J,k}^{(\gamma,0)} x^k = \frac{(J+1)(J+2)(2J+3)}{6(J-1)} + \frac{(J+2)(7J^2+7J-24)}{(J-1)(2J+3)}x$$

$$+ \frac{3}{2}\frac{20J^4+85J^3+85J^2+38J+42}{(J-1)(2J+3)^2(2J+5)}x^2$$

$$+ \frac{9(J+1)(14J^4+84J^3+108J^2-122J-204)}{(J-1)(2J+3)^3(2J+5)(2J+7)}x^3, \quad \text{(C.1)}$$

$$\sum_{k=0}^{3} Q_{J,k}^{(\gamma,1)} x^k = (J+2)^2 + \frac{9J^3+22J^2-10J-6}{(2J+1)(2J+3)}x$$

$$+ \frac{3J(12J^3+53J^2+81J+22)}{(2J+1)^2(2J+3)(2J+5)}x^2$$

$$+ \frac{9J(3J+5)}{(2J+1)^2(2J+3)(2J+5)}x^3, \quad \text{(C.2)}$$

$$\sum_{k=0}^{3} R_{J,k}^{(\gamma,0)} x^k = \frac{1}{12(J-1)}(J-2)(J+1)(J+2)(2J+3)$$

$$+ \frac{44J^5+199J^4+67J^3-748J^2-948J-144}{12(J-1)(J+2)(2J+3)}x$$

$$+ \left[\frac{1}{J+2}(22J^4+59J^3-J^2+82J+288) \right.$$

$$\left. + \frac{3(J+1)}{(2J+3)(2J+5)}(2J^4+4J^3-5J^2-7J-24) \right]$$

$$\times \frac{x^2}{4(J-1)(2J+3)}$$

$$
+ \left[\frac{9(J+1)(34J^4 + 196J^3 + 99J^2 - 959J - 1200)}{(2J+3)^2(2J+5)(2J+7)} \right.
$$

$$
\left. + \frac{39J^3 + 81J^2 - 54J - 120}{J+2} \right] \frac{x^3}{4(J-1)(2J+3)}, \quad \text{(C.3)}
$$

$$
\sum_{k=0}^{3} R_{J,k}^{(\gamma,1)} x^k = \frac{1}{2}(J-1)(J+2)^2 + \frac{11J^4 + 24J^3 - 43J^2 - 100J - 42}{2(2J+1)(2J+3)} x
$$

$$
+ \frac{9J^3 + 25J^2 + 38J + 3}{(2J+1)(2J+3)} x^2 + \frac{9}{2} \frac{J(J-1)^2(J+2)}{(2J+1)^2(2J+3)(2J+5)} x^2
$$

$$
+ 3 \frac{J(12J^3 + 41J^2 + 36J + 31)}{(2J+1)^2(2J+3)(2J+5)} x^3, \quad \text{(C.4)}
$$

$$
\sum_{k=1}^{3} U_{J,k}^{(\gamma,0)} x^k = \frac{4J(J+1)(J+2)}{15(J-1)} x - \frac{8(J+1)(J+2)(J-3)}{5(J-1)(2J+3)} x^2
$$

$$
+ \frac{12}{5} \frac{4J^4 + 23J^3 + 5J^2 - 110J - 120}{(J-1)(2J+3)^2(2J+5)} x^3, \quad \text{(C.5)}
$$

$$
\sum_{k=2}^{3} U_{J,k}^{(\gamma,1)} x^k = \frac{16}{5} x^2 - \frac{48}{5} \frac{J}{(J+1)(2J+3)} x^3, \quad \text{(C.6)}
$$

$$
\sum_{k=0}^{3} Q_{J,k}^{(\beta)} x^k = 3J + 10 + \frac{3}{7} \frac{17J + 15}{2J+3} x + 27 \frac{(J+1)(J+2)}{(2J+3)^2(2J+5)} x^2
$$

$$
+ 81 \frac{(J+1)(J+2)}{(2J+3)^3(2J+5)(2J+7)} x^3, \quad \text{(C.7)}
$$

$$
\sum_{k=0}^{3} R_{J,k}^{(\beta)} x^k = \frac{3}{2} J^2 + 14J + 30 + \frac{72J^2 + 403J + 180}{14(2J+3)} x
$$

$$
+ \frac{3}{14} \frac{160J^3 + 1333J^2 + 2847J + 1680}{(2J+3)^2(2J+5)} x^2
$$

$$
+ \frac{27}{14} \frac{(J+1)(J+2)(48J^2 + 240J + 427)}{(2J+3)^3(2J+5)(2J+7)} x^3, \quad \text{(C.8)}
$$

$$\frac{35}{6}\sum_{k=0}^{3}U_{J,k}^{(\beta)}x^{k}=2J(2J+3)+\frac{-12J^{2}+34J+75}{2J+3}x$$

$$+\frac{2(52J^{3}+313J^{2}+606J+378)}{(2J+3)^{2}(2J+5)}x^{2}$$

$$-216\frac{(J+1)(J+2)(J^{2}+5J+5)}{(2J+3)^{3}(2J+5)(2J+7)}x^{3}, \qquad \text{(C.9)}$$

$$\sum_{k=0}^{3}V_{J,k}^{(\beta)}x^{k}=\frac{3}{5}(9J^{2}+60J+100)+\frac{18}{35}\frac{51J^{2}+236J+150}{2J+3}x$$

$$+\frac{27}{245}\left[123+119\frac{4J^{3}+37J^{2}+78J+42}{(2J+3)^{2}(2J+5)}\right]x^{2}$$

$$+\frac{16524}{35}\frac{(J+1)(J+2)(J^{2}+5J+7)}{(2J+3)^{3}(2J+5)(2J+7)}x^{3}, \qquad \text{(C.10)}$$

$$\sum_{k=1}^{3}B_{J,k}^{(\beta)}x^{k}=\frac{96}{175}\left[J^{2}x-\frac{2J(J+2)}{2J+3}x^{2}+\frac{20J^{3}+107J^{2}+192J+117}{(2J+3)^{2}(2J+5)}x^{3}\right],$$

$$\text{(C.11)}$$

$$\sum_{k=0}^{3}Z_{J,k}^{(\beta)}x^{k}=\frac{48}{5\sqrt{70}}\left[-(3J^{2}+46J+120)+\left(Q_{J,0}^{(\beta)}-\frac{72J^{2}+649J+360}{7(2J+3)}\right)x\right.$$

$$+\left(Q_{J,1}^{(\beta)}-\frac{3}{7}\frac{160J^{3}+1711J^{2}+3981J+2436}{(2J+3)^{2}(2J+5)}\right)x^{2}$$

$$\left.+\left(Q_{J,2}^{(\beta)}-\frac{27}{7}\frac{(J+1)(J+2)(48J^{2}+240J+553)}{(2J+3)^{3}(2J+5)(2J+7)}\right)x^{3}\right],$$

$$\text{(C.12)}$$

$$\sum_{k=1}^{3}T_{J,k}x^{k}=242\frac{J(J+1)(J+2)}{J-1}\left[\frac{x}{6}-\frac{x^{2}}{2J+3}+\frac{3}{2}\frac{4J+7}{(2J+3)^{2}(2J+5)}x^{3}\right],$$

$$\text{(C.13)}$$

$$\sum_{k=0}^{3} X_{J,k} x^k = \frac{(J+1)(J+2)(2J+3)}{6(J-1)} + \frac{3(4J^3 + 11J^2 - 11J - 34)}{(J-1)(2J+3)} x$$

$$+ \left[-\frac{88J^5 + 196J^4 - 460J^3 - 973J^2 - 585J - 396}{4(J-1)(2J+3)^2(2J+5)} \right.$$

$$\left. + \frac{22J^3 + 15J^2 - 31J + 144}{4(J-1)(2J+3)} \right] x^2$$

$$+ \frac{9}{4} \left[\frac{(J+1)(-28J^5 - 24J^4 + 639J^3 + 1176J^2 - 1559J - 2844)}{(J-1)(2J+3)^3(2J+5)(2J+7)} \right.$$

$$\left. + \frac{14J^5 + 81J^4 + 137J^3 - 13J^2 - 191J - 108}{(J-1)(2J+3)^3(2J+5)} \right] x^3.$$

(C.14)

The term ΔE_J accounts for the interaction between the states ϕ^g_{JM} and ϕ^γ_{JM}. In the near vibrational regime this has the expression

$$\Delta E_J = A_1 \frac{\sum_{k=0}^{3} T_{J,k} x^k}{\sum_{k=0}^{3} \left(22 X_{J,k} + 5 U^{(\gamma,0)}_{J,k} \right) x^k},$$

(C.15)

with coefficients $T_{J,k}$ and $X_{J,k}$ given above.

Appendix D: Asymptotic Expansion

Here we give the expressions of the terms ivolved in the asymptotic expansion of the ground, β and γ band energies, used in Chap. 6 (see Eqs. (6.3.15)–(6.3.18)).

$$P^\beta_J = \frac{12}{5} + \frac{171}{35} x - \frac{6}{5x} + \left(\frac{3}{5x} + \frac{1}{x^2} + \frac{13}{5x^3} \right) J(J+1) - \frac{1}{15x^3} J^2(J+1)^2,$$

(D.1)

$$S^\beta_J = \frac{2}{35} \left[1917x^2 + 5946x + 759 - \frac{1937}{x} \right]$$

$$+ \frac{J(J+1)}{35} \left[1125 + \frac{2537}{x} + \frac{14365}{3x^2} + \frac{25181}{3x^3} \right]$$

$$- \frac{J^2(J+1)^2}{7x^2} \left(8 + \frac{1937}{45x} \right),$$

(D.2)

$$F^\beta_J = \frac{54}{1225} \left[-\frac{406}{3} + \frac{1083}{2} x^2 + 826x - \frac{833}{3x} + \left(133 + \frac{714}{3x} + \frac{4403}{9x^2} \right. \right.$$

$$\left. \left. + \frac{10829}{18x^3} \right) J(J+1) - \frac{119}{18x^2} \left(1 + \frac{7}{3x} \right) J^2(J+1)^2 \right],$$

(D.3)

For $J =$ odd we have

$$S_J^\gamma = 198(J+1)x^3 + (J+1)(-66J + 368)x^2 + (J+1)\left(77J^2 - \frac{335}{3}J - \frac{188}{3}\right)x$$

$$+ \frac{1}{9}(-165J^4 + 1023J^3 + 635J^2 - 2219J - 2046)$$

$$+ \frac{(J-1)}{27x}(33J^4 - 688J^3 + 4549J^2 + 7098J - 396)$$

$$+ \frac{11J(J-1)}{27x^2}(2J^4 + 3J^3 - 162J^2 + 499J + 1296)$$

$$- \frac{11}{27x^3}J(J-1)^3(J-2)(J^2 - J - 39), \tag{D.4}$$

$$P_J^\gamma = 9(J+1)x^2 - (3J-4)(J+1)x + \frac{1}{3}(J+1)(6J^2 - 7J - 7)$$

$$+ \frac{1}{9x}(J-1)(-3J^3 + 21J^2 + 28J - 6)$$

$$+ \frac{1}{x^2}J(J-1)(-\frac{1}{9}J^3 - \frac{17}{27}J^2 + \frac{152}{27}J + \frac{20}{3})$$

$$+ \frac{J(J-1)^3}{27x^3}(J^2 - J - 39). \tag{D.5}$$

For $J =$ even we have

$$S_J^\gamma = \sum_{k=0}^{4} U^{(k)} J^k (J+1)^k, \quad P_J^\gamma = \sum_{k=0}^{3} V^{(k)} J^k (J+1)^k, \tag{D.6}$$

where

$$U^{(0)} = -396x^3 - 736x^2 + \frac{376}{3}x + \frac{1364}{3} - \frac{88}{3x},$$

$$U^{(1)} = 198x^3 + 368x^2 - \frac{584}{3}x - \frac{3835}{9} - \frac{4655}{9x} - \frac{1056}{x^2} + \frac{572}{9x^3},$$

$$U^{(2)} = 66x + \frac{1037}{9} + \frac{5702}{27x} + \frac{18847}{54x^2} + \frac{451}{6x^3},$$

$$U^{(3)} = -\frac{47}{54x} - \frac{49}{9x^2} + \frac{539}{162x^3},$$

$$U^{(4)} = -\frac{11}{81x^3}, \tag{D.7}$$

$$V^{(0)} = -18x^2 - 8x + \frac{14}{3} - \frac{4}{3x},$$

$$V^{(1)} = 9x^2 + 4x - \frac{16}{3} - \frac{53}{9x} - \frac{40}{3x^2} + \frac{26}{9x^3},$$

$$V^{(2)} = \frac{3}{2} + \frac{22}{9x} + \frac{169}{27x^2} + \frac{113}{54x^3},$$

$$V^{(3)} = -\frac{7}{54x^2} - \frac{1}{18x^3}. \tag{D.8}$$

The factors $T_J^{n,\beta}$, with n = 4, 5, involved in the equation determining the excitation energies in the beta band have the following expression:

$$T_J^{4,\beta} = \frac{171}{35}x^2 + \frac{195}{7}x + \frac{321}{35} - \frac{361}{35x} - \frac{1949}{105x^2} - \frac{1591}{45x^3}$$

$$+ J(J+1)\left(\frac{99}{70} + \frac{361}{70x} + \frac{1973}{210x^2} + \frac{559}{30x^3}\right)$$

$$- \frac{1}{54x^3}\left(\frac{129}{5} + \frac{108}{35}x\right)J^2(J+1)^2,$$

$$T_J^{5,\beta} = \left[9x^3 + 24x + 16 + \frac{104}{3x} + \frac{74}{3x^2} + \left(6x - 8 - \frac{18}{x} - \frac{13}{x^2}\right)J(J+1)\right.$$

$$\left.+ \frac{x+1}{3x^2}J^2(J+1)^2\right]. \tag{D.9}$$

The function G defining the ground band energies by means of Eq. (6.3.13) has the following expression:

$$G_J = \frac{9}{4}x(x-2) + \left(J + \frac{1}{2}\right)^2 - \frac{4}{9x}\left(3 + \frac{10}{x} + \frac{37}{x^2}\right)$$

$$+ \frac{2}{3x}\left(1 + \frac{10}{3x} + \frac{13}{x^2}\right)J(J+1) - \frac{2}{9x^3}J^2(J+1)^2. \tag{D.10}$$

Appendix E: E2 Transition Operator Matrix Elements

The exact m.e. of the harmonic part of the quadrupole transition operator (6.2.27) can be expressed in terms of the projected state norms:

$$\langle\phi_J^g||Q_2^h||\phi_{J'}^g\rangle = q_h d C_{000}^{J'\,2\,J}\left[\frac{2J'+1}{2J+1}\frac{N_{J'}^g}{N_J^g} + \frac{N_J^g}{N_{J'}^g}\right], \tag{E.1}$$

$$\langle\phi_J^\beta||Q_2^h||\phi_{J'}^\beta\rangle = q_h d C_{000}^{J'\,2\,J}\left[\frac{N_J^\beta}{N_{J'}^\beta} + \frac{18}{5}\frac{N_J^\beta N_{J'}^\beta}{(N_{J'}^g)^2} + \frac{2J'+1}{2J+1}\left(\frac{N_{J'}^\beta}{N_J^\beta} + \frac{18}{5}\frac{N_J^\beta N_{J'}^\beta}{(N_J^g)^2}\right)\right], \tag{E.2}$$

$$\langle\phi_J^g||Q_2^h||\phi_{J'}^\beta\rangle = 0, \tag{E.3}$$

$$\langle\phi_J^\gamma||Q_2^h||\phi_{J'}^g\rangle = q_h d N_J^\gamma\left[\sqrt{\frac{2}{7}}C_{022}^{J'\,2\,J}\frac{1}{N_{J'}^g} + 2\sum_{J_1}\hat{2}\hat{J}C_{-220}^{2\,J\,J_1}C_{000}^{J'\,2\,J_1}\right.$$

$$\left.\times W(22JJ'; 2J_1)\frac{2J'+1}{2J_1+1}\frac{N_{J'}^g}{\left(N_{J_1}^g\right)^2}\right], \tag{E.4}$$

$$\langle\phi_J^\beta||Q_2^h||\phi_{J'}^\gamma\rangle = q_h N_J^\beta N_{J'}^\gamma (2J'+1)\frac{6}{7\sqrt{5}}\left\{C_{2-20}^{J'\,2\,J}\frac{1}{2J+1}\left[3\left(\frac{2}{7}d^2-1\right)(N_J^g)^{-2}\right.\right.$$

$$\left.+\frac{5}{3}\left(N_J^\beta\right)^{-2}\right] - 2d^2 C_{202}^{J'\,2\,J}\sum_{J_1}\frac{1}{2J_1+1}C_{000}^{J\,2\,J_1}C_{2-20}^{J\,2\,J_1}\left(N_{J_1}^g\right)^{-2}\right\}, \quad \text{(E.5)}$$

$$\langle\phi_J^\gamma||Q_2^h||\phi_{J'}^\gamma\rangle = q_h\left[1+\frac{\hat{J}'}{\hat{J}}(-)^{J'-J}(J'\leftrightarrow J)\right]\langle\phi_J^\gamma||b||\phi_{J'}^\gamma\rangle, \quad \text{(E.6)}$$

$$\langle\phi_J^\gamma||b||\phi_{J'}^\gamma\rangle = d(2J'+1)N_J^\gamma N_{J'}^\gamma\left\{\frac{1}{2J+1}C_{202}^{J'\,2\,J}\left(N_J^\gamma\right)^{-2}\right.$$

$$+\sum_{J_1}C_{2-20}^{J'\,2\,J_1}W(J'2J_12;J2)\times\left[2\sqrt{\frac{2}{7}}\frac{\hat{2}}{\hat{J}_1}C_{0-2-2}^{J_1\,2\,J}\left(N_{J_1}^g\right)^{-2}\right.$$

$$\left.\left.+20\sum_{J_2}\frac{\hat{J}_1}{\hat{J}_2}C_{000}^{J_1\,2\,J_2}C_{0-2-2}^{J_2\,2\,J}W(J2J_22;J_12)\left(N_{J_2}^g\right)^{-2}\right]\right\}. \quad \text{(E.7)}$$

The exact expressions for the m.e. of the anharmonic quadrupole transition operator (6.2.27) are following:

$$\langle\phi_J^g||Q_2^{anh}||\phi_{J'}^g\rangle = -q_{anh}d^2\sqrt{\frac{2}{7}}C_{000}^{J'\,2\,J}\left[\frac{2J'+1}{2J+1}\frac{N_{J'}^g}{N_J^g}+\frac{N_J^g}{N_{J'}^g}\right], \quad \text{(E.8)}$$

$$\langle\phi_J^\beta||Q_2^{anh}||\phi_{J'}^\beta\rangle = -q_{anh}d^2\sqrt{\frac{2}{7}}C_{000}^{J'\,2\,J}\left[\frac{N_J^\beta}{N_{J'}^\beta}+\frac{2J'+1}{2J+1}\frac{N_{J'}^\beta}{N_J^\beta}\right], \quad \text{(E.9)}$$

$$\langle\phi_J^\beta||Q_2^{anh}||\phi_{J'}^g\rangle = -6\sqrt{\frac{1}{5}}q_{anh}dC_{000}^{J'\,2\,J}\frac{N_{J'}^g N_J^\beta}{(N_J^g)^2}\frac{2J'+1}{2J+1}, \quad \text{(E.10)}$$

$$\langle\phi_J^\gamma||Q_2^{anh}||\phi_{J'}^g\rangle = q_{anh}N_J^\gamma N_{J'}^g\left[2\left(N_{J'}^g\right)^{-2}C_{022}^{J'\,2\,J}\left(1+\frac{2}{7}d^2\right)\right.$$

$$\left.+20d^2\hat{J}'\sum_{J_1J_2}\hat{J}_2 C_{0-2-2}^{J_1\,J_2\,J}C_{000}^{J_1\,2\,J'}C_{022}^{22\,J_2}(-)^J T_{J_1J_2}^{J\,J'}\right], \quad \text{(E.11)}$$

$$\langle\phi_J^\beta||Q_2^{anh}||\phi_{J'}^\gamma\rangle = \frac{q_{anh}}{q_h}\left[\frac{6}{\sqrt{5}}\langle\phi_J^g||Q_2^h||\phi_{J'}^\gamma\rangle\frac{N_J^\beta}{N_J^g}\right.$$

$$\left.+2d\hat{2}\sum_{J_1}\hat{J}_1 C_{000}^{J_1\,0\,J}W(22JJ';2J_1)\langle\phi_{J_1}^\beta||Q_2^h||\phi_{J'}^\gamma\rangle\frac{N_J^\beta}{N_{J_1}^\beta}\right]. \quad \text{(E.12)}$$

$$\langle\phi_J^\gamma||Q_2^{anh}||\phi_{J'}^\gamma\rangle = q_{anh}\left[1+\frac{\hat{J}'}{\hat{J}}(-)^{J'-J}(J'\leftrightarrow J)\right]\langle\phi_J^\gamma||(bb)_2||\phi_{J'}^\gamma\rangle, \quad \text{(E.13)}$$

$$\langle\phi_J^\gamma||(bb)_2||\phi_{J'}^\gamma\rangle = N_J^\gamma N_{J'}^\gamma\left\{-\sqrt{\frac{2}{7}}C_{202}^{J'\,2\,J}d^2(N_{J'}^\gamma)^{-2}\right.$$

$$+ 20d^2 \sqrt{\frac{2}{7}} \, \hat{J}' \sum_{J_1 J_2} \hat{J}_2 C^{J_1 \, 2 \, J'}_{0-2-2} C^{J_1 \, J_2 \, J}_{0-2-2} C^{2 \, 2 \, J_2}_{0 \, 2 \, 2} T^{J J'}_{J_1 J_2}$$

$$+ 40d^2 2 \hat{J}' \hat{J} \sum_{J_1 J_2 J_3} \hat{J}_2 C^{2 \, 2 \, J_3}_{2 \, 0 \, 2} C^{J \, J_2 \, J_3}_{2 \, 0 \, 2} C^{J_1 \, 2 \, J_2}_{0 \, 0 \, 0} C^{J_1 \, 2 \, J'}_{0-2-2} S^{J J'}_{J_1 J_2 J_3} \Bigg\}.$$

$$(E.14)$$

In the above equations, the following notations were used:

$$T^{J J'}_{J_1 J_2} = W(2222; 2J_2) W(J'2J_1 J_2; J2) \left(N^g_{J_1} \right)^{-2}, \tag{E.15}$$

$$S^{J J'}_{J_1 J_2 J_3} = W(2222; 2J_3) W(J_3 2 J J'; 2J_2) W(22 J' J_2; 2J_1) \left(N^g_{J_1} \right)^{-2}. \tag{E.16}$$

With the analytical expressions listed above, one derives simple relations for the quadrupole moments in the ground and β bands:

$$\frac{\langle \varphi^g_{JJ} | Q^{anh}_{20} | \varphi^g_{JJ} \rangle}{\langle \varphi^g_{JJ} | Q^h_{20} | \varphi^g_{JJ} \rangle} = -\frac{q_{anh}}{q_h} \sqrt{\frac{2}{7}},$$

$$\langle \varphi^\beta_{JJ} | Q^{anh}_{20} | \varphi^\beta_{JJ} \rangle = \langle \varphi^g_{JJ} | Q^{anh}_{20} | \varphi^g_{JJ} \rangle, \tag{E.17}$$

$$\langle \varphi^\beta_{JJ} | Q_{20} | \varphi^\beta_{JJ} \rangle = \left[1 + \frac{18}{5} \left(\frac{N^\beta_J}{N^g_J} \right)^2 \left(1 - d \frac{q_{anh}}{q_h} \sqrt{\frac{2}{7}} \right)^{-1} \right] \langle \varphi^g_{JJ} | Q_{20} | \varphi^g_{JJ} \rangle.$$

From the last equation it results that for $d q_{anh} < q_h \sqrt{\frac{7}{2}}$ the order of the quadrupole moments for the states J^+_β and J^+_g is not affected by supposing an anharmonic structure for $Q_{2\mu}$.

Appendix F: Coefficients of Fractional Parentage

Coefficients of fractional parentage for the boson operators $b^\dagger$ and b, are obtained by using the vibrational limit (i.e. $d \to 0$) of their m.e. with the projected states. The final results are:

$$\langle \frac{J}{2}, \frac{J}{2}, 0, J || b^\dagger || \frac{J-2}{2}, \frac{J-2}{2}, 0, J - 2 \rangle = \left(\frac{J}{2} \right)^{1/2},$$

$$\langle \frac{J+3}{2}, \frac{J+3}{2}, 0, J || b^\dagger || \frac{J+1}{2}, \frac{J+1}{2}, 0, J + 1 \rangle$$

$$= -\frac{J+2}{2J+1} \left[\frac{3(J-1)(J+1)(2J+3)}{J(2J^2 + 5J + 11)} \right]^{1/2}, J = \text{odd},$$

$$\langle \frac{J}{2}+1, \frac{J}{2}+1, 0, J||b||\frac{J}{2}+2, \frac{J}{2}+2, 0, J+2\rangle$$

$$= \left[\frac{J(2J+5)(2J+7)}{2(2J+1)(2J+3)} \right]^{1/2}, \quad J = \text{even},$$

$$\langle \frac{J+3}{2}, \frac{J+3}{2}, 0, J||b||\frac{J+5}{2}, \frac{J+5}{2}, 0, J+2\rangle$$

$$= \left[\frac{(J-1)(J+3)^2(J+4)}{2(J+2)(2J^2+5J+11)(2J^2+13J+29)} \right]^{1/2}$$

$$\times \left(2J+6+\frac{25J+17}{(J+1)(2J+1)} \right), \quad J = \text{odd},$$

$$\langle \frac{J}{2}+1, \frac{J}{2}+1, 0, J||b||\frac{J}{2}+2, \frac{J}{2}+2, 0, J+1\rangle$$

$$= -\left[\frac{18(J+2)(J+3)^3}{J(2J+1)(2J+3)(2J^2+9J+18)} \right]^{1/2}, \quad J = \text{even},$$

$$\langle \frac{J}{2}+3, \frac{J}{2}+1, 0, J||b^\dagger||\frac{J}{2}+2, \frac{J}{2}+2, 0, J+2\rangle$$

$$= \left[\frac{J(2J+5)(2J+7)}{(J+7)(2J+1)(2J+3)} \right]^{1/2},$$

$$\langle \frac{J}{2}+3, \frac{J}{2}+1, 0, J||b^\dagger||\frac{J}{2}+2, \frac{J}{2}+2, 0, J+1\rangle$$

$$= -\left[\frac{36(J+2)(J+3)^3}{J(J+7)(2J+1)(2J+3)(2J^2+9J+18)} \right]^{1/2},$$

$$\langle \frac{J}{2}+3, \frac{J}{2}+1, 0, J||b^\dagger||\frac{J}{2}+2, \frac{J}{2}, 0, J-2\rangle$$

$$= \left[\frac{(J+11)^2(J-2)(2J+3)}{2(J+5)(J+7)(2J-1)} \right]^{1/2},$$

$$\langle \frac{J}{2}+3, \frac{J}{2}+3, 1, J||b^\dagger||\frac{J}{2}+2, \frac{J}{2}+2, 0, J+2\rangle$$

$$= 7\left[\frac{6(2J+5)(2J+7)}{(J+7)(2J+1)(9J^2+199J+490)} \right]^{1/2},$$

$$\langle \frac{J}{2}+3, \frac{J}{2}+3, 1, J||b^\dagger||\frac{J}{2}+2, \frac{J}{2}+2, 0, J+1\rangle$$

$$= \left[\frac{54(J+2)(J+3)^3(J+11)^2}{(J+7)(2J+1)(2J^2+9J+18)(9J^2+199J+490)} \right]^{1/2},$$

$$\langle \frac{J}{2}+3, \frac{J}{2}+3, 1, J||b^\dagger||\frac{J}{2}+2, \frac{J}{2}+2, 1, J-2\rangle$$

$$= [7(J+5)(J+7)(3J+10)-6(J-2)(J+11)(2J+3)]$$

$$\times J^{1/2}[2(J+5)(J+7)(9J^2+199J+490)(9J^2+163J+128)]^{-1/2}.$$

$$(F.1)$$

In the asymptotic regime, the expressions of β and γ states amplitude in terms of the ground state amplitude are:

$$\Gamma_{JK}^{\beta} = \frac{1}{\sqrt{70}}\left[-4\sqrt{2}(k\beta)^3\cos 3\gamma + 6(k\beta)^2 d - 15d + 4d^3\right]\Gamma_{JK}^g$$

$$-\frac{6d}{\sqrt{35}}\left[\left(-\sqrt{2}(k\beta)^2\cos 2\gamma + 2kd\beta\cos\gamma\right)\sum_{J'}C_{0\,0\,0}^{J\,2\,J'}C_{K\,0\,K}^{J\,2\,J'}\Gamma_{J'K}^g \right. \qquad (F.2)$$

$$\left.+ \left((k\beta)^2\sin 2\gamma + \sqrt{2}kd\beta\sin\gamma\right)\sum_{J'}C_{0\,0\,0}^{J\,2\,J'}\left(C_{K\,-2\,K-2}^{J\,2\,J'}\Gamma_{J'K-2}^g + C_{K\,2K+2}^{J\,2\,J'}\Gamma_{J'K+2}^g\right)\right],$$

$$\Gamma_{JK}^{\gamma} = \sqrt{2}\left[\left(-\sqrt{2}(k\beta)^2\cos 2\gamma - k\beta\cos\gamma\right)\sum_{J'}C_{2\,-2\,0}^{J\,2\,J'}C_{K\,0\,K}^{J\,2\,J'}\Gamma_{J'K}^g \qquad (F.3)\right.$$

$$\left.+ \left((k\beta)^2\sin 2\gamma - \frac{kd\beta}{\sqrt{2}}\sin\gamma\right)\sum_{J'}C_{2\,-2\,0}^{J\,2\,J'}\left(C_{K\,-2\,K-2}^{J\,2\,J'}\Gamma_{J'K-2}^g + C_{K\,2K+2}^{J\,2\,J'}\Gamma_{J'K+2}^g\right)\right].$$

The matrix element of the function $(k\beta)^a\cos^b\gamma\sin^c\gamma$ has the expression:

$$I_{JK,J'K'}^{g,g}(,a,b,c) = \sum X_{mn}^{JK}X_{m_1n_1}^{J'K'}$$

$$\times A(m+n+m_1+n_1+a)B(n+n_1+b, m+m_1+c)d^{m+n+m_1+n_1},$$

$$A(t) = \frac{1}{2}\left(\frac{t+3}{2}\right)!\delta_{t,odd} + \frac{(t+3)!}{\left(\frac{t+2}{2}\right)!}\frac{\sqrt{\pi}}{2^{t+4}}\delta_{t,even} \qquad (F.4)$$

$$B(p,k) = \delta_{p,even}\delta_{k,even}\sum_{l=0}^{k/2}\frac{\binom{k/2}{l}(-)^l}{(p+2l+1)(p+2l+3)}\left[\frac{1}{2^{p+2l-3}}+4(3p+6l+1)\right].$$

The indices m, n, m_1, n_1 satisfy the restrictions:

$$n+n_1+b = even, \quad m+m_1+c = even. \qquad (F.5)$$

Consequently,

$$I_{JK,J'K'}^{g,g}(a,b,c) = 0, \text{ if } K\pm K'+2c \neq 4s, \quad s = integer. \qquad (F.6)$$

Appendix G: Single and Multiple Core

Here we consider two particle-core projected states and connect them with the product of two single particle projected states.

Consider first two unprojected states for the particle-core system which generates the projected state:

$$\Psi^{(1)}_{nljI} = |nljI\rangle\Psi_g(d),$$
$$\Psi^{(2)}_{n'l'j'I'} = |n'l'j'I'\rangle\Psi_g(d),\qquad\qquad\text{(G.1)}$$

The product of the two deformed states can be written as

$$\Psi^{(1)}_{nljI}\Psi^{(2)}_{n'l'j'I'} = |nljI\rangle|n'l'j'I'\rangle\Psi_g(2d).\qquad\qquad\text{(G.2)}$$

In the right hand side of the above equation, we used the explicit form for the coherent state Ψ_g which implies the property that the product of two coherent states is a coherent state of a double deformation parameter. In conclusion, due to the addition property of the coherent states the product of two functions describing the particle-core system in the intrinsic frame, each of them carrying a core factor function, is equal to the function describing two particles and a global core. The question which naturally arises is whether this property also holds for the projected states. In order to prove that, let us consider two projected particle core states Φ^{IM}_{nlj} and $\Phi^{I'M'}_{n'l'j'}$. As shown in Eq. (12.1.10) they can be written as:

$$\Phi^{IM}_{nlj} = \mathcal{N}^I_{nlj}\sum_J C^{j\ J\ I}_{I\ 0\ I}\left(N^{(g)}_J\right)^{-1}\left[|nlj\rangle\phi^{(g)}_J\right]_{IM},$$
$$\Phi^{I'M'}_{n'l'j'} = \mathcal{N}^{I'}_{n'l'j'}\sum_{J'} C^{j'\ J'\ I'}_{I'\ 0\ I'}\left(N^{(g)}_{J'}\right)^{-1}\left[|n'l'j'\rangle\phi^{(g)}_{J'}\right]_{I'M'},\qquad\text{(G.3)}$$

where $\phi^{(g)}_{JM}$ denotes the projected states of the CSM core function Ψ_g, with the norm $N^{(g)}_J$. The behavior of the projected states in the large deformation and the vibrational limits are given in Chap. 6. For an easier reading we rewrite these results here:

$$\phi^{(g)}_{JM} = C_J\beta^{-1}e^{-(d-\frac{k\beta}{\sqrt{2}})^2}D^{J*}_{M0}(\Omega_0),\ \text{for d large},$$
$$\lim_{d\to 0}\phi^{(g)}_{JM} = |\frac{J}{2},\frac{J}{2},0,JM\rangle,\qquad\qquad\text{(G.4)}$$

where Ω_0 denotes the Euler angles which define the intrinsic frame of reference with respect to the laboratory frame, and $|N,v,\alpha,JM\rangle$ denotes the SU(5) basis states. C_J is given by Eq. (6.3.3). In the regime of large deformation, the product of two projected states will be a linear combination of functions like $|nljm\rangle|n'l'j'm'\rangle D^{J*}_{M0}(\Omega_0)D^{J'*}_{M'0}(\Omega_0)$. The Wigner function also has an addition property which allows us to transform 2 functions into a linear combination of one function:

$$D^{J^*}_{M0}(\Omega_0) D^{J'^*}_{M'0}(\Omega_0) = \sum_{J_c} C^{J \ J' \ J_c}_{0 \ 0 \ 0} C^{J \ J' \ J_c}_{M \ M' \ M_c} D^{J_c^*}_{M_c 0}. \tag{G.5}$$

This way the product of two projected states is written as linear combinations of terms consisting of two single particle states and one core function. Therefore, in the large deformation regime the product of two projected states can be written as two particles coupled to a single projected core.

A similar conclusion is derived also for the vibrational limit. Indeed, for the case when the projection of the angular momentum on the z-axis is maximum one gets:

$$\left| \frac{J}{2} \frac{J}{2}, 0, J, J \right\rangle = \left[\sqrt{(\frac{J}{2})!} \right]^{-1/2} \left(b^\dagger_{22} \right)^{J/2} |0\rangle, \tag{G.6}$$

Identifying the product of the vacua associated to the two projected states with one vacuum state one obtains:

$$\left| \frac{J}{2} \frac{J}{2}, 0, J, J \right\rangle \left| \frac{J'}{2} \frac{J'}{2}, 0, J', J' \right\rangle = \sqrt{\frac{((J + J')/2)!}{(J/2)!(J'/2)!}} \left| \frac{J + J'}{2}, \frac{J + J'}{2}, 0, J + J', J + J' \right\rangle \tag{G.7}$$

The behavior of the product of two projected functions in the rotational and vibrational limit allows us to generalize this property by inferring that the state

$$|J, J'; J_c M_c\rangle = \sum_{M,M'} C^{J \ J' \ J_c}_{M \ M' \ M_c} \phi^{(g)}_{JM} \phi^{(g)}_{J'M'}. \tag{G.8}$$

obtained with two independent core states $\phi^{(g)}_{JM}, \phi^{(g)}_{J'M'}$, is a state belonging to the core space of projected states. This way, the product of two projected functions can be written as a product of two single particle states and a single core function.

This conclusion can be drawn by a straightforward calculation exploiting Eq. (G.2). Indeed, the core factors appearing in the unprojected states $\Psi^{(1)}$ and $\Psi^{(2)}$ can be written as:

$$\Psi_g(d) = \sum_J \left(N^{(c)}_J(d) \right)^{-1} \phi^{(g)}_{J0}(d),$$

$$\Psi_g(d) = \sum_{J'} \left(N^{(c)}_{J'}(d) \right)^{-1} \phi^{(g)}_{J'0}(d). \tag{G.9}$$

Therefore the equality which holds in the intrinsic frame:

$$\Psi_g(d)\Psi_g(d) = \Psi_g(2d) \tag{G.10}$$

yields, after inserting the expansions for each coherent state:

$$\sum_{J,J'} \left(N_J^{(g)}(d)\right)^{-1} \left(N_{J'}^{(g)}(d)\right)^{-1} \phi_{J0}^{(c)}(d)\phi_{J'0}^{(c)}(d) = \sum_{J_c} \left(N_{J_c}^{(g)}(2d)\right)^{-1} \phi_{J_c0}^{(g)}(2d).$$

(G.11)

Projecting out the good angular momentum in the above equation, one obtains a very simple relation between the product of two projected core states and a projected single core state:

$$\left(N_{J_c}^{(g)}(2d)\right)^{-1} \phi_{J_cM_c}^{(g)}(2d) = \sum_{J,J'} \left(N_J^{(c)}(d)N_{J'}^{(c)}(d)\right)^{-1} C_{0\ 0\ 0}^{J\ J'\ J_c} \left[\phi_J^{(g)}(d)\phi_{J'}^{(g)}(d)\right]_{J_cM_c}.$$

(G.12)

The above equation represents nothing else but the addition equation for the projected coherent states. This equation can be inverted and thereby a product of two core projected states can be expressed as a linear combination of one core projected states. Due to this equation, the projected spherical single particle basis (12.1.9) can be used for treating also the matrix elements of any two body interaction. Indeed, first the product of projected core states is transformed, by means of the above identity, into a projected single core state and then one factorizes the scalar product of the core projected states. To be more concrete, in what follows we describe the application for the scissors mode [REG02], where two single particle-core states are coupled to an angular momentum equal to unity. The projection of the total angular momentum can be performed in several equivalent ways. One way could be to project first the angular momentum from each of the factor states $\Psi_{nljI}^{(1)}$ and $\Psi_{n'l'j'I'}^{(1)}$. Then, the pair of particles of angular momentum equal to one is described by:

$$\Phi_{1M}^{(1)}(nljI; n'l'j'I') = \mathcal{N}^{(1)}(\mathcal{N}_{nlj}^I \mathcal{N}_{n'l'j'}^{I'})^{-1} C_{I\ I'\ I+I'}^{I\ I'\ 1} \left[\Phi_{nlj}^I \Phi_{n'l'j'}^{I'}\right]_{1M},$$

(G.13)

where $\mathcal{N}^{(1)}$ denotes the norm of the state from the left hand side. This expression is simplified if one multiplies first the unprojected core functions and then the angular momentum is projected out from the global core state.

$$\Phi_{1M}^{(1)}(nljI; n'l'j'I') = \mathcal{N}^{(1)} \sum_{J_2,J} C_{I\ I'\ I+I'}^{j\ j'\ J_2} C_{I+I'\ 0\ I+I'}^{J_2\ J\ 1} \left(N_J^{(g)}(2d)\right)^{-1}$$

$$\left[\left[|nlj\rangle|n'l'j'\rangle\right]_{J_2} \phi_J^{(g)}(2d)\right]_{1M}.$$

(G.14)

When a single core is associated with the two spherical shell model particles considered, the projected state with angular momentum equal to unity is:

$$\Phi^{(2)}_{1M}(nljI; n'l'j'I')$$

$$= \mathcal{N}^{(2)} \sum_{J_2, J} C^{j \ j' \ J_2}_{I \ I' \ I+I'} C^{J_2 \ J \ 1}_{I+I' \ 0 \ I+I'} \left(N^{(g)}_J(d) \right)^{-1} \left[[|nlj\rangle |n'l'j'\rangle]_{J_2} \phi^{(g)}_J(d) \right]_{1M}.$$

$$(G.15)$$

The difference between the two projected function consists of their dependence on the parameter d. This dependence is due to the core states and the norms:

$$\left(\mathcal{N}^{(1)} \right)^{-2} = \sum_{J, J_2} \left(N^{(g)}_J(2d) \right)^{-2} \left(C^{j \ j' \ J_2}_{I \ I' \ I+I'} C^{J_2 \ J \ 1}_{I+I' \ 0 \ I+I'} \right)^2,$$

$$\left(\mathcal{N}^{(2)} \right)^{-2} = \sum_{J, J_2} \left(N^{(g)}_J(d) \right)^{-2} \left(C^{j \ j' \ J_2}_{I \ I' \ I+I'} C^{J_2 \ J \ 1}_{I+I' \ 0 \ I+I'} \right)^2, \qquad (G.16)$$

In Ref. [REG02], we investigated how this difference in the deformation dependence manifests itself when a two body matrix element is calculated. Thus, we calculated the matrix elements of a dipole-dipole interaction alternatively with the wave function $\Phi^{(1)}$ and $\Phi^{(2)}$. The resulting matrix elements differ from each other by the factor:

$$F^{(n)}(d) = \sum_J \left(\mathcal{N}^{(n)} \right)^2 \left[N^{(g)}_J(n'd) \right]^{-2} \left(C^{1 \ J \ 1}_{1 \ 0 \ 1} \right)^2,$$

$$n' = n + (-)^{n+1}, \ n = 1, 2; \ J = 0, 2. \qquad (G.17)$$

The factor $F^{(n)}(d)$ is involved in the matrix element corresponding to the function $\Phi^{(n)}$. We calculated the quantities $F^{(n)}(d)$ (n=1, 2) corresponding to different pairs of single particle orbits (j, j') and found out that the differences between n=1 and n=2 factors are negligible.

Appendix H: Solution of the 6th Order Boson Hamiltonian

Here we give the analytical solution of the first Eq. (13.2.30) for an energy value belonging to one of the three domains defined in Sect. 13.2 of Chap. 13. Aiming at a compact presentation of the final results it is useful to introduce the following notations:

$$S_m = \frac{\hbar}{2} \sqrt{\frac{3}{A'F}} \frac{1}{\sqrt[4]{\Delta_m}}, \quad m = U, O,$$

$$S_l = \hbar \sqrt{\frac{3}{A'F}} \frac{1}{\sqrt{(a-c)(b-d)}} = S_r. \qquad (H.1)$$

Here A', F are two of the Hamiltonian coefficients. Δ_m-the second rank Eqs. (13.2.37), (13.2.53) discriminants and a,b,c,d are the roots of the fourth order polynomial $P_4(x; E, L)$ introduced in Chap. 13. Two particular values of the variable x are to be specified:

$$\mu_m = \frac{\lambda_1 u + \frac{1}{2}(a+b)}{\lambda_1 + 1}, \quad \eta_m = \frac{\lambda_2 u + \frac{1}{2}(a+b)}{\lambda_2 + 1}, \quad m = U, O \tag{H.2}$$

λ_1 and λ_2 are the solutions of Eqs. (13.2.37) and (13.2.53) if m is equal to U and O, respectively. Also the following intervals for r are needed:

$$R_U^{(1)} = [\sqrt{b}, \sqrt{\eta_U}], \quad R_U^{(2)} = [\sqrt{\eta_U}, \sqrt{a}],$$
$$R_O^{(1)} = [\sqrt{d}, \sqrt{\eta_O}], \quad R_O^{(2)} = [\sqrt{\eta_O}, \sqrt{a}],$$
$$R_B^{(1)} = [\sqrt{d}, \sqrt{c}], \quad R_B^{(2)} = [\sqrt{b}, \sqrt{a}], \tag{H.3}$$

Integrating the first equation (13.2.30) one obtains the time t as a function of r. In the intervals $R_m^{(1)}$ with $m = U, O$ and $R_B^{(i)}$ with i=1,2 the final result can be written in a compact form:

$$t_m(E, L; r) = S_m F(\Phi_{1m}(E, L; r), k_n(E, L)), \quad m = U, l, r, O,$$
$$n = m(\delta_{m,U} + \delta_{m,O}) + B(\delta_{m,l} + \delta_{m,r}). \tag{H.4}$$

If r belongs to $R_m^{(1)}$ with $m = U, O$, the solution is:

$$t_m(E, L; r) = S_m \left(\frac{\pi}{2} {}_2F_1(\frac{1}{2}, \frac{1}{2}; 1; k_m^2(E, L)) + F(\phi_{2m}(E, L; r), k_m(E, L)) \right). \tag{H.5}$$

$F(\Phi, k)$ denotes the incomplete elliptic integral of the first kind

$$F(\phi, k) = \int_0^\phi \frac{d\theta}{\sqrt{1 - k^2 \sin^2 \theta}}, \tag{H.6}$$

The functions Φ_{1m} and Φ_{2m}, $m = U, O$ have the expressions

$$\phi_{1m}(E, L; r) = \arccos\left(\frac{\eta_m - r^2}{r^2 - \mu_m} \sqrt{\frac{\lambda_1(\lambda_2 + 1)}{\lambda_2(\lambda_1 + 1)}} \right), \tag{H.7}$$

$$\phi_{2\mathrm{m}}(E, L; r) = \arcsin \left(\frac{(\lambda_2 + 1)(\lambda_1 - \lambda_2)}{\lambda_2(\lambda_1 + 1)} \frac{1}{\left(\frac{r^2 - \mu_U}{\eta_U - r^2}\right)^2 - \frac{\lambda_2 + 1}{\lambda_1 + 1}} \right)^{\frac{1}{2}}, \quad m = U, O.$$

For the B energy region the functions Φ are

$$\phi_{1l}(E, L; r) = \arcsin \sqrt{\frac{(a - c)(r^2 - d)}{(c - d)(a - r^2)}}.$$

$$\phi_{1\mathrm{r}}(E, L; r) = \arcsin \sqrt{\frac{(a - c)(r^2 - b)}{(a - b)(r^2 - c)}}. \tag{H.8}$$

Bibliography

[ASP53]   F. Asaro, F.S. Stephen, I. Perlman, Phys, Rev. **92**, 1495 (1953)
[AI76]   A. Arima, F. Iachello, Ann. Phys. (N.Y.) **91**, 253 (1976)
[ArIa76]   A. Arima, F. Iachello, Ann. Phys. (N.Y.) **123**, 468 (1976)
[Ar77]   A. Arima, T. Ohtsuka, F. Iachello, I. Talmi, Phys. Lett. **B66**, 205 (1977)
[Art97]   A. Artna-Cohen, NDS **80**, 723 (1997)
[Akov02]   Y.A. Akovali, NDS **96**, 177 (2002)
[Akov99]   Y.A. Akovali, NDS **87** 249 (1999)
[AMR03]   H. Amro et al., Phys. Lett. B **553**, 197 (2003)
[AR95]   A. Aroua et al., Nucl. Phys. A **728**, 96 (2003)
[ANT05]   A.N. Antonov et al., Phys. Rev. C **72**, 044307 (2005)
[ABST72]   M. Abramowitz, I.A. Stegun (eds.), *Handbook of Mathematical Functions with Formulas, Graphs, and Mathematical Tables, 9th Printing* (Dover, New York, 1972)
[ALL08]   J.M. Allmond et al., Phys. Rev. C **78**, 014302 (2008)
[ARI01]   J.M. Arias, Phys. Rev. C **63**, 034308 (2001)
[AAVG03]   J.M. Arias, C.E. Alonso, A. Vitturi, J.E. Garcia-Ramos, J. Dukelsky, A. Frank, Phys. Rev. C **68**, 041302(R) (2003)
[ART97]   A. Artna-Cohen, NDS **80**, (1997) 723
[AKO93]   Y.A. Akovali, NDS **69**, 155 (1993)
[AKO94]   Y.A. Akovali, NDS **71**, 181 (1994)
[AL57]   G. Alaga, Nucl. Phys. **4**, 625 (1957)
[Art96]   A. Artna-Cohenabc, NDS **79**, 1 (1996)
[BAG12]   C.M. Baglin, Nucl. Data Sheets **113**, 1871 (2012)
[BRJU99]   E. Browne, H. Junde, NDS **87**, 15 (1999)
[BRJU98]   E. Browne, H. Junde, NDS **84**, 337 (1998)
[BR94]   E. Browne, NDS **72**, 221 (1994)
[BaVe78]   M. Baranger, M. Veneroni, Ann. Phys. (NY) **114**, 123 (1978)
[BrJu99]   E. Browne, H. Junde, NDS **87**, 15 (1999)
[BrJu98]   E. Browne, H. Junde, NDS **84**, 337 (1998)
[Ba03]   C.M. Baglina, NDS **99**, 1 (2003)
[Br94]   E. Browne, NDS **72**, 221 (1994)
[Ba02]   C.M. Baglin, NDS **96**, 611 (2002)
[Bl00]   J. Blachot, NDS **91**, 135 (2000)
[Bl91]   J. Blachot, NDS **64**, 1 (1991)

[BM74] A. Bohr, B. Mottelson, *Nuclear Structure*, vol. 2 (W. A. Benjamin Inc, Amsterdam, 1974)

[BE53] H. Bateman, A. Erderly, *Higher Transcedental Functions*, vol. III, Chap. 15 (McGraw-Hill, New York, 1953)

[BM53] A. Bohr, B. Mottelson, Mat. Fys. Medd. Dan. Vidensk. Selsk. **27**, 16 (1953)

[BO52] A. Bohr, Mat. Fys. Medd. Dan. Vid. Selsk **26**, 14 (1952)

[BM81] A. Bohr, B.R. Mottelson, Nucl. Phys. A **354**, 303c (1981)

[BR79] M. Badea, A.A. Raduta, Rev. Roum. Phys. **24**(8), 743 (1979)

[BEL59] S.T. Belyaev, Matt. Phys. Medd. **31**, 5–55 (1959)

[BAY60] B.F. Bayman, Nucl Phys. **15**, 33 (1960)

[BLME62] C. Bloch, A. Messiah, Nucl. Phys. **39**, 95 (1962)

[BMR73] B. Banerjee, H.J. Mang, P. Ring, Nucl. Phys. A **215**, 266 (1973)

[BHM78] R. Bengston, I. Hamamoto, B. Mottelson, Phys. Lett. **73 B**, 259 (1978)

[BZ62] S.T. Belyaev, V.G. Zelevinsky, Nucl. Phys. **39**, 582 (1962)

[BAL04] D.L. Balabanski et al., Phys. Rev. C **70**, 044305 (2004)

[BOMO98] A. Bohr, B. Mottelson, *Nuclear Structure*. Single Particle Motion, vol I (World Scientific, Singapore, 1998), p. 383

[BES59] D.R. Bes, Nucl. Phys. **10**, 373 (1959)

[BONA04] D. Bonatsos, D. Lenis, N. Minkov, D. Petrellis, P.P. Raychev, P.A. Terziev, Phys. Lett. B **584**, 40 (2004)

[BE59] D. Bés, Nucl. Phys. **210**, 373 (1959)

[BFH06] S. De Baerdenmacker, L. Fortunato, V. Hellemans, K. Heyde, Nucl. Phys. A **769**, 16 (2006)

[BCZM03] R. Bijker, R.F. Casten, N.V. Zamfir, E.A. McCutchan, Phys. Rev. C **68**, 064304 (2003)

[BLMPY07] D. Bonatsos, D. Lenis, E.A. McCutchan, D. Petrellis, I. Yigitoglu, Phys. Lett. B **649**, 394 (2007)

[BRD96] V. Baran, A.A. Raduta, D.S. Delion, Phys. Rev. E **54**, 3264 (1996)

[BR98] V. Baran, A.A. Raduta, Int. J. Mod. Phys. E **7**, 527 (1998)

[BE53] H. Bateman, A. Erdely, *Higher Transcendental Functions* (McGraw-Hill Book Company, Inc, New York, 1953), p. 199

[Buc06] D. Bucurescu et al., Phys. Rev. C **73**, 064309 (2006)

[BAG98] C.M. Baglin, NDS **84**, 717 (1998)

[BAG03] C.M. Baglin, NDS **99**, 1 (2003)

[BS96] E. Browne, B. Singh, NDS **79**, 277 (1996)

[BLMPY05] D. Bonatsos, D. Lenis, N. Minkov, D. Petrellis, P. Yotov, Phys. Rev. C **71**, 064309 (2005)

[BB08] P.G. Bizzeti, A.M. Bizzeti-Sona, Phys. Rev. C **77**, 024320 (2008)

[Btz96] H. Baltzer et al., Z. Phys. A **356**, 13 (1996); T. Weber et al., Z. Phys. **A358**, 281 (1997)

[Bak] C. Baktash, J.X. Saladin, J.J. O'Brien, J.G. Alassi, Phys. Rev. C **18**, 131 (1978)

[BN96] P.A. Butler, W. Nazarewicz, Rev. Mod. Phys. **68**, 349 (1996)

[BR78] G. Berrier-Ronsin et al., Phys. Rev. C **17**, 529 (1978)

[BON00] D. Bonatsos et al., Phys. Rev. C **62**, 024301 (2000)

[BRS83] D. Bohle, A. Richter, W. Steffen, A.E.L. Dieprink, N. Lo Iudice, F. Palumbo, O. Scholten, Phys. Lett. B **137**, 27 (1983)

[BBD84] U.E.P. Berg, C. Blassing, J. Drexler, R.D. Heil, U. Kneissl, W. Naatz, H. Ratzek, S. Schennach, R. Stock, T. Weber, H. Wickert, B. Fusher, H. Hollik, D. Kollewe, Phys. Lett. B **149**, 59 (1984)

[BKR84] D. Bohle, G. Kuhler, A. Richter, W. Steffen, Phys. Lett. B **148**, 260 (1984)

[BO86] D. Bohle et al., in *Invited Talk at the International Symposium on Weak and Electromagnetic Interactions in Nuclei*, Heidelberg, 1–5 July 1986

[BOH98] A. Bohrabcde, B. Mottelson, *Nuclear Structure*. Single Particle Motion, vol I (World Scientific, Singapore, 1998), p. 383

[CO99]   J.F.G. Cocks et al., Nucl. Phys. A **645**, 63 (1999)
[CO97]   J.F.G. Cocks et al., Phys. Rev. Lett. **78**, 2920 (1997)
[CH79]   R.R. Chassman, Phys. Rev. Lett. **42**, 630 (1979)
[CHS80]   R.R. Chassman, Phys. Lett. B **96**, 7 (1980)
[CaNi65]   P. Carruthers, M.M. Nieto, Phys. Rev. Lett. **14**, 387 (1965)
[CaNi68]   P. Carruthers, M.M. Nieto, Rev. Mod. Phys. **40**, 411 (1968)
[CAS31]   H.B.G. Casimir, *Rotation of a Rigid Body in Quantum Mechanics* (Wolters, Groningen, 1931)
[CA05]   M.A. Caprio, Phys. Rev. C **72**, 054323 (2005)
[CAR22]   E. Cartan, *Lecons Sur Les Invariants Integraux* (Herman, Paris, 1922)
[CHA63]   R.R. Chasman, Phys. Rev **132**, 343 (1963)
[CCJ66]   P. Camiz, A. Covello, M. Jean, N. Cim. **36**, 663 (1965); **42**, 199 (1966)
[COR12]   Coral M. Baglin, Nucl. Data Sheets **113**, 1871 (2012)
[CRS74]   V. Ceausescu, A.A. Raduta, Progress Theoret. Phys. **52**, 903 (1974)
[CO76]   T. Cooper et al., Phys. Rev. C **13**, 1083 (1976)
[CLAR68]   R.M. Clark et al., Phys. Rev. C **68**, 037301 (2003)
[CHMO76]   E. Chacon, M. Moshinski, R.T. Sharp, J. Math. Phys. **17**, 668 (1976)
[CMW76]   T.M. Corrigan, F.J. Margetan, S.A. Williams, Phys. Rev. C **14**, 2279 (1976)
[CR74]   V. Ceausescu, A.A. Raduta, Progress Theoret. Phys. **52**(3), 903 (1974)
[CR76]   V. Ceausescu, A.A. Raduta, Ann. Phys. **100**, 94 (1976)
[CAIA81]   R.F. Casten, in *Interacting Bose-Fermi Systems in Nuclei*, ed. by F. Iachello (Plenum, New York, 1981), p. 1
[CAZA00]   R.F. Casten, N.V. Zamfir, Phys. Rev. Lett. **85**, 3584 (2000)
[CAZA01]   R.F. Casten, N.V. Zamfir, Phys. Rev. Lett. **87**, 052503 (2001)
[CLCR04]   R.M. Clark, M. Cromaz, M.A. Deleplanque, M. Descovich, R.M. Diamond, P. Fallon, I.Y. Lee, A.O. Macchiavelli, H. Mahmud, E. Rodriguez-Vieitez, F.S. Stephens, D. Ward, Phys. Rev. C **69**, 064322 (2004)
[CCI08]   M.A. Caprio, P. Cejnar, F. Iachello, Ann. Phys. NY, **323**, 1106 (2008). arXiv:0707.0325v1[quant-ph]
[CL03]   R.M. Clark et al., Phys. Rev. C **68**, 037301 (2003)
[CB98]   Coral M. Baglinab, NDS **84**, 717 (1998)
[CA04]   M.A. Caprio, Phys. Rev. C **69**, 044307 (2004)
[CAM93]   M.C. Cambiaggio, in "The Building Blocks of Nuclear Structure", Amalfi, 1992, ed. by A. Covello (World Scientific, Singapore, 1993), p. 293
[CGT88]   Z. Chunmei, W. Gongqing, T. Zhenlan, NDS **83**, 145 (1988)
[CH02]   F.E. Chukreev, V.E. Makarenko, M.J. Martin, NDS **97**, 129 (2002)
[ChSi04]   F.E. Chukreev, B. Singh, NDS **103**, 325 (2004)
[COT87]   P.D. Cottle et al., Phys. Rev. C **36**, 2286 (1987)
[CBH87]   R.F. Casten, D.F. Brener, P.E. Haustein, Phys. Rev. Lett. **58**, 658 (1987); R.F. Casten, K. Heyde, A. Wolf, Phys. Lett. B **208**, 33 (1988)
[Dir27]   P.A.M. Dirac, Proc. Roy. Soc. (Lond.) **A114**, 243 (1927)
[DDK70]   T.D.K. Das, R.M. Dreizler, A. Klein, Phys. Rev. C **2**, 632 (1970)
[Dav32]   P.M. Davidson, Proc. R. Soc. London Ser. A **135**, 459 (1932)
[DF58]   A.S. Davydov, G.F. Filippov, Nucl. Phys. **8**, 237 (1958)
[DAV68]   J.P. Davidson, *Collective Models of the Nucleus* (Academic Press, New York, 1968)
[DYS56]   J.F. Dyson, Phys. Rev. **102**, 1217 (1956)
[DOP82]   S. Drozdz, J. Okolowicz, M. Ploszajczak, Phys. Lett. B **115**, 161 (1982)
[DO81]   J. Dobaczeski, Nucl. Phys. A **369**, 213, 237 (1981); A **380**, 1 (1982)
[DSI80]   A.E.L. Dieperink, O. Scholten, F. Iachello, Phys. Rev. Lett. **44**, 1747 (1980)
[DALI02]   Da-li Zhang, Yu-xin Liu, Phys. Rev. C **65**, 057301 (2002)
[DZ95]   V.Y. Denisov, A. Ya Dzyublik, Nucl. Phys. A **589**, 17 (1995)
[DI83]   A.E.L. Dieperink, Prog. Part. Nucl. Phys. **9**, 121 (1983)

[ERD55]   A. Erdelyi, *Higher Transcedental Functions*, vol. 3 (McGraw-Hill, New York, 1955)
[ERS93]   J.L. Egido, L.M. Robledo, Y. Sun, Nucl. Phys. A **560**, 253 (1993)
[ER03]   J.L. Egido, L.M. Robledo, Lect. Notes Phys. **641**, 269 (2004). arXiv.org/abs/nucl-th/0311106v1, 28 November 2003
[EEP86]   J.P. Elliot, J.A. Evans, P. Park, Phys. Lett. B **169**, 309 (1986)
[EIGR70]   J.M. Eisenberg, W. Greiner, *Nuclear Models*, vol 1 (North-Holland, Amsterdam, 1970) (ch. 6)
[FRA01]   S. Frauendorf, Rev. Mod. Phys. **73**, 463 (2001)
[FOM70]   V.N. Fomenko, J. Phys. A **3**, 8 (1970)
[FLVU63]   B.H. Flowers, M. Vujicic, Nucl. Phys. **49**, 586 (1963)
[FLO52]   B.H. Flowers, Proc. Roy. Soc. A **212**, 248 (1952)
[FDO98]   F. Pan, J.P. Draayer, W.E. Ormand, Phys. Lett. B **422**, 1 (1998)
[FA76]   A. Faessler, K.R. Sandhya Devi, F. Grümmer, K.W. Schmid, R.R. Hilton, Nucl. Phys. A **256**, 106 (1976)
[FG80]   H. Feng, R. Gilmore, Phys. Lett. B **90**, 327 (1980)
[FI72]   M. Finger et al., Nucl. Phys. A **188**, 369 (1972); B. Richter et al., Nucl. Phys. A **319**, 221 (1979)
[FPI84]   G. De Francheschi, F. Palumbo, N. Lo Iudice, Phys. Rev. C **29**, 1496 (1984)
[FRA97]   S. Frauendorf, J. Meng, Nucl. Phys. A **617**, 131 (1997)
[FOVI03]   L. Fortunato, A. Vitturi, J. Phys. G **29**, 1341 (2003)
[FO05]   L. Fortunato, Eur. Phys. J. A **26**, s01 (2005). arXiv.org/abs/Nucl-Th/0411087v1
[FP78]   A. Faessler, M. Ploszajczak, Phys. Lett. B **76**, 1 (1978)
[FAA01]   A. Frank, C.E. Alonso, J.M. Arias, Phys. Rev. C **65**, 014301 (2001)
[FaGr62]   A. Faessler, W. Greiner, Z. Phys. **168**, 425 (1962); **170**, 105 (1962); **177**, 190 (1964); A. Faessler, Nucl. Phys. **59**, 177 (1964); A. Faessler, W. Greiner, R.K. Sheline, ibid **62**, 241 (1965); **70**, 33 (1965)
[FJ98]   D. De Frenne, E. Jacobs, NDS **83**, 535 (1998)
[FUN75]   L. Funke, P. Kemnitz, G. Winter, A.A. Hiorth, A. Johnson, Th Linblad, Phys. Lett. B **55**, 436 (1975)
[FING72]   M. Finger et al., Nucl. Phys. A **188**, 369 (1972)
[FA66]   A. Faessler, Nucl. Phys. **85**, 417 (1966)
[GRF07]   A.C. Gheorghe, A.A. Raduta, A. Faessler, Phys. Lett. B **648**, 171 (2007)
[GRC78]   A. Gheorghe, A.A. Raduta, V. Ceausescu, Nucl. Phys. A **296**, 228 (1978)
[GRC98]   A. Gheorghe, A.A. Raduta, V. Ceausescu, Nucl. Phys. A **637**, 201 (1998)
[GOS64]   A. Goswami, Nucl. Phys. **60**, 228 (1964)
[GOO79]   A.L. Goodman, Adv. Nucl. Phys. **11**, 263 (1979)
[GOO98]   A.L. Goodman, Phys. Rev. C **58**, R3051 (1998)
[GSF79]   F. Grümmer, K.W. Schmid, A. Faessler, Nucl. Phys. **326**, 1 (1979)
[GLNN67]   G. Gustafson, I.L. Lamm, B. Nilsson, S.G. Nilsson, Ark. Fys. **36**, 613 (1967)
[GAR01]   P.E. Garrett, J. Phys. G Nucl. Part. Phys. **27**, R1–R22 (2001)
[GMG69]   G. Gneus, U. Mosel, W. Greiner, Phys. Lett. B **30** 397 (1969)
[GG71]   G. Gneuss, W. Greiner, Nucl. Phys. A **171**, 449 (1971)
[GIKI80]   J.H. Ginocchio, M.W. Kirson, Phys. Rev. Lett. **44**, 1744 (1980)
[GER97]   E. Garrote, J.L. Egido, R.M. Robledo, Phys. Lett. B **410**, 86 (1997)
[GNSC95]   A. Giannatiempo, A. Nannini, P. Sona, D. Cutoiu, Phys. Rev. C **52**, 2969 (1995)
[GrMa96]   W. Greiner, J. Maruhn, *Nuclear Models* (Springer, Berlin, 1996)
[GrRy65]   I.S. Gradshtein, I.M. Ryzhik, *Table of Integrals, Series and Products* (Academic, New York, 1965), pp. 904, 917 and 919
[GRO98]   J. Gröger, T. Weber, J. de Boer, H. Baltzer, K. Freitag, A. Gollwitzer, G. Graw, C. Günter, Acta Phys. Pol. **29**, 365 (1998)
[GHK83]   C. Girit, W.D. Hamilton, C.A. Katfas, J. Phys. G Nucl. Phys. **9**, 797 (1983)
[GER98]   E. Garrote, J.L. Egido, L.M. Robledo, Phys. Rev. Lett. **80**, 4398 (1998)

[GHK77]   C. Gunther, H. Hubel, A. Kleinrahm, D. Mertin, B. Richter, W.D. Schneider, R. Tischler, Phys. Rev. C **15**, 1298 (1977)

[GR64]   W. Greiner, Phys. Rev. Lett. **14**, 599 (1965); W. Greiner, Nucl. Phys. **80**, 417 (1966); A. Faessler, W. Greiner, Z. Phys. **179**, 343 (1964)

[GKP70]   S.I. Gabrakov, A.A. Kuliev, N.I. Pyatov, Yad. Fiz. **12**, 82 (1970); (Sov. J. Nucl. Phys. **12**, 44 (1971)); S.I. Gabrakov, A.A. Kuliev, N.I. Pyatov, D.I. Salamov, H. Schulz, Nucl. Phys. A **182**, 625 (1972)

[GMU91]   E. Garrido, E. Moya de Guerra, P. Sarriguren, J.M. Udias, Phys. Rev. C **44**, R1250 (1991)

[GAR01]   P.E. Garrettab, J. Phys. G Nucl. Part. Phys. **27**, R1–R22 (2001)

[GAC01]   Z. Gacsi et al., Phys. Rev. **64**, 047303 (2001)

[GR04]   A. Gheorghe, A.A. Raduta, J. Phys. A Math. Gen. **37**, 10951 (2004)

[H65]   K.T. Hecht, Nucl. Phys. **63**, 177 (1965)

[HHL70]   P. Haapakoski, T. Honkaranta, P.O. Lipas, Phys. Lett. B **31**, 493 (1970)

[Hol80]   A.S. Holevo, *Probabilistic and Statistical Aspects of Quantum Theory*, 2nd edn. Edizioni della Normale, Pisa, 2011, pp. 204–211, ISBN: 978-88-7642-375-8 Nauka, Moscow, (1980) (Russian translation)

[Harr65] S.M. Harris, Phys. Rev. B **138**, 509 (1965)

[HoLi68] P. Holmberg, P.O. Lipas, Nucl. Phys. A **117**, 552 (1968)

[Hel04]   R.G. Helmer, NDS **101**, 325 (2004)

[HR99]   R.G. Helmer, C.W. Reich, NDS **87**, 317 (1999)

[HA02]   I. Hamamoto, Phys. Rev. C **65**, 044305 (2002)

[HA76]   I. Hamamoto, Nucl. Phys. A **271**, 15 (1976)

[HMO83]   I. Hamamoto, B.R. Mottelson, Phys. Lett. B **127**, 281 (1983)

[HolPr40] T. Holstein, H. Primakoff, Phys. Rev. **58**, 1098 (1940)

[Ho68]   G. Holzwarth, Nucl. Phys. A **113**, 448 (1968) (156 (1970) 511; 174 (1971) 97)

[HMG81]   P. Hess, J. Maruhn, W. Greiner, Phys. Rev. C **23**, 2335 (1981) (J. Phys. G, **7** (1981) 737)

[HHZ89]   I. Hamamoto, J. Holler, X.Z. Zhang, Phys. Lett. B **226**, 17 (1989)

[HM91]   I. Hamamoto, C. Magnusson, Phys. Lett. B **260**, 6 (1991)

[HSMG80] P.O. Hess, M. Seiwert, J. Maruhn, W. Greiner, Z. Physik A **296**, 147 (1980)

[HMG81]   P.O. Hess, J. Maruhn, W. Greiner, J. Phys. G Nucl. Phys. **7**, 737 (1981)

[Iac00]   F. Iachello, Phys. Rev. Lett. **85**, 3580 (2000)

[IA01]   F. Iachello, Phys. Rev. Lett. **87**, 052502 (2001) (ibid. 132502)

[IUPA78] N. Lo Iudice, F. Palumbo, Phys. Rev. Lett. **74**, 1046 (1978)

[IY83]   S. Iida, M. Yamamura, Progress Theoret. Phys. **70**(3), 783–790 (1983)

[ISO73]   A. Ikeda, R.K. Sheline, N. Onishi, Phys. Lett. **44B**, 39 (1973)

[IKMO79] A. Ikeda, M. Kitajima, M. Miyawaki, N. Onishi, Phys. Lett. **85B**, 172 (1979)

[IO83]   A. Ikeda, N. Onishi, Progress Theoret. Phys. **70**, 128 (1983)

[I81]   A. Ikeda, Phys. Rev. C **24**, 1656 (1981)

[IAAR87] F. Iachello, A. Arima, *The Interacting Boson Model* (Cambridge University Press, Cambridge, 1987)

[IA03]   F. Iachello, Phys. Rev. Lett. **91**(132), 502 (2003)

[IPF84]   N. Lo Iudice, F. Palumbo, Phys. Rev. Lett. **74**, 1046 (1978); G. De Franceschi, F. Palumbo, N. Lo Iudice, Phys. Rev. C **29**, 1496 (1984)

[IA81]   F. Iachello, Nucl. Phys. **A358**, 89c (1981)

[IUD95]   N. Lo Iudice, Prog. Part. Phys. **34**, 309 (1995)

[IRD93]   N. Lo Iudice, A.A. Raduta, D.S. Delion, Phys. Lett. B **300**, 195 (1993); Phys. Rev. C **50**, 127 (1994)

[ISS04]   N. Lo Iudice, A.V. Sushkov, N.Y. Shirikova, Phys. Rev. C **70** 064316 (2004)

[JENS02] D.R. Jensen et al., Nucl. Phys. A **703**, 3 (2002)

[JM69]   M. Jean, *Proc* (Predeal Summer School, Predeal, Romania, 1969)

[JDFJ71] D. Janssen, F. Dönau, S. Frauendorf, R.V. Jolos, Nucl. Phys. A **172**, 145 (1971)

[JEN99]   A.P. Jenkins et al., Phys. Rev. Lett. **83**, 500 (1999)

[JZ59]   Z. Jankovic, Nuovo Cimento **14**, 1174 (1959)
[JL95]   J. Jolie, H. Lehmann, Phys. Lett. B **342**, 1 (1995)
[JAJO76]   D. Jansen, V. Jolos, Preprint JINR, E4–9533, Dubna, 1976
[JNH77]   A. Johnson, R. Noah, P.P. Hubert, E. Eichler, D.G. Sarantites, J. Urban, S.W. Yates, T. Linblad, Phys. Rev. C **15**, 1325 (1977)
[JLF76]   A. Johnson, Th Linblad, L. Funke, P. Kemnitz, G. Winter, Nucl. Phys. A **262**, 328 (1976)
[Jol74]   R.V. Jolos, F. Dönau, D. Janssen, Teor. Mat. Fys. **20**, 112 (1974)
[Ja74]   D. Janssen, R.V. Jolos, F. Dönau, Nucl. Phys. A **224**, 93 (1974)
[Jol75]   R.V. Jolos, F. Dönau, D. Janssen, Yad. Fiz. **22**, 965 (1975)
[KLLI81]   A. Klein, C.T. Li, Phys. Rev. Lett. **46**, 895 (1981)
[KS80]   H. Kuratsuji, T. Suzuki, J. Math. Phys. **21**, 472 (1980)
[KLMA91]   A. Klein, E.R. Marshalek, Rev. Mod. Phys. **63**, 375 (1991)
[KISO60]   L.S. Kisslinger, R.A. Sorensen, Mat. Fys. Medd. Dan. Vid. Selsk. **32**, 16 (1960)
[KISO63]   L.S. Kisslinger, R.A. Sorensen, Rev. Mod. Phys. **35**, 853 (1963)
[KMU82]   A. Klein, T. Marumori, T. Une, Phys. Lett. B **109**, 237 (1982)
[KGLD79]   K.K. Kan, J.J. Griffin, P. C. Lichtnerand M. Dworzecka, Nucl. Phys. A **232**, 109 (1979); K.K. Kan, Phys. Rev. C **24**, 279 (1981)
[KS73]   J. Krumlinde, Z. Szymanski, Ann. Phys. **79**, 201 (1973)
[KT71]   T. Kishimoto, T. Tamura, Nucl. Phys. A **163** 100 (1971); A **192**, 246 (1972)
[KY81]   K. Kuriama, M. Yamamura, Progress Theoret. Phys. **65**, 2130 (1981)
[KIR67]   D.A. Kirzhnits, *Field Theoretical Methods in Many-body Systems*, ed. by D.M. Brink (Pergamon Press Ltd., Oxfor, 1967)
[KISP05]   T. Kibedi, R.H. Spear, At. Data Nucl. Data Tables **89**, 77 (2005)
[KR02]   R. Krücken et al., Phys. Rev. Lett. **88**, 232501 (2002)
[KaGr79]   K.K. Kan, J.J. Griffin, P.C. Lichtner, M. Dworzecka, Nucl. Phys. A **232**, 109 (1979); K.K. Kan, Phys. Rev. C **24**, 279 (1981)
[KLM61]   A.K. Kerman, R.D. Lawson, M.H. Macfarlane, Phys. Rev. **124**, 162 (1961); R.K. Richardson, Phys. Rev. **141**, 949 (1966)
[KK02]   J. Katakura, K. Kitao, NDS **97**, 765 (2002)
[Ku67]   K. Kumar, Nucl. Phys. A **92**, 652 (1967), A **231** 189 (1974)
[KT72]   T. Kishimoto, T. Tamura, Nucl. Phys. A **192**, 264 (1972), A **270** 317 (1976)
[KOP81]   Th Koppel, A. Faessler, U. Gotz, Nucl. Phys. A **403**, 263 (1983)
[KB68]   K. Kumar, M. Baranger, Nucl. Phys. A **122**, 273 (1968); M. Baranger, K. Kumar, Nucl. Phys. A **110**, 490 (1969)
[Kch]   K. Kirch, G. Siems, M. Eshenauer, A. Gelberg, R. Kuhn, A. Mertens, U. Neuneyer, O. Vogel, I. Wiedenhover, P. von Bretano, T. Otsuka, Nucl. Phys. A **587**, 211 (1995)
[KP74]   A.A. Kuliev, N.I. Pyatov, Yad. Fiz. **20**, 297 (1974)
[Loui63]   W.H. Louisell, Phys. Lett. **7**, 60 (1963)
[Lev65]   R.D. Levine, J. Chem. Phys. **44**, 3597 (1965)
[LMG]   H.J. Lipkin, N. Meshkov, A.J. Glick, Nucl. Phys. **62**, 188 (1965)
[LA64]   A.M. Lane, *Nuclear Theory* (Benjamin, New York, 1964)
[LNP80]   S. Levit, J.W. Negele, Z. Paltiel, Phys. Rev. C **21**, 1603 (1980); S. Levit, Phys. Rev. C **21**, 1594 (1980); Phys. Lett. B **99**, 444 (1981)
[LOIU97]   N. Lo Iudice, Phys. Part. Nucl. **25**, 556 (1997)
[LES02]   S.R. Lesher et al., Phys. Rev. C **66**, 051305(R) (2002)
[LOPA78]   N. Lo Iudice, F. Palumbo, Phys. Rev. Lett. **41**, 1532 (1978); G. De Francheschi, F. Palumbo, N. Lo Iudice, Phys. Rev. C **29**, 1496 (1984)
[LKH82]   J. Lange, K. Kumar, J.H. Hamilton, Rev. Mod. Phys. **54**, 119 (1982)
[LI83]   P.O. Lipas et al., Phys. Scr. **7**, 8 (1983)
[LEJO95]   H. Lehmann, J. Jolie, Nucl. Phys. A **588**, 623 (1995)
[LA04]   G. Lévai, J.M. Arias, Phys. Rev. C **69**, 014304 (2004)
[LA10]   G. Lévai, J.M. Arias, Phys. Rev. C **81**, 044304 (2010)
[LiMe65]   H.J. Lipkin, N. Meshkov, A.J. Glick, Nucl. Phys. **62**, 188 (1965)

[LaMa94]   R. Landauer, Th Martin, Rev. Mod. Phys. **66**, 217 (1994)
[LRR99]   G.A. Lalazissis, S. Raman, P. Ring, At. Data Nucl. Data Tables **71**, 140 (1999)
[LB06]   D. Lenis, D. Bonatsos, Phys. Lett. B **633**, 474 (2006)
[LS69]   P.O. Lipas, J. Savolainen, Nucl. Phys. A **130**, 77–87 (1969)
[LHH76]   P.O. Lipas, P. Haapakoski, T. Honkaranta, Phys. Scr. **13**, 339 (1976)
[LANC90]   C. Lanczos, J. Res. Natl. Bur. Stand. **45**, 55 (1990)
[LEA82]   G.A. Leander et al., Nucl. Phys. A **388**, 452 (1982)
[LU09]   Y.X. Luo et al., Phys. Lett. B **670**, 307 (2009)
[MN81]   P. Moller, J.R. Nix, Nucl. Phys. A **361**, 117 (1981)
[MSB69]   A.A.J. Mariscotti, G. Scharff-Goldhaber, B. Buch, Phys. Rev. **178**, 1864 (1969)
[MSD74]   J. Meyer-ter-Vehn, F.S. Stephens, R.M. Diamond, Phys. Rev. Lett. **32**, 1383 (1974); J. Meyer-ter-Vehn, Nucl. Phys. A **249** 111, 141 (1975)
[MAK06]   Makito Oi, Phys. Lett. B **635**, 30 (2006)
[MOY86]   E. Moya de Guerra, Phys. Rep. **138**(6), 293 (1986)
[MOY77]   E. Moya de Guerra, F. Villars, Nucl. Phys. A **285**, 297 (1977); A **298**, 109 (1978)
[Ma77]   T. Marumori, Progress Theoret. Phys. **57**, 112 (1977)
[MP82]   A.K. Mukerje, M.K. Pal, Nucl. Phys. A **373**, 289 (1982)
[MSMUH82]   T. Marumori, F. Sakata, T. Maskawa, T. Une, Y. Hashimoto, in *Nuclear Collective Dynamics*, ed. by D. Bucurescu, V. Ceausescu, N. Zamfir. Lecture of the 1982 Rasov International Summer School of Nuclear Physics, Poiana Brasov, Romania
[MV75]   J. Meyer-ter-Vehn, Nucl. Phys. A **249**(111), 141 (1975)
[Ma78]   E.R. Marshalek, Nucleonika **23**, 409 (1978)
[MYT64]   T. Marumori, M. Yamamura, A. Tokynaga, Progress Theoret. Phys. **31**, 1009 (1964)
[MYTT64]   T. Marumori, M. Yamamura, A. Tokynaga, K. Takada, Progress Theoret. Phys. **32**, 726 (1964)
[M7174]   E.R. Marshalek, Nucl. Phys. A **161**, 401 (1971); A **224**, 221, 248 (1974)
[MOCA96]   Enrique Lopez-Moreno, Octavio Castanos, Phys. Rev. C **54**, 2374 (1996)
[MaYaTo64] T. Marumori, M. Yamamura, A. Tokunaga, Progress Theoret. Phys. **31**, 1009 (1964)
[Moz58]   S.A. Moszkovski, Phys. Rev. **110**, 403 (1958)
[MaShBu69] M.A.J. Mariscotti, G. Sharff-Goldhaber, B. Buck, Phys. Rev. **178**, 1864 (1969)
[MATU95]   E. der Mateosian, J.K. Tuli, NDS **75**, 827 (1995)
[MBZC07]   E.A. McCutchan, D. Bonatsos, N.V. Zamfir, R.F. Casten, Phys. Rev. C **76**, 024306 (2007)
[MFK97]   U. Meyer, Amand Faessler, S.B. Khadkikar, Nucl. Phys. A **624**, 391 (1997); Prog. Part. Nucl. Phys. **38**, 241 (1997)
[MRF98]   U. Meyer, A.A. Raduta, A. Faessler, Nucl. Phys. A **637**, 321 (1998)
[MoVa60]   B. Mottelson, T.G. Valatin, Phys. Rev. Lett. **5**, 511 (1960)
[MS67]   W.D. Myers, W.J. Swiatecki, Ark. Fys. **36**, 343 (1967)
[MGM75]   V. Maruhn-Rezwani, W. Greiner, J.A. Maruhn, Phys. Lett **57**, 109 (1975)
[MUK07]   S. Mukhopadhyay et al., Phys. Rev. Lett. **99**, 172501 (2007)
[MOO93]   W.H.L. Moonen et al., J. Phys. G **19**, 635 (1993)
[MNMS95]   P. Möller, J.R. Nix, W.D. Myers, W.J. Swyatecki, At. Data Nucl. Data Tables **59**, 185 (1995)
[MtV79]   J. Meyer-ter-Vehn, in *Interacting Bosons in Nuclear Physics*, ed. F. Iachello (Plenum Press, New York, p. 157)
[NVR75]   K. Neergard, P. Vogel, M. Radomski, Nucl. Phys. A **238**, 231 (1975)
[NIL55]   S.G. Nilsson, Mat. Fys. Medd. K. Dan. Vid. Selsk. **29**(16), 1 (1955)
[Ne85]   John W. Negele, Phys. Today **38**, 24 (1985)
[P73]   I.C. Percival, J. Phys. **B6**, 225 (1973)
[P68]   J. da Providencia, Nucl. Phys. **A108**, 589 (1968)
[PW70]   J. da Providencia, J. Weneser, Phys. Rev. **1**(3), 825 (1970)
[PET96]   C.M. Petrache et al., Nucl. Phys. **A597**, 106 (1996)

[PET06]   C.M. Petrache, G.B. Hegemann, I. Hamamoto, K. Starosta, Phys. Rev. Lett. **96**, 112502 (2006)
[PARA03]   G. Palma, U. Raff, Am. J. Phys. **71**, 956 (2003)
[PBM81]   A.P. Prudnikov, Y.A. Brichkov, O.I. Marichev, *Integrali i riadi* (Moskva, Nauka, 1981), pp. 74,82,84,76,110 and 112
[PL71]   H.C. Pauli, T. Ledergerber, Nucl. Phys. A **175**, 545 (1971)
[PI75]   M. Piiparinen et al., Phys. Rev. Lett. **34**(17), 1110 (1975)
[PA86]   F. Palumbo, in *Symmetries and Semiclassical Features of Nuclear Dynamics*, ed. A.A. Raduta (Springer, Berlin, 1986)
[Par79]   V. Paar, in *Interacting Bosons in Nuclear Physics*, ed. F. Iachello (Plenum Press, New York, 1979), p. 163
[RBD95]   A.A. Raduta, V. Baran, D.S. Delion, Nucl. Phys. A **588**, 431 (1995)
[RBF11]   A.A. Raduta, R. Budaca, A. Faessler, J. Phys. G Nucl. Part. Phys. **38**, 055102 (2011)
[RD76]   A.A. Raduta, R.M. Dreizler, Nucl. Phys. A **258**, 109 (1976)
[RCGD82]   A.A. Raduta, V. Ceausescu, A. Gheorghe, R.M. Dreizler, Nucl. Phys. A **381**, 253 (1981); Phys. Lett. B **99**, 444 (1982)
[RBF12]   A.A. Raduta, R. Budaca, A. Faessler, Ann. Phys. [NY] **327**, (2012) 671
[RS83]   A.A. Raduta, C. Sabac, Ann. Phys. (NY) **148**, 1–31 (1983)
[RSS84]   A.A. Raduta, S. Stoica, N. Sandulescu, Rev. Roum. Phys. **29**, 55 (1984)
[RF05]   A.A. Raduta, A. Faessler, J. Phys. G **31**, 873–901 (2005)
[RGF05]   A.A. Raduta, A. Gheorghe, A. Faessler, J. Phys. G **31**, 337 (2005)
[RGBF09]   A.A. Raduta, A.C. Gheorghe, P. Buganu, A. Faessler, Nucl. Phys. A **819**, 46–78 (2009)
[RH98]   C.W. Reich, R.G. Helmer, NDS **85**, 171 (1998)
[Rei03]   C.W. Reich, NDS **99**, 753 (2003)
[Rei96]   C.W. Reich, NDS **78**, 547 (1996)
[RBB77]   A.A. Raduta, M. Badea, E. Badralexe, J. Math. Phys. **18**, 648 (1977)
[RCG78]   A.A. Raduta, V. Ceausescu, A. Gheorghe, Nucl. Phys. A **311**, 118 (1978)
[RCGP84]   A.A. Raduta, V. Ceuasescu, A. Gheorghe, M.S. Popa, Nucl. Phys. A **427**, 1 (1984)
[RBR07]   A.A. Raduta, R. Budaca, C.M. Raduta, Phys. Rev. C **76**, 064309 (2007)
[RBB76]   A.A. Raduta, E. Badralexe, M. Badea, Revue Roum. Phys. **21**, 959 (1976)
[RISH64]   R.W. Richardson, N. Sherman, Nucl. Phys. **52**, 221 (1964) (it ibid 253)
[RB76]   J. Rowe, R. Basserman, Can. J. Phys. **54**, 1941 (1976)
[RG78]   G. Reinhard, M. Goeke, Nucl. Phys. A **312**, 121 (1978)
[RE80]   H. Reinhardt, Nucl. Phys. **346**, 1 (1980)
[RCD76]   A.A. Raduta, V. Ceausescu, R.M. Dreizler, Nucl. Phys. A **272**, 11 (1976)
[RLF83]   A.A. Raduta, C. Lima, A. Faessler, Phys. Lett. B **121**, 1 (1983); Z. Phys. A **313**, 69 (1983)
[RS77]   P. Ring, P. Schuck, Phys. Rev. C **16**, 801 (1977)
[RCSS73]   A.A. Raduta, V. Ceausescu, G. Stratan, A. Sandulescu, Phys. Rev. C **8**, 1525 (1973)
[RG00]   A.A. Raduta, E. Moya de Guerra, Ann. Phys. **284**, 134 (2000)
[RUD87]   A.A. Raduta, I.I. Ursu, D.S. Delion, Nucl. Phys. A **475**, 439 (1987)
[RD89]   A.A. Raduta, D.S. Delion, Nucl. Phys. A **491**, 24 (1989)
[RUF88]   A.A. Raduta, I.I. Ursu, A. Faessler, Nucl. Phys. A **489**, 20 (1988)
[REG02]   A.A. Raduta, A. Escuderos, E. Moya de Guerra, Phys. Rev. C **65**, 0243121 (2002)
[RIUU95]   A.A. Raduta, N. Lo Iudice, I.I. Ursu, Nucl. Phys. **584**, 84 (1995)
[R95]   A.A. Raduta, Phys. Rev C **A51**, 2973 (1995)
[RRF06]   A.A. Raduta, C.M. Raduta, A. Faessler, Phys. Lett. B **635**, 80 (2006)
[RRR06]   A.A. Raduta, A.H. Raduta, C.M. Raduta, Phys. Rev. C **74**, 044312 (2006)
[RA09]   A.A. Raduta et al., Phys. Rev. C **80**, 044327 (2009)
[ROB94]   L.M. Robledo, Phys. Rev. C **50**, 2874 (1994)
[RER02]   R.R. Guzman, J.L. Egido, L.M. Robledo, Nucl. Phys. A **709**, 201 (2002)
[RFC87]   A.A. Raduta, A. Faessler, V. Ceausescu, Phys. Rev. C **36**, 439 (1987)

[RGB77]   A.A. Raduta, A. Gheorghe, M. Badea, Z. Phys. A **283**, 79 (1977)
[RAD04]   A.A. Raduta, Coherent State Model for several collective interacting bands, in *Recent Research Developments in Nuclear Physics*, vol 1 (Transworld Research Network, Trivandrum, Kerala, India, 2004), pp. 1–70. ISBN:81-7895-124-X
[RGG82]   S.G. Rohozinski, M. Gajda, W. Greiner, J. Phys. G Nucl. Phys. **8**, 787 (1982)
[ROH78]   S.G. Rohozinski, J. Phys. G Nucl. Phys. **4**, 1075 (1978)
[ROGR80]   S.G. Rohozinski, W. Greiner, J. Phys. G Nucl. Phys. **6**, 969 (1980)
[RO04]   D.J. Rowe, Nucl. Phys. A **745**, 47 (2004)
[RORO05]   G. Rosensteel, D.J. Rowe, Nucl. Phys. A **759**, 92 (2005)
[RGF05]   A.A. Raduta, A. Gheorghe, A. Faessler, J. Phys. G Nucl. Part. Phys. **31**, 337 (2005)
[RAU06]   A.A. Raduta, F.D. Aaron, I.I. Ursu, Nucl. Phys. A **772**, 20 (2006)
[RO04]   D.J. Rowe, Nucl. Phys. A **735**, 372 (2004)
[RB98]   D.J. Rowe, C. Bahri, J. Phys. A **31**, 4947 (1998)
[RIUF03]   A.A. Raduta, D. Ionescu, I.I. Ursu, A. Faessler, Nucl. Phys. A **720**, 43 (2003)
[ROSE57]   M.E. Rose, *Elementary Theory of Angular Momentum* (Wiley, New York, 1957)
[RPB03]   A.A. Raduta, L. Pacearescu, V. Baran, Phys. Rev. C **67**, 014301 (2003)
[RiSh80]   P. Ring, P. Schuck, *The Nuclear many Body Problem* (Springer, Berlin, 1980), p. 198
[ReiSc82] H. Reinhardt, H. Schulz, Nucl. Phys. A **391**, 36 (1982)
[RBF10]   A.A. Raduta, R. Budaca, A. Faessler, J. Phys. G; Nucl. Part. Phys., **37**, 085108 (2010)
[RBUG11]   A.A. Raduta, P. Buganu, Phys. Rev. C **83**, 034313 (2011)
[Ra76]   A.A. Raduta, Phys. Lett. B, **63**, 14 (1976)
[RB76]   A.A. Raduta, M. Badea, Z. Phys. A **278**, 81 (1976)
[RCGD81]   A.A. Raduta, V. Ceausescu, A. Gheorghe, R.D. Dreizler, Phys. Lett. B **99**, 444 (1981)
[ROUL78]   C. Roulet et al., Phys. Scr. **17**, 487 (1978)
[RASA86]   A.A. Raduta, N. Sandulescu, Rev. Roum. Phys. **31**(8), 765 (1986)
[RAD83]   A.A. Raduta, Rev. Roum. Phys. **28**(3), 195 (1983)
[RKF83]   A.A. Raduta, A. Faessler, T. Koppel, C. Lima, Z. Phys. A **312**, 233 (1983)
[RRF97]   A.A. Raduta, A.H. Raduta, A. Faessler, Phys. Rev. C **55**, 1747 (1997); J. Phys. G **23**, 149 (1997); A.A. Raduta, A. Faessler, R.K. Sheline, Phys. Rev. C **57**, 1512 (1998)
[RIF02]   A.A. Raduta, D. Ionescu, A. Faessler, Phys. Rev. C **65**, 064322 (2002)
[RI03]   A.A. Raduta, D. Ionescu, Phys. Rev. C **67**, 044312 (2003)
[SGR88]   S.G. Rohozinski, Rep. Prog. Phys. **51**, 541 (1988)
[RRF09]   A.A. Raduta, C.M. Raduta, A. Faessler, Phys. Rev. C **80**, 044327 (2009)
[RS87]   A.A. Raduta, S. Stoica, Z. Phys. A **327**, 275 (1987)
[RBWW79]   B. Richter, H. Backe, F. Weik, R. Willwater, Nucl. Phys. A **319**, 221 (1979)
[ROT80]   G. Rotbard et al., Phys. Rev. C **21**, 1232 (1980)
[RI90]   A. Richter, Nucl. A. Phys. **507**, 99c (1990); A **522**, 139c (1991); A **553**, 417 (1993). Prog. Part. Nucl. Phys. **34**, 261 (1995)
[RICH85]   A. Richter, in *Nuclear Structure*, ed. R. Broglia, G.B. Hagemann, B. Herskind (Benjamin, Reading, 1985)
[RNW71]   N. Rud, K.B. Nielsen, K. Wilsky, Nucl. Phys. A **167**, 401 (1971)
[RRW91]   C. Rangacharyulu, A. Richter, H.J. Wortche, W. Ziegler, R. Casten, Phys. Rev. C **43**, R949 (1991)
[RDI93]   A.A. Raduta, D.S. Delion, N. Lo Iudice, Nucl. Phys. A **564**, 185 (1993)
[RGG01]   A.A. Raduta, E. Garrido, E. Moya de Guerra, Eur. Phys. J. D **15**, 65 (2001)
[REF04]   A.A. Raduta, A. Escuderos, A. Faessler, E. Moya de Guerra, Phys. Rev. C **69**, 064321 (2004)
[RRR99]   A.A. Raduta, A.R. Raduta, A.H. Raduta, Phys. Rev. B **59**, 8209 (1999)
[Rich87]   D. Bohle, G. Kilges, A. Richter, C.W. de Jager, Phys. Lett. B **195**(3), 326-330 (1987)

[RRF14]   A.A. Raduta, C.M. Raduta, A. Faessler, J. Phys. G Nucl. Part. Phys. **41**, 035105 (2014)

[RB14]   A.A. Raduta, R. Budaca, Ann. Phys. **347**, 141 (2014)

[SuGl64]   L. Susskind, J. Glogow, Physics **1**, 49 (1964)

[Schm91]   M.R. Schmorak, NDS **63**, 139 (1991)

[Sch91]   M.R. Schmorak, NDS **63**, 183 (1991)

[ShTi92]   E.N. Shurshikov, N.V. Timofeeva, NDS **67**, 45 (1992)

[SCH03]   G. Schoenwasser et al., Phys. Lett. B **552**, 9 (2003)

[SU83]   T. Suzuki, Nucl. Phys. A **398**, 557 (1983)

[S67]   B. Sorensen, Nucl. Phys. A **97**, 1 (1967); A **119**, 65 (1968); A **142**, 392 (1970)

[SI05]   A.J. Simon et al., J. Phys. G Nucl. Part. Phys. **31**, 541 (2005)

[SGEC98]   P. Sarriguren, E. Moya de Guerra, A. Escuderos, A.C. Carrizo, Nucl. Phys. A **635**, 55 (1998)

[SHI76]   S. Sheng-Ming, Acta Math. Sin. **15**, 296 (1976)

[SHMG81]   M. Seiwert, P. Hess, J. Maruhn, W. Greiner, Phys. Rev. C **23**, 2335 (1981)

[Schw65]   J. Schwinger, in *Quantum Theory of Angular Momentum*, ed. by L.C. Biedenharm, H. Van Dam (Academic Press, New York, 1965)

[SiDe82]   R.S. Simon, R.P. Devito, H. Emling, R. Kulessa, C. Briancon, A. Lefebvre, Phys. Lett. B **108**, 87 (1982)

[Sh60]   R.K. Sheline, Rev. Mod. Phys. **32**, 1 (1960)

[Sa76]   M. Sakai, Nucl. Phys. A **104**, 301 (1976), Nucl. Data Tables A **8**, 323 (1970); A **10**, 511 (1972)

[SHU92]   E.N. Shurshikovab, N.V. Timofeeva, NDS **67**, 45 (1992)

[SI01]   B. Singh, NDS **93**, 243 (2001)

[SI95]   B. Singh, NDS **75**, 199 (1995)

[SiFi95]   B. Singh, R.B. Firestone, NDS **74**, 383 (1995)

[S02]   B. Singh, NDS **95**, 387 (2002)

[S03]   B. Singh, NDS **99**, 275 (2003)

[SuLi185] J. Suhonen, P.O. Lipas, Nucl. Phys. A **442**, 189 (1985)

[SuLi285] J. Suhonen, P.O. Lipas, Phys. Lett. B **150**, 327 (1985)

[Su87]   J. Suhonen, Phys. Lett. **193**, 405 (1987)

[STR68]   V.M. Strutinski, Nucl. Phys. A **122**, 1 (1968)

[SEIF93]   F. Seifert, W. Liebertz, A. Dewald, S. Freund, A. Gelberg, A. Granderath, D. Liebertz, R. Wiroski, P. von Bretano, Nucl. Phys. A **554**, 287 (1993)

[SAP55]   F.S. Stephen Jr, F. Asaro, I. Perlman, Phys. Rev. **100**, 1543 (1955)

[SM95]   J.F. Smith et al., Phys. Rev. Lett. **75**, 1050 (1995)

[SS91]   V.G. Soloviov, A.V. Sushkov, Phys. Lett. B **262**, 189 (1991)

[SAH77]   S.K. Saha et al., Phys. Rev. C **15**, 94 (1977)

[SR77]   T. Suzuki, D.J. Rowe, Nucl. Phys. A **289**, 461 (1977)

[SF06]   B. Singh, A.R. Farhan, Nucl. Data Sheets **107**, 1923 (2006)

[ST05]   N.J. Stone, At. Data Nucl. Data Tables **90**, 75 (2005)

[SING10]   B. Singh et al., Nucl. Data Sheets **111**, 2081 (2010)

[TT73]   K.S. Tanabe, K. Tanabe, Nucl. Phys. A **208**, 317 (1973)

[TATA06]   K. Tanabe, K. Sugawara-Tanabe, Phys. Rev. C **73**, 034305 (2006)

[TAK71]   Y. Takahashi, Progress Theoret. Phys. **46**, 1749 (1971)

[TF75]   H. Toki, A. Faessler, Nucl. Phys. **A253**, 231 (1975)

[TNVF77]   H. Toki, K. Neergard, P. Vogel, AND A. Faessler. Nucl. Phys. A **279**, 1 (1977)

[T81]   M. Tabor, Nucl. Phys. A **353**, 353 (1981)

[TF76]   H. Toki, A. Faessler, Z. Phys. A **276**, 35 (1976)

[TOF76]   H. Toki, A. Faessler, Phys. Lett. B **63**, 121 (1976)

[TYF77]   H. Toki, H.L. Yadav, A. Faessler, Phys. Lett. B **66**, 310 (1977)

[TK73]   R.J. Turner, T. Kishimoto, Nucl. Phys. A **217**, 317 (1973)

[TRO05]   P.S. Turner, D.J. Rowe, Nucl. Phys. A **756**, 333 (2005)

[TMF78]   R. Tischler, D. Mertin, A.H. El Farash, B.V. Thirumala, A. Kleinrahm, C. Gunther, H. Hubel, Z. Phys. A **288**, 67 (1978)
[TAM82]   R. Tamisier et al., Nucl. Phys. A **385**, 430 (1982)
[UF79]   G. Ufert, V. Metag, D. Habs, H.J. Specht, Phys. Rev. Lett. **42**, 1596 (1979)
[VIL66]   F. Villars, in *Many-Body Description of Nuclear Structure and Reactions*, ed. by C. Bloch (Academic Press, New York, 1966)
[Vil77]   F. Villars, Nucl. Phys. A 285 (1977) 269
[VFK04]   C. Vaman, D.B. Fossan, T. Koike, K. Starosta, I.Y. Lee, A.O. Machiavelli, Phys. Rev. Lett. **92**, 032501 (2004)
[VIL68]   N.Y. Vilenkin, in *Special Functions and Theory of Group Representations* (AMS transl., Providence, 1968) (ch. 9)
[VBT69]   L. Varnell, J.D. Bowmann, J. Trishuk, Nucl. Phys. A **127**, 270 (1969)
[YK81]   M. Yamamura, K. Kuriama, Progress Theoret. Phys. **65**, 550 (1981)
[ZAW98]   D. Zawischa, J. Phys. G **24**, 683 (1998)
[ZANE77]   A. Zaringhalam, J.W. Negele, Nucl. Phys. A **288**, 417 (1977)
[ZH90]   W.-M. Zhang, D.H. Feng, R. Gilmore, Rev. Mod. Phys. **62**, 867 (1990)
[ZIB08]   S. Zergine, P. Van Isacker, A. Bouldjedri, S. Heinze, Phys. Rev. Lett. **101**, 022502 (2008)
[ZA02]   N.V. Zamfir et al., Phys. Rev. C **65**, 044325 (2002)
[ZACA91]   N.V. Zamfir, R.F. Casten, Phys. Lett. B **260**, 265 (1991)
[ZK01]   N.V. Zamfir, D. Kusnetzov, Phys. Rev. C **63**, 064306 (2001)
[ZH05]   S. Zhu et al., Phys. Lett. B **618**, 51 (2005)
[ZD93]   A.Y. Dzyublik, V.Y. Denisov, Yad. Fiz. **56**, 30 (1993) [Phys. At. Nucl. **56**, 303 (1993)]
[ZAM86]   L. Zamick, Phys. Lett. B **167**, 1 (1986)
[ZZ90]   D.C. Zheng, L. Zamick, E. Moya de Guerra, A. Richter, Phys. Rev. C **42**, 1408 (1990)
[ZZ91]   L. Zamick, D.C. Zheng, Phys. Rev. C **44**, 2522 (1991); C **44**, 2106 (1992)
[ZFL71]   D.R. Zolnoski, E.C. Funk, J.W. Lihelich, Nucl. Phys. A **177**, 513 (1971)
[WuNi03]   S.-C. Wu, H. Niu, NDS **100**, 483 (2003)
[WIJE56]   L. Wilets, M. Jean, Phys. Rev. **102**, 788 (1956)
[WFS70]   H.H. Wolter, A. Faessler, P.U. Sauer, Phys. Lett. B **31**, 516 (1970)
[W78]   A. Weinstein, Ann. Math. **108**, 507 (1978)
[WZCH99]   J.L. Wood, E.F. Zganjar, C. De Coster, K. Heyde, Nucl. Phys. A **651**, 323 (1999)
[WIM08]   K. Wimmer et al., arXiv:0802.2514v1[nucl-ex]
[WE26]   H. Weyl, Math. A **23**, 271 (1925), ibid **24**, 328, 377 (1926)
[WE46]   H. Weyl, *The Classical Groups* (Princeton University Press, Princeton, 1946) (Chapter 5)
[WW50]   E.T. Whittaker, G.N. Watson, *A Course of Modern Analysis*, 4th edn (Cambridge University Press, Cambridge, 1950), p. 513 (reprinted)
[HJW93]   H.J. Wollershein et al., Nucl. Phys. A **556**, 261 (1993)
[Wi92]   M. Wieland et al., Phys. Rev. C **45**, 1035 (1992)